Power Systems Development Facility

Technical Progress Report For Kellogg Brown & Root Transport Reactor Train With Siemens Westinghouse Particulate Control Device

TC05: January 10 – May 2, 1999

DOE Cooperative Agreement Number
DE-FC21-90MC25140

SOUTHERN COMPANY
Energy to Serve Your World℠

POWER SYSTEMS DEVELOPMENT FACILITY

TECHNICAL PROGRESS REPORT
FOR KELLOGG BROWN & ROOT
TRANSPORT REACTOR TRAIN
WITH SIEMENS WESTINGHOUSE
PARTICULATE CONTROL DEVICE

TC05 REPORT: JANUARY 10 – MAY 2, 1999

DOE Cooperative Agreement Number
DE-FC21-90MC25140

Prepared by:
Southern Company Services, Inc.
Power Systems Development Facility
P.O. Box 1069
Wilsonville, AL 35186

April 2000

DISCLAIMER

This report was prepared as an account of work sponsored by an agency of the United States Government. Neither the United States Government nor any agency thereof, nor any of their employees, nor Southern Company Services, Inc., nor any of its employees, nor any of its subcontractors, makes any warranty, expressed or implied, or assumes any legal liability or responsibility for the accuracy, completeness, or usefulness of any information, apparatus, product, or process disclosed, or represents that its use would not infringe privately owned rights. Reference herein to any specific commercial product, process, or service by trade name, trademark, manufacturer or otherwise, does not necessarily constitute or imply its endorsement, recommendation, or favoring by the United States Government or any agency thereof. The views and opinions of authors expressed herein do not necessarily state or reflect those of the United States Government or any agency thereof.

Available to the public from the National Technical Information Service, U.S. Department of Commerce, 5285 Port Royal Road, Springfield, VA 22161. Phone orders accepted at (703) 487-4650.

CONTENTS

Section Page

Inside Cover
Disclaimer

Listing of Tables and Figures v

1.0 EXECUTIVE SUMMARY 1.1-1

1.1 Summary 1.1-1

1.2 PSDF Accomplishments 1.2-1
1.2.1 Transport Reactor Train 1.2-1
1.2.2 PCD 1.2-2

1.3 Future Plans 1.3-1

2.0 INTRODUCTION 2.1-1

2.1 The Power Systems Development Facility 2.1-1
2.2 Transport Reactor System Description 2.2-1
2.3 Siemens Westinghouse Particulate Control Device 2.3-1
2.4 Operation Status 2.4-1

3.0 PARTICLE FILTER SYSTEM 3.1-1

3.1 TC05 PCD Introduction 3.1-1

3.2 PCD Operation During Test Run TC05 ..... 3.2-1
3.2.1 Introduction 3.2-1
3.2.2 Test Objective 3.2-5
3.2.3 Observations/Events - 1/12/99 Through 1/23/99 ..... 3.2-5
3.2.4 Observations/Events - 1/31/99 Through 2/24/99 ..... 3.2-7
3.2.5 Observations/Events - 3/3/99 Through 3/8/99 ..... 3.2-9
3.2.6 Observations/Events - 3/13/99 Through 3/27/99 ..... 3.2-10
3.2.7 Observations/Events - 4/12/99 Through 5/2/99 ..... 3.2-11
3.2.8 Run Summary 3.2-13
3.2.9 References 3.2-18

3.3 TC05 PCD Inspection Report 3.3-1
3.3.1 Summary 3.3-1
3.3.2 Inspection I 3.3-1
3.3.3 Inspection II 3.3-4

3.3.4 Inspection III 3.3-5
3.3.5 Inspection IV....3.3-7
3.3.6 Inspection V 3.3-7

3.4 TC05 Ash Characteristics and PCD Performance....3.4-1
3.4.1 Measurements of Particulate Mass Loadings....3.4-2
3.4.2 Chemical Analyses 3.4-5
3.4.3 Measurements of Physical Properties 3.4-9
3.4.4 Effect of Particle Size on Drag....3.4-11
3.4.5 Relationship Between Lab-Measured Drag and Actual PCD Performance 3.4-12
3.4.6 Evaluation of Real-Time Particulate Monitors 3.4-13
3.4.7 Measurements of Acid Gases 3.4-16
3.4.8 References....3.4-17

3.5 Fines Handling System....3.5-1
3.5.1 Operational Summary 3.5-1
3.5.2 Spent Fines Transport System (FD0520) Observations and Events 3.5-1
3.5.3 Spent Fines Screw Cooler (FD0502) Observations and Events 3.5-2
3.5.4 Spent Fines Transport System (FD0520) Status and Issues 3.5-3
3.5.5 Spent Fines Screw Cooler (FD0502) Status and Issues 3.5-5

3.6 Candle Filter Material Evaluations....3.6-1

3.7 Ash Bridging in Hot-Gas Filter During Combustion of Petroleum Coke With Dolomite....3.7-1
3.7.1 Background and Observations 3.7-1
3.7.2 Relevant Information From Previous Studies....3.7-3
3.7.3 Chemistry of Ash Bridges and In situ Dust Samples 3.7-6
3.7.4 Laboratory Studies of Ash Consolidation Mechanisms....3.7-8
3.7.5 Conclusions 3.7-13
3.7.6 Future Work 3.7-14
3.7.7 References....3.7-15

4.0 TRANSPORT REACTOR....4.1-1

4.1 Run Summary....4.1-1

4.2 Material Balance....4.2-1

4.3 SO_2, SO_3, and Solids Analyses....4.3-1

4.4 NO_X and N_2O Analysis 4.4-1
4.4.1 NO_X Analysis 4.4-1
4.4.2 N_2O Analysis 4.4-4

4.5 Temperature Profile 4.5-1

TERMS ..... PSDF Terms-1

APPENDIX

This Page Intentionally Left Blank

Listing of Tables

Table | Page

2.2-1 Major Equipment in the Transport Reactor Train 2.2-3
2.2-2 Major Equipment in the Balance-of-Plant 2.2-4

3.2-1 TC05 Run Statistics (1/12/1999 Through 1/22/1999) 3.2-19
3.2-2 TC05 Major Events (1/12/1999 Through 1/22/1999) 3.2-20
3.2-3 TC05 Run Statistics (1/31/1999 Through 2/24/1999) 3.2-21
3.2-4 TC05 Major Events (1/31/1999 Through 2/24/1999) 3.2-22
3.2-5 TC05 Run Statistics (3/3/1999 Through 3/8/1999) 3.2-23
3.2-6 TC05 Major Events (3/3/1999 Through 3/8/1999) 3.2-24
3.2-7 TC05 Run Statistics (3/13/1999 Through 3/27/1999) 3.2-25
3.2-8 TC05 Major Events (3/13/1999 Through 3/27/1999) 3.2-26
3.2-9 TC05 Run Statistics (4/12/1999 Through 5/2/1999) 3.2-27
3.2-10 TC05 Major Events (4/12/1999 Through 5/2/1999) 3.2-28
3.2-11 Operational Data for Pressure Drop Comparison 3.2-29
3.2-12 Calculated Pressure Drop 3.2-30

3.4-1 Summary of Inlet Particulate Loadings Measured During TC05 ....3.4-18
3.4-2 Outlet Particulate Loadings and Collection Efficiencies Measured During TC05 ....3.4-20
3.4-3 Summary of Hot-Gas Filter Performance During Major Portions of TC05 ....3.4-22
3.4-4 Results of Chemical Analyses Performed on Selected TC05 In situ Sample 3.4-23
3.4-5 Results of Chemical Analyses Performed on Selected TC05 Dustcake Sample 3.4-24
3.4-6 Physical Properties of Selected TC05 In situ Samples 3.4-25
3.4-7 Physical Properties of Selected TC05 Dustcake Samples 3.4-26
3.4-8 Measurements of Acid Gases (SO_2, SO_3, HCl, HF) During TC05 ....3.4-27

3.7-1 Chemical Compositions and Molar Ratios of Ash Bridging Samples 3.7-17

4.1-1 TC05 Operating Conditions 4.1-5
4.1-2 Coal Feed Analyses 4.1-6
4.1-3 Sorbent Analyses 4.1-6

4.2-1 Material Balance Periods in TC05 ....4.2-2
4.2-2 Bulk Material Balances in TC05 ....4.2-2
4.2-3 Carbon Component Material Balances in TC05 ....4.2-3
4.2-4 Sulfur Component Material Balances in TC05 ....4.2-3
4.2-5 Oxygen Component Material Balances in TC05 ....4.2-4
4.2-6 Nitrogen Component Material Balances in TC05 ....4.2-4

4.3-1 Test Periods 4.3-16
4.3-2 SO_2 and SO_3 Data and Results 4.3-17
4.3-3 HCI Emissions 4.3-18

4.4-1 Average Conditions for TC05 NO_X and N_2O Data Analysis 4.4-6

4.5-1 Analysis of Each Fuel 4.5-3

Listing of Figures

Figure Page

2.2-1 Flow Diagram of the Transport Reactor Train in Combustion Mode of Operation 2.2-7

2.3-1 Siemens Westinghouse PCD 2.3-2

2.4-1 Operating Hours Summary for Transport Reactor Train Major Test Campaigns 2.4-2

3.2-1 Filter Element Layout for TC05 - January 12 Through January 22 (Layout No. 11) 3.2-31
3.2-2 TC05 Temperature and Pressure for January 12 Through January 18 ..... 3.2-32
3.2-3 TC05 Back-Pulse Pressure and Face Velocity for January 12 Through January 18 ..... 3.2-33
3.2-4 TC05 Pressure Drop and Permeance for January 12 Through January 18 ..... 3.2-34
3.2-5 TC05 Temperature and Pressure for January 18 Through January 23 ..... 3.2-35
3.2-6 TC05 Back-Pulse Pressure and Face Velocity for January 18 Through January 23 ..... 3.2-36
3.2-7 TC05 Pressure Drop and Permeance for January 18 Through January 23 ..... 3.2-37
3.2-8 Filter Element Layout for TC05 - January 31 Through February 24 (Layout 12) 3.2-38
3.2-9 TC05 Temperature and Pressure for January 31 Through February 7 ..... 3.2-39
3.2-10 TC05 Back-Pulse Pressure and Face Velocity for January 31 Through February 7 ..... 3.2-40
3.2-11 TC05 Pressure Drop and Permeance for January 31 Through February 7 ..... 3.2-41
3.2-12 TC05 Temperature and Pressure for February 7 Through February 13 ..... 3.2-42
3.2-13 TC05 Back-Pulse Pressure and Face Velocity for February 7 Through February 13 ..... 3.2-43
3.2-14 TC05 Pressure Drop and Permeance for February 7 Through February 13 ..... 3.2-44
3.2-15 TC05 Temperature and Pressure for February 13 Through February 19 ..... 3.2-45
3.2-16 TC05 Back-Pulse Pressure and Face Velocity for February 13 Through February 19 ..... 3.2-46
3.2-17 TC05 Pressure Drop and Permeance for February 13 Through February 19 ..... 3.2-47
3.2-18 TC05 Temperature and Pressure for February 19 Through February 25 ..... 3.2-48
3.2-19 TC05 Back-Pulse Pressure and Face Velocity for February 19 Through February 25 ..... 3.2-49
3.2-20 TC05 Pressure Drop and Permeance for February 19 Through February 25 ..... 3.2-50
3.2-21 Filter Element Layout for TC05 - March 2 Through March 9 (Layout 13) 3.2-51
3.2-22 TC05 Temperature and Pressure for March 2 Through March 9 ..... 3.2-52
3.2-23 TC05 Back-Pulse Pressure and Face Velocity for March 2 Through March 9 ..... 3.2-53
3.2-24 TC05 Pressure Drop and Permeance for March 3 Through May 2 ..... 3.2-54
3.2-25 TC05 Temperature and Pressure for March 13 Through March 19 ..... 3.2-55
3.2-26 TC05 Back-Pulse Pressure and Face Velocity for March 13 Through March 19 ..... 3.2-56

3.2-27 TC05 Pressure Drop and Permeance for March 13 Through March 19 .....3.2-57
3.2-28 TC05 Temperature and Pressure for March 19 Through March 24.....3.2-58
3.2-29 TC05 Back-Pulse Pressure and Face Velocity for March 19 Through March 24 .....3.2-59
3.2-30 TC05 Pressure Drop and Permeance for March 19 Through March 24 .....3.2-60
3.2-31 TC05 Temperature and Pressure for March 24 Through March 29.....3.2-61
3.2-32 TC05 Back-Pulse Pressure and Face Velocity for March 24 Through March 29 .....3.2-62
3.2-33 TC05 Pressure Drop and Permeance for March 24 Through March 29 .....3.2-63
3.2-34 TC05 Temperature and Pressure for April 11 Through April 17.....3.2-64
3.2-35 TC05 Back-Pulse Pressure and Face Velocity for April 11 Through April 17.....3.2-65
3.2-36 TC05 Pressure Drop and Permeance for April 11 Through April 17 .....3.2-66
3.2-37 TC05 Temperature and Pressure for April 17 Through April 23.....3.2-67
3.2-38 TC05 Back-Pulse Pressure and Face Velocity for April 17 Through April 23....3.2-68
3.2-39 TC05 Pressure Drop and Permeance for April 17 Through April 23 .....3.2-69
3.2-40 TC05 Temperature and Pressure for April 23 Through April 28.....3.2-70
3.2-41 TC05 Back-Pulse Pressure and Face Velocity for April 23 Through April 28....3.2-71
3.2-42 TC05 Pressure Drop and Permeance for April 23 Through April 28 .....3.2-72
3.2-43 TC05 Temperature and Pressure for April 28 Through May 3 .....3.2-73
3.2-44 TC05 Back-Pulse Pressure and Face Velocity for April 28 Through May 3 .....3.2-74
3.2-45 TC05 Pressure Drop and Permeance for April 28 Through May 3.....3.2-75

3.3-1 Tubesheet Map.....3.3-10
3.3-2 Filter Element Layout 11 .....3.3-11
3.3-3 Leak Through a Hole on the Ash Cake 3.3-12
3.3-4 Leak Through a Gap on the Ash Cake.....3.3-12
3.3-5 Leak Through a Gap on the Ash Cake.....3.3-13
3.3-6 Filter Element Layout 12.....3.3-14
3.3-7 Location of the Three Broken AlliedSignal PRD-66 Filter Elements 3.3-15
3.3-8 Broken AlliedSignal PRD-66 Filter Element at B49 .....3.3-15
3.3-9 Broken AlliedSignal PRD-66 Filter Element at B54 .....3.3-16
3.3-10 Small Ash Lumps on Filter Element Surfaces.....3.3-16
3.3-11 Slight Ash Bridging Near the Flanges.....3.3-17
3.3-12 Ash Bridging Between the Shroud and Liner.....3.3-17
3.3-13 Heavy Coverage of Ash on the Shroud.....3.3-18
3.3-14 Filter Element Layout 13.....3.3-19
3.3-15 Locations of the Ash Bridging.....3.3-20
3.3-16 Ash Bridging on the Top Plenum 3.3-21
3.3-17 Ash Bridging Lumps 3.3-21
3.3-18 Ash Lumps on the Filter Element Surfaces.....3.3-22
3.3-19 Ash Build-up on the Shroud and Liner 3.3-22
3.3-20 Filter Elements Inspected from the Lower Manway.....3.3-23
3.3-21 Shroud and Liner Inspected from the Lower Manway.....3.3-23
3.3-22 Filter Elements Inspected from the Top of the PCD.....3.3-24
3.3-23 An Ash Pile on the Top of the Top Plenum.....3.3-24
3.3-24 A Hole on the Body of a 3M Oxide Filter Element.....3.3-25

3.3-25 Filter Element Inspection 3.3-26
3.3-26 Ash Build-up on the Support Column 3.3-27
3.3-27 Cracks on the Gas Inlet 3.3-27
3.3-28 A Buckle on the Liner Near the Gas Inlet 3.3-28
3.3-29 A Buckle on the Liner Near the Bottom of Section B 3.3-28

3.4-1 Effect of Particle Size on Drag Equivalent Diameter of Inlet Dust Samples and Dustcake Samples 3.4-29
3.4-2 Effect of Particle Size on PCD Transient Drag During TC05 In situ Sampling Runs 3.4-29
3.4-3 Lab-Measured Drag Versus Porosity Curves for Various Inlet Dust Samples 3.4-30
3.4-4 Particle-Size Distributions of the Four Inlet Dust Samples With Laboratory Drag Measurements Show in Figure 3.4-3 ..... 3.4-30
3.4-5 Relationships Between Lab-Measured Drag (at Uncompacted Bulk Porosity) and PCD Transient Drag for all TC05 and TC05 Inlet Dust Samples 3.4-31
3.4-6 Relationships Between PCD Residual Dustcake Drag and Lab-Measured Drag at Flow-Compacted Porosity and Between PCD Transient Dustcake Drag and Lab-Measured Drag at Uncompacted Bulk Porosity 3.4-31
3.4-7 Piping and Instrument Diagram of Ash Injection System 3.4-32
3.4-8 Ash Injection System Fluidized-Bed Assembly 3.4-33
3.4-9 Ash Injection System Mass Output 3.4-34
3.4-10 Jonas Particulate Monitor Results 3.4-34

3.5-1 Spent Fines Transport System (FD0520) 3.5-7
3.5-2 Spent Fines Screw Cooler With Original Inlet-side Ceramic Bushing Bearing and Original Inlet-side Seal 3.5-8
3.5-3 Spent Fines Screw Cooler with Modified Inlet-side Bearing Arrangement and Modified Inlet-side Seal 3.5-8

3.7-1 Overall View of Ash Bridging in Top Plenum 3.7-18
3.7-2 Close-up of Ash Bridging in Top Plenum 3.7-19
3.7-3 Overall View of Ash Bridging in Bottom Plenum 3.7-20
3.7-4 Close-up of Ash Bridging in Bottom Plenum 3.7-21
3.7-5 Locations of Retained Ash Bridges 3.7-22
3.7-6 X-ray Diffraction Patterns of Ash Bridging Samples 3.7-23
3.7-7 Relative Strengths of Various Reconsolidated Powders 3.7-23
3.7-8 SEM Photographs of Bridged Material from Hot-Gas Filter 3.7-24
3.7-9 SEM Photographs of In situ Dust Sample Collected at Inlet of Hot-Gas Filter 3.7-25
3.7-10 SEM Photographs of Residual Dustcake from Alabama Coal and Plum Run Dolomite 3.7-26
3.7-11 Close-up of Ash Bridging Showing Variations in Ca/Mg Atomic Ratio 3.7-27
3.7-12 SEM Photographs of Sulfated Dolomite From Flow-Tube Furnace Tests 3.7-28
3.7-13 SEM Photographs of $CaCO_3$ Before and After Treatment in Flow-Tube Furnace 3.7-29

4.3-1 System Pressure, Standpipe, and PCD Temperature 4.3-19
4.3-2 System Pressure, Standpipe, and PCD Temperature 4.3-19
4.3-3 Coal Feed, SO_2 Emissions....4.3-20
4.3-4 Coal Feed, SO_2 Emissions....4.3-20
4.3-5 Alabama Bituminous Coal Sulfur and Ash Contents....4.3-21
4.3-6 Illinois No. 6 Coal Sulfur and Ash Contents....4.3-21
4.3-7 Petroleum Coke Sulfur and Ash Contents....4.3-22
4.3-8 Coal Sulfur and Ash Contents 4.3-22
4.3-9 Fuel Particle Size....4.3-23
4.3-10 Sorbent Particle Size....4.3-23
4.3-11 Sorbent Composition 4.3-24
4.3-12 Sorbent Composition 4.3-24
4.3-13 Reactor and PCD Solids Particle Size....4.3-25
4.3-14 Reactor and PCD Solids Particle Size....4.3-25
4.3-15 Alabama Coal PCD Solids Ca/S, Feeds Ca/S, In situ Ca/S, and Reactor Solids Ca/S 4.3-26
4.3-16 Illinois No. 6 Coal PCD Solids Ca/S, Feeds Ca/S, In situ Ca/S, and Reactor Solids Ca/S 4.3-26
4.3-17 Petroleum Coke PCD Solids Ca/S, Feeds Ca/S, In situ Ca/S, and Reactor Solids Ca/S 4.3-27
4.3-18 PCD Solids Ca/S, Feeds Ca/S, In situ Ca/S, and Reactor Solids Ca/S for Three Fuels....4.3-27
4.3-19 PCD and Reactor Solids $CaCO_3$ and $CaSO_4$ Contents....4.3-28
4.3-20 PCD and Reactor Solids $CaCO_3$ and $CaSO_4$ Contents....4.3-28
4.3-21 PCD and Reactor CaO, CaO•MgO, and MgO Contents 4.3-29
4.3-22 PCD and Reactor CaO, CaO•MgO, and MgO Contents 4.3-29
4.3-23 PCD and Reactor Inerts Contents 4.3-30
4.3-24 PCD and Reactor Inerts Contents 4.3-30
4.3-25 Carbon Monoxide and Unburned Carbon 4.3-31
4.3-26 Carbon Monoxide and Unburned Carbon 4.3-31
4.3-27 Bulk Density of Reactor and PCD Solids 4.3-32
4.3-28 Bulk Density of Reactor and PCD Solids 4.3-32
4.3-29 SO_2-SO_3 Equilibrium 4.3-33
4.3-30 SO_X Removal and PCD Solids Ca/S by Fuel....4.3-33
4.3-31 SO_2 Emissions and PCD Solids Ca/S by Fuel 4.3-34
4.3-32 SO_X Removal and PCD Solids Ca/S by Sorbent....4.3-34
4.3-33 SO_2 Emissions and PCD Solids Ca/S by Sorbent 4.3-35
4.3-34 TC03 SO_X Removal and PCD Solids Ca/S by Sorbent....4.3-35
4.3-35 TC03 SO_2 Emissions and PCD Solids Ca/S by Sorbent....4.3-36

4.4-1 Transport Reactor Train Gas Sample Locations....4.4-8
4.4-2 Effect of Staging Air on NO_X Emissions With Alabama Coal and Longview Limestone 4.4-9
4.4-3 Effect of Staging Air on NO_X Emissions With Illinois Coal and Bucyrus Limestone....4.4-9
4.4-4 Effect of Staging Air on NO_X Emissions With PRB and Bucyrus Limestone....4.4-9

4.4-5 Effect of Staging Air on NO_X Emissions With Pet Coke and Plum Run Dolomite and Bucyrus Limestone 4.4-9
4.4-6 Effect of Excess Oxygen on NO_X Emissions With Alabama Coal and Longview Limestone 4.4-10
4.4-7 Effect of Excess Oxygen on NO_X Emissions With Illinois Coal and Bucyrus and Longview Limestone and Plum Run Dolomite 4.4-10
4.4-8 Effect of Excess Oxygen on NO_X Emissions With Kentucky Coal and Gregg Mine Limestone 4.4-10
4.4-9 Effect of Excess Oxygen on NO_X Emissions With PRB Coal and Bucyrus and Gregg Mine Limestone 4.4-10
4.4-10 Effect of Excess Oxygen on NO_X Emissions With Pet Coke and Plum Run Dolomite and Bucyrus Limestone 4.4-11
4.4-11 Effect of Reactor Temperature on NO_X Emissions With Alabama Coal and Bucyrus and Longview Limestone 4.4-11
4.4-12 Effect of Reactor Temperature on NO_X Emissions With Illinois Coal and Bucyrus and Longview Limestone and Plum Run Dolomite 4.4-11
4.4-13 Effect of Reactor Temperature on NO_X Emissions With KY Coal and Gregg Mine Limestone 4.4-11
4.4-14 Effect of Reactor Temperature on NO_X Emissions With PRB Coal and Bucyrus and Gregg Mine Limestone 4.4-12
4.4-15 Effect of Reactor Temperature on NO_X Emissions With Pet Coke and Plum Run Dolomite and Bucyrus Limestone 4.4-12
4.4-16 Effect of Sorbent Feedrate on NO_X Emissions With Alabama Coal and Bucyrus and Longview Limestone 4.4-12
4.4-17 Effect of Sorbent Feedrate on NO_X Emissions With Illinois Coal and Bucyrus and Longview Limestone and Plum Run Dolomite 4.4-12
4.4-18 Effect of Sorbent Feedrate on NO_X Emissions With Kentucky Coal and Gregg Mine Limestone 4.4-13
4.4-19 Effect of Sorbent Feedrate on NO_X Emissions With PRB Coal and Bucyrus and Gregg Mine Limestone 4.4-13
4.4-20 Effect of Sorbent Feedrate on NO_X Emissions With Pet Coke and Plum Run Dolomite and Bucyrus Limestone 4.4-13
4.4-21 Effect of Sorbent Feedrate on NO_X Emissions With Alabama Coal and Longview Limestone 4.4-14
4.4-22 Effect of Reactor Pressure on NO_X Emissions With Pet Coke and Plum Run Limestone 4.4-14
4.4-23 Effect of Fuel Feed Particle Size on NO_X Emissions With Pet Coke and Bucyrus Limestone 4.4-15
4.4-24 Range of NO_X Emissions With Different Feed Combinations (Data Set L1) 4.4-15
4.4-25 Relationship Between Fuel Nitrogen Conversion to NO_X and Fuel Oxygen and Fuel Nitrogen 4.4-16
4.4-26 Effect of Staging Air on N_2O Emissions With PRB Coal and Bucyrus Limestone 4.4-16
4.4-27 Effect of Staging Air on N_2O Emissions With Illinois Coal and Bucyrus Limestone 4.4-16

4.4-28 Effect of Staging Air on N_2O Emissions With Pet Coke and Bucyrus Limestone and Plum Run Dolomite....4.4-17
4.4-29 Effect of Excess Oxygen on N_2O Emissions With Alabama Coal and Bucyrus and Longview Limestone....4.4-17
4.4-30 Effect of Excess Oxygen on N_2O Emissions With Illinois Coal and Bucyrus and Longview Limestone and Plum Run Dolomite....4.4-17
4.4-31 Effect of Excess Oxygen on N_2O Emissions With Kentucky Coal and Gregg Mine Limestone....4.4-17
4.4-32 Effect of Excess Oxygen on N_2O Emissions With PRB Coal and Bucyrus and Gregg Mine Limestone....4.4-18
4.4-33 Effect of Excess Oxygen on N_2O Emissions With Pet Coke and Plum Run Dolomite and Bucyrus Limestone....4.4-18
4.4-34 Effect of Reactor Temperature on N_2O Emissions With Alabama Coal and Bucyrus and Longview Limestone....4.4-18
4.4-35 Effect of Reactor Temperature on N_2O Emissions With Illinois Coal and Bucyrus and Longview Limestone and Plum Run Dolomite....4.4-18
4.4-36 Effect of Reactor Temperature on N_2O Emissions With Kentucky Coal and Gregg Mine Limestone....4.4-19
4.4-37 Effect of Reactor Temperature on N_2O Emissions With PRB Coal and Bucyrus and Gregg Mine Limestone....4.4-19
4.4-38 Effect of Reactor Temperature on N_2O Emissions With PRB Coal and Bucyrus and Gregg Mine Limestone....4.4-19
4.4-39 Effect of Sorbent Feedrate on N_2O Emissions With Alabama Coal and Longview and Bucyrus Limestone....4.4-19
4.4-40 Effect of Sorbent Feedrate on N_2O Emissions With Illinois Coal and Bucyrus and Longview Limestone and Plum Run Dolomite....4.4-20
4.4-41 Effect of Sorbent Feedrate on N_2O Emissions With Kentucky Coal and Gregg Mine Limestone....4.4-20
4.4-42 Effect of Sorbent Feedrate on N_2O Emissions With PRB Coal and Bucyrus and Gregg Mine Limestone....4.4-20
4.4-43 Effect of Sorbent Feedrate on N_2O Emissions With Pet Coke and Bucyrus Limestone and Plum Run Dolomite....4.4-20
4.4-44 Effect of Sorbent Feedrate on N_2O Emissions With Alabama Coal and Longview Limestone....4.4-21
4.4-45 Effect of Reactor Pressure on N_2O Emissions With Pet Coke and Plum Run Dolomite....4.4-21
4.4-46 Effect of Fuel Feed Particle Size on N_2O Emissions With Pet Coke and Bucyrus Limestone....4.4-22
4.4-47 Range of N_2O Emissions With Different Feed Combinations (Data Set L2)....4.4-22

4.5-1 Riser Temperature Profile for Illinois No. 6 Coal and Petroleum Coke....4.5-4
4.5-2 Standpipe and Dipleg Temperature Profile for Alabama Coal and Petroleum Coke....4.5-4

1.0 EXECUTIVE SUMMARY

1.1 SUMMARY

This report discusses test campaign TC05 of the Kellogg Brown & Root (KBR) transport reactor train with a Seimens Westinghouse Power Corporation (Siemens Westinghouse) particle filter system at the Power Systems Development Facility (PSDF) located in Wilsonville, Alabama. The transport reactor is an advanced circulating fluidized-bed reactor designed to operate as either a combustor or a gasifier using one of two possible particulate control devices (PCD). The transport reactor was operated as a pressurized combustor during TC05.

TC05 was planned as a 1,000-hour test run to demonstrate steady state operations with a variety of feed materials and to perform reactor parametric testing with different feed combinations. The detail objectives of test run TC05 for the transport reactor were:

- Demonstrate stable reactor operations using Alabama Calumet Mine bituminous coal with Ohio Bucyrus limestone and Alabama Longview limestone.
- Demonstrate stable reactor operations using the design coal — Illinois #6 bituminous coal — with Ohio Bucyrus limestone, Alabama Longview limestone (design sorbent), and Plum Run dolomite.
- Demonstrate stable operations using petroleum coke and a Powder River Basin subbituminous coal with a variety of sorbents.
- Evaluate effects of excess air, primary-air distribution, reactor temperature, reactor pressure, and sorbent feed rate on NO_X and N_2O emissions.
- Evaluate effects of sorbent feed rate and reactor conditions on SO_2 emissions.

Test run TC05 was started on January 10, 1999, and was completed May 2, 1999. Overall, this test run was successful, with 10 different feed combinations tested. The reactor temperature was varied between 1,500 and 1,625°F at pressures from 160 to 210 psig. There was agglomeration and clinker formation when using the Powder River Basin coal and Eastern Kentucky coal. The likely cause of the deposits was the presence of excessive fines in the fuel feed. The total hours of solid circulation in TCO5 were 1,627 with 1,429 hours of coal feed attained. The major accomplishments and observations during TC05 included the following:

1. Stable operations were demonstrated using all feedstock combinations tested. There was some agglomerate/clinker formation with the Powder River Basin coal due to a temperature excursion and the presence of excessive fines in the fuel feed. While using the Eastern Kentucky coal, these deposits grew quickly during time periods when excess fines were present and eventually forced a process shutdown.

2. The TC05 test run included the longest continuous trouble-free operations to date without any interruption from the coal feed system or any other subsystem (471 hours).

3. High-carbon conversions along with high throughputs were achieved consistently with different fuels and a multitude of process conditions.

4. Heat-release rates as high as 57 MBtu/hr/ft^2 in the riser were achieved.

5. High-solids-circulation rates (more than 100:1 solids-circulation rate:coal-feed rate) were achieved.

6. A high-sulfur capture, greater than 97 percent, was achieved at a Ca/S molar ratio of 1.5. Low-SO_X emissions were achieved when using PRB without adding sorbent due to high-Ca content in PRB ash.

7. NO_X emissions less than 0.10 lb/MBtu were achieved with the Alabama and Illinois #6 bituminous coals, and NO_X emissions less than 0.15 lb/MBtu were achieved with the Eastern Kentucky bituminous coal and pet coke. Essentially zero-N_2O emissions are achievable at higher operating temperatures.

8. For test purposes, fine sorbent was successfully ground and fed (<40 um mmd).

9. Stable operations were achieved with petroleum coke for 265 hours. Average carbon conversion was 99.2 percent between 1,575 and 1,640°F at high throughputs.

10. The PCD operated on coal for 1,429 hours with relatively few operational problems. The range-of-process conditions include:

    - Temperatures from 700 to 1,400°F.
    - Face velocities from 4 to 8 ft/min.
    - Particulate loadings from 3,000 to 25,000 ppmw.

11. The PCD operated at a face velocity of 8 ft/min for 175 hours. After the initial ~100 hours required for the residual cake to form, the baseline pressure drop was constant.

12. The PCD operated on petroleum coke with dolomite and limestone successfully for 260 hours with a PCD temperature of 750°F.

13. The PCD operated for over 575 hours with an outlet particulate loading below 1 ppmw.

14. Ten different filter elements from seven different manufacturers were tested.

15. Two-meter long 3M oxide filter elements were tested.

16. One McDermott filter element lost a plug in the bottom of the element, which caused leakage. McDermott has redesigned the plug and supplied filter elements for the first gasification run.

17. Three PRD-66 filter elements failed during TC05 and membrane spalling was found on several other PRD-66 filter elements. AlliedSignal has received these filter elements and is evaluating the cause of the failure.

18. One 3M oxide filter element with a pinhole leak was found. This element has been sent back to 3M for evaluation.

19. Ash bridging was experienced when operating with petroleum coke and Plum Run dolomite at a PCD temperature of ~1,400°F. After thorough investigation of the ash, it appears that the root cause of the bridging was sulfation of the PCD dust cake.

1.2 PSDF ACCOMPLISHMENTS

The PSDF has achieved over 4,985 hours of operation on coal feed and about 6,470 hours of solids circulation. The major accomplishments to date have resulted in improved equipment and process design, higher availability, improved process performance, and a better understanding of the transport reactor and PCD operations are summarized below.

1.2.1 Transport Reactor Train

1. Stable reactor operations were demonstrated by successfully addressing the excessive solids-carryover problem.

2. Higher temperatures were achieved with the start-up burner before feeding coal. The start-up burner firing, originally designed for 3.6 MBtu/hr was increased to 7.5 MBtu/hr, which resulted in a PCD-inlet starting temperature of 920°F and a reactor starting temperature of 1,200°F.

3. Coal feed system modifications were effective and the system operated reliably over longer periods of time. Operational problems still occasionally develop with the coal feed system, primarily when (segregated) fine coal moves through the system.

4. Effective solids circulation and higher disengager cyclone collection efficiency were achieved with smaller grind-size start-up bed material (120 μm mmd). Smoother operation in the reactor was achieved with lower grind-size material in the reactor.

5. For test purposes, sorbent was successfully ground to less than 40 μm mmd and was used without any problems in the sorbent feed system to feed into the reactor.

6. Following modifications made to the sealing mechanism on the spheri seal-holding plate the filter ash depressurization and transportation system has performed well.

7. Different legs of an empty reactor loop and combustor heat exchanger were successfully heated to above 1,000°F and the PCD was heated to above 800°F before adding sand through the coal feed system at 110- to 135-psig reactor pressure.

8. Stable operations were demonstrated using the Calumet Mine bituminous coal, the Illinois #6 bituminous coal, the Eastern Kentucky bituminous coal, and Powder River Basin subbituminous coal with Plum Run dolomite, Bucyrus limestone, Longview limestone, and Gregg Mine limestone.

9. Nearly 100-percent carbon conversions were achieved with several different coals at reactor temperatures between 1,525 and 1,625°F.

10. Stable operations were demonstrated using petroleum coke with Plum Run dolomite and Bucyrus limestone. Pet coke conversions ranged from 99.2 to 99.8 percent at reactor temperatures between 1,575 and 1,660°F.

1.2.2 PCD

1. The Seimens Westinghouse PCD operated without ash bridging for about 4,720 hours on coal in combustion mode at PCD-inlet temperatures over 1,350°F. However, ash bridging was experienced for the first time when operating with petroleum coke and dolomite at a PCD temperature of 1,400°F. The PCD then operated on petroleum coke with dolomite and limestone successfully for 265 hours with a PCD temperature of 750°F.

2. The longest continuous run to date without shutdown was experienced at 471 hours.

3. Monitoring and controlling ash level in the PCD continued to be successful.

4. The pulse valves supplied with the PCD were modified and the modifications were proven successful.

5. The 3M Company resolved an issue of dust leaking around the 3M elements, due to the filter vessel-supplied gasketing scheme, by designing a ceramic insert to allow use of the "standard" gasketing scheme.

6. The Seimens Westinghouse PCD was operated for over 1,500 hours with outlet loadings below 1 ppm on coal in combustion.

7. Various feed combinations with four coals and four sorbents were used and demonstrated no negative affects on PCD operation.

8. PSDF has successfully demonstrated the operation of the PCD with design coal and sorbent for the Lakeland CCT project.

9. Several monolithic silicon carbide filter elements have accumulated over 3,200 hours of exposure. Additionally, the composite filter elements have accumulated over 2,200 hours of exposure.

10. Operating with 10 different fuel/sorbent ashes, and at operation up to 8 ft/min face velocity, allowed for the development of models to predict the performance of the PCD under a variety of conditions.

11. Leakage around the failsafe flanges was an issue in the first part of TC05. This lead to the development of a new filter holder by the PSDF staff. The new filter holder is currently undergoing testing.

1.3 FUTURE PLANS

Plans for the remainder of 1999 are shown below.

1. Conversion of the transport reactor and the process for operation in gasification mode of operation will be completed by September 1, 1999.

2. A 100-hour commissioning and characterization test with the transport reactor train operating in gasification mode is planned for the last quarter of the year.

2.0 INTRODUCTION

This report provides an account of the TC05 test campaign with the Kellogg Brown & Root (KBR) transport reactor and the Siemens Westinghouse Power Corporation (Siemens Westinghouse) filter vessel at the Power Systems Development Facility (PSDF) located in Wilsonville, Alabama, 40 miles southeast of Birmingham. The PSDF is sponsored by the U. S. Department of Energy (DOE) and is an engineering-scale demonstration of two advanced coal-fired power systems. In addition to DOE, Southern Company Services, Inc., (SCS), Electric Power Research Institute (EPRI), and Peabody Holding Company are cofunders. Other cofunding participants supplying services or equipment include KBR, Foster Wheeler (FW), Siemens Westinghouse, and Combustion Power Company. SCS is responsible for constructing, commissioning, and operating the PSDF.

2.1 THE POWER SYSTEMS DEVELOPMENT FACILITY

SCS entered into an agreement with DOE/FETC for the design, construction, and operation of a hot-gas clean-up test facility for gasification and pressurized combustion. The purpose of the PSDF is to provide a flexible test facility that can be used to develop advanced power system components, evaluate advanced-turbine system configurations, and assess the integration and control issues of these advanced-power systems. The facility was designed as a resource for rigorous, long-term testing and performance assessment of hot-stream clean-up devices and other components in an integrated environment.

The PSDF will consist of five modules for systems and component testing. These modules include:

- An advanced-pressurized, fluidized-bed combustion module (APFBC).
- A transport reactor module.
- A hot-gas clean-up module.
- A compressor/turbine module.
- A fuel cell module.

The APFBC module consists of FW technology for second-generation PFBC. This module relies on partial conversion of the coal to fuel gas in a carbonizer, with the remaining char converted in a PFBC. Both the fuel gas and PFBC exhaust gas streams are filtered to remove particulates, then combined to fire a combustion turbine. The transport reactor module includes KBR transport technology for pressurized combustion and gasification to provide either an oxidizing or reducing gas for parametric testing of hot-particulate control devices. The filter systems that will be tested at PSDF include particulate control devices (PCDs) supplied by Combustion Power Company and Siemens Westinghouse.

2.2 TRANSPORT REACTOR SYSTEM DESCRIPTION

The transport reactor is an advanced-circulating fluidized-bed reactor acting as either a combustor or as a gasifier using one of two possible hot-gas clean-up filter technologies (particulate control devices or PCDs) at a component size readily scaleable to commercial systems. The transport reactor train operating in the combustion mode is shown schematically in Figure 2.2-1. A taglist of all major equipment in the process train and associated balance-of-plant is provided in Tables 2.2-1 and -2, respectively. Two PCDs are shown in this flow diagram; however, only one PCD is tested with the transport reactor at a given time during operations. The intent is to be able to install, change out, or provide maintenance on a second PCD while one is being tested. This provides increased flexibility for the test facility and reduces downtime. The facility is sized to process nominally 2 tons/hour of coal. This size generates sufficient gas to test the PCD at a nominal 1,000 ACFM of gas at the PCD inlet. Indirect cooling of the gas from the transport reactor allows testing of the PCDs with inlet temperatures between 600 and 1,400°F and at pressures ranging from 150 to 305 psia. The PCD in this train receives particulate-laden gas from the transport reactor, which can operate in either gasification or combustion mode. In the gasification mode, the gas exiting the PCD is oxidized, cooled, and filtered in a baghouse before being discharged from a stack. The ash and char produced in the gasification mode are oxidized in a sulfator prior to disposal.

Coal is ground to a nominal average particle diameter of 100 and 200 μm mass mean diameter (MMD) when the transport reactor is operated in gasification mode and combustion mode, respectively. Sorbent is ground to a nominal average particle diameter of 100 μm MMD. Using feeders to control the rates, both coal and sorbent are pneumatically fed continuously into the transport gasifier/combustor.

Air is compressed to about 350 psia in the main air compressor and fed directly to the transport reactor. For start-up purposes, a burner (BR0201) is provided at the reactor mixing zone. Liquefied propane gas (LPG) is used as start-up fuel. Fuel, sorbent, and gas feeds enter a mixing zone at the bottom of the reactor where they mix with recycled solids from the disengager cyclone. Coal conversion begins in this zone; the reaction mixture then flows upward into the narrower riser section at high velocity, and then flows to the disengager.

The reactor typically operates at temperatures of 1,600 to 1,625°F in combustion mode. Provision is made to inject air at several different points along the riser to control the formation of NO_X. Limestone or dolomitic sorbents are fed into the reactor for sulfur capture, thus eliminating the need for downstream facilities to reduce plant sulfur emissions.

Solids and gases leaving the reactor flow into the disengager for bulk separation of the two phases. Most of the solids collected in the disengager are recycled to the reactor. Coal ash and spent sorbent are discharged from the transport reactor to maintain the solids inventory in the system. In the combustion mode, heat removal from the reactor system is necessary to control the reactor temperature. This is accomplished by removing solids from the disengager, cooling the solids in the combustor heat exchanger (HX0203), and returning the solids to the reactor system.

The gas leaving the disengager, still containing a high loading of particulates, is then sent to a cyclone system for additional solids recovery prior to being fed to the PCD. The cyclone is provided with spoiling gas to vary the solids loading into the effluent gas. The resulting conditioned gas next enters the PCD, where essentially all of the remaining particulates in the gas are removed. The cleaned gas leaving the PCD is sent to a secondary gas cooler (HX0402) and ultimately cooled to about 600°F. All gas-stream cooling is accomplished by generating steam. A portion of the cooled gas is further cooled in the compressor feed cooler (HX0405) and sent to the recycle gas booster compressor (CO0401) where the pressure is increased to about 400 psia. This gas is used for aeration fluidization in the combustor heat exchanger.

The main gas stream from the secondary gas cooler is cooled further by dilution air and cleaned of any remaining particulates in a baghouse before being discharged to the atmosphere through a stack.

Table 2.2-1

Major Equipment in the Transport Reactor Train

TAG NAME	DESCRIPTION
BR0201	Reactor Start-Up Burner
BR0401	Thermal Oxidizer
BR0602	Sulfator Start-Up/PCD Preheat Burner
CO0201	Main Air Compressor
CO0401	Recycle Gas Booster Compressor
CO0601	Sulfator Air Compressor
CY0201	Primary Cyclone in the Reactor Loop
CY0207	Disengager in the Reactor Loop
CY0601	Sulfator Cyclone
DR0402	Steam Drum
DY0201	Feeder System Air Dryer
FD0206	Spent Solids Screw Cooler
FD0210	Coal Feeder System
FD0220	Sorbent Feeder System
FD0502	Fines Screw Cooler
FD0510	Spent Solids Transporter System
FD0520	Fines Transporter System
FD0530	Spent Solids Feeder System
FD0602	Sulfator Solids Screw Cooler
FD0610	Sulfator Sorbent Feeder System
FL0301	PCD — Siemens Westinghouse
FL0302	PCD — Combustion Power
FL0401	Compressor Intake Filter
HX0202	Primary Gas Cooler
HX0203	Combustor Heat Exchanger
HX0204	Transport Air Cooler
HX0402	Secondary Gas Cooler
HX0405	Compressor Feed Cooler
HX0601	Sulfator Heat Recovery Exchanger
ME0540	Heat Transfer Fluid System
RX0201	Transport Reactor
SI0602	Spent Solids Silo
SU0601	Sulfator

Table 2.2-2 (Page 1 of 3)

Major Equipment in the Balance-of-Plant

TAG NAME	DESCRIPTION
BO2920	Auxiliary Boiler
BO2921	Auxiliary Boiler – Superheater
CL2100	Cooling Tower
CO2201A-D	Service Air Compressor A-D
CO2202	Air-Cooled Service Air Compressor
CO2203	High-pressure Air Compressor
CO2601A-C	Reciprocating N_2 Compressor A-C
CR0104	Coal and Sorbent Crusher
CV0100	Crushed Feed Conveyor
CV0101	Crushed Material Conveyor
DP2301	Baghouse Bypass Damper
DP2303	Inlet Damper on Dilution Air Blower
DP2304	Outlet Damper on Dilution Air Blower
DY2201A-D	Service Air Dryer A-D
DY2202	Air-Cooled Service Air Compressor Air Dryer
DY2203	High-Pressure Air Compressor Air Dryer
FD0104	MWK Coal Transport System
FD0111	MWK Coal Mill Feeder
FD0113	Sorbent Mill Feeder
FD0140	Coke Breeze and Bed Material Transport System
FD0154	MWK Limestone Transport System
FD0810	Ash Unloading System
FD0820	Baghouse Ash Transport System
FL0700	Baghouse
FN0700	Dilution Air Blower
HO0100	Reclaim Hopper
HO0105	Crushed Material Surge Hopper
HO0252	Coal Surge Hopper
HO0253	Sorbent Surge Hopper
HT2101	MWK Equipment Cooling Water Head Tank
HT2103	SCS Equipment Cooling Water Head Tank
HT0399	60-Ton Bridge Crane
HX2002	MWK Steam Condenser
HX2003	MWK Feed Water Heater

Table 2.2-2 (Page 2 of 3)

Major Equipment in the Balance-of-Plant

TAG NAME	DESCRIPTION
HX2004	MWK Subcooler
HX2103A	SCS Cooling Water Heat Exchanger
HX2103C	MWK Cooling Water Heat Exchanger
LF0300	Propane Vaporizer
MC3001-3017	MCCs for Various Equipment
ME0700	MWK Stack
ME0701	Flare
ME0814	Dry Ash Unloader for MWK Train
ML0111	Coal Mill for MWK Train
ML0113	Sorbent Mill for Both Trains
PG2600	Nitrogen Plant
PU2000A-B	MWK Feed Water Pump A-B
PU2100A-B	Raw Water Pump A-B
PU2101A-B	Service Water Pump A-B
PU2102A-B	Cooling Tower Make-Up Pump A-B
PU2103A-D	Circulating Water Pump A-D
PU2107	SCS Cooling Water Make-Up Pump
PU2109A-B	SCS Cooling Water Pump A-B
PU2111A-B	MWK Cooling Water Pump A-B
PU2300	Propane Pump
PU2301	Diesel Rolling Stock Pump
PU2302	Diesel Generator Transfer Pump
PU2303	Diesel Tank Sump Pump
PU2400	Fire Protection Jockey Pump
PU2401	Diesel Fire Water Pump #1
PU2402	Diesel Fire Water Pump #2
PU2504A-B	Waste Water Sump Pump A-B
PU2507	Coal and Limestone Storage Sump Pump
PU2700A-B	Demineralizer Forwarding Pump A-B

Table 2.2-2 (Page 3 of 3)

Major Equipment in the Balance-of-Plant

TAG NAME	DESCRIPTION
PU2920A-B	Auxiliary Boiler Feed Water Pump A-B
SB3001	125-V dc Station Battery
SB3002	UPS
SC0700	Baghouse Screw Conveyor
SG3000-3005	4160-V, 480-V Switchgear Buses
SI0101	MWK Crushed Coal Storage Silo
SI0103	Crushed Sorbent Storage Silo
SI0111	MWK Pulverized Coal Storage Silo
SI0113	MWK Limestone Silo
SI0114	FW Limestone Silo
SI0810	Ash Silo
ST2601	N_2 Storage Tube Bank
TK2000	MWK Condensate Storage Tank
TK2001	FW Condensate Tank
TK2100	Raw Water Storage Tank
TK2300A-D	Propane Storage Tank A-D
TK2301	Diesel Storage Tank
TK2401	Fire Water Tank
XF3000A	230/4.16-kV Main Power Transformer
XF3001B-5B	4160/480-V SS Transformer No. 1-5
XF3001G	480/120-V Miscellaneous Transformer
XF3010G	120/208 Distribution Transformer
XF3012G	UPS Isolation Transformer
VS2203	High-pressure Air Receiver

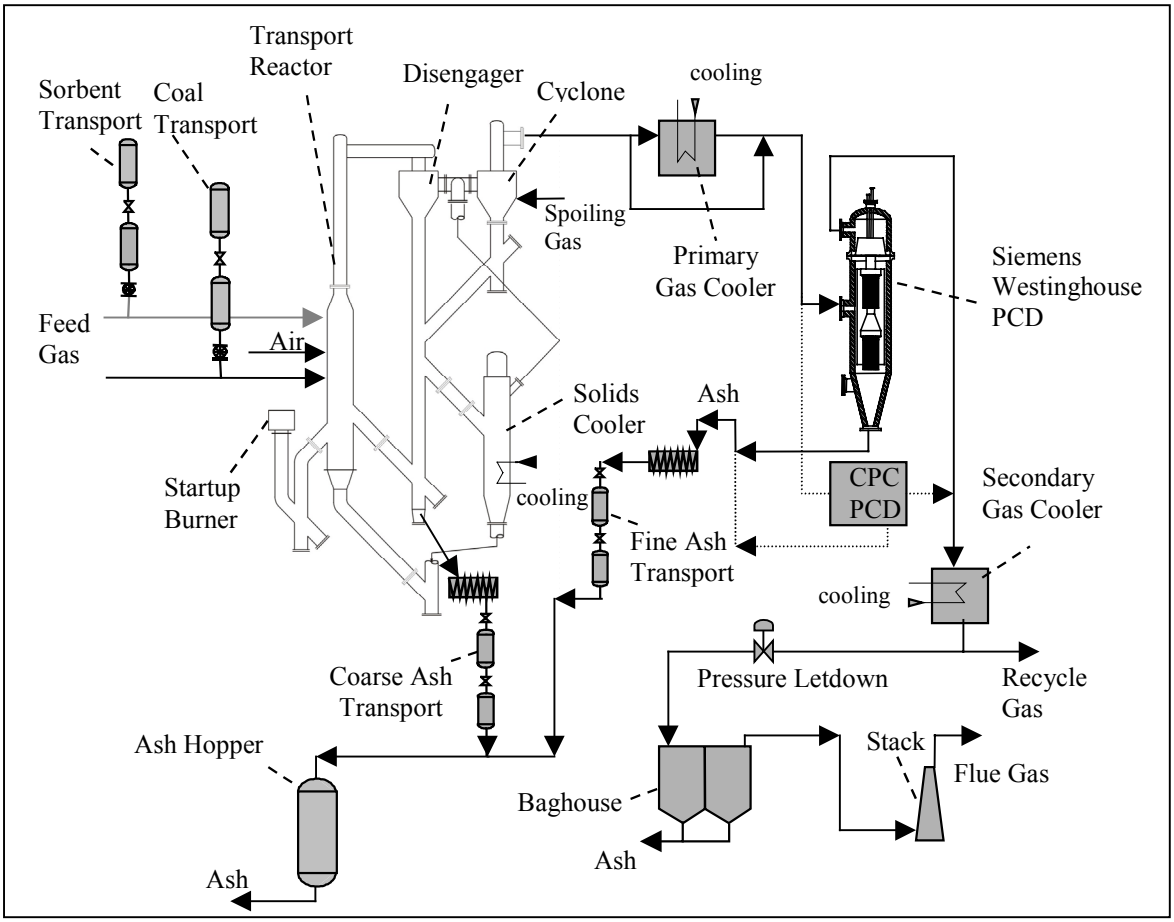

Figure 2.2-1 Flow Diagram of the Transport Reactor Train in Combustion Mode of Operation

2.3 SIEMENS WESTINGHOUSE PARTICULATE CONTROL DEVICE

Several different PCDs will be evaluated on the transport reactor train. The first PCD, commissioned in 1996 and used in all of the testing to date, was the filter system designed by Siemens Westinghouse. The dirty gas enters the PCD below the tubesheet, flows through the filter elements, and the ash collects on the outside of the filter. The clean gas passes from the plenum/filter element assembly through the plenum pipe to the outlet pipe. As the ash collects on the outside surface of the filter elements, the pressure drop across the filter system gradually increases. The filter cake is periodically dislodged by injecting a high-pressure gas pulse to the clean side of the candles. The cake then falls to the discharge hopper.

To date, the transport reactor has been operated only in the combustion mode. Initially, high-pressure air was used as the pulse gas for the PCD. However, the pulse gas was changed to nitrogen early in 1997. The pulse gas was routed individually to the two-plenum/filter element assemblies via injection tubes mounted on the top head of the PCD vessel. The pulse duration was typically 0.1 to 0.5 seconds.

A sketch of the Siemens Westinghouse PCD is shown in Figure 2.3-1.

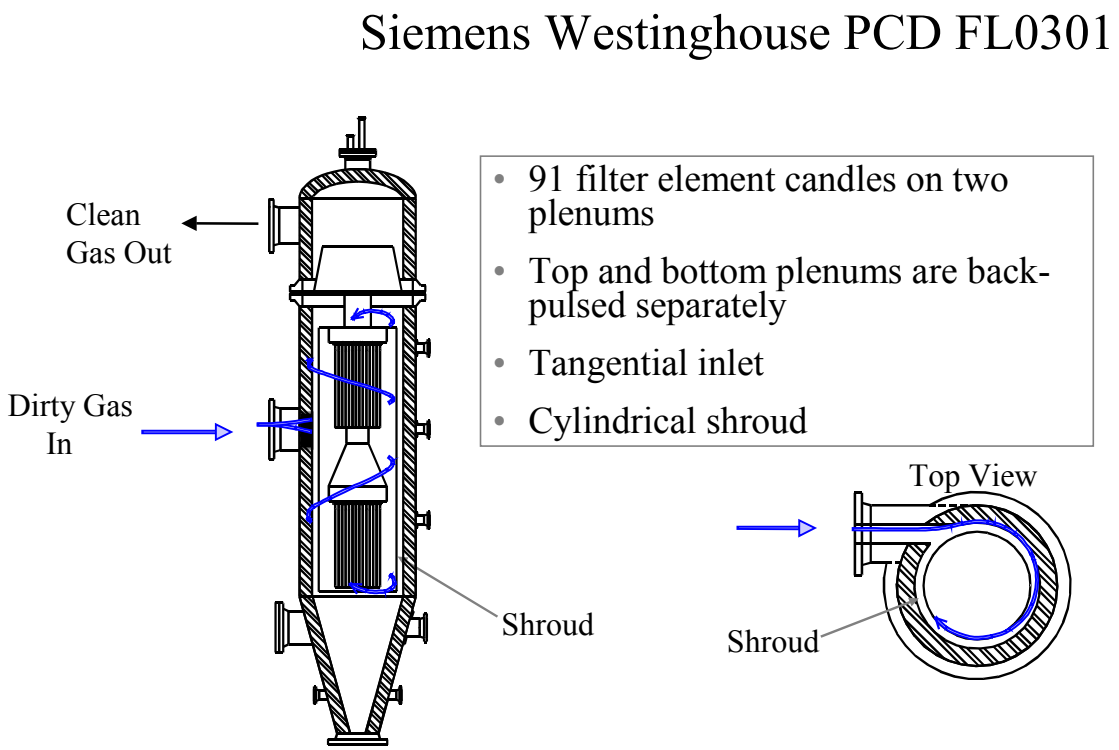

Figure 2.3-1 Siemens Westinghouse PCD

2.4 OPERATION STATUS

Commissioning activities began in September 1995 and proceeded in parallel with construction activities. Design and construction of the transport reactor and associated equipment was completed in early summer of 1996. All separate components and subsystems were fully operational by midsummer and commissioning work was focused on integration issues for the entire transport reactor train. The first coal fire was achieved on August 18, 1996. A series of characterization tests was initiated to develop an understanding of reactor system operations. Test runs CCT1, CCT2, and CCT3 were completed by December 1996. Solids carryover from the reactor to the PCD was found to be excessive during these test runs. A number of start-up and design problems associated with various equipment were successfully addressed.

Three additional sets of characterization test runs (CCT4, CCT5, and CCT6) and one major test campaign (TC01) were undertaken during 1997. TC01 focused on exposing the PCD filter elements to process gas for 1,000 hours at temperatures from 1,350 to 1,400°F and achieving stable reactor operations. An Alabama bituminous coal from the Calumet Mine in the Mary Lee seam and Plum Run dolomite were used in these test runs.

Two test campaigns (TC02 and TC03) were successfully completed during 1998. TC02 was planned for reactor parametric testing to better quantify the effect of different variables on reactor and filter element operation. Test run TC02 was started on April 5, 1998, and was completed on May 11, 1998. Based on TC02 observations, TC03 was planned for additional reactor parametric testing to better quantify the effect of different variables on reactor and PCD operation and to evaluate operation with an Eastern Kentucky bituminous coal and a Gregg Mine limestone from Florida. The third major test campaign, TC03, was performed from May 31, 1998, to August 10, 1998. Stable operations were demonstrated using the Eastern Kentucky coal and Plum Run dolomite, Bucyrus limestone, and Longview limestone during TC03. There were, however, circulation problems using the Eastern Kentucky coal and Florida Gregg Mine limestone because of deposits resulting from excessive fines (segregated) in the Eastern Kentucky feed. One additional test run, TC04, was started on October 14, 1998, but ended prematurely due to a temperature excursion in the PCD during the initial heat-up of the transport reactor system.

TC05 was planned to demonstrate steady state operations using a variety of fuel and sorbent feed materials (including petroleum coke with two different sorbents) and to perform reactor parametric testing using different feed combinations. The test run was started on January 10, 1999, in combustion mode of operation and was completed May 2, 1999. Overall, TC05 was a successful test run with 10 different feed combinations tested. Figure 2.4-1 provides a summary of operating hours for the major test campaigns.

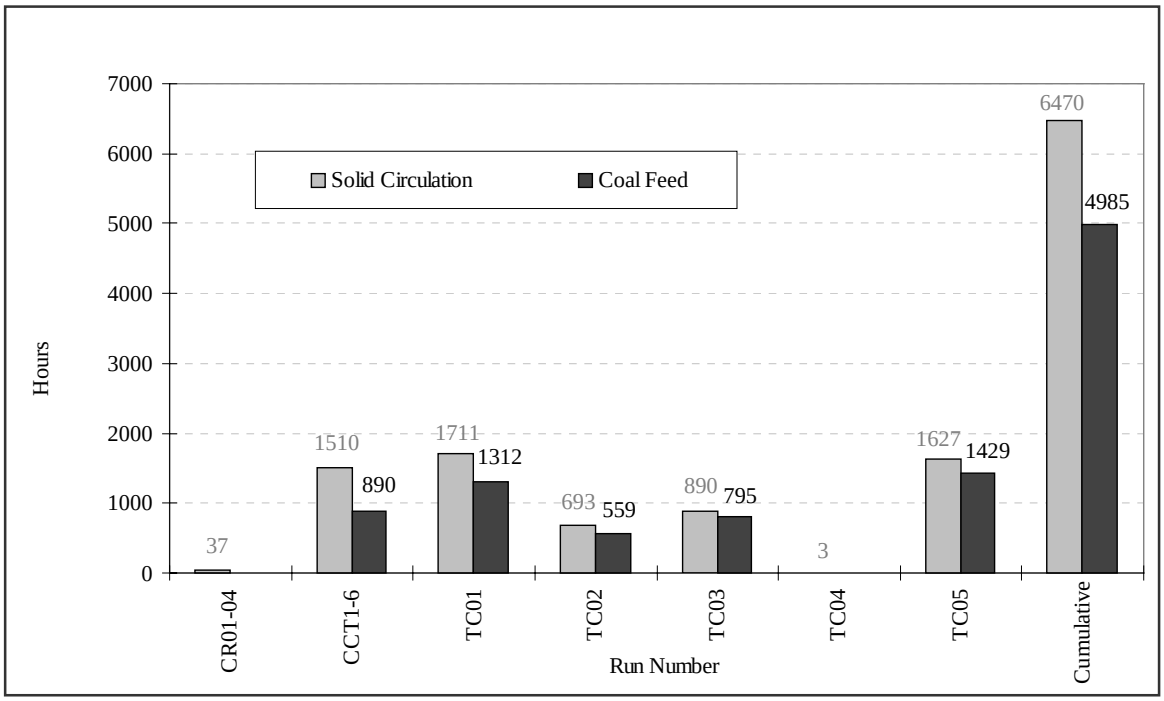

Figure 2.4-1 Operating Hours Summary for Transport Reactor Train Major Test Campaigns

3.0 PARTICLE FILTER SYSTEM

3.1 TC05 PCD INTRODUCTION

The transport reactor and PCD operated on coal for almost 1,500 hours over the 4 months of TC05. Ten different fuel/sorbent combinations were tested during this time under a wide range of PCD operating conditions. Many lessons were learned over the course of the run that should lead to improvements in the reliability of the PCD at the PSDF and in future commercial designs. Some of the experience gained during TC05 includes the following:

- The PCD operated on coal for 1,429 hours with relatively few operational problems. The range-of-process conditions include:
  - Temperatures from 700 to 1,400°F.
  - Face velocities from 4 to 8 ft/min.
  - Particulate loadings from 3,000 to 25,000 ppmw.
- The PCD operated at a face velocity of 8 ft/min for 175 hours. After the initial ~100 hours required for the residual cake to form the baseline pressure drop was constant.
- The PCD operated on petroleum coke with dolomite and limestone successfully for 260 hours with a PCD temperature of 750°F.
- The longest continuous run to date without shutdown was experienced with 471 hours.
- The PCD operated for over 575 hours with an outlet particulate loading below 1 ppmw.
- Operating with 10 different fuel/sorbent ashes and operation at 8 ft/min face velocity allowed for the development of models to predict the performance of the PCD under a variety of conditions.
- Ten different filter element types from seven different manufacturers were tested.
- 2-meter-long oxide filter elements from 3M were tested.
- One McDermott filter element lost a plug in the bottom of the element, which caused leakage. McDermott has redesigned the plug and supplied filter elements for the first gasification run.
- Three AlliedSignal PRD-66 filter elements failed during TC05 and membrane spalling was found on several other PRD-66 filter elements. AlliedSignal has received these filter elements and is evaluating the cause of the failure.

- One 3M oxide filter element was found with a pinhole leak. This element has been sent back to 3M for evaluation.

- Leakage around the failsafe flanges was an issue in the first part of TC05. This led to the development of a new filter holder by PSDF staff. The filter holder is currently undergoing testing.

- Ash bridging was experienced when operating with petroleum coke and Plum Run dolomite at a PCD temperature of ~1,400°F. A thorough investigation of the ash shows that the root cause of the bridging was apparently sulfation of the PCD dust cake.

3.2 PCD OPERATION DURING TEST RUN TC05

3.2.1 Introduction

From a PCD standpoint TC05 proved to be one of the most challenging test runs to date. Ten different fuel/sorbent combinations were filtered by the PCD over the 4 months of this test and 1,429 hours of burning a variety of fuels. There were five test segments from the perspective of the PCD defined by the four outages experienced during the test campaign. The table below is a summary of test conditions during those five test segments.

Test Seg.	Date	Fuel	Sorbent	Nom. Face Vel., ft/min	Nom. PCD Temp, °F	Reason for Outage
1	1/12-22	Calumet Calumet	Bucyrus Longview	8	1,400	High Outlet Loading
2	1/31-2/24	Calumet Illinois #6 Illinois #6 Illinois #6	Longview Bucyrus Longview Plum Run	6	1,400	Broken Filter Elements
3	3/3-8	Illinois #6 Pet. Coke	Plum Run Plum Run	6	1,400	Ash Bridging
4	3/13-27	Pet. Coke Pet. Coke	Plum Run Bucyrus	4	750	Transport Reactor
5	4/12-5/2	Calumet PRB PRB E. Kentucky	Bucyrus Bucyrus Gregg Gregg	5	1,100	End of Campaign

3.2.1.1 Test Segment 1: 1/12 to 1/22/1999

The previous test campaign, TC04, ended during start-up due to a coal fire in the PCD that caused the failure of several elements. When the test plan for TC05 was discussed in the latter part of 1998 it was obvious that it would be the most aggressive to date due to the large number of fuel/sorbent combinations that were planned for testing. There was high concern that there could be another fire in the PCD.

The primary objective for the PCD group was to install a set of filter elements at the beginning of the run that would operate reliably for the entire duration of the test campaign. During 1998 composite oxide filter elements from AlliedSignal (formerly DuPont Lanxide), McDermott, and 3M had operated with few problems. Therefore, it was decided to begin the test campaign with predominantly composite filter elements. In addition to the composites some Industrial Filter and Pump recrystallized silicon carbide (REECER), Pall Iron Aluminide, and Schumacher TF20 filter elements were also installed at the beginning of the test campaign. Dr. Roger Chen of West Virginia University (WVU) had been monitoring the

Schumacher filter elements during 1998 to evaluate his vibrational response nondestructive test, so these were installed to increase the hours of exposure.

At the request of Siemens Westinghouse Power Company (SWPC) and the U. S. Department of Energy (DOE) the test plan called for operating the PCD at a higher face velocity than was tested in 1998. This was accomplished by installing only 57 out of the possible 91 filter elements. The remaining "holes" were plugged with metal blanks. Four of the 3M oxide filters installed on the bottom plenum were 2 meters long rather than the typical 1.5 meters. The tubesheet layout can be seen in Figure 3.2-1.

From the beginning of the test, the outlet particulate loading was higher than desired (> 10 ppm). As the test campaign continued the particulate loading continued to increase and the PCD was shut down when the particulate loading increased above 20 ppm. The higher particulate loading has the potential to damage the pressure let-down valve as well as causing backside blinding of the failsafes and filter elements during pulse cleaning. Over time this blinding would cause an increase in the baseline pressure drop that would ultimately require a shutdown to clean the filter elements and replace the failsafes. The observations and conclusions for this outage can be found in section 3.3 of this report. One significant finding during the outage was that the bottom plug in a McDermott filter had disappeared, producing a 3/16-in. hole in the bottom of the filter, which was a source for some of the leakage. Because of this, all the McDermott filters were removed until this failure could be evaluated and the design of the "plug" improved. These elements were replaced with new Pall and Schumacher silicon carbide filter elements. In addition to the failed McDermott filter element, leakage was also found to occur around the failsafe flanges of several filter elements—primarily the 3M oxide filters.

Operation at 8 ft/min proved to be a challenge due to the higher pressure drop. Initially, this was believed to be much higher than anticipated; however, as explained in section 3.2.8.1 the pressure drop that was experienced could be modeled using the lab data generated by Southern Research Institute (SRI).

Leakage around failsafes had been experienced during several test segments. The higher pressure drop across the failsafe gasket was believed to be contributing to the leakage. Therefore, it was decided to reduce the pressure drop by reducing the face velocity. This was accomplished by increasing the number of filter elements from 57 to 87 for the next test segment. The tubesheet layout can be found in Figure 3.2-8.

3.2.1.2 Test Segment 2: 1/31 to 2/24/1999

With the face velocity reduced, the pressure drop of the PCD was similar to that experienced during TC01 through TC03. The PCD operated well for the approximately 450 hours on coal for this part of TC05. There were four different fuel/sorbent combinations tested with the transition between each fuel and/or sorbent occurring "on-line" (i.e., the PCD was not shut down between the various tests for cleaning). With only minor changes in the pressure drop of the PCD, primarily due to changes in particulate loading, the changes between the various fuels and sorbents had little effect on PCD performance.

However, the lower face velocity and the removal of the McDermott filter elements did not completely eliminate the source of the particulate leakage. The outlet particulate loading through this segment varied from 1.3 to 7.1 ppmw.

On February 21 the ash removal system plugged with fragments from one or more PRD-66 filter elements. These fragments were removed by maintenance and before deciding to shut down a test was performed to see if the failsafe devices had plugged. Dolomite was fed into the transport reactor at a relatively high rate in this test while SRI took a sample downstream of the PCD. The outlet loading for this test was 407 ppmw, so it was decided to shut down. Discussion of the outage can be found in section 3.3. One important observation during the inspection was that there was no gasket found above the PRD-66 filter at tubesheet location B55. Whereas it is possible that the gasket was blown out when the filter element failed, it is more likely that it was never installed. Without this gasket, leakage of gas/particulate around the failsafe flange would be likely and could explain the leakage throughout the test segment.

Due to the failure of three PRD-66 filter elements and the appearance of several "spalled" areas on the membrane of the elements all of the PRD-66 filter elements were removed and replaced with Pall and Schumacher filters. The tubesheet layout after the installation is shown in Figure 3.2-21.

3.2.1.3 Test Segment 3: 3/3 to 8/1999

Test segment 3 was extremely short and consisted primarily of the start-up and transition from Illinois #6 bituminous coal to petroleum coke. During the transition, the most notable change was that operation with petroleum coke and Plum Run dolomite produced essentially no transient pressure drop in the PCD, even though the particulate loading was approximately 15,000 ppm. Since petroleum coke contains about 0.5 percent ash, but also ~5.5 percent sulfur, the particulate reaching the PCD was essentially all dolomite. Because of this, the particulate size distribution was fairly large, producing a filter cake with very little drag. Properties of the particulate generated with petroleum coke/Plum Run dolomite can be found in section 3.4.

The primary reason for the shutdown was due to circulation problems in the transport reactor. However, while the transport reactor was being addressed the PCD ash removal system continued to plug with numerous, hard nodules of ash about 1.0 to 1.5 inches in diameter. The PCD was inspected from the lower manway to determine the source of the nodules and bridging was observed in the lower plenum. The PCD was disassembled, inspected, and then cleaned with air before being reassembled. The outlet loading before shutdown was only 0.1 ppm, so no filter elements were removed during the inspection. Observations from this outage can be found in section 3.3.

The initial hypothesis for the bridging was thought to be due to vanadium. Petroleum coke ash contains about 30 percent vanadium. However, when diluted with sorbent for sulfur control the PCD ash contained about 0.5 percent vanadium. In oil-fired turbines, magnesium is injected with the fuel so the vanadium will form magnesium ortho-vanadate ($Mg_3V_2O_8$), a compound with a high-melting point instead of vanadium pentoxide (V_2O_5) which melts at approximately 1,000°F. Some literature sources and free energy calculations indicated that the

magnesium ortho-vanadate requires the high temperatures of a combustion turbine burner to form and that other magnesium vanadates such as MgV_2O_6 or $Mg_2V_2O_7$, which have low-melting temperatures, may be forming. Conversations with Mike Swanson at UNDEERC indicated that they had successfully tested petroleum coke and Plum Run dolomite with a filter temperature of 1,000°F. It was decided to flow all of the gas through the gas cooler in order to minimize the temperature to the PCD. Hopefully, this would "freeze" any compounds leaving the transport reactor that were not solid.

3.2.1.4 Test Segment 4: 3/13 to 27/1999

With the PCD temperature at nominally 700°F, there were no additional problems operating with petroleum coke. During this test segment, petroleum coke was tested with both Plum Run dolomite and Ohio Bucyrus limestone. With dolomite, the PCD inlet loading exceeded 25,000 ppmw, but as seen in Figures 3.2-27, -30, and -33 there was essentially no transient pressure drop due to a filter cake that had very little drag. When limestone was used as the sorbent, the particulate loading dropped to about 16,000 ppmw. Since limestone has a higher mass percentage of calcium than dolomite, the total sorbent feed was reduced, thus lowering the particulate loading to the PCD. The outlet particulate loading was exceptionally low during this part of the test run, with particulate loadings below 0.2 ppmw.

The run ended on March 27 because the transport reactor cyclone dipleg plugged with refractory. The PCD was inspected through the lower manway but it was not disassembled because there was no evidence of bridging. During the next pressure test the gasket on the PCD leaked and was replaced. When the tubesheet was lifted the top plenum was inspected. There was also no bridging observed on the top plenum.

The next tests involved operation with Powder River Basin (PRB) subbituminous coal. Since this was the first time the coal had been tested at the PSDF there was concern that there could be bridging again at the higher temperatures. The test campaign was scheduled to end at the end of April so maintenance could begin the work required to transition the transport reactor for gasification operations. At this point the main test objective was to maximize the operational hours for the transport reactor and PCD between mid-April and May. Therefore, it was decided to increase the PCD temperature to nominally 1,200°F by partially bypassing the gas cooler.

3.2.1.5 Test Segment 5: 4/12 to 5/2/1999

The last test segment turned out to be the longest continuous run to date at the PSDF. The run lasted for 471 hours on coal and the PCD operated trouble-free for this entire test segment. During this segment four different coal/sorbent combinations were tested. The majority of the testing was with PRB coal. Since the PRB coal has relatively low ash (<5 percent) and low sulfur (~0.3 percent) the total solids to the PCD were low during this test. Typical particulate loadings to the PCD were 4,000 to 10,000 ppmw.

Even though there was no maintenance to the PCD filter elements during the outage, the outlet loading was 1 to 2 ppmw during the first part of the run. The outlet loading decreased to about 0.2 ppmw at the end of the run, indicating that the leak had plugged the failsafe

during operation. Upon inspection, one 3M oxide filter element with a pinhole through the filter mat was found.

3.2.2 Test Objective

The primary test objective for TC05 was to operate the PCD with high reliability. To meet this objective, the filter elements chosen for the run were primarily composites. The reason for this selection was that composite filters had performed essentially trouble-free during 1998. All of the filter elements installed in 1999 were new, and almost from the beginning of the test problems with the composite filters were detected. The PCD was opened four times during the run (including the last outage in May) and materials problems were found with composite filters in three of the four outages as described above.

A second objective was to operate the PCD at high (8 ft/min or higher) face velocities and assess performance. Operating at high-face velocities is important to the economics of these filter systems. The number of filter elements sets the face velocity in the system – the higher the face velocity, the fewer the number of filter elements. The number of filter elements in the PCD determines the size of the filter vessel. The pressure vessel is approximately 80 percent of the total PCD capital cost, so determining the maximum face velocity is important.

Operation of the PCD at high-face velocities produced higher differential pressures than experienced during previous runs. There was concern expressed by SWPC and PSDF staff that these pressure drops were higher than expected, but as discussed in section 3.2.8.1 pressure drops were predictable. The larger problem was the leakage through the failed McDermott filter and the failsafe flanges.

Another test objective was to operate the PCD with a variety of fuel/sorbent combinations and determine the impact to PCD performance. Instead of cleaning the filter elements between different fuel/sorbent combinations, it was decided to switch the fuel and sorbent "on-line" to see if the pressure drop changed. Typically, there was very little change in the baseline pressure drop, indicating that the drag of the residual cake remained fairly constant during operation. However, changes in the transient pressure drop were observed with changing particulate loading and with different ashes.

3.2.3 Observations/Events – 1/12/99 Through 1/23/99

A. Main Air Compressor (MAC) Started – 1/12/99 at 15:00. After the initial start, the (MAC) was stopped and restarted on 1/13/99 at 17:00.

B. PCD Pulse System Started – 1/13/99 at 15:00.

C. Start-up Burner Lit – 1/13/99 at 19:15. Like the MAC, the start-up burner was lit, stopped, and then restarted on 1/13/99 at 19:15.

D. Coal Feed Started – 1/14/99 at 23:00. The coal and sorbent fed into the transport reactor at the beginning of the test was Calumet Alabama bituminous coal and Ohio Bucyrus limestone.

E. Reduced Coal Feed – 1/16/99 at 15:30. Due to plugging between FD0104 and FD0210 coal feed to the transport reactor was decreased to avoid running out of coal and having to relight the start-up burner. Additionally, circulation of the transport reactor was reduced. The effect of this on the PCD was a decrease in temperature (reduced load in reactor), a decrease in face velocity due to the decrease in volumetric flow, and a decrease in pressure drop due to the reduced face velocity and particulate loading to the PCD.

F. Decreased Pulse Interval/Increased Pulse Pressure – 1/18/99 at 08:45 and 09:40. Due to the increased face velocity (8 ft/min) the baseline and peak pressure drops were higher than previously experienced. At this time, the baseline pressure drop was increasing and the peak pressure drop was approaching 250 inWG. The ΔP alarm is set at 277 inWG (10 psi), so it was decided to increase the pulse pressure from 425 to 475 psig and decrease the pulse interval from 40 to 30 minutes. Increasing the pulse pressure would help stabilize the baseline pressure drop and decreasing the pulse interval would decrease the peak ΔP.

An additional concern was raised when SRI reported that the PCD outlet loading was 10.9 ppm, indicating that there was a leak in the PCD. This was watched carefully as the outlet loading increased to 21.8 ppm over the next 4 days.

G. Coal Feeder Tripped – 1/19/99 at 08:15. The coal feeder FD0210 tripped briefly.

H. Changed From Bucyrus to Longview Limestone – 1/20/99 at 05:00. As part of the test plan the limestone was changed "on-line" from Ohio Bucyrus limestone to Alabama Longview limestone. The Calumet Alabama bituminous coal was used for both test segments.

I. Increased Pulse Pressure/Decreased Pulse Interval – 1/20/99 at 10:50 and 12:10. Once again the pulse parameters were adjusted to stabilize the baseline pressure drop and decrease the maximum ΔP. The pulse pressure was increased from 475 to 525 psig and the pulse interval decreased from 30 to 20 minutes. The test ended roughly 2 days later due to the increasing outlet loading, but a review of the permeance graph (Figure 3.2-7) for January 18 through 23 indicates that the baseline pressure drop was stabilizing. The permeance is the face velocity divided by the baseline pressure drop and corrected for temperature. The permeance reflects the stability of the filter element residual cake. If there is no change in the permeance over time the pressure drop due to the residual cake, filter element, vessel losses, etc., is constant and any changes in baseline pressure drop are due to changes in the gas volumetric flow. The permeance beginning

on January 20 and until the end of the run appears to have been approaching a steady state, and the slope of the permeance vs. time over the 2 days was essentially zero.

J. Run Ended – 1/22/99 at 13:00. Due to the increasing outlet loading it was decided to shut down to find the leak and repair it before continuing the run. The details of this inspection are found in section 3.3.

When the run ended there was concern that the higher outlet loading was due to the higher pressure drop, which in turn was caused by the higher face velocity. There was also concern that the pressure drop was higher than expected, which will be discussed in section 3.2.8.1. Since one of the primary overall objectives of TC05 was to maximize the run hours of the transport reactor it was decided to lower the face velocity by installing additional filter elements.

3.2.4 Observations/Events – 1/31/99 Through 2/24/99

A. Main Air Compressor Started – 1/31/99 at 14:00.

B. Start-up Burner On – 2/1/99 at 06:25.

C. Coal Feed Started – 2/2/99 at 03:50 (resumed after initial brief periods on February 1). The initial coal fed for this run was Calumet Alabama bituminous coal. The initial sorbent was Alabama Longview limestone.

D. Increased Pulse Pressure – 2/4/99 at 08:15. Due to the experience of the previous run it was decided to start at a slightly higher backpulse pressure. The pulse pressure was increased from 425 to 475 psig.

Two outlet particulate samples from SRI indicated that there was still a minor leak in the PCD. Although it was on an order of magnitude less than the first part of TC05 it was watched carefully throughout the run and ultimately the leak reached a maximum of 7 ppm.

E. Coal Feeder Outage – 2/5/99 at 08:30. Due to a mechanical problem with the coal feeder spheri valve the coal feeder was out of service for approximately 30 to 45 minutes.

F. Changed To Illinois #6 Coal With Ohio Bucyrus Limestone – 2/7/99 at 04:00. Over a period of about a day both the coal and sorbent were changed.

G. Changed Pulse Pressure – 2/9/99 at 11:40. Due to a slightly increasing baseline pressure drop, the pulse pressure was changed from 475 to 525 psig. The first backpulse after the change caused a dipleg upset dumping solids into the PCD. It was decided to lower the pulse pressure back to 475 psig, where it remained for the rest of the run.

H. Changed From Bucyrus to Longview Limestone – 2/13/99 at 06:00. Without changing the coal (still Illinois #6) the sorbent was changed from Ohio Bucyrus limestone to Alabama Longview limestone.

I. FD0520 System Tripped – 2/15/99 at 17:30. The PCD ash lockhopper tripped due to a high-dispense vessel pressure, which typically indicates plugging in the discharge line or vessel. While troubleshooting this problem the lockhopper vent valve was determined to be leaking as a result of valve wear. Coal feed was stopped and the reactor depressurized in order to replace the valve and do maintenance on the lockhopper.

J. Reactor Depressurized – 2/15/99 at 22:00.

K. Start-up Burner On – 2/16/99 at 02:15. With the maintenance complete the start-up burner was lit to continue the test.

L. Coal Feed Started – 2/16/99 at 14:00.

M. Changed From Bucyrus Limestone To Plum Run Dolomite – 2/20/99 at 17:15.

N. FD0520 Plugs With PRD-66 Filters – 2/21/99 at 23:30. The PCD ash lockhopper tripped again due to plugging of the discharge line. The discharge line was plugging with hard pieces of ash, fiberfrax (from the degradation of the PCD liner), and fragments of three PRD-66 filter elements. Coal feed and circulation was stopped and the reactor depressurized. During the inspection of the lockhopper it was found that the upper spheri valve was leaking so the valve was disassembled and the seal replaced.

It was mutually agreed to restart circulation with only the start-up burner with feed dolomite at an excessive rate. This would allow SRI to take an outlet particulate sample. If the outlet loading was acceptable the run would continue; otherwise the PCD would be disassembled.

O. Start-up Burner Lit – 2/24/99 at 01:14.

P. Dolomite Feed Begins – 2/24/99 at 08:00.

Q. Run Ended – 2/24/99 at 11:30. SRI measured an outlet particulate loading of over 400 ppm so it was decided to shut down, disassemble the PCD, and remove the broken filter elements. Discussion of the inspection is in section 3.3.
The most significant finding was that the top gasket on one of the broken filter elements was missing. The design of the SWPC holding mechanism would prevent the sealing of the failsafe flange and allow gas and dust to flow around the failsafe instead of through it

The failsafe was fairly clean on the broken filter element that was missing a gasket. The failsafes of the other two broken filters were dirty, but not plugged

(insufficient exposure to ash prevented their plugging due to the quick shutdown). This is a further indication that the failsafe was not sealed against the tubesheet and the dirty gas was flowing around the failsafe instead of through it. It was also probably the source of the 1- to 7-ppm leak that was experienced throughout the run.

3.2.5 Observations/Events – 3/3/99 Through 3/8/99

A. Main Air Compressor Started – 3/3/99 at 16:15.

B. Start-up Burner On – 3/3/99 at 17:00.

C. Coal Feed Started – 3/4/99 at 13:45. The initial coal fed for this run was Illinois #6 bituminous coal. The initial sorbent was Plum Run dolomite.

D. Changed From Illinois #5 Coal to Petroleum Coke – 3/5/99 at 08:15.

E. Low-PCD ΔP – 3/6/99 at 06:30. Probably the most dramatic change in operation of the PCD with petroleum coke was the very small change of the transient differential pressure over the 40-minute pulse cycle. As indicated on Figure 3.2-24 and in section 3.4 the inlet loading was about 14,800 ppm, which is a fairly "typical" inlet loading for the PCD. The mass-median-particle size was approximately 40 microns due to the agglomeration of smaller particles. The large, sticky particles formed a transient filter cake with very low drag.

F. Circulation Problems In Transport Reactor – 3/6/99 at 13:00. Due to increasing difficulty in operating the transport reactor the unit was briefly shut down at 16:10 to drain the standpipe and reactor J-leg, and to open some plugged aeration nozzles.

G. Began Reheating PCD – 3/7/99 at 23:30. The sulfator burner was lit to begin reheating the PCD and continue the run.

H. FD0520 Plugs With Hard Ash – 3/8/99 at 06:00. The discharge line on the PCD ash removal system (FD0520) was continually plugging with hard ash. When maintenance began cleaning the line many small (~1.0 to 1.5 in.) chunks of very hard ash were found in the line. Based on the quantity and size of the chunks, the source of these chunks was felt to be the PCD, so the decision was made to inspect the PCD through the lower manway.

I. Run Ended – 3/8/99 at 14:00. When the PCD manway was opened bridging of the lower plenum was observed in several locations. There were no broken filter elements, but the decision was made to disassemble the PCD to clean the ash from between the filters and to take some samples of the bridged ash. The observations from this outage can be found in section 3.3 and a description of the ash samples taken found in section 3.4.

3.2.6 Observations/Events – 3/13/99 Through 3/27/99

A. Main Air Compressor Started – 3/13/99 at 12:40.

B. Start-up Burner Lit – 3/13/99 at 13:15.

C. Fuel Feed Started – 3/14/99 at 13:30. This run was a continuation of the previous run. The fuel feed was petroleum coke and the sorbent was Plum Run dolomite.

D. PCD Temperature At ~700°F. In the previous run the PCD had bridged at ~1,400°F. At the time of this run the assumption was that the vanadium in the petroleum coke was in an oxide form (V_2O_5) and not magnesium-vanadate (such as $Mg_3V_2O_8$) as originally thought. The fusion point of vanadium pentoxide is approximately 1,000°F. Conversations with Mike Swanson of UNDEERC indicated successful operation of petroleum coke with Plum Run dolomite in combustion in their testing with the PCD operating at 1,000°F. However, the temperature control of the PCD at the PSDF is fairly crude, involving an uncontrolled bypass around the primary gas cooler (HX0202). With the gas cooler partially bypassed in 1997, the PCD operating temperature was nominally 950°F. However, the transport reactor was operating at a much higher load for this test and there was concern that the temperature of the PCD would be 1,100 to 1,200°F. Therefore, it was decided to remove the bypass and flow all of the gas through the gas cooler for this run. This produced a PCD temperature of nominally 700 to 750°F.

   Because of the lower gas temperature the gas density was higher than 1,400°F and therefore the volumetric gas flow as well as the face velocity was lower than in the previous test segment. Operation of the PCD at this temperature with petroleum coke and Plum Run dolomite was successful.

E. Low PCD ΔP – 3/15/99 at 00:00. During the previous test the change in the PCD-transient-pressure drop dramatically decreased when the fuel was switched from Illinois #6 coal to petroleum coke. This is primarily due to the large particle size with a mass median diameter of 40 microns entering the PCD. The large particles are agglomerates formed inside the transport reactor. Even though the particulate loading to the PCD was slightly higher than "typical" the change in transient-pressure drop was much less. As described in section 3.4 the larger particulate forms a filter cake with a much lower drag or resistance.

F. Pressure Raised in Transport Reactor – 3/15/99 at 16:45, 3/16/99 at 14:05, 3/17/99 at 14:25, and 3/19/99 at 08:15. Several times during the run the pressure was raised in the transport reactor. Depending on the change in pressure this has an impact on the PCD. First of all, the pulse pressure is typically held at ~225 psi above the reactor pressure so the pulse pressure changes. Second, increasing the transport reactor pressure increases the gas density. The increased gas density decreases the actual volumetric flow of the gas , which reduces the

face velocity. A decrease in face velocity produces a corresponding decrease in pressure drop.

G. Changed From Plum Run Dolomite to Bucyrus Limestone – 3/20/99 at 05:30. The sorbent was changed from Plum Run dolomite to Ohio Bucyrus limestone. The fuel used was still petroleum coke. This change in sorbent had little affect on the PCD operation.

H. Coal Feeder Tripped – 3/23/99 at 00:00. Due to the accumulation of fines in the coal feeder the feeder tripped and could not be restarted. The reactor was shut down and depressurized so maintenance could repair the feeder.

I. Start-up Burner Lit – 3/24/99 at 16:30 and 19:15.

J. Fuel Feed Started – 3/25/99 at 06:20. The fuel and sorbent were still petroleum coke and Ohio Bucyrus limestone.

K. Pressure Raised in Transport Reactor – 3/26/99 at 14:45.

L. Run Ended – 3/27/99 at 20:00. The run ended because the transport reactor cyclone dipleg would not drain into the standpipe. Upon inspection, a piece of refractory was found blocking the cyclone solids outlet return line. The PCD was inspected through the manway but it was not disassembled. No bridging or deposition of ash was observed during the inspection. During the next pressure test the PCD girth flange (84-in. flange) gasket leaked and had to be replaced prior to start-up.

3.2.7 Observations/Events – 4/12/99 Through 5/02/99

A. Main Air Compressor Started – 4/12/99 at 01:05.

B. Start-up Burner On – 4/12/99 at 7:10.

C. Fuel Feed Started – 4/12/99 at 14:33. The initial coal fed for this run was the Calumet Alabama bituminous coal. The initial sorbent was Ohio Bucyrus limestone.

D. PCD Temperature at ~1,200°F. For the remainder of the run the gas cooler was partially bypassed, i.e. gas was flowing through both the gas cooler and the bypass line. The primary reason for this was to maximize the run hours prior to the end of the run while burning Powder River Basin subbituminous coal. After the experience with the petroleum coke in early March there was a hesitancy to burn subbituminous coal at the higher PCD temperature, given that there was only 3 weeks available for operation. The PCD operated well at this temperature with the PRB coal.

E. Increased Pulse Pressure – 4/13/99 at 09:30 and 11:50. Due to the rapidly increasing PCD pressure drop the back-pulse pressure was increased from 425 to 475 psig at 09:30 and to 525 psig at 11:50.

F. Change in Circulation, Coal, and Sorbent Feeds Reduces PCD Loading – 4/15/99 at 10:45. After a significant upset in the transport reactor dipleg the circulation rate as well as the coal and sorbent feedrates were reduced. This significantly decreased the particulate loading to the PCD and lowered the rate of pressure drop rise in the PCD. The particulate loading on April 15 was 16,200 ppm and on April 16 the particulate loading was 10,200 ppm.

G. Gas Flow Reduced – 4/16/99 at 12:35.

H. Decreased Pulse Pressure – 4/16/99 at 17:40. The increased pulse pressure had an adverse affect on the cyclone dipleg, which caused large quantities of particulate to be carried into the PCD. Because of the lower pressure drop in the PCD it was decided to decrease the PCD backpulse pressure to 475 psig. The backpulse pressure was again lowered on 4/17 to 450 psig.

I. Changed From Calumet Alabama Bituminous Coal to Powder River Basin (PRB) Subbituminous Coal – 4/18/99 at 10:00.

J. Low-PCD ΔP – 4/19/99 at 18:00. Swapping to the PRB coal had a positive impact on the PCD operation. The low ash and sulfur content of the PRB coal reduced the total particulate loading to the PCD. With the Alabama coal and Bucyrus limestone the particulate loading was typically 14,000 to 16,000 ppm. While feeding the PRB coal the "typical" particulate loading was 3,200 to 9,900 ppm.

K. Decreased Pulse Pressure – 4/20/99 at 14:00. Due to a couple of dipleg upsets the back-pulse pressure was reduced further to 425 psig.

L. Decreased Reactor Pressure – 4/26/99 at 10:00. Decreasing the reactor pressure increased the volumetric flow by decreasing the gas density. The increase in volumetric flow increased the face velocity and the pressure drop.

M. Changed From Bucyrus Limestone to Gregg Limestone – 4/26/99 at 12:10.

N. Changed From Powder River Basin Subbituminous Coal to Eastern Kentucky Bituminous Coal – 4/29/99 at 12:00. Switching coals increased the loading to the PCD due to the increased sorbent feedrate.

O. Run Ended – 5/2/99 at 06:15. Over the last part of the run a clinker in the mixing zone formed that eventually blocked the coal feed line and ended the run.

3.2.8 Run Summary

3.2.8.1 High-Pressure During Test Segment 1

In the first test segment of TC05 the face velocity was nominally 8 ft/min, about 35 percent greater than any face velocity tested to date. Because of the higher velocity the baseline and transient pressure drop was much higher than previously experienced. The high- pressure drop caused concern for both the PSDF and SWPC staffs and there was concern that perhaps there was some phenomena such as cake compressibility that may have been responsible for the change in differential pressure.

During the first segment of TC05 two different fuel/sorbent combinations were tested (see Table 3.2-1). One of these combinations, Calumet bituminous coal and Bucyrus limestone, was tested again during the last segment of TC05. In the last segment the face velocity was approximately 4.5 ft/min so it is interesting to compare the pressure drop during the two run segments. The PCD flow, face velocity, loading, and pressure drop for the two dates are shown in Table 3.2-11.

Pressure Drop Calculations

The total pressure drop across the PCD is made up of several components, as shown below:

$$\Delta P_{PCD} = \Delta P_{vessel} + \Delta P_{failsafe} + \Delta P_{element} + \Delta P_{residual} + \Delta P_{transient}$$

The vessel pressure drop consists of the inlet and outlet losses, flow through the plenum piping, shroud, etc., and is proportional to the square of velocity:

$$\Delta P_{vessel} = K_{vessel}\, \rho v^2$$

Where:

K_{vessel}	is the flow resistance constant
ρ	is the gas density
v	is the gas velocity

The flow through the failsafe is also proportional to the square of the velocity:

$$\Delta P_{failsafe} = K_{failsafe}\, \rho v^2$$

Together, the pressure drops of the failsafe and the vessel account for about 10 to 15 percent of the baseline pressure drop.

Since the gas velocity through the filter element is so low the flow is laminar and the pressure drop is linearly proportional to flow. Therefore, the pressure drop can be estimated by using Darcy's Law:

$$\Delta P_{element} = \frac{\mu v L}{D_e}$$

Where:

- μ is the gas viscosity.
- L is the wall thickness.
- D_e is the specific permeability of the filter element.

Typically, the filter element accounts for about 2 to 5 percent of the total baseline pressure drop. However, some types of filter elements have low permeabilities and can account for up to 10 percent of the total baseline pressure drop.

SRI reports the lab measured pressure drop of residual and transient filter cakes as a normalized drag, which is the pressure drop divided by the face velocity and the areal loading (see section 3.4). This measured drag is determined at ambient conditions so it must be corrected for gas viscosity. Therefore, to calculate the pressure drop of either the residual or transient filter cake the following equation is used:

$$\Delta P_{cake} = \text{Drag} * \text{Face Vel} * \text{Areal Loading} * \frac{\mu}{\mu_{amb}}$$

Where:

Drag	is the lab measured dustcake drag.
Face Vel	is the filter face velocity.
μ_{amb}	is the gas viscosity at ambient temperature.
Areal Loading	is pounds particulate per ft^2 surface area

Typically, the ambient drag for the residual cake has been measured at 15 inWG/((ft/min)* (lb/ft^2))[1]. The areal loading for the residual cake was determined by weighing a known area of residual cake from the filter elements during shutdown. The areal loading is typically 0.57 lb/ft^2 [1].

The drag for the transient cake of several fuel/sorbent combinations, including Calumet coal and Bucyrus limestone, is shown in Figure 3.4-3. As shown by the graph, the drag is a function of the cake porosity. To date, determining the actual transient cake porosity has proven to be a challenge. For the calculated pressure drop shown in Table 3.2-12 the porosity was varied until the calculated transient pressure drop agreed with the measured transient pressure drop. Once the drag was determined by trial and error the same drag was used for both cases.

The areal loading for the transient cake is calculated using the following formula:

$$A.L._{Trans} = \frac{\text{Loading} * \text{Gas Flow}}{1{,}000{,}000} \frac{(1 - \eta)}{\text{Surface Area}} \text{ Pulse Interv.}$$

Where:

$A.L._{Trans}$	is the areal loading of the transient cake.
Loading	is the particulate loading ppmw (mass solids/mass gas).
Gas Flow	is the gas mass flow rate.
η	is the fraction of particulate that separates before reaching the filter elements.
Surface Area	is the filtration surface area.
Pulse Interv	is the pulse interval.

As reported in the TC03 Run Report[2], the fraction of particulate that separates before reaching the filter elements is approximately 0.25.

Conclusions

In comparing the calculated pressure drops for the two cases (Table 3.2-12) with the measured pressure drops (Table 3.2-11) there is good agreement between the two cases. The conclusions of this analysis are:

- Using lab- and field-measured values of drag and areal loading allows the performance of the PCD to be estimated accurately.

- The high-pressure drop at the higher face velocity was caused by the relatively high drag of the ash produced by burning Calumet coal with Bucyrus limestone.

- In general, the baseline-pressure drop is linearly proportional to the face velocity. This is not exactly true since the pressure drop of the piping and failsafe losses are proportional to the velocity squared. However, these losses are minor compared to the pressure drop due to the residual cake, which is linearly proportional to flow. Therefore, the baseline-pressure drop is proportional to the face velocity raised to the 1.0 to 1.2 power.

- However, it can be derived that if the loading and pulse interval are held constant the pressure drop of the transient cake is proportional to the face velocity squared. The face velocity can be changed either by increasing the gas velocity or reducing the filtration area. If the gas flow is increased and the loading is constant the mass of particulate entering the PCD increases and therefore the cake thickness increases at a faster rate. If the gas flow and loading are constant but the surface area is decreased the cake thickness also increases at a faster rate. In both cases the increased rate of

cake thickness growth is linearly proportional to gas flow and therefore, by Darcy's Law, the transient-pressure drop is proportional to the face velocity squared.

- The maximum allowable face velocity depends on the properties of the filter cake. Figure 3.4-3 shows that the transient cake drag depends not only on the cake porosity but also on the fuel and sorbent used in the combustor. The maximum allowable pressure drop is determined by the construction of the PCD. Therefore, if the fuel and sorbent being burned in the combustor produces a dustcake with low drag the filter system can be operated at higher face velocities before exceeding the maximum allowable pressure drop.

  As an example, if the maximum allowable pressure drop for the PCD was 250 inWG the maximum allowable face velocity for the Calumet/Bucyrus ash would be 7.8 ft/min if the parameters in Table 3.2-12, particulate loading and pulse interval, were held constant. However, if the fuel being burned in the transport reactor was Powder River Basin coal with no sorbent and the residual cake properties and particulate loading were held constant the maximum face velocity in the PCD would be 9.5 ft/min. This has very important commercial implications since the maximum face velocity determines the size of the PCD and therefore the capital cost.

3.2.8.2 Ash Bridging

As mentioned in section 3.2.1 it was initially assumed that the high concentration of vanadium in the petroleum coke ash contributed to the ash bridging. However, as the ash nodules were removed from the PCD and analyzed it became apparent that the cause of the ash bridging was not due to vanadium but sulfidation of the dust cake in the PCD. As described in section 3.4.2 the SO_x in the gas entering the PCD reacted with the dolomite to produce a binary sulfate – $Mg_3Ca(SO_4)_4$. At the operating temperature of the PCD it is believed that the binary sulfate formed a low-melting eutectic with $CaSO_4$ that caused the bridging in the PCD. A preliminary report on the analysis of the bridged filter deposits is included in section 3.7.

3.2.8.3 Particulate Leakage

In the first two months of TC05 particulate leakage through the PCD was a continual problem. In general, the leak path was around the outside of the failsafe flange. The failsafe/tubesheet gasket is the primary dirty side seal for the PCD. Throughout the test program at the PSDF, getting a reliable seal on this gasket has been difficult. The sealing mechanism used is dependent upon all of the components (filter element flange, gaskets, failsafe, spacer nuts, etc.) being within a tight dimensional tolerance. Leakage through the tubesheet/failsafe gasket at the PSDF has been present under any of the following conditions:

- Filter element flange out of specification – Primarily a problem with the 3M oxide filter elements.

- Improper installation – When a filter element is not properly installed, the tubesheet/failsafe gasket cannot properly seat and leakage can occur.

- Missing gasket – During the second test segment of TC05 it appeared that a top gasket was missing on an AlliedSignal PRD-66 filter element. This prevented the tubesheet/failsafe gasket from properly seating.

A new filter element holder has been developed by the PSDF staff in order to improve the reliability of the filter element seal. This filter holder is currently undergoing testing and it is hoped that it will prevent leakage through the failsafe/tubesheet gasket in future runs.

In addition to the above reasons for leakage a "pinhole" was discovered in a 3M oxide filter element at the end of TC05. It is very likely that the leakage that occurred towards the end of the test run was caused by the pinhole.

3.2.8.4 Filter Element Performance

Since there were no major thermal events in the PCD during the run there were few problems related to the filter elements. Ten different types of filter elements were tested during TC05. The majority of these filter elements were typically 1.5-meter long, but 2.0-meter 3M oxide filter elements were also tested at the beginning of TC05. Evaluation of these filter elements by SRI is ongoing and the results will be reported in a later report.

Overall, most of the filter elements performed well. Problems developed with some of the filter elements tested including the following:

- 3M oxide (1.5 meter) – Initially there was leakage around the failsafes on some of these elements due to an undersized flange. This was corrected by installing a thicker gasket on top of the filter element and removing spacer nuts to improve compression of the tubesheet/failsafe gasket.

  In addition, a pinhole was found in one 3M filter element at the end of TC05 that lead to some minor particulate leakage in the PCD.

- 3M oxide (2.0 meter) – The failsafes on these filter elements also leaked at the beginning of TC05.

- Allied Signal PRD-66 – Three filter elements failed at the end of the second test segment on February 21, 1999. One of these filter elements was missing the top gasket and this may have allowed movement of the failsafe. This movement may have contributed to the failure of this filter element.

  In addition, membrane "spalling" occurred on several PRD-66 filter elements as described in section 3.3.

- McDermott – The bottom "plug" on one McDermott filter element failed during the first test segment of TC05 producing a 3/16-in. hole in the bottom of the filter element. McDermott has redesigned and tested the plug and supplied filter elements with the improved design to the PSDF for testing in GCT1, the next planned testing phase, which will be in gasification mode.

3.2.9 References

1. R. S. Dahlin and Landham, E. C., *Effects of Dust Characteristics on Hot-Gas Filter Performance In A Transport Reactor System*, Proceedings of the 4th International High Temperature Gas Cleaning Conference, Karlsruhe, Germany, September 22-24, 1999.

2. Technical Progress Report for Kellogg Brown and Root Transport Reactor With Siemens Westinghouse Particulate Control Device: TC03: May 1998 – August 1998, Section 3.4.2. Prepared by Southern Company Services, DOE Cooperative Agreement Number DE-FC21-90MC25140.

Table 3.2-1

TC05 Run Statistics
1/12/1999 Through 1/22/1999

Start Time:	1/12/1999 at 15:15
End Time:	1/22/1999 at 14:00
KBR Sub Tests:	TC05A-1 Through TC05B-5
Coal/Sorbent Type:	
1/12 to 1/20	Calumet Alabama Bituminous/Ohio Bucyrus Limestone
1/20 to 1/22	Calumet Alabama Bituminous/Alabama Longview Limestone
Hours On Coal	182.0
Number of Filter Elements:	57
Filtration Area:	164.7 ft^2 (15.3 m^2)
Filter Element Layout Number:	11 (Figure 3.2-1)
Pulse Valve Open Time:	0.2 sec.
Pulse Time Trigger:	20 to 40 minutes
Pulse Pressure:	425 to 525 psig (29 to 36 bar, g)
Pulse Logic:	Pulse On Timer

Table 3.2-2

TC05 Major Events
1/12/1999 Through 1/22/1999
(Refer to Figures 3.2-2 Through 3.2-7)

Event	Description	Date at Time
A	Main Air Compressor Started	1/12/99 at 15:00 1/13/99 at 17:00
B	PCD Pulse System Started	1/13/99 at 15:00
C	Startup Burner On	1/12/99 at 15:15 1/13/99 at 19:15
D	Coal Feed Started	1/14/99 at 23:00
E	Reduced Coal Feed	1/16/99 at 15:30
F	Decreased Pulse Interval Increased Pulse Pressure	1/18/99 at 08:45 1/18/99 at 09:40
G	Coal Feeder Tripped	1/19/99 at 08:15
H	Changed From Bucyrus to Longview Limestone	1/20/99 at 05:00
I	Increased Pulse Pressure Decreased Pulse Interval	1/20/99 at 10:50 1/20/99 at 12:10
J	Run Ended	1/22/99 at 13:00
*	Data Outage	

Table 3.2-3

TC05 Run Statistics
1/31/1999 Through 2/24/1999

Start Time:	1/31/1999 at 14:00
End Time:	2/24/1999 at 11:30
KBR Sub Tests:	TC05B-6 Through TC05E-1
Coal/Sorbent Type:	
1/31 to 2/7	Calumet Alabama Bituminous/Alabama Longview Limestone
2/7 to 2/13	Illinois #6 Bituminous/Ohio Bucyrus Limestone
2/13 to 2/20	Illinois #6 Bituminous/Alabama Longview Limestone
2/20 to 2/24	Illinois #6 Bituminous/Plum Run Dolomite
Hours On Coal	460.1
Number of Filter Elements:	87
Filtration Area:	247.1 ft^2 (23.0 m^2)
Filter Element Layout Number:	12 (Figure 3.2-8)
Pulse Valve Open Time:	0.2 sec.
Pulse Time Trigger:	40 minutes
Pulse Pressure:	425 to 525 psig (29 to 36 bar, g)
Pulse Logic:	Pulse On Timer

Table 3.2-4

TC05 Major Events
1/31/1999 Through 2/24/1999
(Refer to Figures 3.2-9 Through 3.2-20)

Event	Description	Date at Time
A	Main Air Compressor Started	1/31/99 at 14:00
B	Startup Burner On	2/1/99 at 06:25
C	Coal Feed Started	2/2/99 at 03:50
D	Increased Pulse Pressure	2/4/99 at 08:15
E	Coal Feeder Outage	2/5/99 at 08:30
F	Changed to Illinois #6 Coal With Ohio Bucyrus Limestone	2/7/99 at 04:00
G	Changed Pulse Pressure	2/9/99 at 11:40
H	Changed From Bucyrus to Longview Limestone	2/13/99 at 06:00
I	FD0520 System Tripped	2/15/99 at 17:30
J	Reactor Depressurized	2/15/99 at 22:00
K	Startup Burner On	2/16/99 at 02:15
L	Coal Feed Started	2/16/99 at 14:00
M	Changed From Bucyrus Limestone to Plum Run Dolomite	2/20/99 at 17:15
N	FD0520 Plugs With PRD-66 Filters	2/21/99 at 23:30
O	Startup Burner Lit	2/24/99 at 01:15
P	Dolomite Feed Begins	2/24/99 at 08:00
Q	Run Ended	2/24/99 at 11:30
*	Data Outage	

Table 3.2-5

TC05 Run Statistics
3/3/1999 Through 3/8/1999

Start Time:	3/3/99 at 16:15
End Time:	3/8/99 at 14:00
KBR Sub Tests:	TC05E-2 Through TC05F-1
Fuel/Sorbent Type:	
3/3 to 3/5	Illinois #6 Bituminous/Plum Run Dolomite
3/5 to 3/8	Petroleum Coke/Plum Run Dolomite
Hours On Coal	50.4
Number of Filter Elements:	87
Filtration Area:	247.1 ft^2 (23.0 m^2)
Filter Element Layout Number:	13 (Figure 3.2-21)
Pulse Valve Open Time:	0.2 sec.
Pulse Time Trigger:	40 minutes
Pulse Pressure:	425 psig (29 bar, g)
Pulse Logic:	Pulse On Timer

Table 3.2-6

TC05 Major Events
3/3/1999 Through 3/8/1999
(Refer to Figures 3.2-22 Through 3.2-24)

Event	Description	Date at Time
A	Main Air Compressor Started	3/3/99 at 16:15
B	Startup Burner On	3/3/99 at 17:00
C	Coal Feed Started	3/4/99 at 13:45
D	Changed From Illinois #6 Coal to Petroleum Coke	3/5/99 at 08:15
E	Low PCD ΔP	3/6/99 at 09:30
F	Circulation Problems In Transport Reactor	3/6/99 at 13:00
G	Began Reheating PCD	3/7/99 at 23:30
H	FD0520 Plugs With Hard Ash	3/8/99 at 06:00
I	Run Ended	3/8/99 at 14:00

Table 3.2-7

TC05 Run Statistics
3/13/1999 Through 3/27/1999

Start Time:	3/13/99 at 12:40
End Time:	3/27/99 at 20:00
KBR Sub Tests:	TC05F-2 Through TC0G-6
Fuel/Sorbent Type:	
3/13 to 3/20	Petroleum Coke/Plum Run Dolomite
3/20 to 3/27	Petroleum Coke/Ohio Bucyrus Limestone
Hours On Coal	265.0
Number of Filter Elements:	87
Filtration Area:	247.1 ft^2 (23.0 m^2)
Filter Element Layout Number:	13 (Figure 3.2-21)
Pulse Valve Open Time:	0.2 sec.
Pulse Time Trigger:	40 minutes
Pulse Pressure:	400 to 450 psig (28 to 31 bar, g)
Pulse Logic:	Pulse On Timer

Table 3.2-8

TC05 Major Events
3/13/1999 Through 3/27/1999
(Refer to Figures 3.2-25 Through 3.2-33)

Event	Description	Date at Time
A	Main Air Compressor Started	3/13/99 at 12:40
B	Startup Burner On	3/13/99 at 13:15
C	Fuel Feed Started	3/14/99 at 13:30
D	PCD Temperature At ~700°F	3/14/99 at 18:00
E	Low PCD ΔP	3/15/99 at 00:00
F	Pressure Raised In Transport Reactor	3/15/99 at 16:45 3/16/99 at 14:05 3/17/99 at 14:25 3/19/99 at 08:15
G	Changed From Plum Run Dolomite to Bucyrus Limestone	3/20/99 at 05:30
H	Coal Feeder Tripped	3/23/99 at 00:00
I	Startup Burner Lit	3/24/99 at 16:30 3/24/99 at 19:15
J	Fuel Feed Started	3/25/99 at 06:20
K	Pressure Raised In Transport Reactor	3/26/99 at 14:45
L	Run Ended	3/27/99 at 20:00

Table 3.2-9

TC05 Run Statistics
4/12/1999 Through 5/2/1999

Start Time:	4/12/99 at 01:05
End Time:	5/2/99 at 06:15
KBR Sub Tests:	TC05H-1 Through TC05K-2
Fuel/Sorbent Type:	
4/12 to 4/18	Calumet Alabama Bituminous Coal/Ohio Bucyrus Limestone
4/18 to 4/26	Powder River Basin Subbituminous Coal/Ohio Bucyrus Limestone
4/26 to 4/29	Powder River Basin Subbituminous Coal/Florida Gregg Limestone
4/29 to 5/2	Eastern Kentucky Bituminous Coal/Florida Gregg Limestone
Hours On Coal	471.3
Number of Filter Elements:	87
Filtration Area:	247.1 ft^2 (23.0 m^2)
Filter Element Layout Number:	13 (Figure 3.2-21)
Pulse Valve Open Time:	0.2 sec.
Pulse Time Trigger:	40 minutes
Pulse Pressure:	425 to 525 psig (29 to 36 bar, g)
Pulse Logic:	Pulse On Timer

Table 3.2-10

TC05 Major Events
4/12/1999 Through 5/2/1999
(Refer to Figures 3.2-34 Through 3.2-45)

Event	Description	Date at Time
A	Main Air Compressor Started	4/12/99 at 01:05
B	Startup Burner On	4/12/99 at 07:10
C	Fuel Feed Started	4/12/99 at 14:33
D	PCD Temperature at ~ 1,200°F	4/13/99 at 00:00
E	Increased Pulse Pressure	4/13/99 at 09:30 4/13/99 at 11:50
F	Change In Circulation, Coal and Sorbent Feeds Reduces PCD Loading	4/15/99 at 10:45
G	Gas Flow Reduced	4/16/99 at 12:35
H	Decreased Pulse Pressure	4/16/99 at 17:40
I	Changed From Calumet Alabama Bituminous to Powder River Basin Subbituminous Coal	4/18/99 at 10:00
J	Low PCD ΔP	4/19/99 at 18:00
K	Decreased Pulse Pressure	4/20/99 at 14:00
L	Decreased Reactor Pressure	4/26/99 at 10:00
M	Changed From Bucyrus Limestone to Gregg Limestone	4/26/99 at 12:10
N	Changed From Powder River Basin Subbituminous Coal to Eastern Kentucky Bituminous Coal	4/29/99 at 12:00
O	Run Ended	5/2/99 at 06:15

Table 3.2-11

Operational Data For Pressure Drop Comparison

Operating Period	1/18/1999	4/16/99
Coal	Calumet Bituminous	Calumet Bituminous
Sorbent	Bucyrus Limestone	Bucyrus Limestone
Filter Elements Installed	57	87
Total Filtration Area, ft^2	164.7	247.1
Avg. Volumetric Flow, ACFM	1,210	1,186
Avg. Face Velocity, ft/min	7.3	4.8
Pulse Interval, min	30	40
Particulate loading, ppmw	12,000	10,800
Baseline pressure drop, inWG	148	91
Transient pressure drop, inWG	221	125

Table 3.2-12

Calculated Pressure Drop

Operating Period	1/18/1999	4/16/99
Vessel/Failsafe ΔP (inWG)	21	11
Residual Cake		
Areal Loading (lb/ft^2 1)	0.57	0.57
Drag (inWG/((ft/min)*(lb/ft^2)) 1)	15	15
Viscosity Correction	2.2	2.0
ΔP (inWG)	137	82
Baseline Pressure Drop (inWG)	158	93
Transient Cake		
Areal Loading, lb/ft^2	0.66	0.59
Drag (inWG/((ft/min)*(lb/ft^2)) 2)	6.6	6.6
Viscosity Correction	2.2	2.0
ΔP (inWG)	70	37
Peak Pressure Drop, inWG	228	130

Note 1: See Reference 1.
Note 2: Figure 3.4-4 of this report at a porosity of 76%.

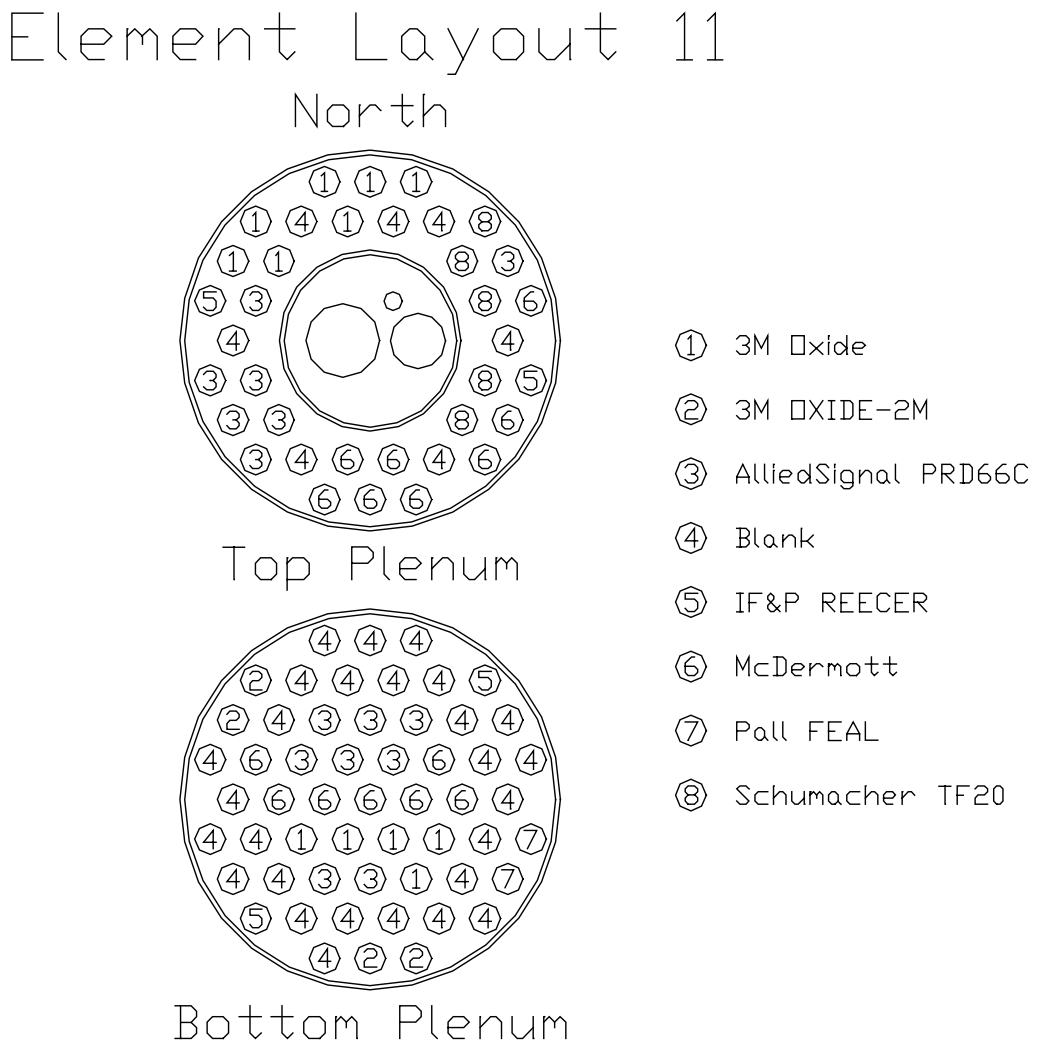

Figure 3.2-1 Filter Element Layout For TC05 – January 12 Through January 22 (Layout 11)

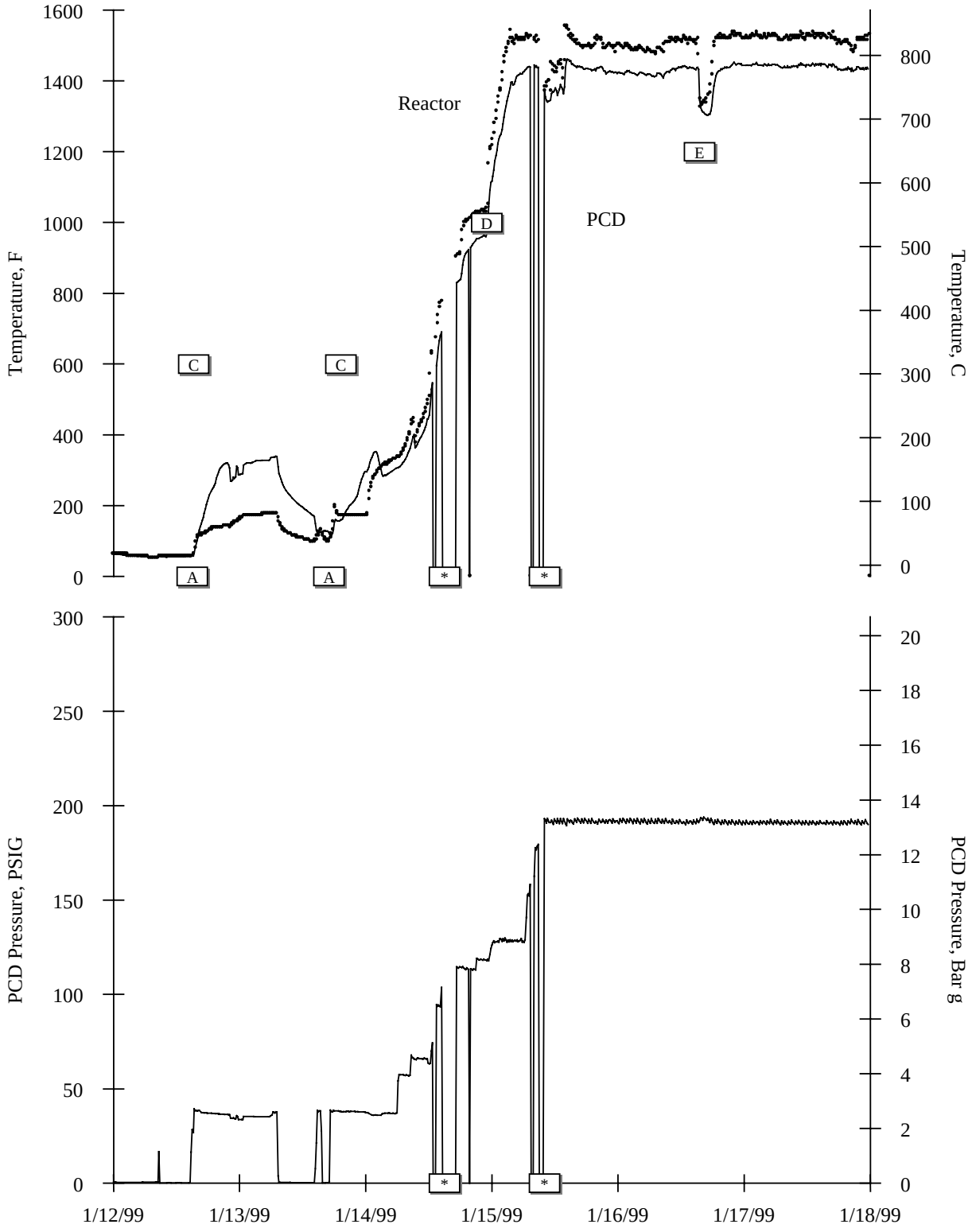

Figure 3.2-2 TC05 Temperature and Pressure For January 12 Through January 18

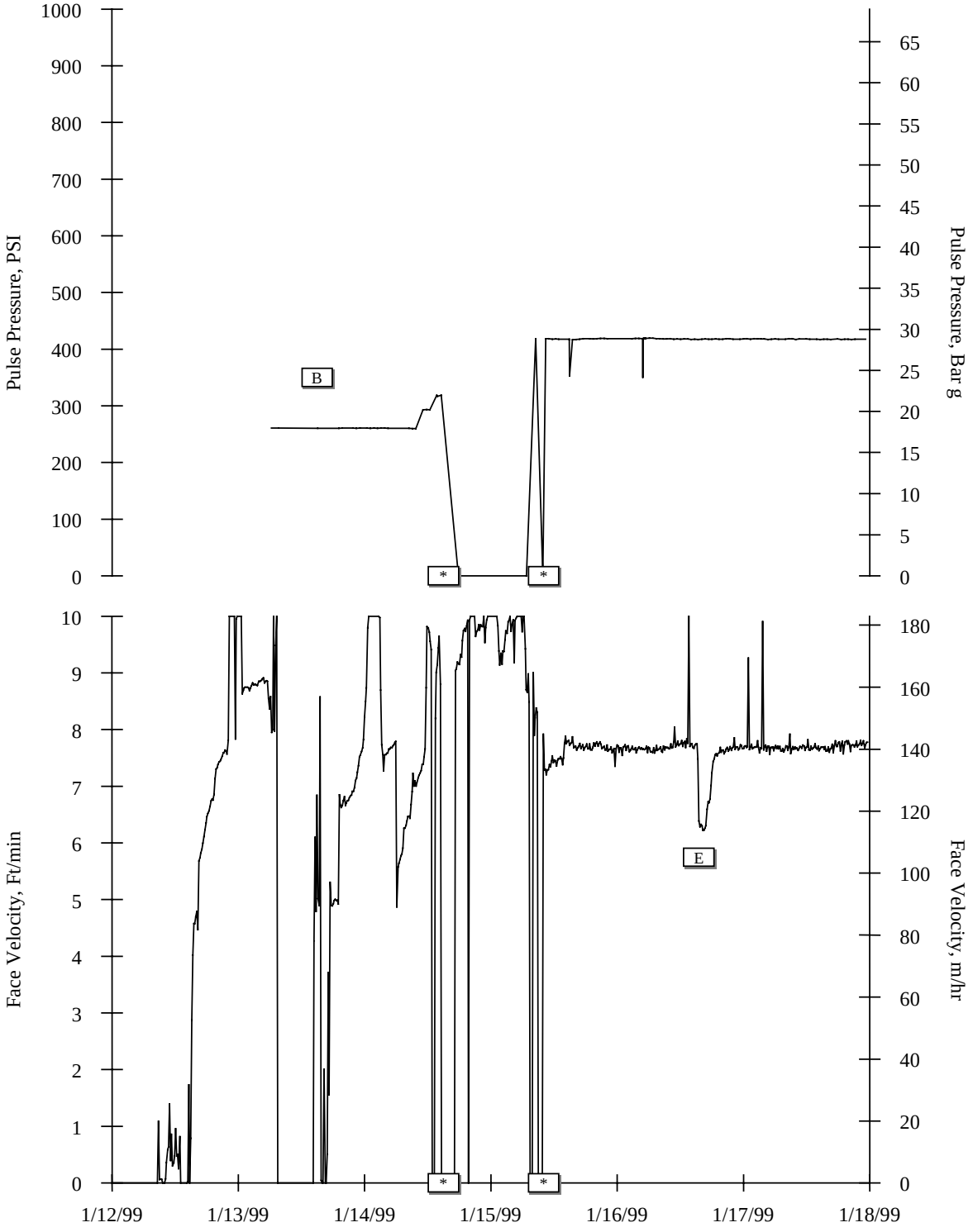

Figure 3.2-3 TC05 Back-Pulse Pressure and Face Velocity For January 12 Through January 18

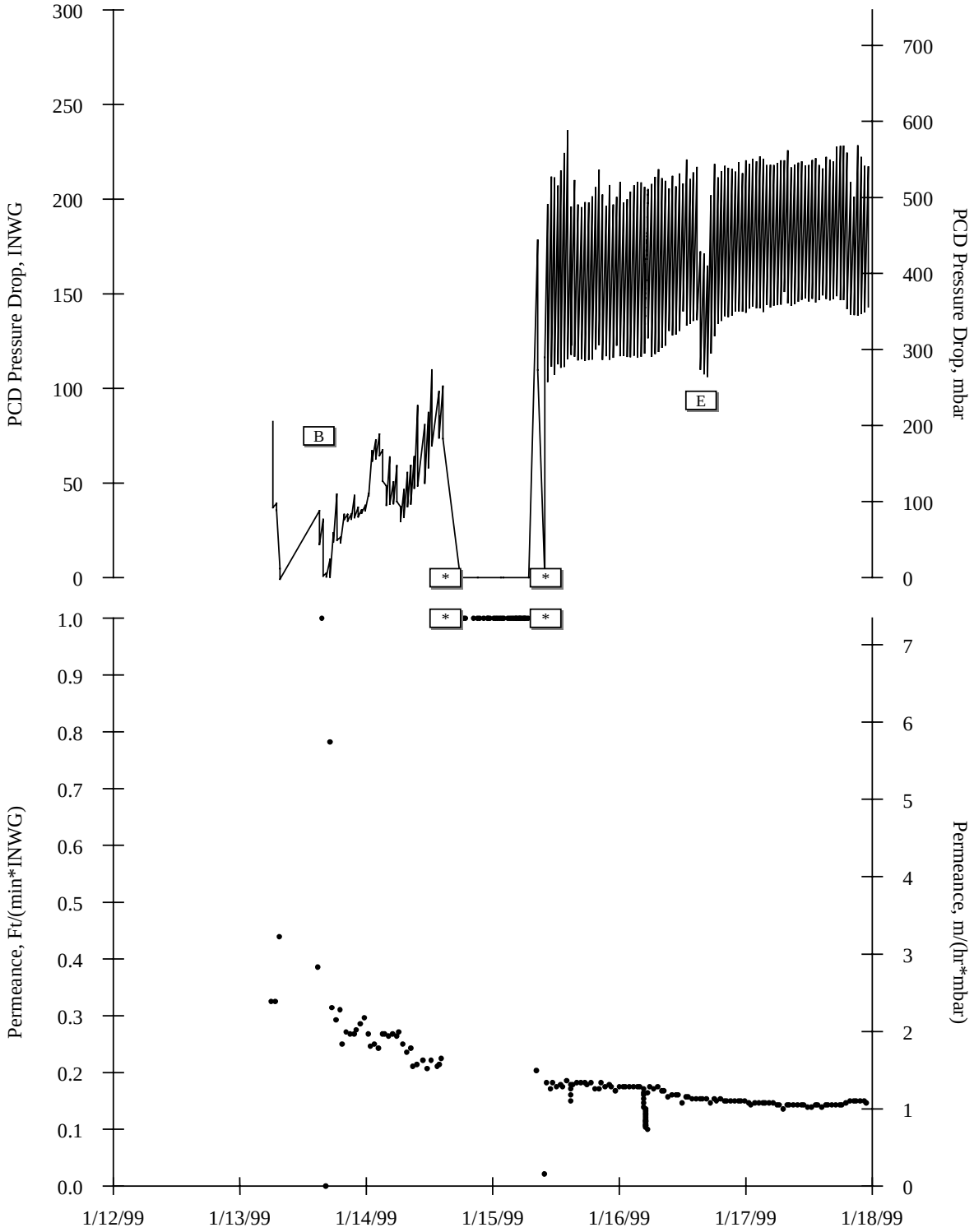

Figure 3.2-4 TC05 Pressure Drop and Permeance for January 12 Through January 18

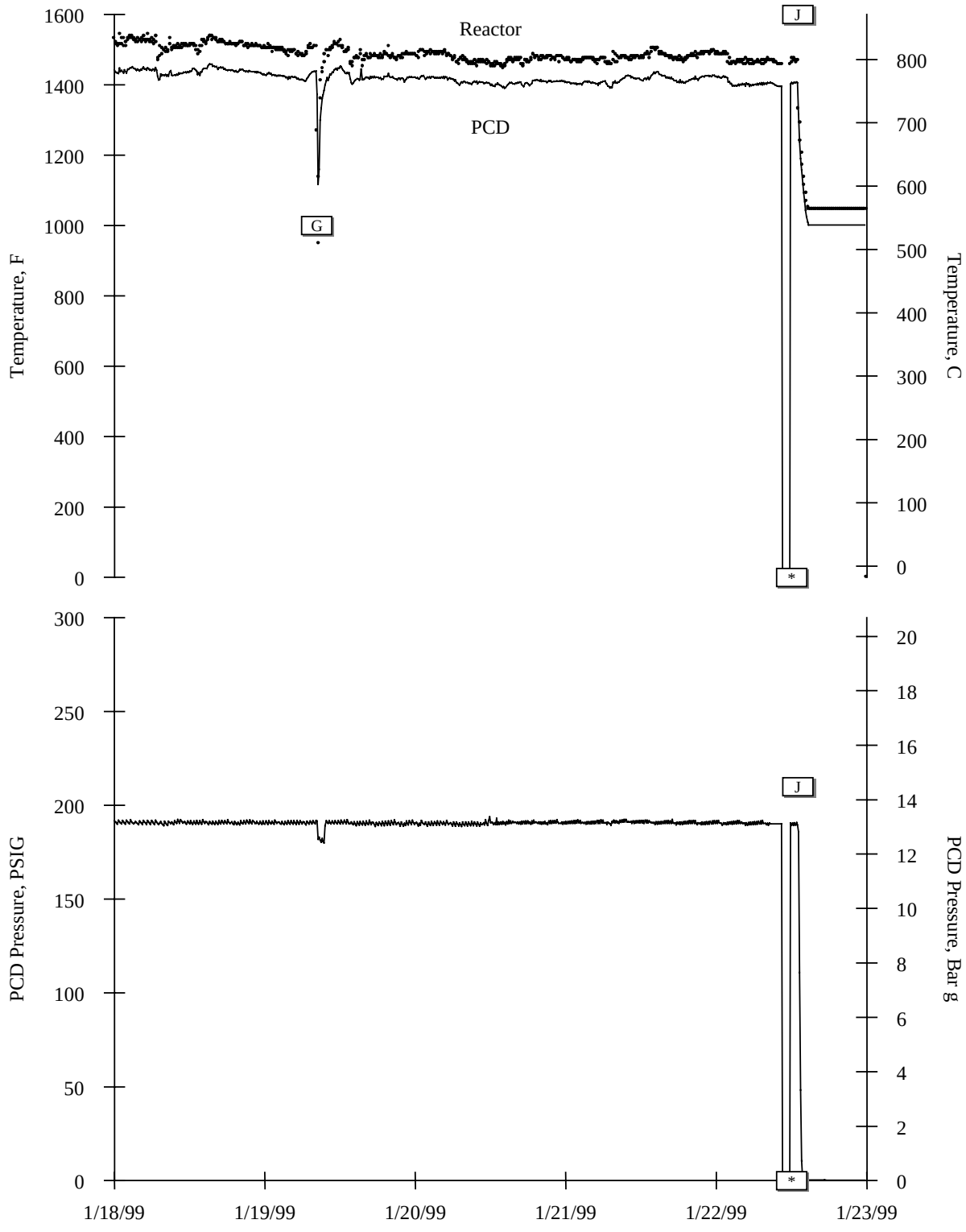

Figure 3.2-5 TC05 Temperature and Pressure for January 18 Through January 23

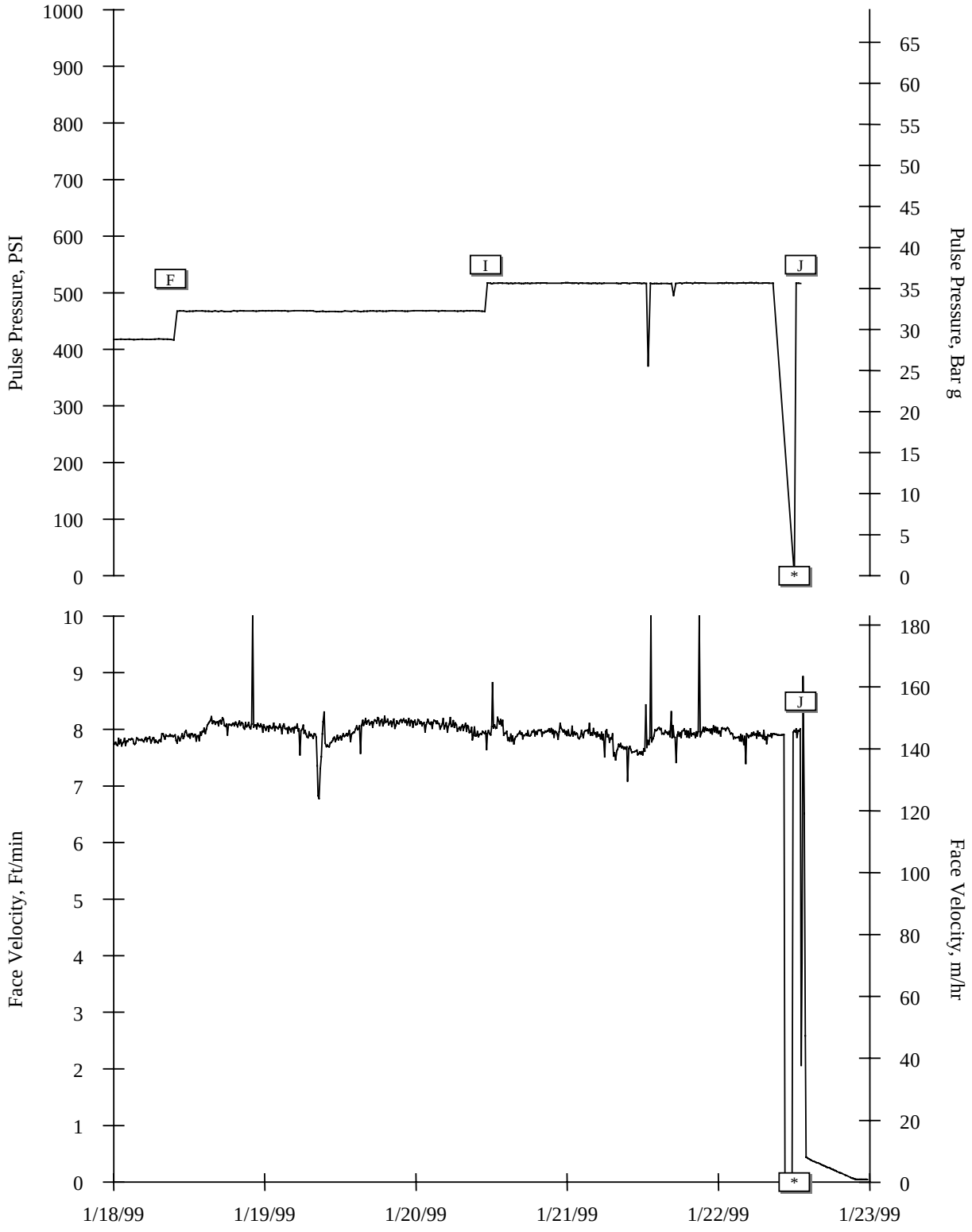

Figure 3.2-6 TC05 Back-Pulse Pressure and Face Velocity for January 18 Through January 23

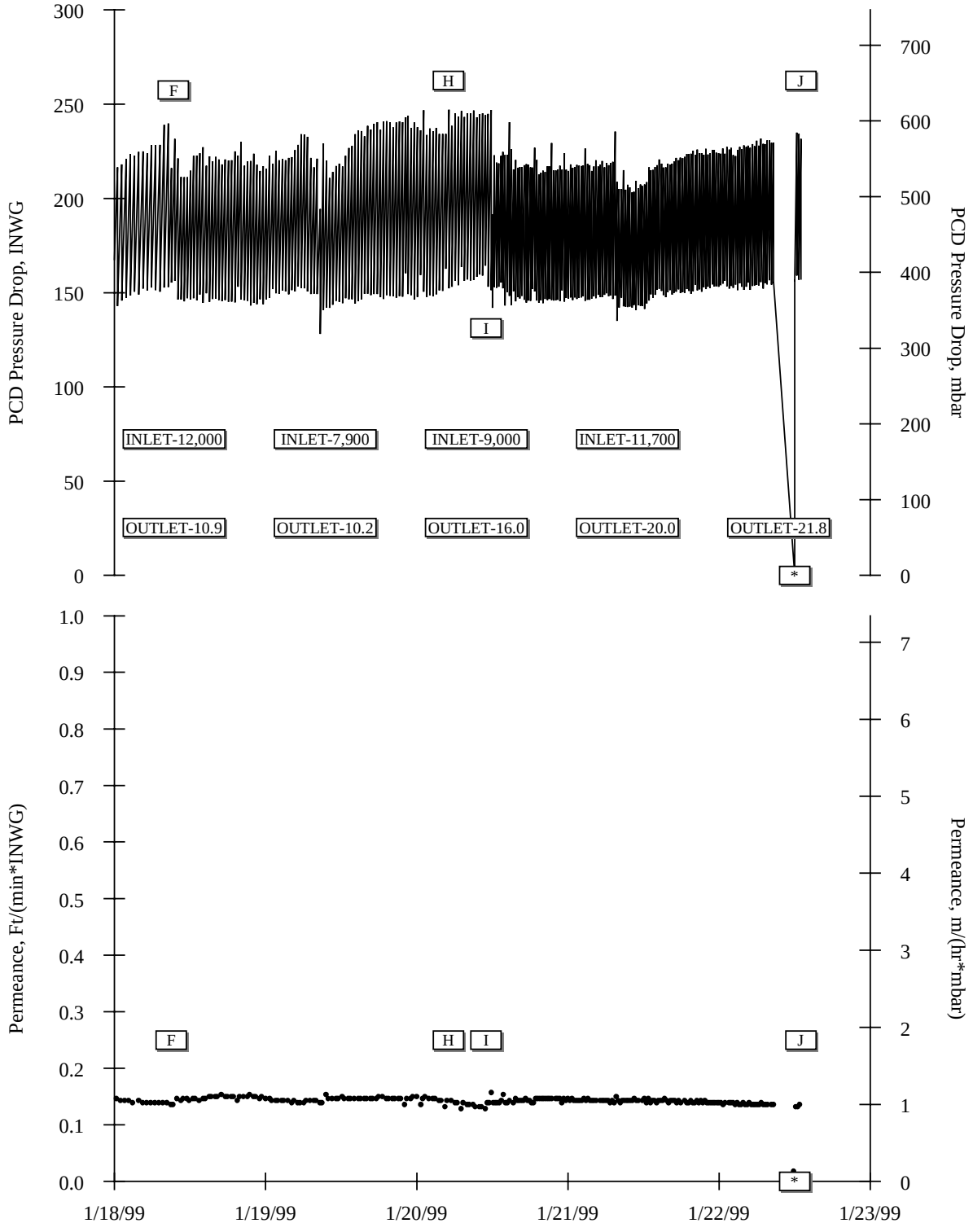

Figure 3.2-7 TC05 Pressure Drop and Permeance for January 18 Through January 23

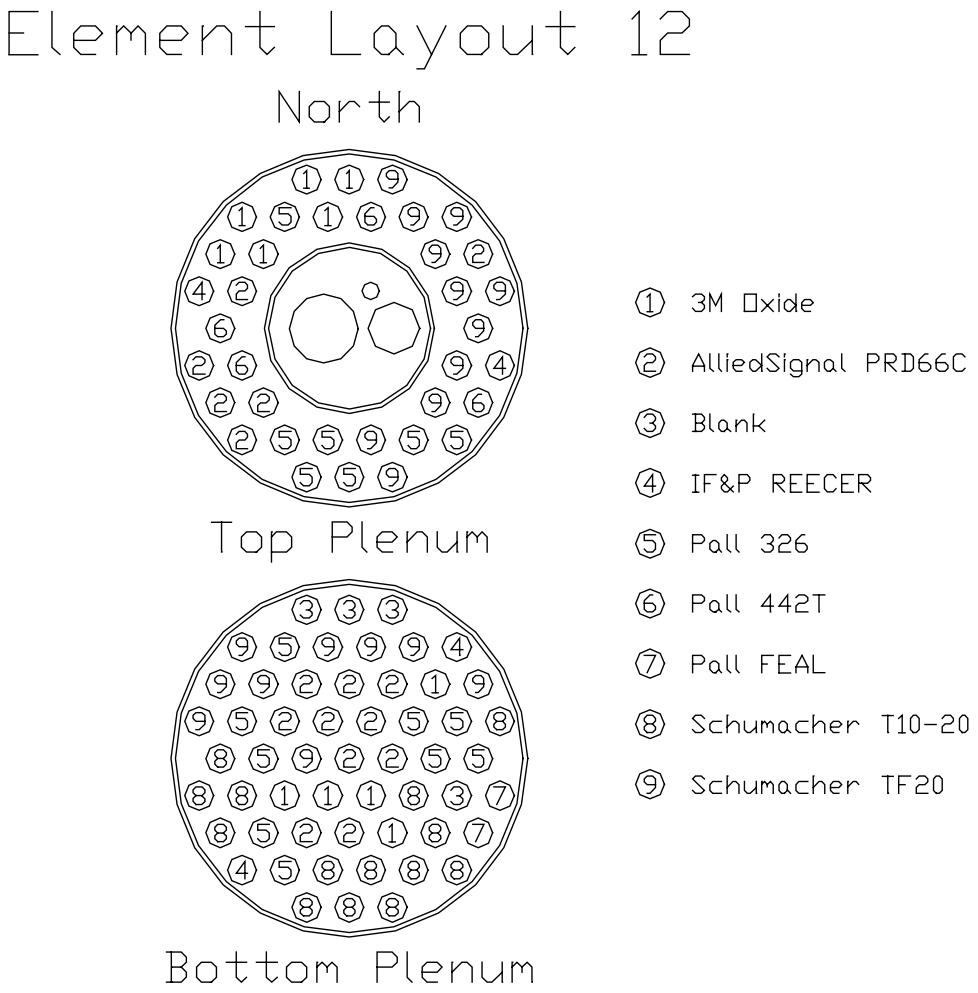

Figure 3.2-8 Filter Element Layout For TC05 – January 31 Through February 24

(Layout 12)

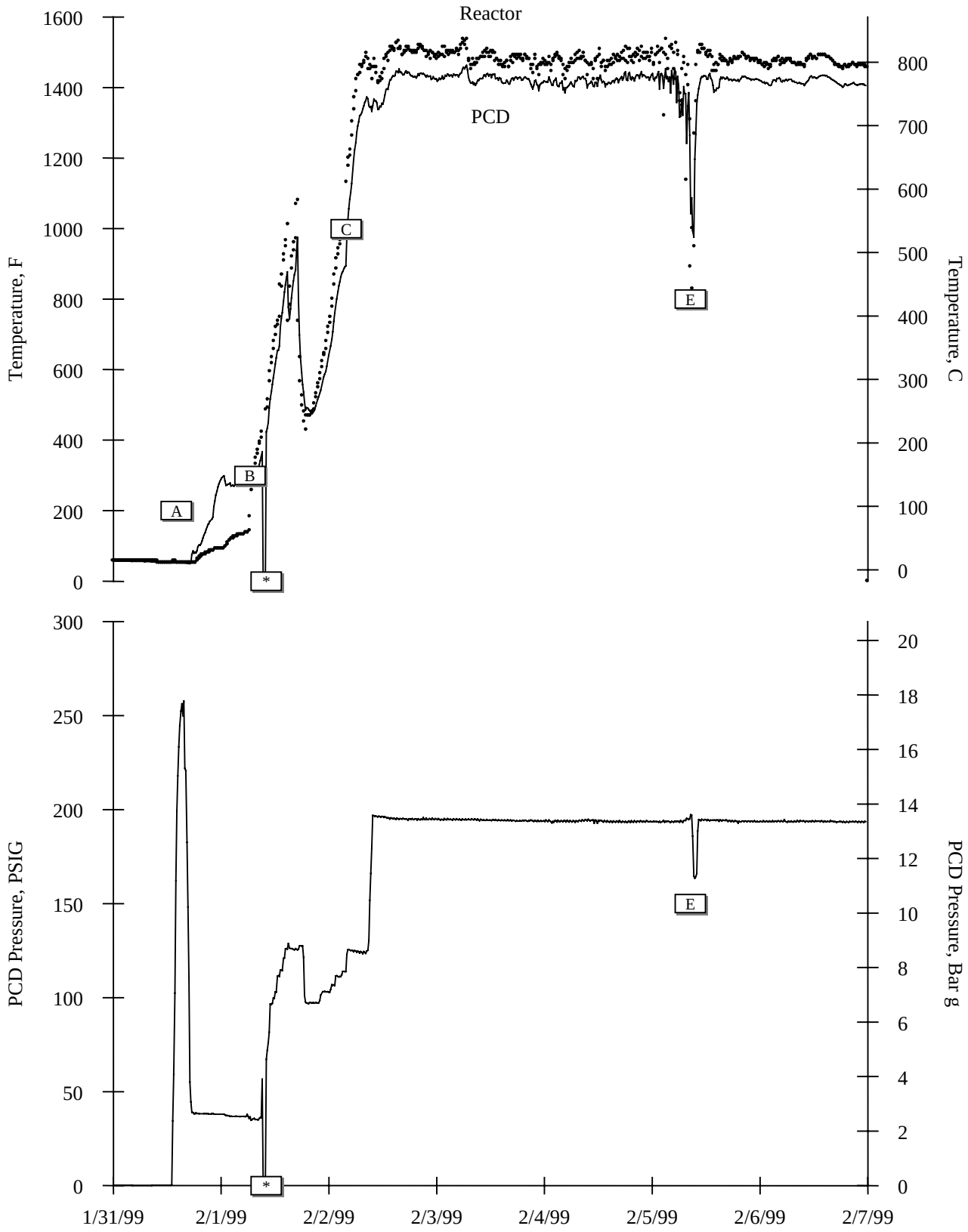

Figure 3.2-9 TC05 Temperature and Pressure For January 31 Through February 7

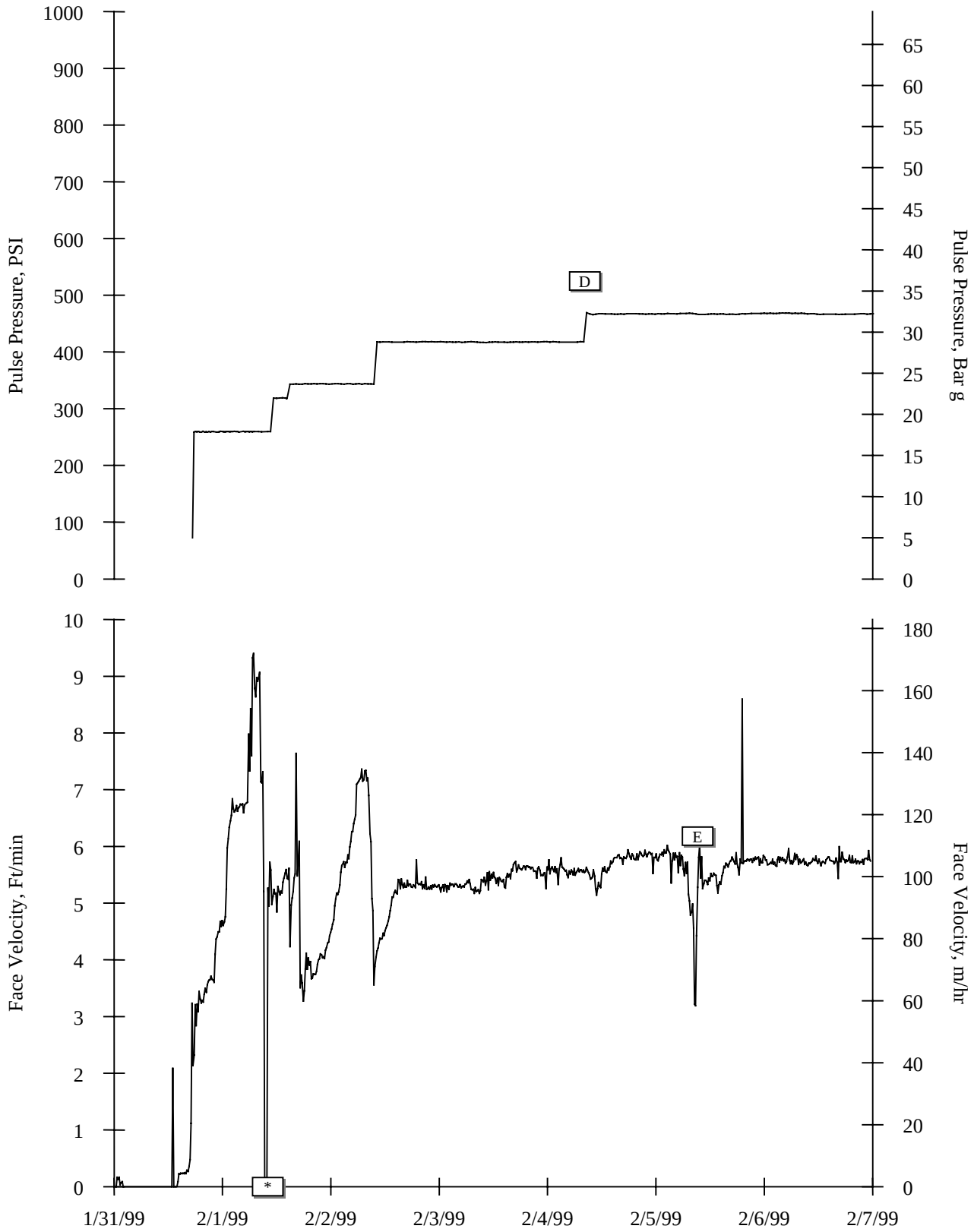

Figure 3.2-10 TC05 Back-Pulse Pressure and Face Velocity for January 31 Through February 7

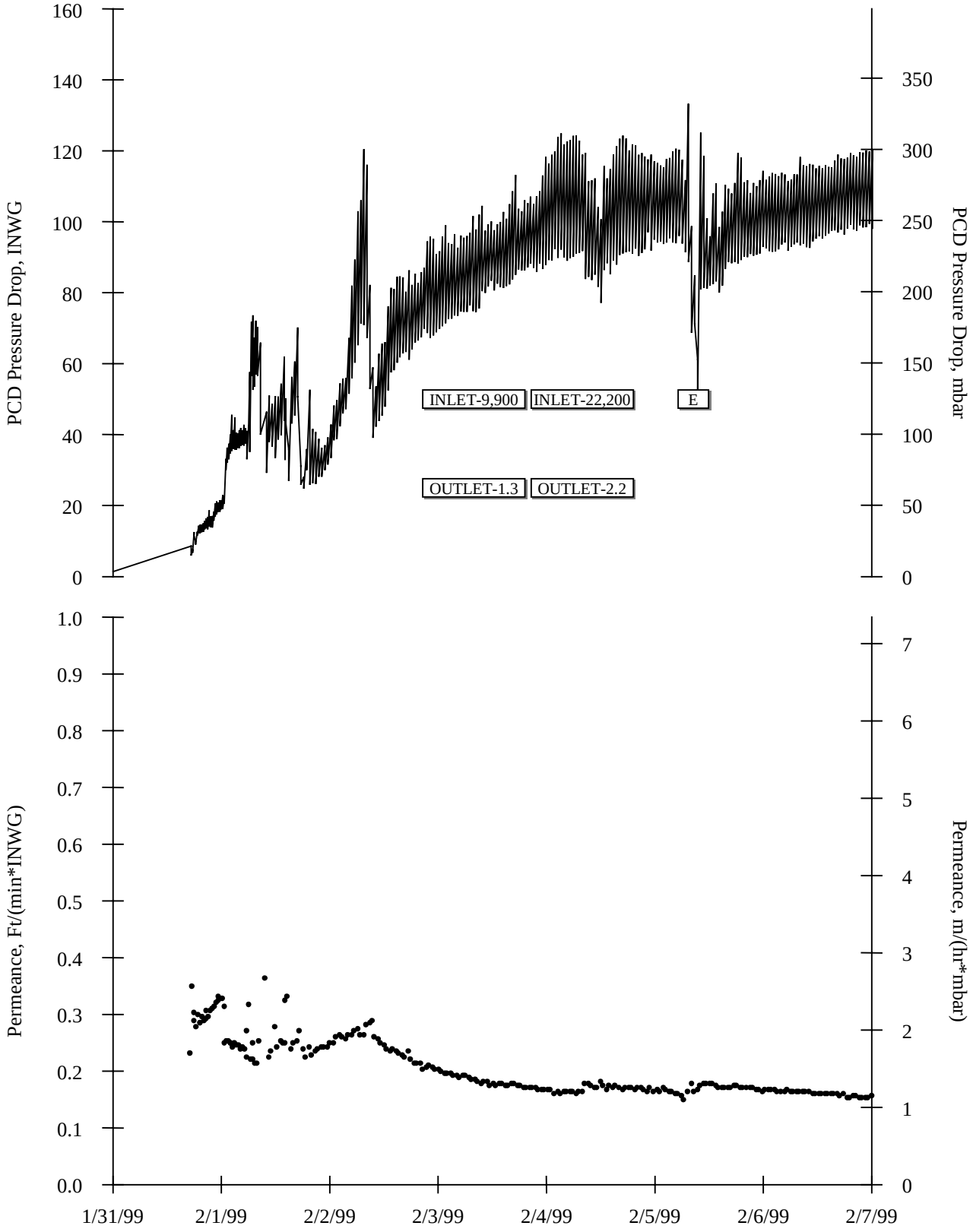

Figure 3.2-11 TC05 Pressure Drop and Permeance for January 31 Through February 7

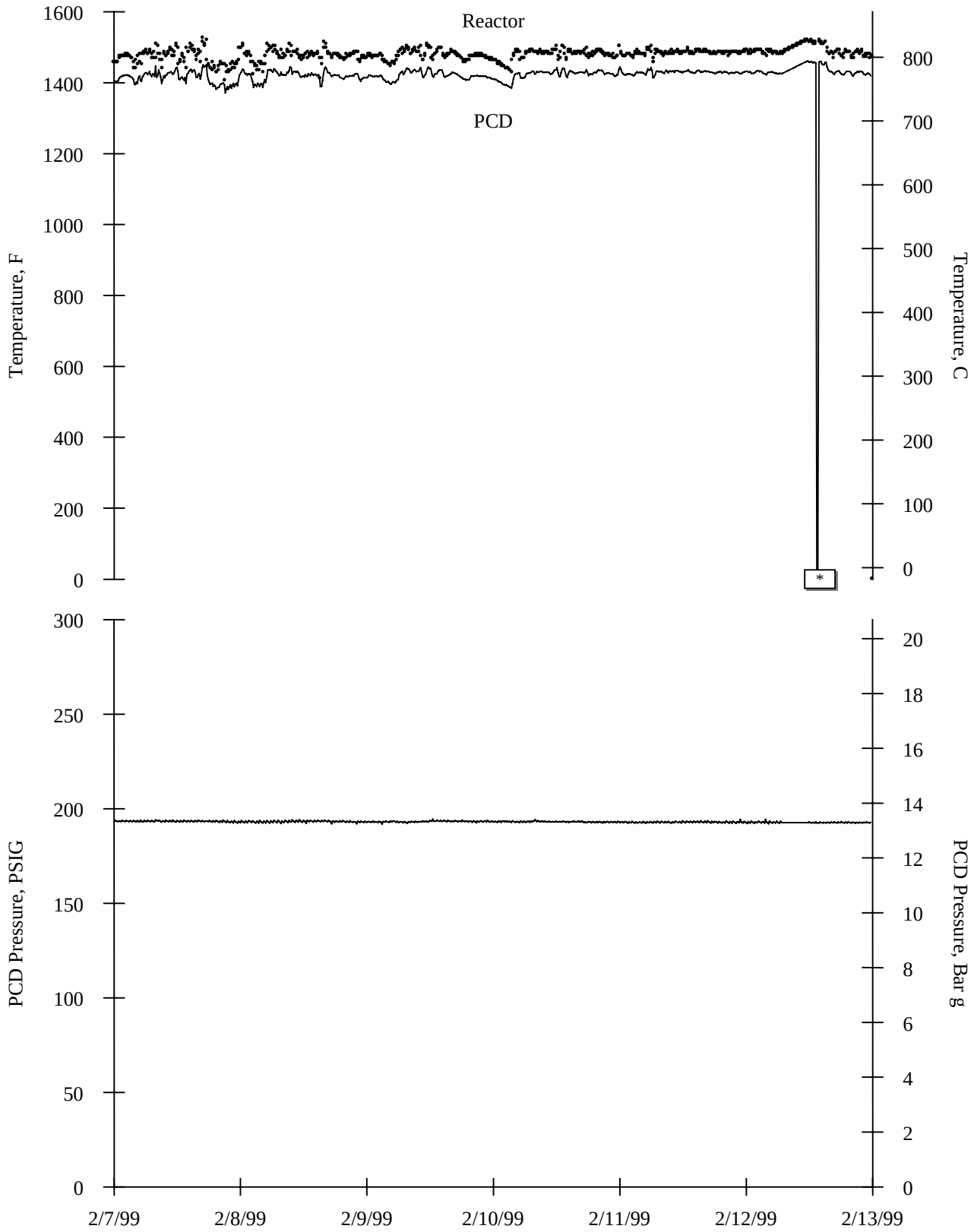

Figure 3.2-12 TC05 Temperature and Pressure for February 7 Through February 13

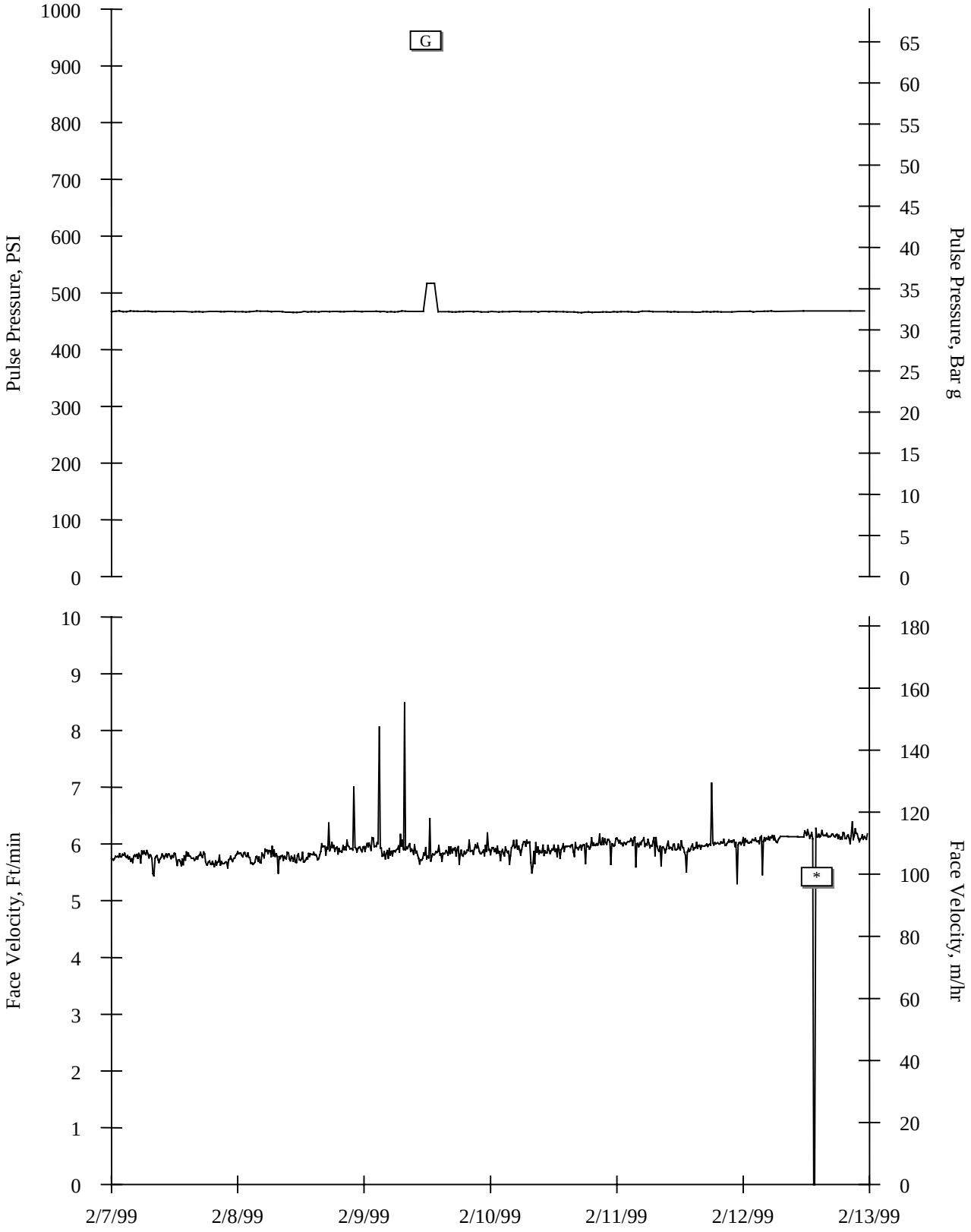

Figure 3.2-13 TC05 Back-Pulse Pressure and Face Velocity for February 7 Through February 13

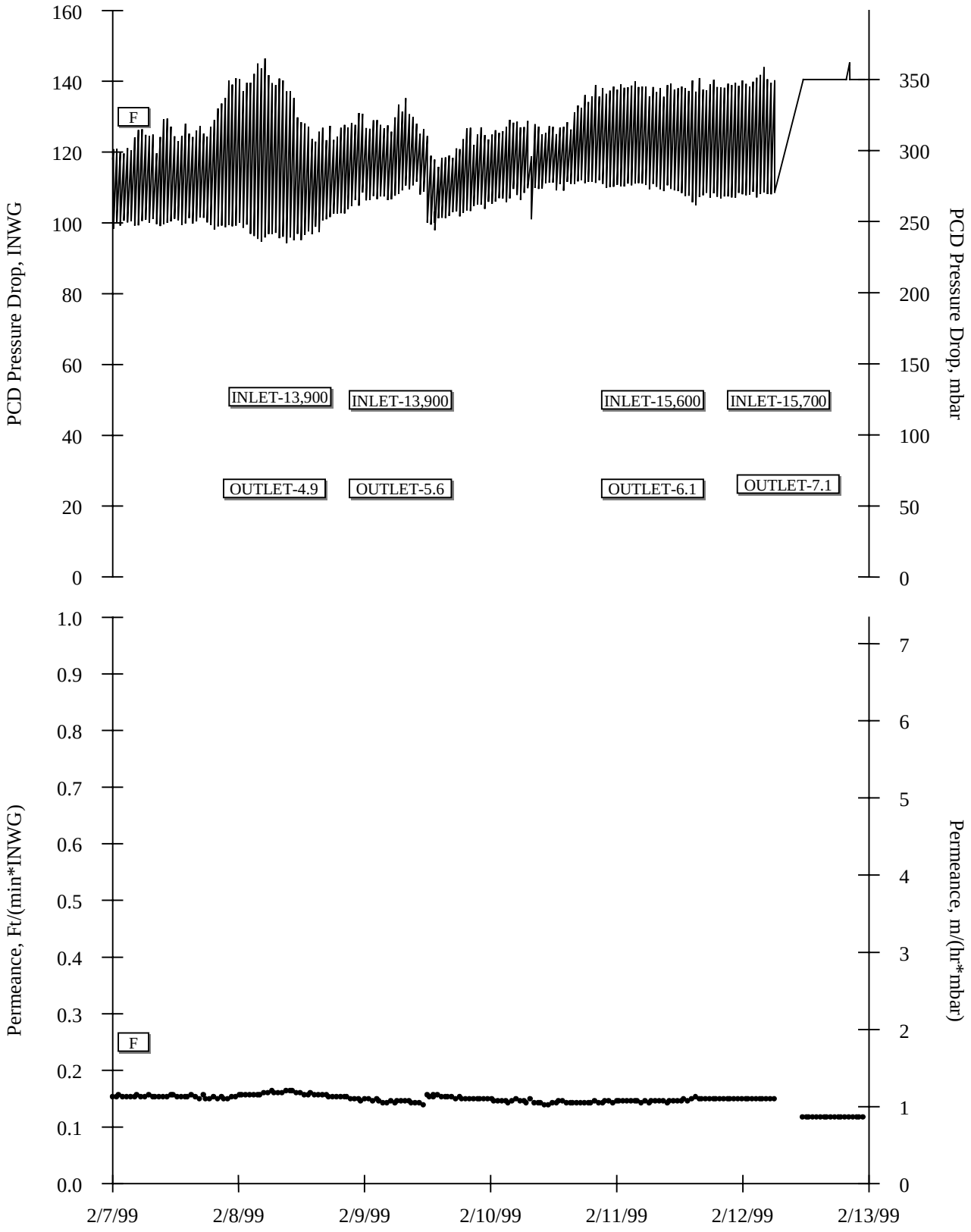

Figure 3.2-14 TC05 Pressure Drop and Permeance for February 7 Through February 13

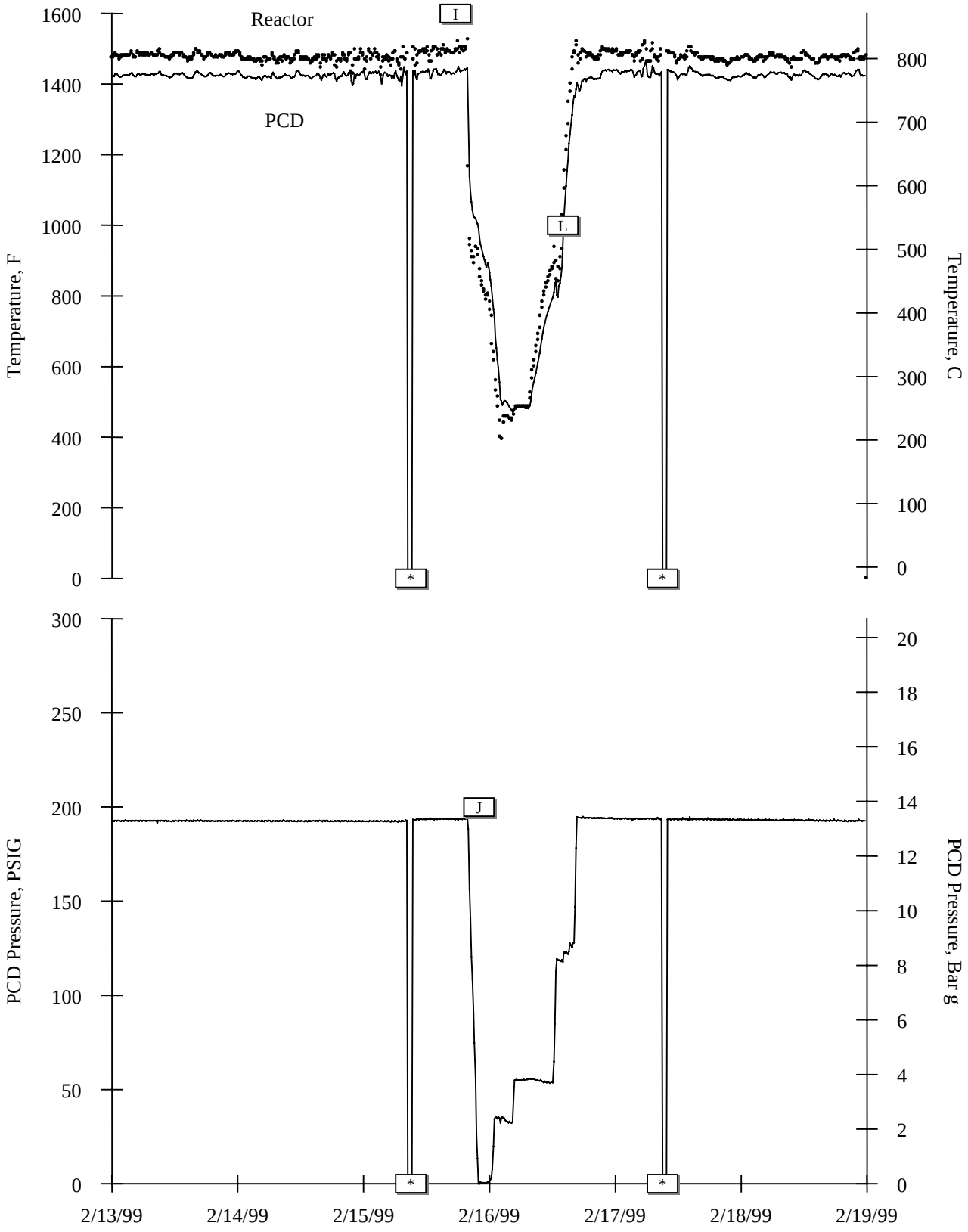

Figure 3.2-15 TC05 Temperature and Pressure for February 13 Through February 19

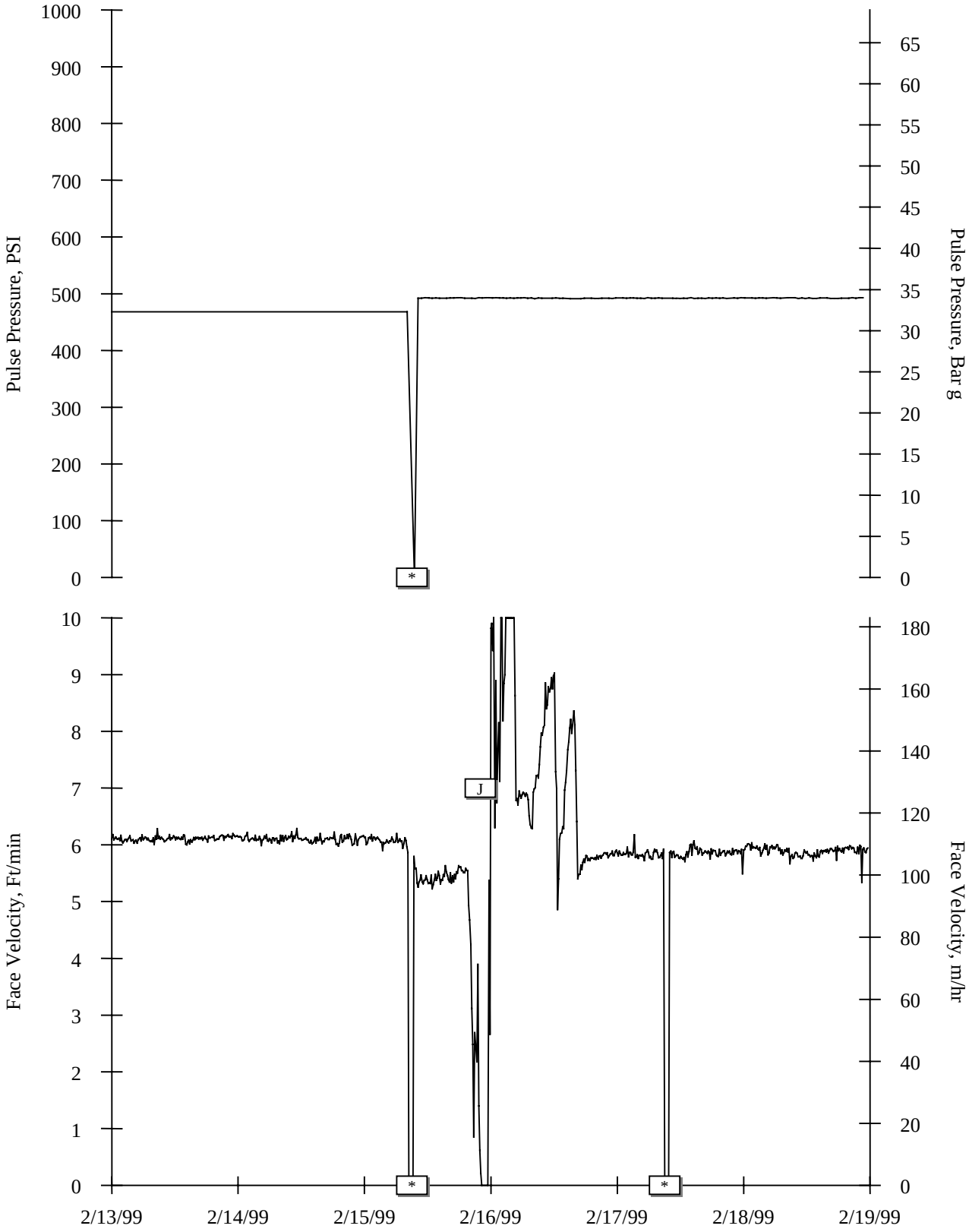

Figure 3.2-16 TC05 Back-Pulse Pressure and Face Velocity for February 13 Through February 19

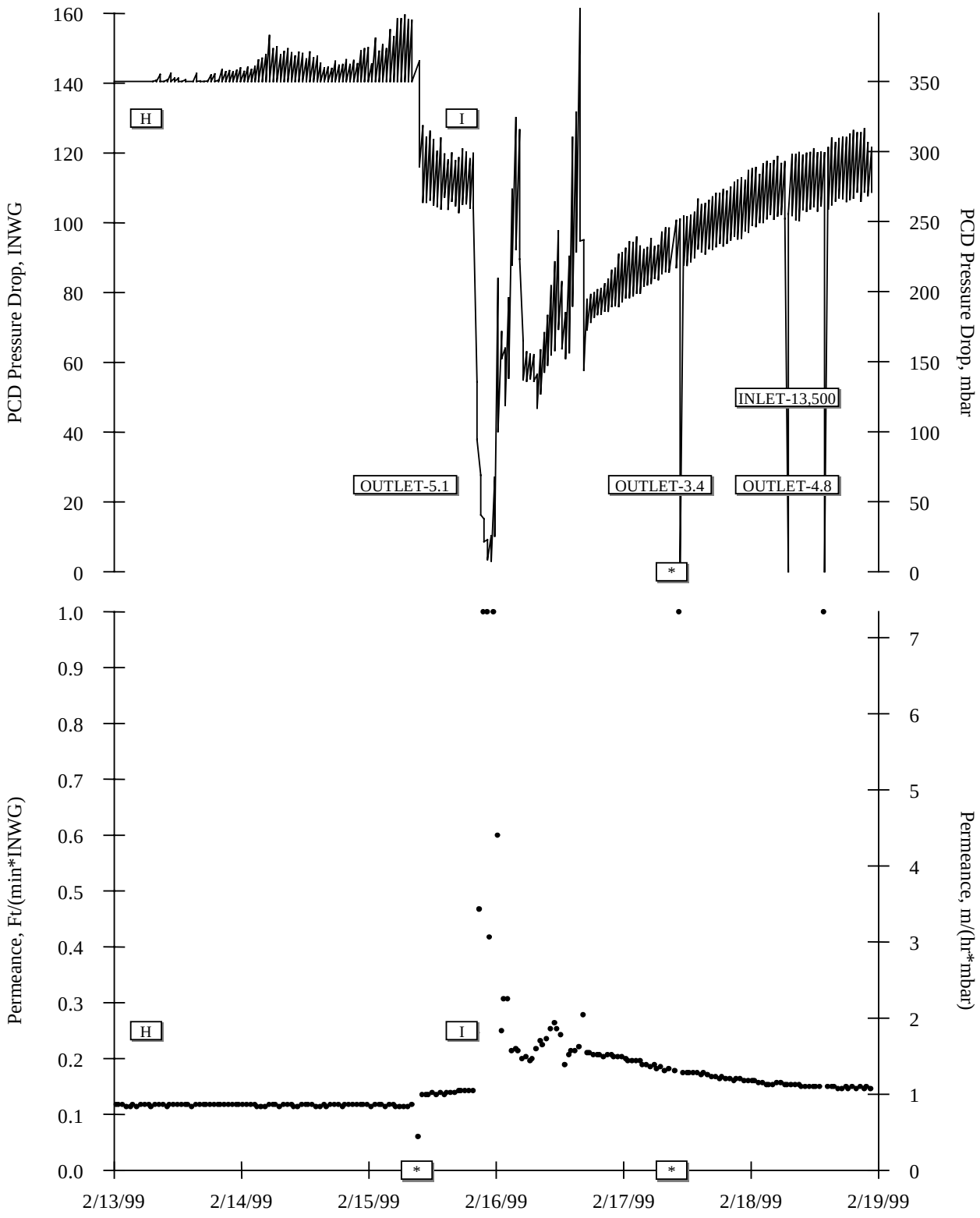

Figure 3.2-17 TC05 Pressure Drop and Permeance for February 13 Through February 19

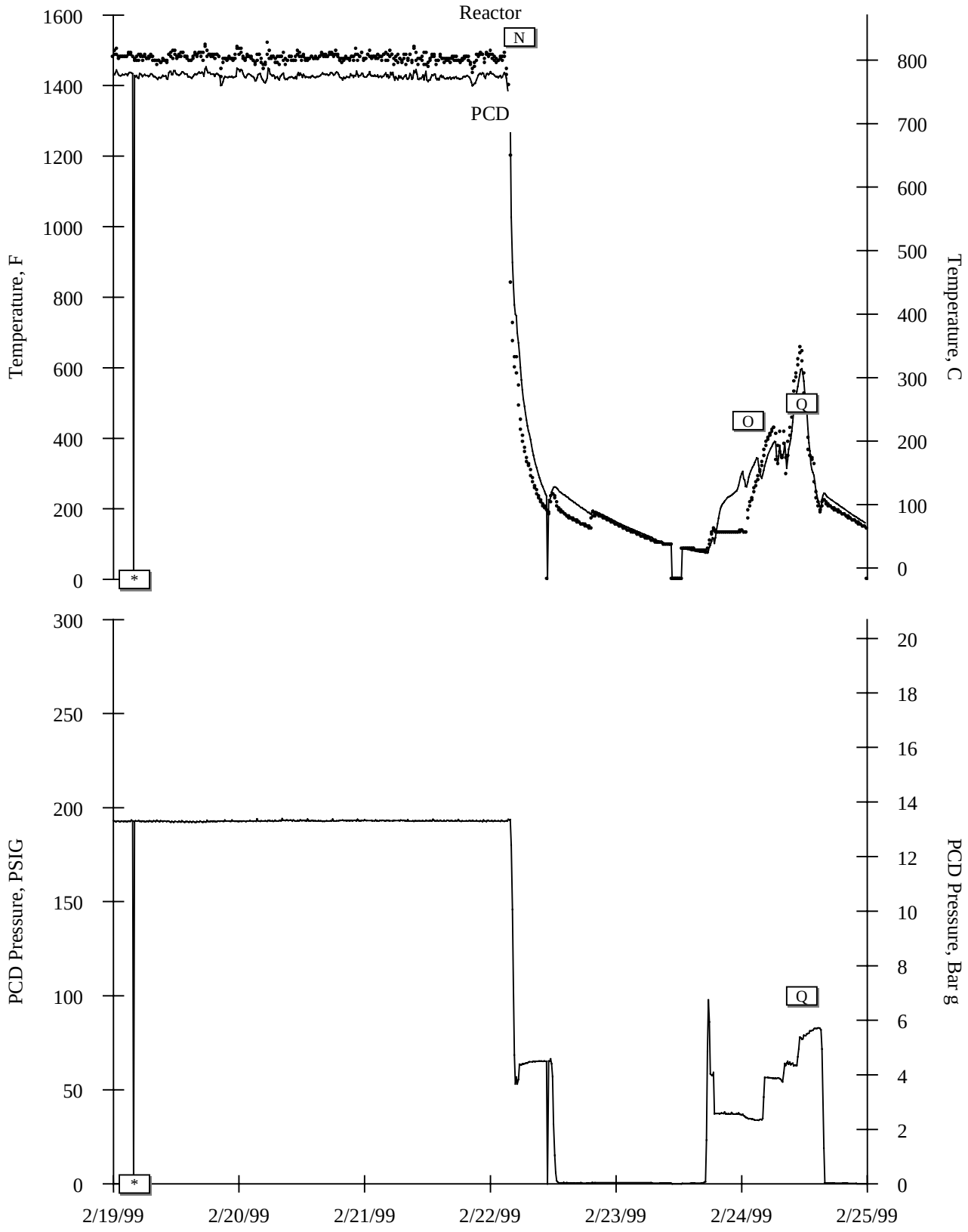

Figure 3.2-18 TC05 Temperature and Pressure for February 19 Through February 25

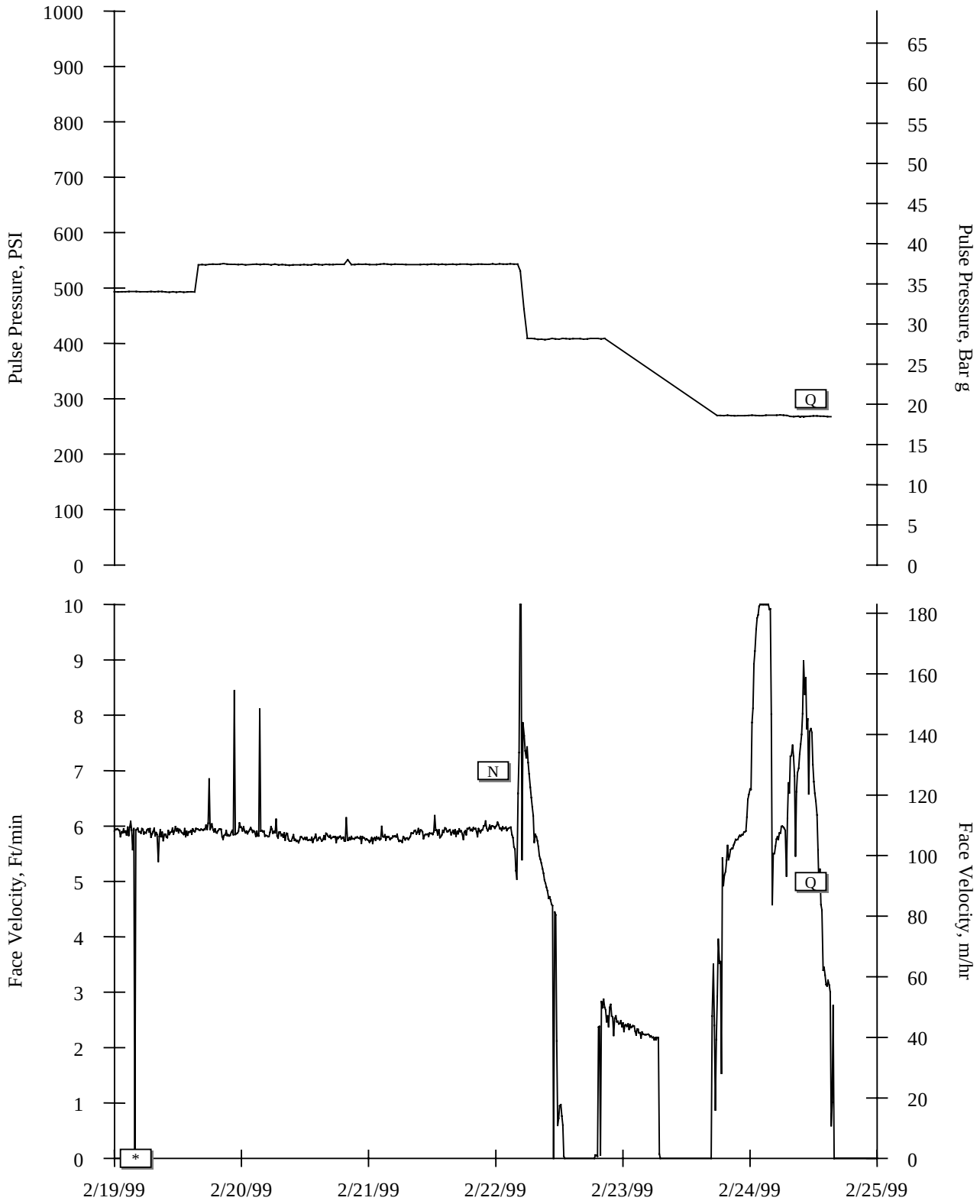

Figure 3.2-19 TC05 Back-Pulse Pressure and Face Velocity for February 19 Through February 25

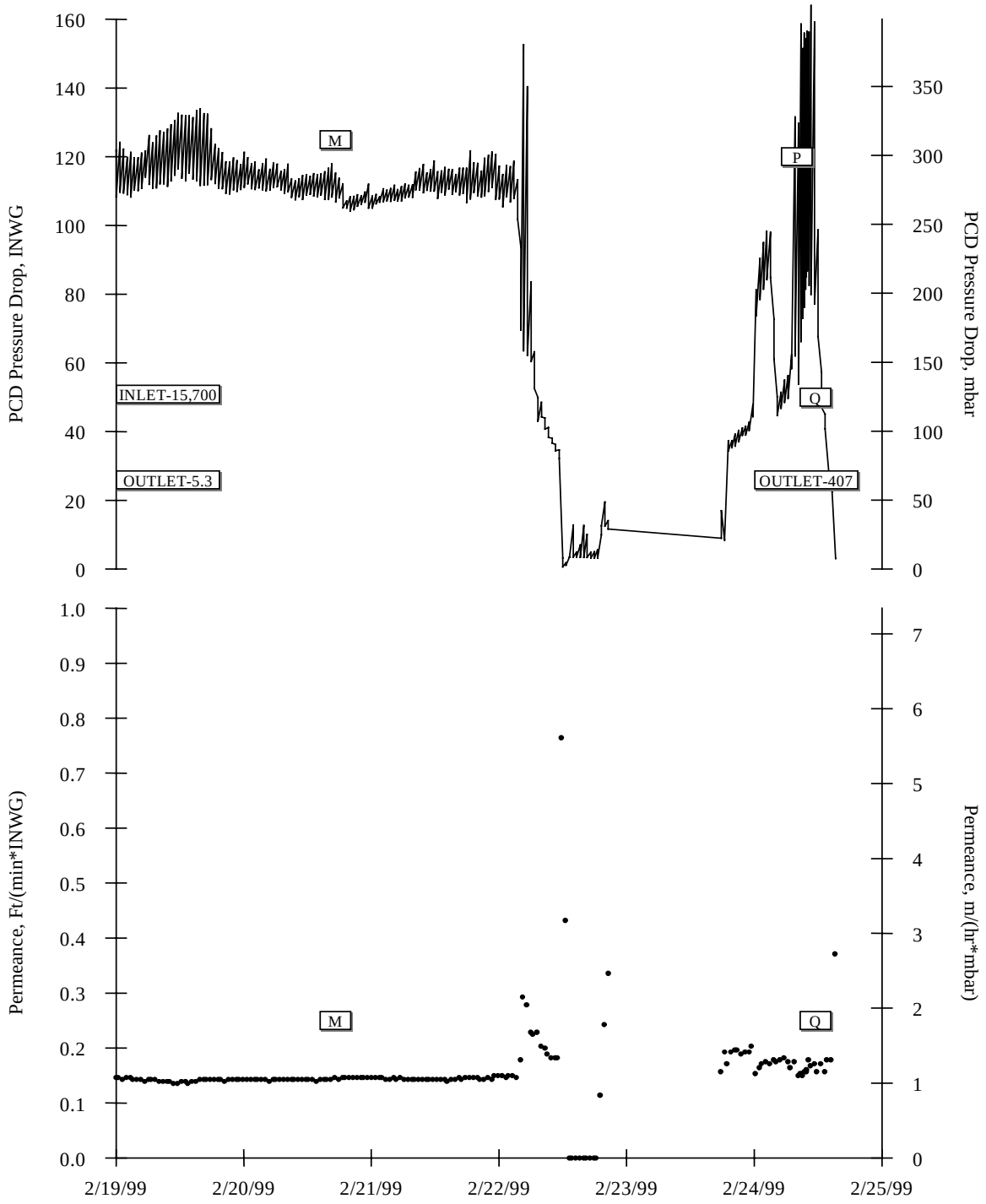

Figure 3.2-20 TC05 Pressure Drop and Permeance for February 19 Through February 25

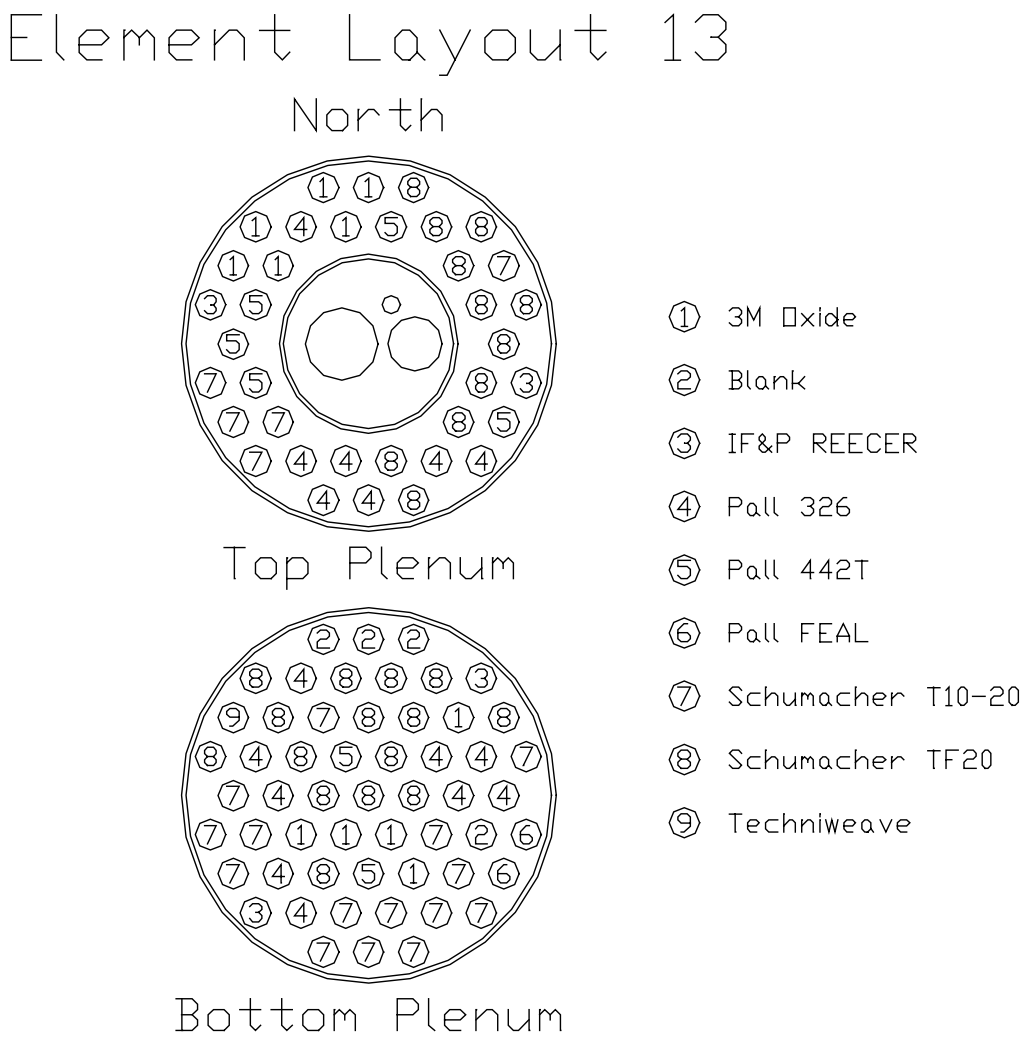

Figure 3.2-21 Filter Element Layout For TC05 – March 3 Through May 2

(Layout 13)

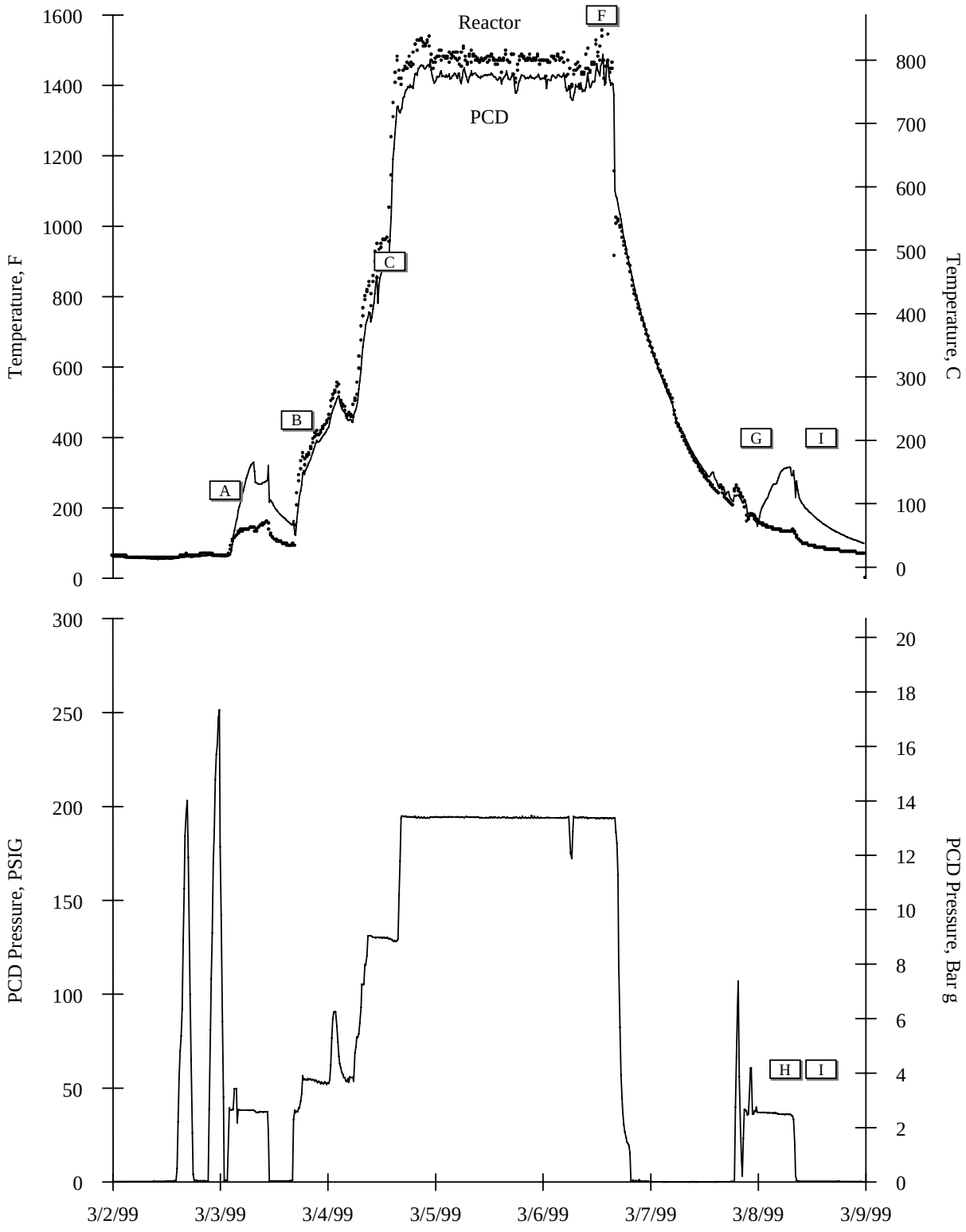

Figure 3.2-22 TC05 Temperature and Pressure for March 2 Through March 9

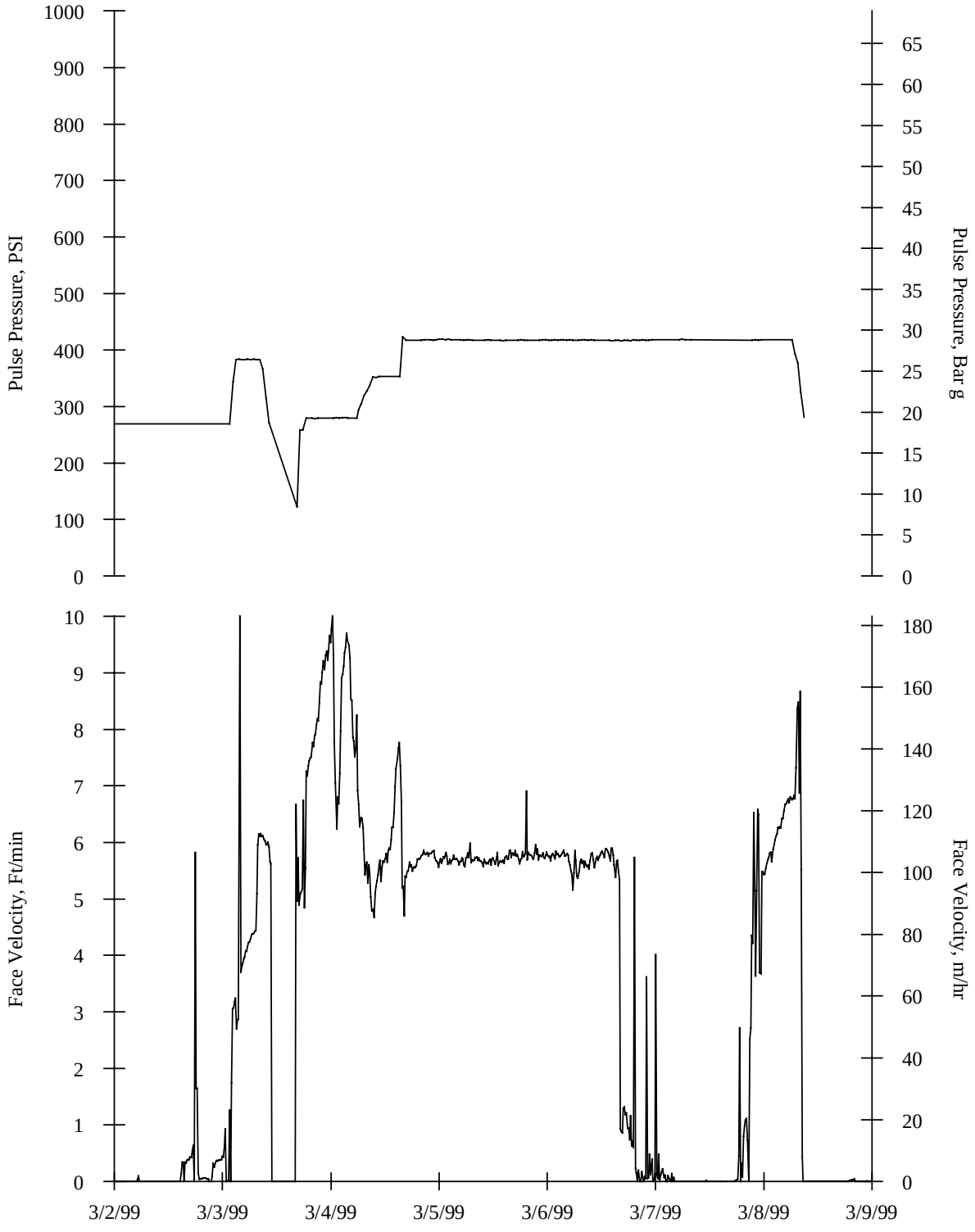

Figure 3.2-23 TC05 Back-Pulse Pressure and Face Velocity for March 2 Through March 9

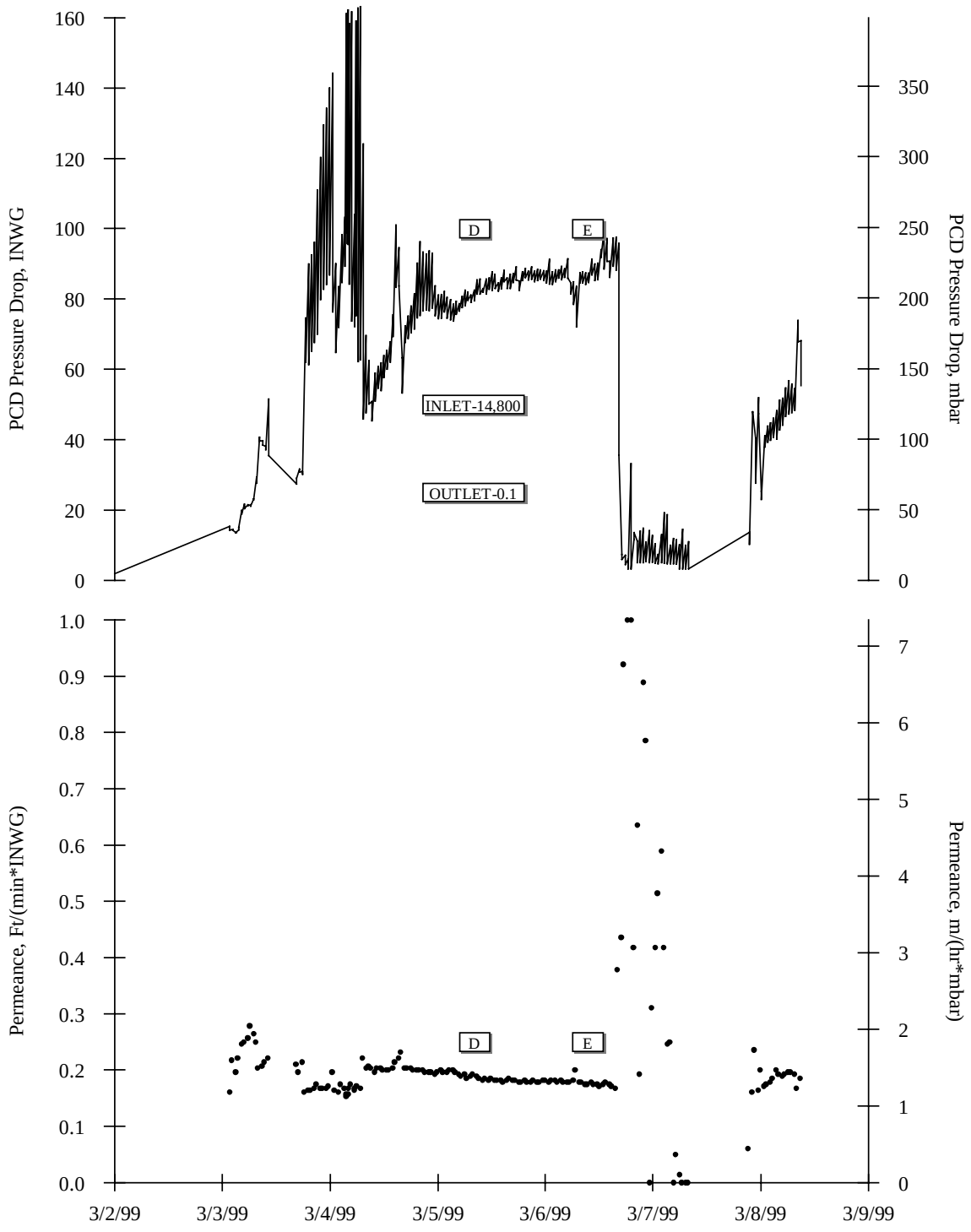

Figure 3.2-24 TC05 Pressure Drop and Permeance for March 2 Through March 9

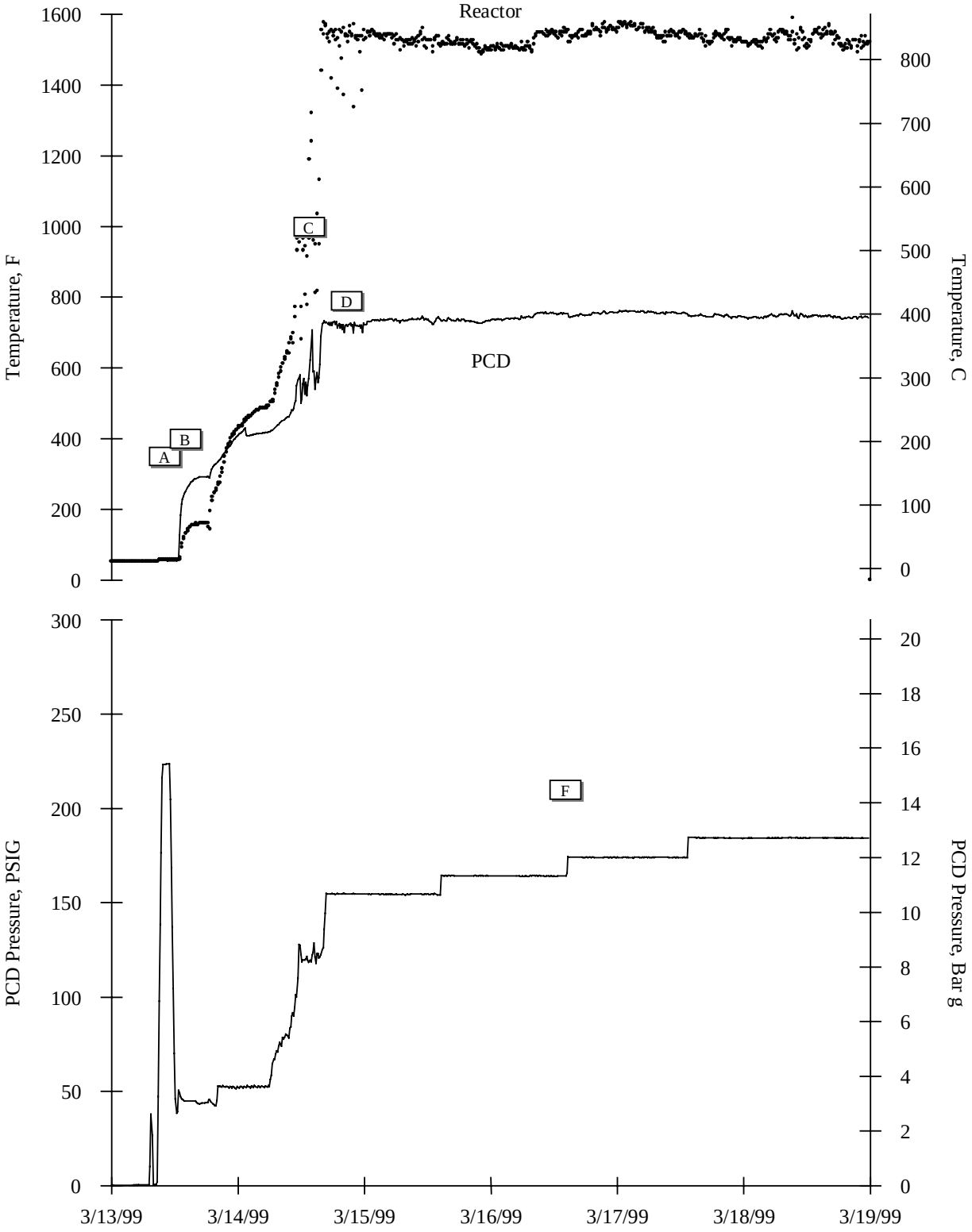

Figure 3.2-25 TC05 Temperature and Pressure for March 13 Through March 19

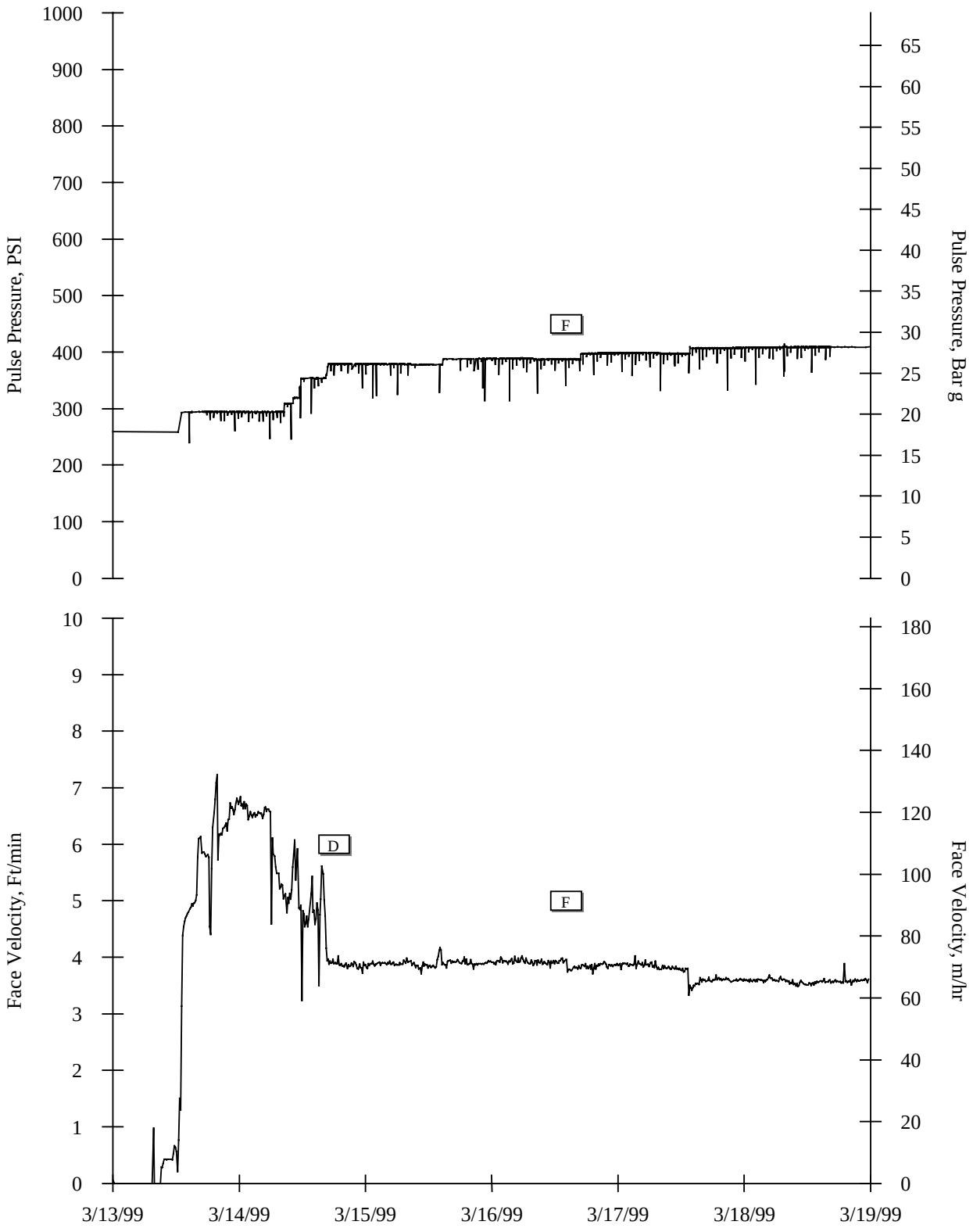

Figure 3.2-26 TC05 Back-Pulse Pressure and Face Velocity for March 13 Through March 19

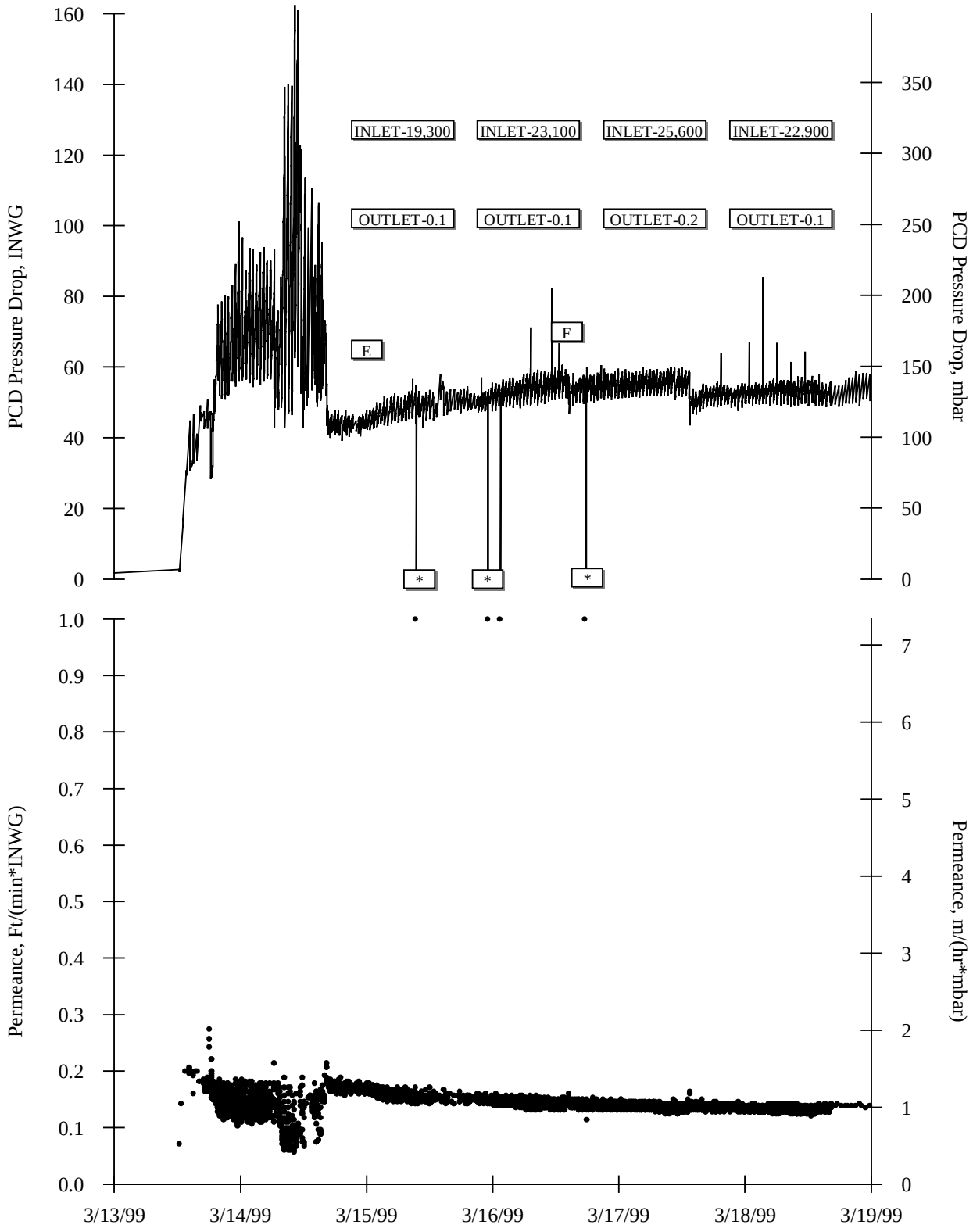

Figure 3.2-27 TC05 Pressure Drop and Permeance for March 13 Through March 19

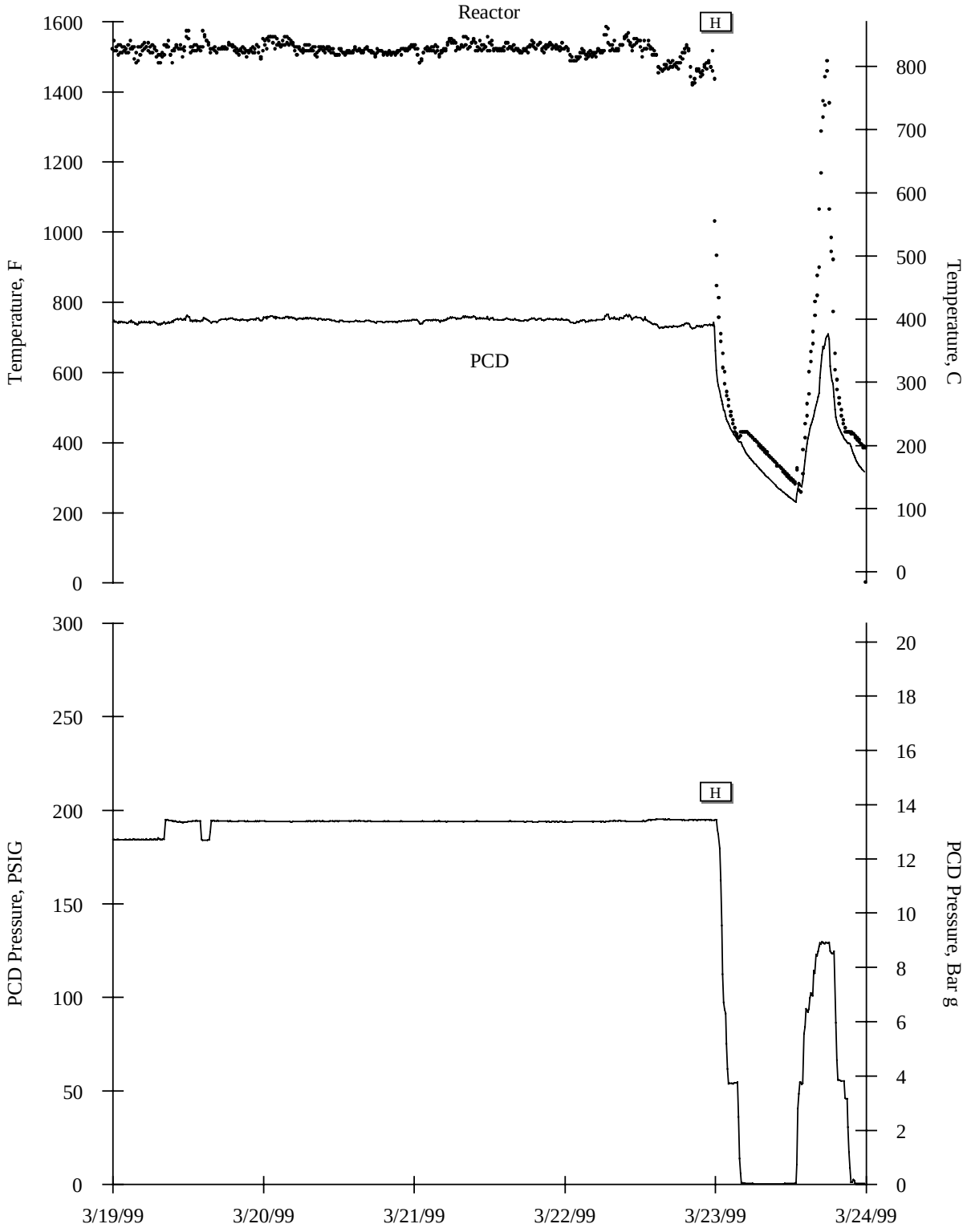

Figure 3.2-28 TC05 Temperature and Pressure for March 19 Through March 24

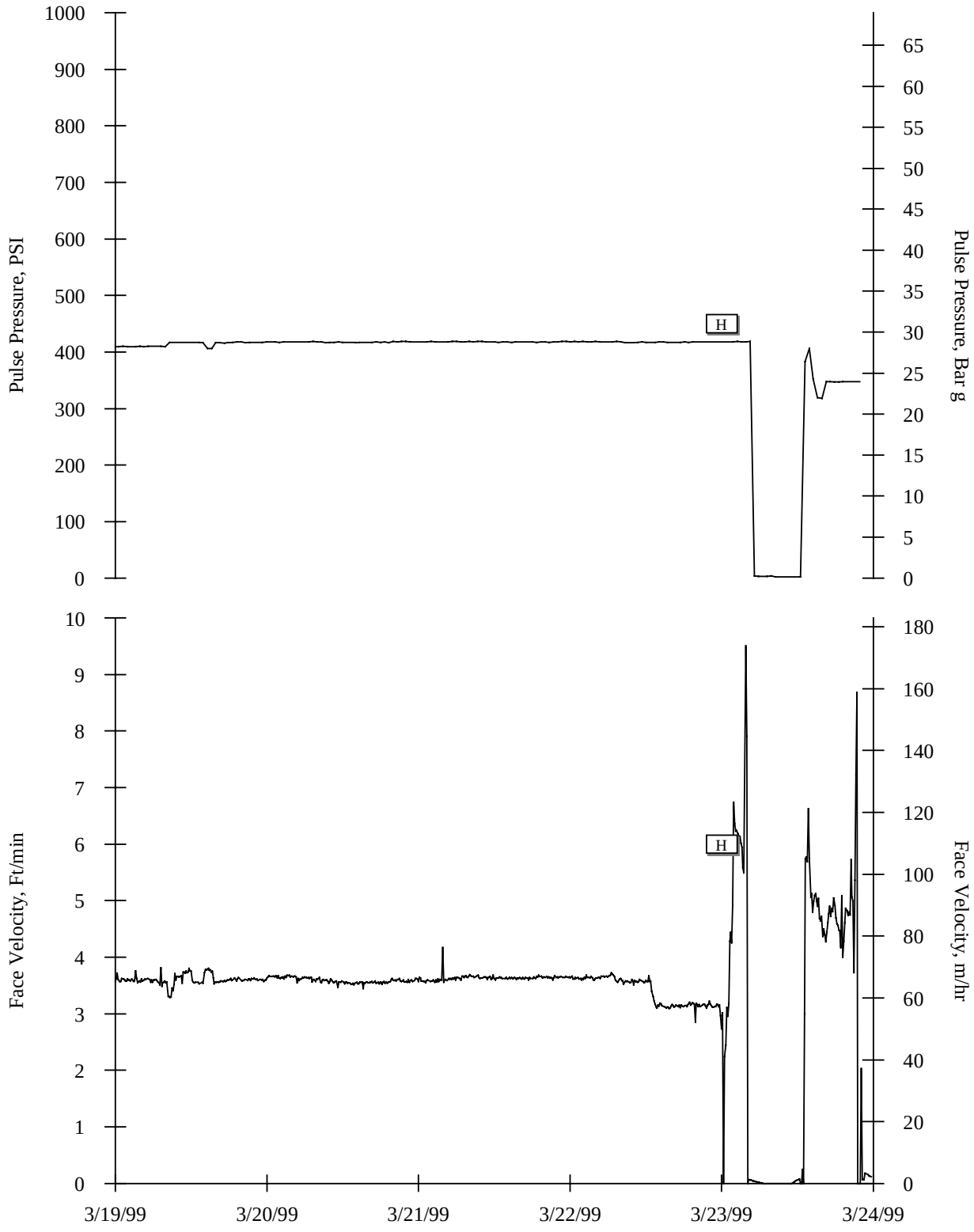

Figure 3.2-29 TC05 Back-Pulse Pressure and Face Velocity for March 19 Through March 24

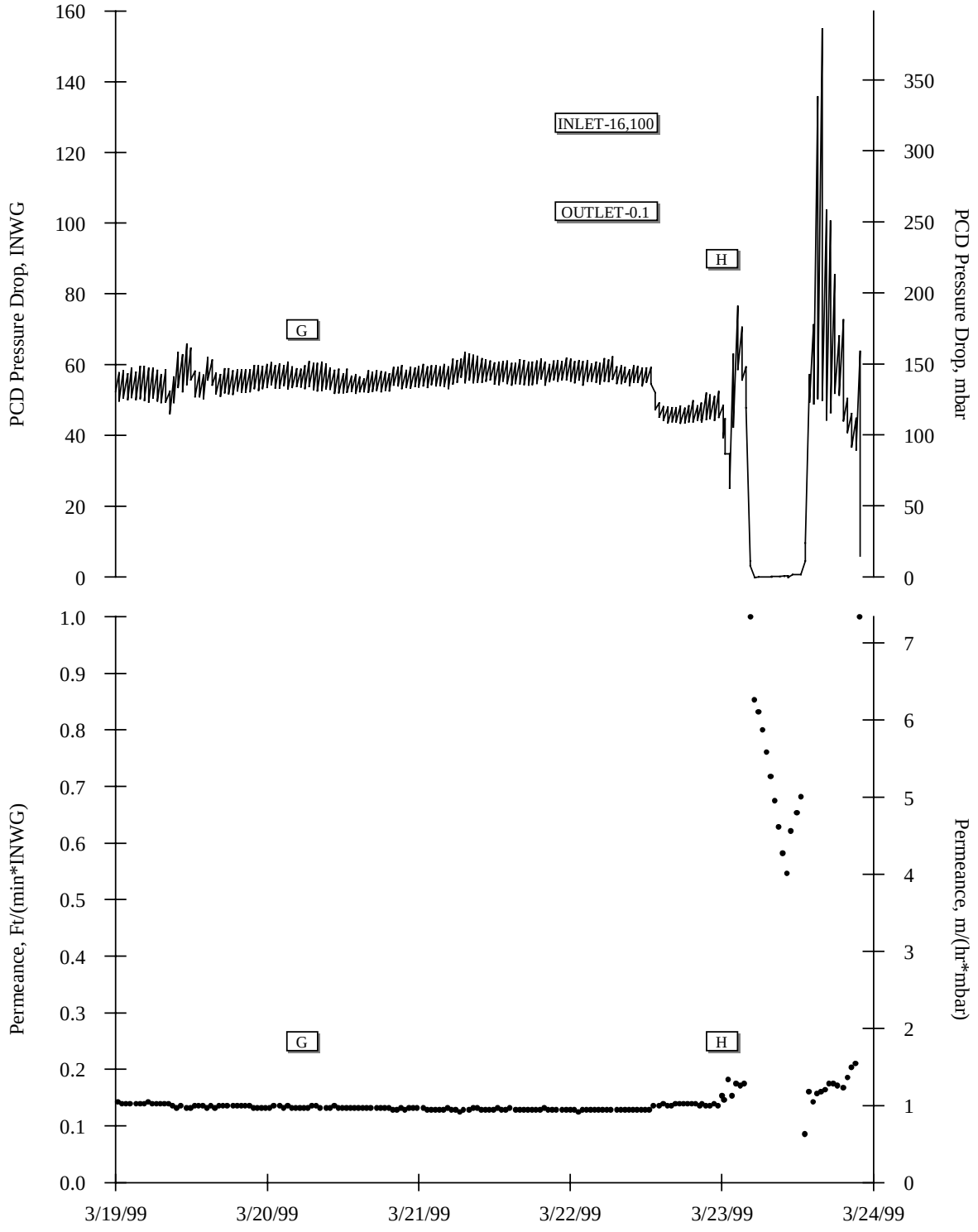

Figure 3.2-30 TC05 Pressure Drop and Permeance for March 19 Through March 24

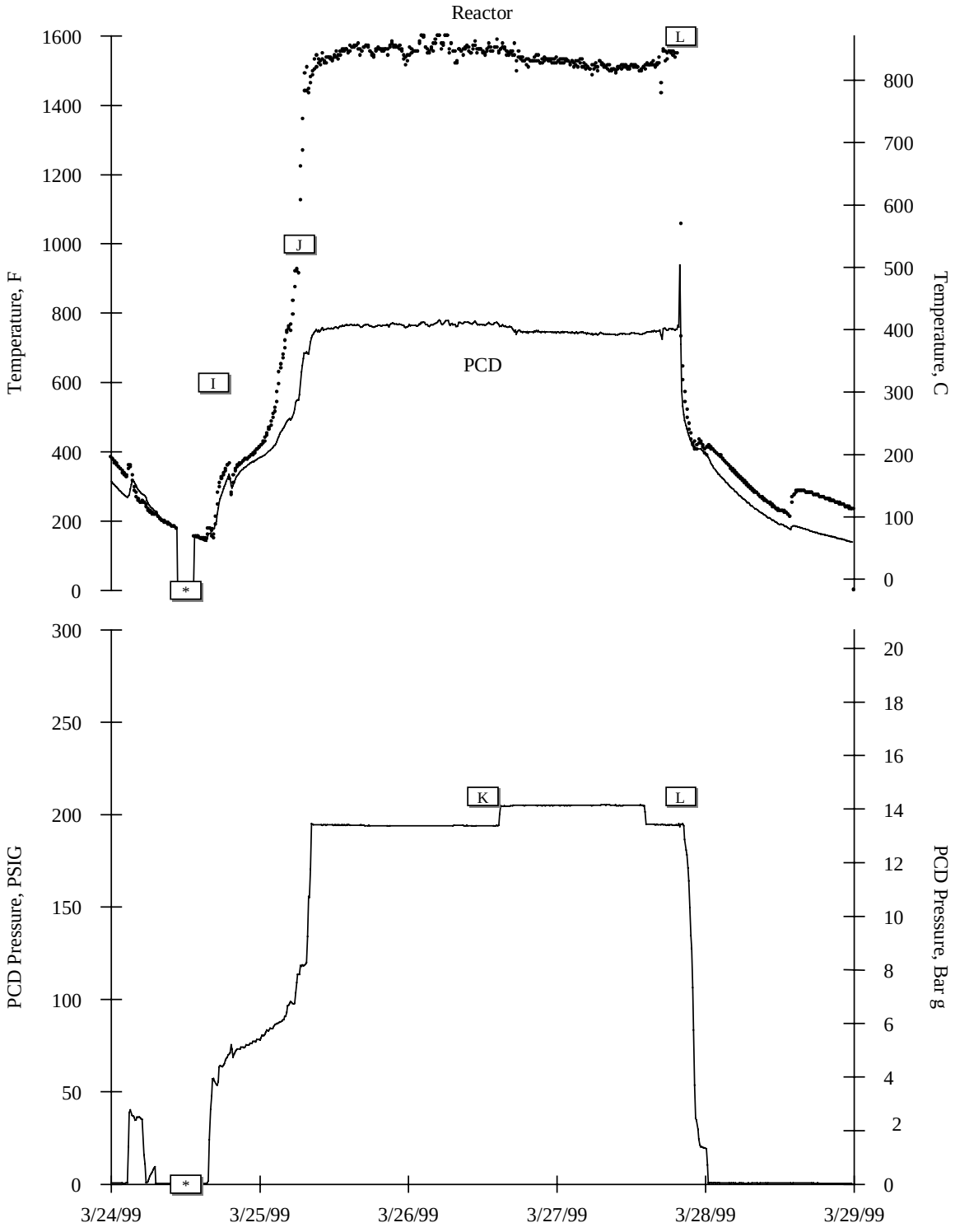

Figure 3.2-31 TC05 Temperature and Pressure for March 24 Through March 29

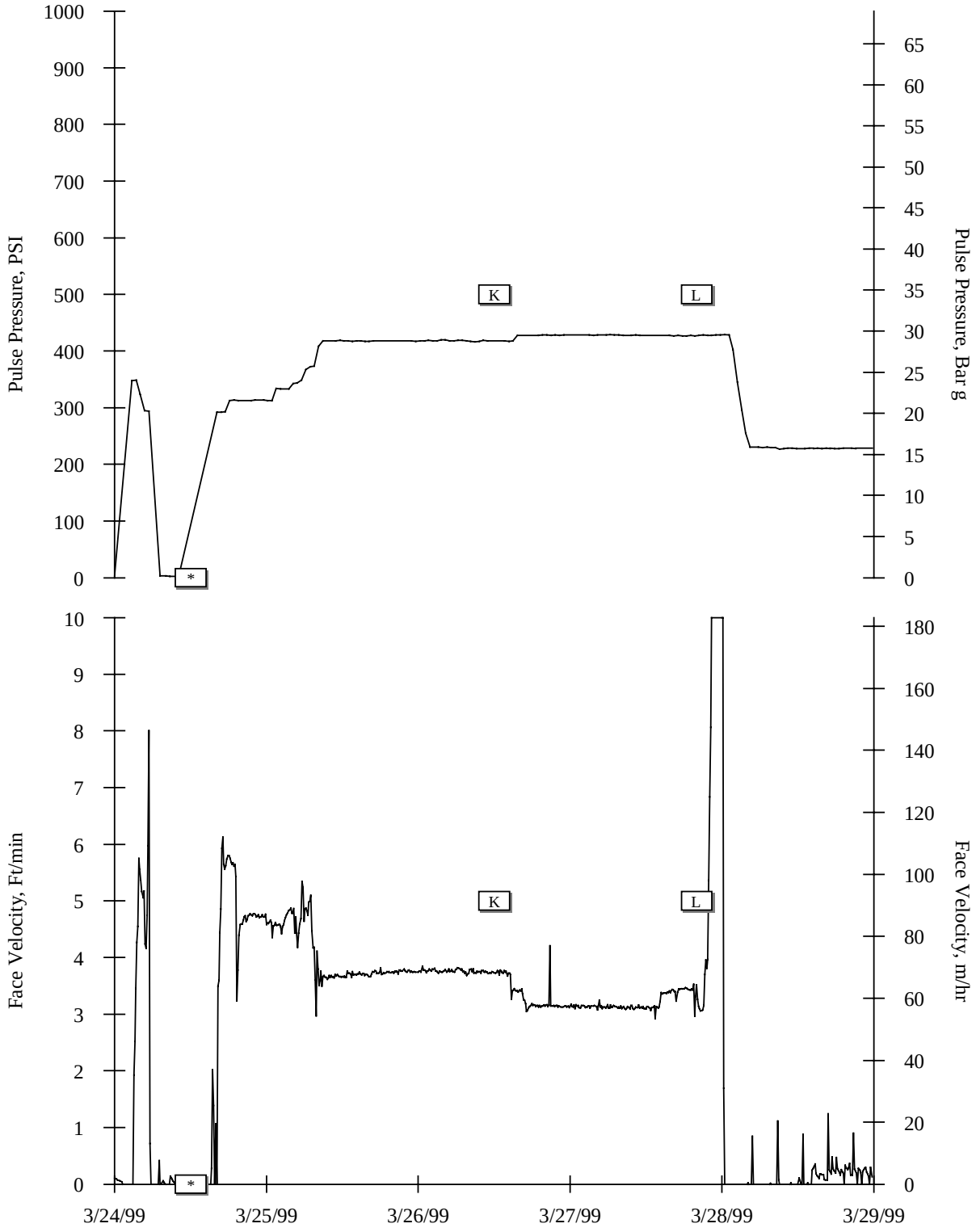

Figure 3.2-32 TC05 Back-Pulse Pressure and Face Velocity for March 24 Through March 29

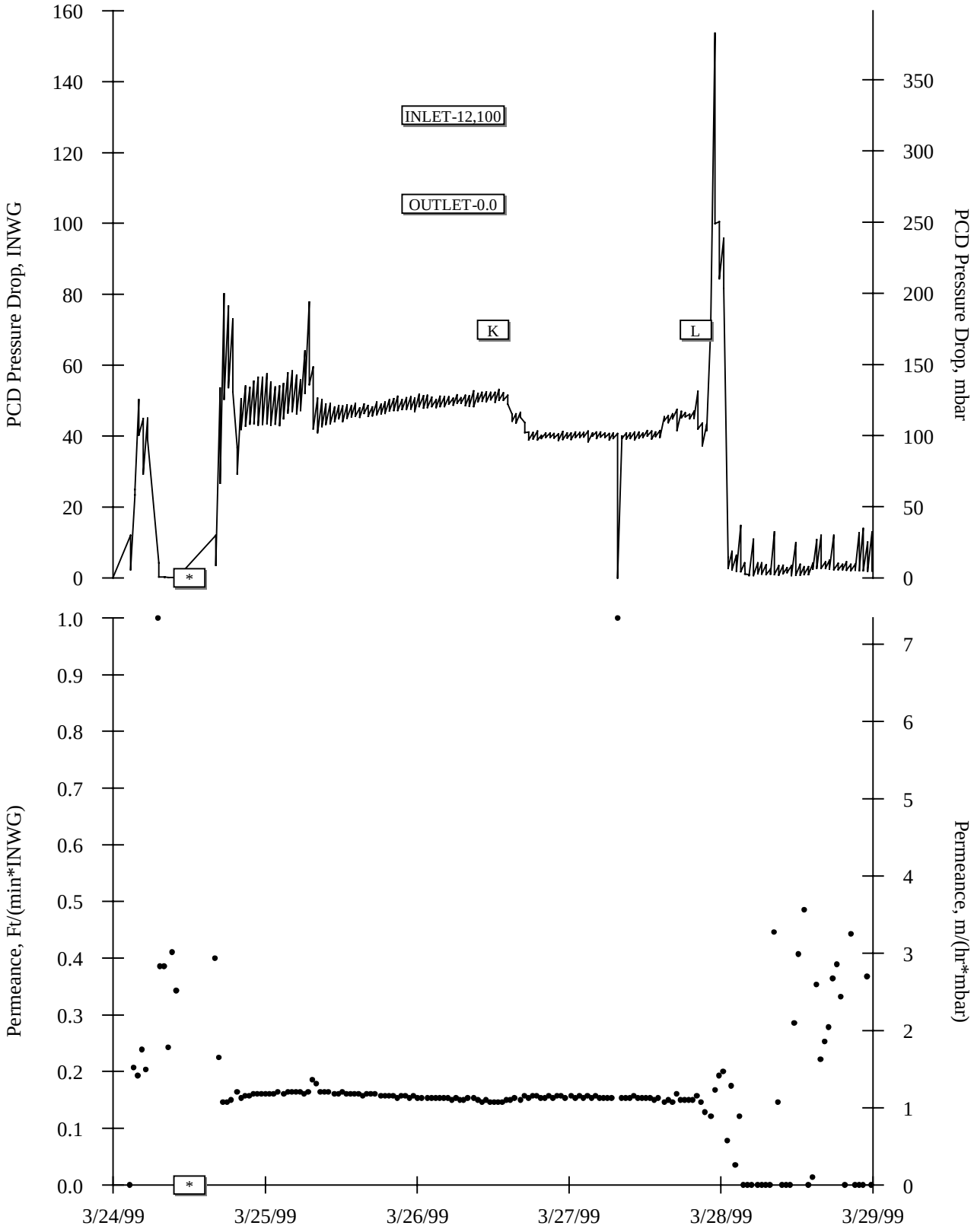

Figure 3.2-33 TC05 Pressure Drop and Permeance for March 24 Through March 29

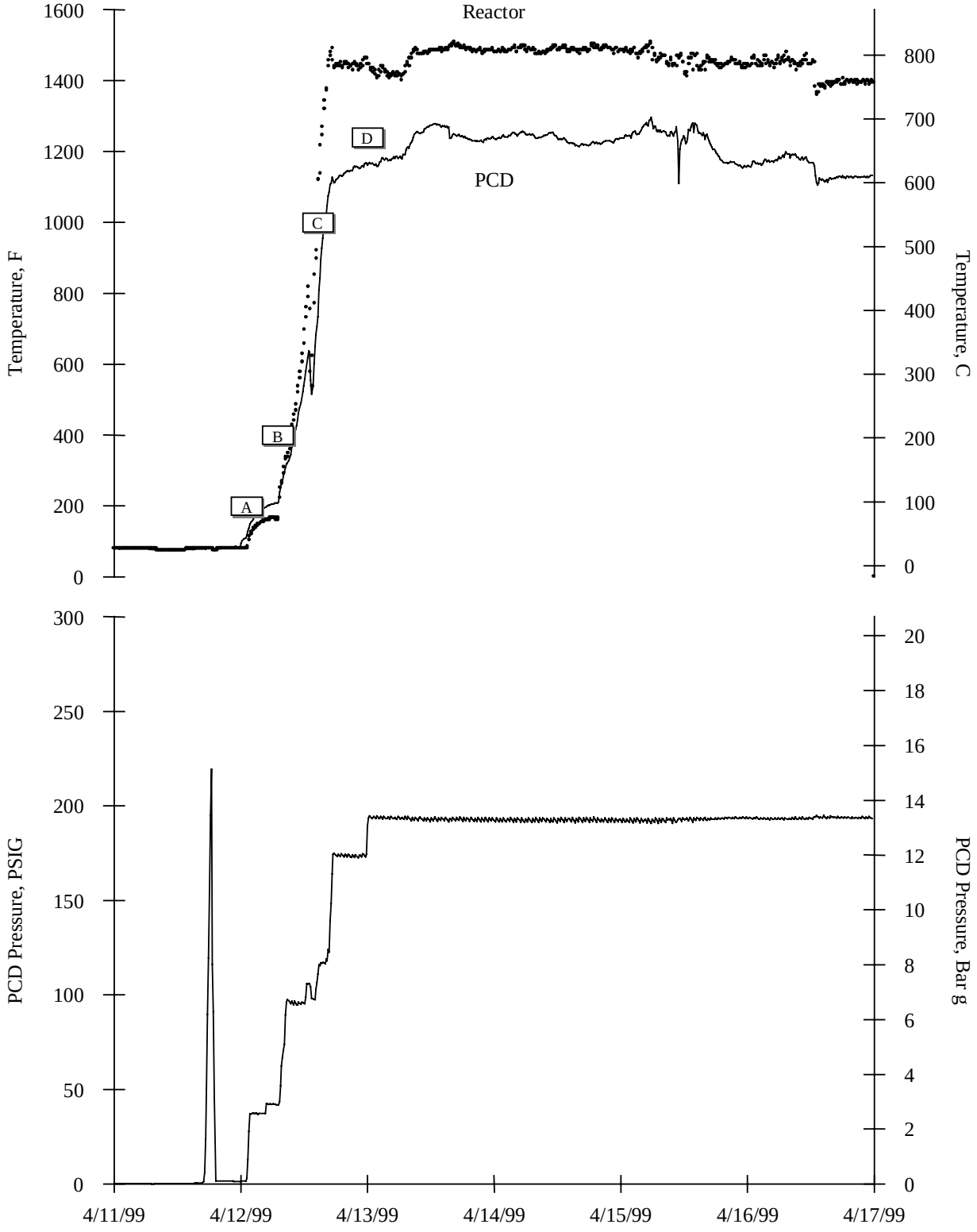

Figure 3.2-34 TC05 Temperature and Pressure for April 11 Through April 17

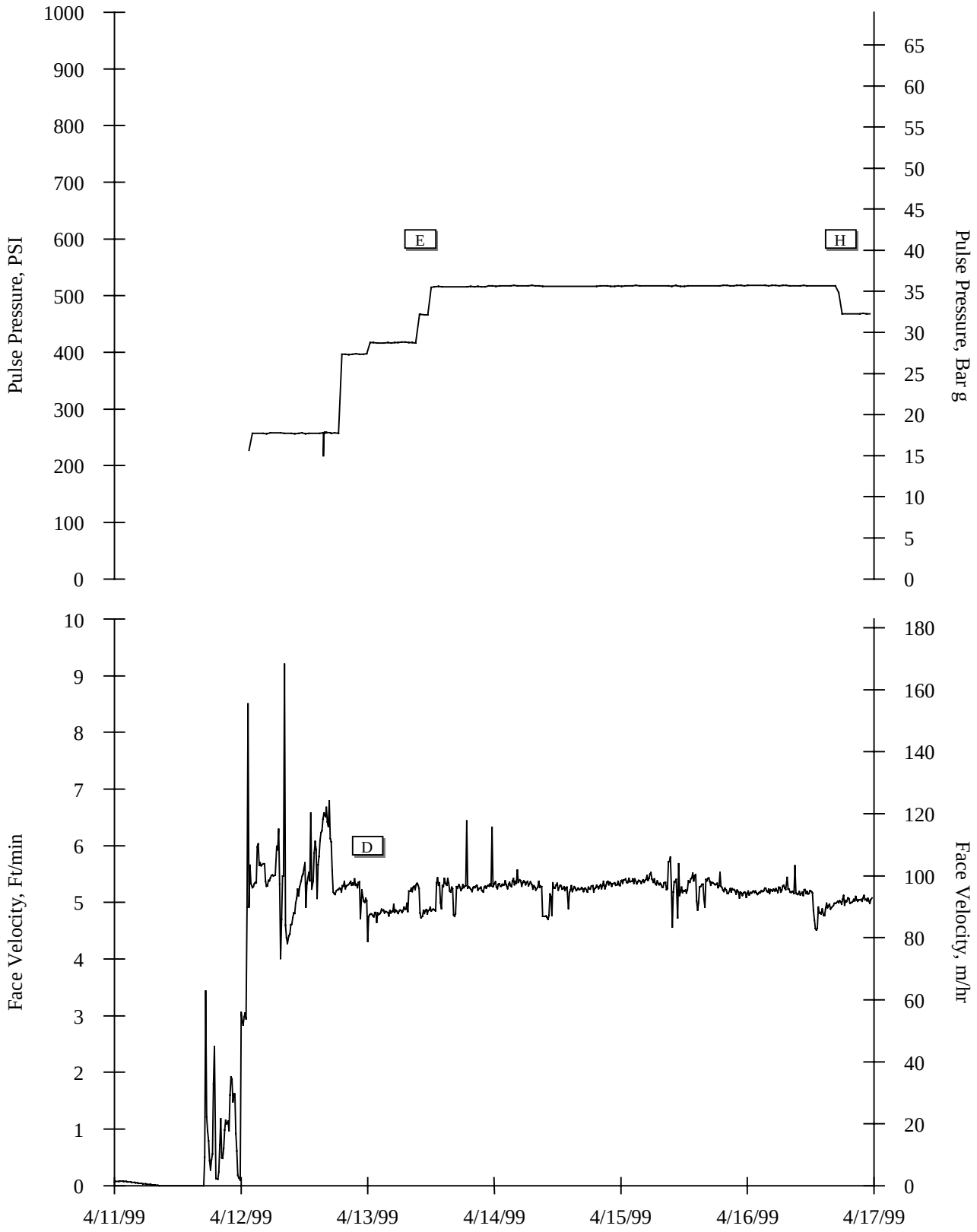

Figure 3.2-35 TC05 Back-Pulse Pressure and Face Velocity for April 11 Through April 17

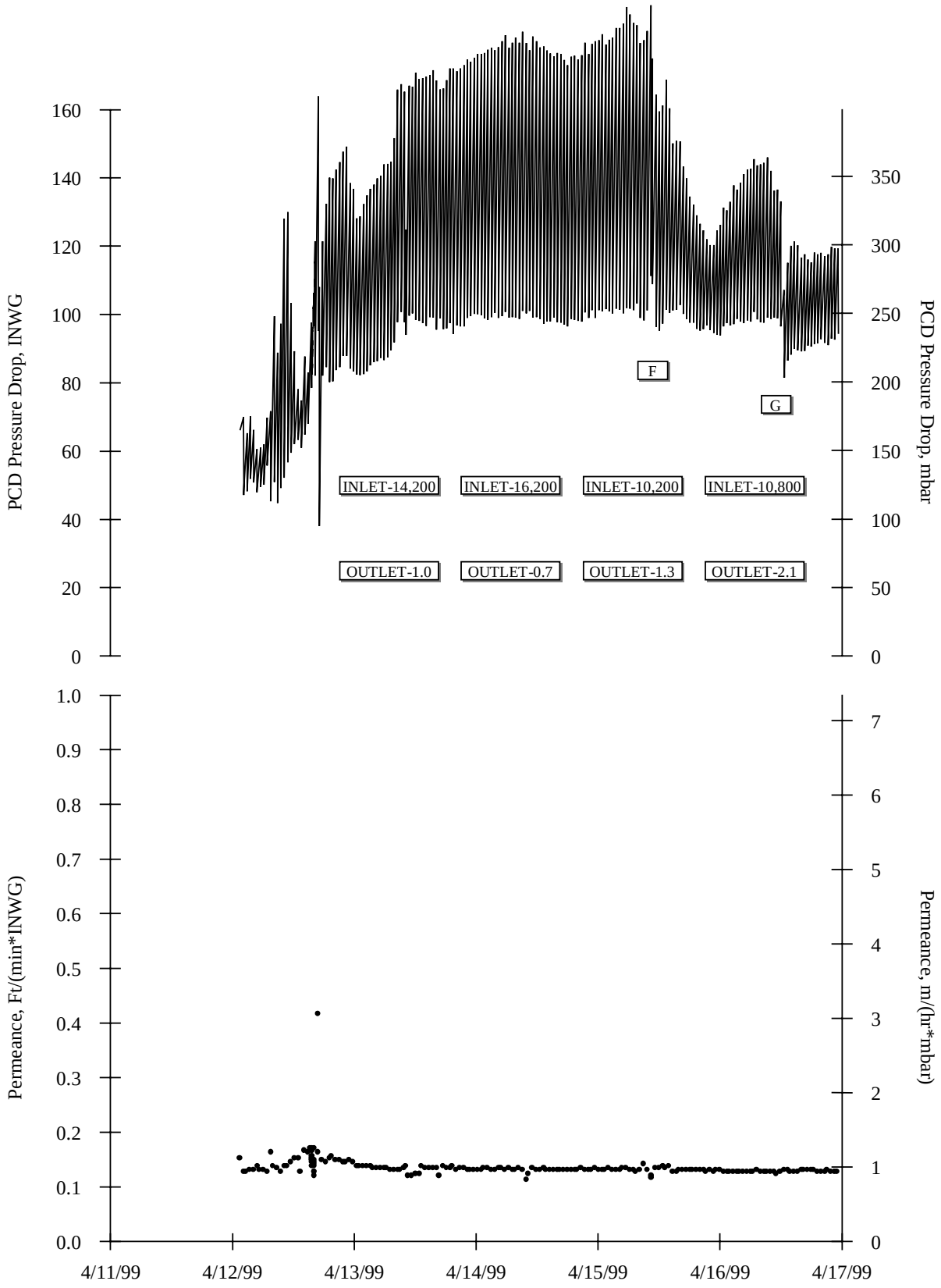

Figure 3.2-36 TC05 Pressure Drop and Permeance for April 11 Through April 17

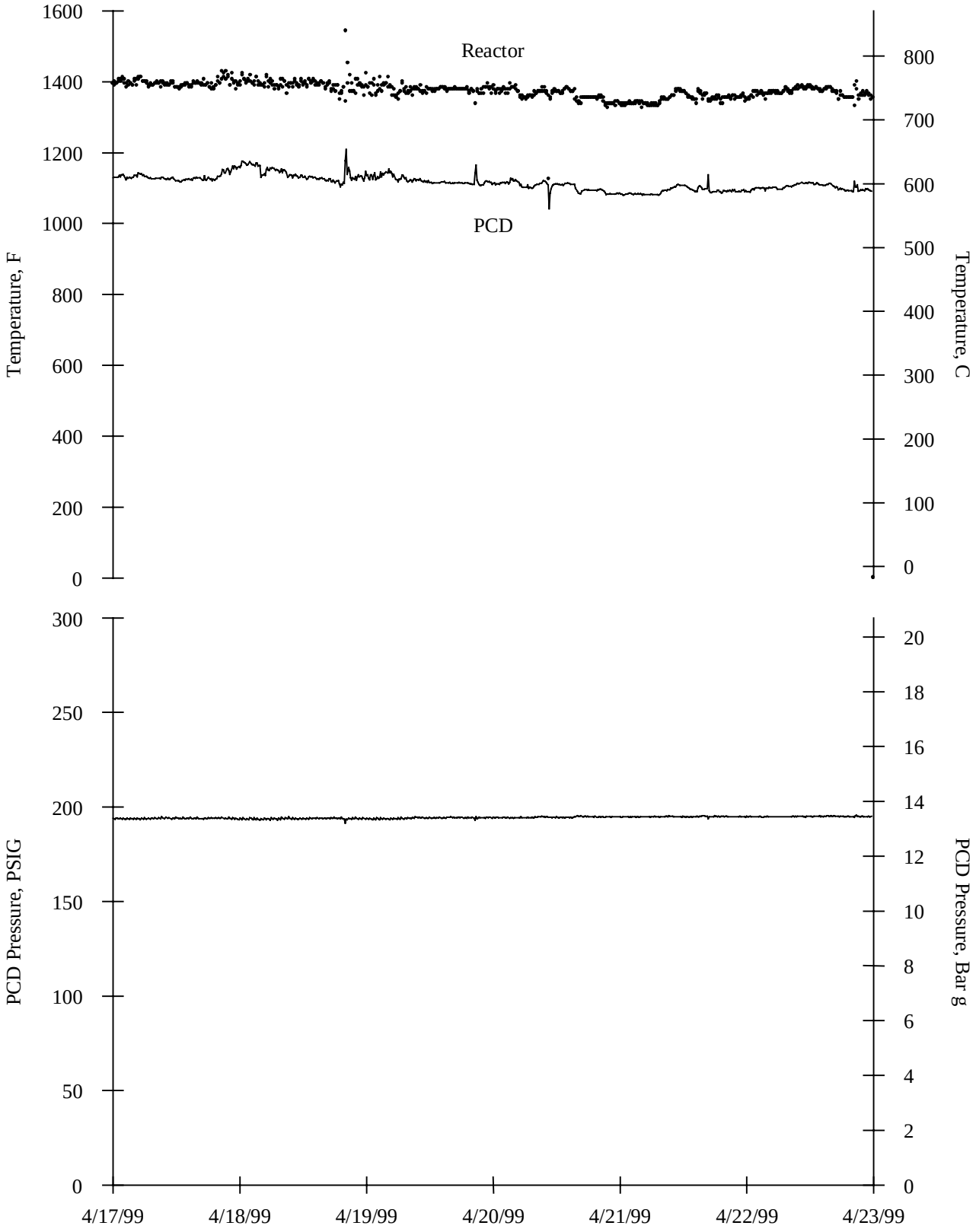

Figure 3.2-37 TC05 Temperature and Pressure for April 17 Through April 23

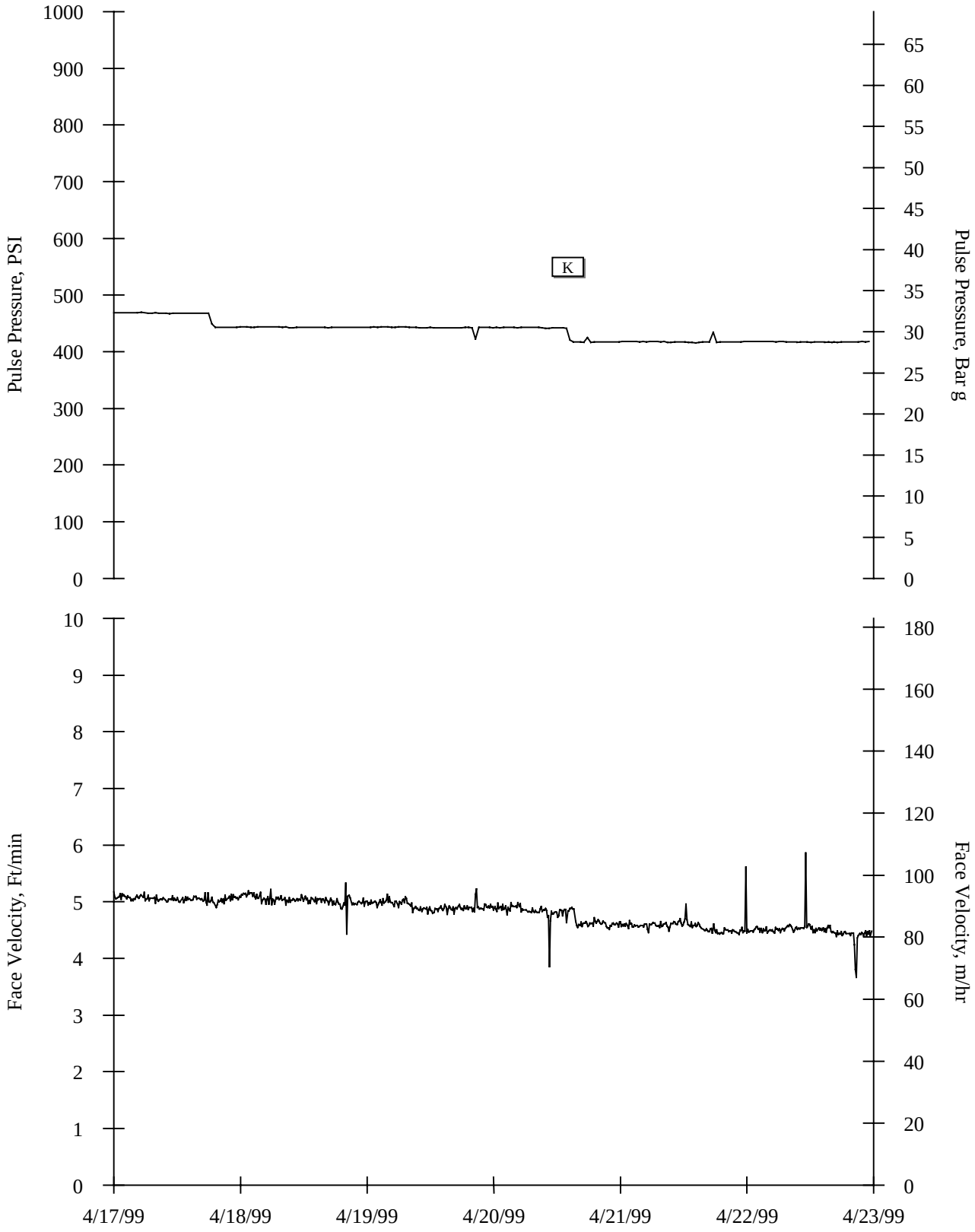

Figure 3.2-38 TC05 Back-Pulse Pressure and Face Velocity for April 17 Through April 23

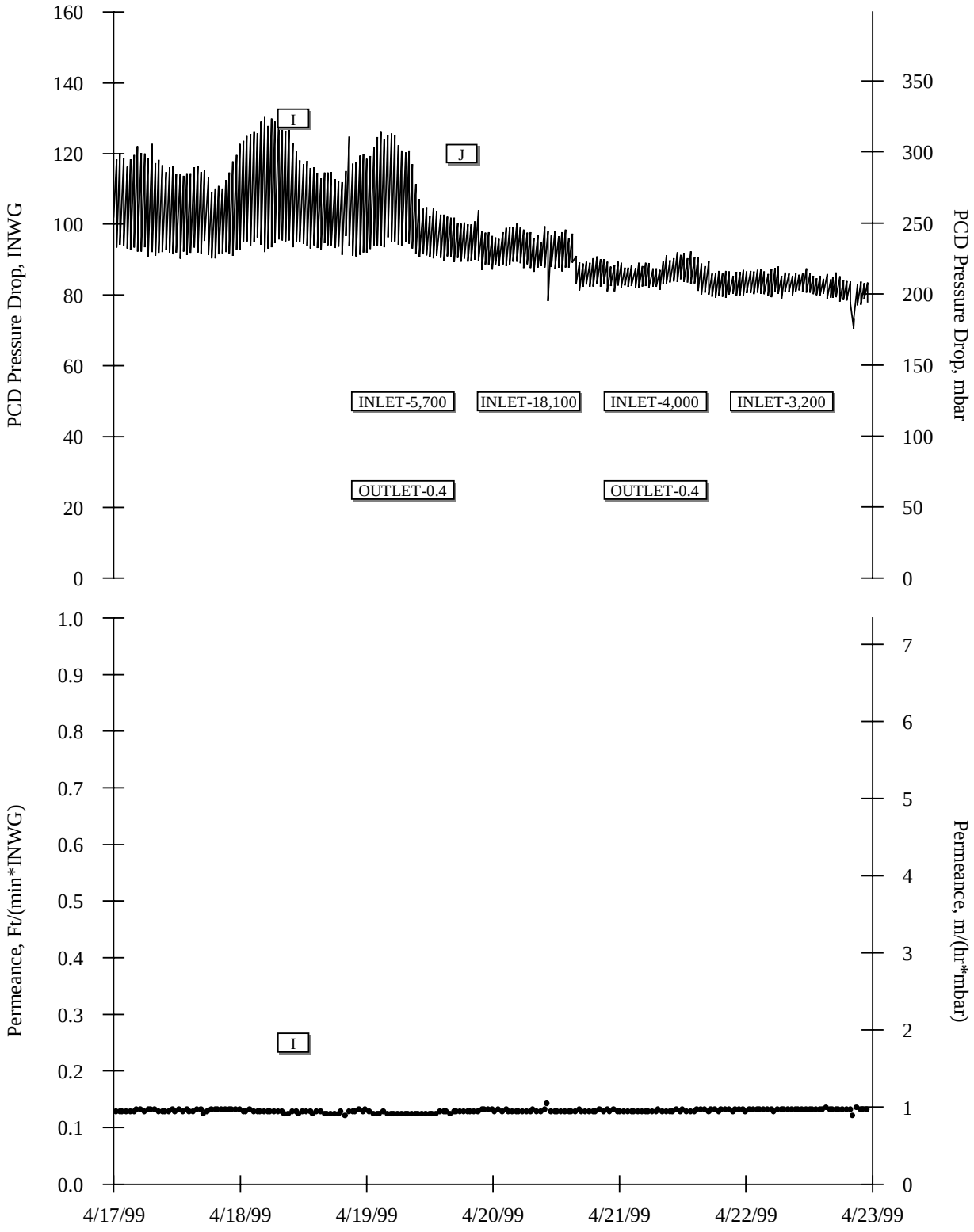

Figure 3.2-39 TC05 Pressure Drop and Permeance for April 17 Through April 23

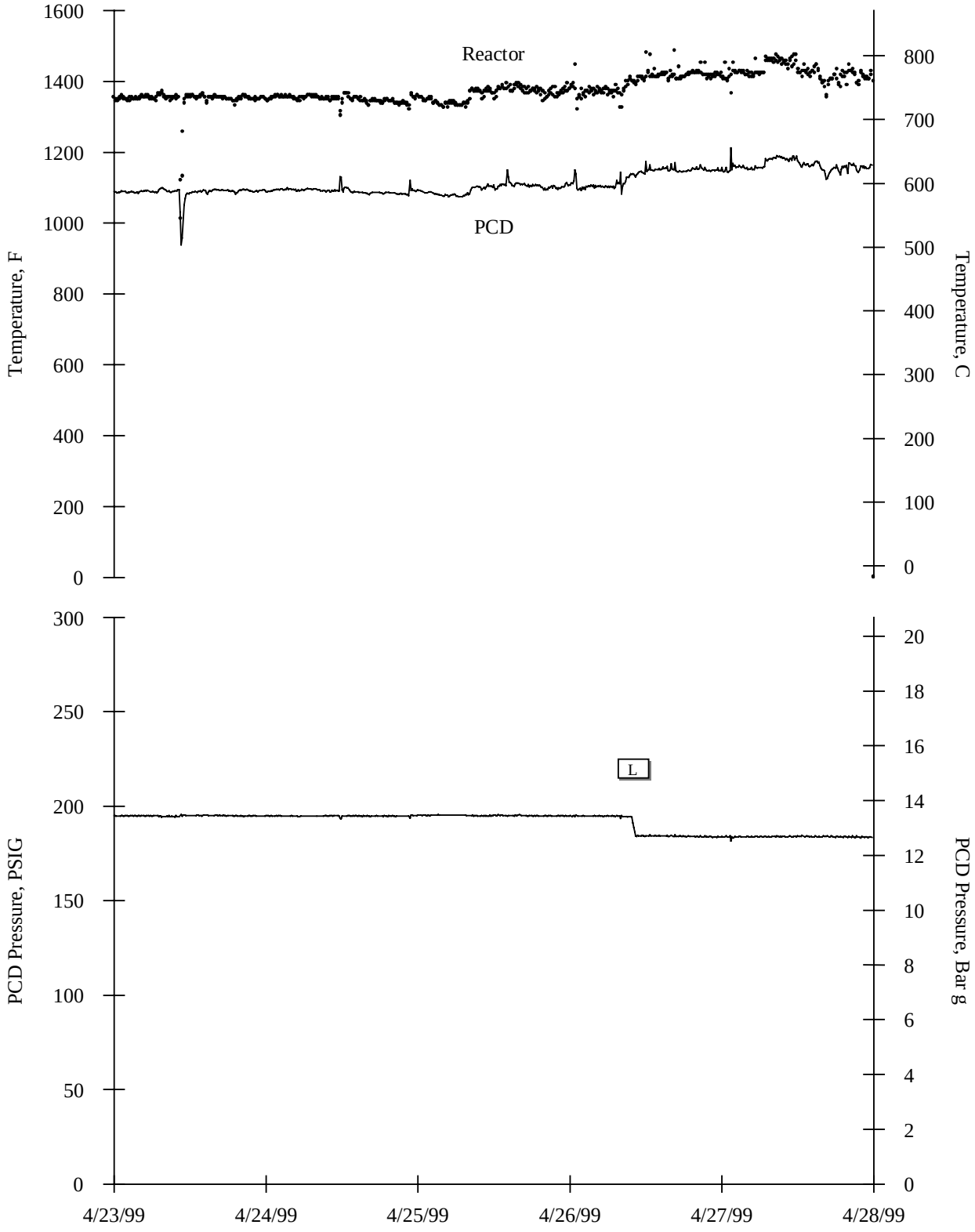

Figure 3.2-40 TC05 Temperature and Pressure for April 23 Through April 28

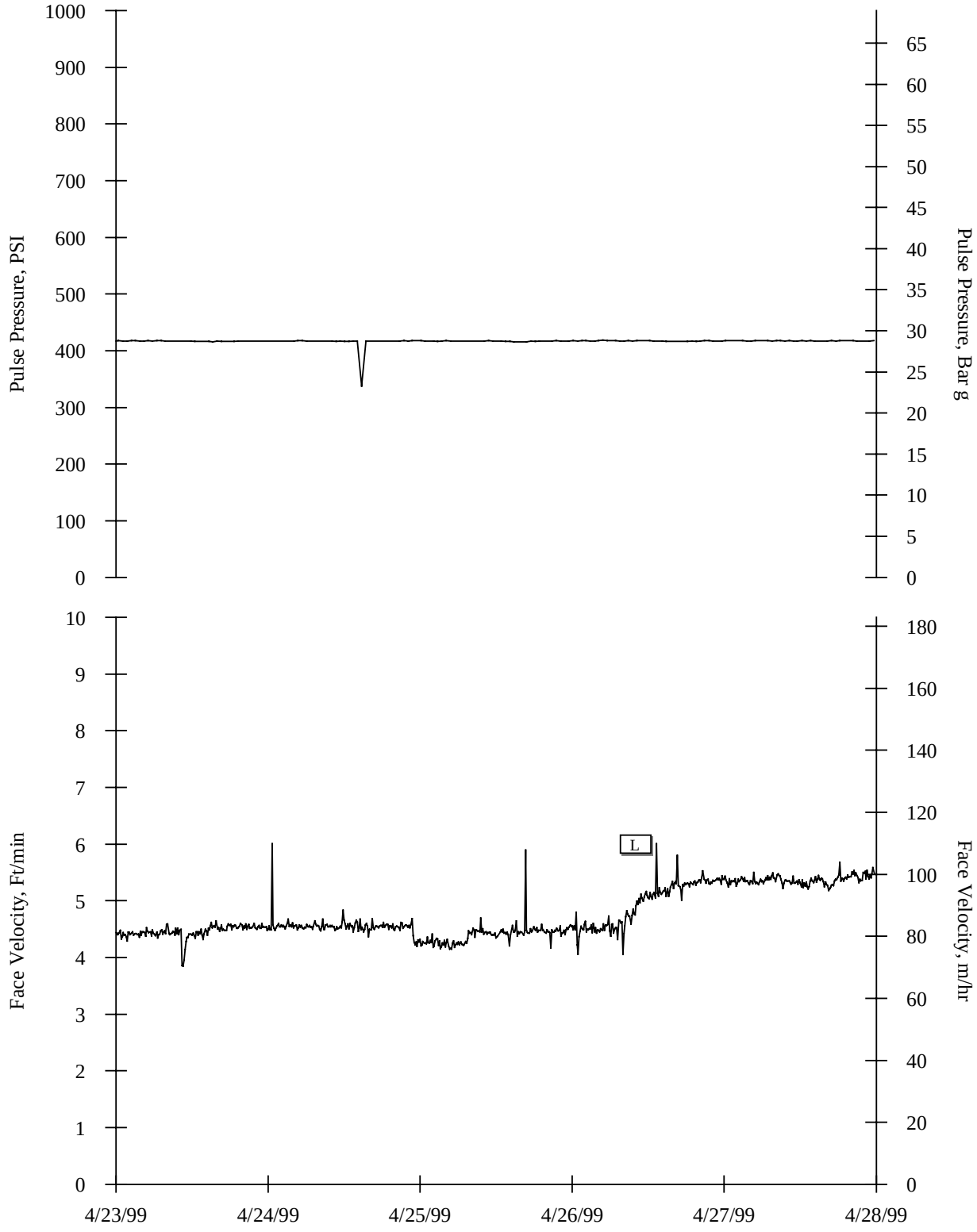

Figure 3.2-41 TC05 Back-Pulse Pressure and Face Velocity for April 23 Through April 28

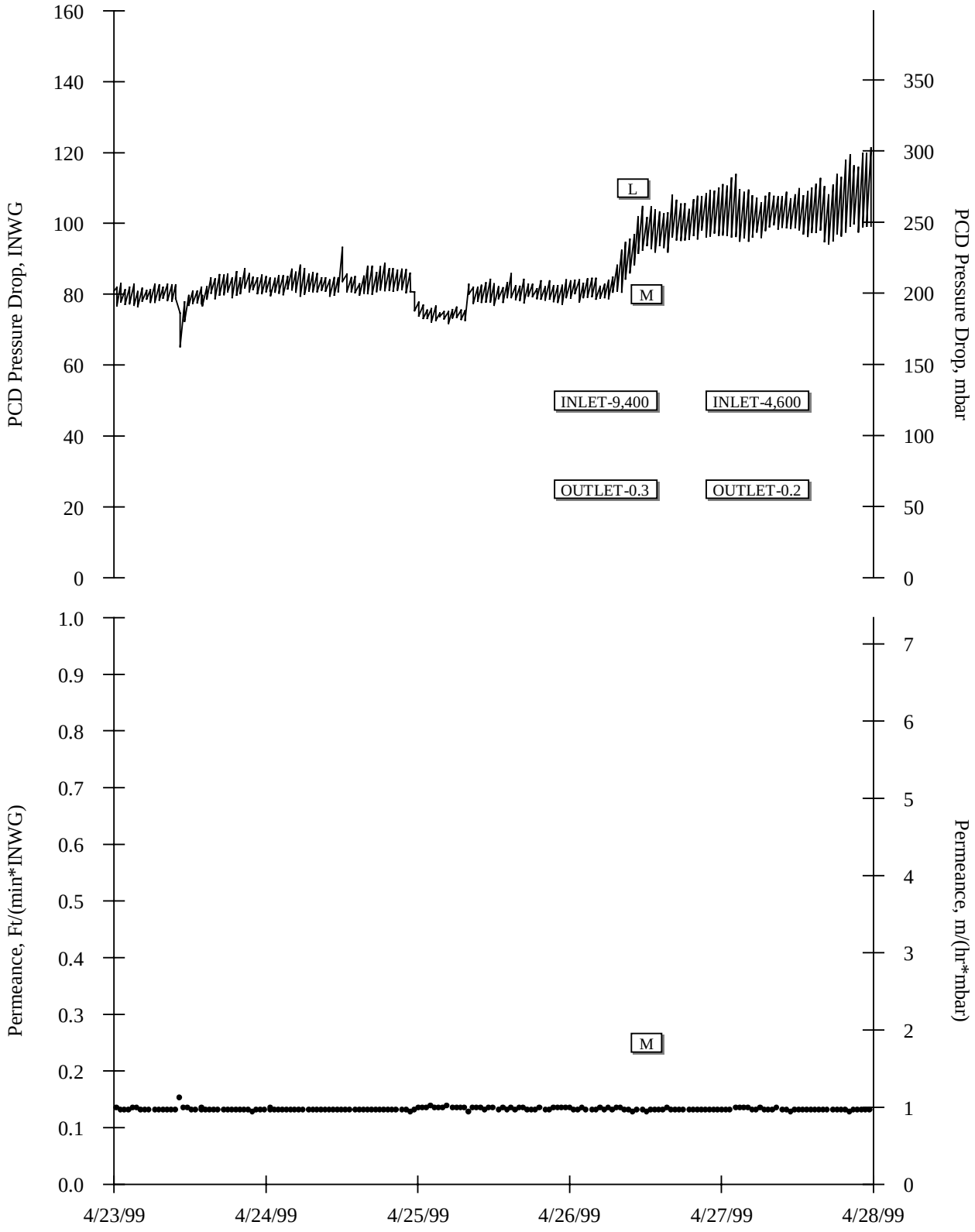

Figure 3.2-42 TC05 Pressure Drop and Permeance for April 23 Through April 28

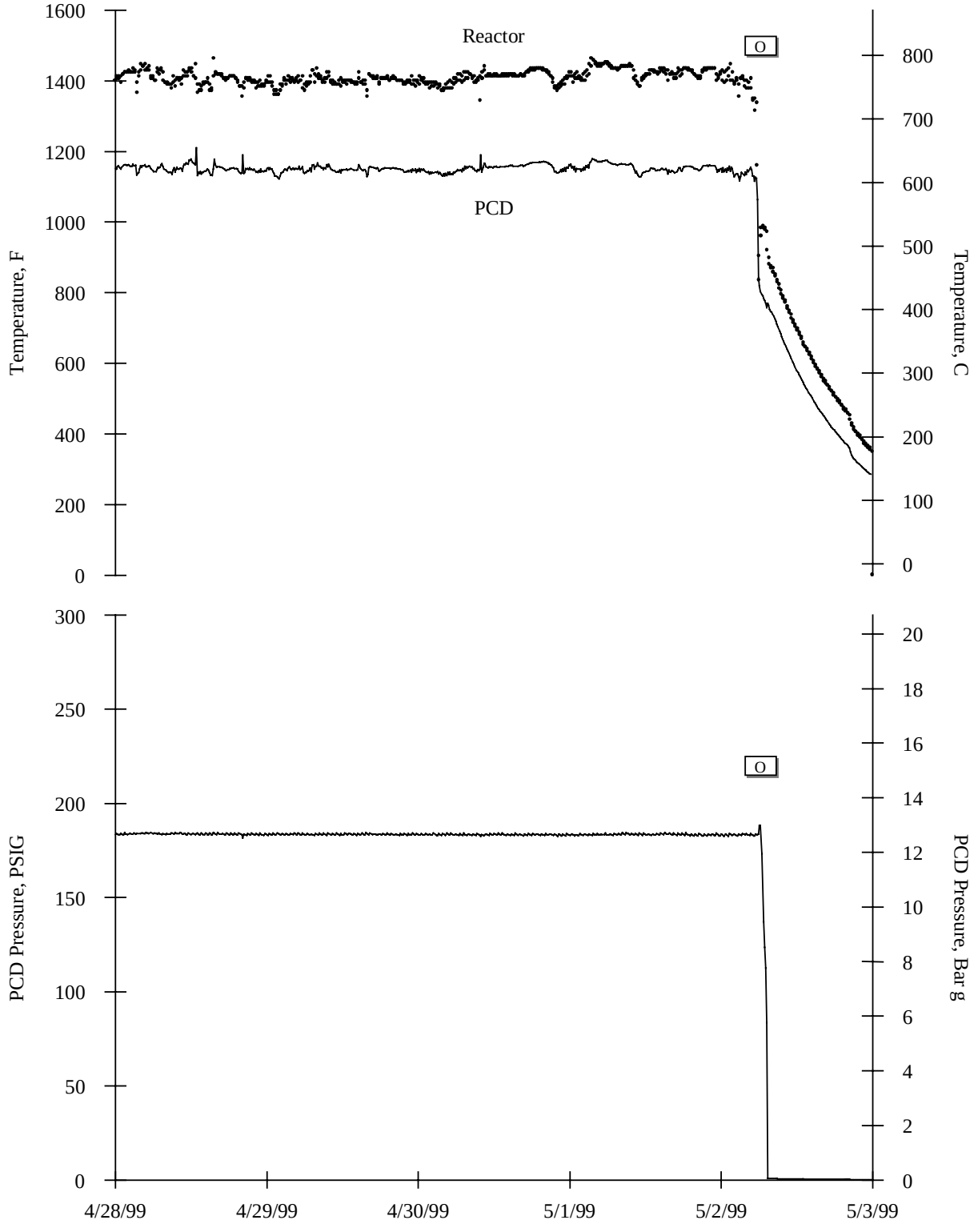

Figure 3.2-43 TC05 Temperature and Pressure for April 28 Through May 3

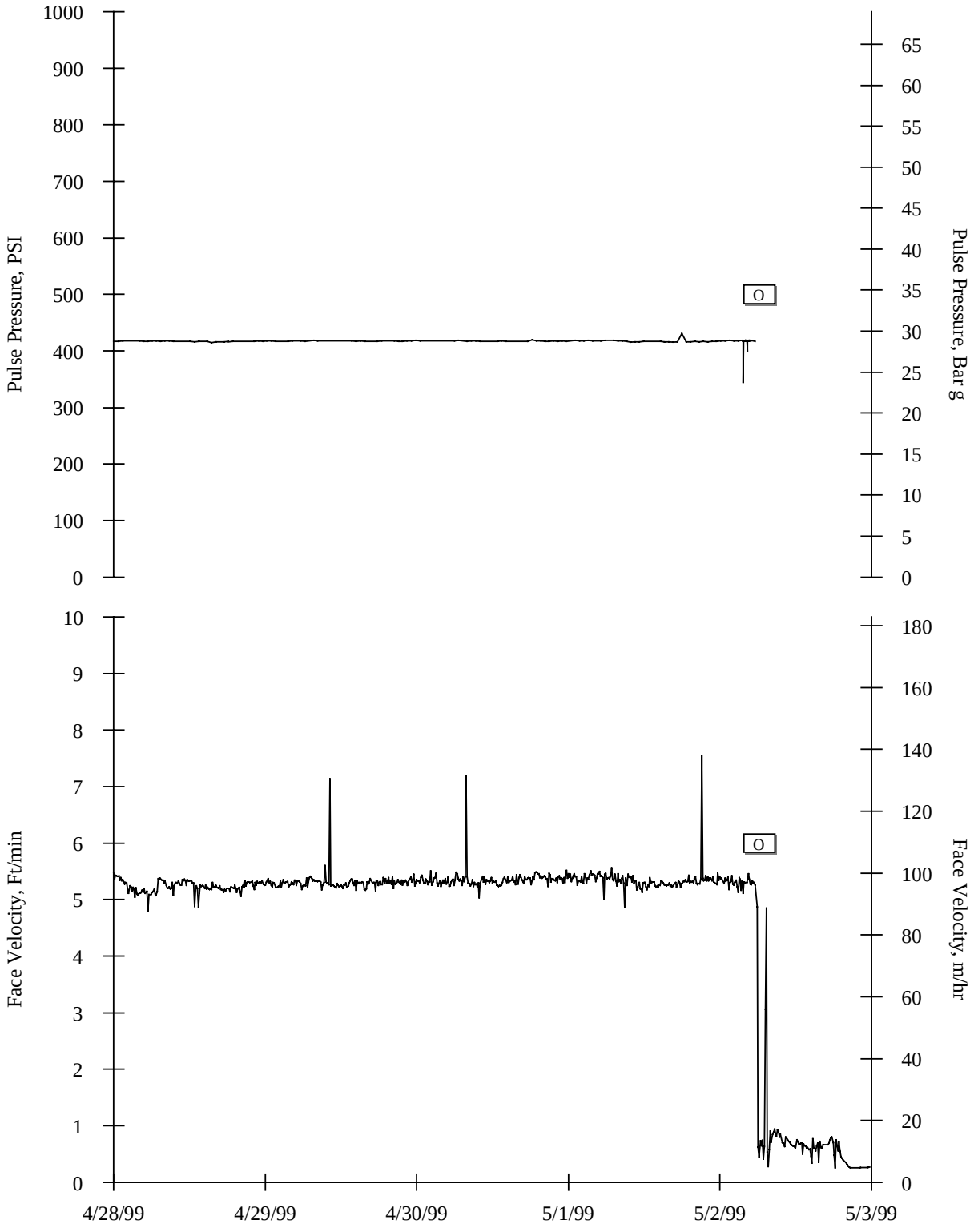

Figure 3.2-44 TC05 Back-Pulse Pressure and Face Velocity for April 28 Through May 3

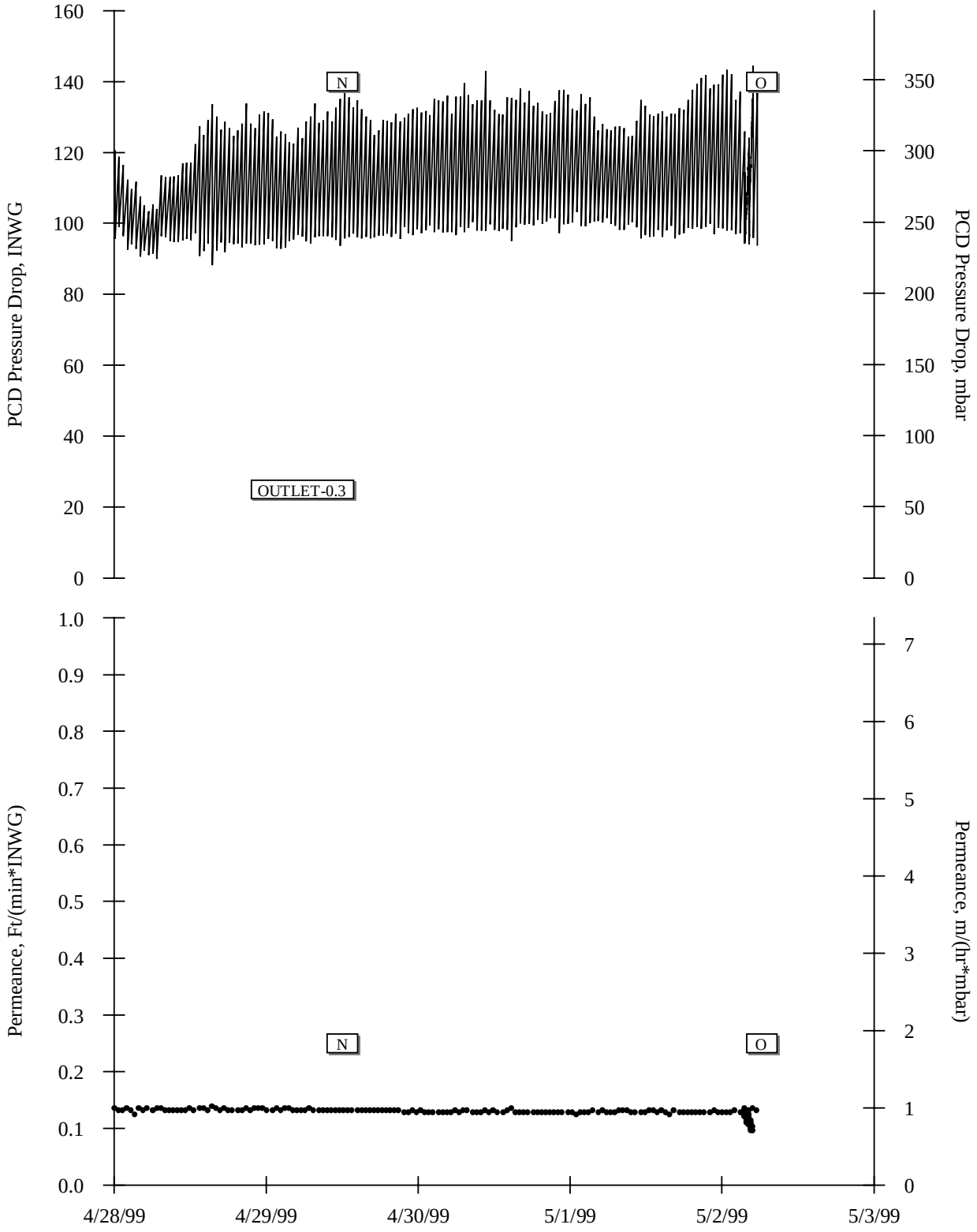

Figure 3.2-45 TC05 Pressure Drop and Permeance for April 28 Through May 3

3.3 TC05 PCD INSPECTION REPORT

3.3.1 Summary

During and after the entire TC05 test run the PCD was inspected five times. Each inspection corresponded to a system shutdown due to either a PCD or transport reactor related problem. The main reasons of the inspections are listed below and described in details in the following subsections:

- Inspection I - system shutdown due to a high-PCD-outlet loading.
- Inspection II - system shutdown due to a high-PCD-outlet loading caused by AlliedSignal PRD-66 filter element failures.
- Inspection III - system shutdown due to transport reactor J-leg upsets. Ash bridging in the PCD was found after the shutdown.
- Inspection IV – system shutdown due to circulation losses in the transport reactor.
- Inspection V – final inspection at the end of the TC05 test run.

In general, the inspections included examinations for integrity of the filter elements, their fixtures to the plenums, ash deposition, shroud and liner distortion, and back-pulse pipes.

After the final inspection minor repairs were performed for the liner. New filter elements were then installed for the gasification test run. Some components of the PCD and ash removal system were also modified to address the operation and safety issues related to the upcoming gasification run.

3.3.2 Inspection I

This inspection was performed in the week of January 25, 1999, after the system shutdown on January 24, 1999. High-PCD-outlet loading had been observed and it was increasing near the end of this run segment (from 10 to 22 ppmw). The PCD had been running at a high-face velocity (~8 ft/min) and, therefore, the filter pressure drop was higher. It was decided to shut down the system to identify the leak sources. The system was shut down in a dirty state, which means that there was no back-pulse cleaning after the shutdown. In this way, the ash cake on filter elements would be thicker so that the leak paths could be easily identified.

To facilitate the discussion a tubesheet map and the filter element layout (Layout 11) are shown in Figures 3.3-1 and -2. The letter T and B preceding the numbers denote the top and bottom plenums, respectively.

The PCD was opened on January 25, 1999. There were no broken filter elements. No ash bridging was found. The ash layer on the filter elements was thicker due to the dirty shutdown.

The holder flanges were covered by ash and the ash cake tended to merge together near the flanges as was usually seen in the previous dirty shutdowns.

Upon opening the PCD, multiple suspected leak paths were found near the flanges of several different types of filter elements. These filter elements were located at T1, T2, T3, T11, T13, T17, T18, T30, T31, B9, B10, B17, B37, B38, and B40. Among these filter elements B9, B10, and B17 are 2-meter long 3M oxide filter elements. The suspected leak paths exhibited holes and gaps on the ash cake showing potential gas flow through the gasket fixtures (see Figures 3.3-3 to -5).

The fifteen filter elements mentioned above were then removed for further inspection. It was found that there were at least four distinct leaks, i.e., T1, T17, B9, and B10. The worst one was B10, where the failsafe and the holder were covered by a thick layer of ash. On the outside of the failsafe there was a clear ash layer formed by leaking gas through the fiberfrax ring (the major seal).

During the inspection it was found that one McDermott filter element (T7) had a 3/16-in. hole at the bottom. Apparently the plug, part of the filter element structure, fell off from the bottom end and left the hole open. The failsafe above this filter element was partially covered by ash and the holder was clean. A flow test later confirmed that the failsafe was not completely plugged. Therefore, the hole must have contributed to the high-outlet ash loading.

An AlliedSignal PRD-66 filter element (T31) broke when it was reinstalled. The fracture was near the neck of the flange. There was no ash on the main section of the crack except for a thin fiber layer with tan color on the ID surface due to ash penetration.

It was found that the compression on the gaskets was quite different from one filter element to another. This can be evidenced from the different thickness of the gasket on top of the filter element flange. Some gaskets had a thickness almost twice that of the average thickness. Among other possible reasons, less compression might have negated the sealing effect, especially for the fiberfrax ring on the failsafe. It was speculated that the insufficient compression resulted in the leakage under the high-filter-pressure drop. The serial arrangement of the gaskets made it difficult to adjust the compression separately and securely. Possible damage of the weak fiberfrax ring during installation may also contribute to the leakage.

On the inside surface of many filter elements an ash layer was found. The ash may be entrained from the leak sources by back-pulse gas. Some of these filter elements were not immediately close to the leak sources.

In this test run two Conax fittings were installed to seal the thermocouples. The inspection revealed that the Conax fittings were not leaking. Two thermocouple wires were cut off by the corner of the pipe connection to the top plate inside the top plenum. These two thermocouple readings were lost during the run. The cut point on the wire looked like a sharp bending damage. The back-pulse induced vibration of the wires may have played a role on the damage. In the future the wires should be kept loose to prevent the wires from being cut off.

After the inspection the filter element layout was rearranged and new filter elements were installed. Before installing the new filter elements all filter holders were brush-cleaned to remove the ash build-up caused by the leaking. The new layout (Layout 12) is shown in Figure 3.3-6. Several considerations were taken into account.

1. All the blanks were removed and replaced with filter elements. These blanks were used in the previous run segment to increase the face velocity, which induced relatively high-filter-pressure drop. Since the reason for the leakage was not clear and still under investigation a decision was made to lower the face velocity to continue the test run. The four blanks that were used for sample posts and support post remained in the plenums.

2. All the McDermott filter elements were removed and replaced by other types of filter elements. The concern was raised by the falling plug on the McDermott filter element (T7).

3. All four 2-meter 3M oxide filter elements were removed and replaced by other 1.5-meter filter elements. It was speculated that the vibration of the long filter elements might have exacerbated the leakage.

4. The Conax fittings were removed and replaced with filter elements. All six thermocouples were removed since some of them were damaged during the operation.

In the new layout there were 87 filter elements. The face velocity was lowered to its nominal value, 4.5 to 6.0 ft/min.

The liner and shroud were also inspected. The shroud was relatively round and there was no apparent distortion. However, the bottom end moved toward the northwest side and its stiffening ring touched the liner. This displacement caused the gap between the shroud and liner to be wider on the other side. The gas flow might have been altered near the cone region. Visual inspection for the liner revealed that two buckles (one was at the inlet and the other was about 15 degree downstream of the gas inlet) had been growing and seemed to be touching the shroud. They may have exerted a force pushing the shroud toward the northwest side. Since the shroud is supported at the top the buckles forced the shroud to move until its bottom end touched the liner. If this trend continued the shroud would be distorted. Regarding the cone liner, it had moved up slightly but the gap between the cone liner (Section A) and the middle liner (Section B) was still sufficiently large (roughly 3.5 inches on one side). The moving liner sheared off one of the fluffing nozzles on the cone; however, the nozzle could have been sheared off prior to this test segment.

The back-pulse pipes were in good condition. There were no cracks except for scattered shallow corrosion spots. The spots were located near the flanges where the outer pipes support the back-pulse pipes.

During the reassembling of the instrument tubing one pressure tap tube on the tubesheet broke. A new connection was welded and the tubing was reinstalled.

In summary, multiple leak paths were identified in this inspection. The leakage was generic to different types of filter elements. High-face velocity, and thus high-filter-pressure drop, caused the ash leak through gasket fixtures resulting in a high-outlet-ash loading. Some possible reasons of the leakage through the gasket fixtures were insufficient compression, damage of the fiberfrax ring on failsafe, and vibration induced deterioration of the sealing effect. The structural failure of one McDermott filter element (hole at bottom) contributed to the high-ash loading. Further investigation is needed, although several speculations were proposed. In the new layout all blanks were replaced with filter elements to lower the face velocity. The PCD was reassembled on January 28, 1999.

3.3.3 Inspection II

This inspection was conducted after the system shutdown due to the failure of AlliedSignal PRD-66 filter elements. Before the shutdown the system had been running continuously for 6 days (February 16 to 22, 1999) with an outlet loading of 1.32 to 7.46 ppmw. On February 22 the ash removal system (FD0520) was plugged several times by broken PRD-66 filter elements. While maintenance was working on unplugging the system the PCD cone was partially filled with ash. The system was then shut down due to the concerns of the interrupted ash-removal-system operation and the PCD cone capacity.

After FD0520 was cleared up the system was restarted on February 24, 1999, to verify the failsafe performance with the broken filter elements. During the heat-up period dolomite was fed into the system and an outlet ash sample was taken. The sampling showed that the PCD-outlet-loading was 400 ppmw. The system was then shut down for the PCD inspection.

The PCD was opened on February 25, 1999. Three AlliedSignal PRD-66 filter elements were found broken when the PCD was opened (see Figure 3.3-7). The failed filter elements were located at B49, B54, and B55. B49 and B55 broke at the lower edge of the filter nut and B54 broke at 1 to 2 in. below that edge (see Figures 3.3-8 and -9). B49 and B54 were installed at the beginning of TC05 and B55 was installed on January 29, 1999.

All 16 AlliedSignal PRD-66 filter elements, including the failed ones, were removed for further inspection and testing. Since most PRD-66 filter elements were located near the center of the bottom plenum other types of filter elements at the outside had to be temporarily removed to access the PRD-66 filter elements.

During the removal one PRD-66 filter element (T4) broke with almost zero force acting on it. It broke at the same point as B49 and B55.

The top donut gasket on B55 was missing when the remaining part of the filter element was removed. Clear ash trace was found on the top surface of the filter flange and failsafe flange. However, the failsafe and the filter holder were relatively clean compared with adjacent ones. Flow test on the three failsafes (B49, B54, and B55) revealed that B55 was the least plugged (failsafe B55 was also a shorter one from Karhula). It is unclear at this point whether the gasket was not installed originally or it fell off after the filter element failure.

This time the system was shut down in a clean state, which means the filter was back-pulse cleaned after the shutdown. The filter element surfaces were relatively clean. However, numerous small ash lumps were scattered on the filter element surfaces (see Figure 3.3-10). The filter elements on top plenum had more numerous and larger lumps. The lumps were harder than the ash usually seen and were not easily removed by hand. It is speculated that these lumps were not removed by back-pulsing during the operation and, therefore, the actual filtration surface was less than the nominal value. The true face velocity was higher than the calculated value so the filter DP baseline was higher during the operation.

Slight ash bridging was found between filter elements near the flanges (see Figure 3.3-11). The ash build-up was harder. No apparent filter element failure resulted from this slight ash bridging. The ash was later cleared by blowing air through the filter element arrays.

Ash bridging was also found between the shroud and liner (see Figure 3.3-12). The shroud was heavily covered with a thick ash layer (~1 inch) (see Figure 3.3-13). The PCD cone liner was also covered with a thick ash layer. The bridging ash and the ash layer were cleared later.

During the examination of the removed AlliedSignal PRD-66 filter elements several spalling spots were found on the OD surfaces (membrane) of three filter elements. The spots were located 10 ½ to 16 inches below the flange. They might be caused by the operation of pneumatic wrenches during the installation and removal.

Before the PCD internal was put back into the vessel the PCD cone liner was inspected. No visible changes were found except that several pieces of fiberfrax were sheared out at the lower manway.

The back-pulse pipes were visually inspected. The OD surfaces had been continuously corroded (~1x1 inch^2 spots) since the last inspection. There were no cracks found on the surfaces. The corroded areas were located about .05 to 1.0 ft from the flange. The spots were covered by rust, which was contacting both the OD surface of the back-pulse pipe and the ID surface of the outside pipe (support pipe) during the operation.

After the inspection new Schumacher, Pall, and Techniweave filter elements were installed to replace the removed AlliedSignal PRD-66 filter elements. The new layout (Layout 13) is shown in Figure 3.3-14. The PCD was reassembled on February 26, 1999.

3.3.4 Inspection III

This inspection followed the finding of the ash bridging between filter elements after a shutdown. The direct reason for the system shutdown on March 6, 1999, resulted from a need to inspect the transport reactor after several J-leg upsets. The transport reactor had been running for about 50 hours, with 32 hours on petroleum coke and dolomite before the shutdown. The system was restarted on March 8, 1999, after the reactor inspection. However, the system start-up could not proceed due to a start-up burner problem.

During that start-up period the exit line of the ash removal system (FD0520) kept plugging. Several objects were found from the exit line, including small pieces of the AlliedSignal PRD-66 filter elements (remaining in the system since the last shutdown), small pieces of refractory, and many hard ash chunks. Due to the concerns about the hard ash the lower manway was opened to inspect the PCD. It was found from the manway inspection, that the filter elements in the bottom plenum were bridged by ash. Therefore, a decision was made to open the PCD for further inspection. The PCD was opened and the plenum was pulled to the maintenance bay on March 9, 1999.

The inspection revealed that both the top and bottom plenums had ash bridging. A sketch of the bridging locations is shown in Figure 3.3-15. In general, the ash lumps were located at the upper portion of the filter elements (see Figure 3.3-16). The ash cake was loosely trapped between the filter elements at the time of the inspection. The hard ash layers, once grown from the surfaces of the filter elements, contacted each other with a loose ash layer sandwiched in between. The hard layers were also separated from the surfaces of the filter elements (see Figure 3.3-17). On the part not covered by the bridging ash lumps the filter element surfaces were clean except that numerous small ash lumps were scattered, as shown in Figure 3.3-18. These small ash lumps looked similar to the ones observed in the last shutdown.

On the plenum surfaces (filter holder flanges and bolts and nuts) there were many "fluff-like" ash build-ups. These build-ups indicated that the ash layer may also grow from these surfaces and contribute to the ash bridging.

The overall ash bridging is speculated to be driven by the chemical reaction and physical process (refer to Section 3.4 Ash Report for details). However, from a mechanical point of view the ash bridging located near the top portion of the filter elements may be due to at least three reasons. First of all, the ash lumps near the plenum had more places to bind, i.e., plenum, filter holder fixture, and filter element surfaces. These binding surfaces held the ash lumps more firmly than other locations. Second, there was a dead space between the filter holder flanges. The back-pulse gas could not reach there, directly resulting in a weak blowout to the ash build-up. Third, the filter element vibration during a back-pulse had the smallest effect on crushing and shaking down the ash build-up at the top portion of the filter element. As the filter elements were fixed at the flange and kept free at the bottom end, the maximum lateral displacement of the filter element during the vibration would occur at the bottom end. The top end was almost stationary. If any ash bridging formed near the bottom portion it would have been removed earlier than that in the top portion.

The ash coverage on the vessel was also inspected. Heavy ash build-up on the shroud had been observed (see Figure 3.3-19). Ash bridging was found between the liner and the shroud.

The inspection confirmed that there were no filter element failures and therefore, a removal and reinstallation was not necessary. After the inspection and ash sampling the filter elements, plenum, liner, and shroud were thoroughly cleaned to remove the ash build-up. The total ash amount removed from these locations occupied almost half of the PCD cone. The ash was then removed from the PCD before the start-up. The PCD was reassembled on March 11, 1999.

The primary gas cooler was put in service upstream of the PCD to lower the inlet temperature while the causes of the ash bridging would be investigated.

The back-pulse pipes were inspected and they were in a good condition. A piece of fiberfrax slid down from behind the liner near the lower manway. It was cut off and removed.

In summary, ash bridging was found in the PCD. No filter elements were damaged due to the bridging. The ash build-up was hard but kept loose from the binding surfaces when inspected. It should be noted that the observations made in this inspection reflected only about 32 hours of operation on petroleum coke and dolomite. A longer operation might have had a quite different result. The worst case would have been filter element failures due to the ash bridging if the hard ash build-up had been allowed to grow without being effectively cleaned. Unfortunately, no indications of the ash bridging were shown in the plant information (PI) system, making it difficult to monitor the situation. The only indication was the hard ash pieces discharged from the ash removal system. It was not until the restart of the system that the hard ash pieces were found.

3.3.5 Inspection IV

This was a brief inspection conducted after a system shutdown. The transport reactor had experienced circulation losses before being shutdown on March 27, 1999. Although there was no indication of filter element failure the PCD was inspected due to a concern of the ash build-up. During this run segment the reactor still ran on petroleum coke and dolomite but the PCD temperature was ~700˚F. In the previous run segment ash bridging occurred with the same fuel and sorbent at ~1,400˚F PCD temperature. The objective of this inspection was to check if the ash bridging formed in the PCD at this low temperature.

The PCD lower manway was opened on March 29, 1999. The filter elements on the bottom plenum were inspected. There was no ash bridging. The ash was dry and easy to flow. The filter elements were clean (see Figure 3.3-20). No heavy ash deposit was found on the shroud, liner, and PCD cone (see Figure 3.3-21).

The top plenum was inspected when the tubesheet gasket was replaced on April 10, 1999. The PCD internal was lifted about 2 feet. The filter elements, shroud, and liner were inspected through that opening and appeared to be clean (see Figure 3.3-22). A pile of loose ash was found on the top of the top plenum (see Figure 3.3-23).

No filter element failures were found in this inspection. The PCD was returned to service without removal and installation. The bypass pipe was installed to the primary gas cooler upstream of the PCD to bring the PCD temperature up to 1,100˚F.

3.3.6 Inspection V

This was the post inspection following the TC05 test run. The system was shut down in a dirty state on May 2, 1999. The transport reactor had run with the Powder River Basin coal and limestone and then switched to the East Kentucky coal before the shutdown.

The PCD was opened and placed in the maintenance bay for inspection on May 5, 1999. No filter element breakage was found. All the filter elements were removed from the plenums to have the plenums ready for the installation for the gasification run. One Schumacher SiC filter element broke during the removal. Upon further inspection a small hole was found on a 3M oxide filter element, as shown in Figure 3.3-24. The hole was located at 10.3 inches from top of the flange. It was not clear at the time what caused this damage. More investigation is needed to analyze the damage.

The ash cake on filter elements was about 0.25 to 0.50-in. thick. The appearance of the ash cake was smooth (see Figure 3.3-25). A pile of loose ash was found on top of the top plenum. Ash deposit was also found on the support column (see Figure 3.3-26).

After all the filter elements were removed the inspection was focused on the shroud and liner. Visual inspection revealed that the shroud was pushed toward the northwest side at the bottom by two big buckles on the liner. One buckle was located near the gas inlet and one at the bottom. The bottom end of the shroud contacted the liner so that the shroud was slightly deformed. The shroud was pulled out of the PCD on May 10, 1999. During the pulling the shroud was caught at several places by the deformed liner. One pin at the shroud support bracket was found broken, probably due to the movement of the shroud caused by the distortion of the liner. This brought the total damaged pins to two. The other one had broken before TC05.

The PSDF engineers and a Siemens Westinghouse representative then inspected the liner. Compared to the inspection results in October 1998 several key points should be noted as follows.

1. The cracks at the gas inlet grew bigger (see Figure 3.3-27).

2. The buckle near the gas inlet grew bigger (see Figure 3.3-28).

3. The bottom portion of the middle liner (Section B) further deformed and three buckles were formed starting from the three openings for the thermocouples (see Figure 3.3-29).

All four supports on the top liner (Section C) were still in good condition. The cone liner (Section A) did not grow further. The gap between Sections A and B was at least 3.5 inches. The patched plates for the cone liner supports were still in place. These plates were installed before TC04 to patch the holes left after the supports were sheared by the cone liner.

Based on the inspection results a decision was made not to conduct major repairs for the liner at this time. Minor fix-ups, however, were performed to maintain the operability of the PCD. The repairs included the following items. (1) The biggest buckle located at the bottom of middle liner was cut and patched so that the shroud could be reinstalled without interference with the liner. (2) The cracks at the gas inlet were patched to prevent further growing. (3) The opening on the liner for a thermocouple near the gas inlet was patched to stop any gas flow behind the

liner where a buckle was located leaving a big gap between the liner and refractory. (4) All four supports on the middle liner were welded back in place. These support plates were previously sheared off. This would release some load on the gas inlet and prevent the cracks from growing. (5) Two new pins were installed on the supports for the shroud.

A dye-penetration inspection was made for the major welds on the tubesheet and cluster. The tubesheet cover and insulation were removed from the tubesheet before the inspection. The welds inspected on the tubesheet included the inner cone-to-inner cone radial welds, inner cone-to-inner disk circumferential weld, and outer cone-to-outer cone radial welds. The one linear indication noted in February 1998 did not extend. No other relevant indications were shown. On the cluster, four welds joining the support ring and the top plenum and the support ring and the support column were also dye penetration inspected. No relative indications were found.

A plenum pressure test was conducted on August 2, 1999. The filter holders and the Venturi devices were plugged with rubber plugs and the top and bottom plenums were pressurized with air separately. The pressure was varied between 10 and 20 psig. At 10 psig both plenums held the pressure for at least 45 minutes without significant leakage (pressure dropped less than 0.9 psig).

In summary, the PCD was inspected at the end of TC05 test run. No filter element failed during the last run segment. The major PCD components were inspected and minor repairs were conducted. The PCD was ready for the first gasification test run. Detailed preparation for the gasification run and installation of the filter elements will be described in a later report.

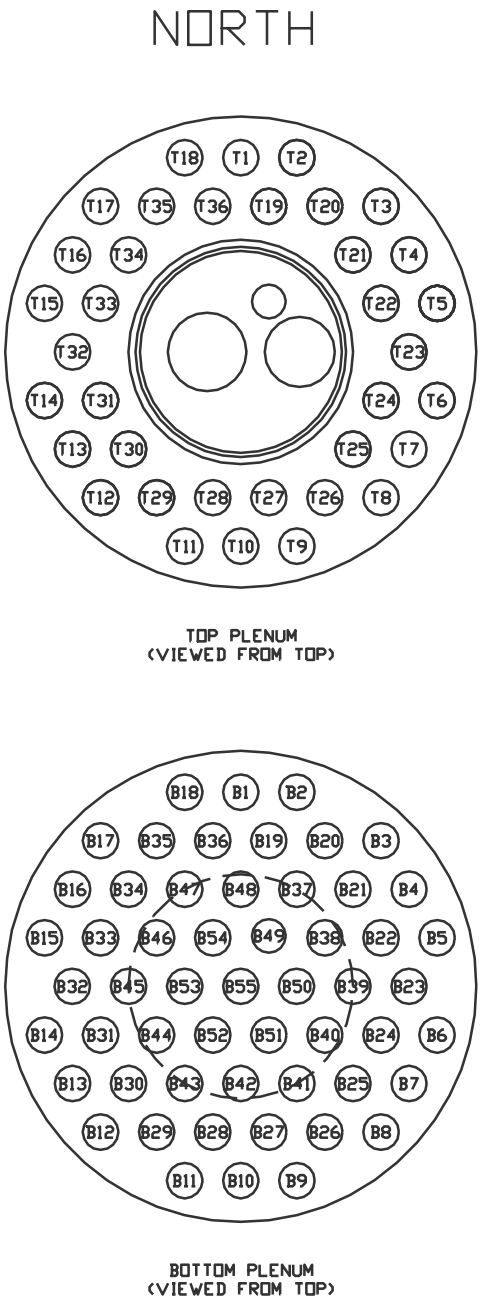

Figure 3.3-1 Tubesheet Map

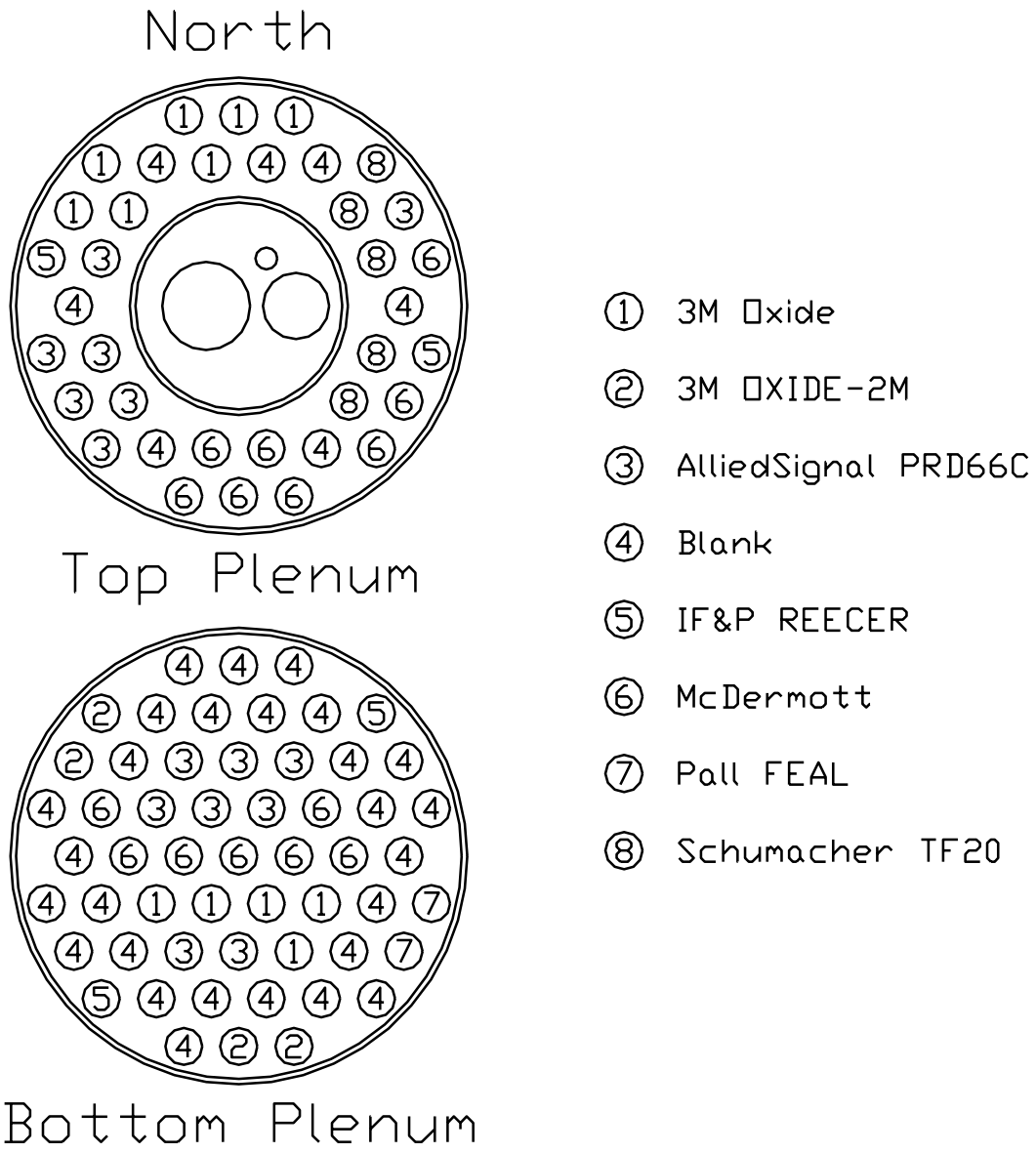

Figure 3.3-2 Filter Element Layout 11

Figure 3.3-3 Leak Through a Hole on the Ash Cake

Figure 3.3-4 Leak Through a Gap on the Ash Cake

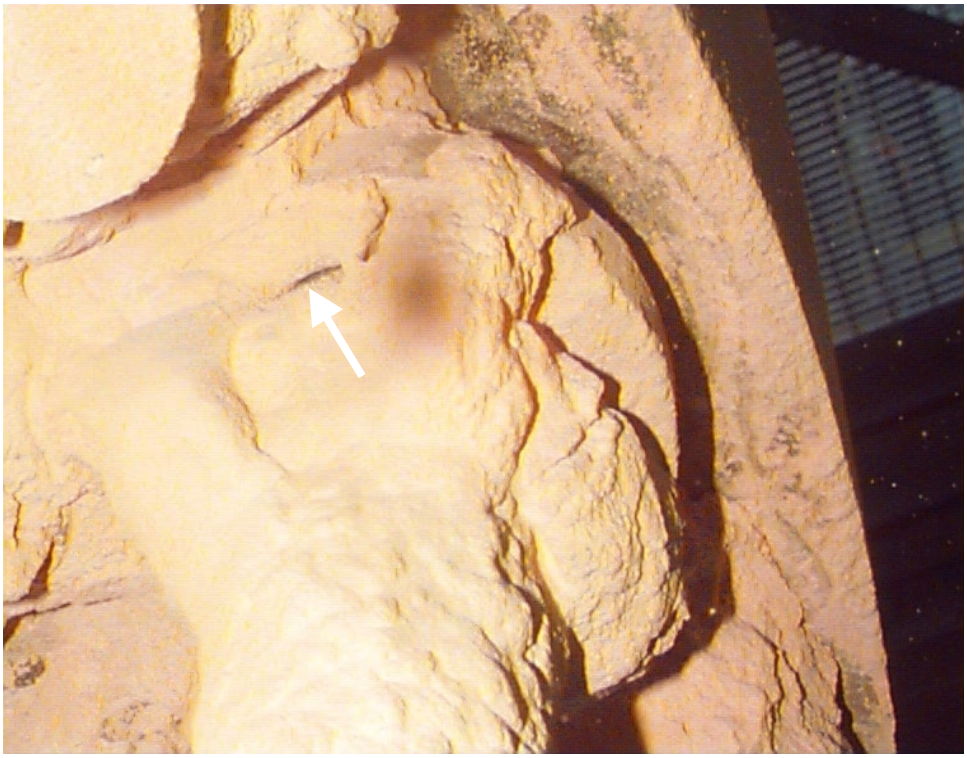

Figure 3.3-5 Leak Through a Gap on the Ash Cake

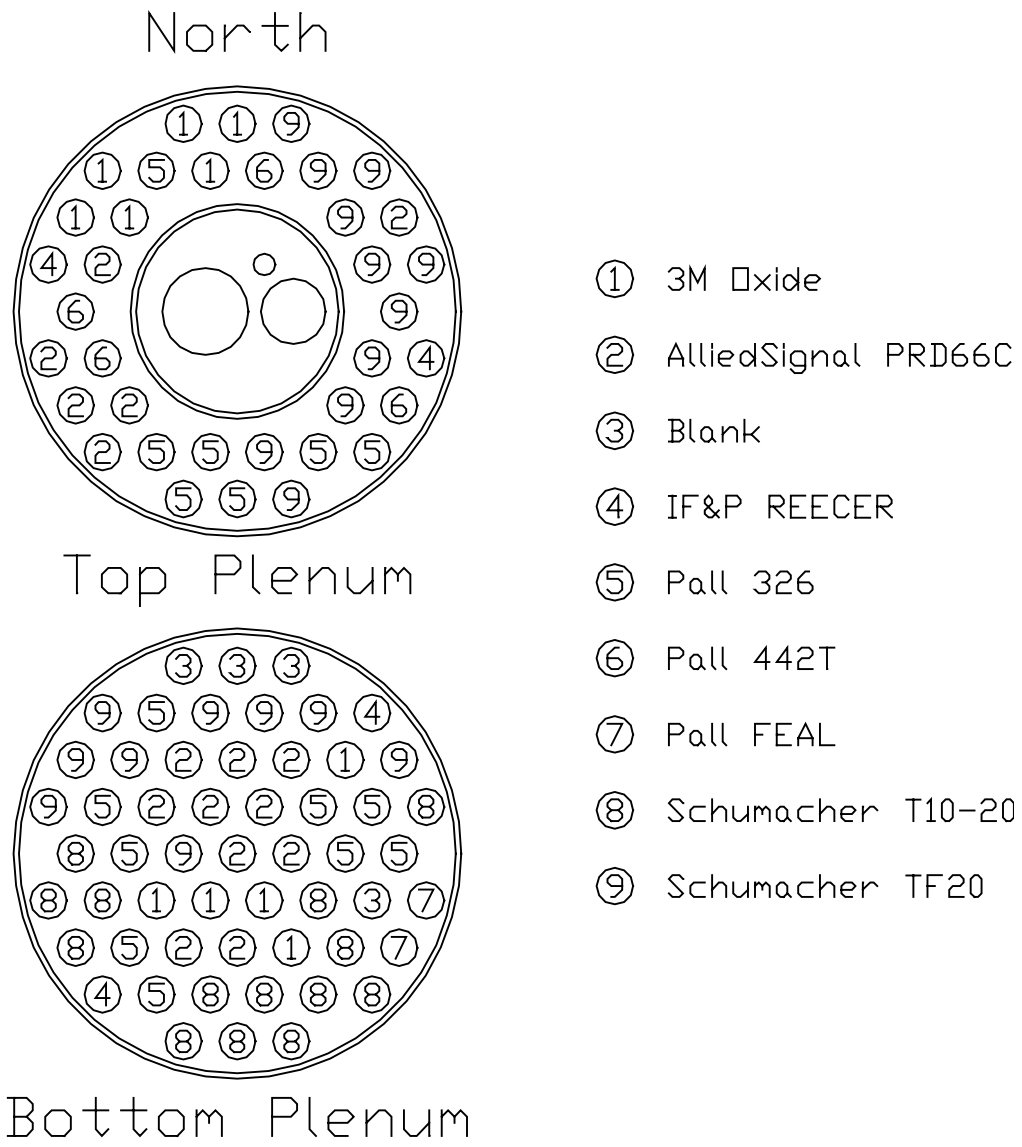

Figure 3.3-6 Filter Element Layout 12

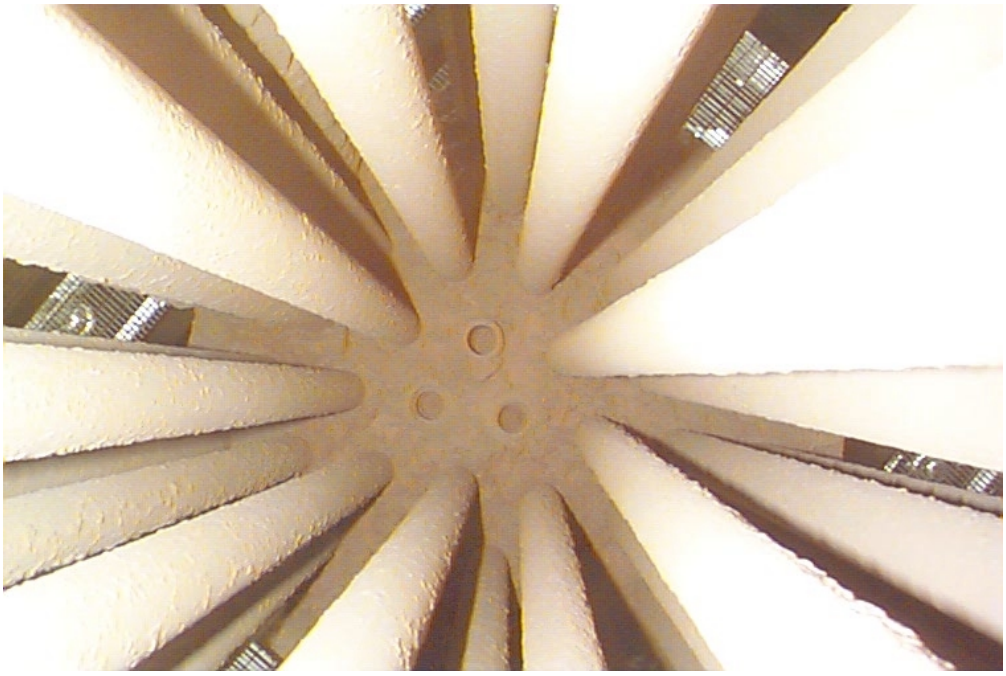

Figure 3.3-7 Location of the Three Broken AlliedSignal PRD-66 Filter Elements

Figure 3.3-8 Broken AlliedSignal PRD-66 Filter Element at B49

Figure 3.3-9 Broken AlliedSignal PRD-66 Filter Element at B54

Figure 3.3-10 Small Ash Lumps on Filter Element Surfaces

Figure 3.3-11 Slight Ash Briding Near the Flanges

Figure 3.3-12 Ash Bridging Between the Shroud and Liner

Figure 3.3-13 Heavy Coverage of Ash on the Shroud

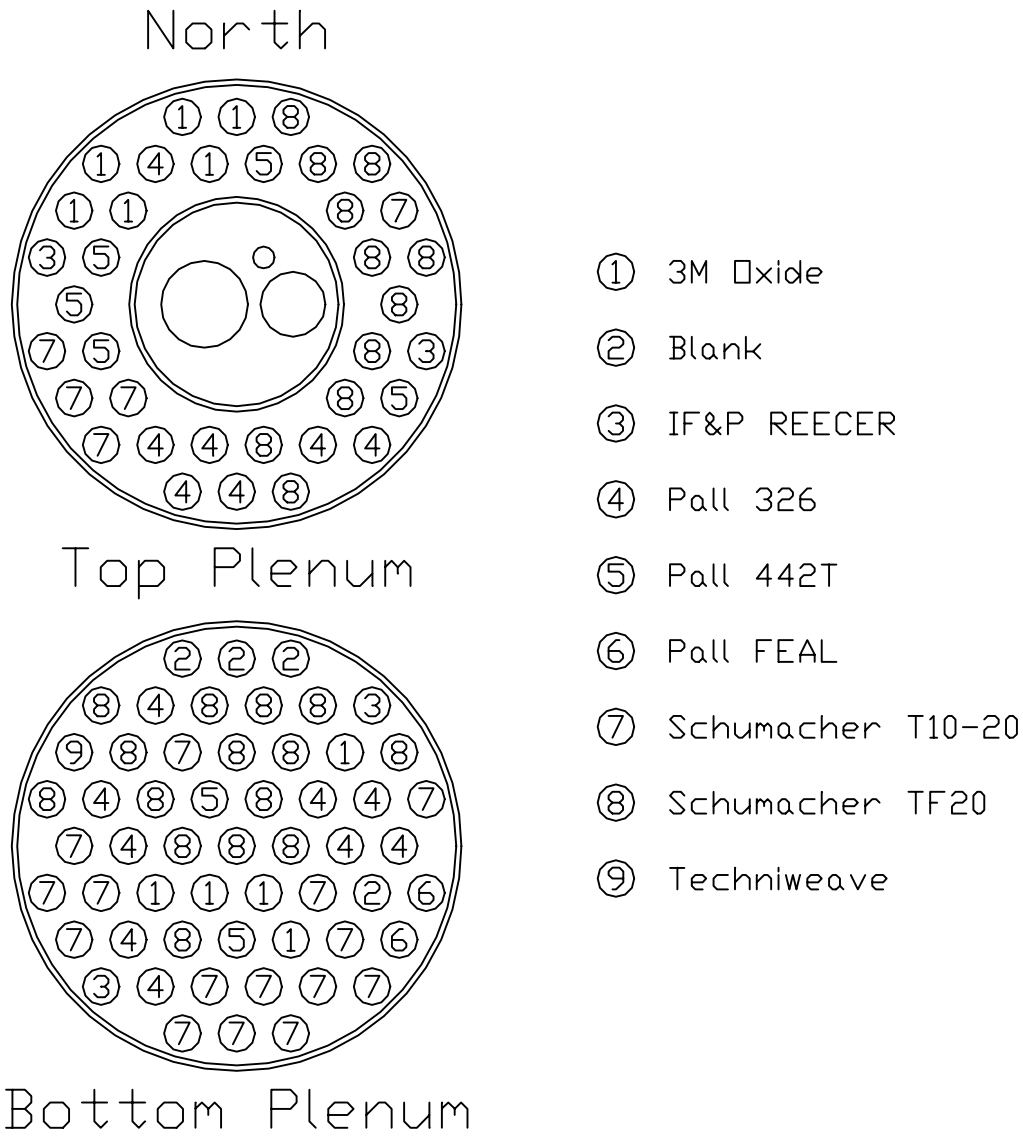

Figure 3.3-14 Filter Element Layout 13

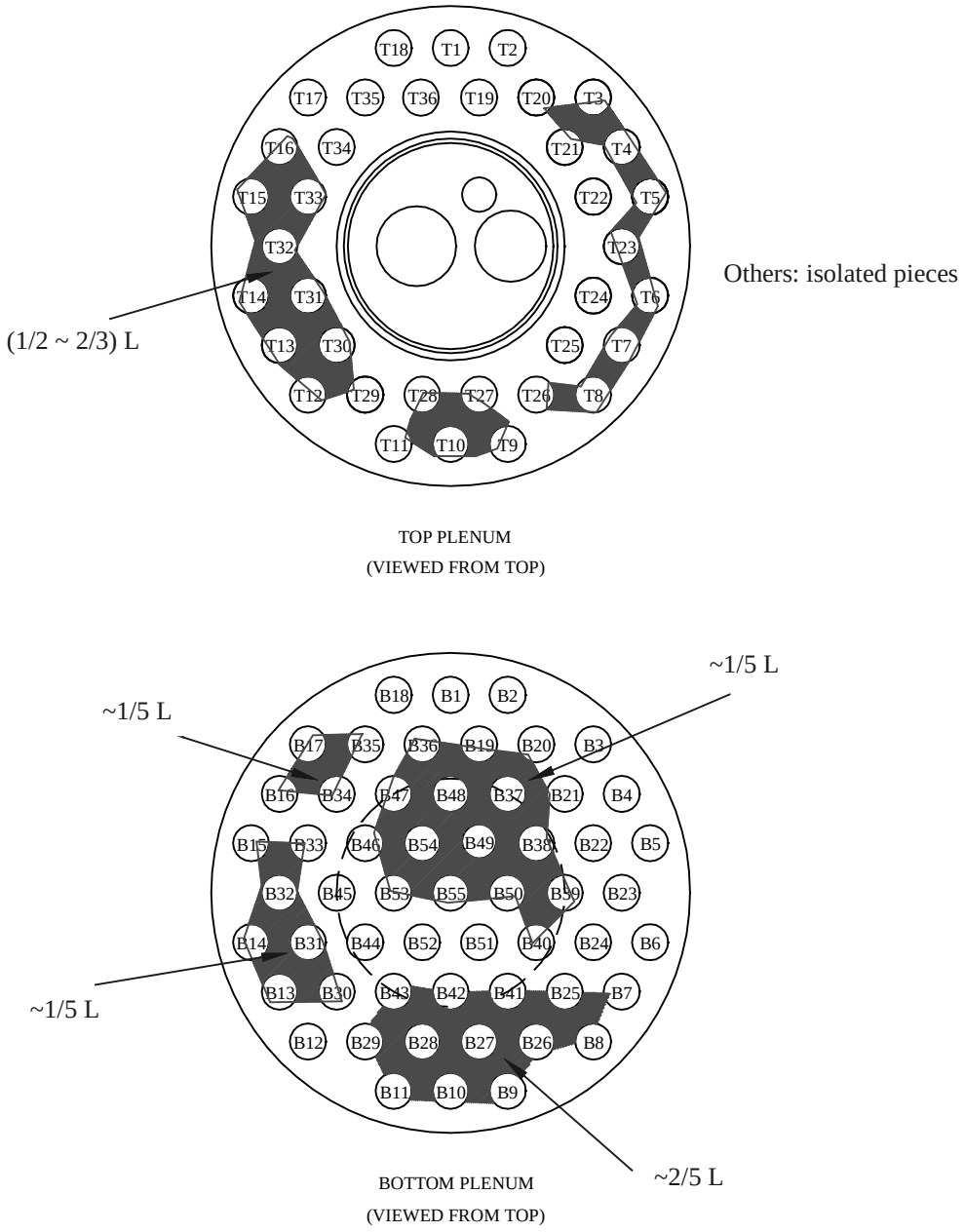

Figure 3.3-15 Locations of the Ash Bridging (Electronic copies show numbers in blue that Indicate the lengths of the ash lumps measured from the top as a portion of the length of the filter element.)

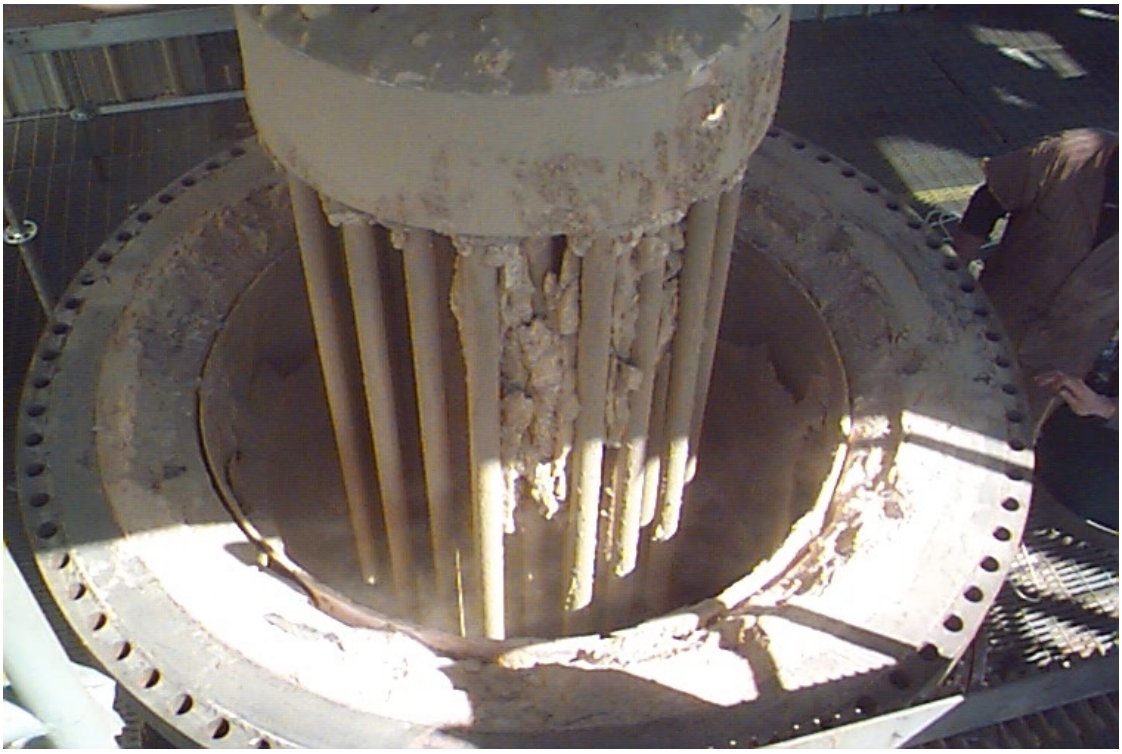

Figure 3.3-16 Ash Bridging on the Top Plenum

Figure 3.3-17 Ash Bridging Lumps

Figure 3.3-18 Ash Lumps on the Filter Element Surfaces

Figure 3.3-19 Ash Build-up on the Shroud and Liner

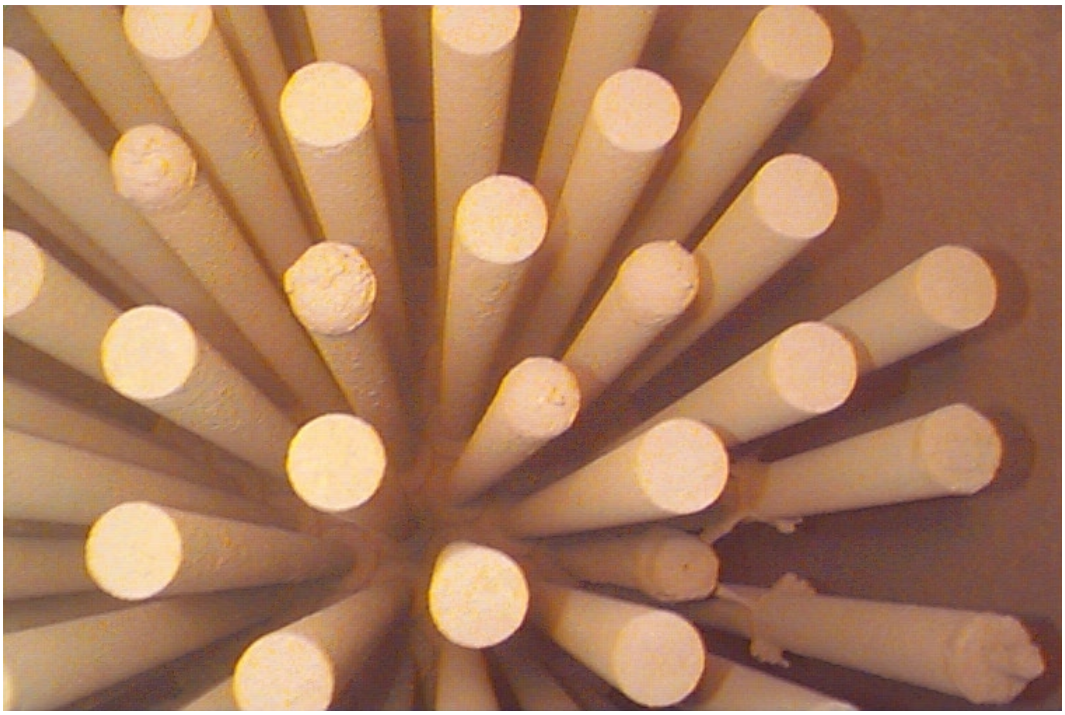

Figure 3.3-20 Filter Elements Inspected from the Lower Manway

Figure 3.3-21 Shroud and Liner Inspected from the Lower Manway

Figure 3.3-22 Filter Elements Inspected from the Top of the PCD

Figure 3.3-23 An Ash Pile on the Top of the Top Plenum

Figure 3.3-24 A Hole on the Body of a 3M Oxide Filter Element

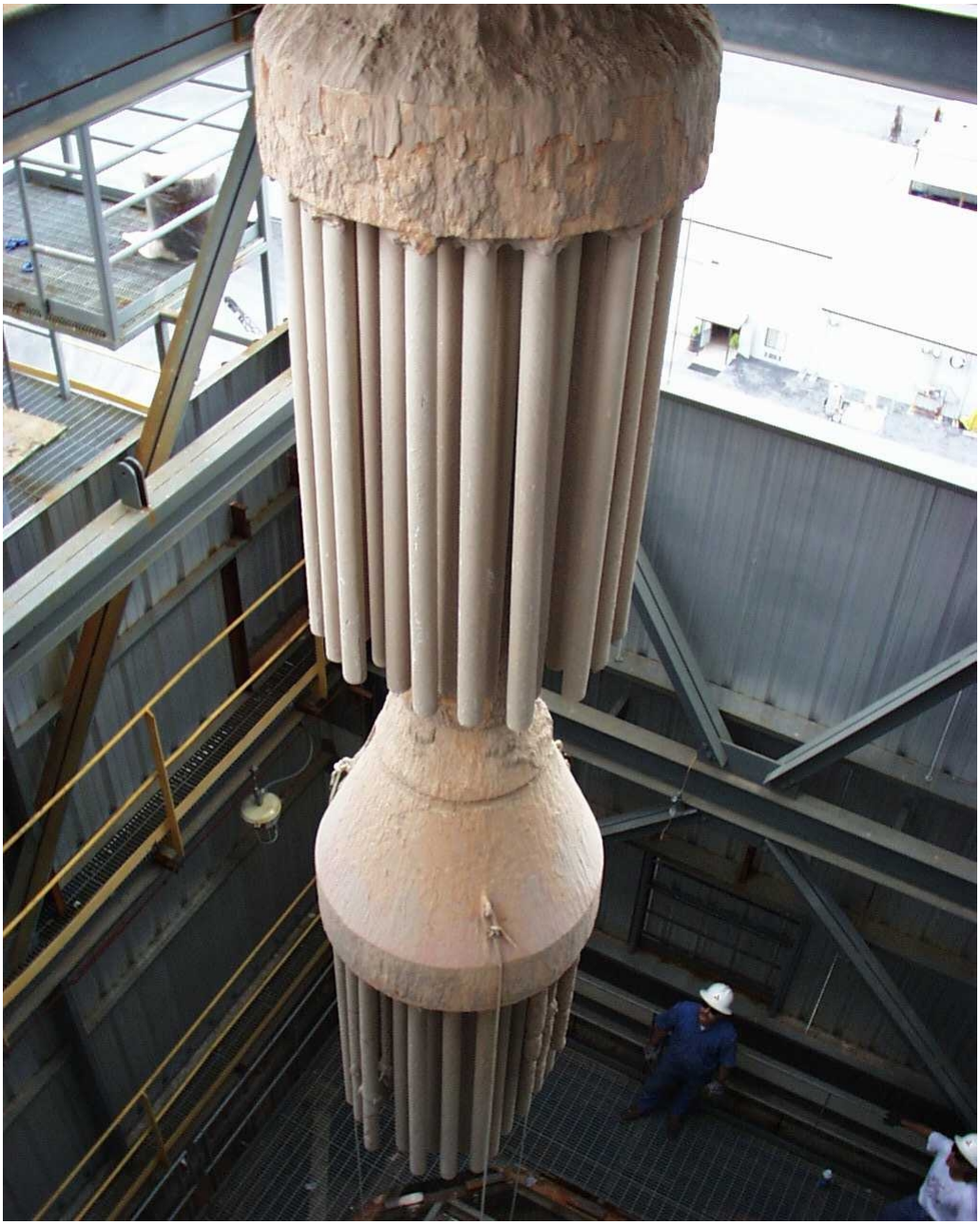

Figure 3.3-25 Filter Element Inspection

Figure 3.3-26 Ash Build-up on the Support Column

Figure 3.3-27 Cracks on the Gas Inlet

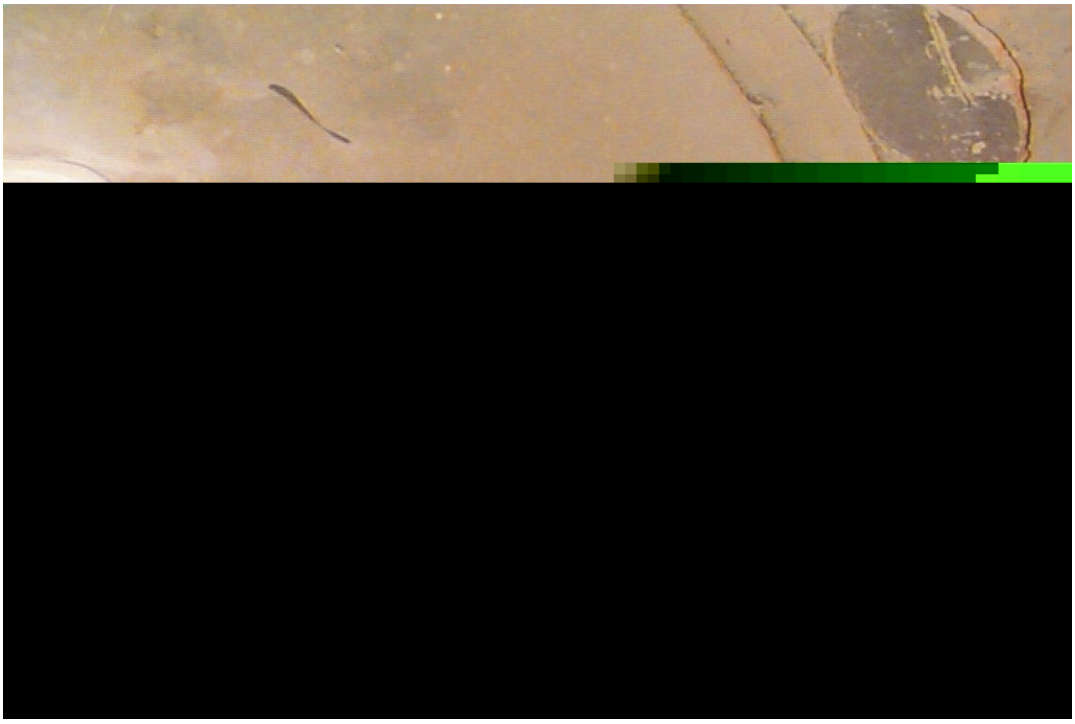

Figure 3.3-28 A Buckle on the Liner Near the Gas Inlet

Figure 3.3-29 A Buckle on the Liner Near the Bottom of Section B

3.4 TC05 ASH CHARACTERISTICS AND PCD PERFORMANCE

As in previous test campaigns, in situ particulate sampling runs were performed on a regular basis at the PCD inlet and at the PCD outlet throughout TC05. Measurements of the particulate loadings in the process gas streams entering and leaving the PCD were obtained with seven different combinations of fuels and sorbents, including: Alabama coal and Ohio limestone, Alabama coal and Alabama limestone, Illinois coal and Ohio limestone, Illinois coal and Alabama limestone, petroleum coke and dolomite, petroleum coke and limestone, and Powder River Basin (PRB) coal with Ohio limestone.

In addition to the in situ particulate sampling dustcake samples were collected on three occasions when the PCD-filter cluster was removed during an outage. The first set of dustcake samples was collected in January after about 1 week of operation with a reduced number of filter elements to evaluate PCD performance at high-face velocity. In this case the PCD was shut down dirty and both transient and residual dustcake samples were collected using the methods described in previous reports. The second set of samples was collected in March after an incident of severe PCD-ash bridging that occurred after about 30 hours of operation on petroleum coke and dolomite. The third and final set of dustcake samples was collected at the conclusion of TC05 in May.

Selected in situ samples and dustcake samples were thoroughly characterized in an effort to better understand the effects of dust characteristics on PCD performance. Dust characterization tests included chemical analysis; particle-size analysis; laboratory measurements of drag as a function of dustcake porosity; and measurements of the true particle density, bulk density, uncompacted bulk porosity, and specific surface area. The results of these tests were used to document the effects of particle size and dustcake porosity on dustcake drag and to develop a better understanding of the relationship between laboratory drag measurements and PCD performance.

In carrying out the analysis of dust characteristics and their effect on PCD performance PCD hopper samples collected during TC05 were intentionally omitted from the analysis. As discussed in the TC03 report, previous testing has shown that PCD hopper samples do not accurately reflect process-operating conditions at the time when the sample was taken. Because of intermittent and variable solids retention in the PCD hopper and ash discharge system hopper samples frequently do not reflect the properties of the dust being collected in the PCD during a given time period. Therefore, it is probably best to avoid the use of hopper samples in the analysis of PCD operation.

In addition to the dust sampling and characterization mentioned above work continued on the evaluation of a real-time particulate monitor for turbine protection. A fluidized-bed dust injection system was built, calibrated, and used to systematically test the response of the Jonas Model 5 Particle Flow Monitor. The results of this testing were used to evaluate the suitability of the monitor for use in PCD leak detection and turbine protection.

To document the emissions of acid gases from the transport reactor/PCD system, measurements of SO_2, SO_3, HCl, and HF were made with five of the fuel/sorbent combinations mentioned previously: Alabama coal and Alabama limestone, Illinois coal and Ohio limestone,

Illinois coal and Alabama limestone, petroleum coke and dolomite, and PRB coal with no sorbent.

The remainder of this report will focus on the results of the in situ particulate sampling, measurements of PCD collection efficiency, characterization of the in situ particulate samples and dustcake samples, the effect of dust characteristics on dustcake drag, and the relationship between laboratory drag measurements and PCD performance. The results of the real-time particulate monitor evaluation and the results of the acid gas measurements will also be discussed.

3.4.1 Measurements of Particulate Mass Loadings

Inlet Measurements. Table 3.4-1 gives a summary of the particulate loadings measured in the process gas stream entering the PCD during TC05. During the first six sampling runs the transport reactor was fired with the Alabama (Calumet) coal used in previous testing. Ohio (Bucyrus) limestone was used as the sorbent during the first two runs, while Alabama (Longview) limestone was used during the four remaining runs. As in previous tests the sampling runs were timed to avoid the effects of back-pulse-induced upsets in the primary cyclone dipleg. Nevertheless, run TC05IMT-06 was inadvertently started before the effects of the back-pulse had completely dissipated, resulting in contamination of the sample with the carryover of bed material. Otherwise, the inlet particulate loadings measured during this portion of TC05 were generally in the same range as those measured previously with the same types of coal and limestone. The results do not suggest any significant difference in the particulate loadings obtained with the two types of limestone.

Sampling runs TC05IMT-7 to -13 were performed with Illinois coal and the same two types of limestone (Alabama and Ohio). Inlet particulate loadings measured with the Illinois coal were in the range of about 14,000 to 16,000 ppmw with both types of limestone. Although the Illinois coal contains less ash than does the Alabama coal (about 9 versus 15 percent), the Illinois coal contains much more sulfur (3.5 versus 0.9 percent). Because of the higher sulfur content the rate of limestone addition must be substantially higher with the Illinois coal, resulting in the higher particulate loadings (14,000 to 16,000 ppmw with the Illinois coal versus 8,000 to 12,000 ppmw with the Alabama coal).

During sampling runs TC05IMT-14 to -20 the transport reactor was fired with petroleum coke. Plum Run dolomite was injected at a Ca/S molar ratio of 1.3:1 during the first five of these sampling runs (TC05IMT-14 to -18). During the last two coke runs (TC05IMT-19 and –20) Ohio limestone was injected at a Ca/S molar ratio of 1.7:1. Because of the very high-sulfur content of the petroleum coke (≅ 5 wt percent) the sorbent feedrates were substantially higher than those used in all previous tests, resulting in average inlet particulate loadings of 21,100 ppmw with dolomite and 14,100 ppmw with limestone.

During the first inlet sampling run with petroleum coke and dolomite (TC05IMT-14) the primary gas cooler was bypassed, resulting in a flue gas temperature of about 1,400°F at the PCD inlet. While unloading the sampler it was noted that a portion of the particulate sample had formed a weakly bonded bridge in the precutter and the particulate sample appeared to be stickier than any dust sample collected previously at the PSDF. After about 30 hours of PCD

operation under these conditions the ash discharge system became plugged with ash deposits. Subsequent inspection of the PCD internals revealed substantial ash bridging between the filter elements. In an effort to minimize the ash bridging in the PCD the primary gas cooler was placed in service during the outage. As a result of this change all of the remaining sampling runs on petroleum coke (TC05IMT-15 to -20) were done with the PCD operating at a nominal temperature of 750°F. None of the dust samples collected at this temperature exhibited the bridging behavior or stickiness of the sample collected at 1,400°F and there were no apparent problems with ash bridging in the PCD at 750°F.

During sampling runs TC05IMT-21 to -24 the transport reactor was again fired with Alabama (Calumet) coal and Ohio limestone was added to maintain SO_2 emissions below about 20 ppm. The PCD temperature was increased to 1,100 to 1,200°F for the remainder of TC05. Cyclone dipleg upsets occurred during the first two particulate sampling runs (TC05IMT-21 and -22), resulting in abnormally high-particulate loadings (14,200 ppmw and 16,200 ppmw). Particulate loadings of 10,200 ppmw and 10,800 ppmw were measured in the next two runs (TC05IMT-23 and -24), which were free of any process upsets. The latter measurements were in good agreement with the results of previous sampling runs with Alabama coal and Ohio limestone which gave an average loading of 10,000 ppmw.

The last six sampling runs of TC05 (TC05IMT-25 to -30) were performed with a Powder River Basin (PRB) coal. As noted in the table, four of the runs (TC05IMT-25, -26, -27, and –29) were performed with Ohio limestone. One run (TC05IMT-28) was done with no sorbent addition and one run (TC05IMT-30) was done with Florida limestone. Unusually high-particulate loadings were measured in run TC05IMT-26 and -29 as a result of upsets in the cyclone dipleg seal. Excluding these measurements, the particulate loadings were: 4,000 to 5,700 ppmw with Ohio limestone; 4,600 ppmw with Florida limestone; and 3,200 ppmw with no sorbent addition. These results suggest that about 20 to 40 percent of the solids generated from the PRB coal with limestone addition were associated with the limestone. The particulate loadings measured with the PRB coal were generally lower than those measured with the Alabama coal. This result was expected based on the ash and sulfur contents of these coals.

Outlet Measurements and PCD Collection Efficiency. Table 3.4-2 gives a summary of the particulate loadings measured in the process gas stream leaving the PCD during TC05 and the corresponding particulate collection efficiencies. The first five runs (TC05OMT-1 to -5) were done while the PCD was operated with a reduced number of filter elements, resulting in a nominal face velocity of 8 ft/min. Under this test condition the initial sampling runs (TC05OMT-1 and -2) revealed that there was definitely measurable particle penetration through the PCD, resulting in an outlet loading of 10 to 11 ppmw. Subsequent sampling runs (TC05OMT-3 to -5) performed over the next few days showed that the leakage was increasing, reaching a level of about 22 ppmw. At that point operations personnel decided to shut down the transport reactor system to correct the PCD leakage.

Subsequent inspection of the PCD revealed what appeared to be several pinhole leaks around several flanges connecting the filter elements to the tubesheet. These pinholes were apparently caused by leakage of the gasket between the failsafe and the tubesheet. Additionally, a 3/16-in. hole was also found in the bottom of one McDermott filter element. In response to these problems the filter elements in question were removed and replaced and all of the McDermott

elements were replaced with other types of elements. In addition to these changes, new filter elements were installed in place of all blanks. The latter change was made to reduce the filter face velocity and thereby lessen the pressure drop across the filter element gaskets and minimize the attendant risk of leakage between the elements and the tubesheet.

The transport reactor system was restarted in early February with the PCD operating at a lower face velocity of 5 to 6 ft/min (versus 8 ft/min in January). Under the lower face velocity conditions the measured outlet loading was initially in the range of 1.3 to 2.2 ppmw, as indicated in Table 3.4-2. While maintaining stable operating conditions with the lower face velocity the measured outlet loading gradually increased to about 7 ppmw over a 10-day period (sampling runs TC05OMT-6 to -11). The outlet loading then seemed to decrease slightly into the range of 3 to 5 ppmw over the next 8 days (sampling runs TC05OMT-12 to -15). These results show that the changes made during the January outage in combination with the reduction in face velocity were successful in reducing particle penetration by an order of magnitude compared to the leakage experienced at high-face velocity. Nevertheless, there was still significant particle penetration.

On February 22 the transport reactor system was shut down to clear a stoppage in the ash discharge system and fragments of at least one broken filter element were recovered. After clearing the stoppage the unit was restarted on propane on February 24. Dolomite was fed to the reactor and an outlet-sampling run was performed to check for particle penetration through the PCD. The results of this run revealed a leakage rate of about 400 ppmw. Subsequent inspection of the PCD confirmed that three Allied Signal PRD-66 filter elements had been broken and the top donut gasket was found to be missing on one of the broken elements when it was removed. Ash patterns on the filter element flange and contacting failsafe surface suggested that ash was leaking around the failsafe of the element with the missing gasket. Flow tests later revealed that this particular failsafe had a flow resistance that was similar to the flow resistance exhibited by a new, unused failsafe. The most likely explanation seems to be that a substantial portion of the dust leaked around the failsafe. No dustcake sampling was performed since the PCD had been back-pulsed extensively during shutdown, resulting in an extremely thin residual cake.

The first sampling run performed after the February outage (TC05OMT-17) was done with the transport reactor operating on petroleum coke and dolomite. The PCD was operating at a nominal temperature of 1,400°F and at a nominal face velocity of 5.7 ft/min. The result of this run showed that there was virtually no particle penetration through the PCD, confirming that the leakage that had occurred previously in February had been eliminated. After this run the transport reactor system was again shut down. Subsequent inspection of the PCD internals revealed severe ash bridging between the filter elements as mentioned earlier. The cause of the ash bridging in the PCD has been the subject of an extensive laboratory study that will be described in a separate topical report.

The remaining outlet sampling runs with petroleum coke (TC05OMT-18 to -23) were done with the primary gas cooler in service, producing a nominal temperature of 750°F and a nominal face velocity of 3.8 ft/min. The reduced operating temperature of the PCD was successful in eliminating the ash bridging that occurred at 1,400°F. The results of the outlet sampling runs at

the lower operating temperature confirmed that there was no significant leakage through the PCD. PCD collection efficiency was consistently greater than 99.999 percent during these tests.

After sampling run TC05OMT-23 the transport reactor system was shut down for about 3 weeks for maintenance. During the outage leaks were discovered at the flanged connection between the head of the PCD vessel and the vessel shell. The leaks were eliminated by replacing the PCD head gasket. An orifice was installed in the bypass line around the primary gas cooler to provide intermediate gas temperatures to the PCD and the transport reactor system was restarted in this configuration on April 12. During the first four sampling runs after the start-up (TC05OMT-24 to -27) the transport reactor was fired with Alabama coal and Ohio limestone. With the primary gas cooler partially bypassed the PCD operating temperature varied from about 1,170 to 1,250°F and the face velocity varied from about 5.0 to 5.2 ft/min. Under these conditions the outlet particulate loading varied from 0.68 to 2.1 ppmw, and PCD collection efficiency varied from 99.98 to 99.994 percent.

The next four sampling runs at the PCD outlet (TC05OMT-28, -30, -34, and -35) were done with the PRB coal and the last run (TC05OMT-37) was done while Eastern Kentucky coal was burned in the transport reactor. Ohio limestone was used as the sorbent during all but the last two runs (TC05OMT-35 and -37), which were done with Florida limestone. During the tests with the PRB and Eastern Kentucky coals (TC05OMT-28 to -37) the PCD operating temperatures varied from about 1,100 to 1,180°F, which were generally somewhat lower than the temperatures recorded during the tests with Alabama coal. The face velocities varied from about 4.6 to 5.3 ft/min and were also generally somewhat lower than the face velocities recorded during the tests with the Alabama coal as a result of the difference in operating temperatures. During the runs on the PRB and Eastern Kentucky coals the outlet particulate loading varied from 0.22 to 0.41 ppmw and the PCD collection efficiency varied from 99.991 to 99.996 percent.

The previous inlet and outlet results and the PCD performance during the major portions of the TC05 test period are summarized in Table 3.4-3.

3.4.2 Chemical Analyses

As in previous test runs chemical analyses were performed on selected in situ particulate samples and dustcake samples from TC05. PCD hopper samples were also analyzed but the compositions of the hopper samples will not be considered in this report since previous tests have shown that the hopper samples are of very limited usefulness in the analysis of PCD performance. The analytical results contained in this report are expressed as the corresponding oxides on an ignited basis. These results were then converted into a calculated chemical composition using the following assumptions.

1. All sulfur contained in a sample up to a molar S/Ca ratio of 1:1 is assumed to be present as $CaSO_4$.

2. Any unsulfated calcium in the sample is assumed to take the form of $CaCO_3$ if the sorbent being used is limestone or $CaCO_3 \bullet MgO$ if the sorbent being used is dolomite.

3. Any sulfur that is present in a sample in excess of a molar S/Ca ratio of 1:1 is assumed to be present as the binary sulfate compound $Mg_3Ca(SO_4)_4$.

4. Any magnesium that was not accounted for in the binary sulfate was presumed to be in the form of MgO or $CaCO_3$●MgO.

The assumptions listed above are different from the assumptions used in previous reports, which did not take into account the existence of the binary sulfate compound in some highly sulfated samples. This change in assumptions affects the calculated compositions only when the molar S/Ca ratio in the sample exceeds 1:1. In the case of the TC05 samples this was true for only two types of samples: (1) the ash bridging material formed during high-temperature (1,400°F) operation of the PCD on petroleum coke and dolomite and (2) two of the in situ particulate samples generated from the same operating period.

The basis for calculating the chemical composition of particulate and dustcake samples was changed as indicated above because x-ray diffraction studies confirmed the presence of the binary sulfate compound in the ash bridging material and in the in situ particulate samples from the high-temperature PCD operation on petroleum coke and dolomite. A literature search on the binary sulfate compound revealed that significant levels of the compound had been found in ash bridging samples from the hot-gas filter at the Tidd PFBC Plant (Smith et al., 1997a). Earlier laboratory studies had confirmed that the binary sulfate compound could be formed by the sulfation of half-calcined dolomite (Hubble et al., 1977) and by the reaction of mixtures of $CaSO_4$ and $MgSO_4$ (Rowe et al., 1967). A more recent laboratory study also demonstrated that heating mixtures of $CaSO_4$ and $MgSO_4$ powders in air at 1,400°F produced the binary sulfate compound along with consolidation of the mixture into a bonded deposit similar to the ash bridges formed in the PCD during the high-temperature petroleum coke/dolomite run (Smith, et al., 1997b).

<u>In situ Particulate Samples</u>. Table 3.4-4 summarizes the analytical results and calculated compositions for selected in situ particulate samples obtained during TC05. As indicated in the table fractional calcium utilization (or S/Ca molar ratio) varied from a low of 0.36 with PRB coal and limestone to a high of 1.07 to 1.15 with petroleum coke and dolomite. The low-calcium utilization obtained with the PRB coal is to be expected based on the very low-sulfur content of this fuel. It is interesting that the sample produced from PRB coal without sorbent addition contained significantly more $CaSO_4$ than did the sample produced from PRB coal with limestone addition (about 40 versus 20 percent). This result suggests that the inherent calcium in the PRB coal ash is removing most or all of the sulfur, so that the addition of sorbent only has a diluting effect on the level of $CaSO_4$ in the reaction products. The very high utilizations obtained with the petroleum coke and dolomite are attributed to complete sulfation of the calcium in combination with the partial sulfation of magnesium in the form of the binary sulfate compound. The chemistry of these solids will be discussed in more detail in a separate topical report on the investigation of the ash bridging that occurred with the petroleum coke and dolomite.

Aside from the very high values of sorbent utilization there are several other features of the ash chemistry that distinguish the petroleum coke/dolomite samples from the other samples. As expected, the petroleum coke/dolomite samples contain a significant amount of magnesium

(about 15 to 20 percent as MgO compared to 2 to 6 percent for the samples produced with coal and limestone). Second, the petroleum coke/dolomite samples contain much lower concentrations of the mineral constituents normally associated with coal ash (SiO_2, Al_2O_3, etc) since the petroleum coke contains only about 0.5 percent ash. Finally, the samples generated from the petroleum coke contain about 0.6 to 0.8 percent vanadium (expressed as V_2O_5) while the coal/sorbent samples contain less than 0.04 percent vanadium (expressed as V_2O_5). This vanadium comes from the petroleum coke ash which typically contains 30 to 50 percent vanadium as V_2O_5.

Results obtained with the various coals and limestones suggest that the Alabama limestone may have been somewhat more highly utilized than was the Ohio limestone (S/Ca = 0.85 to 0.88 with Alabama limestone versus S/Ca = 0.51 to 0.62 with Ohio limestone). The utilizations achieved with the Ohio limestone in TC05 appear to be similar to those achieved with the same limestone and Eastern Kentucky coal in TC03 (S/Ca = 0.59 to 0.64 in TC03 versus 0.51 to 0.62 in TC05). The utilizations achieved with the Alabama limestone in TC05 appear to be somewhat higher than those achieved with the same limestone and with Eastern Kentucky coal in TC03 (S/Ca = 0.58 to 0.68 in TC03 versus 0.85 to 0.88 in TC05). Overall, it appears that the best utilization obtained with any limestone was achieved with the Alabama limestone in TC05.

Dustcake Samples. Table 3.4-5 summarizes the analytical results and calculated chemical compositions for the dustcake samples removed during the various TC05 PCD inspections. The samples collected on January 26 were obtained after a dirty shutdown of the PCD in which the coal and sorbent feeds to the transport reactor were discontinued at the end of a filtration cycle without any subsequent pulsing of the PCD. This procedure made it possible to preserve the entire (residual plus transient) dustcake for characterization. The resulting dustcake was separated into so-called residual and transient layers using the scraping procedure described in the TC03 report. Two sets of the residual/transient dustcake samples were subjected to chemical analysis (and a variety of physical tests discussed later). The first set was taken from the inner side of element T-12 (i.e., along the element surface facing the centerline of the element array). The second set was taken from the windward side of the same element (i.e., the side on which the swirling gas flow impinges). As shown in the table, calcium utilization (S/Ca molar ratio) was much higher in the residual dustcake from the inner side than it was in the transient dustcake from the same side (S/Ca = 0.76 in residual cake versus S/Ca = 0.47 in transient cake). This result was consistent with previous analyses of transient and residual ash layers and demonstrated that the residual layer is much more highly sulfated than is the transient layer. This result is to be expected in view of the prolonged residence time of the residual layer compared to that of the transient layer.

Different results were obtained with residual and transient layers removed from the windward surface of the element. In this case identical values of calcium utilization were obtained from the two layers (S/Ca = 0.66 in both layers). This result was inconsistent with previous analyses of transient and residual layers but none of the previous samples were collected specifically from the windward surface of an element. Additional sampling of transient and residual dustcake layers will be performed during future dirty shutdowns to investigate the validity of this result.

As suggested earlier, very interesting analytical results were obtained on the ash bridging material removed after the high-temperature run with petroleum coke and dolomite. The molar S/Ca

ratio of 1.57 suggests that all of the calcium has been sulfated and 57 percent of the magnesium has been sulfated. X-ray diffraction analysis detected two primary compounds in the ash bridging material: $CaSO_4$ and $Mg_3Ca(SO_4)_4$ (the so-called binary sulfate). No $MgSO_4$ was detected. These results suggest that the sulfated calcium took the form of the binary sulfate as well as $CaSO_4$ while the binary sulfate alone must account for all of the sulfated magnesium (i.e., there is no evidence of $MgSO_4$ per se). Based on the ratio of areas under the x-ray diffraction peaks and the known concentration of $CaSO_4$ it appears that all of the sulfated magnesium is indeed contained in $Mg_3Ca(SO_4)_4$. Using the calculation basis outlined previously the concentration of $Mg_3Ca(SO_4)_4$ in the bridged material was estimated to be 35 percent by weight. Using x-ray diffraction in combination with the analysis of water extracts the concentration of $Mg_3Ca(SO_4)_4$ in ash bridges removed from the hot-gas filter at the Tidd PFBC was estimated to be 37 percent by weight (Smith et al., 1997). Thus, the apparent concentration of binary sulfate in the PCD ash bridging material does not appear to be unreasonable compared to the ash bridging material from Tidd.

As was the case with the in situ particulate samples only the dustcake sample from the petroleum coke run contained a significant level of vanadium (0.66 percent as V_2O_5). The dustcake sample removed after the conclusion of TC05 contained only 0.04 percent vanadium as V_2O_5.

Samples of the ash bridging that occurred in the PCD during the high-temperature run with petroleum coke and dolomite have been subjected to much more extensive examination by scanning electron microscopy with energy-dispersive x-ray analysis (SEM/EDX). The SEM/EDX studies have successfully documented the changes in particle morphology and in the distribution of calcium and magnesium that occur during the formation of the ash bridges, and the formation of the binary sulfate compound has been confirmed by x-ray diffraction. The morphological changes, changes in calcium/magnesium distribution, and production of the binary sulfate compound have also been reproduced by exposing the dolomite to simulated flue gas environments in flow-tube furnace tests in the laboratory. Very similar changes in morphology and in calcium/magnesium distribution have also been observed in $CaSO_4/MgSO_4$ mixtures heated to 1,400°F. The results of all these tests suggest that the bridging that occurred in the PCD may be related to the migration of calcium and magnesium, which is associated with the formation of the binary sulfate compound $CaMg_3(SO_4)_4$. It is possible that the dolomite particles are being bonded together by the migration of calcium and/or magnesium across the interfaces between particles. The mechanism by which this migration occurs is not understood but it is possible that the mobility of the calcium and magnesium is enhanced by the formation of a low-melting eutectic mixture containing $CaSO_4$ and $CaMg_3(SO_4)_4$.

A literature search on the binary sulfate compound revealed that the binary sulfate could form eutectic mixtures with $CaSO_4$. One such eutectic mixture contains 55 wt percent $CaSO_4$ and 45 wt percent binary sulfate (Rowe, et al., 1967). In this eutectic mixture the $CaSO_4$ and the binary sulfate are present in a weight ratio of 55:45, or 1.2:1, which is the same weight ratio found in the bridged material. Thus, $CaSO_4$ and binary sulfate are present in the bridged material in proportions that would form a low-melting eutectic mixture. The formation of this low-melting eutectic mixture may help explain the morphological changes and the migration of calcium and magnesium that were revealed by the SEM/EDX studies. The results of these SEM/EDX studies and the flow-tube furnace tests will be discussed in more detail in a topical report on the investigation of the ash bridging problem with petroleum coke and dolomite.

3.4.3 Measurements of Physical Properties

Selected in situ particulate samples and dustcake samples were subjected to the standard suite of physical measurements used in previous tests. The measurements included true particle density, bulk density, uncompacted bulk porosity, specific surface area, particle-size analysis, and dustcake drag measurements as a function of dustcake porosity. The methods used for making these measurements have been described in previous reports.

In situ Particulate Samples. Physical properties of the in situ particulate samples are summarized in Table 3.4-6. Uncompacted bulk porosities, which indicate the tendency of the dust to pack, were generally within the range of previous measurements (76 to 81 percent), with the exception of the sample generated with Alabama coal and Alabama limestone (68.4 percent), the samples generated with petroleum coke and dolomite (71.5 percent), and the sample generated with petroleum coke and limestone (69.8 percent). These particular samples also have relatively low-specific surface areas (0.67 to 1.01 m^2/g) and relatively high levels of calcium utilization (S/Ca molar ratio = 0.80 to 1.15). The relatively high levels of sulfation in these samples would be expected to produce relatively low-specific surface areas as the $CaSO_4$ reaction product seals off pores in the sorbent particles. This pore-closure mechanism would reduce the internal porosity within the sorbent particles but it may not necessarily have any effect on bulk porosity (i.e., the void space between particles). It is also possible, however, that the void space between particles could be reduced by the buildup of $CaSO_4$ reaction product, which could explain the reduced uncompacted bulk porosities of these samples.

The mass median diameters (mmd) determined from the particle-size analyses were in the range of 18 to 24 μm for the samples generated with the various coals and limestones, while the mmd of the samples generated from the petroleum coke were in the range of 28 to 37 μm. This difference has been confirmed by SEM examination and is presumably attributable to the very low-ash content of the petroleum coke, which means that the PCD solids generated from petroleum coke are predominantly composed of sulfated sorbent particles. The samples generated from coal and limestone contain a significant amount of coal ash, which apparently has a finer particle-size distribution than does the sorbent.

As expected, the difference in physical particle size (MMD) leads to a corresponding difference in drag equivalent diameter (DED) as shown in the table. (The DED is the diameter of a spherical particle that would produce the same drag versus porosity characteristics exhibited by the dust sample if it were packed in a bed of identical spherical particles, all of which have a diameter equal to DED.) Previous reports have shown that the DED may be correlated with the MMD or the mean physical size of the particles. The relationship between MMD and DED and the effects of particle size and porosity on dustcake drag will be examined in more detail after discussing the physical properties of the dustcake samples.

Dustcake Samples. Table 3.4-7 gives a summary of the physical properties of the selected dustcake samples. All of the uncompacted bulk porosities were within the range of previous dustcake measurements (79 to 83 percent for TC05 dustcakes versus 76 to 83 percent for TC03 dustcakes). Specific surface areas were also generally in the same range as those measured on TC03 dustcakes (1.4 to 3.9 m^2/g for TC05 dustcakes versus 1.8 to 4.6 m^2/g for TC03

dustcakes). As shown in the tables, the dustcake samples generally had higher specific surface areas than the in situ particulate samples collected during the preceding test period. This result reflects the finer particle-size distribution of the dustcake samples compared to that of the in situ particulate samples. This difference in physical particle size is also reflected in the drag characteristics of the samples as indicated by the following comparison of samples collected during the time period of January 19 to 26.

Test Parameter	In situ Particulate	Transient Dustcake	Residual Dustcake
Mass Median Diameter (μm)	19.9	11.1-15.8	11.4-18.2
Drag-Equivalent Diameter (μm)	2.7	1.7-2.1	1.9-2.6
Lab Drag @ UBP (in. H_2O/(ft/min)/(lb/ft^2))	4.7	5.5-8.7	—
Lab Drag @ FCP (in. H_2O/(ft/min)/(lb/ft^2))	—	—	26-30

As expected, the dustcakes have smaller mass median diameters than does the inlet dust, as a result of particle dropout in the PCD vessel. As a consequence of this particle-size difference the dustcakes exhibit more resistance to gas flow than does the inlet dust. This difference in drag characteristics is reflected in the drag equivalent diameters and the lab-measured drag values shown above. For this comparison, the lab-measured drag values for the inlet dust and for the transient dustcake samples were determined at the uncompacted bulk porosity (UBP). The lab-measured drag values for the residual dustcake samples were determined at the flow-compacted porosity (FCP), which is the lowest porosity achieved in the laboratory tests. The flow-compacted porosities of the residual dustcakes were in the range of 64.3 to 69.5 percent, while the uncompacted bulk porosities of the inlet dust and transient dustcake samples were in the range of 68.4 to 81.7 percent. It seems reasonable that the flow-compacted porosity would be more appropriate for the residual dustcake since the residual cake should reach a steady-state porosity determined by long-term exposure to the ultimate compressive force exerted by the flowing gas. During the buildup of the transient dustcake the transient cake porosity varies as the pressure drop increases. Therefore, the average compressive force exerted on the transient dustcake during a given filtration cycle is substantially lower than the compressive force that is achieved at the end of each filtration cycle just before back-pulsing.

Our lack of knowledge concerning the true dustcake porosity obviously imposes severe limitations on the analysis of PCD performance using laboratory drag measurements. In an effort to alleviate some of these limitations a new apparatus has been developed to give a better indication of the true dustcake porosity to be expected at a given face velocity. The new apparatus has been termed the RAPTOR, which stands for Resuspended Ash Permeability Tester for Operational Research). In the RAPTOR, a dust sample is resuspended in air and collected on a filter under flow conditions that simulate the flow-induced compressive forces operative in the PCD. The resuspension and collection of the dust sample is done in air at room temperature and the operating face velocity is adjusted to simulate the drag exerted by the flue gas under process conditions. From the thickness and weight of the resulting cake the dustcake porosity can then be determined. Because of the effect of operating temperature on dust stickiness and the effects of prolonged sulfation and other chemical reactions this value of porosity may not be an accurate representation of the dustcake porosity developed in the PCD. Nevertheless, the value of porosity determined by this method is almost certainly a better

indication of the compressed dustcake porosity than is the FCP determined from conventional drag measurements based on compaction of the dust sample using a piston. Systematic testing of dust samples with the RAPTOR system has just begun and will be discussed in more detail in future reports. All of the remaining analyses of dustcake drag included in this report are based on the conventional permeability test procedures used throughout all previous test campaigns.

3.4.4 Effect of Particle Size on Drag

Relationship between Particle Size and Drag Equivalent Diameter. Figure 3.4-1 shows the effect of physical particle size (MMD) on the characteristic drag of the dust as determined by the drag equivalent diameter (DED). This plot is based on data for both inlet dust samples and dustcake samples collected during TC05. The linear regression suggests that there is a reasonably good correlation between MMD and DED even though the data were obtained with a variety of coals and sorbents and the data represent both in situ samples and dustcake samples. This result suggests that all of these samples have similar morphologies except possibly for the ash bridging material from the petroleum coke/dolomite run. The data point for the ash-bridging sample is the farthest point from the regression line and it could be considered an outlier. SEM examination of the ash bridging material has also shown that it has a morphology that is significantly different from the morphologies of typical coal/sorbent samples.

Effect of Particle Size on PCD Transient Drag. The effect of particle size on drag is shown more directly in Figure 3.4-2, which shows PCD transient drag versus MMD. The PCD transient drag shown here is based on the PCD pressure drop buildup occurring during the time period when the corresponding in situ sample was collected. The transient drag was determined by dividing the pressure drop buildup by the PCD face velocity and by the areal loading of dust accumulated during the same time period. The areal dust loading was calculated from the measured inlet dust loading, corrected for particle dropout, and the total active surface area of the filter elements. For these calculations 25 percent dropout was assumed. As shown in the plot, most of the data points agree fairly well with the trend predicted by SRI modification of the Carman-Kozeny Equation for pressure drop in beds of particles. The two outliers are both data points obtained with Alabama coal and Ohio limestone. These points are obviously characterized by unexpectedly high values of transient drag. The cause for this unexpected high drag is unknown.

Effect of Fine Particles on Drag. As shown in previous reports dustcake drag is particularly sensitive to the concentration of fine particles in the dust. The effect of fine particles on drag may be seen by examining the lab-measured drag-versus-porosity curves for various inlet dust samples (Figure 3.4-3) and the particle-size distributions of the same samples (Figure 3.4-4). The in situ particulate sample generated from petroleum coke and dolomite exhibited the lowest drag and also had the lowest concentration of fine particles. The in situ particulate sample generated from Alabama coal and Ohio limestone exhibited the highest drag and also had the highest concentration of fine particles (D_p <6 μm). The samples generated from Illinois coal and Ohio limestone and from PRB coal with no sorbent had similar concentrations of fine particles but the latter had a higher concentration of large particles, explaining its lower drag. Thus, the characteristic flow resistance of a dust sample appears to be strongly related to the particle-size distribution of the sample.

3.4.5 Relationship Between Lab-Measured Drag and Actual PCD Performance

Transient Drag and PCD Performance. Figure 3.4-5 shows the relationship between the lab-measured drag of in situ particulate samples and actual PCD transient drag. The lab-measured drag values are the values obtained for the in situ particulate samples at the uncompacted bulk porosity and corrected to the viscosity of the process gas at PCD conditions. The PCD transient drag values were calculated from the pressure drop buildup during the time period of the in situ sample collection, the measured inlet particulate loading based on the corresponding sample (corrected for 25-percent dropout), the PCD face velocity, and the total active surface area of the filter elements. At low values of PCD transient drag—less than about 5 to 10 in. $H_2O/(ft/min)/(lb/ft^2)$—the lab measurements appear to over-predict the flow resistance of the transient dustcake. At higher values of PCD transient drag the lab measurements appear to under-predict the transient dustcake drag. The most likely explanation for this behavior is that the transient dustcake becomes more highly compacted at higher values of transient drag, producing flow-compacted porosities that are increasingly farther and farther from the uncompacted bulk porosity. Good agreement between the lab-measured drag values and the PCD transient drag values could probably be achieved by taking into account the effect of the transient drag (i.e., the compressive force) on the dustcake porosity. Such calculations could be done given sufficient information on the compressibility of the dustcake (i.e., the relationship between applied force and dustcake porosity). Standard laboratory procedures are available for measuring the compressibility of powders but these procedures may not accurately simulate the drag forces exerted on the particles by the gas flowing through the dustcake. This limitation points again to the need for a measurement system like the RAPTOR which offers the potential for a better understanding of true dustcake porosity and the relationship between flow conditions and flow compaction of dustcakes.

Residual Dustcake Drag and PCD Baseline Pressure Drop. Figure 3.4-6 illustrates the relationship between actual PCD dustcake drag and lab drag measurements on both residual and transient dustcake samples. In this plot the lab-measured drag values were determined at the flow-compacted porosity for residual dustcake samples and at the uncompacted bulk porosity for transient dustcake samples. In the case of the residual dustcake samples the PCD residual dustcake drag was determined from the baseline ΔP prior to shutdown. The residual dustcake ΔP was calculated as the difference between the baseline ΔP and the clean filter ΔP. The clean-filter ΔP was based on ΔP measurements made during the TC01 start-up, with appropriate corrections for the effects of gas velocity and gas viscosity on the ΔP. The areal loading of the residual dustcake was estimated assuming that the residual dustcake porosity was equal to the flow-compacted porosity determined from the lab measurements and that the dustcake thickness was 1/8 in. For the residual dustcakes that remained after the January portion of TC05 the residual dustcake ΔP calculated in this manner was 125 in. H_2O. The areal loading of the residual cake was estimated to be 0.53 to 0.61 lb/ft^2 and the residual dustcake drag was estimated to be 26 to 30 in. $H_2O/(ft/min)/(lb/ft^2)$. As shown in the plot, these values were in substantial agreement with the lab-measured drag values for the residual dustcake samples.

PCD dustcake drag for the transient dustcakes was determined from the pressure drop buildup during the filtration cycles, the estimated areal loading of the transient cake, and the PCD face velocity. The lab-measured drag values for the transient dustcakes were determined at the

uncompacted bulk porosity and corrected for gas viscosity. The lab drag values determined in this manner varied from 5.5 to 8.7 in. $H_2O/(ft/min)/(lb/ft^2)$ for the transient dustcakes removed after the January portion of TC05. The corresponding PCD transient dustcake drag was estimated to be 7.1 in. $H_2O/(ft/min)/(lb/ft^2)$, which is in reasonably good agreement with the corrected lab drag measurements on the transient cakes. As noted in the plot, the outliers are the ash bridging material from the petroleum coke/dolomite run and the residual dustcake sample collected at the conclusion of TC05. The latter sample may have been altered by exposure to blowing rain.

3.4.6 Evaluation of Real-Time Particulate Monitors

Protection of the combustion turbine located downstream of the PCD from particulates is of paramount importance. Accordingly, an instrument that could provide particle concentration monitoring at the exit of the PCD in near real time is desirable to minimize turbine damage resulting from a filter failure or other high-mass-emission event. Unfortunately, the conditions under which such an instrument must operate are severe and the choices are limited. The first in–situ particulate monitor evaluated for possible use in this application was the Jonas Model 5 Particle Flow Monitor.

The Jonas Monitor determines particle concentration by measuring the shock waves of particles that have impacted into a probe that protrudes into the process stream. The shock waves are transmitted through a waveguide to an accelerometer located outside the duct. The shock wave signatures are analyzed and converted to particle mass by a proprietary algorithm running on a PC-compatible computer. The monitor is rated by the manufacturer for particle concentrations as low as 0.4 ppmw. Probes were installed at both the inlet and outlet of the PCD on the Kellogg system but our main interest here is in the results from the outlet probe.

The Jonas monitors were originally installed during the summer of 1997 with initial operation during TC01 in September 1997. Commissioning of the probes was performed by a representative of Jonas Inc. After commissioning, the inlet probe appeared to indicate approximately the correct mass concentration although this value was obtained by adjustment of that probe to agree with our measured value. The outlet probe was indicating zero, which was in general agreement with the true outlet concentration at that time of 0.1 ppmw given the lower limit of resolution of the probe (0.4 ppmw).

Unfortunately, the original Jonas design used graphoil to provide the high-pressure seal between the probe body and the waveguide. Although graphoil is rated for high temperature in a reducing environment it is not acceptable for use under oxidizing conditions. After only a few hours of operation at 1,400°F the seal in the outlet probe failed and flue gas began to leak from the back of the probe. Although the quantity of gas leaking was small because of the small clearance between the waveguide and its housing this was a safety hazard and the hot gases destroyed the accelerometer in any case. Therefore, all external connections were removed from the probe, all ports into the probe housing were plugged, and the probe housing was allowed to equilibrate with the duct pressure. Although the inlet probe had not yet failed it was also sealed as a safety precaution. Since the signal wires had to be cut to seal the housings no further data could be collected.

During the next outage both probes were removed from the process duct and shipped back to Jonas for repair and modification. The transducer was replaced on the outlet probe as were both sets of signal wires. The seal problem was resolved by installing a metal bellows seal at the flue gas end of the probe. A second line of defense was provided by adding a bulkhead near the back end of the probe with a Swagelok fitting to seal around the waveguide. In addition, the back end of the probe was sealed by passing the electrical feed through a Conax fitting. No additional leakage problems were encountered after these modifications were made.

The modified Jonas probes were reinstalled prior to TC02. Several problems were identified during evaluation. First, there was considerable crosstalk between the two probes through their common power supply. Because of the much higher mass concentration, and thus much higher signal level on the inlet probe, the crosstalk swamped the signal to the outlet probe although this was not initially obvious. Second, based on the particle-size distribution measured with cascade impactors at the PSDF Jonas decided that the outlet probe was not sensitive enough to accurately detect the particles at the PCD outlet. The probes were again shipped back to Jonas for modification to reduce crosstalk and to fit and recalibrate them with more sensitive transducers.

Just prior to the start of TC05 the Jonas probes were received with the modifications and were reinstalled on the transport reactor. To further increase the chance of obtaining meaningful results the outlet probe was moved to a new location in the outlet duct. The new location was much better for collection of an accurate sample with at least 10 duct diameters of straight pipe both upstream and downstream of the probe.

The mass concentration indicated by the outlet probe was monitored during the initial part of TC05 as natural changes in mass concentration occurred. During January and February of 1999 the PCD outlet mass concentration varied from 1 to 22 ppmw. Although there was some output from the Jonas probe it was not consistent and could not be correlated with the changes in mass concentration. That is, the probe could be adjusted to agree with one known concentration but when the concentration subsequently changed the probe did not track the change accurately. However, on February 24, 1999, during operation with a large leak through the PCD the outlet probe responded in a meaningful way. During this leakage period the probe indicated 200 ppmw while manual measurements with SRI sampling systems indicated a true mass concentration of 400 ppmw. Considering past results agreement within a factor of two was encouraging. At least it appeared that the probe could detect massive leaks.

The lack of ability to control the particle concentration in the range important for turbine protection (1 to 100 ppmw) at the Jonas probe was a significant limitation in our ability to evaluate its performance. During March 1999 a system for injecting dust into the PCD outlet gas stream at known concentrations was installed. The drawings of the injection system are shown in Figures 3.4-7 and -8. The system uses medium-pressure nitrogen to fluidize a column of fly ash and create a controlled carryover of ash particles into the process stream. The fluidizing velocity is adjusted to provide a predetermined rate of ash injection. The dust was injected approximately 50 feet upstream from the SRI batch sampling system and 100 feet upstream of the Jonas probe.

Figure 3.4-9 shows the result of calibration measurements made on the ash injection system. Over the range of mass concentrations of interest the relationship between bed flow and mass emission was quite well defined. The bed was refilled after each test to ensure that the output did not vary as the ash was consumed and the bed level dropped.

In late April 1999 the final push to validate the Jonas probe was undertaken. A Jonas technician was brought to the PSDF to ensure that every possible effort was made to provide a fair test of the instrument capabilities. The technician tested all aspects of the system operation and optimized the configuration of the probe for the existing operating conditions.

During the period of these tests, in the absence of dust injection, the mass concentration in the PCD outlet duct was approximately 0.4 ppmw. With the Jonas probe adjusted to agree with this background concentration a series of tests with dust added to the gas stream were conducted. During each test a manual measurement of the in situ mass concentration was made to determine the true mass loading. The output from the Jonas probe was averaged over the same time period as the in situ sample. The results of this test are illustrated in Figure 3.4-10. The data point collected from the gasket leak during TC05 with a concentration of 400 ppmw is also shown on the graph. As indicated in the graph, the Jonas probe did not respond to mass concentrations below 100 ppmw. The dust injection system was not used to purposefully generate dust concentrations in excess of 100 ppmw because of the potentially harmful effects on the pressure letdown valve. The Jonas technician admitted that the particles in the duct were simply too small to generate a signal that the system could accurately measure.

Siemens Westinghouse has reported that turbine life is shortened by particle concentrations above 1 ppmw, with drastic life reductions above 10 ppmw. Therefore, even though the Jonas probe can detect larger leaks of a few hundred ppmw it does not appear to be useful for true turbine protection.

No further work is planned with the Jonas instrument at this time but SRI will continue to evaluate other real-time monitors. Based on further evaluation of available monitors a new instrument has already been selected to replace the outlet Jonas probe. (The Jonas probe installed at the PCD inlet will be left in place and will continue to be used for monitoring of dipleg seal losses and other process upsets.) The new instrument, an electrodynamic particle monitor, has recently been installed in the same port where the outlet Jonas probe was installed previously. The electrodynamic particle monitor, manufactured by PCME Ltd, detects the current flow that is induced on the probe as charged particles pass around the probe. One advantage of this type of system is that the particle detection does not depend on particles impacting the probe. Even very fine particles that will follow the gas streamlines around the probe should still be detected as long as the particles possess a net electrical charge.

A low-temperature, low-pressure version of the PCME probe has been widely used as a baghouse leak detector in Europe and elsewhere. The high-temperature, high-pressure version of the device currently installed at the PSDF has not been used commercially although one is currently installed at Sierra Pacific's Piñion Pines IGCC demonstration plant. Sierra Pacific has not yet generated any definitive information on the performance of the PCME probe at Piñion Pines. Evaluation of the probe at Piñion Pines may be difficult since the Sierra Pacific facility is not equipped with an ash injection system for generating known particulate concentrations in

the process gas. Using the ash injection system described earlier SRI will evaluate the PCME probe during upcoming tests at the PSDF. Evaluation of this instrument and other real-time monitors will continue until an instrument can be identified that has the sensitivity and reliability needed for turbine protection.

3.4.7 Measurements of Acid Gases

Concentrations of acid gases (SO_2, SO_3, HCl, and HF) were measured using the modified Cheney-Homolya sampling train and analytical procedures described in previous reports. The primary purpose of these measurements was to quantify the levels of SO_3, HCl, and HF produced with each fuel-sorbent combination. A secondary goal was to provide SO_2 measurements for evaluating the performance of the on-line SO_2 analyzer.

As shown in Table 3.4-8, the SO_2 concentrations measured by the Cheney-Homolya procedure were consistently higher than the SO_2 concentrations recorded by the on-line analyzer. The cause of this discrepancy remains unknown. One possible explanation is loss of SO_2 across the in-line filter or in the sampling line leading to the on-line analyzer. Another possible explanation is some other problem with the on-line analyzer or with the calibration of the analyzer. It seems unlikely that the Cheney-Homolya procedure would produce an artificially high-SO_2 reading because the titration operation used in the Cheney-Homolya procedure is specific for the sulfate anion (i.e., it is not subject to interference from anions generated by the absorption of other acid gases such as chloride, fluoride, etc).

The measured SO_3 concentrations seemed to track the measured SO_2 concentrations with the highest levels of both gases obtained with the Alabama coal and Alabama limestone (36 to 67 ppm of SO_2 and 14 to 50 ppm of SO_3). The lowest levels of SO_2 and SO_3 were obtained with the PRB coal without sorbent addition (7 to 9 ppm of SO_2 and 0.7 to 1.2 ppm of SO_3). These levels of SO_2 and SO_3 reflect a relatively high degree of sulfur capture by the limestone or by the inherent calcium content of the ash in the case of the PRB. In all cases except the PRB and the petroleum coke the remaining SO_3 is still present at sufficiently high levels to be of concern from the standpoint of the acid dewpoint and potential for low-temperature corrosion.

Measured SO_3 concentrations were very low during petroleum coke combustion with dolomite addition (0.3 to 1 ppm). Given the high-sulfur content of the petroleum coke (about 5 percent by weight) the low levels of SO_3 are somewhat surprising and probably reflect a low degree of catalytic conversion of SO_2 to SO_3. The apparent lack of catalytic activity may result from the very low-ash content of the petroleum coke (about 0.5 percent by weight). Because of the combination of high-sulfur content, low-ash content, and high-sorbent addition rates much of the SO_2 may be captured by the dolomite before it comes into contact with any catalytic sites on the ash particles. This result is significant because it suggests a low potential for back-end corrosion problems with petroleum coke and dolomite. Measured HCl and HF concentrations were also relatively low with petroleum coke and dolomite compared to the combinations of coal and limestone.

Measured HCl concentrations were highest with the Illinois coal and Alabama limestone (48 to 52 ppm) and lowest with the PRB coal with no sorbent addition (< 2.2 ppm, which was the detection limit under these conditions). This result is consistent with the relatively high-chlorine

content of the Illinois coal and the relatively low-chlorine content of the PRB coal. There was no statistically significant difference in measured HF concentrations with the various combinations of Alabama coal, Illinois coal, Ohio limestone, and Alabama limestone, all of which gave values in the range of 5 to 8 ppm. The PRB coal, however, produced significantly lower levels of HF, which were in fact below the detection limit (< 1.2 ppm).

3.4.8 References

1. B. R. Hubble, Siegel, S., Fuchs, L. H., Hoekstra, H. R., Tani, B., and Cunningham, P.T, "The Formation of $Mg_3Ca(SO_4)_4$ During the Sulfation Reaction of Dolomite," J. Air Pollut. Control Assoc., Vol. 27, No. 4, pp. 343-346 (1977).

2. J. J. Rowe, Morey, G. W., and Silber, C. C., "The Ternary System K_2SO_4—$MgSO_4$—$CaSO_4$.," J. Inorg. Nucl. Chem., Vol. 29, No. 4, pp. 925-942 (1967).

3. D. H. Smith, Haddad, G. J., and Grimm, U., "Composition and Chemistry of Particulates from a PFBC Demonstration Plant," Fuel, Vol. 76, No. 8, pp. 727-732 (1997a).

4. D. H. Smith, Haddad, G. J., and Ferer M., "Shear Strengths of Heated and Unheated Mixtures of $MgSO_4$ and $CaSO_4$ Powders," Energy & Fuels, Vol. 11, No. 5, pp. 1006-1011 (1997b).

Table 3.4-1

Summary of Inlet Particulate Loadings Measured During TC05

SRI Run No.	Date	Start Time	End Time	Coal	Limestone	Test Condition	PCD Pulse	Loading, ppmw
TC05IMT-01	1/18/99	13:15	13:31	Alabama	Ohio	Stable	No	12,000
TC05IMT-02	1/19/99	10:10	10:35	Alabama	Ohio	Stable	No	7,900
Average With Alabama Coal And Ohio Limestone								**10,000**
TC05IMT-03	1/20/99	9:55	10:20	Alabama	Alabama	Stable	No	9,000
TC05IMT-04	1/21/99	10:25	10:40	Alabama	Alabama	Stable	No	11,700
System shut down on 1/22/99 to repair PCD leaks and install additional filter elements.								
TC05IMT-05	2/3/99	14:30	15:00	Alabama	Alabama	Stable	No	9,000
TC05IMT-06	2/4/99	11:15	11:45	Alabama	Alabama	Stable	Yes	22,200[1]
Average With Alabama Coal And Alabama Limestone[2]								**9,900**
TC05IMT-07	2/8/99	10:35	11:05	Illinois	Ohio	Stable	No	13,900
TC05IMT-08	2/9/99	10:40	11:00	Illinois	Ohio	Stable	No	13,900
TC05IMT-09	2/11/99	9:20	9:50	Illinois	Ohio	Stable	No	15,600
TC05IMT-10	2/12/99	12:55	13:15	Illinois	Ohio	Stable	No	15,700
Average With Illinois Coal And Ohio Limestone								**14,800**
TC05IMT-11	2/15/99	12:21	12:41	Illinois	Alabama	Stable	No	-----[3]
TC05IMT-12	2/18/99	11:05	11:25	Illinois	Alabama	Stable	No	13,500
TC05IMT-13	2/19/99	9:45	10:05	Illinois	Alabama	Stable	No	15,700
Average With Illinois Coal And Alabama Limestone								**14,600**
System shut down on 2/24/99 to replace broken filter elements and repair other PCD leaks.								
TC05IMT-14	3/05/99	12:18	12:48	Pet Coke	Dolomite	Stable	No	14,800
System shut down on 3/06/99 to inspect PCD. Severe ash bridging in PCD.								
TC05IMT-15	3/15/99	10:42	11:12	Pet Coke	Dolomite	Stable	No	19,300

Continued on next page

Table 3.4-1 (Page 2 of 2)

Summary of Inlet Particulate Loadings Measured During TC05

SRI Run No.	Date	Start Time	End Time	Coal	Limestone	Test Condition	PCD Pulse	Loading, ppmw
TC05IMT-16	3/16/99	10:05	10:35	Pet Coke	Dolomite	Stable	No	23,100
TC05IMT-17	3/17/99	10:45	11:15	Pet Coke	Dolomite	Stable	No	25,600
TC05IMT-18	3/18/99	9:33	10:03	Pet Coke	Dolomite	Stable	No	22,900
Average With Pet Coke And Dolomite								**21,100**
TC05IMT-19	3/22/99	10:00	10:30	Pet Coke	Ohio LS	Stable	No	16,100
System shut down on 3/23/99 due to failure of coal feeder and start-up burner.								
TC05IMT-20	3/26/99	9:38	10:38	Pet Coke	Ohio LS	Stable	No	12,100
Average With Pet Coke and Ohio Limestone								**14,100**
End of Pet Coke Testing. Shut down system to drain reactor and combustion heat exchanger.								
TC05IMT-21	4/13/99	9:52	10:22	Alabama	Ohio LS	Unstable	No	14,200[1]
TC05IMT-22	4/14/99	11:30	12:00	Alabama	Ohio LS	Unstable	No	16,200[1]
TC05IMT-23	4/15/99	11:48	12:18	Alabama	Ohio LS	Stable	No	10,200
TC05IMT-24	4/16/99	9:18	9:48	Alabama	Ohio LS	Stable	No	10,800
Average With Alabama Coal and Ohio Limestone								**10,500**
TC05IMT-25	4/19/99	11:26	11:51	PRB	Ohio LS	Stable	No	5,700
TC05IMT-26	4/20/99	10:15	11:00	PRB	Ohio LS	Unstable	Yes	18,100[1]
TC05IMT-27	4/21/99	9:30	11:00	PRB	Ohio LS	Stable	Yes	4,000
TC05IMT-28	4/22/99	9:28	11:28	PRB	None	Stable	Yes	3,200
TC05IMT-29	4/26/99	9:20	11:20	PRB	Ohio LS	Unstable	Yes	9,400[1]
TC05IMT-30	4/27/99	9:30	10:00	PRB	Florida LS	Stable	No	4,600
Average With PRB Coal and Ohio Limestone								**4,800**

1. Sample included bed material from loss-of-cyclone dipleg seal.
2. Average excludes run TC05IMT-06 which was contaminated with bed material.
3. Sampler leaked; result invalid.

Table 3.4-2

Outlet Particulate Loadings and Collection Efficiencies Measured During TC05

SRI Run No.	Date	Start Time	End Time	Inlet Loading, ppmw	Outlet Loading, ppmw	Blank, ppmw	Collection Efficiency, %
TC05OMT-01	1/18/99	9:30	14:00	12,000	10.9	-0.02	99.91
TC05OMT-02	1/19/99	10:00	13:00	7,900	10.2	0.01	99.87
TC05OMT-03	1/20/99	9:30	13:00	9,000	16.0	0.06	99.82
TC05OMT-04	1/21/99	9:30	12:30	11,700	20.0	-0.05	99.83
TC05OMT-05	1/22/99	8:32	10:02	9,900[1]	21.8	0.01	99.78
System shut down on 1/22/99 to repair PCD leaks and install additional filter elements.							
TC05OMT-06	2/3/99	9:15	13:15	9,000	1.32	0.20	99.99
TC05OMT-07	2/4/99	10:05	13:45	9,900[1]	2.24	0.10	99.98
TC05OMT-08	2/8/99	9:30	13:30	13,900	4.92	0.00	99.96
TC05OMT-09	2/9/99	9:20	13:20	13,900	5.61	0.09	99.96
TC05OMT-10	2/11/99	9:00	13:15	15,600	6.11	0.05	99.96
TC05OMT-11	2/12/99	10:30	13:30	15,700	7.14	0.07	99.95
TC05OMT-12	2/15/99	9:30	13:30	14,800	5.12	0.14	99.96
TC05OMT-13	2/17/99	9:00	13:00	13,300	3.37	0.12	99.97
TC05OMT-14	2/18/99	10:22	13:22	13,500	4.83	0.14	99.96
TC05OMT-15	2/19/99	9:00	13:00	15,700	5.34	0.13	99.97
System shut down on 2/22/99 because of ash discharge plugging and broken filter elements.							
Sorbent injected on 2/24/99 without coal fire to test PCD leakage.							
TC05OMT-16	2/24/99	9:15	10:15	14,600[1]	407	-1.19	97.21
System shut down on 2/24/99 to replace broken filter elements and repair other PCD leaks.							
TC05OMT-17	3/05/99	9:25	13:25	14,800	0.09	-0.05	99.9994
System shut down on 3/06/99 to inspect PCD. Severe ash bridging in PCD.							

Table 3.4-2 (Page 2 of 2)
Outlet Particulate Loadings and Collection Efficiencies Measured During TC05

SRI Run No.	Date	Start Time	End Time	Inlet Loading (ppmw)	Outlet Loading (ppmw)	Blank (ppmw)	Collection Efficiency (%)
TC05OMT-18	3/15/99	9:50	13:50	19,300	0.08	-0.14	99.9996
TC05OMT-19	3/16/99	9:15	13:15	23,100	0.10	-0.06	99.9996
TC05OMT-20	3/17/99	9:20	13:30	25,600	0.17	0.01	99.9993
TC05OMT-21	3/18/99	9:25	13:35	22,900	0.11	-0.09	99.9995
TC05OMT-22	3/22/99	8:45	12:46	16,100	0.14	-0.07	99.9991
System shut down on 3/23/99 due to failure of coal feeder and start-up burner.							
TC05OMT-23	3/26/99	9:00	13:00	12,100	0.01	-0.11	99.9999
End of Pet Coke Testing. Shut down system to drain reactor and combustion heat exchanger.							
TC05OMT-24	4/13/99	9:00	13:10	10,500[2]	1.00	0.14	99.990
TC05OMT-25	4/14/99	11:20	14:20	10,500[2]	0.68	0.17	99.994
TC05OMT-26	4/15/99	10:15	13:20	10,200	1.27	0.17	99.988
TC05OMT-27	4/16/99	8:20	12:20	10,800	2.13	0.13	99.980
TC05OMT-28	4/19/99	9:30	13:30	5,700	0.41	0.09	99.993
TC05OMT-30	4/21/99	9:20	11:50	4,000	0.38	0.14	99.991
TC05OMT-34	4/26/99	9:00	11:15	4,800[2]	0.28	-0.02	99.994
TC05OMT-35	4/27/99	9:28	13:28	4,600	0.22	0.06	99.995
TC05OMT-37	4/29/99	9:35	12:35	6,500[3]	0.29	0.05	99.996

1. No inlet loading was measured on this day. Collection efficiency was calculated using the average inlet loading for this coal-sorbent combination.
2. Inlet loading was measured during a dipleg upset. Collection efficiency was calculated using average inlet loading excluding runs during dipleg upsets.
3. No inlet loading was measured on this day. Collection efficiency calculated using the average inlet loading from TC03 tests with Eastern Kentucky coal and Florida limestone.

Table 3.4-3

Summary of Hot-Gas Filter Performance During Major Portions of TC05

Dates	Fuels	Sorbents	Filter Operating Temperature (°F)	Filter Face Velocity (ft/min)	Avg Inlet Loading (ppmw)	Outlet Loading (ppmw)	Collection Efficiency (%)
Beginning of TC05. Some filter elements blanked off to increase filter face velocity.							
1/18/99 to 1/19/99	**Alabama**	**Ohio LS**	**1,400**	**8**	**10,000**	**10.6**	**99.9**
1/20/99 to 1/22/99	**Alabama**	**Alabama LS**	**1,400**	**8**	**10,200**	**19.3**	**99.8**
System shut down due to increasing outlet loading. Found several pinhole leaks at element flanges and one hole in McDermott element. Leaking elements and all McDermott elements replaced. Full set of elements installed to reduce filter face velocity.							
2/03/99 to 2/04/99	**Alabama**	**Alabama LS**	**1,400**	**5-6**	**9,500**	**1.8**	**99.98**
2/08/99 to 2/12/99	**Illinois**	**Ohio LS**	**1,400**	**5-6**	**14,800**	**5.8**	**99.96**
2/15/99 to 2/19/99	**Illinois**	**Alabama LS**	**1,400**	**5-6**	**14,300**	**4.7**	**99.97**
Shut down due to ash discharge plugging. Found element fragments. Sampling with sorbent feed with no coal revealed leak of about 400 ppmw. Found three broken DuPont elements and one missing gasket. Gasket and all DuPont elements replaced.							
3/05/99 to 3/06/99	**Pet Coke**	**PR Dolomite**	**1,400**	**6**	**14,800**	**0.09**	**99.9994**
System shut down due to ash discharge plugging Found severe ash bridging between filter elements after 30 hours on pet coke and dolomite. Deposits removed and primary gas cooler placed in service to reduce filter operating temperature.							
3/15/99 to 3/22/99	**Pet Coke**	**PR Dolomite**	**750**	**3-4**	**21,400**	**0.12**	**99.9994**
3/26/99	**Pet Coke**	**Ohio LS**	**750**	**3-4**	**12,100**	**0.01**	**99.9999**
System shut down to drain reactor and combustion heat exchanger. Restarted with primary gas cooler partially bypassed (?).							
4/13/99 to 4/16/99	**Alabama**	**Ohio LS**	**1,190-1,250**	**4-5**	**10,500**	**1.3**	**99.99**
4/19/99 to 4/26/99	**PRB**	**Ohio LS**	**1,100-1,140**	**4-5**	**4,800**	**0.36**	**99.993**
4/27/99	**PRB**	**Florida LS**	**1,180**	**4-5**	**4,600**	**0.22**	**99.995**
End of TC05							

Table 3.4-4

Results of Chemical Analyses Performed on Selected TC05 In situ Sample

SRI Run No.	Date Sampled	Coal Type	Sorbent Type	Gas Cooler in Service	Wt % Al_2O_3	Wt % CaO	Wt % Fe_2O_3	Wt % MgO	Wt % P_2O_5	Wt % K_2O	Wt % SiO_2	Wt % Na_2O	Wt % SO_3	Wt % TiO_2	Wt % V_2O_5	Sum of Oxides, Wt %
TC05IMT-2	01/19/99	Alabama	Ohio L.S.	No	20.10	10.45	4.59	3.05	0.27	2.25	42.66	0.15	9.25	0.88	0.04	93.69
TC05IMT-6	02/04/99	Alabama	Alabama L.S.	No	11.03	11.77	4.52	2.29	0.25	1.19	47.39	0.67	14.75	0.62	0.04	94.52
TC05IMT-9	02/11/99	Illinois	Ohio L.S.	No	7.44	23.17	6.42	5.77	0.02	1.05	20.02	0.31	20.00	0.33	0.02	84.55
TC05IMT-12	02/18/99	Illinois	Alabama L.S.	No	8.86	20.37	6.39	3.53	0.14	0.99	26.66	0.97	24.70	0.38	0.04	93.03
TC05IMT-14	03/05/99	Pet Coke	P.R. Dolomite	No	4.89	23.90	2.06	15.84	0.02	0.75	11.25	0.22	39.25	0.10	0.79	99.07
TC05IMT-14[1]	03/05/99	Pet Coke	P.R. Dolomite	No	2.13	24.27	1.38	15.73	0.03	0.67	14.36	0.15	37.00	0.09	0.64	96.45
TC05IMT-16[1]	03/16/99	Pet Coke	P.R. Dolomite	Yes	0.99	32.24	0.92	20.22	0.05	0.28	5.76	0.10	36.50	0.05	0.59	97.70
TC05IMT-20	03/26/99	Pet Coke	Ohio L.S.	Yes	2.49	37.09	0.80	9.14	0.02	0.01	6.74	0.01	42.33	0.10	0.80	99.53
TC05IMT-23	04/15/99	Alabama	Ohio L.S.	Yes[2]	17.50	11.70	4.20	3.10	0.30	2.40	39.70	0.10	8.60	0.80	N.M.	88.40
TC05IMT-27	04/21/99	PRB	Ohio L.S.	Yes[2]	15.19	22.32	5.42	5.01	0.53	0.64	31.64	0.59	11.50	1.07	N.M.	93.91
TC05IMT-28	04/22/99	PRB	None	Yes[2]	17.01	23.27	5.15	4.33	1.26	0.47	24.50	1.74	23.60	1.38	N.M.	102.71

Calculated Parameters

SRI Run No.	Date Sampled	Coal Type	Sorbent Type	Gas Cooler in Service	S/Ca Molar Ratio	Wt % $CaSO_4$	Wt % $Mg_3Ca(SO_4)_4$	Wt % $CaCO_3$	Wt % MgO
TC05IMT-2	01/19/99	Alabama	Ohio L.S.	No	0.62	15.73	0.00	7.10	3.05
TC05IMT-6	02/04/99	Alabama	Alabama L.S.	No	0.88	25.08	0.00	2.58	2.29
TC05IMT-9	02/11/99	Illinois	Ohio L.S.	No	0.60	34.00	0.00	16.38	5.77
TC05IMT-12	02/18/99	Illinois	Alabama L.S.	No	0.85	41.99	0.00	5.50	3.53
TC05IMT-14	03/05/99	Pet Coke	P.R. Dolomite	No	1.15	55.15	10.58	0.00	13.27
TC05IMT-14[1]	03/05/99	Pet Coke	P.R. Dolomite	No	1.07	57.62	4.82	0.00	14.56
TC05IMT-16[1]	03/16/99	Pet Coke	P.R. Dolomite	Yes	0.79	62.05	0.00	11.95	20.22
TC05IMT-20	03/26/99	Pet Coke	Ohio L.S.	Yes	0.80	71.96	0.00	13.32	9.14
TC05IMT-23	04/15/99	Alabama	Ohio L.S.	No	0.51	14.62	0.00	10.14	3.10
TC05IMT-27	04/21/99	PRB	Ohio L.S.	No	0.36	19.55	0.00	25.48	5.01
TC05IMT-28	04/22/99	PRB	None	No	0.71	40.12	0.00	12.05	4.33

Procedure for Calculating Chemical Composition

Let X, Y, Z = Wt % CaO, SO_3, MgO from chemical analysis as oxides

From solution of component mass balance equations for Ca, Mg, and S:

If S/Ca < 1:

Wt % $CaSO_4$ = 136 * Y / 80

Wt % $Mg_3Ca(SO_4)_4$ = 0

Wt % $CaCO_3$ = 100 * (X / 56 - Wt % $CaSO_4$ / 136)

Wt % MgO = Z

If S/Ca > 1:

Wt % $CaSO_4$ = 136 * (4 * X / 56 - Y / 80)/3

Wt % $Mg_3Ca(SO_4)_4$ = 497 * (Y / 80 - X / 56) / 3

Wt % $CaCO_3$ = 0

Wt % MgO = 40.3 * (Z / 40.3 - Y / 80 + X / 56)

1. Analysis done in SRI's Birmingham Laboratories. 2. Gas cooler partially bypassed.

Table 3.4-5

Results of Chemical Analyses Performed on Selected TC05 Dustcake Sample

Type of Shutdown and Dustcake Sample	Sample Location (Element No./ Location on Element)	Date Sampled	Wt % Al_2O_3	Wt % CaO	Wt % Fe_2O_3	Wt % MgO	Wt % P_2O_5	Wt % K_2O	Wt % SiO_2	Wt % Na_2O	Wt % SO_3	Wt % TiO_2	Wt % V_2O_5	Sum of Oxides, Wt %
Dirty/Residual	T-12/Inner Surface	01/26/99	20.14	9.51	4.89	2.14	0.34	2.06	42.63	0.19	10.29	1.07	N.M.	93.26
Dirty/Transient	T-12/Inner Surface	01/26/99	21.69	12.22	5.42	2.42	0.37	2.06	44.79	0.22	8.24	1.10	N.M.	98.53
Dirty/Transient	T-12/Outer Surface	01/26/99	22.88	9.30	5.52	2.21	0.37	2.02	46.40	0.19	9.51	1.10	N.M.	99.50
Dirty/Residual	T-12/Windward Surface	01/26/99	20.50	10.83	5.13	2.25	0.37	1.99	43.08	0.16	10.14	1.07	N.M.	95.52
Dirty/Transient	T-12/Windward Surface	01/26/99	22.43	9.44	3.79	1.51	0.57	2.42	50.59	0.18	8.91	0.87	N.M.	100.71
Dirty/Transient	T-12/Leeward Surface	01/26/99	21.39	12.16	5.39	2.37	0.37	2.02	43.57	0.19	7.39	1.08	N.M.	95.93
Ash Bridging	Upper Tier/Bridged Mass	03/10/99	2.61	20.88	1.74	13.24	0.03	0.49	8.26	0.20	46.80	0.12	0.66	95.03
Normal/Residual	T-12/Entire Surface	05/07/99	11.34	30.05	4.12	1.04	0.02	1.45	24.52	0.19	26.08	0.60	0.04	99.45

Calculated Parameters

Type of Shutdown and Dustcake Sample	Sample Location (Element No./ Location on Element)	Date Sampled	S/Ca Molar Ratio	Wt % $CaSO_4$	Wt % $Mg_3Ca(SO_4)_4$	Wt % $CaCO_3$	Wt % MgO	Calculation Procedures (Refer to Table 1 for Definitions of X, Y, and Z)	
Dirty/Residual	T-12/Inner Surface	01/26/99	0.76	17.49	0.00	4.12	2.14	If S/Ca < 1:	Wt % $CaSO_4$ = 136 * Y / 80
Dirty/Transient	T-12/Inner Surface	01/26/99	0.47	14.01	0.00	11.52	2.42		Wt % $Mg_3Ca(SO_4)_4$ = 0
Dirty/Transient	T-12/Outer Surface	01/26/99	0.72	16.17	0.00	4.72	2.21		Wt % $CaCO_3$ = 100 * (X / 56 - Wt % $CaSO_4$ / 136)
Dirty/Residual	T-12/Windward Surface	01/26/99	0.66	17.24	0.00	6.66	2.25		Wt % MgO = Z
Dirty/Transient	T-12/Windward Surface	01/26/99	0.66	15.15	0.00	5.72	1.51	If S/Ca > 1:	Wt % $CaSO_4$ = 136 * (4 * X / 56 - Y / 80)/3
Dirty/Transient	T-12/Leeward Surface	01/26/99	0.43	12.56	0.00	12.48	2.37		Wt % $Mg_3Ca(SO_4)_4$ = 497 * (Y / 80 - X / 56) / 3
Ash Bridging	Upper Tier/Bridged Mass	03/10/99	1.57	41.09	35.15	0.00	4.69		Wt % $CaCO_3$ = 0
Normal/Residual	T-12/Entire Surface	05/07/99	0.61	44.34	0.00	21.06	1.04		Wt % MgO = 40.3 * (Z / 40.3 - Y / 80 + X / 56)

Table 3.4-6

Physical Properties of Selected TC05 In situ Samples

SRI Run No.	Date Sampled	Chem Lab ID No.	Coal Type	Sorbent Type	Gas Cooler in Service	Bulk Density, g/cm^3	True Density, g/cm^3	Uncom-pacted Bulk Porosity, %	BET Specific Surface Area, m^2/g	Mass Median Diameter, μm	Drag-Equivalent Diameter, μm	Lab-Measured Drag, in.H_2O/(ft/min.)/(lb/ft^2)	Viscosity-Corrected Lab Drag, in.H_2O/(ft/min.)/(lb/ft^2)	PCD Transient Drag, in.H_2O/(ft/min.)/(lb/ft^2)
TC05IMT-2	01/19/99	AB05406	Alabama	Ohio L.S.	No	0.53	2.50	78.8	1.96	19.9	2.7	4.7	10.8	22.2
TC05IMT-6	02/04/99	AB04692	Alabama	Alabama L.S.	No	0.85	2.69	68.4	0.80	20.7	5.2	4.7	10.8	3.0
TC05IMT-9	02/11/99	AB05407	Illinois	Ohio L.S.	No	0.68	2.86	76.2	2.56	21.6	3.7	3.3	7.6	5.3
TC05IMT-12	02/18/99	AB04789	Illinois	Alabama L.S.	No	0.57	2.86	80.1	1.78	17.6	3.0	2.6	6.0	3.6
TC05IMT-14	03/05/99	AB04851	Pet Coke	P.R. Dolomite	No	0.82	2.88	71.5	0.67	37.0	9.9	0.8	1.8	0.1
TC05IMT-16	03/16/99	AB05408	Pet Coke	P.R. Dolomite	Yes	0.87	3.05	71.5	1.01	27.5	6.1	2.0	3.4	1.5
TC05IMT-20	03/26/99	AB05409	Pet Coke	Ohio L.S.	Yes	0.88	2.91	69.8	0.69	28.4	8.2	1.4	2.4	0.7
TC05IMT-23	04/15/99	AB05260	Alabama	Ohio L.S.	Yes[1]	0.53	2.55	79.2	1.78	19.8	2.8	4.0	8.6	19.8
TC05IMT-27	04/21/99	AB05410	PRB	Ohio L.S.	Yes[1]	0.64	2.78	77.0	1.02	21.8	4.2	2.3	4.9	4.2
TC05IMT-28	04/22/99	AB05411	PRB	None	Yes[1]	0.72	2.78	74.1	0.46	24.2	5.2	2.2	4.7	4.1

1. Gas cooler partially bypassed.

Table 3.4-7

Physical Properties of Selected TC05 Dustcake Samples

Type of Shutdown and Dustcake Sample	Sample Location (Element No./ Location on Element	Date Sampled	Chem Lab ID No.	Bulk Density, g/cm^3	True Density, g/cm^3	Uncom-pacted Bulk Porosity, %	BET Specific Surface Area, m^2/g	Mass Median Diameter, μm	Drag-Equivalent Diameter, μm	Lab Drag* @FCP (Residual) or UBP (Transient)	PCD Face Velocity Prior to Shutdown, ft/min.	Residual PCD Drag (Res) or Transient PCD Drag (Transient)
Dirty/Residual	T-12/Inner Surface	01/26/99	AB04366	0.51	2.68	81.0	2.00	11.4	1.9	30.0	7.8	30.2
Dirty/Transient	T-12/Inner Surface	01/26/99	AB04367	0.47	2.72	82.7	2.51	11.8	1.7	5.8	7.8	7.1
Dirty/Transient	T-12/Outer Surface	01/26/99	AB04369	0.47	2.57	81.7	2.75	11.0	1.9	5.5	7.8	7.1
Dirty/Residual	T-12/Windward Surface	01/26/99	AB04370	0.55	2.63	79.1	1.35	18.2	2.6	29.0	7.8	26.3
Dirty/Transient	T-12/Windward Surface	01/26/99	AB04371	0.56	2.63	78.7	3.06	15.8	2.1	7.2	7.8	7.1
Dirty/Transient	T-12/Leeward Surface	01/26/99	AB04373	0.53	2.63	79.8	3.40	11.1	1.8	8.7	7.8	7.1
Ash Bridging	Upper Tier/Bridged Mass	03/10/99	AB04909	0.54	2.60	79.2	1.59	24.4	8.7	8.8	6.0	0.03
Normal/Residual	T-12/Entire Surface	05/07/99	AB05413	0.55	2.80	80.4	3.91	6.7	1.8	37.7	5.3	27.7

* Drag corrected to viscosity of process gas.

Table 3.4-8

Measurements of Acid Gases (SO_2, SO_3, HCl, HF) During TC05 (Page 1 of 2)

Date	Time Period [1]	Coal	Limestone	Measured Concentration, ppmv				
				SO_2 Manual Meas.	SO_2 Plant Analyzer	SO_3 Manual Meas.	HCl Manual Meas.	HF Manual Meas.
2/4/99	10:02 to 10:54	Alabama	Alabama	36	12	14	27	7.0
2/4/99	11:13 to 12:22	Alabama	Alabama	67	16	50	17	5.4
2/4/99	12:55 to 13:36	Alabama	Alabama	53	10	44	16	4.8
--	**Average**			52	13	36	20	5.7
--	**Standard Deviation**			16	3.1	19	6.1	1.1
2/9/99	9:20 to 10:19	Illinois	Ohio	29	9	26	26	8.2
2/9/99	10:35 to 11:38	Illinois	Ohio	26	10	26	35	5.4
2/9/99	11:57 to 12:58	Illinois	Ohio	27	12	26	30	7.9
--	**Average**			27	10	26	30	7.2
--	**Standard Deviation**			1.5	1.5	0	4.5	1.5
2/18/99	10:22 to 11:20	Illinois	Alabama	12	1.6	8	52	5.6
2/18/99	11:45 to 12:42	Illinois	Alabama	12	0	7.0	50	5.0
2/18/99	13:44 to 14:47	Illinois	Alabama	11	1.2	6.0	48	6.0
--	**Average**			12	0.9	7.0	50	5.5
--	**Standard Deviation**			0.6	0.8	1.0	2.0	0.5
3/17/99	9:26 to 10:30	Pet Coke	Dolomite	22	13	1.0	15	< 1.9
3/17/99	10:52 to 11:45	Pet Coke	Dolomite	8.7	4.2	0.4	17	< 1.8
3/17/99	12:23 to 13:02	Pet Coke	Dolomite	3.4	0.5	0.3	12	< 2.7
--	**Average**			11	5.9	0.6	15	< 2.1
--	**Standard Deviation**			10	6.4	0.4	3	< 0.5

Continued on next page

Table 3.4-8

Measurements of Acid Gases (SO_2, SO_3, HCl, HF) During TC05 (Page 2 of 2)

Date	Time Period [1]	Coal	Limestone	Measured Concentration, ppmv				
				SO_2 Manual Meas.	SO_2 Plant Analyzer	SO_3 Manual Meas.	HCl Manual Meas.	HF Manual Meas.
4/15/99	10:17 to 11:37	Alabama	Ohio	13	4.3	5.9	11	< 2.1
4/15/99	12:31 to 13:26	Alabama	Ohio	53	14	31	15	3.7
4/15/99	13:49 to 14:41	Alabama	Ohio	22	4.8	13	14	5.0
--	**Average**			29	7.7	17	13	3.6
--	**Standard Deviation**			21	5.5	13	2.1	1.5
4/22/99	9:02 to 9:50	PRB	None	6.8	4.3	0.7	< 2.2	< 1.2
4/22/99	10:07 to 10:55	PRB	None	8.2	4.8	0.8	< 2.2	< 1.2
4/22/99	11:11 to 12:01	PRB	None	8.9	5.1	1.2	< 2.2	< 1.2
	Average			8.0	4.7	0.9	< 2.2	< 1.2
--	**Standard Deviation**			1.1	0.4	0.3	< 1.2	< 0.7

1. Measurements were not taken over the entire time period. Typically, SO_2/SO_3 was measured first, for about 15 minutes, then HCl/HF was measured the final 15 minutes of the time period. The balance of time was spent changing the test apparatus.

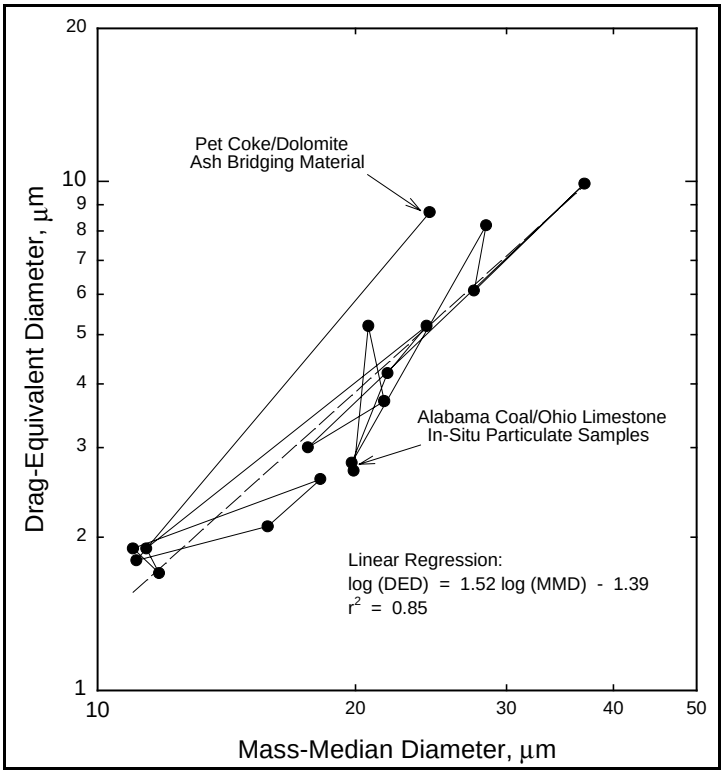

Figure 3.4-1 Effect of Particle Size on Drag Equivalent Diameter of Inlet Dust Samples and Dustcake Samples

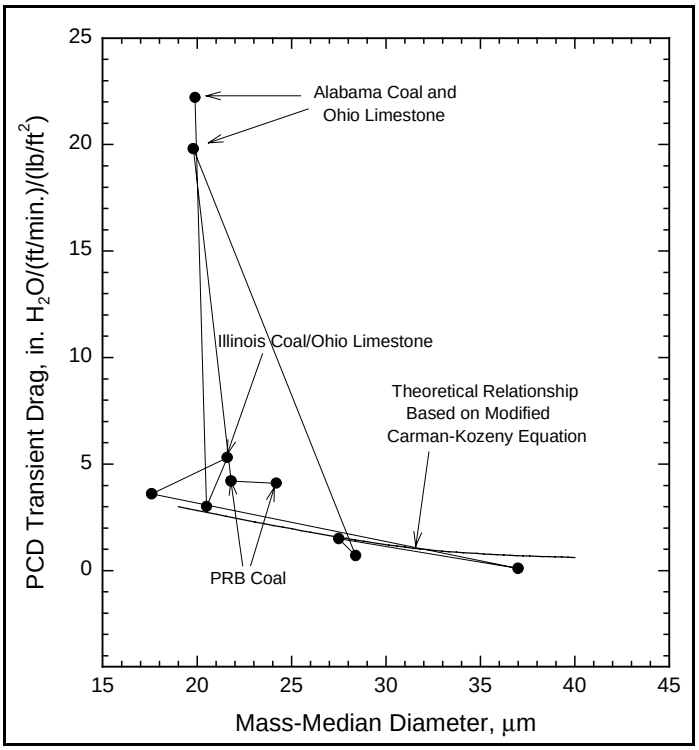

Figure 3.4-2 Effect of Particle Size on PCD Transient Drag During TC05 In situ Sampling Runs

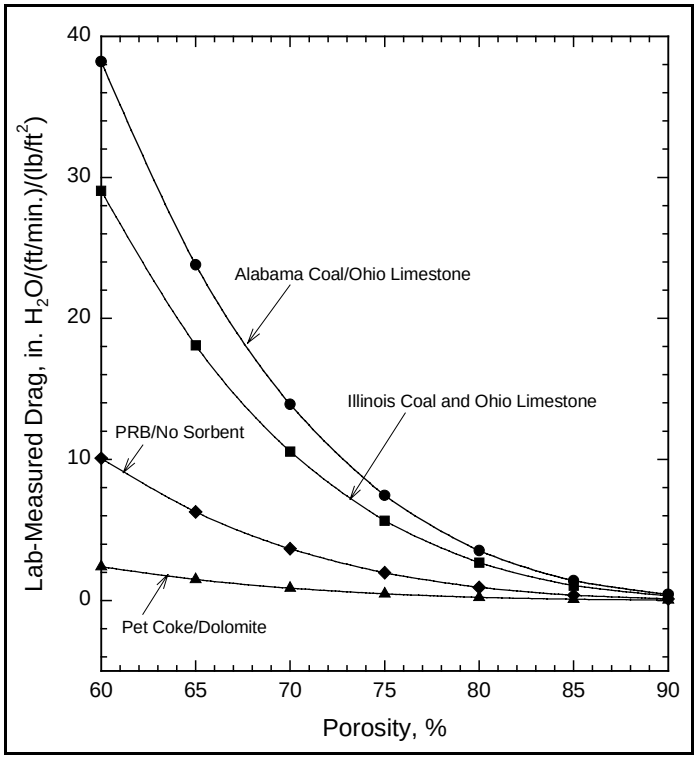

Figure 3.4-3 Lab Measured Drag Versus Porosity Curves for Various Inlet Dust Samples

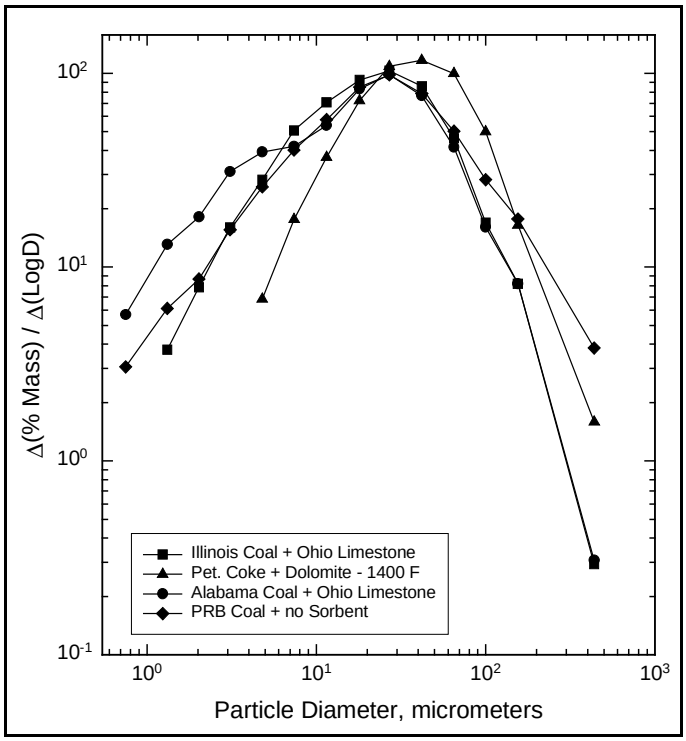

Figure 3.4-4 Particle-Size Distributions of the Four Inlet Dust Samples With Laboratory Drag Measurements Shown in Figure 3.4-3

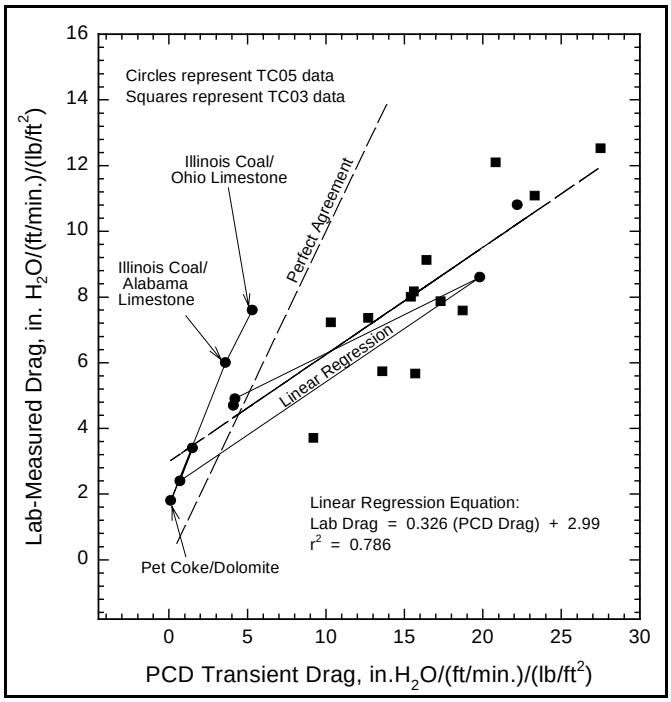

Figure 3.4-5 Relationship Between Lab Measured Drag (at Uncompacted Bulk Porosity) and PCD Transient Drag for all TC05 and TC03 Inlet Dust Samples

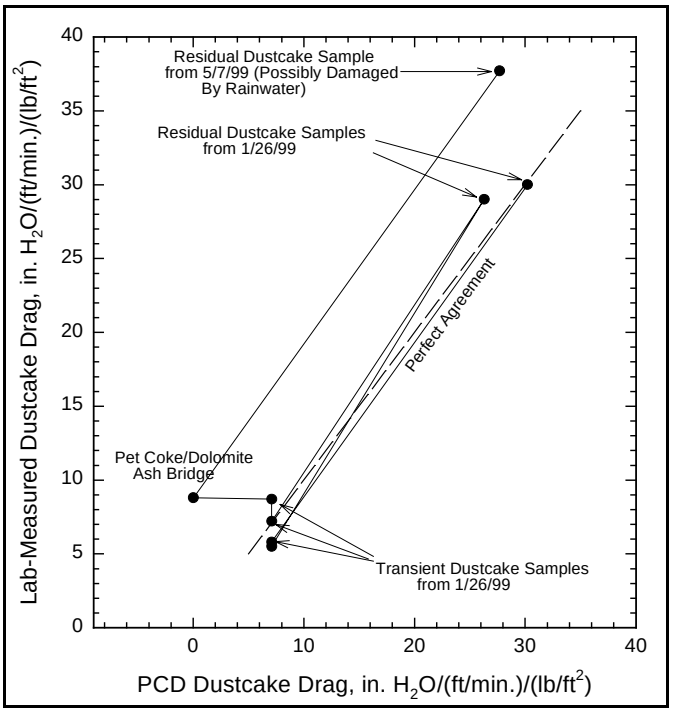

Figure 3.4-6 Relationships Between PCD Residual Dustcake Drag and Lab-Measured Drag at Flow-Compacted Porosity and Between PCD Transient Dustcake Drag and Lab-Measured Drag at Uncompacted Bulk Porosity

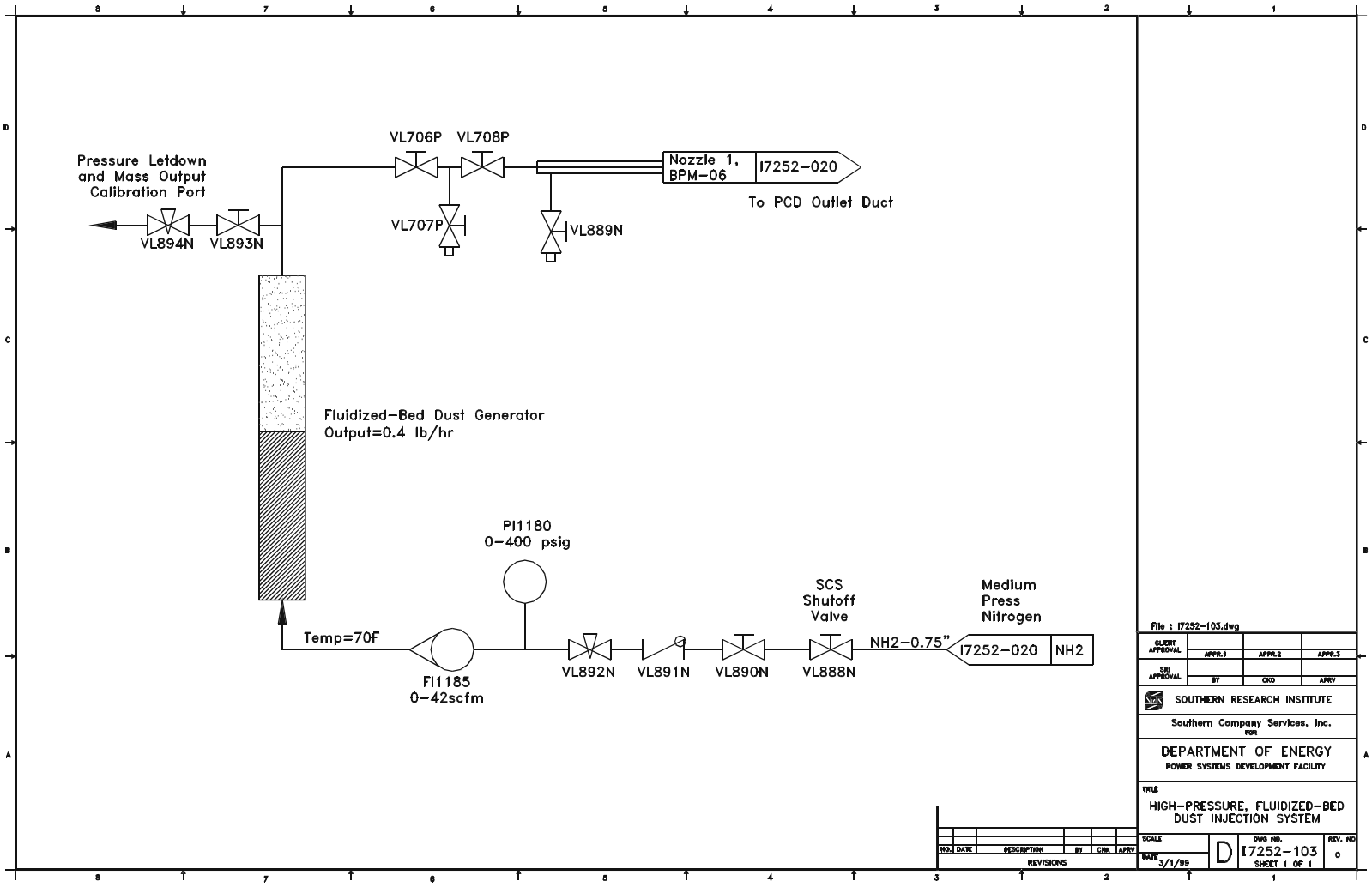

Figure 3.4-7 Piping and Instrument Diagram of Ash Injection System

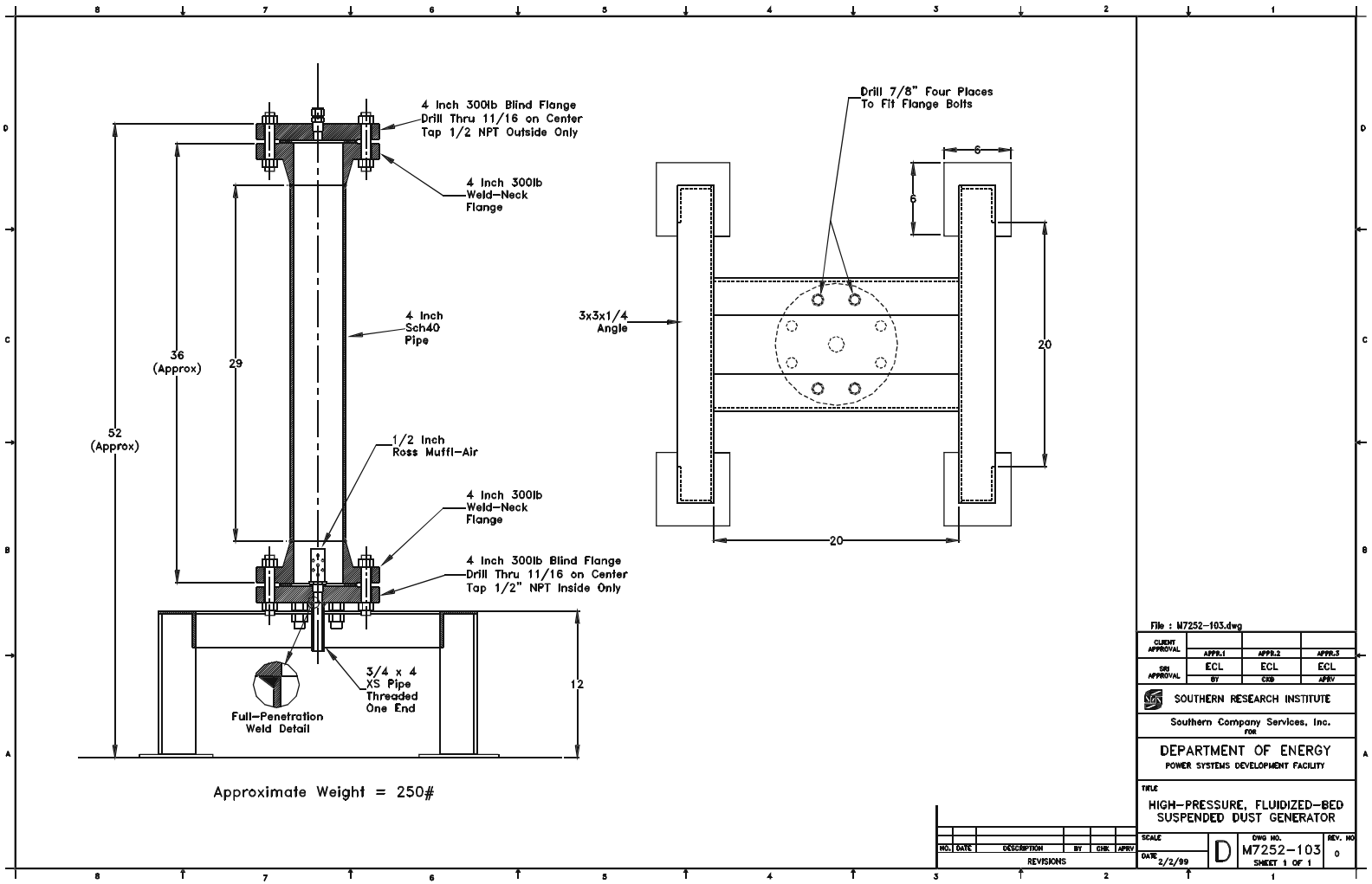

Figure 3.4-8 Ash Injection System Fluidized-Bed Assembly

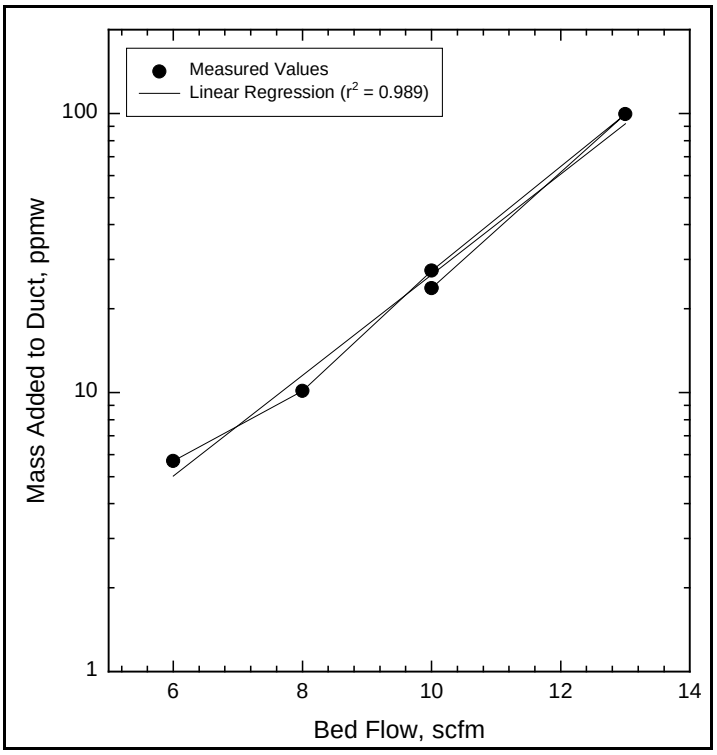

Figure 3.4-9 Ash Injection System Mass Output

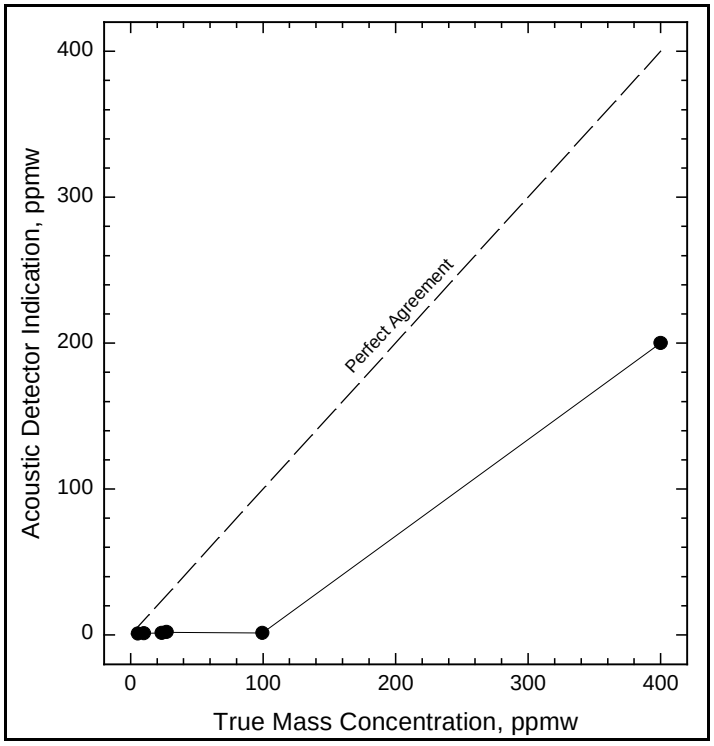

Figure 3.4-10 Jonas Particulate Monitor Results

3.5 FINES HANDLING SYSTEM

3.5.1 Operational Summary

The spent fines transport system (FD0520) required significant maintenance during the test campaign. Most of the problems were related to the following issues:

1. The dense-phase dispense vessel outlet line would plug and the ash could not be transferred to the spent-solids surge bin (FD0530).

2. The lock-vessel vent valve (XV8539) would wear and lose the ability to seal.

Performing on-line maintenance on the FD0520 system was often possible due to certain piping and valving changes implemented at the PSDF. This on-line maintenance allowed the run to continue on several occasions. Figure 3.5-1 shows the FD0520 system. The system was manufactured by Clyde Pneumatic Conveying Ltd. of England.

The spent fines screw cooler (FD0502) showed some operational improvements during the test campaign. During 1998 FD0502 was modified as follows:

1. The screw pitch was changed from 3 to 6 inches. The goal was to increase the ash removal rate.

2. The inlet-side internal ceramic bushing bearing was replaced with an external pillow block bearing similar to the drive-side arrangement. The goal was to eliminate the excessive wear associated with the ceramic bushing and thereby eliminate the noise and vibration experienced during previous runs. Figure 3.5-2 shows FD0502 with the original ceramic bushing bearing and the original inlet-side seal. Figure 3.5-3 shows FD0502 with the modified external pillow block bearing and the modified inlet-side seal.

The TC05 operational experience suggests that these two modifications were successful. However, the drive-side seal was a continuous operational challenge. There was repeated leakage between the packing and the shaft. This leakage required constant monitoring but did not force a stoppage of the run. The system was manufactured by Christian Engineering.

3.5.2 Spent Fines Transport System (FD0520) - Observations and Events

A. *January 15 at 11:20:* Level Probe Malfunction – The level probe continuously read a high level. This caused the lock vessel spheri valve to remain closed.

B. *January 16 at 06:00*: Lock Vessel Spheri Valve Leakage.

C. *January 21 at 14:30*: Lock Vessel Vent Valve Failure.

D. *February 03 at 08:00:* Discharge Line Plugged – The discharge line was cleaned out using a rod. A small piece of fused ash was removed.

E. *February 12 at 01:55:* Discharge Line Plugged – The discharge line was cleaned out using a rod.

F. *February 15 at 17:26:* FD0520 System Trip – The system tripped on high-dispense vessel pressure.

G. *February 15 at 23:07:* Lock Vessel Vent Valve Failure – The lock vessel vent valve was not sealing. The valve was replaced.

H. *February 16 at 05:30:* Discharge Line Plugged – The discharge elbow was removed. A broken fluffing nozzle from the PCD Cone was found in the discharge piping.

I. *February 16 at 12:00:* Pressurization Valve Failure – It was determined that the pressurization valve was leaking. No spare valve was available. The run was not interrupted to replace/repair this valve.

J. *February 16 at 22:45:* Discharge Line Plugged – Solids were cleared from the discharge line.

K. *February 23:* Discharge Line Plugged – The discharge line was plugged with fiberfrax, ash, and pieces of an Allied Signal PRD-66 candle. The line was cleared and FD0520 was put back into service.

L. *February 23:* Lock Vessel Spheri Valve Leakage – Ash penetrated past the seal and O-rings causing the leakage. The seals were replaced, the valve was cleaned, and it was put back into service.

M. *March 06 at 07:45:* Discharge Line Plugged – A broken candle piece was cleared from the discharge line. The candle piece was from the PRD-66 filters broken on February 23, 1999.

N. *March 08 at 06:05:* Discharge Line Plugged – The discharge line repeatedly plugged due to packed ash.

O. *April 12 at 18:00:* Lock Vessel Vent Valve Failure – The lock vessel vent valve was not sealing. The valve was replaced.

3.5.3 Spent Fines Screw Cooler (FD0502) - Observations and Events

A. *February 16 at 00:30 to 04:00:* Ash Removal Rate – FD0502 was required to handle a significant amount of material that was carried over to the PCD from the transport reactor. It was noticed that the modified 6-in. pitch on the screw increased the ash removal rate. (The screw pitch was originally 3 inches.)

B. *February 16 at 07:30:* Drive-Side Seal Leakage – The seal leaked between the packing and the shaft. The bolts on the packing follower were tightened and the leakage dissipated. The seal pressure regulator was also readjusted to 15 psi above the system pressure.

C. *February 17 at 14:30:* Drive-Side Seal Leakage – The seal leaked between the packing and the shaft. The bolts on the packing follower were tightened and the leakage dissipated.

D. *February 19 at 09:15:* Drive-Side Seal Leakage – The seal leaked between the packing and the shaft. The bolts on the packing follower were tightened and the leakage dissipated.

E. *February 21 at 14:15:* Drive-Side Seal Leakage – The seal leaked between the packing and the shaft. The bolts on the packing follower were tightened and the leakage dissipated.

F. *February 24 to March 03 (Outage):* Drive-Side Seal Repair – In an attempt to minimize the ongoing seal leakage, the John Crane C-VH packing was replaced on the drive-side seal.

G. *March 08 to March 13 (Outage):* Seal Purge Modification – In an attempt to minimize the ongoing seal leakage, the seal purge line orifice size was increased from 3/32 to 3/8 inches.

H. *March 17 at 14:30:* Seal Purge Pressure Setting Error – It was noticed that the seal purge pressure was 5 psi below the system pressure. The pressure regulator was adjusted so that the seal purge pressure would be 15 psi above the system pressure.

I. *April 18 at 06:55:* Drive-Side Seal Leakage – The seal leaked between the packing and the shaft. The bolts on the packing follower were tightened and the leakage dissipated.

J. *Friday April 30:* Drive-Side Seal Modification – In an attempt to minimize the ongoing seal leakage, a temporary jackbolt was added to the drive-side bearing. The jackbolt was used to center the shaft inside the seal by moving the bearing.

3.5.4 Spent Fines Transport System (FD0520) - Status and Issues

The spent fines transport system (FD0520) has experienced operational and design changes that have increased the reliability of the system. However, the operation continues to be maintenance intensive. The discussions listed below highlight the problems encountered during TC05 and any currently proposed and/or initiated solutions.

1. The discharge of FD0520 repeatedly plugged. Oversized pieces of fused ash or broken candles normally caused the blockage. This blockage caused the transfer of ash from the PCD to the spent solids surge bin (FD0530) to be either limited or stopped. Generally, the blockage would occur either in the 2-in. XXS discharge line downstream of the outlet spheri valve or in the spheri valve port. The blockage was cleared by opening the pipe flanges and manually removing the obstruction(s) with a rod and/or pressurized air. This maintenance was often performed on-line without stopping the run by closing the manual block valve (MV0910) in the FD0520 drop pipe.

Proposed Solution(s):

- There is a 90° elbow that connects the dispense vessel discharge hopper outlet and the outlet spheri valve. This 90° elbow could be replaced with a "tee." The 2-in. horizontal branch of the tee would connect to the inlet of the existing outlet spheri valve. The vertical run of the tee would be connected to a larger 6-in. pipe. The 2-in. branch would be used during normal operation. Then, when blockage of the 2-in. line occurs, the 6-in. line would be opened and used to transport the oversized pieces. After the oversized pieces were cleared, the 6-in. line would be closed and the 2-in. line would be reopened.

- The lock vessel is depressurized to near atmospheric pressure before the ash is fed to the dispense vessel. Since the ash is no longer under pressure it can be handled with equipment designed for atmospheric pressure. Therefore, the dispense vessel and the dense-phase transport piping could be removed and replaced with an enclosed shaker. The ash could be transported to FD0530 via this shaker and the oversized pieces would be automatically separated. (Figure 3.5-1 shows the FD0520 lock vessel and dispense vessel.)

2. The lock vessel is depressurized by venting through a 1-in. vent line. The lock vessel vent valve (XV8539) controls the flow through this line. During depressurization some solids were transported through XV8539. The solids caused the valve to wear and lose its ability to seal. Once XV8539 began to leak, the ability to pressurize the lock vessel was limited. To correct the problem the FD0520 system was then isolated and the valve replaced.

   Initiated Solution(s):

   - The FD0520 system would be isolated during TC05 to replace a damaged vent valve. A parallel and redundant vent line was added so that a damaged vent valve could be replaced on-line.

   - The flow orifice was upstream of the vent valve during TC05. The vent valve was exposed to the higher velocity gas downstream of the flow orifice. The flow orifice was moved downstream of the vent valve as one initiative to limit the wear on the valve by lowering the gas velocity through the valve.

   - The vent valve will be exposed to solids during depressurization of the lock vessel. The valve should be designed to accommodate some wear. Therefore, the existing valve was replaced with a heavy-duty ball valve with stellite seats and a hard-coated ball.

3. The lock vessel level probe readings were not reliable. A back-up timer cycle was also used to avoid overfilling the lock vessel. If the level probe did not read a "high level" within 6 minutes the timer would close the lock vessel spheri valve. However, the back-up timer could not <u>open</u> the lock vessel spheri valve. Therefore, if the level

probe incorrectly read a high level, the lock vessel spheri valve would remain closed and the ash would accumulate in the FD0520 drop pipe. To clear the incorrect probe reading, the sensitivity of the probe was adjusted or the vessel was struck to clear the ash from the probe.

4. The lock vessel spheri valve leaked on two different occasions. On one occasion ash had penetrated past the seal and O-rings, causing a leakage. The seals were replaced and the valve was cleaned and put back into service. The seals operated without significant problems for the remainder of TC05. Two different silicone seal types were used during TC05. PSDF continues to test different seal designs developed by Clyde Pneumatic Conveying Ltd. of England.

3.5.5 Spent Fines Screw Cooler (FD0502) - Status And Issues

The spent fines screw cooler (FD0502) operated well during TC05 with the exception of the drive-side seal leakage. Stopping the seal leakage required significant maintenance attention. It was suspected that the leaking gas was purge nitrogen, not process gas. Ash was not noticed in the leaking gas. For this combustion test run the leakage did not negatively affect the run. However, for future gasification runs the leakage of process gas could be a safety concern and could impede the run progress. Therefore, efforts were made to determine how the leakage could be eliminated. Discussions regarding the leakage and any currently proposed and/or initiated solution(s) are listed below.

1. The modified inlet-side seal is similar to the drive-side seal but the inlet-side seal has experienced only minimal leakage. It has been postulated that the inlet-side seal does not leak because the shaft is always "centered" in the seal. On the drive-side the shaft tends to be pulled in the direction of the drive motor and ultimately loses the center alignment relative to the seal.

   Proposed Solution(s):

   - It is possible that the bearing may be moving due to the force of the chain-drive. The drive-side bearing is currently held with two bolts. A jackbolt arrangement and/or a four-bolt bearing could be used to more securely hold the bearing in place. Alternatively, a larger diameter sprocket could be used to decrease the chain-drive force.

   - A different packing material could be used that would accommodate the misalignment of the shaft inside the seal.

   - The drive arrangement is currently a chain-and-sprocket type design that inherently pulls the shaft toward the drive motor. The drive arrangement could be changed to a direct-coupled type drive that would not offset the shaft alignment.

2. If the seal-purge pressure falls below the system pressure the seals can be permanently damaged. To maintain a purge on the packing the purge pressure must be 10 to 15 psi above the system pressure. The purge pressure is controlled by a regulator and is

manually monitored in the plant. A low-purge pressure situation could exist for hours before being noticed.

Initiated Solution(s):

- A seal purge pressure indicator was added. The pressure can now be monitored on the distributed control system (DCS).

3. If it is determined that "zero-leakage" is required for gasification operation the existing shaft rider seals may be inadequate. New seal designs were investigated that would provide zero-leakage.

   Proposed Solution(s):

   - A totally enclosed, pressurized seal could be used on both ends of the screw cooler housing. The screw would be driven by a hydraulic drive and the external shaft drive would be eliminated. However, retrofitting these seals on the existing housing might not be practical. It is possible that a new screw cooler would be required. The assessment of potential solutions is continuing.

Figure 3.5-1 Spent Fines Transport System (FD0520)

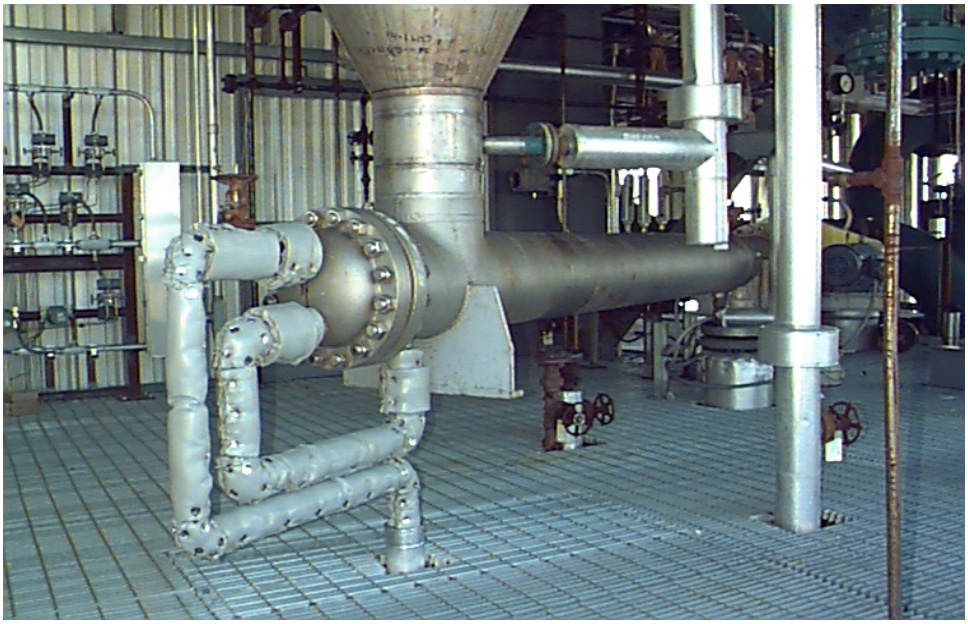

Figure 3.5-2 Spent Fines Screw Cooler With Original Inlet-Side Ceramic Bushing Bearing and Original Inlet-Side Seal

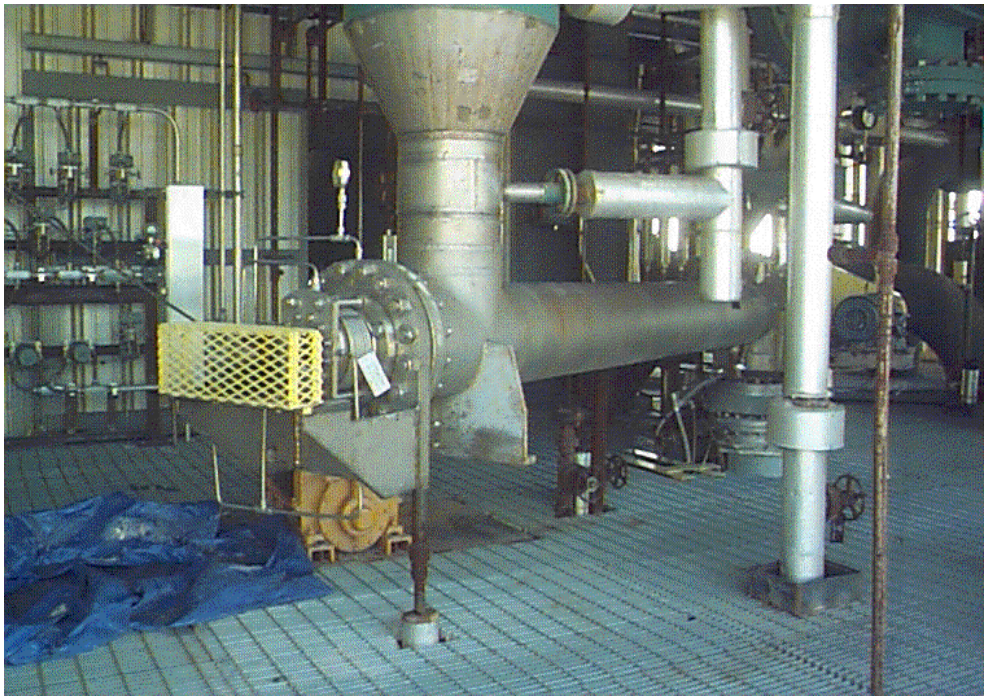

Figure 3.5-3 Spent Fines Screw Cooler With Modified Inlet-Side Bearing Arrangement and Modified Inlet-Side Seal

3.6 CANDLE FILTER MATERIAL EVALUATIONS

Mechanical and thermal evaluation of several candle filter materials is a portion of the ongoing testing being conducted at the PSDF. The latest evaluation results are included in a report prepared by SRI and presented in this TC05 report as the appendix. A brief summary of this appendix report is included here as section 3.6.

The overall objectives of the mechanical and thermal testing are as follows: a) provide material characterization to develop an understanding of the physical, mechanical, and thermal behavior of these materials; b) develop a materials property data base from which the behavior of these materials in the hot-gas cleanup environment may be predicted; c) perform testing and analysis of filter materials after operation in the PSDF to determine the effects of the thermal and chemical environments on these materials; and d) explain candle filter failures in the PSDF.

The materials evaluated were:

- Pall 442T, 326, and 181.
- Schumacher TF20 and T10-20.
- Coors P-100A-1.
- Industrial Filter and Pump (IF&P) Recrystallized SiC (REECER™).
- Ensto aluminum oxide.

All of the Pall and Schumacher filter materials discussed in this report are made from clay-bonded silicon carbide (SiC). The filter elements have an ID of ~1.575 in. (40 mm) and a wall thickness of ~0.400 in. (10 mm). The filters have a membrane layer of ~100 μm thickness. The microstructure of both Schumacher and Pall materials consists of individual SiC particles connected by clay or glass bridges and providing a toughness that slows microcrack propagation. The differences in materials include SiC particle size, binder chemistry, and outer membrane composition. Pall 326 and Schumacher TF20 have higher temperature, creep resistant binders (in comparison with Pall 442T and Schumacher F40) and were developed in response to creep failures and binder degradation experienced previously by the latter two elements in other PFBC facilities. The reduced creep rates come at the expense of room temperature tensile strength as both Schumacher TF20 and Pall 326 had lower tensile strengths than Schumacher F40 and Pall 442T. Testing has been conducted on Schumacher TF20 and Pall 326 and 442T after operation in the PSDF to assess lifetime issues and to evaluate their performance during thermal transient events. Pall 181 is manufactured with a crystalline binder containing more mullite than Pall 326. Schumacher T10-20 has the same support body as the Schumacher TF20 but a different membrane.

Coors P-100A-1 is a monolithic alumina/mullite filter material. The Coors filters have the same nominal dimensions as the Pall and Schumacher clay-bonded SiC particle filters but have no

membrane layer applied to the OD. The Coors material allows higher temperature operations by eliminating the creep and chemical degradation of the binder observed in the clay-bonded materials. Experience in the SCS-PSDF, however, has resulted in failure of many Coors candles, especially during transition from start-up burner operation to coal. Testing was conducted in the program to explain these failures. Test results showed that the Coors P-100A-1 has a much lower thermal conductivity than the clay-bonded SiC materials; therefore under the same thermal transient conditions more severe temperature gradients develop in the Coors material. Further, cracks propagate more readily since the microstructure of the Coors material does not provide the same inherent toughness as the clay-bonded SiC materials.

The IF&P REECER™ consists of SiC grains fused together without the use of a clay binder. Processing consists of heating SiC grains to temperature above 3,500°F (1,930°C) in an inert environment so that the grains fuse and form a monolithic material. Ensto candle filters consist of aluminum oxide particles with a mullite binder to form a microstructure similar to the clay-bonded SiC materials. IF&P recrystallized SiC and Ensto alumina oxide are newer candidate materials with little or no prior testing experience.

Results obtained for IF&P material showed that it has a thermal conductivity that is more than twice the conductivity of any other candidate material. Therefore, it may perform better than materials with similar thermal expansion and strain-to-failure during thermal transients because temperature gradients will be less severe than in other materials. Additional testing is required to address long-term operation issues such as oxidation of the SiC particles. Results obtained for Ensto indicate that it has relatively high coefficient of thermal expansion and a low-thermal conductivity. Therefore, it will be quite susceptible to thermal stress failure during transient events.

The characteristics investigated generally included tensile strength, thermal expansion, thermal conductivity, and density. The overall conclusions obtained from test results to date in this program include:

- During operation at the PSDF, Coors P-100A-1 elements failed due to accumulated microcracking probably caused by coal burning in the PCD during several transitions to coal feed.

- Coors P-100A-1, Blasch 4-270, and Ensto filter elements are likely to experience failure from thermal transients because the elements have low-thermal conductivities and the homogeneous microstructures in the Coors and Blasch elements allow microcracks to readily propagate.

- For operation at up to 1,400°F (760°C), and in the absence of major process upsets and temperature excursions, the clay-bonded SiC particle materials from Schumacher and Pall have a potentially long life (thousands of hours).

- More operating experience will be required to adequately predict lifetimes for clay-bonded SiC materials of 9,000 and 18,000 hours, etc.

- The use of clay-bonded SiC materials above 1,400°F (760°C) will be limited by creep, static fatigue, and degradation.

- Although possessing low-thermal conductivity, McDermott and PRD-66C oxide composites have high strain-to-failure and toughness, at least in as-manufactured condition, allowing these materials to survive the thermal transients experienced at the PSDF.

- More experience in operation is required to assess long-term operation of the composite materials.

Please read the complete report on these mechanical and thermal evaluations in the appendix of this report. The appendix report is organized to include the following: background information; material issues and system requirements; material descriptions; test matrices and cutting plans; test methods; experimental results; material comparisons; conclusions; and references.

3.7 ASH BRIDGING IN HOT-GAS FILTER DURING COMBUSTION OF PETROLEUM COKE WITH DOLOMITE

In March 1999 an episode of severe ash bridging occurred in the hot-gas filter on the KBR transport reactor system during the combustion of petroleum coke with the addition of dolomite for sulfur capture. This ash-bridging event was the only episode of ash bridging that has occurred in a hot-gas filter at the Power Systems Development Facility (PSDF). Prior to this episode, ash bridging had been avoided by limiting the maximum operating temperature of the hot-gas filter to about 1,400°F (760°C) and by the selection of nonfouling fuels. Petroleum coke had not been used in the transport reactor system prior to this incident.

This report discusses the conditions leading up to the ash-bridging incident and summarizes the results of various laboratory studies directed at determining the cause of the ash bridging and at identifying practical methods of avoiding ash bridging in the future. The chemistry associated with the ash-bridging problem is discussed in terms of analytical data obtained on the bridged material and on in situ dust samples collected during the formation of the ash bridges. Changes in particle morphology and in the distribution of certain elements are discussed through the use of photomicrographs and elemental maps obtained by scanning electron microscopy (SEM) with energy-dispersive x-ray (EDX) analysis. To investigate the mechanism of the ash bridging, additional SEM/EDX studies were employed in conjunction with a series of flow-tube furnace tests in which the dolomite was exposed to a synthetic flue gas mixture simulating the process gas produced by the transport reactor system. These tests successfully reproduced the morphological and chemical changes observed in the bridged material, thereby illuminating the mechanism of the ash bridging. Based on the results of these studies a mechanism is put forth to explain the ash bridging that occurred in the hot-gas filter at the PSDF and a means of avoiding the ash bridging in the future is suggested.

Please note that the results described in this report are very preliminary. Work is still in progress to study and explain the bridging mechanisms occuring at the PSDF. The results and discussion that follow relate specifically to the ash-bridging incident that occurred at the PSDF during combustion of petroleum coke with dolomite addition. These results and conclusions may not apply to other fuel/sorbent combinations or other operating conditions. Extreme caution is advised in attempting to apply these results to the analysis of ash-bridging events at other facilities.

3.7.1 Background and Observations

3.7.1.1 Conditions Leading Up to Ash Bridging

The ash bridging occurred during combustion-mode operation of the KBR transport reactor system on petroleum coke and dolomite with the hot-gas filter operating at a temperature of 1,400°F (760°C). The transport reactor was operating at a temperature of 1,600 to 1,650°F (870 to 900°C) and a total system pressure of 200 psig (14.6 atm). Plum Run dolomite was being added to produce a nominal calcium-to-sulfur (Ca/S) molar ratio of 1.3:1. The CO_2 content of the flue gas was typically about 9-vol. percent, producing a CO_2 partial pressure of 1.4 atm. Thermodynamically, it should not be possible to calcine the $CaCO_3$ portion of the dolomite

under these conditions even at the temperatures generated in the transport reactor itself (Baker, 1962). Although there may have been localized regions within the reactor where the local CO_2 concentration was much lower than 9-vol. percent, thermodynamics would ultimately favor the production of $CaCO_3 \bullet MgO$ (i.e., half-calcined dolomite) prior to sulfation. The half-calcined dolomite should have been rapidly sulfated when exposed to the high concentrations of SO_2 generated from the petroleum coke, which typically contains about 5-wt-percent sulfur. Based on a sulfur-mass balance, the flue gas generated from the petroleum coke combustion would have contained about 6-vol.-percent SO_2 without any SO_2 capture. This concentration of SO_2 would correspond to an SO_2 partial pressure of 0.9 atm. Previous studies have shown that the sulfation of half-calcined dolomite under conditions very similar to these will produce $CaSO_4$ along with the binary sulfate compound $Mg_3Ca(SO_4)_4$ (Hubble, et al, 1977).

Because of the high-sulfur content of the petroleum coke, the dolomite addition rate used during this run was substantially higher than the dolomite-addition rates used in previous tests with coal. Since the petroleum coke contains very little ash (about 0.5-wt percent), the solids leaving the transport reactor system were predominantly composed of the sulfated dolomite reaction products ($CaSO_4$ and, in high-temperature operation, $Mg_3Ca(SO_4)_4$) along with some unsulfated sorbent in the form of $CaCO_3 \bullet MgO$ or $CaCO_3$ and MgO. This assertion was confirmed by chemical analyses of in situ solids samples, which showed that these reaction products accounted for 79-to 94-wt percent of the solids entering the hot-gas filter. The molar ratio of sulfur-to-calcium (S/Ca) in the in situ solids sample collected at 1,400°F (760°C) was about 1.1:1, indicating that there was definitely sulfation of both the calcium and magnesium portions of the dolomite. The in situ solids sample collected at 1,400°F (760°C) formed a low-strength bridge in the particulate sampler, suggesting that the solids entering the hot-gas filter were somewhat sticky at this temperature. In the bridged material removed from the hot-gas filter elements, the sulfur-to-calcium ratio was about 1.6:1, indicating that additional sulfation was occurring with the continued exposure of the solids to the flue gas in the hot-gas filter. In view of this high-S/Ca ratio, and the previous work reported in the literature, it was strongly suspected that the bridged material contained a significant amount of the binary sulfate compound mentioned earlier.

After about 30 hours of operation under these conditions, large clumps of ash were detected in the ash discharge system, suggesting that ash deposits could be forming in the hot-gas filter. At this point other problems with the transport reactor caused a forced shutdown of the system. During the subsequent outage the hot-gas filter internals were removed and inspected, revealing the presence of self-supporting ash bridges between some of the filter elements and around the filter holders.

After the ash-bridging incident the deposits were removed from the filter elements and the transport reactor system was again operated with the same petroleum coke and dolomite. This time, however, the primary gas cooler was placed in service, resulting in a flue gas temperature of 750°F (400°C) at the inlet to the hot-gas filter. The system was operated in this mode for about a week before switching from dolomite to limestone and then operated for approximately another week with the limestone addition. There was no ash bridging in the hot-gas filter during

these runs at the lower gas temperature and none of the in situ dust samples collected during the low-temperature (750°F/400°C) operation appeared to be sticky.

3.7.1.2 Observations Recorded During Filter Inspection

Figures 3.7-1 and -2 show overall and close-up views of the bridged material retained in the top plenum of the hot-gas filter after the high-temperature (1,400°F/760°C) run. Similar views of the ash bridging in the bottom plenum are shown in Figures 3.7-3 and -4. The retained bridges were strong enough to be self-supporting and to resist removal by back-pulse cleaning, but they could be easily broken apart by hand. In some areas, an interface was apparent where the consolidated dustcakes on adjacent elements had grown outward from the element surfaces to the point where they came into contact. In other areas, some of the bridged material had apparently been dislodged from the filter elements, had fallen downward, and had been trapped by other bridged material located farther down the element length. Some of the bridged material had obviously been dislodged during removal of the filter internals or during back-pulsing of the filter.

Figure 3.7-5 illustrates the locations of the areas where significant amounts of bridged material were retained between the filter elements. The numbers on the drawing indicate the approximate fraction of the filter element length that was covered by the ash bridges in each area where there was significant ash retention. The filter elements that are blackened were newly installed prior to this run. The unshaded elements had been used in previous runs and were already covered with ash from previous tests with various coals and sorbents. Originally, it was thought that the presence of the newly installed elements might have been a factor in determining the locations of the retained ash bridges, because the new elements may have collected a disproportionate amount of the "new" ash from the petroleum coke/dolomite run. This theory is not supported by Figure 3.7-5, which clearly shows that there are large areas of ash bridging that do not include any of the new filter elements.

3.7.2 Relevant Information From Previous Studies

3.7.2.1 Ash Fouling Associated With Petroleum Coke Combustion

The occurrence of ash bridging during the petroleum coke run is not surprising since the use of petroleum coke has been associated with problems of ash agglomeration and fouling of heat transfer surfaces in atmospheric fluidized-bed combustors (Anthony, 1992). When the ash fouling problems associated with petroleum coke were first reported it was generally believed that the problems were associated with the vanadium content of the coke ash and the formation of low-melting vanadium compounds (Zierold and Voyles, 1993). However, field and laboratory studies conducted by researchers at the CANMET Energy Technology Centre suggested that the agglomeration of coke/limestone solids can take place in the absence of vanadium and actually results from extensive sulfation of the sorbent (Anthony, et al., 1997). The CANMET researchers referred to this mechanism as "molecular cramming" because the change in molar volume that occurs with sulfation causes deposits that are trapped between boiler tubes (or other surfaces) to become tightly compacted.

3.7.2.2 Ash Fouling During Limestone Injection Into PC-Fired Boilers

In a study of limestone injection into pulverized coal-fired boilers Åbo Åkademi University and Tampella Power Ltd showed that the strength of boiler-tube deposits increased with an increasing degree of sulfation (Skrifvars, et al., 1991). They suggested that recarbonation of the deposits was also a factor in strength development in the temperature range of 1,300 to 1,470°F (700 to 800°C) and they used the term "chemical-reaction sintering" to refer to the combined effects of sulfation and recarbonation. In the absence of either sulfation or recarbonation (i.e., in a nitrogen atmosphere) they found that there was no significant sintering of the ash/limestone deposits within this temperature range.

3.7.2.3 Sintering of PFBC Dustcakes

In flow-tube furnace tests performed at a temperature of 1,500°F (820°C) researchers at the Westinghouse (now Siemens Westinghouse) Science and Technology Center showed that sulfation had a much greater effect on the sintering of PFBC dustcakes than did recarbonation (Newby, et al., 1995). The Westinghouse researchers also showed that there was negligible sintering of the PFBC dustcakes in the absence of SO_2 and CO_2 (i.e., in pure nitrogen). These results seem to be consistent with the results reported by CANMET, Åbo Åkademi University, and Tampella Power. All of these results show that ash consolidation and strength development are influenced by reactions between the solids and the SO_2 (and to a lesser extent the CO_2) in the flue gas. An important underlying theme of these studies is that the ash consolidation, or sintering, is insignificant in the absence of these gases (at least at temperatures up to 1,500°F or 820°C). The inability to produce ash consolidation in a nitrogen atmosphere at these temperatures implies not only that the flue gas interactions with the solids play a dominant role, but also that the consolidation is not based on reactions between solid components. This is an important point because it refutes theories that the consolidation results solely from reactions between solid-phase components that form low-melting compounds or eutectics (cf. Snyder and Pontius, 1997; Hurley, et al., 1998).

3.7.2.4 Low-Melting Compounds and Eutectics

While the molecular cramming and chemical-reaction sintering mechanisms can explain the consolidation of trapped ash deposits they cannot explain why the solid material adheres to a surface (a boiler tube or a filter element) initially. To explain the ability of the ash to stick to surfaces one must imagine some mechanism in which the surface of the ash particles becomes sticky. Moreover, the mechanism must be temperature-dependent since the particles were obviously more sticky at 1,400°F (760°C) than they were at 750°F (400°C). (The bridged material adhered to the filter elements at the higher temperature but not at the lower temperature.) Formation of low-melting compounds or eutectics on the particle surface could account for this type of particle stickiness (Snyder and Pontius, 1997; Hurley, et al., 1998). For example, certain magnesium-vanadium compounds and certain alkali-metal-containing compounds have melting points that are below the operating temperature of the hot-gas filter at the PSDF but x-ray diffraction analysis has failed to detect any of these compounds in the solids from fluidized-bed combustors burning petroleum coke (Anthony, et al., 1995). Moreover, the

concentrations of vanadium and alkali metals in the hot-gas filter solids are apparently too low to produce a substantial amount of any magnesium-vanadium compound or any alkali salt. The bridged material taken from the hot-gas filter contained only 0.6-to 0.8-wt-percent vanadium (as V_2O_5) and only 0.8-to 1.0-wt-percent alkali metals (as Na_2O plus K_2O). Therefore, it seems unlikely that the presence of these components, or their reaction products, could explain the observed bonding between particles or the adherence of the solids to the filter elements unless these materials were highly concentrated on the particle surface.

If the concentrations of vanadium and alkali metals are too low to form significant amounts of a low-melting eutectic perhaps there is a eutectic mixture created from the reaction products of the dolomite and SO_2. One possibility is a eutectic mixture of $CaSO_4$ and $Mg_3Ca(SO_4)_4$ that has been reported in the literature (Rowe, et al., 1967). Their phase equilibrium study of the system K_2SO_4-$MgSO_4$-$CaSO_4$ suggested the presence of two low-melting eutectic mixtures of $CaSO_4$ and $Mg_3Ca(SO_4)_4$. They suggested that the eutectic mixtures occurred at 15-wt-percent $CaSO_4$ and at 55-wt-percent $CaSO_4$. The formation of either one of these eutectics would obviously require the presence of a significant amount of the binary sulfate $Mg_3Ca(SO_4)_4$. Since this compound could only be formed via extensive sulfation of the dolomite the formation of sticky ash deposits involving one of the $CaSO_4/Mg_3Ca(SO_4)_4$ eutectics could only take place in the presence of SO_2. This may explain why interactions with the flue gas species (SO_2 and CO_2) appear to play a key role in ash consolidation/sintering and why the consolidation/sintering does not take place in an inert atmosphere. Of course, it is also possible that the "initial" stickiness of the dolomite particles results from other low-melting components concentrated on the particle surface. In any case, the involvement of low-melting components or eutectics is strongly suggested by the effect of temperature on particle stickiness (sticky at 1,400°F/760°C and not sticky at 750°F/400°C).

3.7.2.5 Ash Bridging at the Tidd PFBC

At the Tidd PFBC demonstration plant severe ash bridging was encountered in the hot-gas filter at an operating temperature of about 150°F (840°C). The ash bridging occurred during combustion of Pittsburgh No. 8 coal with Plum Run dolomite (the same dolomite used at the PSDF). Researchers at the U.S. Department of Energy (DOE) analyzed the ash deposits from the Tidd hot-gas filter by x-ray diffraction (XRD) and found a substantial concentration of a binary sulfate compound, which they originally reported to be $Mg_3Ca(SO_4)_4$ (Smith, et al., 1997a). The DOE researchers subsequently used the analysis of aqueous extracts to suggest the compound may actually be a different binary sulfate compound $Mg_2Ca(SO_4)_3$ and that the concentration of this compound in the bridged solids was about 37-wt percent. In a later study (Smith, et al., 1997b) the same DOE researchers produced the binary sulfate compound by heating mixtures of $CaSO_4$ and $MgSO_4$ in air at 1,380°F (750°C). After heating various mixtures for 1 hour, the reaction products that were formed had unconfined yield strengths in excess of 3 psi (20 kPa). If the mixture was first compacted under a pressure of 3 psi (20 kPa) the unconfined yield strength after 1 hour of heating was increased to about 6 psi (40 kPa). X-ray diffraction (XRD) analysis confirmed that the reaction products contained the binary sulfate compound. SEM examination of the reaction products revealed the presence of necks between the $CaSO_4$ and $MgSO_4$ particles and EDX analysis of the necks showed that they were enriched

in calcium and sulfur. These results suggest that there is a migration of calcium and magnesium associated with the reaction that forms the binary sulfate compound. The necks observed under the SEM are presumably the result of this reaction and the resulting migration across particle boundaries. These results coupled with the strength measurements imply that the particle neck formation is a contributing factor in the ash consolidation (or sintering).

It is interesting that the DOE researchers were able to sinter mixtures of $CaSO_4$ and $MgSO_4$ in air but the Westinghouse researchers were unsuccessful in sintering PFBC dustcakes in nitrogen. The apparent contradiction in these results may be associated with the degree of sulfation of the solids. Perhaps fully sulfated materials can be sintered in the absence of SO_2, while partially sulfated materials require additional sulfation before they will sinter. This assertion cannot be proven but it is consistent with both sets of results. All of the results are consistent with a requirement for extensive sulfation prior to the development of stickiness and consolidation.

3.7.3 Chemistry of Ash Bridges and In situ Dust Samples

3.7.3.1 X-ray Diffraction Analysis

To identify the chemical compounds actually present in the bridged material from the PSDF hot-gas filter a sample of the material was sent to the Georgia Institute of Technology (Georgia Tech) for analysis by XRD. The in situ dust samples collected during both the high- and low-temperature runs were also sent for comparison. When the samples were originally submitted the investigators at PSDF and Georgia Tech were unaware of the previous work related to the binary sulfate compound and its potential role in ash bridging. The original intent of the XRD studies was to search for low-melting vanadium compounds that might be involved in the bridging. The researchers at Georgia Tech failed to detect any vanadium compounds but they found the binary sulfate compound in the PSDF samples without any prior knowledge of its existence in the ash bridges from Tidd or from the other studies.

Figure 3.7-6 shows the XRD patterns obtained for the sample of bridged material and the two in situ dust samples. In all of the samples only two compounds were detected: $CaSO_4$ and $Mg_3Ca(SO_4)_4$. This result does not mean that these two compounds are the only compounds present. Other compounds are surely present but they could not be detected either because their concentration is too low or are amorphous. (XRD will only detect crystalline compounds.) In any case the XRD results clearly show that there is a substantial amount of $Mg_3Ca(SO_4)_4$ present in the bridged material and a much lower amount present in the in situ dust sample from the 1,400°F (760°C) run. No $Mg_3Ca(SO_4)_4$ was detected in the in situ dust sample from the 750°F (400°C) run. These results suggest that none of the $Mg_3Ca(SO_4)_4$ is formed in the transport reactor and only a small fraction of the $Mg_3Ca(SO_4)_4$ is formed upstream of the hot-gas filter during high-temperature filter operation. The $Mg_3Ca(SO_4)_4$ is primarily formed in the hot-gas filter.

It is interesting that no $MgSO_4$ was detected in either the bridged material or in the in situ dust samples. Any $MgSO_4$ that was present should have been in crystalline form so it should have been detectable by XRD. Therefore, the failure to detect $MgSO_4$ could be interpreted to mean

that sulfation of the magnesium takes place by direct formation of the binary sulfate or that any $MgSO_4$ that is formed instantaneously reacts with $CaSO_4$ to form the binary sulfate.

3.7.3.2 Calculation of Chemical Composition

Standard ash mineral analyses were used to determine the complete elemental composition of the bridged material and of the in situ dust samples by standard ash mineral analysis. The chemical composition of each sample was calculated using the following assumptions.

1. If the S/Ca molar ratio was less than 1:1 then all of the sulfur was in the form of $CaSO_4$, and any unsulfated calcium was in the form of $CaCO_3$ or $CaCO_3$•MgO.

2. If the S/Ca molar ratio was greater than 1:1 then all of the calcium was sulfated and some of the magnesium was sulfated in the form of $Mg_3Ca(SO_4)_4$. In other words, any $MgSO_4$ that was formed reacted with $CaSO_4$ and formed $Mg_3Ca(SO_4)_4$.

3. Any remaining magnesium was in the form of MgO or $CaCO_3$•MgO depending upon the extent to which the $CaCO_3$ was sulfated.

4. Calcium and magnesium were not present in any other forms (e.g., silicates, aluminosilicates, ferrites, etc.).

Based on these assumptions the chemical compositions of the various samples were calculated from the standard ash mineral (elemental) analyses using straightforward mass-balance techniques. The results, summarized in Table 3.7-1, show that the bridged material contained about 41-wt-percent $CaSO_4$ and 35-wt-percent $Mg_3Ca(SO_4)_4$. (Recall that the DOE researchers estimated that the ash bridges from the Tidd hot-gas filter contained about 37-wt-percent of the binary sulfate although they disagreed on the formula for this compound.) The in situ dust from the high-temperature run contained about 58-wt-percent $CaSO_4$ and 5-wt-percent $Mg_3Ca(SO_4)_4$. The in situ dust from the low-temperature run contained about 62-wt-percent $CaSO_4$ and no $Mg_3Ca(SO_4)_4$. The in situ sample from the low-temperature run would represent quenched material from the transport reactor, indicating that there is no binary sulfate formed in the reactor itself. Even during the high-temperature operation without the quenching there is apparently only a very small amount of the binary sulfate (about 5-wt percent) formed upstream of the hot-gas filter. In all cases most of the $Mg_3Ca(SO_4)_4$ is formed in the hot-gas filter. None was formed ahead of the filter during the low-temperature run. These results may help explain why the in situ dust from the high-temperature run was somewhat sticky while the in situ dust from the low-temperature run was not sticky at all.

The weight ratio of $CaSO_4$ to $Mg_3Ca(SO_4)_4$ in the bridged material was 41:35 (= 1.2:1), which is exactly the same as the weight ratio found in one of the eutectic mixtures reported by Rowe, et al., (55:45 = 1.2:1). Thus, it is very conceivable that this combination of $CaSO_4$ and $Mg_3Ca(SO_4)_4$ formed a low-melting eutectic mixture, which could help explain the stickiness of the ash and the apparent ability of calcium and magnesium to migrate as discussed later. Unfortunately, Rowe, et al., did not measure the melting point of this eutectic mixture. Based

on extrapolation of their phase equilibrium diagram the melting point should be in the range of 900 to 1,000°C. Although the operating temperature of the hot-gas filter is well below this melting point it is common for materials to soften and become sticky at temperatures well below their melting point.

Various studies of sintering phenomena have shown that particles can begin to stick together at absolute temperatures that are about 75 percent of the absolute melting point (Philibert, 1991). If the melting point of the aforementioned eutectic were 900°C (1,173°K), consolidation could begin at temperatures as low as 880°K (607°C)–well below the operating temperature of the hot-gas filter at the PSDF. Even if the melting point were 1,000°C (1273°K) consolidation could begin at temperatures as low as 955°K (682°C), which is still well below the operating temperature of the hot-gas filter. Moreover, it is also possible that the presence of small amounts of sodium and potassium compounds, vanadium compounds, or other unidentified compounds could further reduce the melting point of the mixture and further enhance particle stickiness, particularly if they were concentrated on the particle surface (Snyder and Pontius, 1997; Hurley, et al., 1998).

3.7.4 Laboratory Studies of Ash Consolidation Mechanisms

A series of laboratory tests were undertaken to determine the cause of the ash bridging in the hot-gas filter at the PSDF. These tests included the production and strength testing of consolidated pellets, SEM/EDX studies of changes in particle morphology and distribution of calcium and magnesium, and flow-tube furnace tests designed to reproduce the consolidation and particle morphology changes in a simulated flue gas environment.

3.7.4.1 Ash Reconsolidation and Strength Testing

The initial portion of the laboratory test program involved a series of crude experiments designed to determine whether the bridged material would reconsolidate after being dispersed into a powder and reheated in air. These experiments were also run on ashes from various coal/sorbent combinations to better understand the differences between materials produced from coal ash and those produced from petroleum coke ash. The material was first run through a 150-μm sieve to break up any clumps. The resulting powder was then dumped into a small crucible which was then tapped to remove any trapped air and to even out the layer of powder. The crucible was then placed in a muffle furnace and heated for 30 minutes at temperatures ranging from 800 to 1,600°F (430 to 870°C). After baking at the prescribed temperature, the crucible was allowed to cool, and the material was carefully removed from the crucible. If the material appeared to be consolidated the strength of the consolidated material was evaluated by applying a series of increasing weights to a piston pressing on the center of the consolidated disk. The piston diameter was ¼ in. (6.4 mm). The diameter of the consolidated disk varied from about 1 in. (2.5 cm) at the top surface where the piston was applied to about 1.5 in. (3.8 cm) at the bottom. (The disk was inverted when it was removed from the crucible.)

The test described above was a crude fracture test that was used to rank the relative strengths of consolidated materials. The test suffered from numerous limitations. The load was applied to

only a small fraction of the surface–the two faces of the consolidated disks were not exactly parallel, and the cross-sectional area of the disk was variable. Therefore, this test was not intended to provide accurate measurements of compressive strength but was simply a relative ranking of the degree of consolidation of the various materials.

As shown in Figure 3.7-7, the reconsolidation tests showed that the bridged material could be dispersed into a powder and then reconsolidated by heating in air. Based on the relative strength measurements described above the reconsolidated disks made from the bridged material began to develop measurable strength at about 1,000°F (540°C) and the strength increased significantly as the consolidation temperature was increased. When an ash produced from Illinois coal and limestone was subjected to the same procedures there was no significant strength development at temperatures up to 1,400°F (760°C). The coal/limestone ash developed measurable strength at 1,600°F (870°C) but the strength was far below that of the petroleum coke/dolomite ash. When an ash produced from Alabama coal and dolomite was tested a slightly higher strength was developed but the strength was still well below that of the petroleum coke/dolomite ash produced using the same dolomite (Plum Run). Based on these results it is clear that petroleum coke/dolomite ash consolidates at lower temperatures than does ash from coal/dolomite or ash from coal/limestone. It is also clear that the petroleum coke/dolomite ash develops greater strength at equivalent temperatures, at least up to a temperature of 1,600°F (870°C).

These results appear to be generally consistent with the Åbo Åkademi study cited previously, which showed that coal/sorbent ashes did not develop significant strength when heated in nitrogen at a temperature of 1,400°F (760°C). There is an apparent conflict with the results of the previously cited Westinghouse study which found no significant strength development in PFBC dustcakes when they were heated in nitrogen at temperatures up to 1,550°F (840°C). This apparent discrepancy could possibly be related to differences in the coal ash properties. (The Westinghouse study used ash from Pittsburgh No. 8 coal with Plum Run dolomite while the tests performed at the PSDF used Alabama coal with Plum Run dolomite.) One other difference was that the Westinghouse studies of strength development were done in nitrogen while the PSDF studies were done in air. This difference in test environments probably did not have any significant impact on the test results, however, since the Åbo Åkademi studies were also done in nitrogen and were consistent with the PSDF results.

3.7.4.2 SEM Studies of Bridged Material

Figure 3.7-8 shows SEM photographs of the bridged material taken from the hot-gas filter after the high-temperature (1,400°F/760°C) run. This material was collected on and between the filter elements during the high-temperature run and may have been exposed to the hot-flue-gas environment for up to 30 hours before shutdown. For comparison, Figure 3.7-9 shows SEM photographs of an in situ dust sample collected at the inlet of the hot-gas filter during the same run. This material was collected at a constant rate during a 30-minute sampling run so the average exposure to the hot flue gas was about 15 minutes. As indicated previously, most of the particles in both samples are partially sulfated dolomite particles with the bridged material having a substantially higher degree of sulfation (S/Ca ≅ 1.6:1 in bridged material versus S/Ca ≅ 1.1:1 in the incoming dust). Comparison of Figures 3.7-8 and -9 suggests that there is a substantial

morphological change associated with the additional sulfation and additional exposure to process conditions within the hot-gas filter.

This type of morphological change was not observed among adjacent particles in the residual dustcakes produced from Alabama coal and the same (Plum Run) dolomite as shown in Figure 3.7-10. The dolomite particles in the coal/dolomite dustcake are covered with dozens of small fly ash particles while there are only a few fly ash particles on each dolomite particle in the coke/dolomite bridged material. Based on these SEM photographs the coating of fly ash in the coal/dolomite dustcake appears to be so extensive that it could virtually eliminate any possibility for intimate contact between the dolomite particles. In this manner the fly ash could actually serve to block any bridging that might occur between dolomite particles. This may explain why the bridging occurred with coke and dolomite but not with coal and dolomite. (The petroleum coke contains about 0.5-percent ash while the Alabama coal contains about 15-percent ash.)

3.7.4.3 SEM/EDX Studies of Calcium and Magnesium Distributions

Figure 3.7-11 shows a close-up SEM view of the bridged material in which several particles appear to be bonded together. Energy-dispersive x-ray (EDX) analysis was used to study variations in the Ca/Mg atomic ratio in this sample. As shown on the photograph, the ratio varied considerably from one area of the sample to the next. In raw dolomite the calcium and magnesium are distributed in alternating layers at the atomic level, resulting in a more-or-less uniform distribution of these elements with Ca/Mg molar ratio ≅ 1:1 (Boynton, 1966). Thus, the appearance of substantial variations in Ca/Mg ratio in the bridged material implies that there has been movement of the calcium and/or magnesium. This movement may be associated with the formation of the binary sulfate compound discussed previously which has a molar Ca/Mg ratio of 1:3. To produce this stoichiometry, magnesium would have to migrate to the areas where the binary sulfate is formed and calcium would have to migrate away from those areas. As the binary sulfate is formed a relatively high concentration of magnesium is produced in the vicinity of the binary sulfate, creating a concentration gradient that serves as the driving force for migration of magnesium away from the area. Smith, et al. (1997b) suggested that this type of migration was responsible for the necks that they observed between particles in heated mixtures of $CaSO_4$ and $MgSO_4$.

It is interesting that SEM studies of coal/dolomite solids do not reveal any interparticle necks under the same conditions that produce interparticle necks in coke/dolomite solids. In the coal/dolomite solids it is obvious that the sulfated dolomite particles are coated with numerous fine fly ash particles that prevent intimate contact between sulfated dolomite particles. This observation explains why interparticle necks do not develop between sulfated dolomite particles in the coal/dolomite solids, but not why are there no interparticle necks between sulfated dolomite particles and fly ash particles in the coal/dolomite solids. If the interparticle necks were formed by ionic, solid-phase diffusion of calcium and magnesium then they <u>should</u> be formed between sulfated dolomite particles and fly ash particles and not just between adjacent sulfated dolomite particles. This is a strong argument against purely ionic, solid-phase diffusion and in favor of the type of sintering that occurs as the temperature exceeds 75 percent of the absolute-melting temperature of the eutectic phase. As the binary sulfate formation occurs,

calcium and magnesium must migrate as discussed previously. Some of this migration will naturally occur at the points where adjacent sulfated dolomite particles are in contact. This migration is facilitated by the development of the low-melting eutectic mixture of $CaSO_4$ and $Mg_3Ca(SO_4)_4$. In the absence of this eutectic the absolute melting point of the reaction products would be so high that it would be impossible to achieve the 75-percent approach discussed earlier and there would be no interparticle neck formation.

In addition to the SEM/EDX studies performed at the PSDF an independent SEM/EDX examination of the bridged material from the PSDF was performed by Professor Brent Carter at the Georgia Tech. Professor Carter's work confirmed that there was considerable variation in the Ca/Mg ratio and showed that the bridges or necks between particles were primarily composed of calcium, sulfur, and oxygen. This observation led Professor Carter to speculate that $CaSO_4$ was the main ingredient in the "glue" holding the particles together. The amorphous, globular appearance of the necks suggested that the material forming the necks had been molten, or at least softened, at one time. Pure $CaSO_4$ by itself could not possibly become molten, however, since its melting point is 2,640°F (1,450°C). Therefore, the most likely explanation appears to be that the $CaSO_4$ is involved in a low-melting eutectic mixture–possibly the eutectic mixture with the binary sulfate. As mentioned earlier, this mixture would have a melting point of around 1,650°F (900°C) but the formation of interparticle necks could commence at temperatures well below the operating temperature of the hot-gas filter. Additionally, it is also possible that the melting point of the mixture could be further reduced by the presence of other low-melting species.

The appearance of the interparticle necks and the scale of the morphological changes relative to the particle sizes strongly suggest that the migration of calcium and magnesium is being facilitated by the formation of a low-melting eutectic. If it is assumed that the interparticle necks originate at the points where calcium and magnesium atoms in adjacent particles are in contact, then it is a simple matter to explain why the consolidation is so pronounced in a system that is dominated by sulfated dolomite particles and why the consolidation is insignificant in a system where the sulfated dolomite particles are separated by fly ash particles. As mentioned earlier, the lack of neck formation between particles in the system containing fly ash suggests that the migration of the calcium and magnesium does not occur purely by ionic diffusion in the solid state. If it did there would be neck formation between fly ash particles and sulfated dolomite particles which has not been observed in any of the samples discussed here. The facilitating effect of the eutectic formation is not operative at fly ash/dolomite interfaces because there is no way to produce the binary sulfate and the associated eutectic mixture at these interfaces. Formation of interparticle necks between fly ash particles has been observed at higher temperatures (Snyder and Pontius, 1997) presumably because ionic diffusion rates increase with increasing temperature. At a temperature of 1,400°F (760°C), however, the rate of purely ionic diffusion in the solid state is apparently too low to result in significant neck formation between particles. Therefore, it seems most likely that eutectic formation is promoting the calcium and magnesium migration and interparticle neck formation in the hot-gas filter deposits discussed here.

Professor Carter also used electron spectroscopy for chemical analysis (ESCA) to examine the surface of the particles in the bridged material. Examination of the top few atom layers of the surface revealed no significant enrichment of vanadium or alkali metals on the particle surfaces. This observation casts further doubt on the theory that the particle stickiness could be attributed to low-melting vanadium compounds, alkali salts, or eutectics involving these species. Considering all of the evidence from XRD, SEM/EDX, and previous studies, the most likely source of the stickiness appears to be the low-melting eutectic mixture produced from $CaSO_4$ and $Mg_3Ca(SO_4)_4$. Both of these compounds have been positively identified in the bridged material from the PSDF and in bridged material from the Tidd hot-gas filter (Smith, et al., 1997). The existence of a low-melting eutectic mixture of these compounds has been confirmed through phase-equilibrium studies of the $CaSO_4/MgSO_4$ system (Rowe, et al., 1967). SEM/EDX analysis of the bridged material has revealed an enrichment of calcium, sulfur, and oxygen in the bridges or necks between particles and no enrichment in vanadium or alkali metals in these areas.

3.7.4.4 Flow-Tube Furnace Tests to Define Consolidation Mechanism

In view of the SEM/EDX results obtained on the bridged material a series of flow-tube furnace tests were performed to determine whether the consolidation and morphological changes observed in the bridged material could be reproduced by exposing dolomite to synthetic flue gas (in the absence of any fly ash, vanadium, and alkali metals). A small sample (~5 to 10 g) of the Plum Run dolomite was placed in an alumina combustion boat which was then placed in a Thermolyne Model 21100 tube furnace that had been preheated to 1,400°F (760°C). A synthetic flue gas mixture containing 6-vol.-percent SO_2, 40-vol.-percent CO_2, 20-vol.-percent O_2, and 34-vol.-percent N_2 was passed through the tube furnace and over the dolomite for time periods ranging from 22 to 65 hours. The formulation of the synthetic flue gas mixture was chosen to simulate the partial pressure of SO_2 generated by the combustion of the petroleum coke, to provide a partial pressure of CO_2 that is high enough to prevent calcination of $CaCO_3$, and to provide excess O_2 for the sulfation reaction. Similar tests were also conducted with reagent-grade $CaCO_3$ so that the morphology changes observed in the dolomite particles could be compared to those occurring in $CaCO_3$ containing a minimal level of magnesium. (The $CaCO_3$ that was used for this experiment was a special, chelometric standard, Alfa-Aesar stock no. 36399, that contained less than 0.05-percent magnesium.)

SEM photographs of the sulfated-dolomite particles produced after a 22-hour exposure in the flow-tube furnace are shown in Figure 3.7-12. For comparison, Figure 3.7-13 shows the sulfated $CaCO_3$ produced after an identical treatment. After the 22-hour exposures to the simulated flue gas at 1,400°F (760°C) the sulfated dolomite was noticeably consolidated while the sulfated $CaCO_3$ remained a loose powder with no apparent consolidation. Comparison of the SEM photographs shows that the dolomite underwent a much more pronounced morphological change than did the $CaCO_3$. The dolomite particles were converted into globular clusters while the $CaCO_3$ particles retained their basic, cubical shape. This result implies that the presence of the magnesium may play a role in the consolidation which would be expected if the mechanism involves the formation of the binary sulfate $Mg_3Ca(SO_4)_4$ as suggested previously. When taken together with all of the other results the flow-tube furnace tests suggest that the bridges between

the particles are the result of the migration of calcium and magnesium that takes place when the binary sulfate is formed. All of the results seem to consistently point to this explanation except for the EDX results that suggest the bridges are predominantly $CaSO_4$. Based on the chemical analysis of the bridged material the bulk composition should comprise about 41-wt-percent $CaSO_4$ and 35-wt-percent $Mg_3Ca(SO_4)_4$. EDX analysis suggests that the composition of the bridges is closer to 85-wt-percent $CaSO_4$ and 15-wt-percent $Mg_3Ca(SO_4)_4$. (This composition is roughly equivalent to a 9:1 atomic ratio of Ca/Mg.) Although EDX analyses performed on very small areas of the sample should not be expected to match the bulk chemical composition of the sample it is surprising that the bridges apparently contain less binary sulfate than does the bulk sample. If the bridges or necks are very thin (< 1 μm) it is possible that the x-ray beam is penetrating completely through the bridges and the EDX analysis is actually detecting material that lies under the bridges. To investigate this possibility additional EDX studies were done in which the depth of penetration of the x-ray beam was varied. These studies did not reveal any apparent bias of the particle neck analysis by underlying materials.

Although significant morphological changes were not observed in the reagent-grade $CaCO_3$ after treatment at 1,400°F (760°C) this result does not mean that morphological changes would not occur in the $CaCO_3$ at higher temperatures. Similarly, the results obtained with the reagent-grade $CaCO_3$, which contains essentially no magnesium should not be extrapolated to commercial limestones which generally contain some amount of magnesium. In fact, consolidated deposits have been formed in fluidized-bed boilers fired with petroleum coke with limestone addition for in-bed sulfur capture (Anthony, et al., 1992). Of course, temperatures in the fluidized-bed boilers are significantly higher than the temperature in the hot-gas filter at the PSDF and the temperature used in the tube furnace tests (1,400°F/760°C).

3.7.5 Conclusions

The results of this study have shown that a loose powder of dolomite particles can be consolidated, or bridged together, by exposing the powder to a synthetic flue gas mixture at a temperature of 1,400°F (760°C). Under conditions simulating the flue-gas environment in the hot-gas filter the consolidation takes place within 22 hours and does not depend on the presence of fly ash, vanadium, or alkali metals. Interactions with the flue gas, especially with the SO_2, are an essential aspect of the consolidation mechanism. Magnesium also apparently plays an enabling role in the mechanism since pure $CaCO_3$ does not consolidate under the same conditions. Migration of calcium and magnesium during the consolidation process may be inferred from the nonuniform distribution of these elements within the consolidated material. The migration may be facilitated by the formation of a low-melting eutectic mixture involving $CaSO_4$ and $Mg_3Ca(SO_4)_4$. Consolidation presumably takes place when this migration occurs between adjacent particles, therefore forming a neck or bridge between the particles. There are many factors that can influence this process, in particular the presence of other particles that can prevent intimate contact between the dolomite particles. In the case of coal/dolomite solids the presence of fly ash particles around the dolomite particles apparently blocks the consolidation by preventing intimate contact between adjacent dolomite particles. This "blocking effect" is not operative in the coke/dolomite solids because of the very low ash content of petroleum coke. Thus, the difference in ash content of the fuels partly explains why coal/dolomite solids do not

consolidate under the conditions that produce consolidation of coke/dolomite solids. The failure of coal/dolomite solids to consolidate suggests that the mechanism of calcium and magnesium migration is not purely ionic, solid-phase diffusion. If this type of diffusion were the dominant mechanism of migration there should be interparticle necks between fly ash and sulfated dolomite particles but no such necks have been observed under the SEM. The formation of interparticle necks at 1,400°F (760°C) has only been observed between sulfated dolomite particles.

Although vanadium can react with dolomite at the temperatures of interest, the EDX studies showed that there was no enrichment of vanadium in the bridges between particles. Moreover, the ESCA analysis showed that there was no enrichment of vanadium on particle surfaces. Therefore, the results of this study conclusively demonstrate that vanadium did not play a significant role in the ash bridging that occurred in the hot-gas filter at the PSDF at 1,400°F (760°C). That is not to say that vanadium is never a contributing factor in ash consolidation but that it was not a significant factor in the bridging that occurred in the hot-gas filter at the PSDF. Based on the EDX and ESCA results the same may be said for the contribution of alkali metals.

The results of this study suggest that ash bridging may be ameliorated by the addition of an inert material that will prevent intimate contact between the dolomite particles. The material could be fly ash, sand, or some other inert material. Operating experience at the PSDF has shown that the consolidation of coke/dolomite solids can also be avoided by operating the hot-gas filter at 750°F (400°C). Although this temperature may be too low to be of practical interest it is possible that other temperatures between 750 and 1,400°F (400 and 760°C) may result in satisfactory filter operation without bridging. If a suitable inert material is used it may even be possible to operate at higher temperatures with petroleum coke and dolomite, but additional transport reactor/hot-gas filter tests would be required before this type of operation could be recommended. These conclusions apply strictly to cases where petroleum coke is used with dolomite and should not be extrapolated to situations involving petroleum coke and limestone or cases involving various types of coal with dolomite or limestone. Because of differences in fuels, sorbents, and operating conditions the mechanisms of ash bridging discussed here may not apply to incidents of ash bridging that have occurred at other facilities.

In addition to the above caution not to extrapolate these results to other fuels/sorbents and facilities, please note that the reported results are preliminary. Work is ongoing to better define these bridging mechanisms and may ultimately produce different conclusions from the results being reported at this time.

3.7.6 Future Work

Additional flow-tube furnace tests are needed to better define the maximum operating temperature at which ash bridging can be avoided when burning petroleum coke with dolomite. Additional tests are also needed to better define the levels of magnesium that lead to bridging problems. This determination could be made through a series of flow-tube furnace tests using limestones with various magnesium contents and using various mixtures of $CaCO_3$ and $MgCO_3$. The sulfated products from the tests should be subjected to detailed SEM/EDX examination to

document the calcium and magnesium contents of the bridges between particles and to compare the elemental distributions in the particles to those in the bridges. To further elucidate the bridging mechanism, melting-point determinations should be made on various mixtures of $CaSO_4$ and $Mg_3Ca(SO_4)_4$ with and without trace additions of vanadium and alkali metals. These measurements would better define the melting point of the eutectic and verify that it is low enough to facilitate the observed migration of calcium and magnesium. The potential roles of ionic diffusion and grain-boundary diffusion in the migration of calcium and magnesium need to be investigated further to confirm the apparent temperature limitations of these diffusion mechanisms and verify that they cannot produce interparticle necks in the absence of low-melting compounds or eutectics.

3.7.7 References

Anthony, E. J., "Petroleum Coke Burning in FBC Systems," CANMET Energy, Mines, and Resources Canada, Report No. ERL 92-36(CF), 1992.

Anthony, E. J., A. P. Iribarne, and J. V. Iribarne, "A New Mechanism for FBC Agglomeration and Fouling When Firing 100% Petroleum Coke," *Proceedings of the 13th International Conference on Fluidized-Bed Combustion*, Vol. 1, pp. 523-533 (1995).

Anthony, E. J., F. Preto, L. Jia, and J. V. Iribarne, "Agglomeration and Fouling in Petroleum Coke Fired Boilers," *Proceedings of the 15th International Conference on Fluidized-Bed Combustion*, Vol. 2, pp. 839-846 (1997).

Baker, E. H., "The Calcium Oxide–Carbon Dioxide System in the Pressure Range 1–300 Atmospheres," *J. Chem. Soc.*, pp. 464-469 (1962).

Boynton, R. S., "Chemistry and Technology of Lime and Limestone," John Wiley & Sons, New York (1966).

Hubble, B. R., S. Siegel, L. H. Fuchs, H. R. Hoekstra, B. Tani, and P. T. Cunningham, "The Formation of $Mg_3Ca(SO_4)_4$ During the Sulfation Reaction of Dolomite," *J. Air Pollut. Control Assoc.*, Vol. 27, No. 4, pp. 343-346 (1977).

Hurley, J. P., J. W. Nowok, J. A. Bieber, and B. A. Dockter, "Strength Development at Low Temperatures in Coal Ash Deposits," *Prog. Energy Combust. Sci.*, Vol. 24, pp. 513-521 (1998).

Newby, R. A., M. A. Alvin, D. M. Bachovchin, E. E. Smeltzer, and T. E. Lippert, "Integrated Low Emissions Cleanup System for Coal-Fueled Turbines, Phase III Topical Report: Bench-Scale Testing and Evaluation," U.S. DOE/METC, Contract No. DE-AC21-87MC24257, 1995.

Philibert, J., "Atom Movements, Diffusion, and Mass Transport in Solids," Les Éditions de Physique, Les Ulis, France (1991).

Rowe, J. J., G. W. Morey, and C. C. Silber, "The Ternary System K_2SO_4-$MgSO_4$-$CaSO_4$," *J. Inorg. Nucl. Chem.*, Vol. 29, No. 4, pp. 925-942 (1967).

Skrifvars, B-J., M. Hupa, and P. Hyöty, "Superheater Fouling Due To Limestone Injection in Coal-Fired Boilers," *J. Inst. Energy*, Vol. 64, No. 12, pp. 196-201 (1991).

Smith, D. H., G. J. Haddad, and U. Grimm, "Composition and Chemistry of Particulates From a PFBC Demonstration Plant," *Fuel*, Vol. 76, No. 8, pp. 727-732 (1997a).

Smith, D. H., G. J. Haddad, and M. Ferer, "Shear Strength of Heated and Unheated Mixtures of $MgSO_4$ and $CaSO_4$ Powders," *Energy & Fuels*, Vol. 11, No. 5, pp. 1006-1011 (1997b).

Snyder, T. R. and D. H. Pontius, "Particulate Hot Gas Stream Cleanup Technical Issues," *Proceedings of the Advanced Coal-Based Power and Environmental Systems '97 Conference*, U.S. DOE/FETC, Pittsburgh, PA, July 22-24, 1997.

Zierold, D. M. and R. W. Voyles, "NISCo Cogeneration Facility," *Proceedings of the 12th International Conference on Fluidized-Bed Combustion*, Vol. 1, pp. 501-510 (1993).

Table 3.7-1

Chemical Compositions and Molar Ratios of Ash Bridging Samples

	Ash Bridge	High-Temperature In situ Dust	Low-Temperature In situ Dust
Ca/Mg Molar Ratio	1.13	1.11	1.15
S/Ca Molar Ratio	1.57	1.07	0.79
S/(Ca+Mg) Molar Ratio	0.83	0.56	0.42
CaSO4(Wt %)	41.09	57.62	62.05
$Mg_3Ca(SO_4)_4$ (Wt %)	35.14	4.82	0
MgO (Wt %)	4.69	14.56	20.22
$CaCO_3$ (Wt %)	0	0	11.95

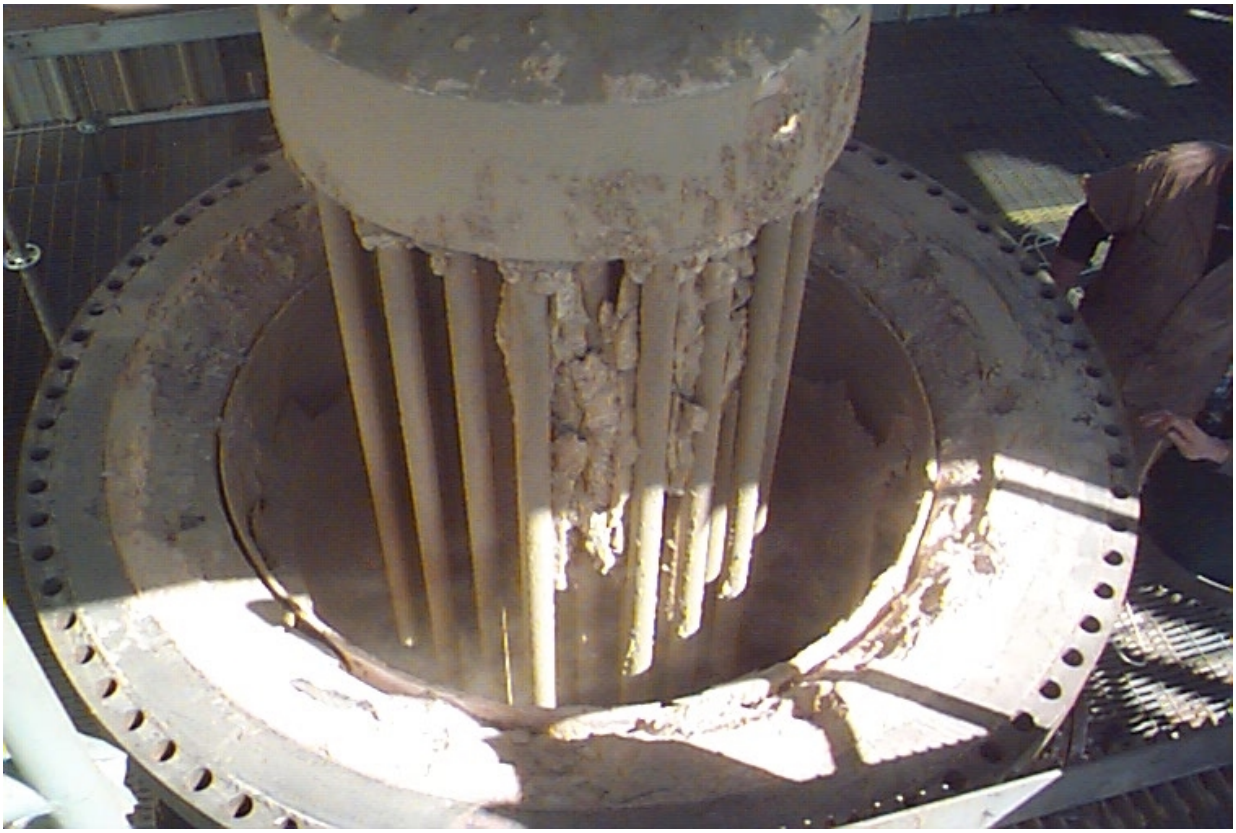

Figure 3.7-1 Overall View of Ash Bridging in Top Plenum

Figure 3.7-2 Close-up of Ash Bridging in Top Plenum

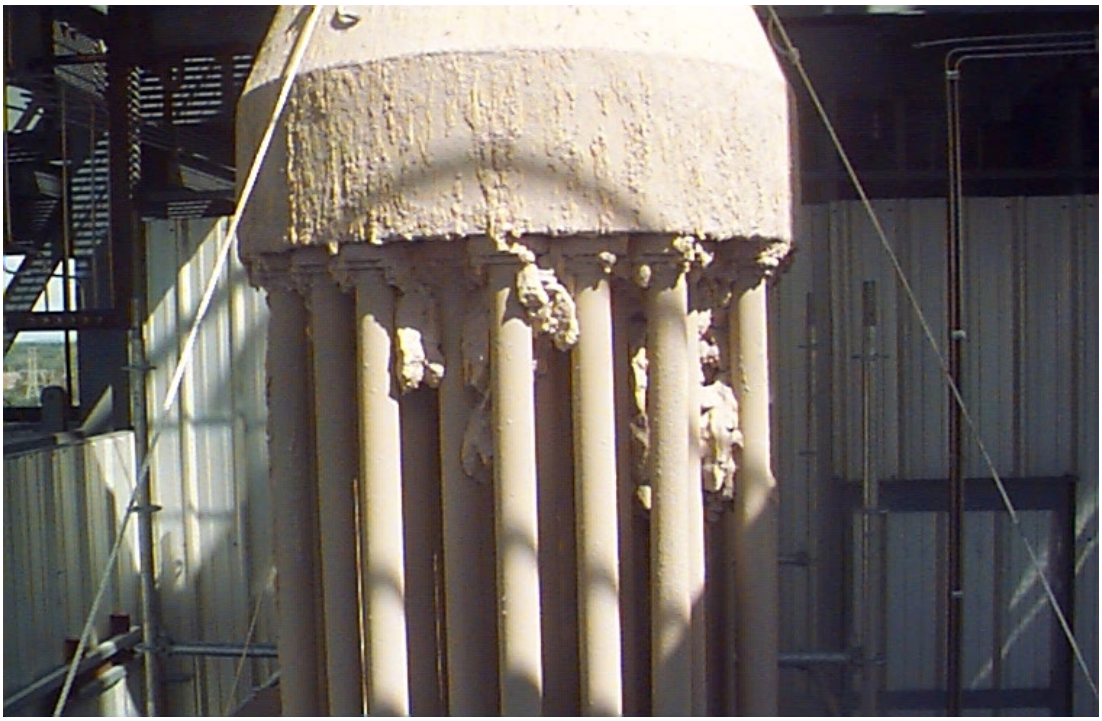

Figure 3.7-3 Overall View of Ash Bridging in Bottom Plenum

Figure 3.7-4 Close-up of Ash Bridging in Bottom Plenum

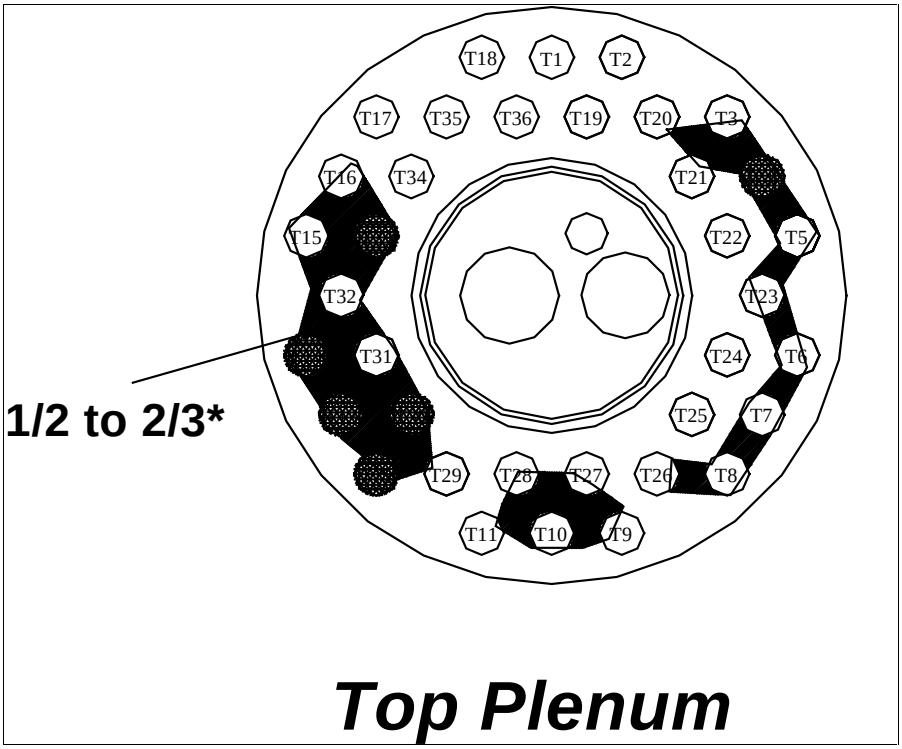

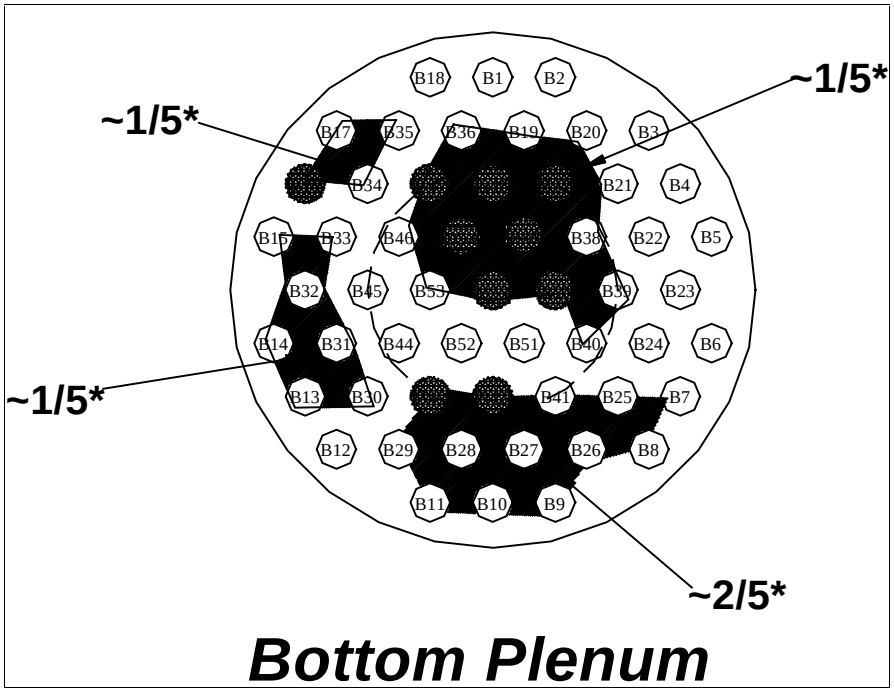

Figure 3.7-5 Locations of Retained Ash Bridges

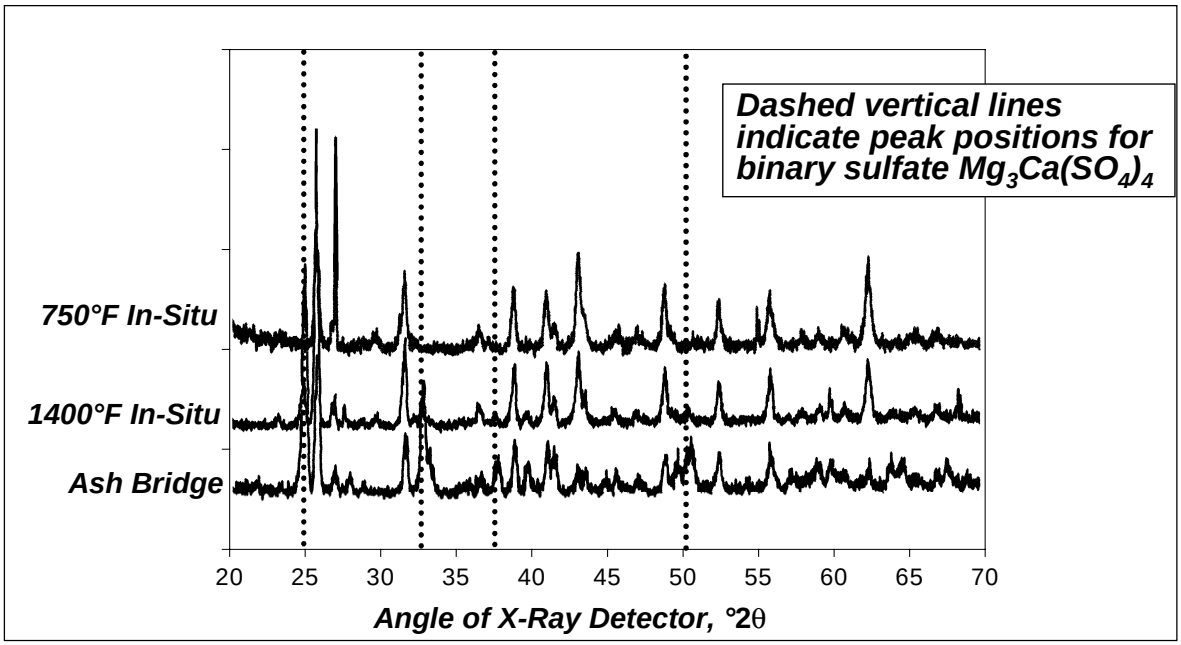

Figure 3.7-6 X-ray Diffraction Patterns of Ash Bridging Samples

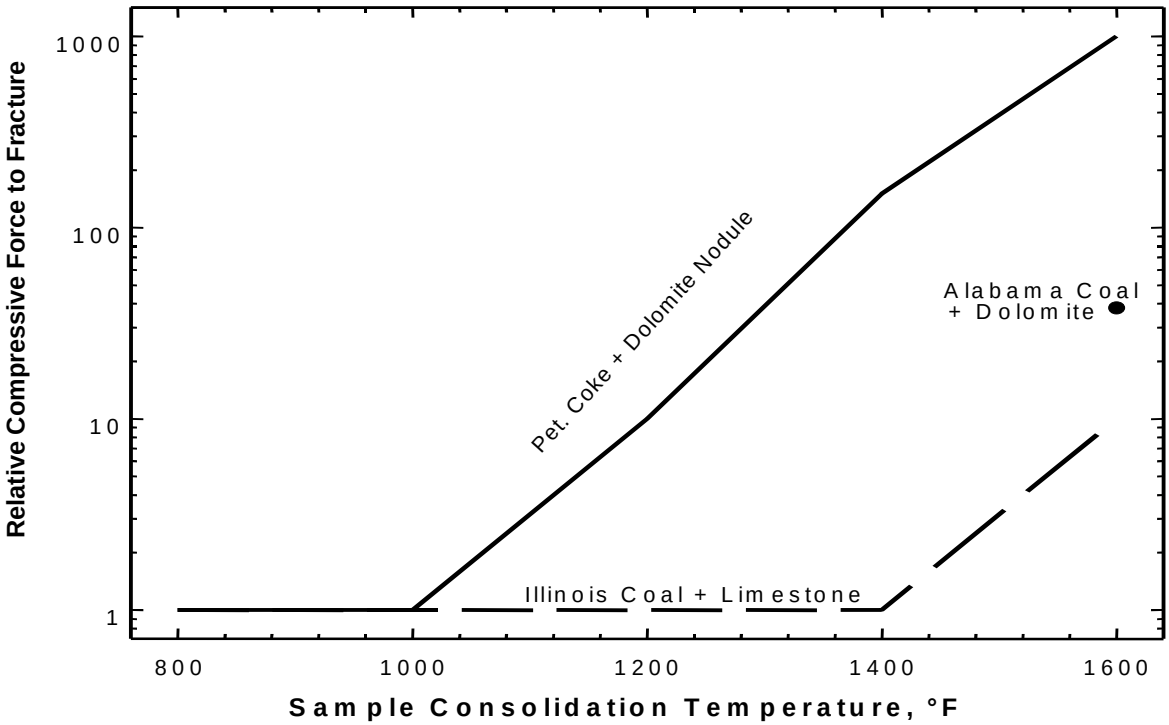

Figure 3.7-7 Relative Strengths of Various Reconsolidated Powders

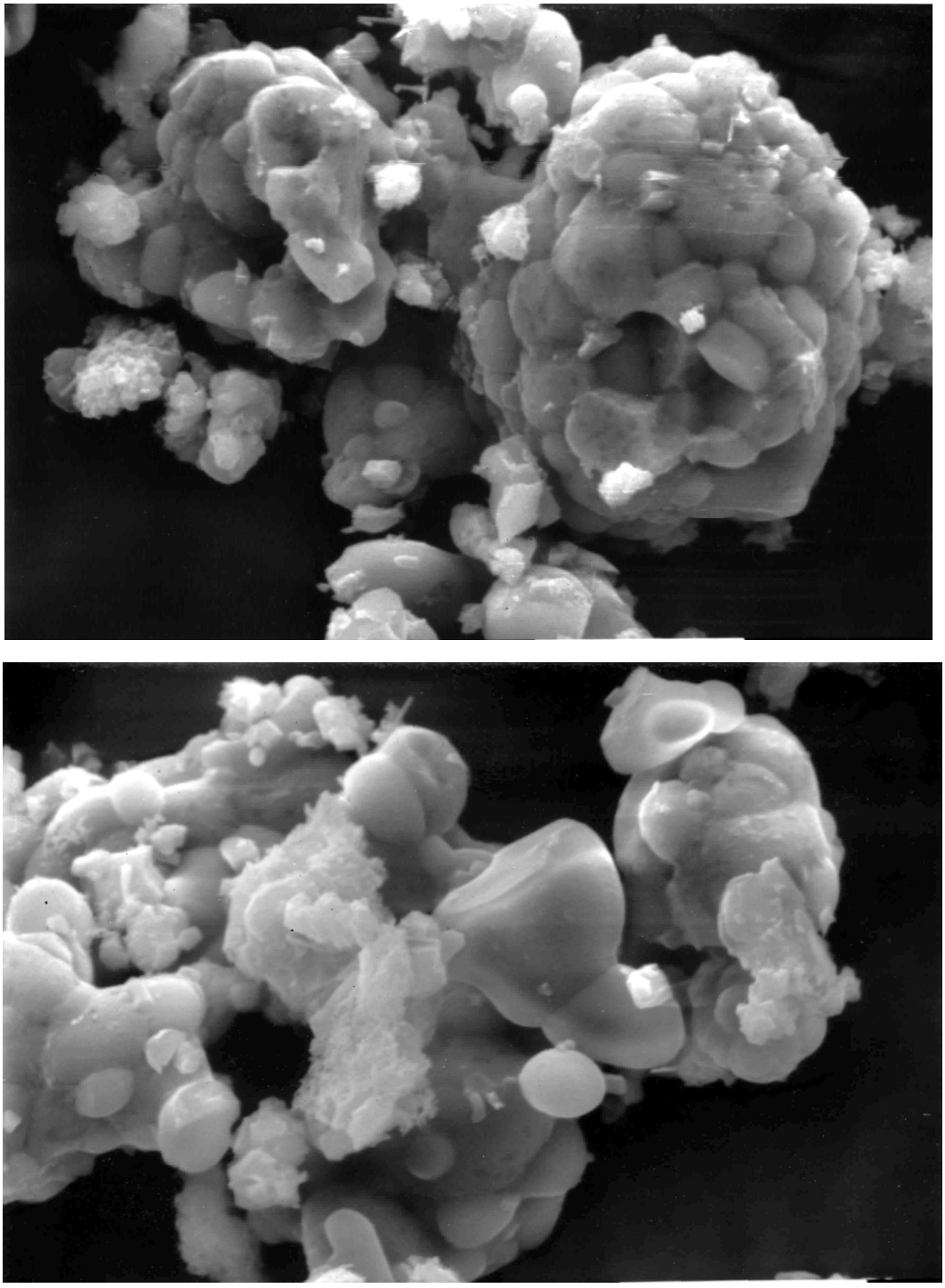

Figure 3.7-8 SEM Photographs of Bridged Material from Hot-Gas Filter
(Top Photo at 2600x and Bottom Photo at 3100x)

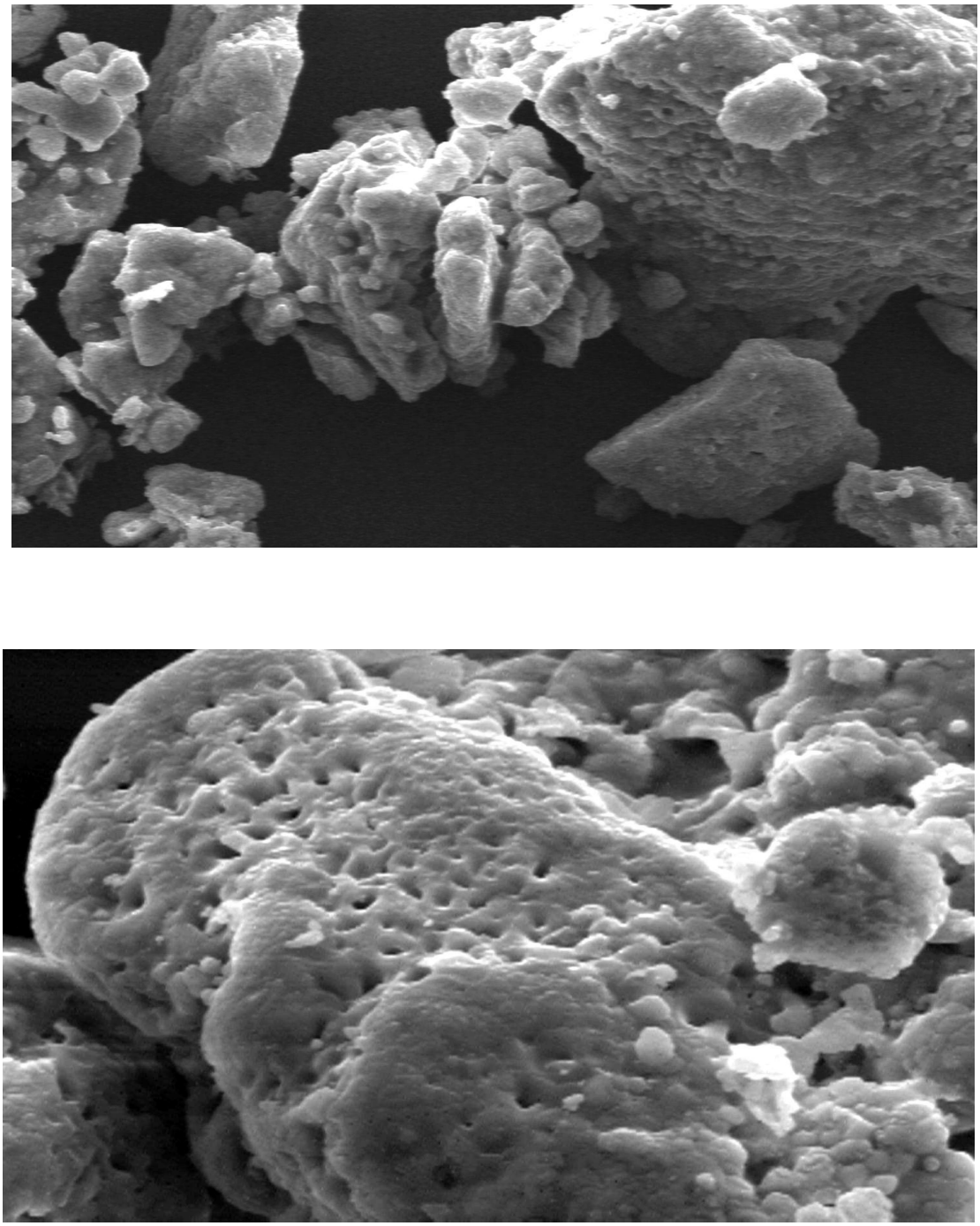

Figure 3.7-9 SEM Photographs of In situ Dust Sample Collected at Inlet of Hot-Gas Filter
(Top Photo at 1300x and Bottom Photo at 2600x)

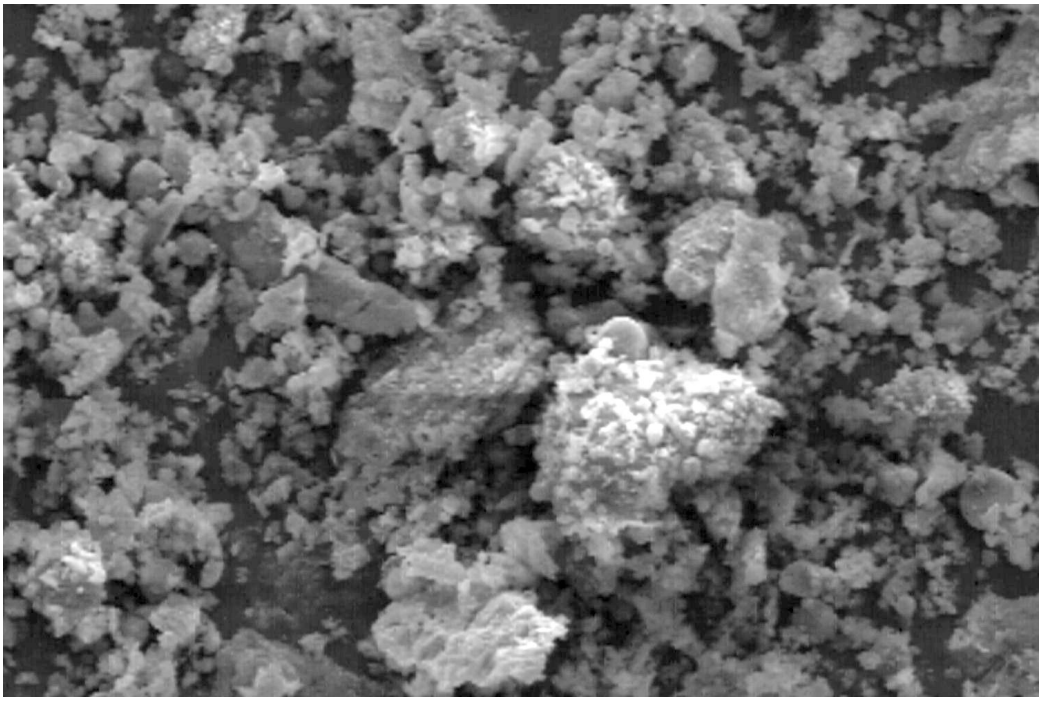

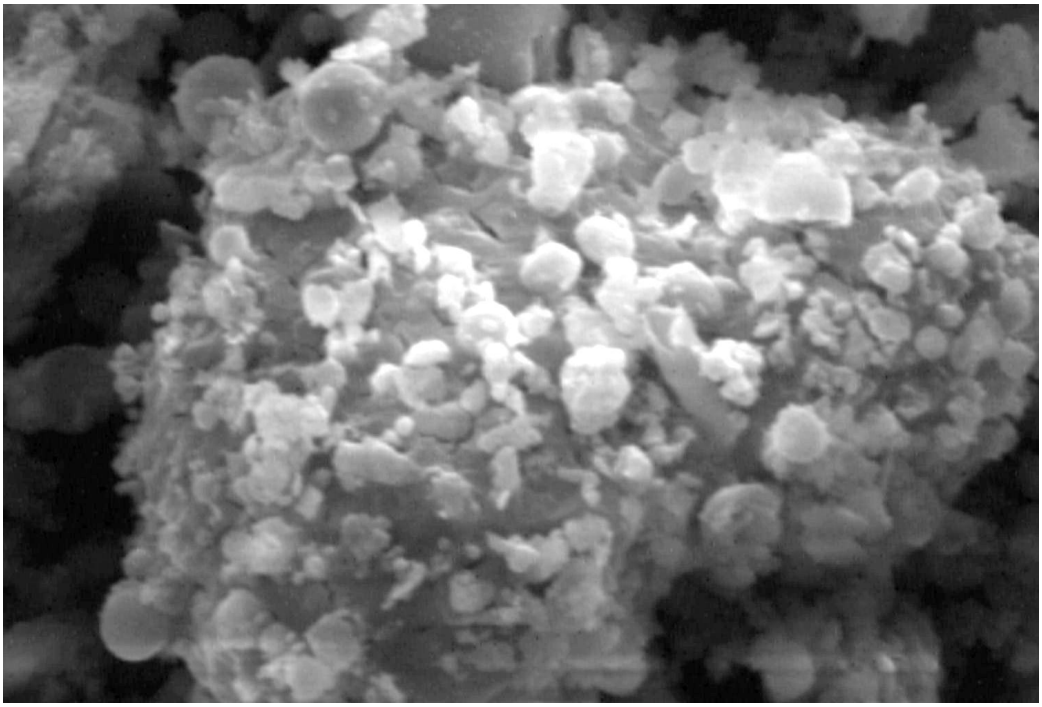

Figure 3.7-10 SEM Photographs of Residual Dustcake from Alabama Coal and Plum Run Dolomite (Upper Photo at 600x and Bottom Photo at 2600x)

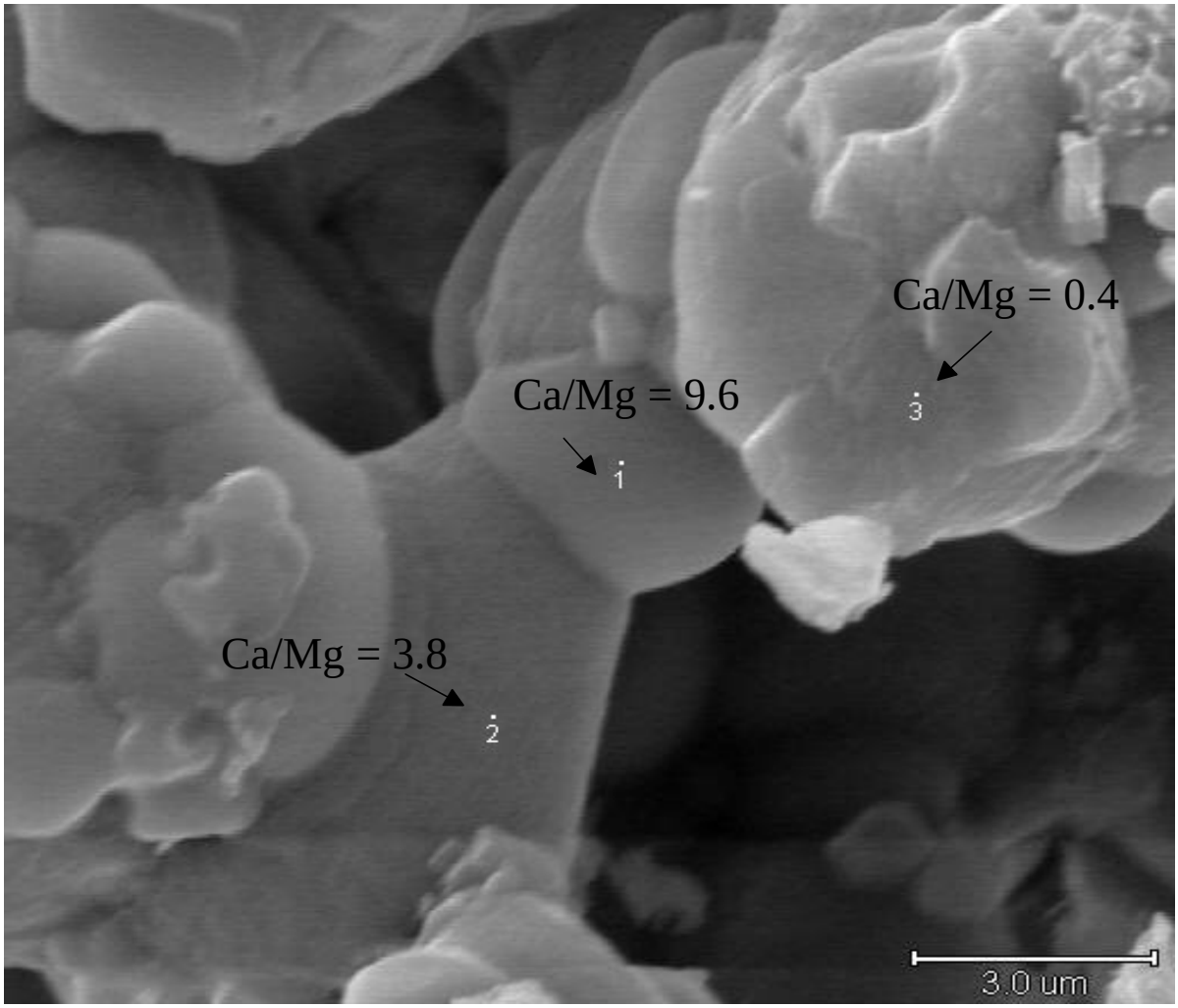

Figure 3.7-11 Close-up of Ash Bridging Showing Variations in Ca/Mg Atomic Ratio (Photo at 10,000x)

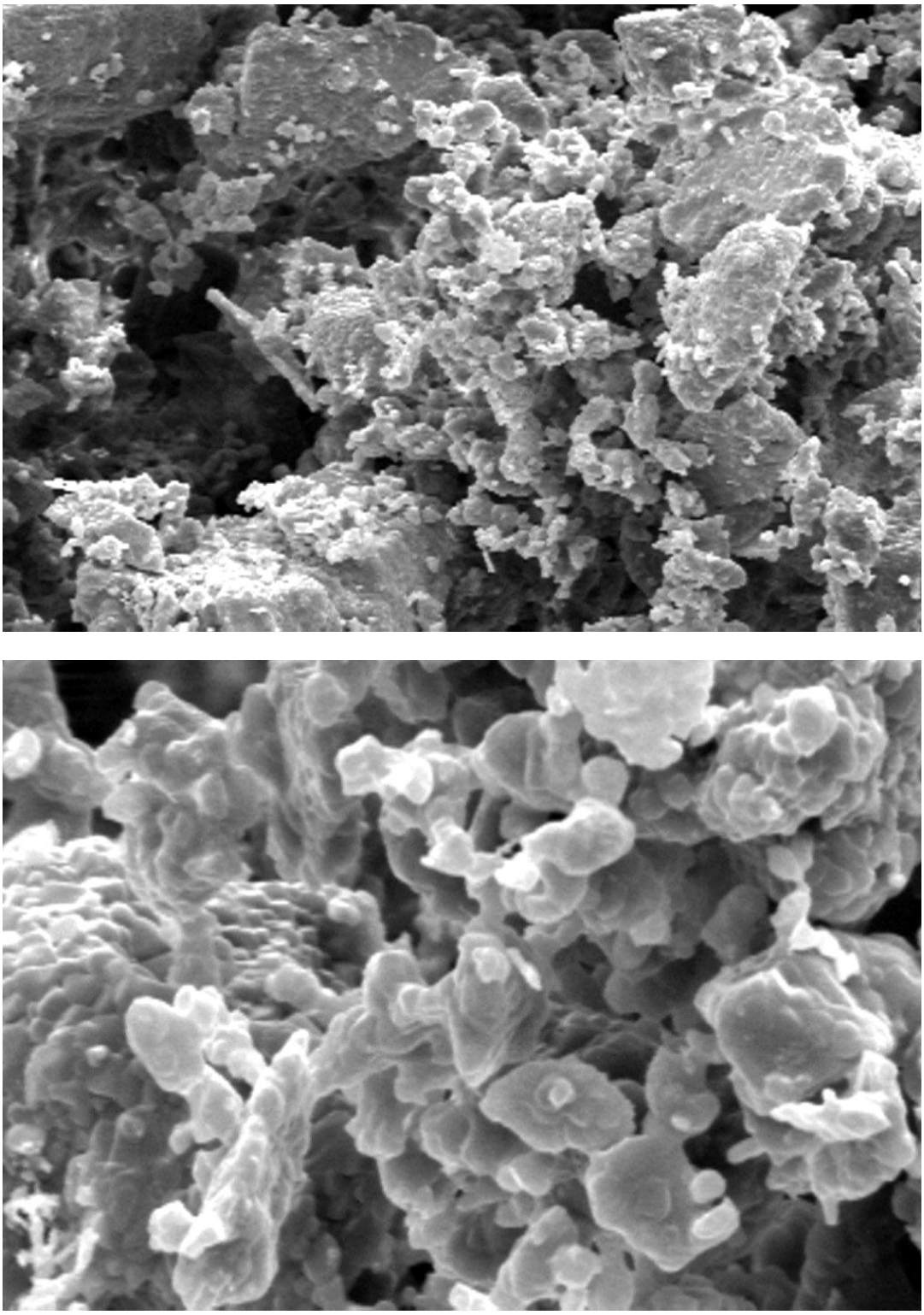

Figure 3.7-12 SEM Photographs of Sulfated Dolomite From Flow-Tube Furnace Tests
(Top Photo at 600x and Bottom Photo at 2600x)

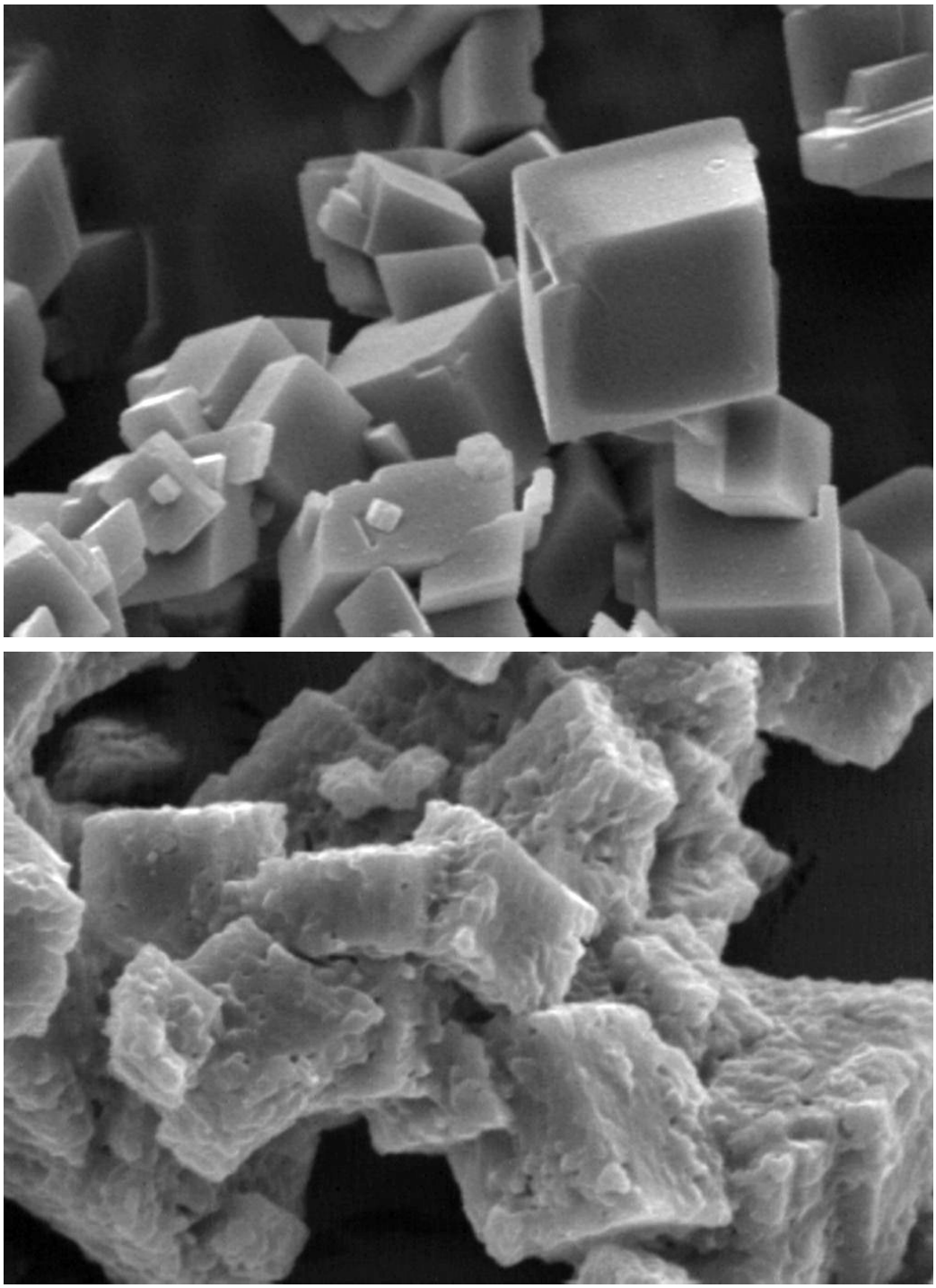

Figure 3.7-13 SEM Photographs of $CaCO_3$ Before and After Treatment in Flow-Tube Furnace (Top Photo Before Treatment and Bottom Photo After Treatment, Both Photos at 3000x)

4.0 TRANSPORT REACTOR

4.1 TC05 RUN SUMMARY

Test run TC05 coal feed was started on January 14, 1999, and ended on May 2, 1999, with 1,429 hours on coal feed. The mode of operation was combustion. See Table 4.1-1 for the TC05 operating conditions. The objectives of test run TC05 for the transport reactor were as follows:

- *Different feedstock combinations* – Demonstrate stable reactor operations using Alabama Calumet Mine coal and Eastern Kentucky coal with Ohio Bucyrus limestone, Alabama Longview limestone, and Florida Gregg Mine limestone.

- *Design coal* – Demonstrate stable reactor operations using the design coal, Illinois No. 6 with Plum Run dolomite, Ohio Bucyrus limestone, Alabama Longview limestone, and Florida Gregg Mine limestone.

- *Effects of reactor conditions on NO_X emissions* – Vary excess air, air distribution, sorbent type and feedrates, and operation temperature.

- *Effects of reactor conditions on SO_2 emissions* – Vary Ca/S molar ratio, solids inventory, solid circulation rate, and operation temperature.

- *Alternate fuels* – Demonstrate stable operations using petroleum coke and a Powder River Basin (PRB) coal with different sorbents.

Preliminary work included pressure check of the reactor and repair of leaks, pressure balance of the PDTs, and filling the reactor and heat exchanger with 122 μm mmd sand. The coal at the start of the test run was Calumet Mine coal with Bucyrus limestone sorbent. The coal and sorbent analyses are listed in Tables 4.1-2 and -3. The reactor heatup and the start of coal feed on January 14 and 15 were smooth and was similar to previous test runs. On the morning of January 15 the standpipe level and circulation were unusually high, which was later determined to be a result of the combustor heat exchanger vent valve being closed. Subsequent start-ups have used this technique to increase the standpipe level and preferentially induce high-solids-circulation rates through the reactor J-leg when necessary.

Test runs TC05A-1 through TC05A-25 (some transient conditions are also numbered), conducted between January 15 and January 20, 1999, tested the effects of sorbent rate on SO_X emissions, the effects of temperature, and air distribution on NO_X emissions.

On January 20, 1999, the Bucyrus limestone was stopped and the SO_X was allowed to increase before introducing Longview limestone. Test runs TC05B-1 through -5 were conducted on sorbent rate and on staging air effects on NO_X. The PCD showed a high-particulate-outlet loading of 22 ppm at the high-face-velocity test. The system was shutdown on January 22, 1999.

Alabama coal feed resumed on February 1, 1999, after adding a full set of candles to get the normal 3 ft/min face velocity. At start-up, the start-up burner tripped two times with subsequent stopping of the coal feed. Coal feed resumed early on February 2 but sorbent was not added until February 3. On February 5 the middle valve on FD0210 coal feeder did not indicate that it was closed, resulting in intermittent coal feed from 01:45 to 09:15. The valve position indicator arm was discovered to be bent from its normal position and was subsequently placed back in the normal position. Tests were run on the effect of sorbent rate on SO_X, N_2O, and NO_X and the effects of staging air for tests TC05B-1 through -21 for January 20 to February 6. Reactor stability continued to improve.

On February 6, Longview limestone ran out and was switched to Bucyrus limestone. Illinois No. 6 coal was added to the remaining Alabama coal. Coal was changed from Alabama to Illinois No. 6 coal on February 7. Reactor operation was smoother. Tests TC05C-1 through -10 were conducted for sorbent rate on SO_X, N_2O, NO_X, staging air, and the effects of coal-feed rate, higher reactor and PCD temperatures as well as lower coal-feed rates.

On February 13, the sorbent was changed to Longview limestone. Tests TC05D-1 through -9 were conducted to observe the effect of higher temperature, staging air, and sorbent rate. The FD0520 vent valve failed and the unit was taken off coal on February 15 for 20 hours to repair the vent valve. A broken fluffing nozzle from the PCD was found in the FD0520 exit. Coal feed resumed on February 16. On the morning of February 20 the reactor temperature began to alternately drop and rise by 50 to 70°F. That afternoon, feeding of dolomite was started for test TC05E-1. On February 22 there were a number of problems. The discharge line on FD0520 (PCD ash) plugged frequently, the reactor circulation was decreased, and the coal feeder tripped due to a dispense vessel spheri valve not indicating its position closed. The compressor surged a couple of times. On the second surge the dipleg was lost and did not recover. A significant amount of solids was passed to the PCD. The FD0520 was plugged with fiberfrax and filter element pieces. Although operations were briefly resumed, PCD outlet loadings were too high and testing was discontinued on February 24 to inspect the PCD. The fluffing nozzle and the fiberfrax in FD0520 were the result of the shifting shroud in the PCD. Three broken filter elements were replaced.

On March 4, coal feed was started in FD0220 with a fuel mixture of Illinois No. 6 and pet coke with dolomite as the sorbent on top of sand. Test number TC05E-2 was run on a mixture of Illinois No. 6 coal and pet coke. As the fuel transitioned completely to pet coke the TC05F test series began. On March 6 the reactor circulation was very erratic as evidenced by sudden temperature drop from 1,370 to 970°F in 3 minutes. The temperature would then return to normal in 10 minutes (these occurred at 00:40, 08:10, 09:45, 11:45, 13:08, and 14:15). The reactor was shut down at 16:10 and drained of solids. No clinkers were found. Refractory inspections were OK. Three nozzles on the reactor J-leg were unplugged and had to be drilled out.

On March 7 the reactor was refilled with 3,500 lb of sand; however, the start-up burner pilot would not light. An outage was taken from March 8 to 13 to repair the start-up burner pilot and place the primary gas cooler, HX0202, in service to keep PCD temperatures low. On restart the start-up burner tripped three times but could be relit. Pet coke and dolomite feeds were started on March 14. For this segment of the pet coke run the standpipe aeration was reduced. The

theory for the loss-of-circulation in the previous segment was that the standpipe was overly aerated. The coal feeder tripped two times due to a sticking shuttle valve that controlled the lock vessel spheri valve. Data on the effects of pet coke, oxygen, reactor pressure, and reactor temperature were taken via TC05F-1 through -6 from March 5 through 20.

On March 20 sorbent feed was switched to Bucyrus limestone. TC05G-1 through -4 were performed to test Ohio limestone, pressure effect, oxygen effect, and lower circulation rate. The unit was running well until March 22 when the coal feeder lock vessel began to plug with fines and the motor speed was increased form 8.30 to 11.4 rpm. The unit was taken off line at 00:00 on March 23.

Upon restart, the start-up burner would not light. The pilot tip and shroud were burned out. Pet coke and Bucyrus limestone feeds were started on March 25. Tests TC05G-5 and -6 were completed to test oxygen effect and lower circulation rates. On March 27 the dipleg would not drain into the standpipe. The reactor was shut down, ending the pet coke tests. Upon inspection, refractory pieces from the primary cyclone roof were found blocking the cyclone dipleg. Other parts of the reactor were clean. When the reactor was depressurized a heat transfer fluid started leaking from FD0206 (screw cooler for standpipe solids) into FD0510 and FD0530. The rotofeed on FD0530 would not turn with the wet solids. The leak was a cracked weld at the solids inlet to the screw cooler where there is an annular heat transfer cooling section. Repairs included cutting off the outer shell, welding the weld crack on the inner side of the annulus, and replacing the shell. Some carbonization of the heat transfer fluid was found. Since the annular area does not have a high-point drain, a 2-in. nozzle was added to drain gas. During the outage the primary gas cooler was partially bypassed by connecting the bypass orifice in parallel to the cooler. All of the pet coke was removed.

Upon restart, 12,000 lb of sand was added to the reactor and heat exchanger with another 3,000 lb of sand added from FD0220 during start-up. Alabama coal and Bucyrus limestone feeds were started on April 12. Tests for Alabama coal and Bucyrus limestone, lower heat-exchanger level, and low-circulation and lower reactor temperature were completed (tests TC05H-1 through -4).

PRB coal was ground and added on top of the Alabama coal. The transition from Alabama coal to PRB occurred between 18:00 on April 16 and 19:00 on April 17. Test series TC05I began on PRB at 10:00 on April 18. The staging air effect, lower circulation rate, no-sorbent effect, and higher reactor temperature are included in runs TC05I-1 through -11. During this period and throughout the rest of the run the heat exchanger could not be filled up because at least once a day a dipleg upset would cause the loss of accumulated solids. Due to the low-solids level sand was fed along with the Bucyrus limestone as a mixture from FD0220.

On April 26 the mixing-zone-pressure drop started to increase after one of the dipleg upsets, indicating that some degree of a clinker had formed. Also, Bucyrus limestone had run out and was replaced with Florida limestone. Tests TC05J-1 through -4 were run between April 26 and 29.

On April 28, the coal feeder again ran into problems transporting fine coal, as observed by the lower weights of coal that would go into the lock vessel. Since the coal would not drop into the dispense vessel the dispense vessel ran out of coal with no feed to the reactor. When the coal

feed was brought back the feed rate was too high, resulting in a temperature spike to 1,600°F. On April 28 more dipleg upsets occurred due to coal feeder problems in handling fines. Four tons of Alabama coal were ground at 07:35 and fed in the interim until the Eastern Kentucky coal could be delivered to the site. Eastern Kentucky coal was ground at 14:00, resulting in blends of three different coals fed on April 28.

Feeding of the Eastern Kentucky coal with Florida limestone began on April 29. Tests for sorbent rate and coal type were done in TC05K-1 and -2. On April 30 to May 2, the mixing-zone-pressure drop continued to increase, indicating the mixing zone was mostly plugged with clinkers. The coal-feed line plugged at 05:52 on May 2 and the reactor was shut down. Upon inspection, the mixing zone was mainly filled with clinkers, with only a small passage through the middle for flow. The length of this zone was about 6 feet.

Major accomplishments and observations from TC05 include the following:

1. Stable operations were demonstrated in all feedstock combinations tested. There was some agglomerate/clinker formation with the Powder River Basin coal due to a temperature excursion and the presence of excessive fines in the fuel feed. Deposits grew quickly while using the Eastern Kentucky coal during time periods when excess fines were present and eventually forced a process shutdown.

2. The TC05 test run included the longest continuous trouble-free operation to date without any interruption from the coal-feed system or any other subsystem (471 hours).

3. High-carbon conversions along with high throughputs were achieved consistently with different fuels and a multitude of process conditions.

4. Heat release rates as high as 57 MBtu/hr/ft^2 in the riser were achieved.

5. High-solids circulation rates (more than 100:1 solids circulation rate:coal-feed rate) were achieved.

6. A high-sulfur capture (greater than 97 percent) was achieved at a Ca/S molar ratio of 1.5. Low-SO_X emissions were achieved when using PRB without adding sorbent due to high-Ca content in PRB ash.

7. NO_X emissions of less than 0.10 lb/MBtu were achieved with the Alabama and Illinois No. 6 bituminous coals and NO_X emissions of less than 0.15 lb/MBtu were achieved with the Eastern Kentucky bituminous coal and pet coke. Essentially zero-N_2O emissions are achievable at higher operating temperatures.

8. For test purposes, fine sorbent was successfully ground and fed (<40 um mmd).

9. Stable operations were achieved with petroleum coke for 257 hours. Average carbon conversion was 99.2 percent between 1,575 and 1,640°F at high throughputs.

Table 4.1-1

TC05 Operating Conditions

Start-up Bed Material	140 μm SMD Sand
Fuel	• Alabama Calumet Mine Bituminous Coal From Mary Lee Seam. • Illinois No. 6 Bituminous Coal From Marissa Mine in Washington County. • Eastern Kentucky Coal From Clover Mine (Hazard No. 4 Seam) in Hazard County. • Petroleum Coke. • Powder River Basin Coal From Belle Ayre, Jacobs Ranch, and North Antelope Mines in Wyoming.
Fuel Particle Size	275 to 400 μm SMD
Average Fuel Feed Rate	1,000 to 1,800 lb/hr
Sorbent	• Ohio Bucyrus Limestone. • Alabama Longview Limestone. • Gregg Mine Florida Limestone. • Plum Run Dolomite.
Sorbent Particle Size	10 to 20 μm SMD
Average Sorbent Feed Rate	50 to 300 lb/hr
Ca/S Molar Ratio	Amount Required for 95 to 99-%-Sulfur Capture
Reactor Temperature	1,500 to 1,625°F
Reactor Pressure	150 to 220 psig
Primary/Secondary Air Split	0.25 to 1.0
HX0203 Inventory	Half-Full — Nearly Full
Planned Duration of Coal Feed	Nominally 1,000 Hours

Table 4.1-2

Coal Feed Analyses

	Alabama	Illinois No. 6	Pet Coke	PRB	E. Kentucky
Moisture (%)	2.2	4.2	1.2	15.4	1.8
Ash	16.9	11.8	2.8	8.5	10.0
Sulfur	0.9	2.9	5.6	0.6	1.3
C	66.4	67.0	76.4	58.6	73.9
H	4.3	4.4	3.7	4.0	4.8
N	1.6	1.4	1.6	1.0	1.6
O	7.8	8.3	8.7	11.9	6.6
Vol	31.2	38.3	15.2	36.1	36.1
Fix C	49.5	45.7	80.8	40.1	52.1
Calculated Heating Value (Btu/lb)	11,911	11,947	12,938	10,091	12,722

Table 4.1-3

Sorbent Analyses

	Plum Run Dolomite From Ohio	Gregg Mine Limestone From Florida	Bucyrus Limestone From Ohio	Longview Limestone From Alabama
$CaCO_3$ (wt %)	49.7	90.4	73.0	88.7
$MgCO_3$ (wt %)	41.9	1.1	15.8	5.5
Inerts (wt %)	8.4	8.5	11.2	5.8

4.2 MATERIAL BALANCE

Four separate periods during TC05 were selected for material balances. The periods were selected to provide data on a relatively steady-state, 24-hour interval for each of four different fuels fired during the campaign. Table 4.2-1 lists the intervals and operating information for the interval. The periods will be referred to by the fuel in subsequent discussions. Data was not suitable for analysis on the fifth fuel/sorbent combination in TC05 (Eastern Kentucky coal) due to brevity of the run caused by deposits blocking the mixing zone.

The bulk material balances closed to within 1.0 percent for all four periods. Table 4.2-2 gives detailed information on the bulk material balances.

The most difficult flow to calculate is the fine ash flow. The fine ash flows presented are derived from a combination of weigh cell readings on the ash removal system and component balances. The error margin, based on the extremes for the ash flow that are found using only the weigh cells or only a single component, is estimated at around 50 percent. This error margin is only relevant in component balances in which a majority of a component is found in the ash leaving the reactor. The sorbent for the PRB balance includes sand that was added to maintain bed level while firing the low-ash PRB coal. The component balances attempt to use the correct sorbent flow. Because of the sand, the fine ash flow was determined solely from the weigh cells.

The performance of the transport reactor can best be seen by looking at the sulfur and carbon component balances. Table 4.2-3 gives data on the carbon balances. The petroleum coke test had the lowest carbon conversion, which was still 99.3 percent. Notably, the PRB test achieved a carbon conversion of 99.9 percent at a temperature of 1,520°F.

The sulfur balances are in Table 4.2-4. The sulfur capture in each case was very high. The large error in the mass balance in the Illinois No. 6 case could be evidence that the fine ash flowrate calculated is too high.

The oxygen component balance is shown in Table 4.2-5. All of the oxygen balances closed to within 5 percent.

The excess air used during the balance periods ranged from 12 percent for the Alabama coal to 49 percent for PRB.

The nitrogen component balance is shown in Table 4.2-6.

Table 4.2-1

Material Balance Periods in TC05
(February 17 - April 22, 1999)

Date	February 17	March 18	April 14	April 22
Fuel	Illinois No. 6 Coal	Petroleum Coke	Alabama Bituminous Coal	Powder River Basin Coal
Sorbent	Alabama Longview Limestone	Plum Run Dolomite	Ohio Bucyrus Limestone	Ohio Bucyrus Limestone
Temperature (Degree F)	1,535	1,585	1,610	1,520
Pressure (psig)	200	190	200	200

Table 4.2-2

Bulk Material Balances in TC05

Period (Fuel)		Illinois No. 6 Coal	Petroleum Coke	Alabama Bituminous Coal	Powder River Basin Coal
Feeds (pph)	Coal	1,456	1,247	1,681	1,365
	Sorbent	187	435	115	66
	Air	20,479	18,960	20,264	19,267
	N_2	5,316	4,712	5,285	4,824
	Totals	**27,438**	**25,354**	**27,345**	**25,522**
Products (pph)	Flue Gas	26,816	24,550	26,630	25,309
	Fine Ash	290	510	350	208
	Coarse Ash	5	25	13	20
	Accumulation	74	2	–7	–41
	Totals	**27,185**	**25,087**	**26,986**	**25,496**
In/Out		1.01	1.01	1.01	1.00

Table 4.2-3

Carbon Component Material Balances in TC05

Period (Fuel)	Illinois No. 6 Coal	Petroleum Coke	Alabama Bituminous Coal	Powder River Basin Coal
In (pph)	1,003.3	999.7	1,114.3	797.6
Out (pph)	1,000.5	1,144	1,213.4	817.9
In/Out	1.00	0.87	0.92	0.98
Unburned (pph)	1.8	6.3	1.3	1.1
Conversion (%)	99.8	99.3	99.9	99.9

Table 4.2-4

Sulfur Component Material Balances in TC05

Period (Fuel)	Illinois No. 6 Coal	Petroleum Coke	Alabama Bituminous Coal	Powder River Basin Coal
In (pph)	47.5	72.9	14.1	6.4
Out (pph)	24.6	68.6	15.2	7.6
In/Out	1.93	1.06	0.93	0.84
Ca/S (Feed)	1.2	1.3	2.2	*
Sulfur Capture (%) (Based on SO_2)	99.4	99.4	97.9	98.7

* Mixture of sand and sorbent was fed to the reactor.

Table 4.2-5

Oxygen Component Material Balances in TC05

Period (Fuel)	Illinois No. 6 Coal	Petroleum Coke	Alabama Bituminous Coal	Powder River Basin Coal
In (pph)	4,953	4,659	4,870	4,686
Out (pph)	4,929	4,809	5,141	4,926
In/Out	1.00	0.97	0.95	0.95
O_2 (Flue Gas %)	5.3	4.2	3.9	7.9
Excess O_2 (%)	18	23	12	49

Table 4.2-6

Nitrogen Component Material Balances in TC05

Period (Fuel)	Illinois No. 6 Coal	Petroleum Coke	Alabama Bituminous Coal	Powder River Basin Coal
In (pph)	20,844	19,089	20,656	19,426
Out (pph)	22,137	19,935	21,778	20,869
In/Out	0.94	0.96	0.95	0.93
N_2 (Flue Gas %)	85.5	84.1	84.7	85.4
NO_X (ppm)	59	86	37	152
NO_X (lb/MBtu)	0.09	0.12	0.05	0.28

4.3 SO_2, SO_3 AND SOLIDS ANALYSES

During TC05 solids were collected from the fuel feed system (FD0210), the sorbent feed system (FD0220), the standpipe spent solids transport system (FD0510), and the PCD fine solids transport system (FD0520). These solids were analyzed for chemical composition and particle size. The SO_2 emissions were also continuously measured and recorded by the Plant Information System (PI). This section will use the chemical analysis data and SO_2 emissions data to show:

- Chemical composition changes during a test.
- Effect of sorbent on sulfur dioxide removal.
- Particle-size and solids-bulk-density changes during a test.
- Sulfur and calcium balances.
- Thermodynamic equilibrium in the sulfur dioxide–sulfur trioxide system.
- Levels of unburned carbon–combustion efficiency.
- Sulfur trioxide (SO_3) emissions.
- Hydrochloric acid (HCl) emissions.

Coal feed for run TC05 began on January 14, 1999; this run consisted of 11 separate test periods (A to K) distinguished by the fuel and sorbent used. The start and end time of each test as well as the fuel and sorbent are shown on Table 4.3-1. Note that tests A and H have the same fuel and sorbent. The exact test start and end times are not precise because each new fuel and sorbent was placed on top of the previous fuel or sorbent in the feed-bin system. There is some rat holing and backmixing of solids that could result in solids arriving at times other than those expected. The feeds solids analyses show that there were periods when mixtures of two fuels or two sorbents were fed.

The fuels used during TC05 were:

- Alabama Calumet Mine bituminous coal (tests A, B, and H).
- Illinois No. 6 coal from the Pattiki Mine owned by the White County Coal Corporation (tests C, D, and E).
- Petroleum coke from the Hunt Oil Company in Tuscaloosa, Alabama (tests F and G).

- PRB Coal (a mixture of four different coals; tests I and J).
- Eastern Kentucky bituminous coal (test K).

The 8-hour averages for standpipe temperature, PCD temperatures, and reactor pressures are shown in Figures 4.3-1 and -2. The Alabama bituminous tests (A and B) were characterized by 1,600°F reactor temperatures, 200-psig reactor pressure, and 1,350°F PCD temperatures. The Illinois No. 6 coal tests (C, D, and E) were characterized by 200-psig reactor pressure and slowly decreasing reactor temperatures from 1,600 to 1,500°F. The reactor temperature was typically controlled to maintain the PCD below 1,350°F. The first petroleum coke test (F) was started at the same reactor conditions as the last Illinois coal test (E). The reactor was shut down after a few days of petroleum coke operation due to unstable reactor conditions. When the PCD was inspected the candles were bridged with ash. As a result, the blind was placed in the bypass around the primary gas cooler (HX0202) to cool the PCD to around 725°F. The reactor pressure was slowly increased from 160 to 200 psig during petroleum coke testing with dolomite (F) and maintained at 200 psig during petroleum coke test with limestone (G) until nearly the end of test G when the pressure was raised to 210 psig. The reactor temperature was slowly increased from 1,525 to 1,600°F during petroleum coke test with dolomite (F) and maintained at 1,600°F during the petroleum coke test with limestone (G).

At the beginning of test H an orifice was placed in the bypass around the primary gas cooler (HX0202) to increase the PCD temperature. The Alabama bituminous test H started at 1,600°F reactor temperature but was decreased to 1,525°F. Reactor temperature was decreased during test H to prepare for PRB coal operation. The reactor temperature decrease in turn reduced the PCD temperature from 1,200 to 1,100°F. The PRB with Ohio limestone test I was at 200 psig and reactor temperature of 1,500°F and a PCD temperature of 1,025°F. During PRB operation with Florida limestone (J) the reactor pressure was lowered to 190 psig, which then continued through the Eastern Kentucky coal test (K). The reactor temperature was maintained constant during the last two tests (J and K) at around 1,550°F. The PCD temperature increased about 75°F (to a temperature of 1,100°F) at the start of PRB operation with Florida limestone (J) on March 26.

The 8-hour averages for the fuel-feed rate (by CO_2) and the SO_2 PCD-exit concentrations are shown in Figures 4.3-3 and -4. The fuel-feed rate is calculated from the flue-gas rate, CO_2 content of the flue gas and the carbon content of the fuel. During periods when the gas analyzers were being serviced the fuel rates shown on Figures 4.3-3 and -4 were determined by the weigh cell differences.

The coal rate generally increased from January 15 through February 15 (tests A, B, and C) from 1,000 to 1,800 lb per hour coal. After the brief shutdown in test D the coal rate again was slowly increased to 1,750 lb per hour. The fuel rate is usually controlled to maintain the reactor at a desired temperature. The fuel rate on petroleum coke (test F) from March 5 to 7 was 1,250 to 1,500 lb per hour. From March 14 to March 17 (test F) the fuel rate increased from 1,000 to 1,400 lb and then decreased to 1,150 lb on March 20. The fuel rate was steady for a few days

during the beginning of petroleum coke test G until the outage on March 23. The final 2 days of petroleum coke began at 1,500 lb per hour and then decreased to 1,150 lb per hour.

The Alabama bituminous coal test H started at a fuel rate of 1,800 lb per hour, then was decreased to 1,500 lb per hour. Note that the reactor temperature decreased at the same time that fuel-feed rate was decreased. The fuel rate was varied between 1,100 and 1,800 lb per hour during the PRB coals tests (I and J). This was because it was difficult to maintain the transport reactor bed height due to daily dipleg upsets which decreased the solids circulation rate and the fuel feed rate. There were several days at a constant fuel rate of 1,500 lb per hour during test I. The Eastern Kentucky coal test K had a coal feed rate of 1,200 lb per hour.

The SO_2 emissions were generally below 20 ppm for all the fuels except the petroleum coke tests (tests F and G). The unit was operated in TC05 to minimize SO_2 emissions and to prevent SO_3 plumes and, therefore, potential damage to downstream carbon steel equipment.

Figures 4.3-5 through -8 show the fuel sulfur and ash as sampled from the fuel feed system during TC05. Figure 4.3-5 shows the data for Alabama bituminous coal tests (A and B). The first week of testing (January 15 to 22) resulted in analyses consistent with previous Alabama bituminous at 1-percent sulfur and 17-percent ash. On February 3 the coal sulfur increased to 2 percent and ash decreased to 14 percent and continued at these levels until the switch to Illinois No. 6 coal. The Illinois No. 6 coal data is shown in Figure 4.3-6 where the trend of 2-percent sulfur and 14-percent ash continued for a few days and then changed to 3.2-percent sulfur and 10-percent ash. It appeared that there were two different seams of Alabama bituminous coal. The Illinois No. 6 coal sulfur and ash both leveled out until February 19, when the levels rose to 4.0-percent sulfur and decreased to 8.0-percent ash, possibly due to mixing with petroleum coke.

Figure 4.3-7 shows the sulfur and ash analyses contents of petroleum coke for tests F and G. The transition was quick to petroleum coke as the sulfur increased to about 5.5 percent and ash decreased to 1.5 percent a few days after the fuel switch. The actual petroleum coke ash (1.5 percent) was larger than expected (less than 0.5 percent).

Figure 4.3-8 shows the fuel sulfur and ash analyses of the last four tests (H, I, J, and K) on Alabama bituminous, PRB, and Eastern Kentucky coals. The sulfur data showed all the fuel switches: from petroleum coke (5.5 percent) to Alabama bituminous (1 percent), to PRB (0.5 percent), to Eastern Kentucky (1.3 percent). The ash content never leveled out for the last four tests but varied from 11- to 16-wt percent for Alabama bituminous, then slowly decreased to 6.0 percent for PRB, and increased to 9.5 percent for Eastern Kentucky coal.

The Sauter mean diameter (SMD) of the fuel sampled from the fuel feeder FDO210 is plotted on Figure 4.3-9. The fuel grind size was steady during the first week of Alabama coal operation (A) with an average SMD diameter of about 350 μm. On February 4 (B) there appeared to be a period of coal fines with SMD of 160 to 250 μm. On February 5 there were problems with the coal feeder. Operation on Illinois coal had the SMD increase gradually up to 375 from 350 μm and then drop down to 340 μm. The fuel SMD dropped below 300 μm on March 21 and 22, indicating the presence of fines. A system outage on March 22 was blamed on fuel fines in

FD0210. The petroleum coke tests (F and G) averaged about 340 μm at the beginning of the run, then decreased to 300 μm near the end of the run.

The SMD of the Alabama coal test H started at 350 μm, then decreased to 275 μm. The PRB SMD had a wider size variation than the other fuels and generally decreased from 425 to 325 μm during tests I and J. There was a period of coal fines at the end of the PRB test J with a low SMD of 125 μm. The Eastern Kentucky coal SMD also had a wide variation in values (175 to 375 μm) and seemed to have the lowest average SMD of around 200. Fines were certainly present during Eastern Kentucky coal operation. There was an outage on May 2 due to a coal line plug.

FD0220 was used during TC05 to feed:

- Ohio Bucyrus limestone (A, C, G, H, and I).
- Alabama Longview limestone (B and D).
- Ohio Plum Run dolomite (E and F).
- Florida Gregg Mine limestone (J and K).
- Wisconsin sand.

Limestone and dolomite were fed as both sulfur control and to maintain reactor inventory. Sand was fed during start-up and to maintain reactor inventory when the fuel sulfur level was low enough that sulfur emissions control did not require enough sorbent to maintain reactor level.

The Sauter mean diameter of the solids sampled from the sorbent feeder FD0220 are plotted on Figure 4.3-10. The solids were typically less than 20 μm, except when sand was added to FD0220 on start-up or to maintain bed height. During the PRB tests (I and J), from April 16 to 30, sand and limestone were alternately added to FD0220 to maintain bed height. This resulted from the lower sorbent requirement for the low-sulfur PRB coal.

Figures 4.3-11 and -12 show the $CaCO_3$, $MgCO_3$, $CaCO_3$•$MgCO_3$ and inert contents of FDO220 solids. Whenever the sorbent solids inerts content was above 10 percent, this coincided to when sand was added to FDO220. These periods are shown on Figures 4.3-11 and -12. The $MgCO_3$ content of the sorbent is the best indication of when limestones were changed, while the $CaCO_3$ content is the best indication of whether limestone and dolomite are used.

Ohio limestone has a higher magnesium content than Alabama limestone, as is shown in the transition from test A to B, test B to C, and test C to D. The dolomite appeared to come a bit early in the transition from test D to E on February 19 and the Ohio limestone came several days early in the transition of test F to test G. The addition of sand during startups after outages are seen clearly in the high inerts in the solids sampled from FD0220. Note the high inerts during start-ups on February 17, March 4, and March 14. During the period from April 16 to

April 26 for the PRB and from April 26 to April 30 for the Eastern Kentucky coal, sand and limestone were added alternately into FD0220, as can be seen by the wide variations in FD0220 solids compositions.

The Sauter mean diameter (SMD) of the reactor bed solids taken from the standpipe using the spent solids transport system FD0510 and of the solids collected by the PCD and sampled from the fine solids transport system FD0520 are shown in Figures 4.3-13 and -14. The reactor solids had a larger SMD than the PCD solids, as expected since the larger solids are collected by the cyclone and disengager and remain in the reactor.

The reactor solids SMD were very constant for the Alabama bituminous coal and Ohio limestone operation (A) at 150 μm. The reactor solids SMD was steady at 170 μm until midway through the Illinois coal and Ohio limestone test (C), when it jumped down to 140 μm. The reactor SMD stayed constant at 140 μm until the beginning of the Illinois No. 6 coal and dolomite test (E), when the reactor SMD then dropped down to 120 μm. The second start on petroleum coke with dolomite (F) has a constant reactor SMD of about 140 μm with several points around 80 μm. Once Ohio limestone was added (G), the reactor SMD increased to 170 μm and then decreased to about 140 μm after several days operation.

The Alabama bituminous–Ohio Limestone test (H) had a reactor SMD of 155 to 165 μm. The reactor SMD for the PRB coal–Ohio limestone (I) increased from 165 to 200 μm and then decreased back to about 170 μm just after the introduction of the Florida limestone (J). The higher SMDs were probably due to the sand additions. During tests J and K the reactor SMD was constant at about 170 μm.

The PCD solids for the Alabama bituminous–Ohio limestone test started at around 20 μm then increased for several days to 80 to 100 μm before decreasing back to 20 μm at the introduction of Alabama limestone (B). After test B was restarted on February 1 the PCD SMDs were fairly constant at 15 to 30 μm. The introduction of Illinois coal (C) increased the PCD SMD to 60 to 80 μm, and then the SMD decreased back to 20 μm where its was steady at 20 μm during the Alabama limestone test D. The PCD SMD increased to 50 μm with the introduction of dolomite (E). Petroleum coke–dolomite operations (F) on March 5 to 7 had a PCD SMD of 60 to 80 μm. For the remainder of the petroleum coke tests, with dolomite (F) and Ohio limestone (G), the PCD SMD was about 40 μm with a few outliers. The start of the Alabama bituminous–Ohio limestone (H) test had a PCD SMD of 20 to 40 μm, then settled down to 15 μm. The start of the PRB operation with Ohio limestone (I) had a wide variation of PCD SMD with SMD from 20 to 175 μm. This was probably due to the intermittent feeding of sand with the Ohio limestone. Once the sand addition stopped during the Florida limestone test K, the PCD SMD was steady at 20 μm.

The molar ratio of calcium to sulfur (Ca/S) was calculated for each sample from the fine ash system (FD0520) and the reactor solids from the standpipe (FD0510). For dolomite addition,

the Ca/S ratio is the measure of excess sorbent required for sulfur removal according to equation (1):

$$SO_2 + CaCO_3 \bullet MgCO_3 + (1/2)O_2 \rightarrow CaSO_4 + 2CO_2 + MgO \quad (1)$$

While for limestone addition, the equation is:

$$SO_2 + CaCO_3 + (1/2)O_2 \rightarrow CaSO_4 + CO_2 \quad (2)$$

To react all the dolomite or limestone calcium requires an equal molar amount of calcium and SO_2, which would result in the same molar amount of calcium in the solids as sulfur (Ca/S = 1.0). Solids with the minimum amount of sorbent required would then have calcium only present as $CaSO_4$ and there would be neither $CaCO_3$ nor CaO•MgO present. The higher the Ca/S ratio, the more excess sorbent is used than theoretically required for 100-percent SO_2 capture.

Ca/S ratios from four different streams are plotted in Figures 4.3-15 through -18:

1. Based on spent PCD (FD0520) solids analysis.
2. Based on spent reactor (FD0510) solids analysis.
3. Calculated from the fuel and sorbent feed rates.
4. Based on in situ sample collected at the PCD inlet.

The two solids analyses are based on chemical analysis of the solids, specifically the calcium and sulfur analysis. The feed Ca/S is calculated from the feed calcium and feed sulfur. The fuel sulfur and the fuel calcium are calculated from the fuel feed rate and fuel analysis. The sorbent feed rate is determined from a correlation between sorbent weigh cell readings and sorbent feeder speed. The sorbent calcium feed rate is then determined from the sorbent feed rate and the amount of calcium in the sorbent. The Ca/S ratio based on the feeds was not calculated when sand and limestone were alternately added to FD0220 since the FD0220 solids calcium content was varying so much. (See Figure 4.3-12.) The in situ soilds were collected during the PCD inlet particulate sampling. Analyses of the collected solids are given in Table 3.4-4.

The majority of the solids flowed from the reactor through FD0520 (PCD solids) during TC05 since operating FD0510 (reactor solids) was not necessary to control reactor solids level. The sampled reactor solids tended to sit in the bottom dead leg of the reactor and were often not representative of the actual reactor solids. There often was a large time lag in the reactor solids reaching the actual sample point.

Figure 4.3-15 shows the Ca/S ratios for the first two Alabama bituminous coal tests (A and B). The feeds-Ca/S-ratio at the start of test A were near 1.5, while the PCD solids Ca/S ratio was between 2.0 and 3.0 until January 20 when they decreased to around 1.5. This may have been the purging of a large amount of limestone added on start-up. The Alabama limestone and Alabama limestone (B) test started with a Ca/S based on feed of about 1.8 and PCD solids Ca/S

ratio of 1.5. The January 19 in situ sample Ca/S ratio of 1.6 agreed well with the feed. Just prior to the outage on January 22, the Ca/S ratio based on the feeds, PCD solids, and reactor solids were all in agreement at about 1.8. The reactor was started up on February 2 with the feed Ca/S, PCD Ca/S, and reactor Ca/S in agreement at 1.8. After several days of operation ending on February 4, the feed in situ samples and PCD solids Ca/S ratio were in good agreement at 1.3. Following the outage, the feed and PCD Ca/S ratios were again in agreement at 1.2 until the sorbent feed rate was increased on February 6 at the end of test B. The reactor Ca/S ratios were consistently higher (1.5 to 2.2) than the feed and PCD Ca/S ratios, possibly due to reaction products collecting in the reactor.

Figure 4.3-16 provides the Ca/S ratio for the Illinois No. 6 coal tests (C, D, and E). The Illinois tests PCD solids were very constant at about 1.2 for the entire test on Ohio limestone (C). The feed Ca/S ratio started test C at 1.75 and held constant for several days until February 9 when it decreased to 1.4 and then closely tracked the PCD solids Ca/S. The reactor solids Ca/S started test C at about 2.0, then decreased to 1.2 on February 8 where it closely tracked the other two ratios. The agreement between feed, PCD, and reactor Ca/S in Illinois coal and Alabama limestone (D) was excellent from February 9 to 18. The February 11 in situ sample Ca/S ratio at 1.7 was higher than the other three Ca/S ratios at 1.3. On February 18 the feed Ca/S ratios dropped to below 1.0 and remained consistent until midway through the petroleum coke tests on March 15. The reactor and PCD solids Ca/S were in excellent agreement to the end of the Illinois coal tests.

Figure 4.3-17 provides the petroleum coke feed Ca/S, PCD solids Ca/S, and reactor solids PCD Ca/S results. All four Ca/S ratios were in agreement on March 5. The first short test on petroleum coke and dolomite from March 5 to 7 had the feed Ca/S ratio still less than 1.0 and dropping. By the end of the March 5 to 7 period, the PCD solids Ca/S had increased to 1.9, the feed Ca/S ratios had decreased to 0.6, and the reactor solids Ca/S were still at 1.0. The restart of the petroleum coke and dolomite run (F) began with high-PCD Ca/S ratios (2.0) which then decreased to about 1.5 on March 17 and 18. The feed-Ca/S ratios slowly increased from March 15 (1.25) to March 22 (1.8). The March 16 in situ Ca/S ratio was in good agreement with the feed Ca/S ratio, less than the PCD Ca/S ratio, and greater than the standpipe Ca/S ratio. The feeds and PCD Ca/S solids ratios were in agreement from March 17 to 19 at 1.4. The reactor Ca/S ratios during test F were at 1.0 and consistently below the feed and PCD Ca/S ratios. The petroleum coke–Ohio limestone tests (G) started with the feed Ca/S ratios increasing from 1.5 to 2.0 and with the reactor and the PCD Ca/S ratios either being in stark disagreement on March 21 (1.25 vs. 2.6) or in good agreement on March 22 (1.25). The final 2 days of petroleum coke operation from March 26 to March 28 showed excellent agreement between the feed, PCD, in situ, and reactor Ca/S ratios at about 1.25.

Figure 4.3-18 shows the feed, PCD solids, and reactor solids Ca/S ratios for the last three fuels tested during TC05 (Alabama bituminous, PRB, and Eastern Kentucky). The Alabama coal–Ohio limestone test was purposely run at high-Ca/S ratios. The PCD and reactor Ca/S ratios were in good agreement between 2.0 and 2.5. The Ca/S ratios based on the feeds were all below 1.0 for the first 2 days of operation, but on April 15 they were in good agreement with the PCD, in situ, and reactor solids Ca/S ratios at 2.0. The last several days of Alabama coal–Ohio limestone (H) had PCD Ca/S ratios from 1.8 to 2.5. From April 16 to 30 sand was added

alternately to the reactor with the sorbent. Ca/S ratios based on the feeds were not calculated during that time because the calcium content of the solids fed through FD0220 varied so much (see Figure 4.3-12).

The PRB tests with Ohio limestone (I) had high PCD Ca/S ratios that started at 2.0 and went up to 3.0. This was due to the very low sulfur of the PRB coal, which did not require much sorbent to control sulfur. The April 21 in situ sample Ca/S ratio was in agreement with the slow increase in Ca/S ratio shown by the reactor and PCD samples. The April 22 Ca/S ratio was below this general trend. Excess sorbent was added to the reactor, despite the alternate addition of sand and sorbent in an attempt to reduce sorbent to the reactor. The PRB coal with Florida limestone (J) had both reactor and PCD Ca/S ratios up to 4.0 for the reactor solids and to 6.2 for the PCD solids. Again the reactor was overfed with sorbent due to the low-sulfur level of the PRB coal. During the Kentucky coal–Florida limestone test (K), limestone-only feed through FD0220 was resumed, and the Ca/S ratio by the feeds could be again calculated. The PCD and feed Ca/S ratios were in good agreement at 3.0 during test K.

The solid compounds produced by the reactor were determined using the solids analysis and several assumptions. The assumptions were different for the dolomite and limestone operation.

1. All carbon dioxide measured came from $CaCO_3$, hence moles CO_2 = moles $CaCO_3$.

2. All sulfur measured came from $CaSO_4$, hence moles sulfur = moles $CaSO_4$.

3. All calcium not taken by $CaSO_4$ and $CaCO_3$ came from CaO•MgO for dolomite. All calcium not taken by $CaSO_4$ and $CaCO_3$ came from CaO for limestone.

4. All remaining magnesium not taken by CaO•MgO came from MgO for dolomite. All magnesium in the sample came from MgO for limestone.

5. All carbon dioxide measured was also measured as carbon, hence unburned carbon in the solids is moles measured carbon minus moles measured CO_2.

Figures 4.3-19 and -20 show a plot of the weight percent of $CaCO_3$ and $CaSO_4$ in the PCD solids, in situ solids, and reactor solids against time. Another way of looking at these plots is that $CaCO_3$ is the amount of CO_2 in the solids and $CaSO_4$ is the amount of sulfur in the solids.

During operation on petroleum coke and dolomite, the reactor Ca/S ratio dropped below 1.0 for several samples, indicating that there had to be another sulfur species other than $CaSO_4$ in the solids. Analyses using X-ray diffraction identified the presence of $CaMg_3(SO_4)_4$. For solids which have a Ca/S ratio less than 1.0, the following calculation procedure was used to determine the species present in the solids:

1. All carbon dioxide measured came from $CaCO_3$, hence moles CO_2 = moles $CaCO_3$.

2. The remaining calcium (not in the $CaCO_3$) and all sulfur are distributed between $CaSO_4$ and $CaMg_3(SO_4)_4$.

3. The remaining magnesium (not in $CaMg_3(SO_4)_4$) is present as MgO.

The in situ solids were not analyzed for CO_2, hence the $CaO/CaCO_3$ split cannot be determined for the in situ solids. Table 3.4-4 assumes that all left over calcium is present as $CaCO_3$, while the above analysis assumes that the left over calcium is split between CaO and $CaCO_3$. Only the $CaSO_4$ in situ values will be compared with the PCD and reactor solids, since the comparison between $CaCO_3$ and $CaMg_3(SO_4)_4$ would not be meaningful.

Both reactor and PCD solids began TC05 at low-$CaSO_4$ and -$CaCO_3$ levels. The PCD solids $CaSO_4$ climbed to 18 percent by the end of the Alabama bituminous–Ohio limestone test (A). The PCD $CaCO_3$ and reactor $CaCO_3$ values were very low during the first two Alabama bituminous coal tests (A and B). The January 19 in situ $CaSO_4$ was a few percent higher than the PCD solids $CaSO_4$, while the February 4 in situ $CaSO_4$ amount agreed very well with the PCD solids. The reactor $CaSO_4$ values held constant during the last 5 days of test B at about 8 percent. The PCD $CaSO_4$ values increased from 20 to 40 percent from the resumption of the Alabama bituminous–Alabama limestone test (B) to the end of test B. The reactor $CaSO_4$ values rose from 10 to 60 percent during the Illinois No. 6–Ohio limestone testing (C). During the same time the PCD $CaSO_4$ values rose from 40 to 50 percent. The February 11 in situ analyses had $CaSO_4$ 15 percent less than the PCD solids analysis. Prior to February 13 the reactor $CaSO_4$ values were lower than the PCD values, after February 13 they were nearly the same. The PCD $CaSO_4$ values were climbing after the short outage in test D, up to 60 percent at the beginning of the Illinois No. 6–dolomite testing (E). During the entire Illinois No. 6 coal testing (C, D, and E), the $CaCO_3$ values for both the PCD and reactor were very low, usually under 5 percent, indicating excellent limestone utilization. The February 18 in situ $CaSO_4$ agreed very well with the PCD solids.

The first 3 days of the petroleum coke testing (F) on March 5 through 7 were very unstable. Note that PCD $CaSO_4$ values increased from 28 to 45 percent and then decreased back to 30 percent in just 2 days. The two March 5 in situ solids $CaSO_4$ were 10 percent higher than the PCD solids. This might have been due to the unsteady nature of this period of operation. The resumption of petroleum coke–dolomite testing on March 15 showed a general trend of increasing PCD and reactor $CaSO_4$ values through the end of the petroleum coke testing with both dolomite (F) and Ohio limestone (G). The reactor $CaSO_4$ increased from 10 to 52 percent and the $CaSO_4$ PCD increased from 30 to 68 percent. During both petroleum coke tests (F and G), the PCD $CaCO_3$ values were constant at 10 to 15 percent, while the reactor $CaCO_3$ values were very low at nearly zero percent. Petroleum coke testing had the highest PCD $CaCO_3$ values (10 percent) during TC05 on both limestone and dolomite. The March 16 and 26 in situ $CaSO_4$ analyses agreed with the PCD solids.

The Alabama bituminous–Ohio limestone tests (H) had very constant PCD $CaSO_4$ values at about 17 percent and PCD $CaCO_3$ values of 5 percent. The reactor $CaCO_3$ values were very low

for test H at less than 5 percent, while the reactor $CaSO_4$ values were at 2 to 12 percent. The April 15 in situ $CaSO_4$ agreed well with the PCD solids.

The PRB coal tests (I and J) had very low reactor $CaCO_3$ values (less than 5 percent) while the $CaSO_4$ values were at 5 to 10 percent for test I and 5 percent for test J. The PCD $CaCO_3$ values for the PRB coal tests were 2.0 to 5.0 percent for Ohio Limestone (I) and 5 to 10 percent for Florida limestone (J). The comparable PCD $CaSO_4$ values were 15 percent for test I and 5 to 12 percent for test J. The amount of $CaSO_4$ in the in situ sample of April 21 and 22 was larger than that in the PCD solids. This may have been due to the alternating sand and limestone feeds during this time. The in situ analyses might have been sampled during a period of limestone feed.

The Eastern Kentucky coal tests had PCD $CaSO_4$ values of 18 to 20 percent and PCD $CaCO_3$ values of 8.0 to 15.0 percent. The end-of-run reactor solids had very low values of $CaCO_3$ and 10 percent $CaSO_4$.

Figures 4.3-21 and -22 plot the weight percent CaO, MgO, and CaO•MgO for the TC05 testing. This is essentially the "left over" calcium that is not part of $CaCO_3$ or $CaSO_4$. It is also an indication of the excess magnesium for the dolomite tests. The first 8 days of Alabama coal operation on both Alabama and Ohio limestones (A and B) had low-PCD CaO and MgO at 1 to 5 percent and the reactor CaO and MgO were extremely low at less than 2 percent. The end of the Alabama bituminous test on Alabama limestone (B) after February 2 had the PCD MgO at 3 to 5 percent and the PCD CaO at 2 percent. In test B the reactor CaO and MgO were less than 4 percent. The Illinois coal–Ohio limestone (C) tests had PCD MgO at 4 to 6 percent and the PCD CaO at less than 2.0 percent, probably due to the higher MgO of Ohio limestone. The reactor CaO and MgO were both less than 4 percent for these tests. On the change in Illinois coal operation to Alabama limestone (D) the CaO and MgO in both the PCD and reactor solids were from 2 to 4 percent. The change to dolomite as a sorbent at the start of test E brought a quick rise to 14 percent in the PCD MgO. For the dolomite testing, it was assumed that all excess calcium not taken by $CaCO_3$ or $CaSO_4$ was present as CaO•MgO. Note that right before the introduction of dolomite the PCD CaO•MgO at first increased to 6 percent then decreased to nearly zero.

The first 3 days of petroleum coke–dolomite operation (F) had very high PCD MgO values of 7 to 16 percent. The CaO•MgO values increased from near zero to 16 percent from March 5 to 7. The reactor MgO value was 8 percent. Note that there was no reactor CaO•MgO because there was more sulfur and CO_2 than calcium in the sample, so that the presence of $MgSO_4$ was assumed (see Figure 4.3-19). The restart on March 14 of the petroleum coke–dolomite test (F) had high PCD CaO•MgO values of 15 to 27 percent, which then decreased at the end of test F to 8 percent. The reactor MgO increased to about 6 percent during F. The PCD MgO increased from 12 to 20 percent on March 17, then decreased to 10 percent at the end of test F on March 20. The decrease in MgO was probably due to the early arrival of Ohio limestone. During the petroleum coke–Ohio limestone test (G) the PCD MgO decreased to 8 percent, the PCD CaO decreased to less than 6.0 percent, and both reactor MgO and reactor CaO were less than 5 percent.

The Alabama coal–Ohio limestone tests (H) had constant PCD CaO at 7 percent, constant PCD MgO at 4.0 percent, and reactor CaO and MgO at less than 5 percent. The switch to PRB coal (I) led to an increase in PCD CaO, which was a reflection on the excess limestone used for PRB. The reactor MgO, reactor CaO, and PCD MgO stayed the same as in test H. The PCD CaO for test J with Florida limestone seemed to hold steady at 10 to 15 percent, while the MgO decreased from 5 to 2 percent, probably due to the lower magnesium content of the Florida limestone. The switch to Eastern Kentucky coal (K) produced the same results as J, which was PCD CaO at 10 to 15 percent and PCD MgO at a very low level.

Figures 4.3-23 and -24 plot the weight percent inerts for both the PCD and reactor solids against time. The inerts are defined as a mixture of sand, fuel ash, and sorbent inerts, and are any bed compounds not containing calcium, magnesium, or sulfur. The inerts will go down when the sorbent feed rate is larger than the fly ash and sand feed rates, which would be typical for the higher sulfur fuels such as Illinois No. 6 and petroleum coke. Inerts should go up when sand is added or low-sulfur, high-ash fuels such as PRB are used.

The PCD inerts began TC05 at a very high level during the beginning of the Alabama bituminous–Ohio limestone test (A). As coal reaction products replaced the startup sand during the Alabama bituminous tests (A and B) the PCD inerts slowly decreased from 90 to 42 percent and the reactor inerts decreased from 95 to 85 percent. The reactor inerts were constant at 85 percent for the last several days of Alabama bituminous operation (B). The switch to Illinois No. 6 coal with its higher sulfur level than the Alabama coal slowly reduced the PCD inerts to 30 percent and quickly reduced the reactor inerts from 85 to 65 percent. The change of limestones lowered the reactor inerts from 65 to 40 percent. During the Illinois No. 6–Ohio limestone (D) test, the PCD and reactor inerts were about the same at 40 to 45 percent. Most of the inserts were replaced by $CaSO_4$ (see Figure 4.3-19). With the introduction of dolomite at the beginning of test E, the PCD inerts dropped to 20 percent due to the presence of the high amount of magnesium compounds in dolomite that do not participate in sulfur capture.

The first short petroleum coke–dolomite (F) test had rapidly dropping PCD inerts from 45 to 25 percent, while the reactor inerts were constant at 32 percent. The restart of test F started with high reactor inerts at 78 percent, which dropped quickly to 60 percent. The PCD inerts started at 25 percent on March 15 and dropped to below 10 percent, then rose to 25 percent at the end of the dolomite test. FDO220 was run at nearly its maximum rate during test F to keep up with the high sulfur and low ash of the petroleum coke. The PCD inerts held steady at about 25 percent from March 20 to March 23.

The Alabama bituminous–Ohio limestone test (H) started with the PCD inerts at 78 percent and the reactor inerts at 65 percent. During the entire PRB coal testing (I and J), the limestone was alternated with sand in FD0220 to maintain bed height, so the reactor inerts remained at a high level (75 to 85 percent). During test I, the reactor inerts dropped from 87 to 72 percent. The PCD inerts started test I at 65 percent, then dropped to 50 percent, then rose to 70 percent. During test J, the PCD inerts were 60 to 75 percent and the reactor inerts held constant at about 80 percent. During the eastern Kentucky coal tests (K), the PCD inerts dropped from 75 to 50 percent due to only sorbent being fed to the reactor.

The laboratory reported carbon in two forms, elemental carbon and carbon dioxide (CO_2). The measured elemental carbon is the total carbon in the sample and includes unburned carbon and carbon dioxide. The actual elemental carbon in the solids is the difference between the measured elemental carbon and the measured carbon dioxide. The elemental carbon in the solids is a measure of combustion efficiency. Zero carbon in the solids would indicate 100-percent combustion efficiency. The carbon content of the solids is calculated as the difference of two small numbers, which are typically close to each other in value. Hence there is a lot of relative variation in the carbon content of the solids. Sometimes the CO_2 content of solids is larger than the total carbon, resulting in a "negative" unburned carbon.

The unburned carbon contents for both the PCD and reactor solids are plotted on Figures 4.3-25 and -26 as the difference between the elemental carbon and the carbon dioxide of the solids. Also plotted on Figures 4.3-25 and -26 are the measured carbon monoxide (CO) values, which is another measure of combustion efficiency. As with previous combustion testing in TC01, TC02, and TC03, Alabama bituminous (A, B, and H) had low-unburned carbon indicating about 99.9-percent combustion efficiency. There are a few outlier points indicating either high- or low-unburned carbons for both the reactor and PCD solids. The carbon monoxide during test A was between 5 and 32 ppm and seemed to be increasing. Illinois No. 6 coal (C, D, and E) also had low-unburned carbons. There appeared to be a slight increasing trend of unburned carbon from February 2 (-0.05 percent) to February 21 (+0.05 percent). The end of the Alabama bituminous coal (B) and the Illinois coal–Ohio limestone (C) had low-CO values of 15 ppm. Before the outage on February 15 the CO values had drifted up to 30 ppm. The end of the Illinois coal testing (D) had low-CO values of 10 ppm.

The petroleum coke tests (F and G) did have some reactor unburned carbons of about 0.05 percent. The long-term testing of petroleum coke from March 17 to 23 had low-CO values of 15 to 20 ppm, indicating excellent combustion efficiency. The PCD solids from the PRB coal with Ohio limestone (I) and Florida limestone (K) had very low-unburned carbon. PRB had low-CO values of 5 to 10 ppm indicating excellent carbon conversion. The Eastern Kentucky coal (K) seemed to line out at 15 ppm CO. The few points of higher unburned carbon of 0.2 and 0.3 percent from the reactor solids were probably related to the minimal draw off of reactor solids during the Alabama coal test (H) and the PRB coal tests (I and J).

The bulk densities of the reactor and PCD solids are plotted in Figures 4.3-27 and -28. The bulk density of the Alabama coal and Ohio Limestone (A) PCD solids started at around 60 lb per cubic foot and then dropped off to 40 lb/ft^3, while the reactor solids were constant at 90 lb/ft^3. The switch to Alabama limestone (B) did not produce any change in bulk densities of the PCD and reactor solids. The switch to Illinois No. 6 coal and Ohio limestone (C) increased the PCD bulk density to about 55 lb/ft^3, while the reactor solids bulk density remained constant at around 85 lb/ft^3. The switch to Alabama limestone (D) decreased the PCD solids bulk density to about 40 lb/ft^3, while the reactor solids density increased to about 90 lb/ft^3. The change to dolomite (E) increased the PCD solids bulk density to 70 lb/ft^3, while the reactor bulk density increased slightly to 93 lb/ft^3. The start of the petroleum coke–dolomite (F) tests on March 15 had PCD bulk densities of 62 lb/ft^3, while the reactor bulk densities were about 95 lb/ft^3. The switch to Ohio limestone (G) reduced the reactor bulk density to 82 to 90 lb/ft^3, while the PCD solids

varied from 58 to 78 lb/ft^3. The resumption of testing on Alabama coal and Ohio limestone (H) repeated the bulk densities of test (A) with reactor bulk densities of 90 lb/ft^3 and PCD solids of 40 lb/ft^3. During the PRB coal tests (I and J), the sand addition caused a wide variation in PCD solids bulk destinies from 44 to 90 lb/ft^3. The reactor solids bulk densities were fairly constant at 90 lb/ft^3 during test I and J. The Kentucky coal–Florida limestone tests had PCD solids bulk densities of 50 lb/ft^3 and reactor solids bulk densities of 90 lb/ft^3.

Southern Research Institute (SRI) obtained both SO_2 and SO_3 data from the cyclone outlet (PCD inlet). SRI used extractive and wet chemical techniques to obtain SO_2 and SO_3 concentrations.

Table 4.3-2 compares the six extractive SO_2 and SO_3 tests during TC05. The average extractive SO_2 and SO_3 data are shown as well as the average SO_2 gas analyzer data. The SO_X emissions in lb of SO_X per MBtu fired, SO_2 emissions in pounds of SO_2 per MBtu fired, and SO_X removal based on the calculated SO_X from the fuel sulfur is provided in this table. The Ca/S ratios are taken from Figures 4.3-15 through -18. There was poor agreement between the extractive and analyzer SO_2 readings, with the extractive SO_2 data at nearly twice the plant SO_2 analyzer. Note the high-SO_X removals and low-SO_2 emissions for the two high-sulfur fuels at low-Ca/S ratios (1.2 to 1.4).

A useful way to analyze SO_2/SO_3 data is to look at the thermodynamics of the SO_2 to SO_3 reaction:

$$SO_2 + (1/2)O_2 \leftrightarrow SO_3 \tag{3}$$

Higher pressure and oxygen concentrations will lead to higher SO_3 concentrations. Equation (3) leads to the equilibrium constant, which combines the effects of pressure, sulfur oxide concentration, and oxygen concentration. The equilibrium constant K_p is defined as:

$$K_P = \frac{SO_3}{SO_2\sqrt{P(O_2)}} \tag{4}$$

The concentrations SO_3 and SO_2 are in ppm and $P(O_2)$ is the partial pressure of oxygen in atmospheres.

The measured K_p is shown in Table 4.3-2 for the six TC05 SO_3 data points.

The equilibrium constant is a function of temperature. Wheeldon, et al., 1985, used the equation:

$$K_P = 2.1x10^{-5}\exp(20520/T) \tag{5}$$

The temperature, T, is in degrees Rankine. According to this equation, plotting the logarithm of the equilibrium constant against reciprocal temperature will result in a straight line. At high temperatures the formation of SO_2 is favored, while at low temperatures the formation of SO_3 is favored. Measured equilibrium constants are plotted in Figure 4.3-29 for TC02, TC03, and

TC05 data with the thermodynamic equilibrium line. Note that most of the data is clustered around one point. The general trend of TC05 data is to be near equilibrium around 1,350°F and much less than equilibrium values at lower temperatures. The only exceptions are a few TC02 data at Kp = 10^{-1}. The lower Kp tends to decrease SO_3.

TC05 data was searched to find periods of steady operations with respect to the SO_2 emissions to relate the Ca/S ratio to the SO_2 emissions. The periods of operations varied from 9 to 28 hours with the average period of 14 hours. To estimate the SO_2 and SO_3 concentrations and calculate percent SO_X removal and SO_2 emissions during these periods the following assumptions were made:

- Since the extractive SO_2 analysis consistently gave a higher SO_2 reading than the plant analyses, the extractive SO_2 and plant analyzer SO_2 data in Table 4.3-2 were used to determine a correlation between the plant analyzers and the extractive samples. The values for the extractive samples were used to determine the SO_2 emissions and SO_X removal.

- A correlation was made between the reciprocal temperature and SO_2/SO_3 equilibrium constant for the data shown in Table 4.3-2 and Figure 4.3-29. The SO_3 concentration could then be determined from the corrected SO_2, PCD temperature, and oxygen concentration using equation (4).

The plot of PCD solids Ca/S ratio and SO_X removal is shown on Figure 4.3-30 with the data sorted by fuels. The PCD Ca/S ratios were taken from Figures 4.3-15 to 18. The SO_X removal should have increased with increasing Ca/S but did not, based on all the data. The reason that it did not is that the fuel sulfurs varied so much and there was no effort to obtain any steady state data at higher than 40 ppm SO_2 emissions. The Alabama bituminous coal shows the expected trend of increasing removal with increasing Ca/S ratio, if the 91-percent removal, 2.2-Ca/S ratio point is ignored. The Illinois coal shows SO_X removal above 96 percent at Ca/S ratios of less than 1.5. Petroleum coke has excellent SO_X removal—greater than 98 percent for a range of Ca/S ratios from 1.2 to 2.2. The PRB coal showed good SO_X removal for such a low-sulfur coal and was operated at high-Ca/S ratios of above 2.1. There were only two Eastern Kentucky coal points at about the same Ca/S.

Figure 4.3-31 plots the SO_2 emissions in pounds of SO_2 emission per MBtu fuel fired for the various fuels used in TC05. The expected trend of increasing Ca/S ratios resulting in lower SO_2 emissions is only seen for the Alabama bituminous coal if the 0.08 lb SO_2 per MBtu, 2.2-Ca/S ratio point is ignored.

Figure 4.3-32 replots the same data as in Figure 4.3-30 and shows the different sorbents used in TC05. Most of the data was with Ohio limestone. Note that all of the Plum Run dolomite removals were above 98 percent. Figure 4.3-33 replots the same data as in Figure 4.3-31 and shows the different sorbents used in TC05. There does not appear to be much difference between the sorbents in these tests, again because the SO_2 concentration was held to below 40 ppm.

Test runs TC01, TC02, and TC03 were also analyzed for long periods of steady-SO_2 emissions. Only data from TC03 were found to be acceptable. The data are plotted on Figures 4.3-34 for SO_X removal and -35 for SO_X emissions. All data were taken with Eastern Kentucky coal and three different limestones. The data are very similar to the TC05 data in that the overall trend is the opposite of the expected trend of decreasing SO_X emissions with increasing Ca/S ratio. Note that the Florida limestone data have the expected trend of decreasing SO_X emissions with increasing Ca/S ratio.

During TC03 and TC05, HCl emissions data were obtained while taking SO_3 and SO_2 data (see Table 3.4-8). The data are provided in Table 4.3-3. The expected emissions based on the measured-fuel chlorine content and fuel-flow rates also are shown in Table 4.3-3. The measured and the calculated values are approximately the same, indicating minimal-HCl removal in the transport reactor.

Reference

J. M. Wheeldon, Burdett, N. A., Freidman, M. A., and Stantan, J. E., "SO_3 measurements at the Grimethorpe PFBC," Proceeding of the Eighth International Conference on Fluidized-Bed Combustion, Vol. II, July 1985, p. 715.

Table 4.3-1

Test Periods

Test No.	Fuel	Sorbent	Start Time	End Time
A	Alabama Coal	Ohio Limestone	01/15/99 03:50	01/20/99 05:00
B	Alabama Coal	Alabama Limestone	01/20/99 05:00	02/07/99 04:00
C	Illinois Coal	Ohio Limestone	02/07/99 04:00	02/13/99 05:00
D	Illinois Coal	Alabama Limestone	02/13/99 05:00	02/20/99 17:15
E	Illinois Coal	Dolomite	02/20/99 17:15	03/05/99 08:15
F	Pet Coke	Dolomite	03/05/99 08:15	03/20/99 05:30
G	Pet Coke	Ohio Limestone	03/20/99 05:30	03/27/99 20:09
H	Alabama Coal	Ohio Limestone	04/12/99 14:33	04/18/99 10:00
I	PRB Coal	Ohio Limestone	04/18/99 10:00	04/26/99 12:10
J	PRB Coal	Florida Limestone	04/26/99 12:10	04/29/99 12:00
K	Kentucky Coal	Florida Limestone	04/29/99 12:00	05/02/99 05:52

Table 4.3-2

SO_2 and SO_3 Data and Results

Date	02/04/99	02/09/99	02/18/99	03/17/99	04/15/99	04/22/99
Extractive Data Points	3	3	3	3	3	3
Fuel	Alabama Coal	Illinois Coal	Illinois Coal	Pet Coke	Alabama Coal	PRB Coal
Sorbent	Alabama Limestone	Ohio Limestone	Dolomite	Dolomite	Ohio Limestone	Sand
PCD Outlet Temp (°F)	1,355	1,368	1,361	716	1,188	1,051
Pressure (psig)	200	200	200	180	200	200
O_2 (%)	5.9	6.4	4.5	4.0	6.1	8.0
Extractive SO_3 (ppm)	36	26	7	0.6	17	0.9
Extractive SO_2 (ppm)	52	27	12	11	29	8
Analyzer SO_2 (ppm)	13	11	1	6	8	5
SO_X Emissions (lb/MBtu)	0.32	0.21	0.06	0.03	0.18	0.04
SO_2 Emissions (lb/MBtu)	0.17	0.10	0.04	0.03	0.10	0.03
SO_X From Fuel (ppm)	984	1,344	1,821	2,786	496	283
SO_X Removal (%)	95.1	97.3	99.6	99.8	94.9	98.0
Feed Solids Ca/S Ratio	1.2	1.3	0.8	1.6	1.9	0.0
PCD Solids Ca/S Ratio	1.3	1.2	1.3	1.4	2.1	2.5
Reactor Solids Ca/S Ratio	2.1	1.2	1.3	0.9	2.4	2.1
K_p ($atm^{-0.5}$)	0.71	0.98	0.74	0.08	0.57	0.10

Notes: 1. Extractive data collected by Southern Research Institute for about 10 minutes.
2. K_p defined in Equation (4).

Table 4.3-3

HCl Emissions

Date	07/28/98	07/30/98	02/04/99	02/09/99	02/18/99	03/17/99	04/15/99	04/22/99
Extractive Data Points	3	3	3	3	3	3	3	3
Coal	Eastern Kentucky	Eastern Kentucky	Alabama	Illinois	Illinois	Pet Coke	Alabama	PRB
Sorbent	Ohio Limestone	Ohio Limestone	Alabama Limestone	Ohio Limestone	Alabama Limestone	Dolomite	Ohio Limestone	Ohio Limestone
Extractive HCl (ppm)	56	42	20	30	50	15	13	<2.2
Calc HCl/From Fuel (ppm)	61	61	14	43	48	7	15	2
Fuel C1/(ppm)	1,600	1,600	325	1,000	1,000	154	325	43
Pressure (psig)	145	145	200	200	200	180	200	200

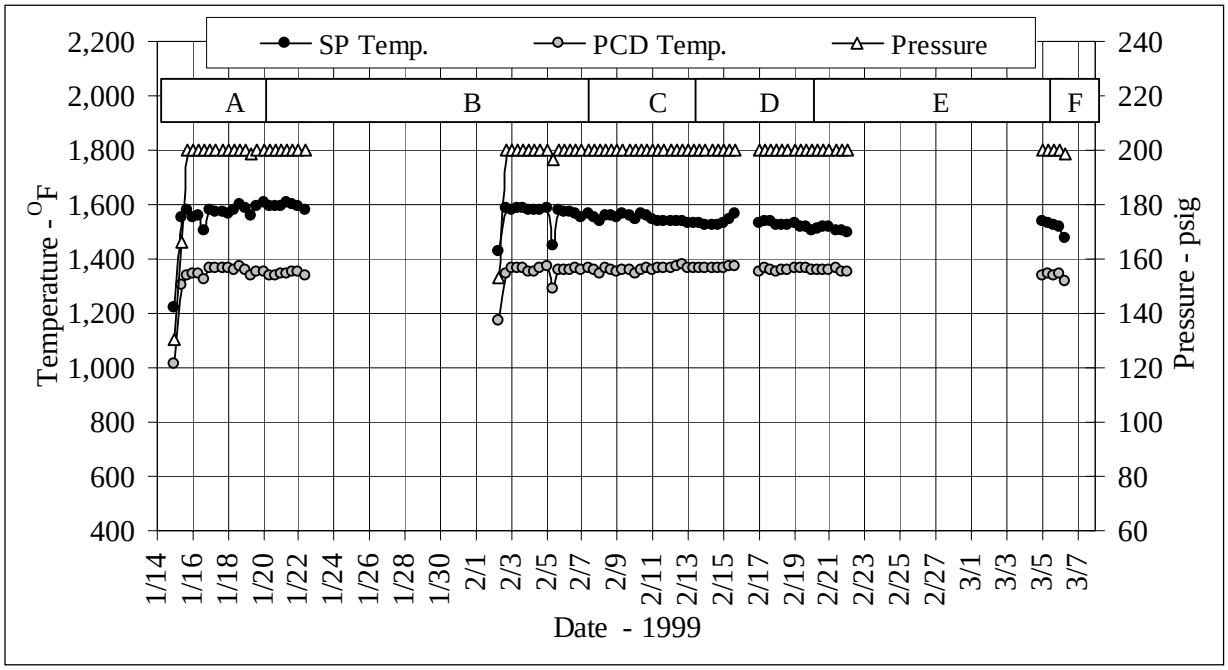

Figure 4.3-1 System Pressure, Standpipe, and PCD Temperature

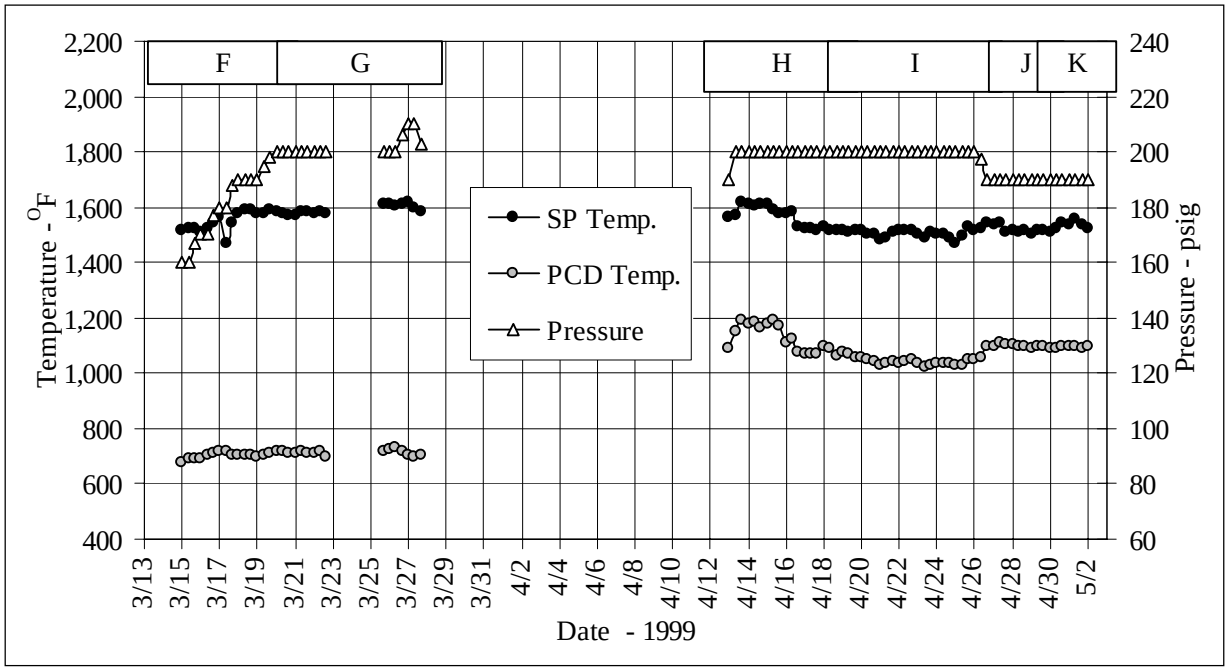

Figure 4.3-2 System Pressure, Standpipe, and PCD Temperature

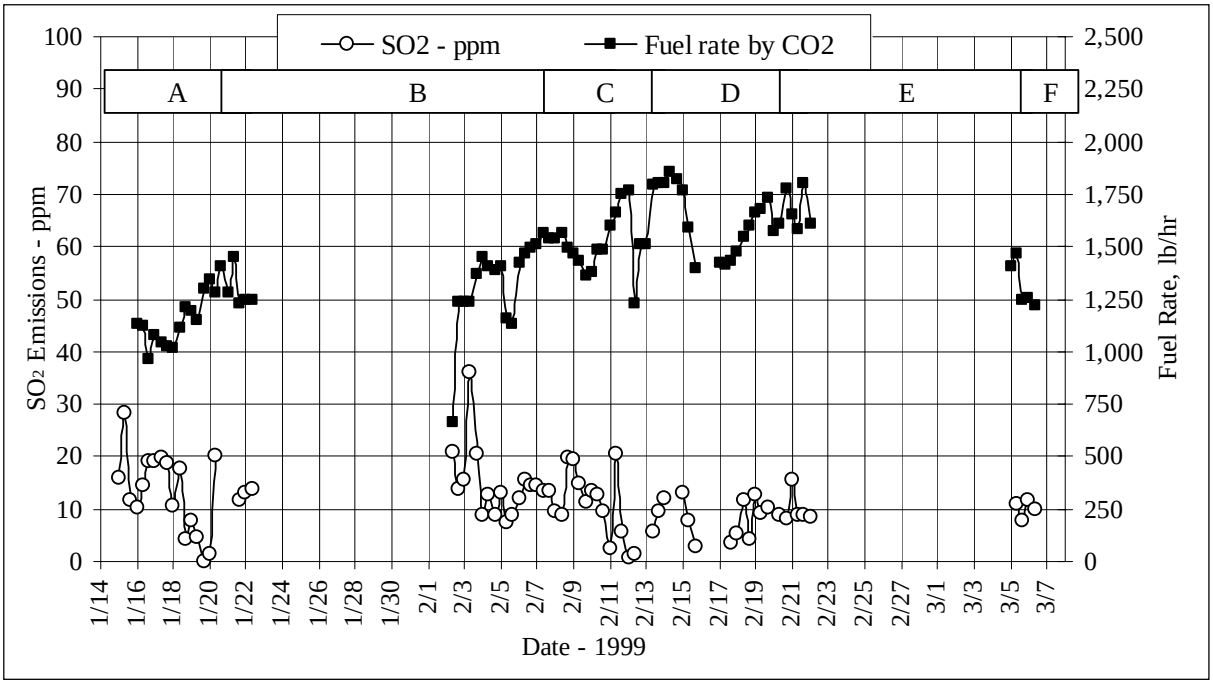

Figure 4.3-3 Fuel Feed, SO_2 Emissions

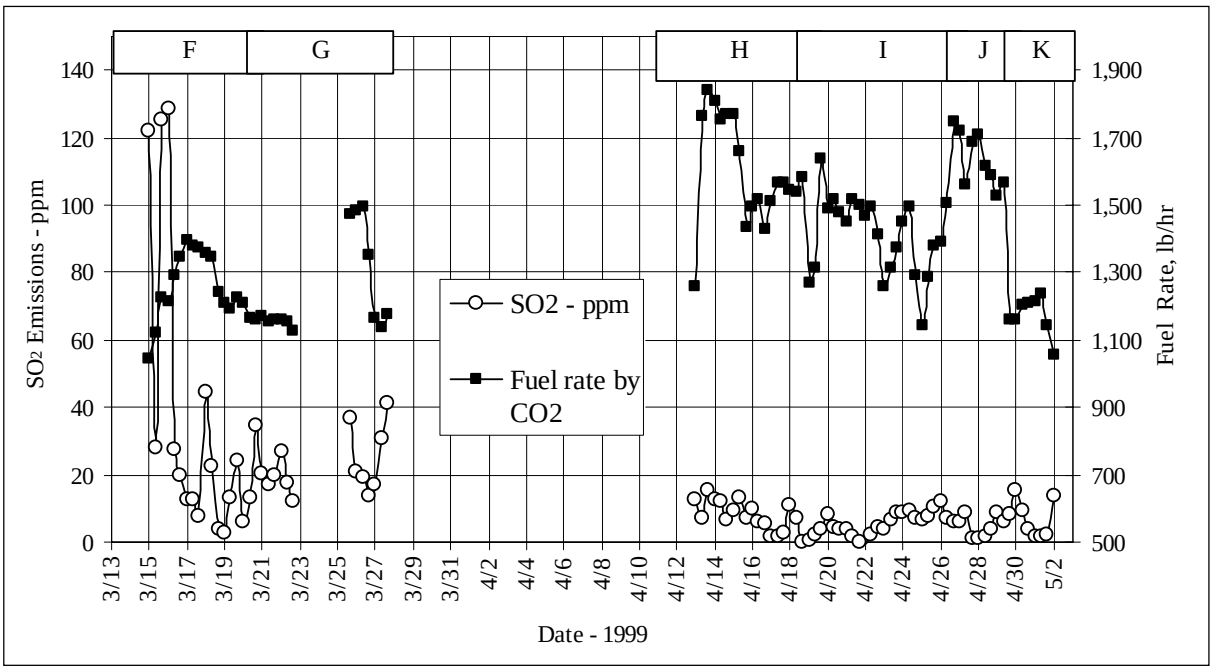

Figure 4.3-4 Fuel Feed, SO_2 Emissions

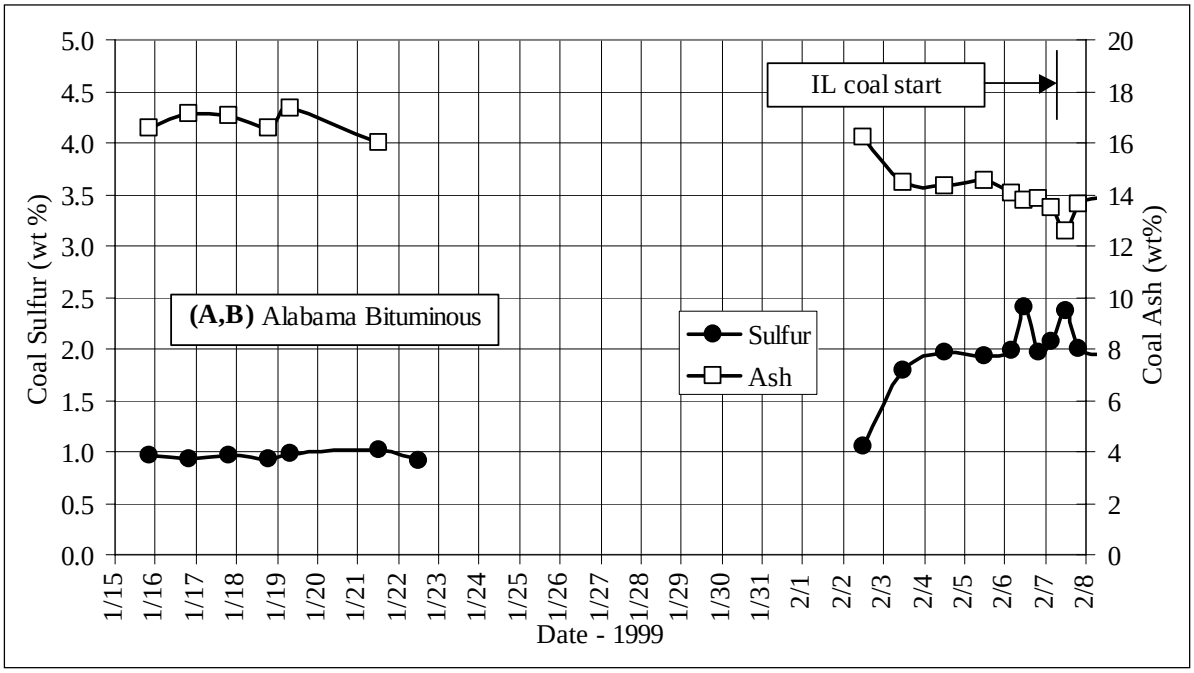

Figure 4.3-5 Alabama Bituminous Coal Sulfur and Ash Contents

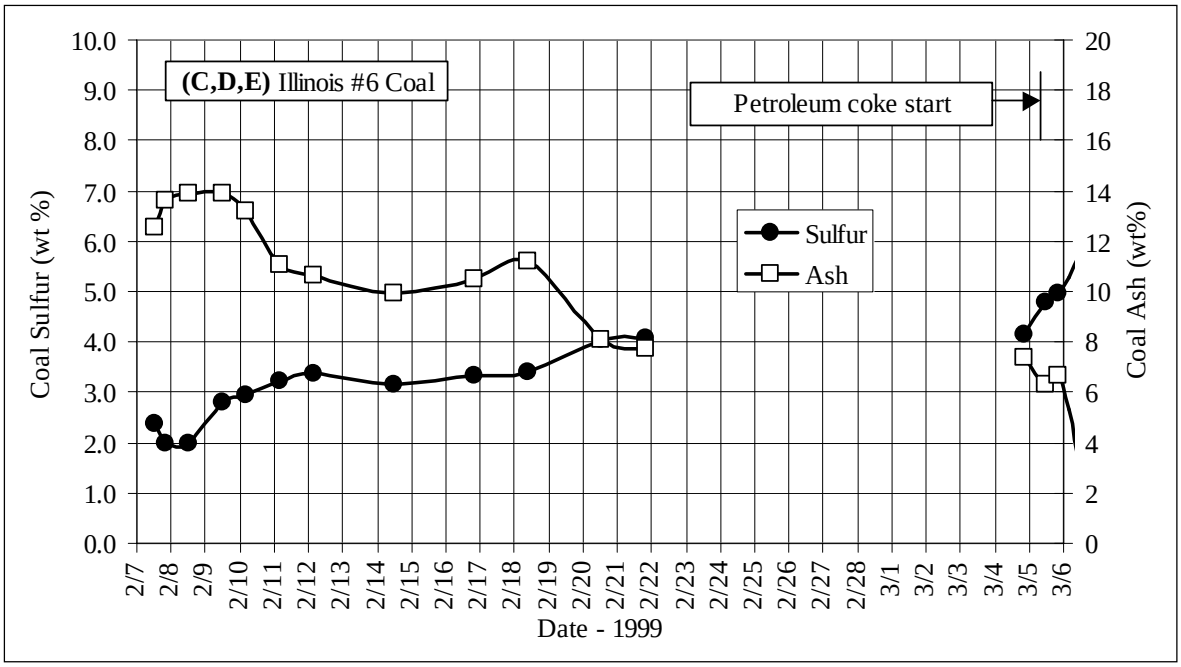

Figure 4.3-6 Illinois No. 6 Coal Sulfur and Ash Contents

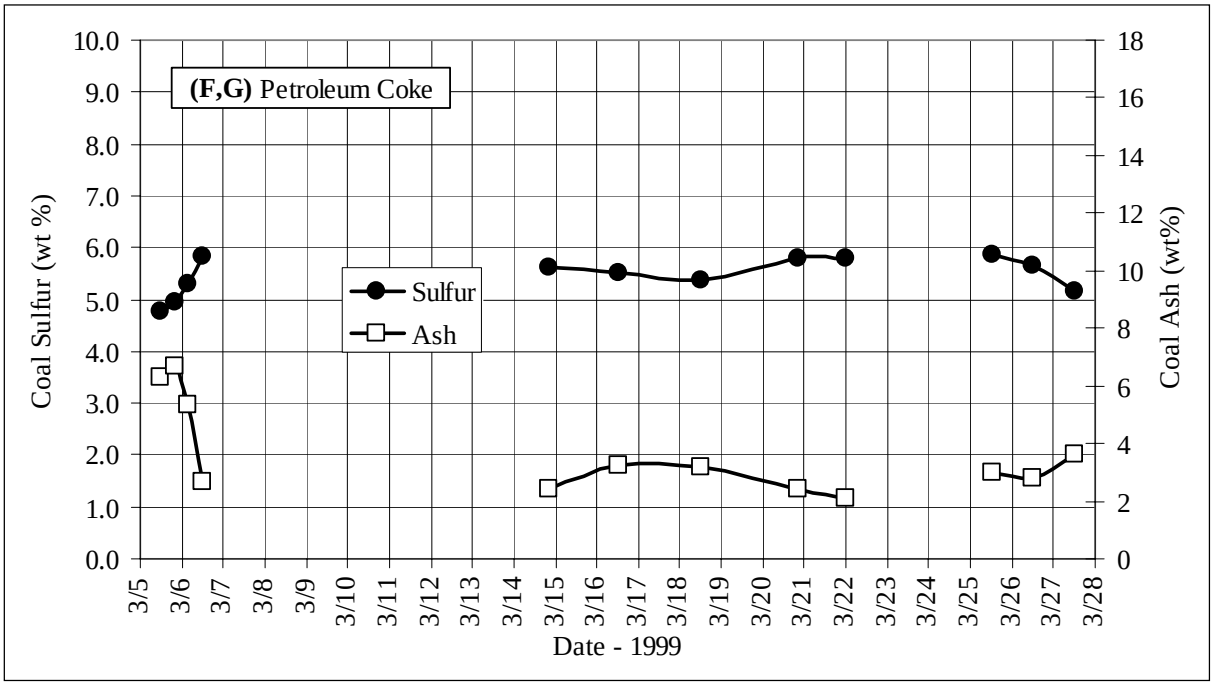

Figure 4.3-7 Petroleum Coke Sulfur and Ash Contents

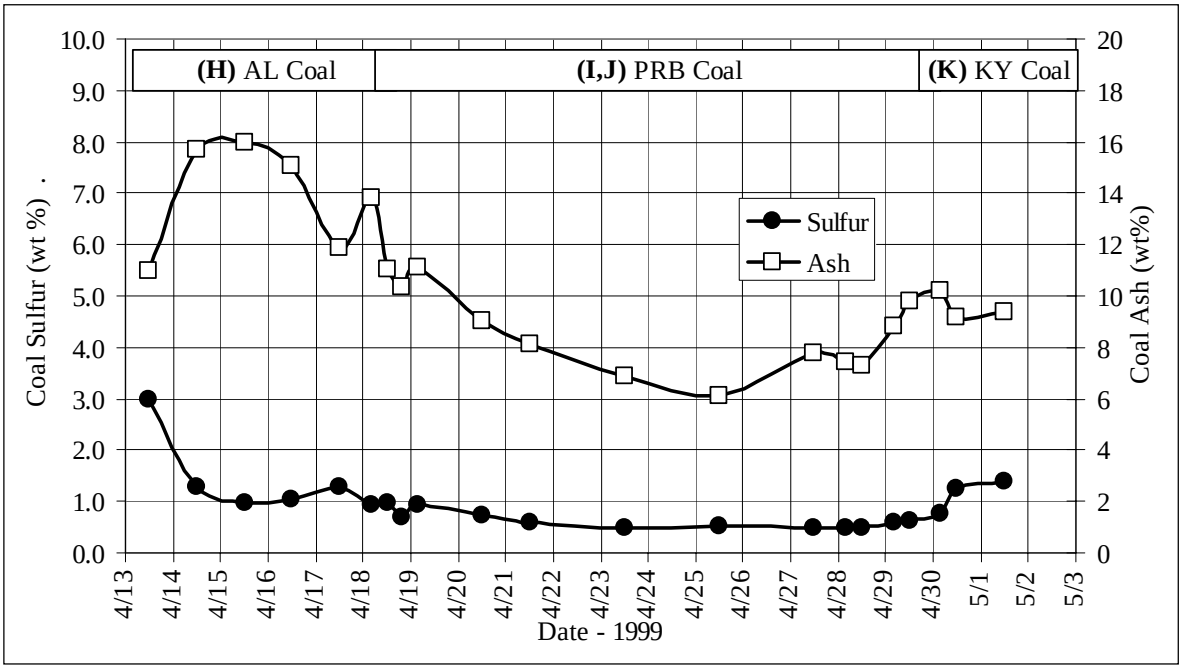

Figure 4.3-8 Coal Sulfur and Ash Contents

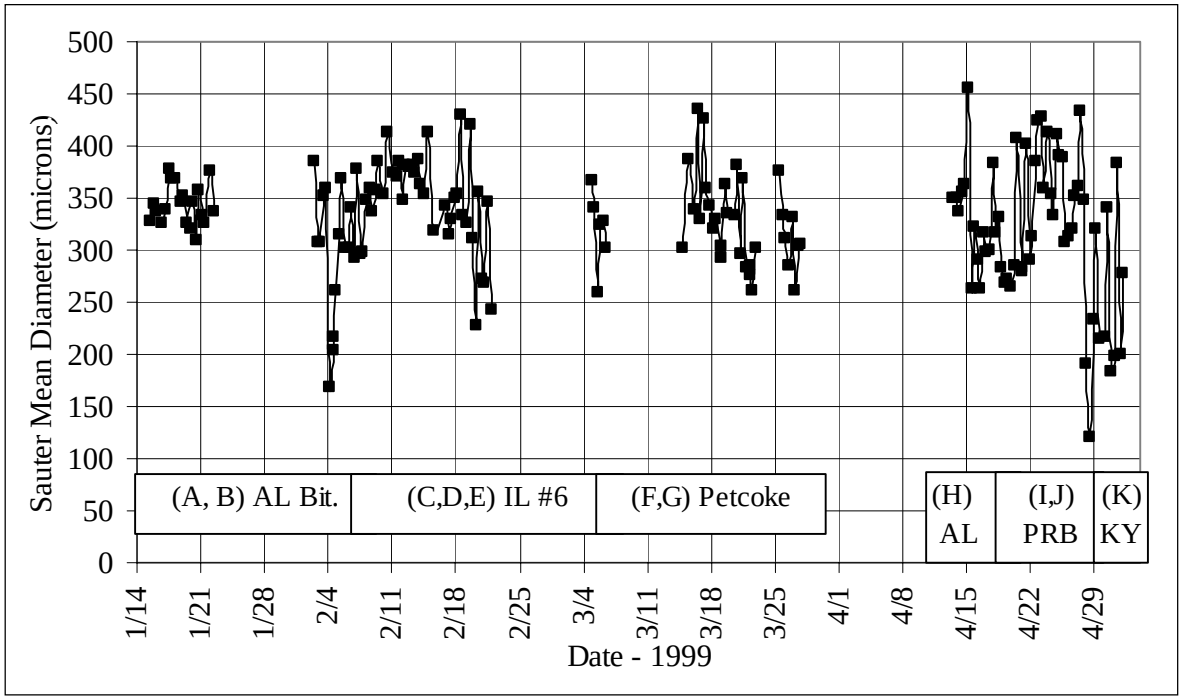

Figure 4.3-9 Fuel Particle Size

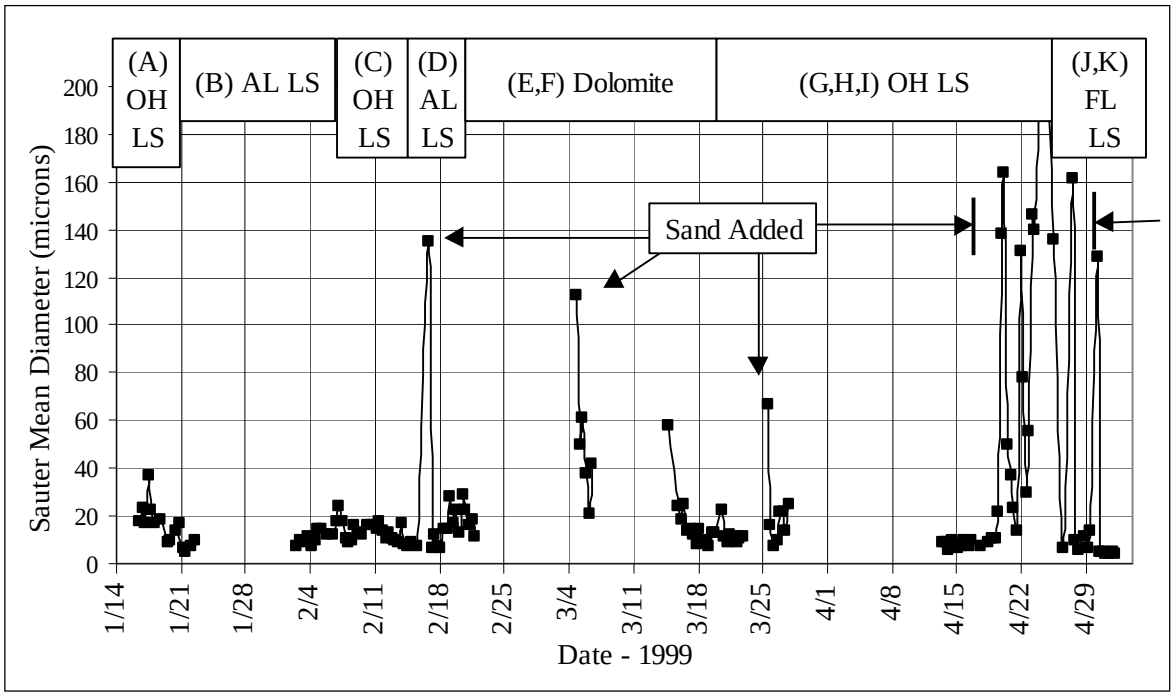

Figure 4.3-10 Sorbent Particle Size

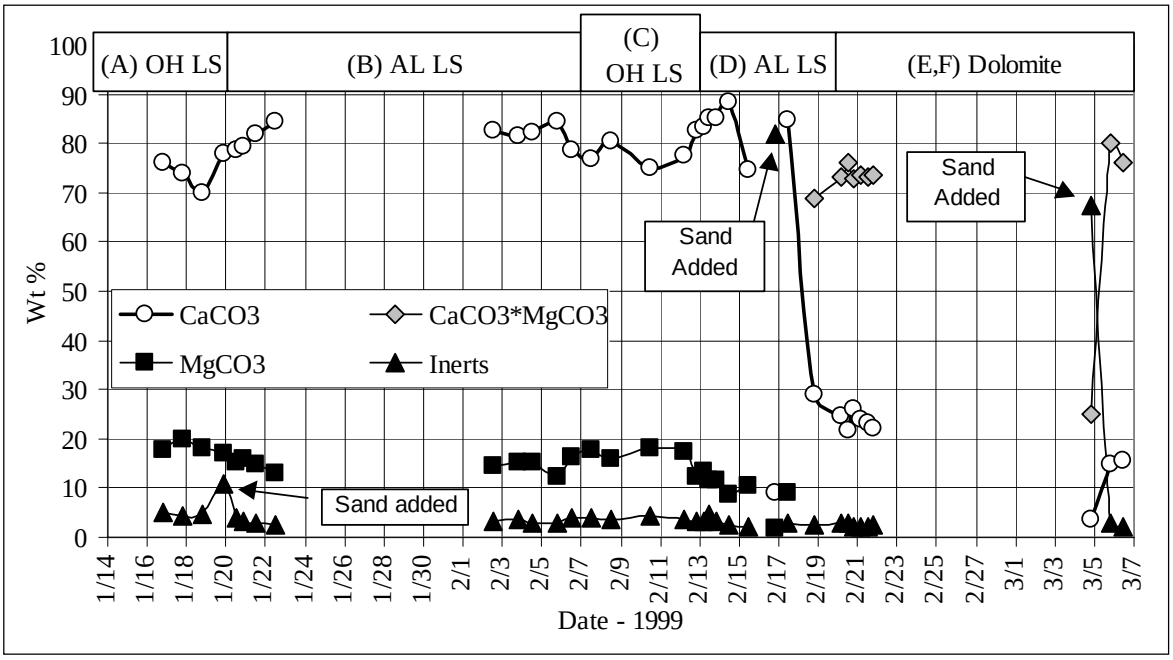

Figure 4.3-11 Sorbent Composition

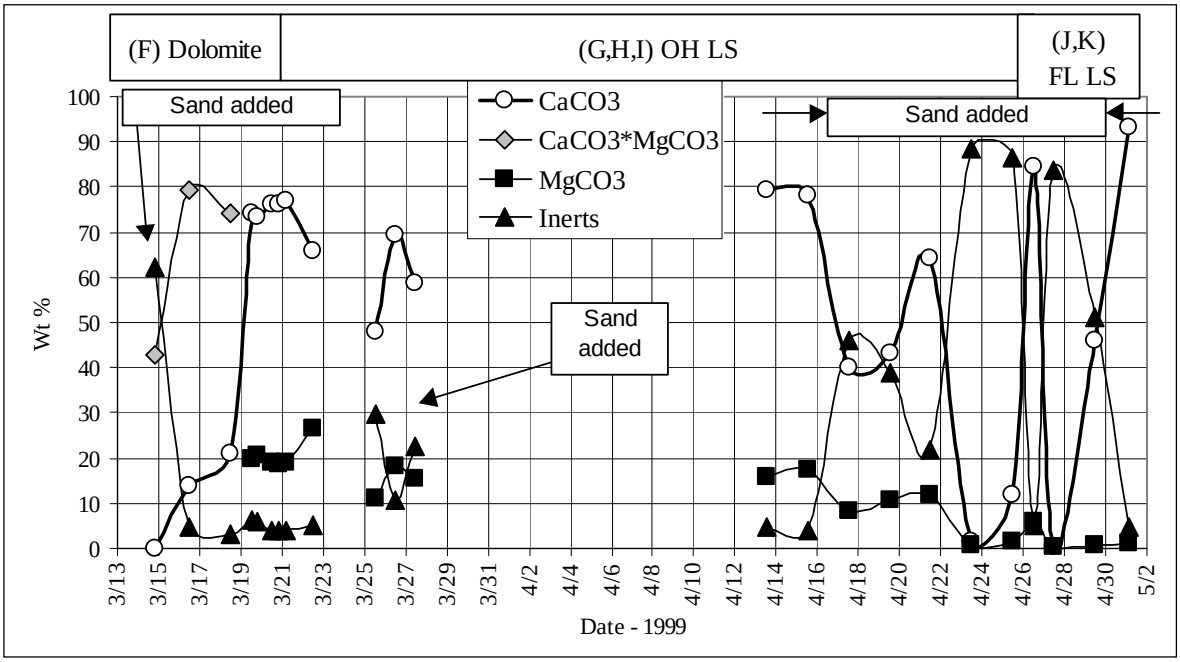

Figure 4.3-12 Sorbent Composition

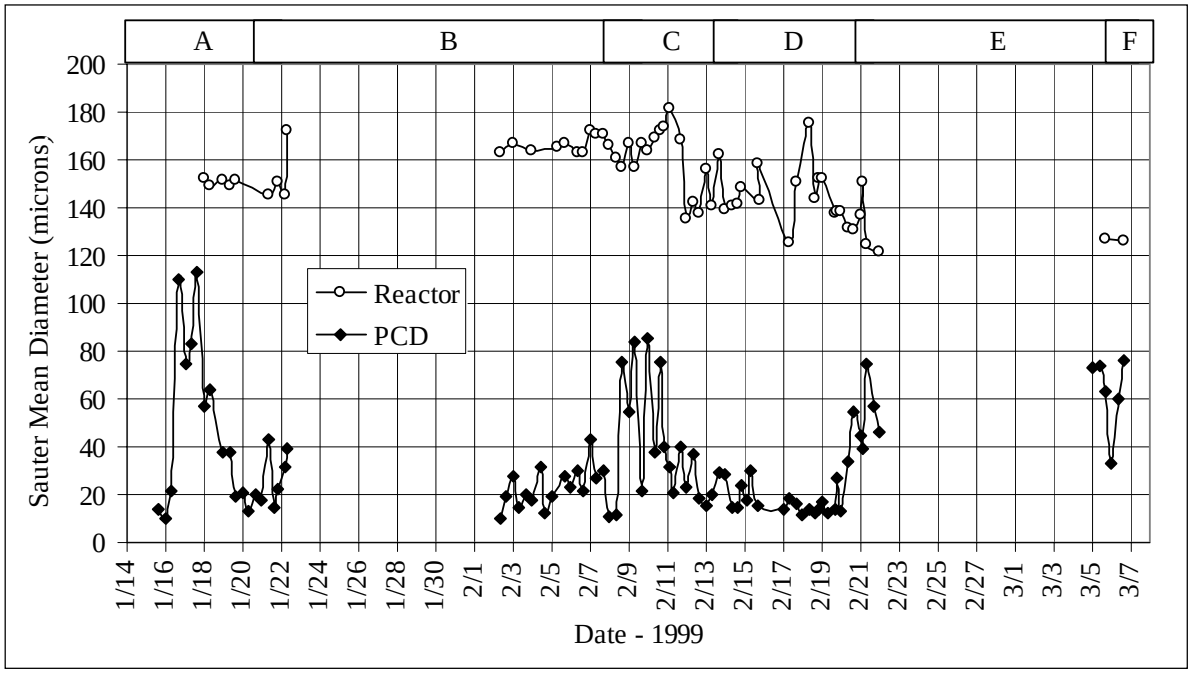

Figure 4.3-13 Reactor and PCD Solids Particle Size

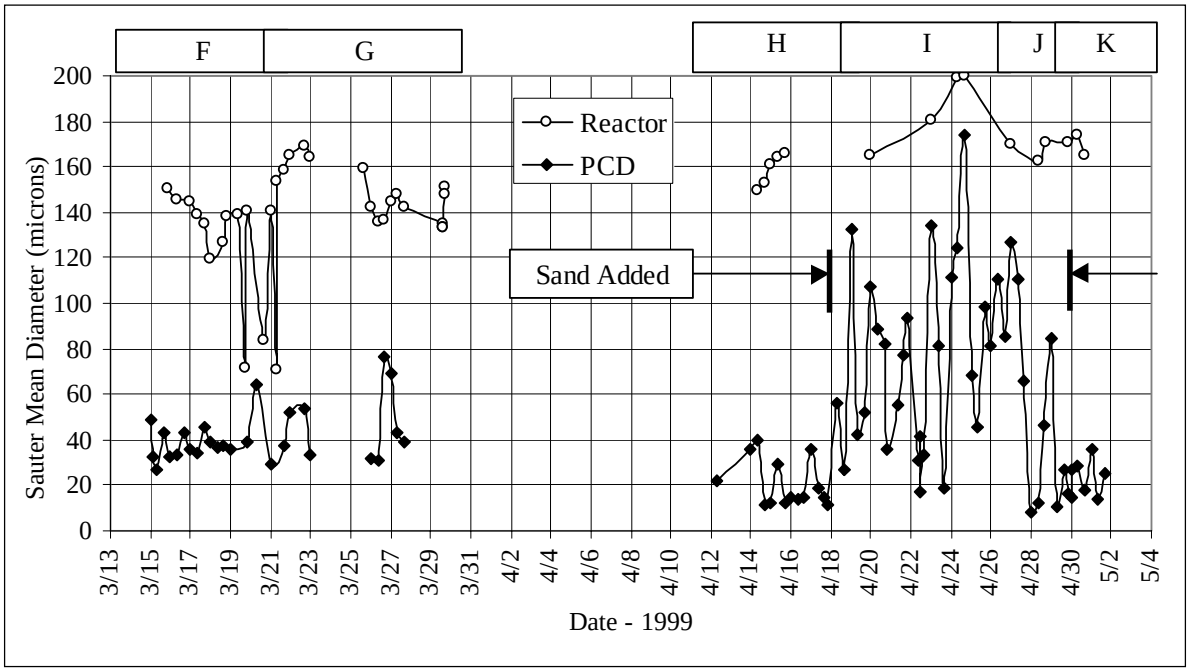

Figure 4.3-14 Reactor and PCD Solids Particle Size

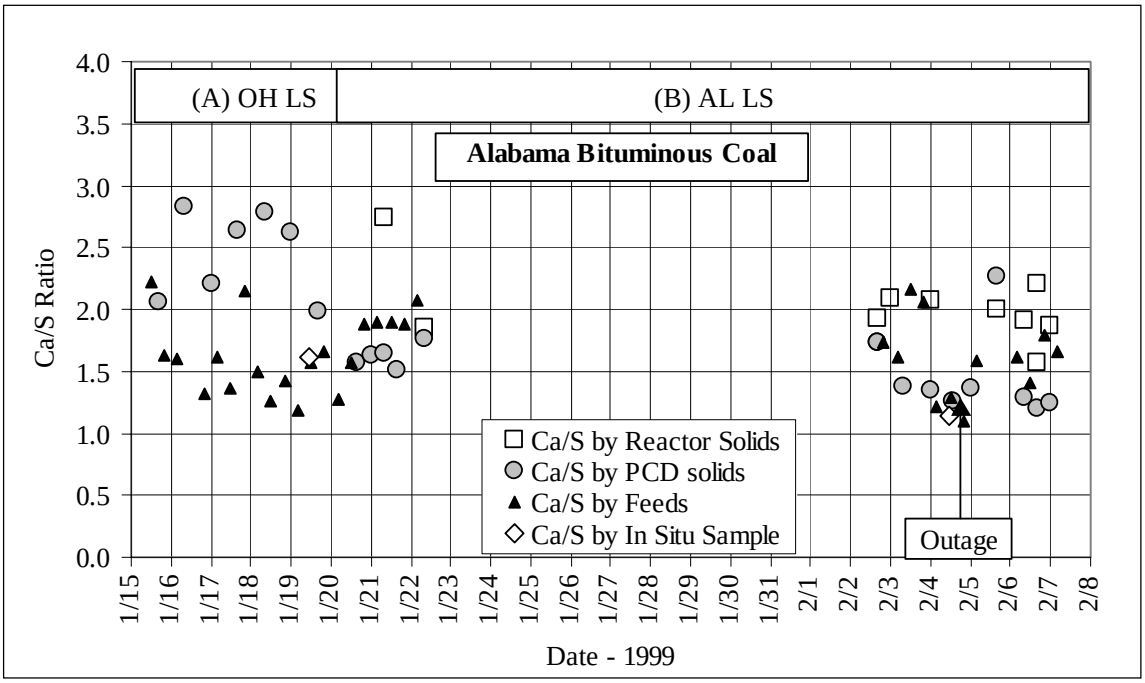

Figure 4.3-15 Alabama Coal PCD Solids Ca/S, Feeds Ca/S, In situ Ca/S, and Reactor Solids Ca/S

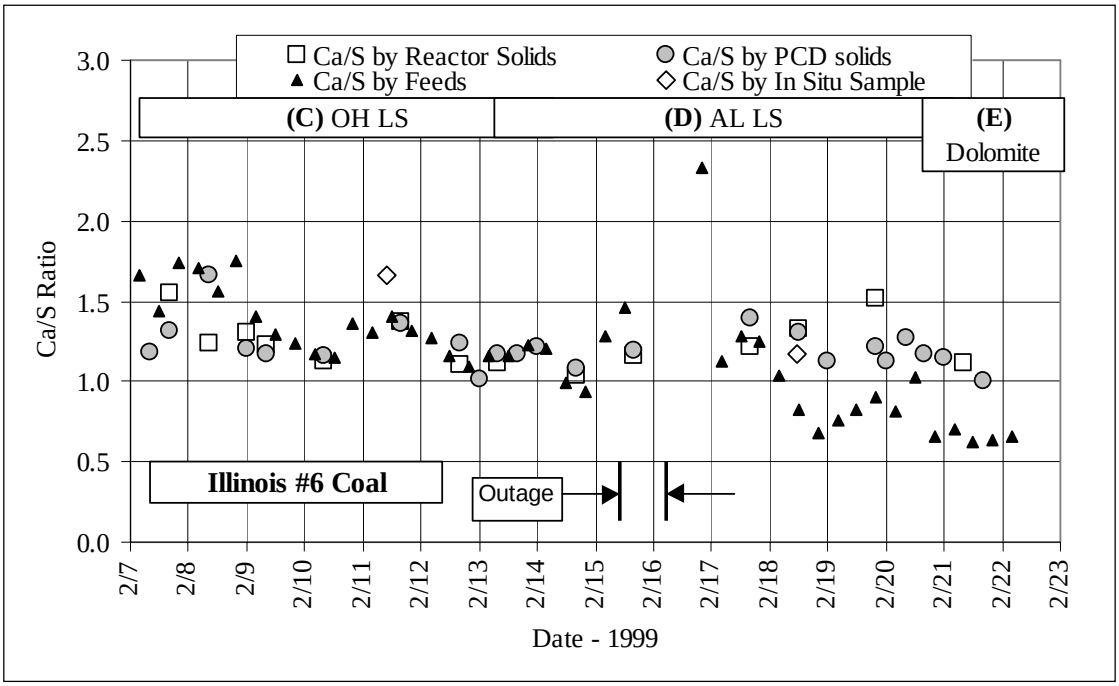

Figure 4.3-16 Illinois No. 6 Coal PCD Solids Ca/S, Feeds Ca/S, In situ Ca/S, and Reactor Solids Ca/S

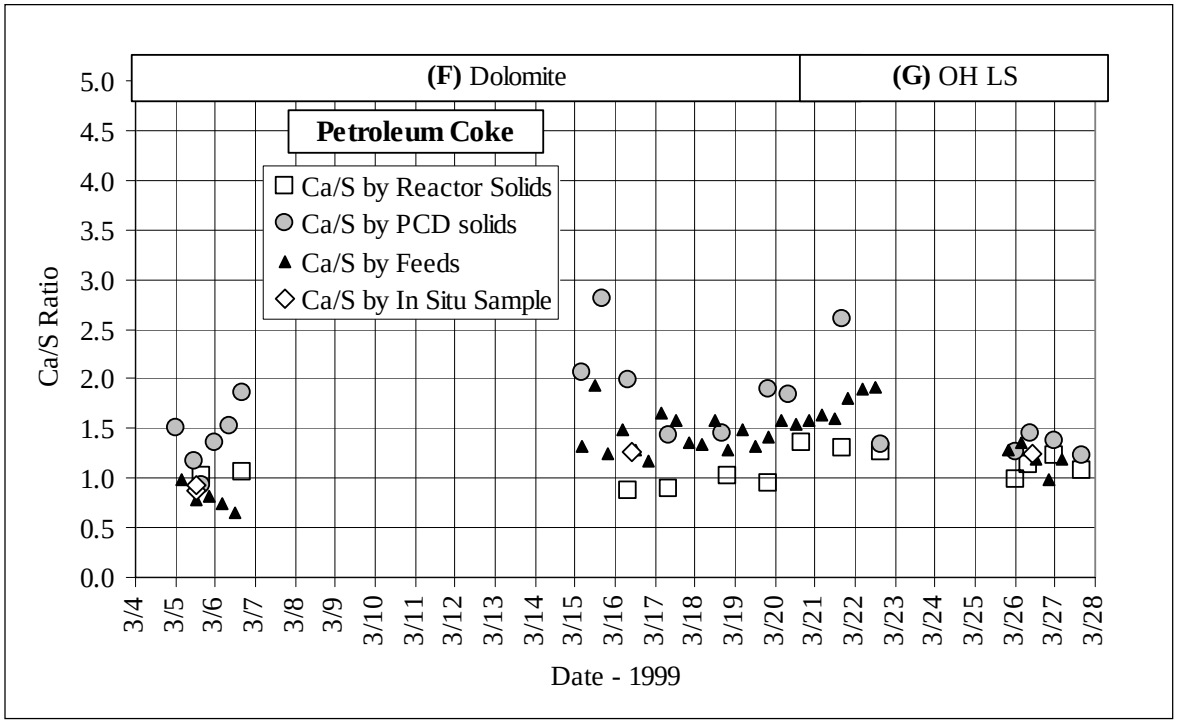

Figure 4.3-17 Petroleum Coke PCD Solids Ca/S, Feeds Ca/S, In situ Ca/S, and Reactor Solids Ca/S

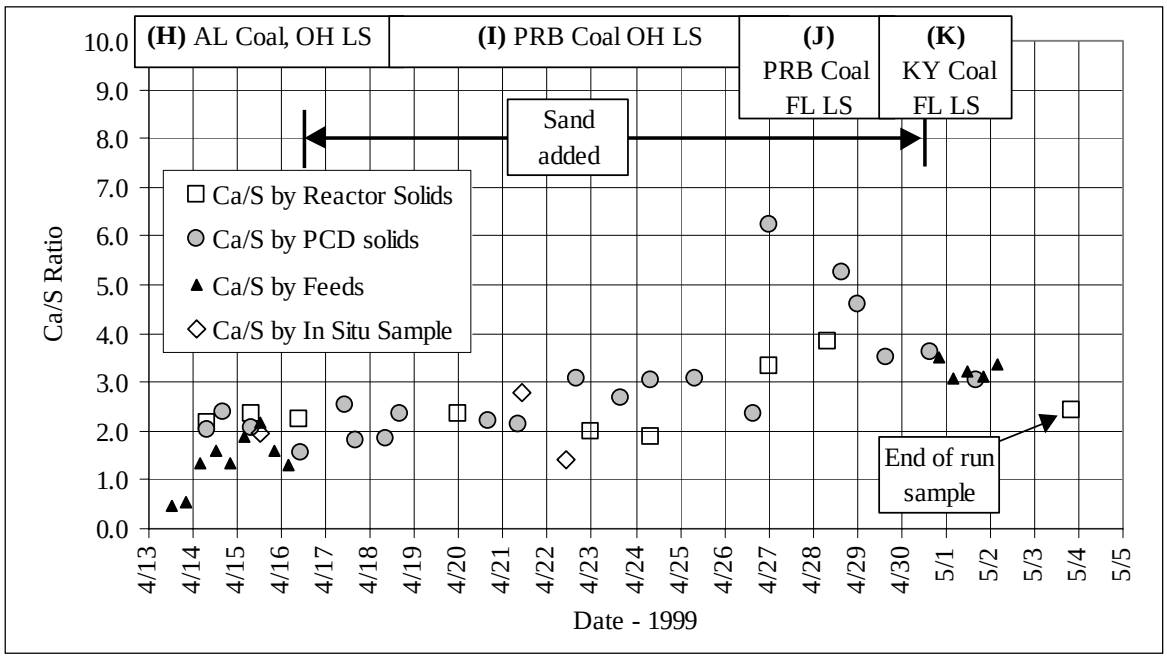

Figure 4.3-18 PCD Solids Ca/S, Feeds Ca/S, In situ Ca/S, and Reactor Solids Ca/S for Three Fuels

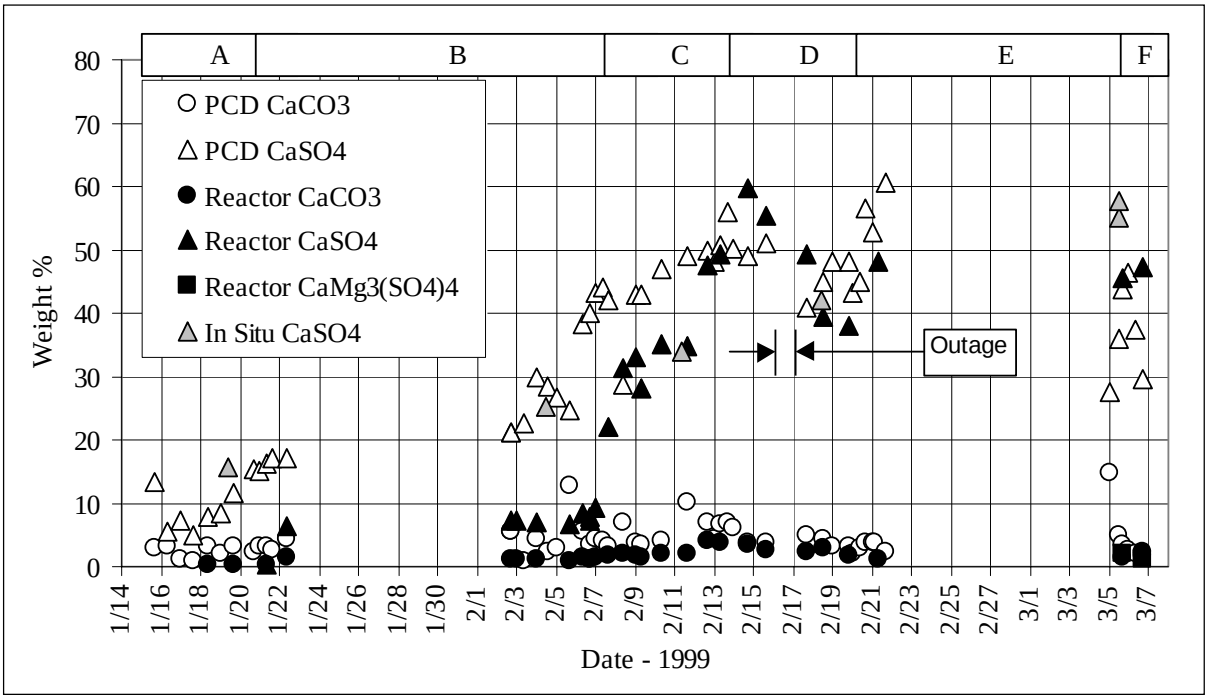

Figure 4.3-19 PCD and Reactor Solids $CaCO_3$ and $CaSO_4$ Contents

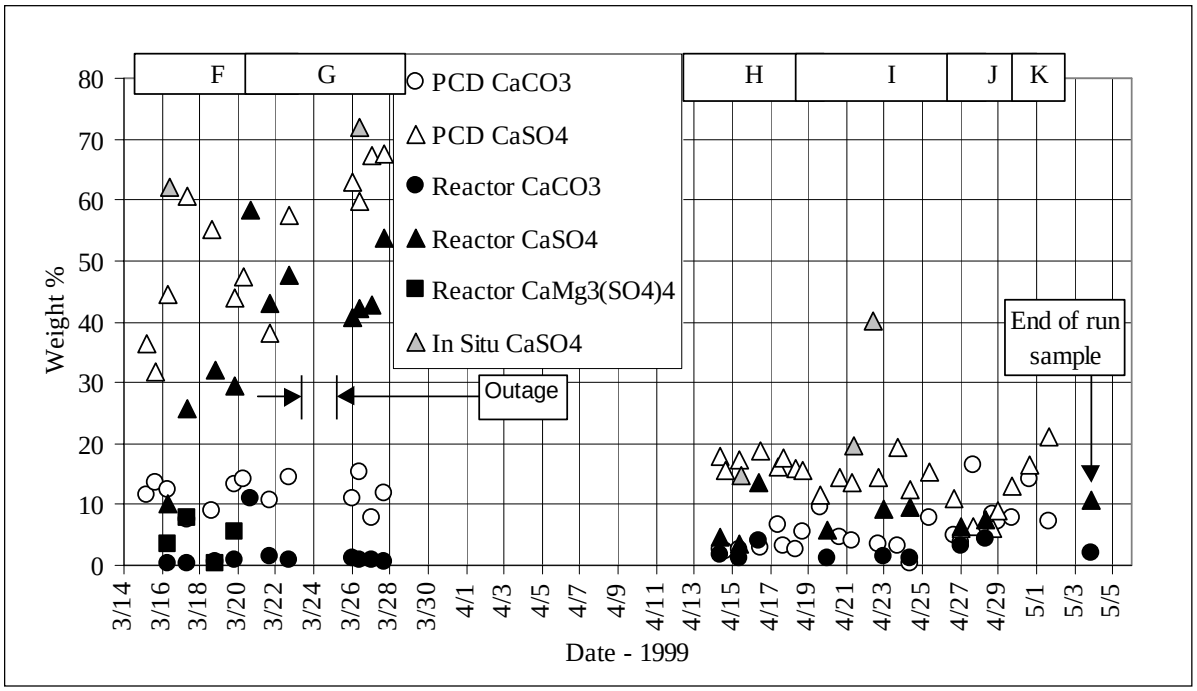

Figure 4.3-20 PCD and Reactor Solids $CaCO_3$ and $CaSO_4$ Contents

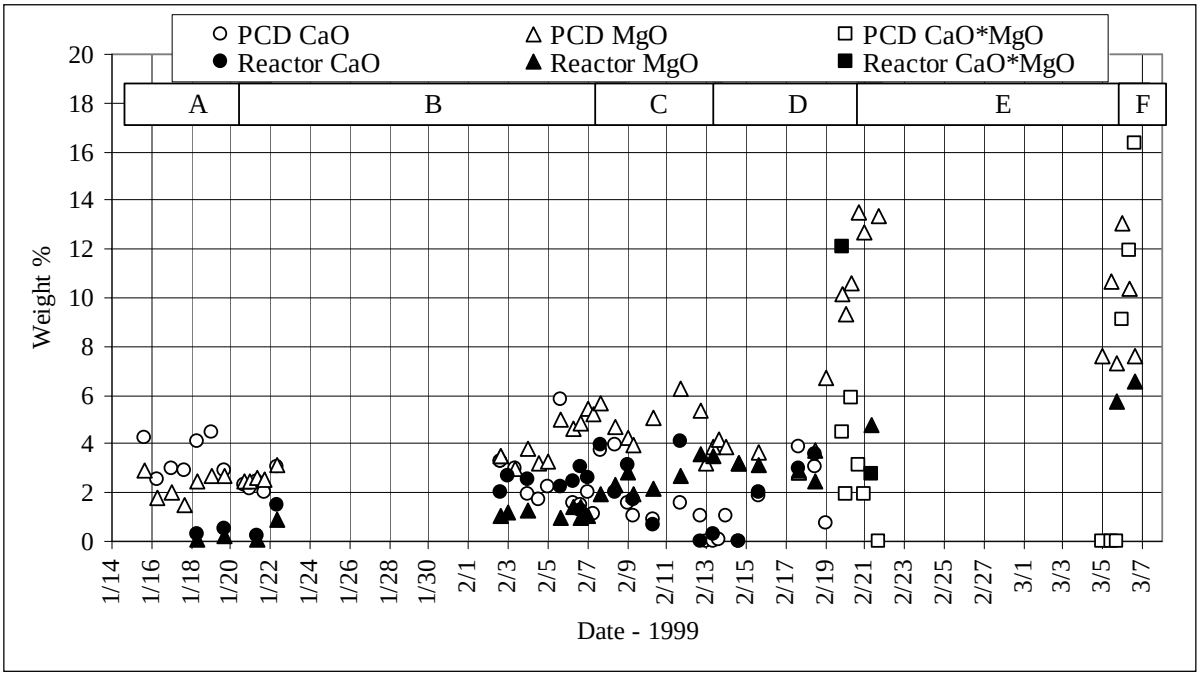

Figure 4.3-21 PCD and Reactor CaO, CaO•MgO, and MgO Contents

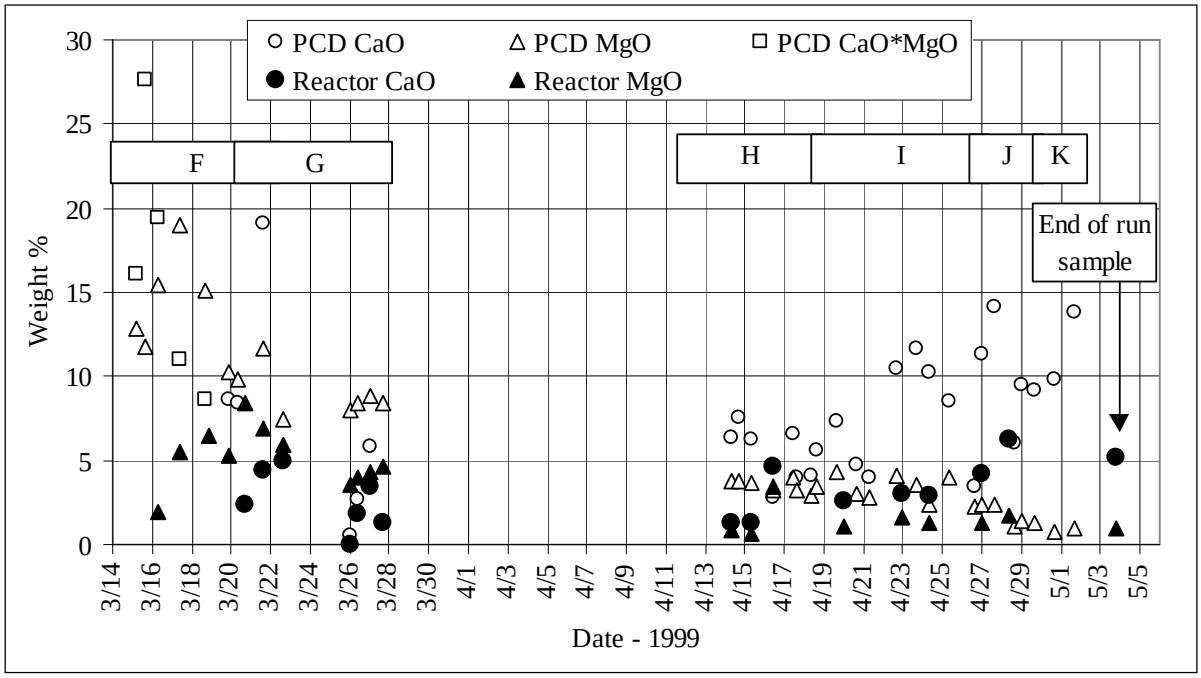

Figure 4.3-22 PCD and Reactor CaO, CaO•MgO, and MgO Contents

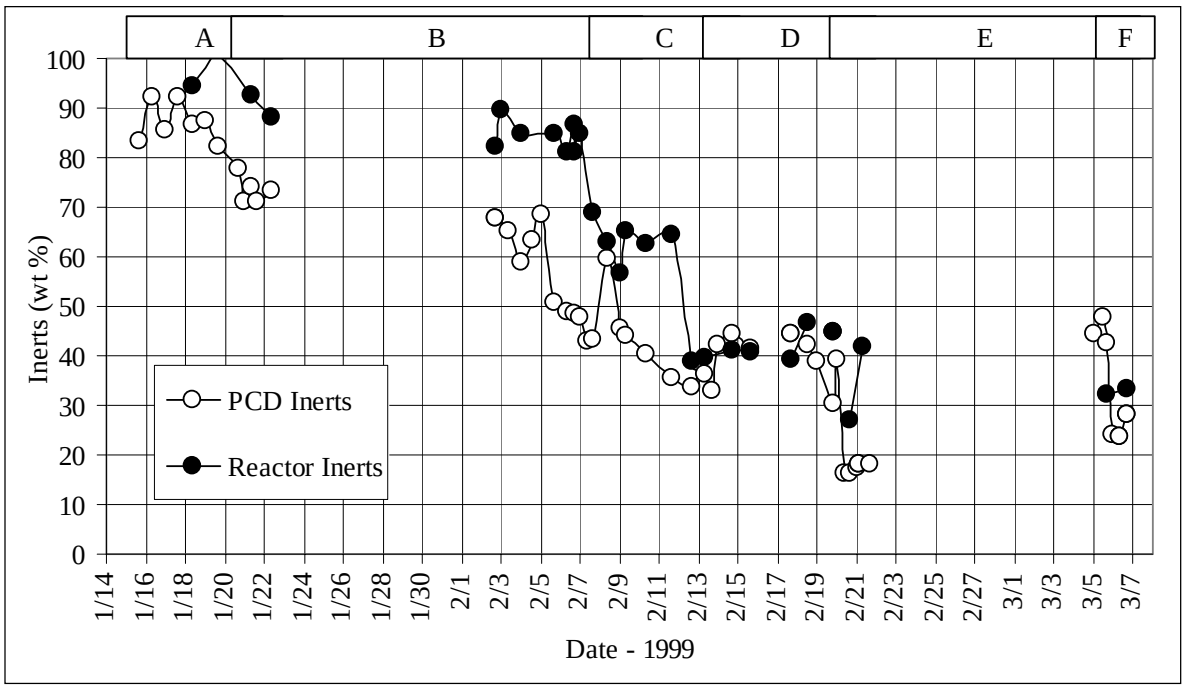

Figure 4.3-23 PCD and Reactor Inerts Contents

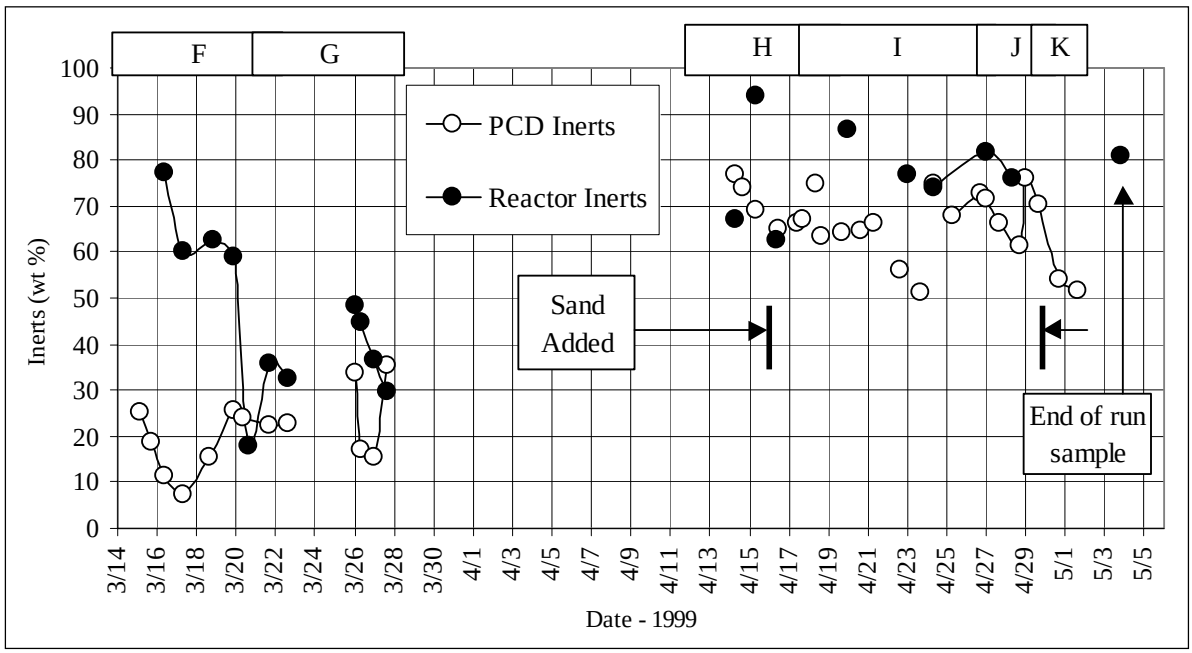

Figure 4.3-24 PCD and Reactor Inerts Contents

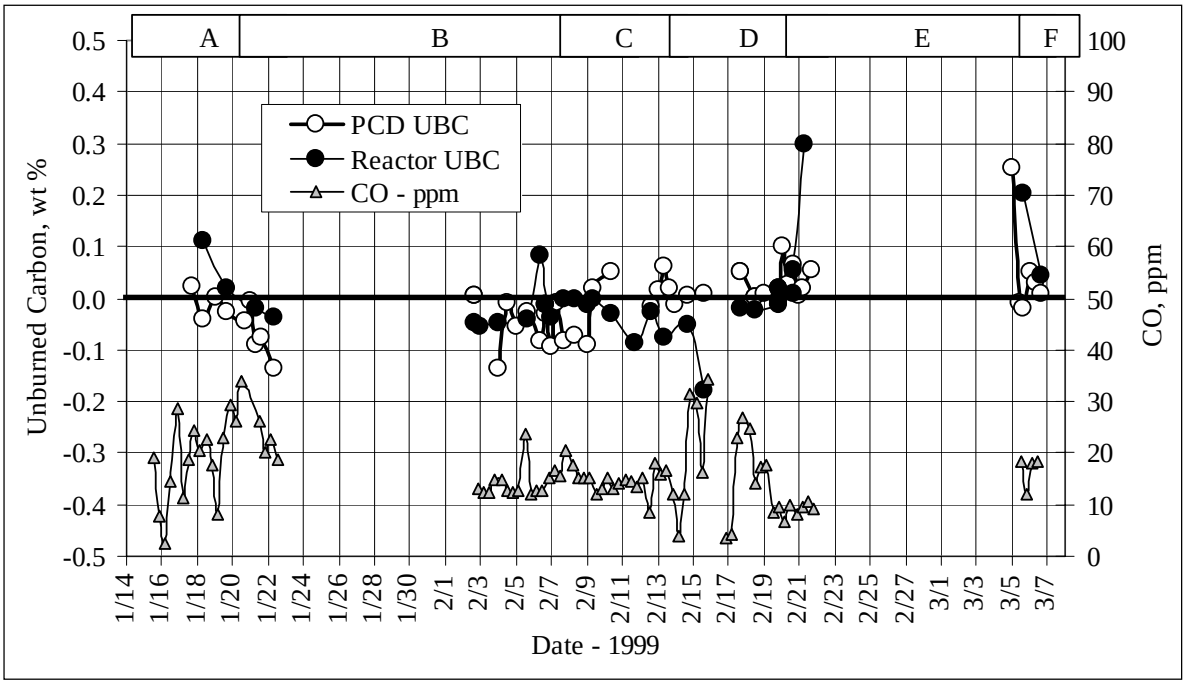

Figure 4.3-25 Carbon Monoxide and Unburned Carbon

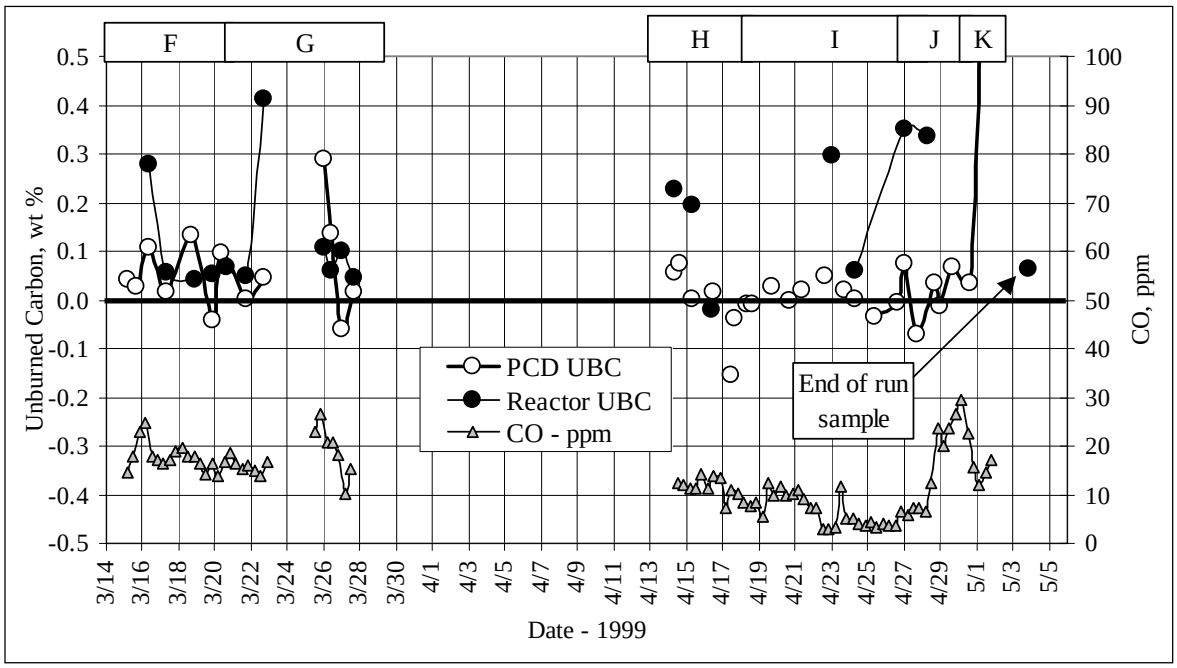

Figure 4.3-26 Carbon Monoxide and Unburned Carbon

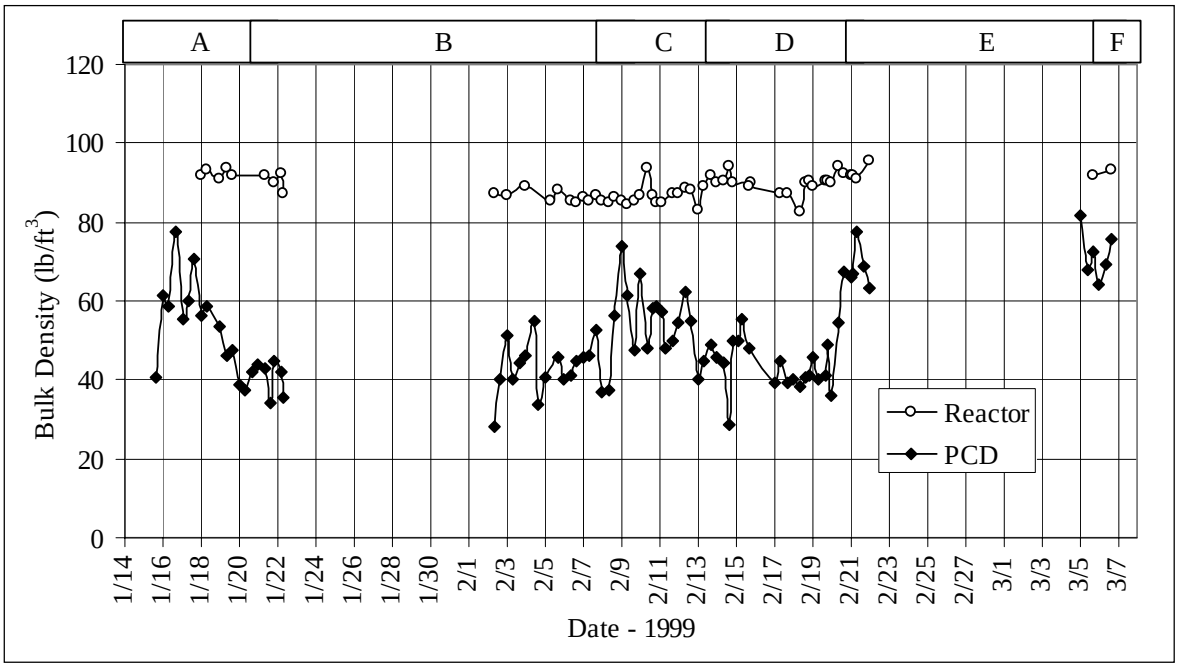

Figure 4.3-27 Bulk Density of Reactor and PCD Solids

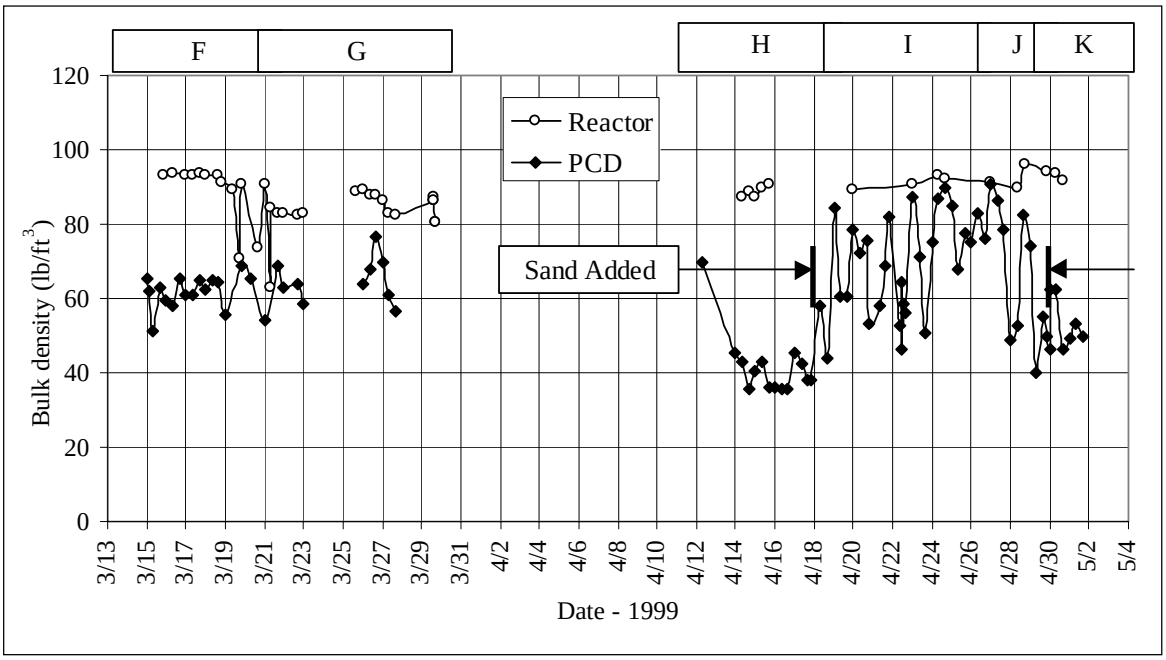

Figure 4.3-28 Bulk Density of Reactor and PCD Solids

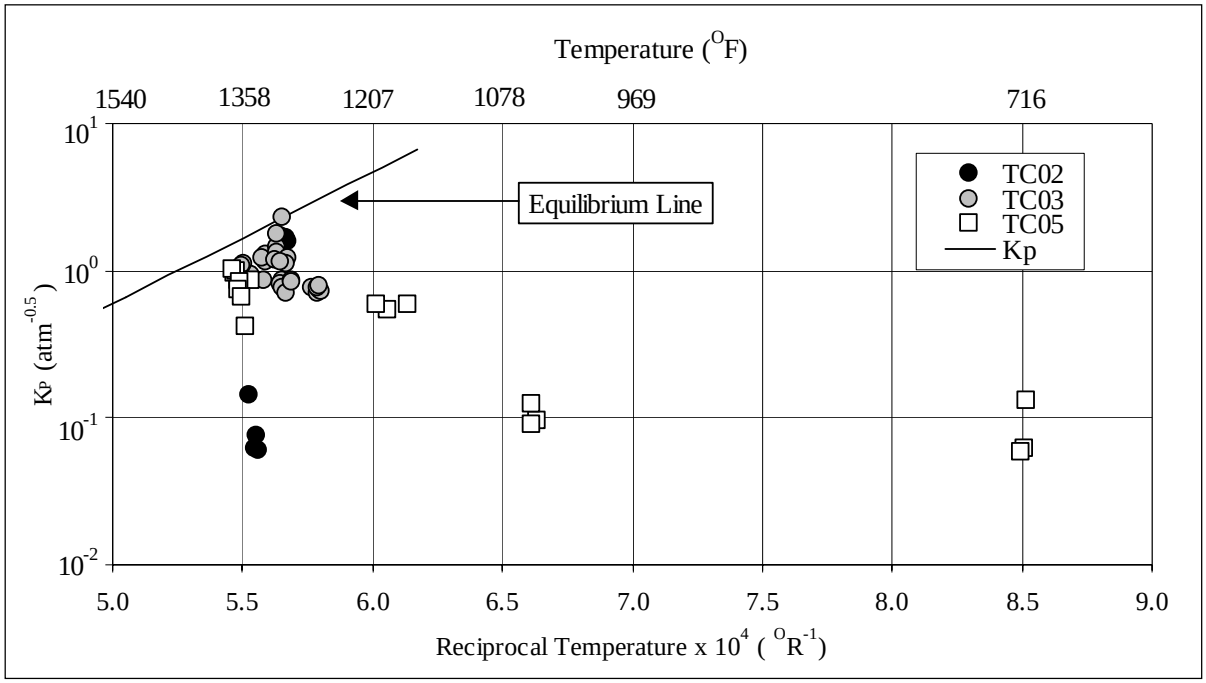

Figure 4.3-29 SO_2-SO_3 Equilibrium

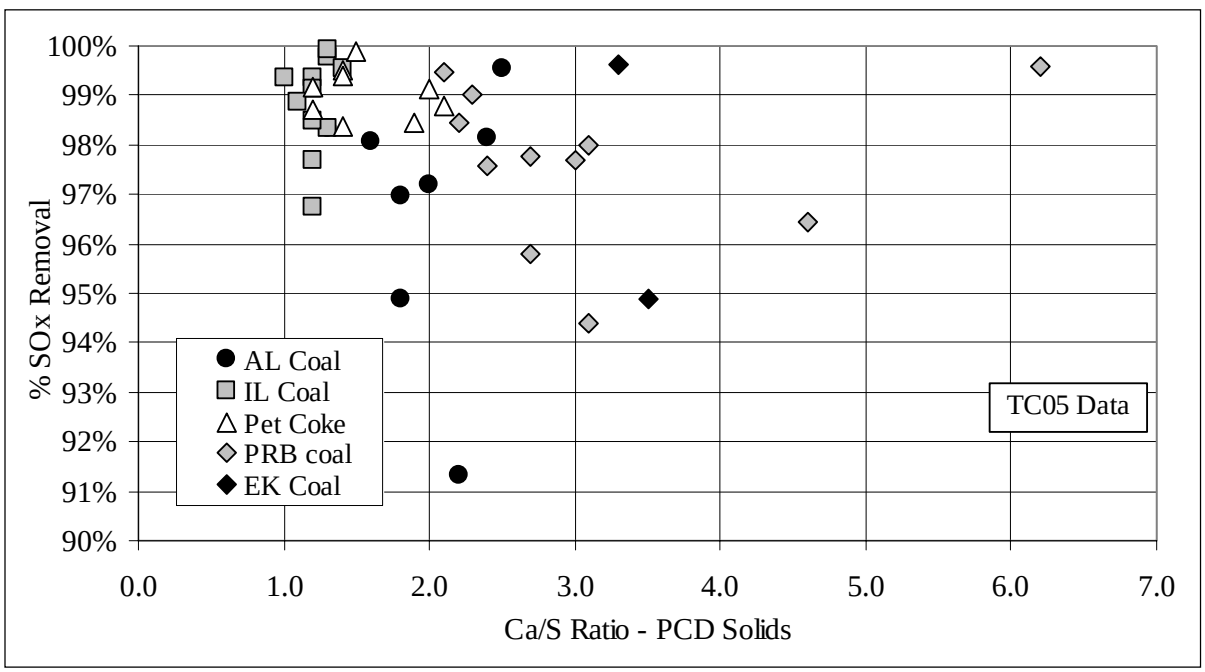

Figure 4.3-30 SO_x Removal and PCD Solids Ca/S by Fuel

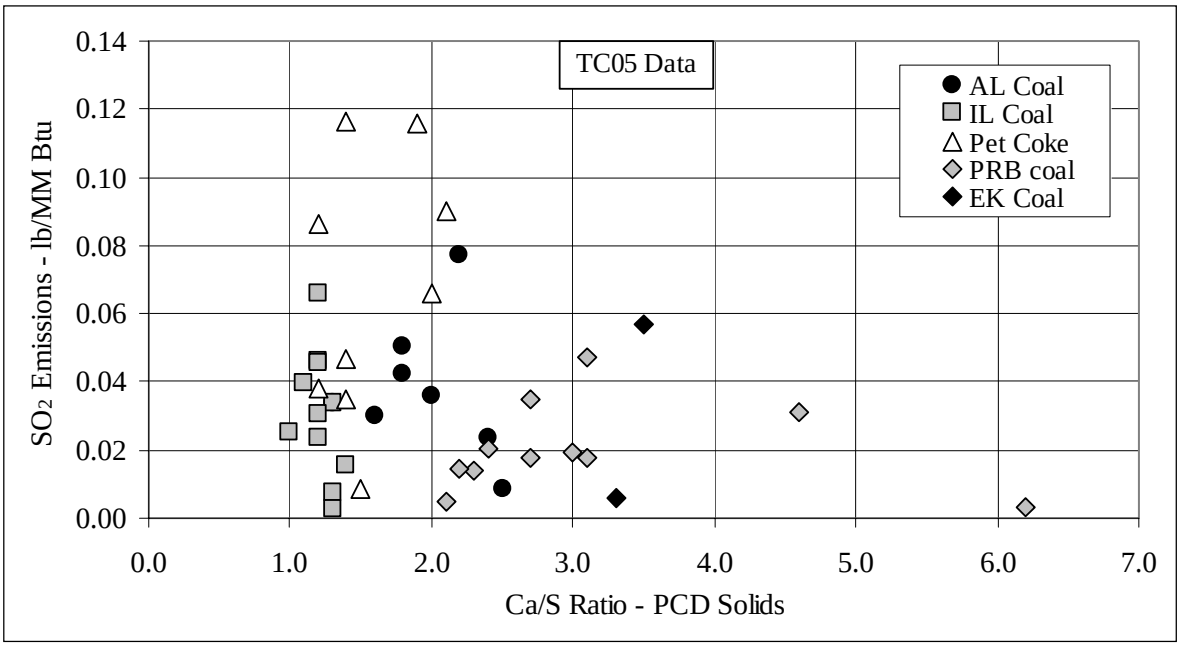

Figure 4.3-31 SO_2 Emissions and PCD Solids Ca/S by Fuel

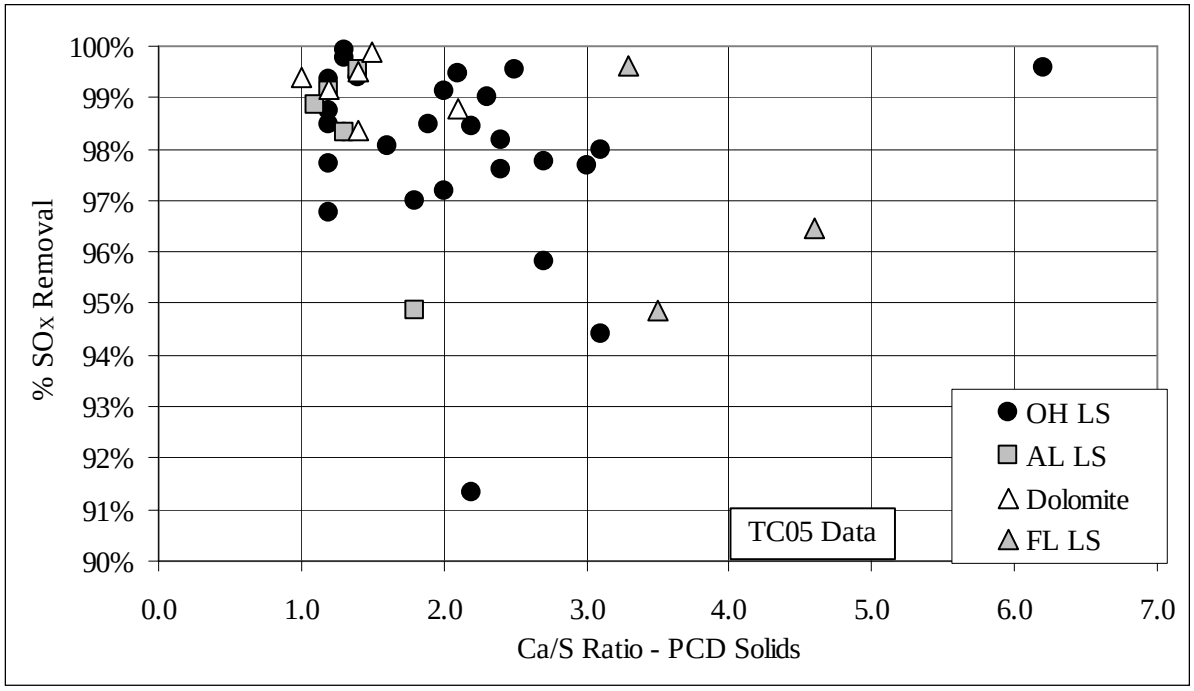

Figure 4.3-32 SO_X Removal and PCD Solids Ca/S by Sorbent

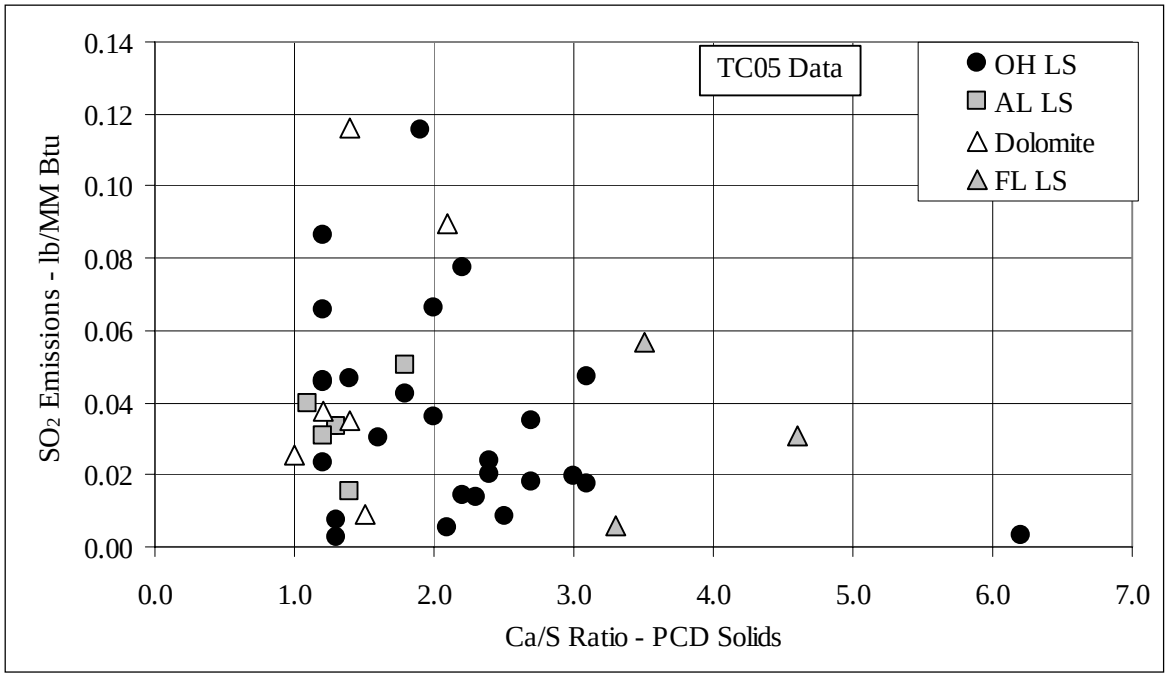

Figure 4.3-33 SO_2 Emissions and PCD Solids Ca/S by Sorbent

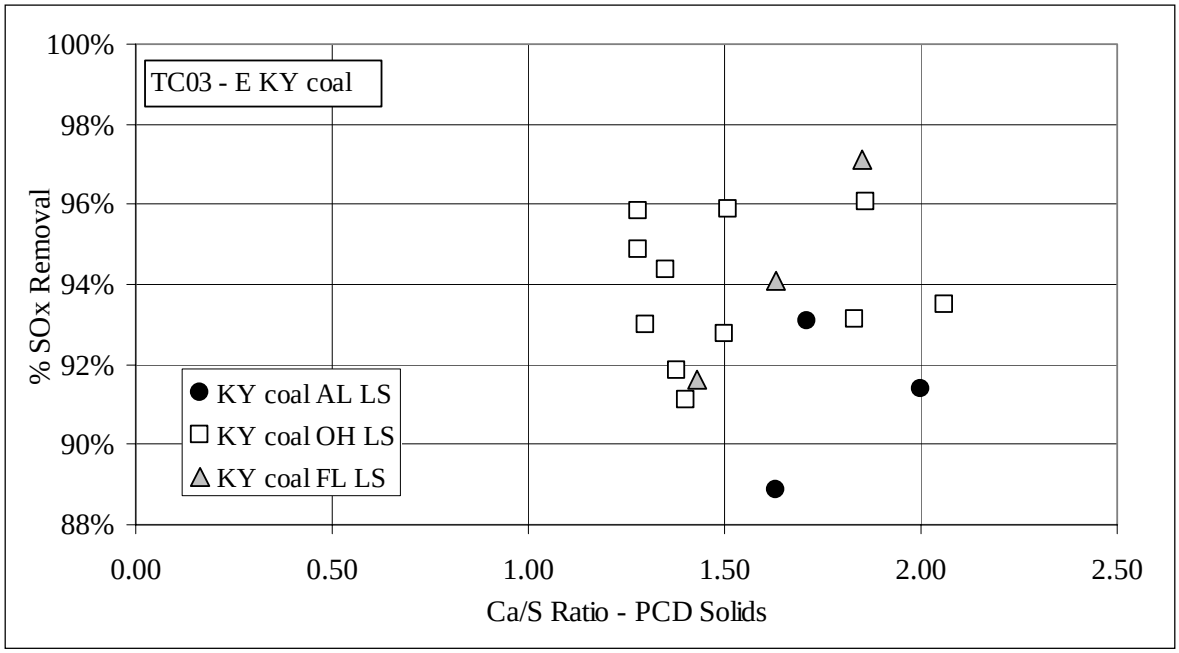

Figure 4.3-34 TC03 SO_x Removal and PCD Solids Ca/S by Sorbent

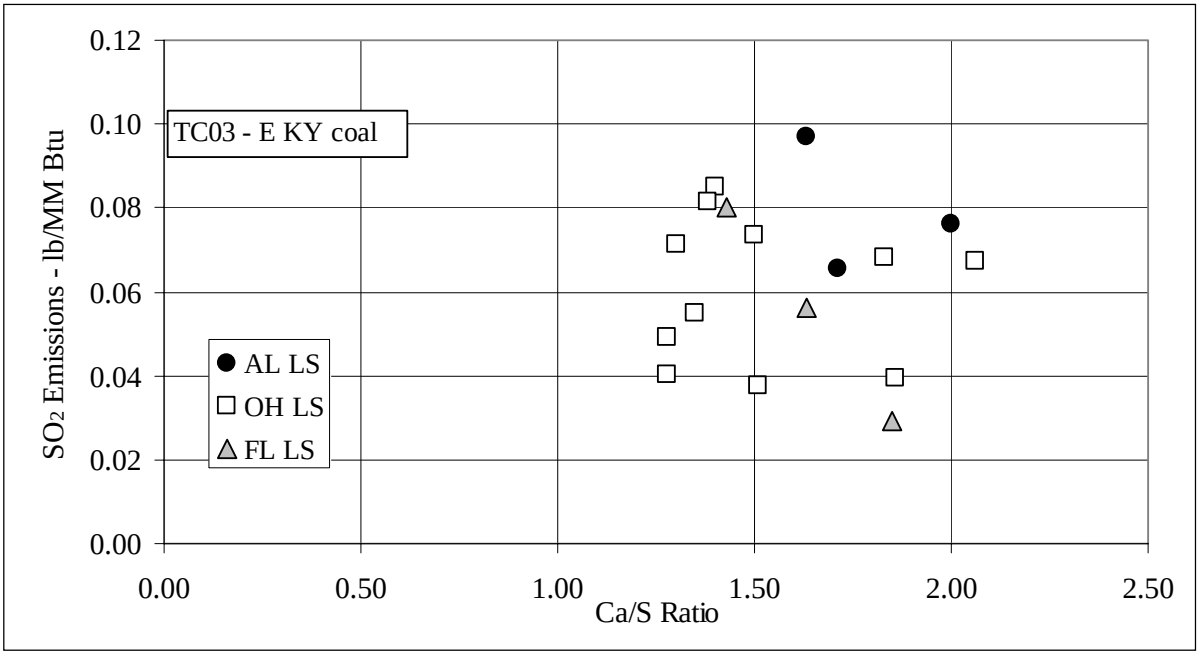

Figure 4.3-35 TC03 SO_2 Emissions and PCD Solids Ca/S by Sorbent

4.4 TC05 NO_X AND N_2O ANALYSIS

Data collected during TC05 was analyzed to evaluate the effect of different operating parameters on the NO_X and N_2O emissions. The operating parameters evaluated include:

- Staging air.
- Primary air distribution.
- Excess air.
- Reactor temperature.
- Reactor pressure.
- Fuel feed particle size.
- Ca/S molar ratio.
- Feed types.

The gas samples used for analysis can be taken from the two locations shown in Figure 4.4-1. Sample point 1, immediately downstream of the Siemens Westinghouse PCD, was used for the first days following an outage and sample point 2, downstream of the secondary gas cooler, was used due to plugging of the sample point 1 sample line with ash. There was no noticeable difference in measurements from sample point 1 and 2.

As discussed in section 4.1 each TC05 subtest was based on a certain feed combination. Thus, each subtest was analyzed separately. Since the NO_X and N_2O emissions behavior is different they are discussed individually. The NO_X analysis is shown in section 4.4.1 while the N_2O analysis is discussed in section 4.4.2. All data points were based on 15-minute averages with the relevant operating conditions of each data set listed in Table 4.1.

4.4.1 NO_X Analysis

A chemiluminescence analyzer was used to measure NO and NO_2 recorded as NO_X (ppm) and calculated as pounds of NO_2 divided by the heat input in MBtu. This chemiluminescence analyzer can be set to measure only NO. NO alone was measured for short times in various test runs.

Effect of Air Staging

Figures 4.4-2 to -5 show the NO_X emissions versus the staging factor. The staging factor is defined as the secondary-airflow divided by the total airflow rate to the mixing zone. An increase in air staging showed only moderate decreases in NO_X emissions for the ranges tested. With the Alabama coal and Longview limestone (data set B3) the NO_X emissions decreased

about 15 percent (0.13 to 0.11 lb/MBtu) as the staging factor was increased from 14 to 44. There was only the slight decrease of 6 percent (0.16 to 0.15 lb/MBtu) in NO_X emissions with the Illinois coal and Bucyrus limestone (data set C2) as the staging factor was increased from 9 to 37. With the PRB coal and Bucyrus limestone (data set I3) the NO_X emissions decreased about 10 percent (0.44 to 0.40 lb/MBtu) as the staging factor was increased from 9 to 31. Decreases of 13 to 14 percent in NO_X emissions were observed with both the pet coke and Plum Run dolomite (data set F2) and with the pet coke and Bucyrus limestone (data set G2). Small changes in the primary air distribution (air-to-mixing zone) had no effect on NO_X emissions.

Effect of Excess Air

An increase in excess air was found to increase the NO_X emissions with varying degrees depending on the range of variation and other operational parameters such as fuel/sorbent combination. Figures 4.4-6 to -10 plot the NO_X emissions (lb/MBtu) versus the oxygen concentration in the flue gas (percent). With the Alabama coal and Bucyrus limestone (data set H1) the NO_X emissions increased from 0.06 to 0.15 lb/MBtu as the oxygen concentration was increased from 3.6 to 6.4 percent. With the Alabama coal and Longview limestone (data set B2) the NO_X emissions increased from 0.12 to 0.13 lb/MBtu as the oxygen concentration was increased from 5.3 to 6.1 percent. Similar increases in NO_X emissions as the oxygen concentration increased were observed with all feed combinations.

Effect of Temperature

The reactor operating temperature was found to have little or no effect on NO_X emissions. Figures 4.4-11 to -15 plot the NO_X emissions (lb/MBtu) versus the reactor temperature (°F). With the Alabama coal and Bucyrus limestone (data set A1) (Figure 4.4-11) shows no increase in NO_X emissions as the reactor temperature was increased from 1,575 to 1,620°F. However, in some cases the NO_X decreased when the operating temperature was increased. For example, with PRB coal and Bucyrus limestone (data set I2) the NO_X emissions decreased from 0.45 to 0.42 (lb/MBtu) as the reactor temperature increased from 1,470 to 1,545°F. However, this increase in the reactor operating temperature coincided with an increase in coal feed rate and thus a decrease in oxygen concentration (Figure 4.4-9). Thus, the decrease in NO_X cannot be attributed solely to the decrease in temperature.

Effect of Sorbent Feed Rate

The sorbent feedrate effect on NO_X emissions differed dependent upon other operating conditions. Figures 4.4-16 to -20 plot the NO_X emissions (lb/MBtu) versus the Ca/S molar ratio (calculated based on feeds) at constant oxygen concentrations. With the Alabama coal and Longview limestone at 8-percent oxygen concentration (data set A3) the NO_X emissions increased almost linearly from 0.13 to 0.31 lb/MBtu as the Ca/S molar ratio was increased from zero to 4.5. At 7-percent oxygen (data set A2) the NO_X emissions increased as the Ca/S molar ratio was increased from zero to 0.7, but as the Ca/S molar ratio was increased further there were no additional increases in NO_X emissions. A similar effect was observed with the Alabama coal and Longview limestone at 6-percent oxygen (data set B4). It was also noted that although

the NO_X might be insensitive to changes in Ca/S molar ratio in lower ranges, very high Ca/S molar ratios would cause additional increases in NO_X emissions. (See data set I4 on Figure 4.4-19.) The transient response of NO_X emissions to changes in the sorbent feedrate is shown in Figure 4.4-21.

Effect of Pressure

Increasing the reactor pressure decreased the NO_X emissions. Figure 4.4-22 plots the NO_X emissions versus the reactor pressure using pet coke and Plum Run dolomite. The NO_X emissions decreased from 0.25 to 0.19 lb/MBtu as the reactor pressure was increased from 160 to 200 psig.

Effect of Fuel-Feed-Particle Size

NO_X emissions decreased as the fuel-feed particle size was reduced with the Eastern Kentucky coal, the Powder River Basin coal, and pet coke. Fines in the fuel feed are detected by comparing the coal feeder speed and the fuel feed rate. Since fines have a lower density the coal feeder speed had to be increased to maintain a constant feed rate. Figure 4.4-23 plots the coal feeder speed (rpm), coal feed rate (lb/hr), oxygen concentration in the flue gas (percent), and the NO_X concentration (ppm) versus time. From 0:30 to 8:00 on March 21, 1999, the coal feed speed was increased from 7.5 to 10.2 rpm while the coal feed rate remained constant around 1,175 lb/hr. The NO_X decreased from 122 ppm (0.32 lb/MBtu) to 95 ppm (0.24 lb/MBtu). When all of the fine material had been fed the feeder speed was decreased to 7.5 rpm and the NO_X increased to 130 ppm.

Effect of Fuel and Sorbent Type

Fuel type has a big influence on NO_X emissions while sorbent type appears to have some lesser effect. Figure 4.4-24 plots the NO_X emissions with different feed combinations at similar operating conditions (data set L1). The NO_X emissions with the bituminous coals were the lowest while NO_X emissions with PRB were the highest. The NO_X emissions with the bituminous coals were comparable to the NO_X emissions from other facilities with no additional control technologies. The fuel-N-conversion to NO_X correlated well with the fuel-oxygen-to-fuel-nitrogen ratio (see Figure 4.4-25). Similar correlations can be found in the literature.

Conclusions

Excess air had a large influence on NO_X emissions. The NO_X emissions could be decreased significantly by lowering the excess air. The NO_X emissions could also be decreased somewhat by increasing the reactor pressure and by increasing the staging air. The reactor temperature had little or no effect on NO_X emissions. Sorbent addition appeared to increase NO_X emissions initially but as feedrate is increased further there was little or no increase in NO_X. However, at very high sorbent feedrates there were additional increases in NO_X emissions. It was also noted that decreases in the fuel feed particle size caused decreases in the NO_X emissions. Without any additional reduction control systems NO_X emissions <0.10 lb/MBtu can be achieved with the Alabama and Illinois #6 bituminous coals and NO_X emissions <0.15 lb/MBtu can be achieved

with the Eastern Kentucky bituminous coal and pet coke. The NO_X was composed of 80- to 90-percent NO and 10- to 20-percent NO_2.

4.4.2 N_2O Analysis

A nondispersive infrared analyzer was used to measure N_2O. CO and CO_2 were also measured since they are interference gases with N_2O measurements at the absorption wavelength used.

Effect of Air Staging

An increase in air staging showed decreases of about 0.02 lb/MBtu in N_2O emissions for the ranges tested. Figures 4.4-26 through -28 show N_2O emissions versus the staging factor. Small changes in the primary air distribution (air-to-mixing-zone) had no effect on N_2O emissions.

Effect of Excess Air

Figures 4.4-29 through -33 plot the N_2O emissions (lb/MBtu) versus the oxygen concentration in the flue gas (percent). An increase in excess air was found to have little or no effect on N_2O emissions. For example, the N_2O emissions with the Alabama coal (data sets B1, B2, and H10) could vary as much as 0.03 lb/MBtu at a constant-oxygen concentration. Another example is with the Kentucky coal and Gregg Mine limestone (data set K1). The N_2O emissions were around 0.25 lb/MBtu at oxygen concentrations of both 6.8 and 7.8 percent. Other plots show a large degree of scatter in the data.

Effect of Temperature

Figures 4.4-34 through -39 plot the N_2O emissions (lb/MBtu) versus the reactor temperature in the flue gas (°F). The N_2O emissions are highly dependent on reactor temperature. As the reactor temperature increased the N_2O emissions decreased significantly independent of fuel and sorbent. For instance, with the Illinois coal and Bucyrus limestone, the N_2O emissions decreased from 0.12 to 0.03 lb/MBtu as the temperature increased from 1,510 to 1,560°F.

Effect of Sorbent Feed Rate

There was no strong influence of sorbent feed rate on N_2O emissions (Figures 4.4-40 through -44). However, some data showed a slight decrease in N_2O emissions as the sorbent feedrate was increased. For example, with pet coke and Bucyrus limestone the N_2O emissions decreased about 0.01 MBtu as the Ca/S molar ratio was increased from 0.8 to 1.6

Effect of Pressure

Increasing the reactor pressure decreased the N_2O emissions. Figure 4.4-45 plots the N_2O emissions versus the reactor pressure at constant temperatures using pet coke and Plum Run dolomite. At 1,550°F the N_2O emissions decreased from 0.12 to 0.06 lb/MBtu as the reactor

pressure was increased from 160 to 200 psig. There was a similar decrease at higher temperatures also.

Effect of Fuel-Feed-Particle Size

The effect of fuel-feed-particle size on N_2O emissions was inconclusive due to the high-temperature dependency of N_2O on temperature. Figure 4.4-46 plots the coal feeder speed (rpm), coal-feed rate (lb/hr), oxygen concentration in the flue gas (percent), and the N_2O concentration (ppm) versus time.

Effect of Fuel and Sorbent Type

Figure 4.4-47 plots the N_2O emissions with different feed combinations at 1,560°F (data set L2). At 1,560°F the N_2O emissions were lowest with Illinois coal and highest with Kentucky coal. However, very low-N_2O emissions are achievable at higher temperatures independent of feed types.

Conclusions

N_2O emissions decrease significantly as reactor temperature is increased. Essentially zero-N_2O emissions are achievable at higher operating temperatures. N_2O emissions were also decreased by increasing staging air and increasing reactor pressure. The excess air and sorbent feedrate appeared to have little influence on N_2O emissions.

Table 4.4-1

Average Conditions for TC05 NO_x and N_2O Data Analysis (Page 1 of 2)

Data Set	Fuel Type	Sorbent Type	Reactor Temp (°F)	Coal-Feed Rate (lb/hr)	Ca/S Molar Ratio	Oxygen Conc (%)	Reactor Pres (psig)	Staging Factor
A1	Calumet Mine Bit (AL)	Bucyrus ls (OH)	1570-1620	1230	1.8	6.9	200	14
A2	Calumet Mine Bit (AL)	Bucyrus ls (OH)	1575-1590	1190-1230	0-1.8	6.7-7.3	200	14
A3	Calumet Mine Bit (AL)	Bucyrus ls (OH)	1525-1570	1050-1135	0.1-4.5	7.7-8.3	200	14
B1	Calumet Mine Bit (AL)	Longview ls (AL)	1550-1580	1285	0	5.6-6.2	200	20
B2	Calumet Mine Bit (AL)	Longview ls (AL)	1525-1570	1450	3.0	5.3-6.1	200	27
B3	Calumet Mine Bit (AL)	Longview ls (AL)	1550-1560	1270-1380	1.2-1.7	6.1-6.4	200	14-44
B4	Calumet Mine Bit (AL)	Longview ls (AL)	1550-1580	1280-1450	0-4.2	5.7-6.2	200	20-27
B20	Calumet Mine Bit (AL)	Longview ls (AL)	1560-1570	1280-1500	0-4.2	5.6-6.4	200	20-33
C1	IL No. 6 Bit Coal	Bucyrus ls (OH)	1550-1580	1515-1715	1.3	3.7-5.75	200	37
C2	IL No.6 Bit Coal	Bucyrus ls (OH)	1555	1460-1480	0.9	5.6	200	9-37
C3	IL No. 6 Bit Coal	Bucyrus ls (OH)	1530-1555	1480-1500	0.4-1.4	4.8-5.2	200	33-37
C4	IL No. 6 Bit Coal	Bucyrus ls (OH)	1530-1555	1430-1450	0.7-1.4	4.8-5.2	200	33-37
C20	IL No. 6 Bit Coal	Bucyrus ls (OH)	1525-1535	1350-1525	0.6-1.4	5.0-6.3	200	33-37
D1	IL No. 6 Bit Coal	Longview ls (AL)	1530-1580	1615-1800	0.9-1.2	3.7-5.8	200	36-40
D2	IL No. 6 Bit Coal	Longview ls (AL)	1510-1530	1675-1760	0.9-1.9	3.8-4.2	200	36-40
D3	IL No. 6 Bit Coal	Longview ls (AL)	1550-1565	1375-1430	0.9-1.4	6.8-7.2	200	35-37
D20	IL No. 6 Bit Coal	Longview ls (AL)	1515-1525	1730-1760	1.0-1.7	3.7-4.0	200	37
E1	IL No. 6 Bit Coal	Plum Run Dol (AL)	1500-1550	1600-1665	0.6-0.8	4-5	200	36
E2	IL No. 6 Bit Coal	Plum Run Dol (AL)	1515-1535	1610-1690	0.6-0.8	4.2-4.9	200	36
E20	IL No. 6 Bit Coal	Plum Run Dol (AL)	1525-1535	1600-1665	0.6-0.8	4-5	200	36
F1	Pet Coke	Plum Run Dol (AL)	1575-1600	1170-1190	0.8-1.2	3.2-5.4	200	32-36
F2	Pet Coke	Plum Run Dol (AL)	1565	1130	1.4	4.5-4.8	160	6-22
F3	Pet Coke	Plum Run Dol (AL)	1540-1570	1200-1270	1.0-1.3	4.8-5.2	190	31
F4	Pet Coke	Plum Run Dol (AL)	1545-1585	1170-1200	0.7-1.4	4.0-5.3	160-200	20-30
F15	Pet Coke	Plum Run Dol (AL)	1545-1555	1770-1330	1.2-1.3	3.8-4.8	160-180	22-31

Table 4.4-1

Average Conditions for TC05 NO_X and N_2O Data Analysis (Page 2 of 2)

F16	Pet Coke	Plum Run Dol (AL)	1595-1605	1170-1330	0.9-1.3	3.6-6.0	160-190	22-31
F20	Pet Coke	Plum Run Dol (AL)	1595-1605	1170-1360	0.9-1.2	3.6-5.4	190	31
G1	Pet Coke	Bucyrus Is (OH)	1540-1560	1180-1200, 1425-1500	1.2-1.5	2.5-6.3	200	30-37
G2	Pet Coke	Bucyrus Is (OH)	1565-1575	1180	1.4	6.2-6.4	200	13-36
G3	Pet Coke	Bucyrus Is (OH)	1570-1600	1375-1500	0.8-1.6	2.8-3.2	200	35-37
G4	Pet Coke	Bucyrus Is (OH)	1540-1570	1180-1200	1.2-1.6	5.8-6.2	200	37
G20	Pet Coke	Bucyrus Is (OH)	1595-1605	1590-1600	0.9-1.6	3.0-3.5	200	29-31
H1	Calumet Mine Bit (AL)	Bucyrus Is (OH)	1560-1610	1470-1480, 1740-1770	1.3-1.4	3.6-6.4	200	24-30
H2	Calumet Mine Bit (AL)	Bucyrus Is (OH)	1580-1610	1700-1770	1.4-2.5	3.7-4.3	200	24-30
H10	Calumet Mine Bit (AL)	Bucyrus Is (OH)	1555-1620	1480-1700	2.1	3.5-4.4	200	30
H20	Calumet Mine Bit (AL)	Bucyrus Is (OH)	1598-1602	1735-1745	0-2.0	3.9-4.1	200	30
I1	PRB	Bucyrus Is (OH)	1500-1560	1125-1510	0	6.0-10.6	200	9
I2	PRB	Bucyrus Is (OH)	1470-1525	1360-1535	0.7-1.1	7.2-8.9	200	8-10
I3	PRB	Bucyrus Is (OH)	1480-1500	1480-1500	0.7	7.9-8.2	200	9-31
I4	PRB	Bucyrus Is (OH)	1495-1530	1125-1410	0-4.6	8.7-9.3	200	9-15
I20	PRB	Bucyrus Is (OH)	1495-1505	1440-1500	0-0.7	6.6-7.8	200	9
J1	PRB	Gregg Mine Is (FL)	1510-1540	1570-1840	0.6-3.0	5.4-7.5	190	15
J2	PRB	Gregg Mine Is (FL)	1535-1565	1570-1620	0-18	6.8-7.2	190	15
J20	PRB	Gregg Mine Is (FL)	1525-1535	1570-1580	0-18	5.7-7.4	190	15
K1	KY bituminous coal	Gregg Mine Is (FL)	1470-1560	1125-1260	0.6-3.1	5.8-8.1	190	26
K2	KY bituminous coal	Gregg Mine Is (FL)	1490-1520	1220-1260	0.5-2.6	6.8-7.2	190	26
K20	KY bituminous coal	Gregg Mine Is (FL)	1510-1525	1120-1280	1.6-3.1	6.5-7.8	190	26
L1	Overall comparison NO_X		1550-1600	1300-1800	1.5-2.5	6	200	20-30
L2	Overall comparison N_2O		1555-1565	1170-1700	1.5-2.5	4.5-7	200	20-30

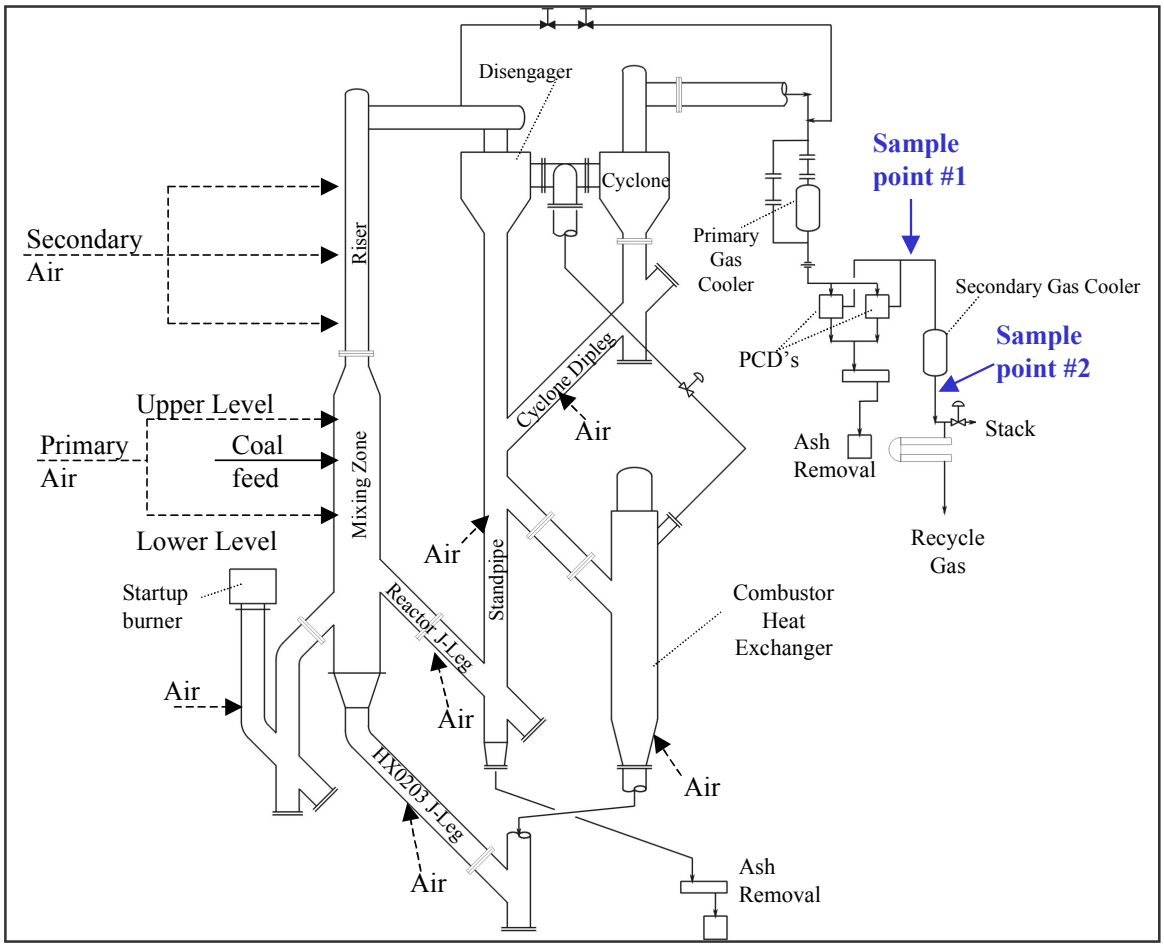

Figure 4.4-1 Transport Reactor Train Gas Sample Locations

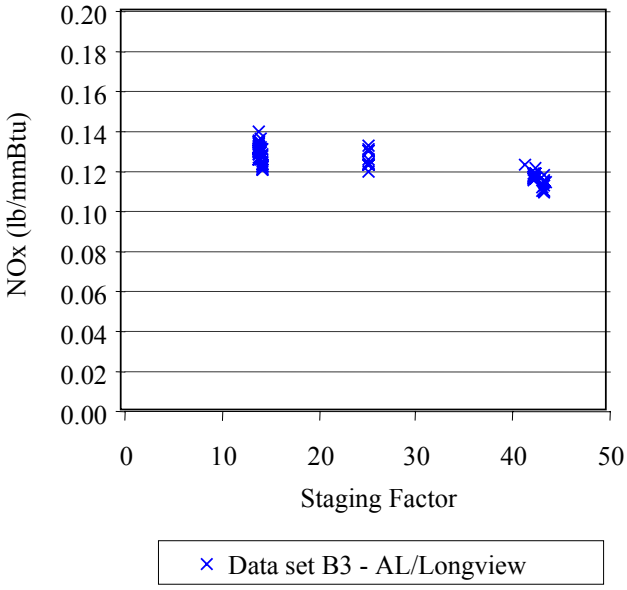

Figure 4.4-2 Effect of Staging Air on NOx Emissions With Alabama Coal and Longview Limestone

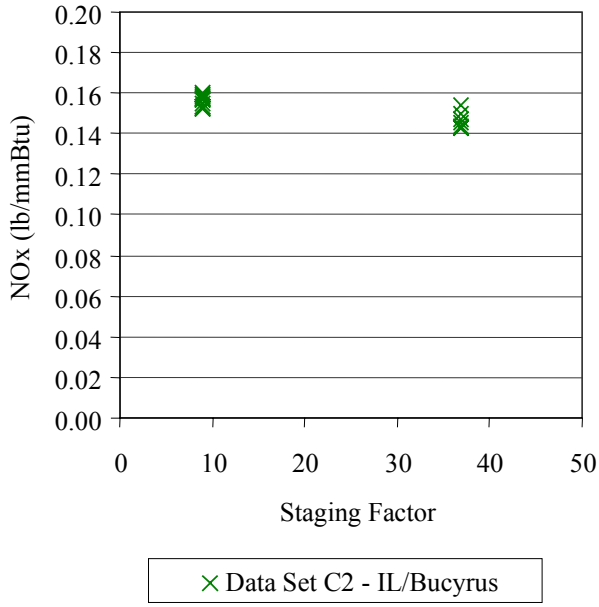

Figure 4.4-3 Effect of Staging Air on NOx Emissions With Illinois Coal and Bucyrus Limestone

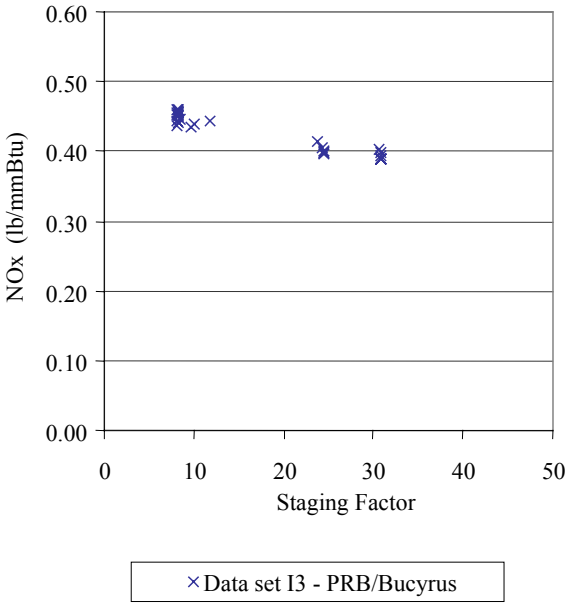

Figure 4.4-4 Effect of Staging Air on NOx Emissions With PRB and Bucyrus Limestone

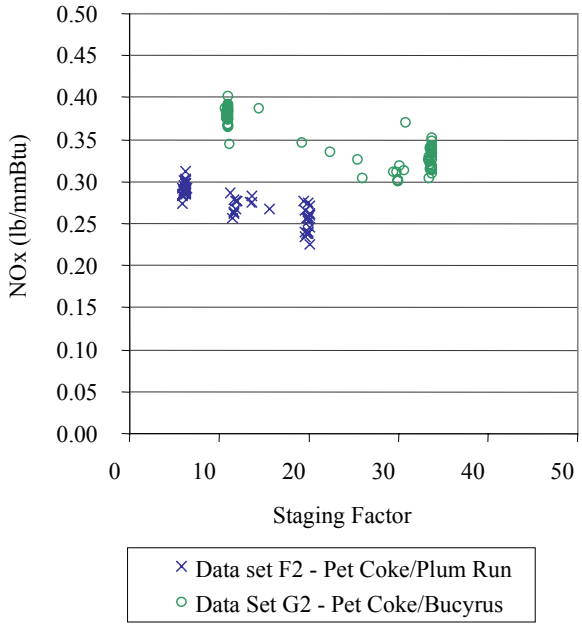

Figure 4.4-5 Effect of Staging Air on NOx Emissions With Pet Coke and Plum Run Dolomite and Bucyrus Limestone

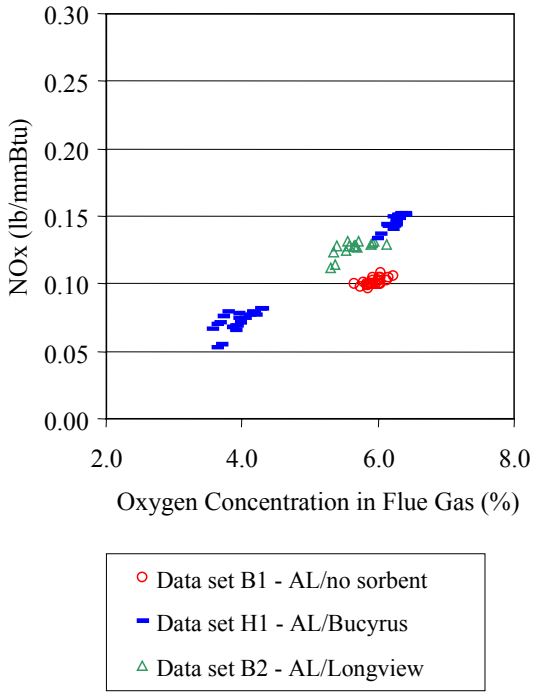

Figure 4.4-6 Effect of Excess Oxygen on NOx Emissions With Alabama Coal and Bucyrus and Longview Limestone

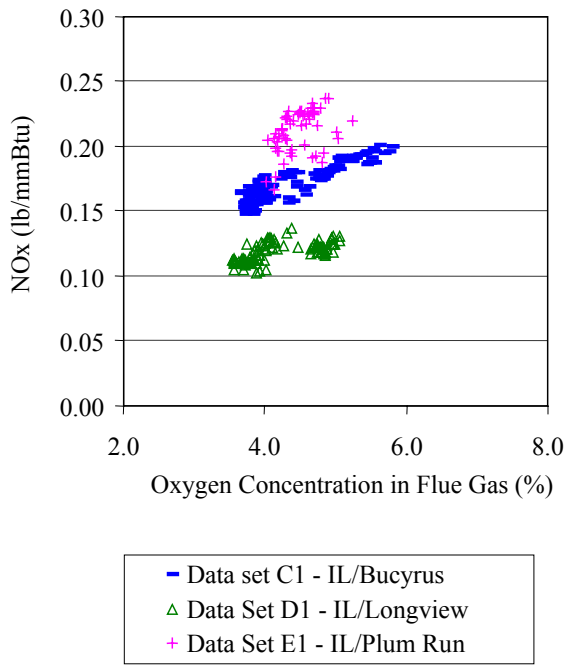

Figure 4.4-7 Effect of Excess Oxygen on NOx Emissions With Illinois Coal and Bucyrus and Longview Limestone and Plum Run Dolomite

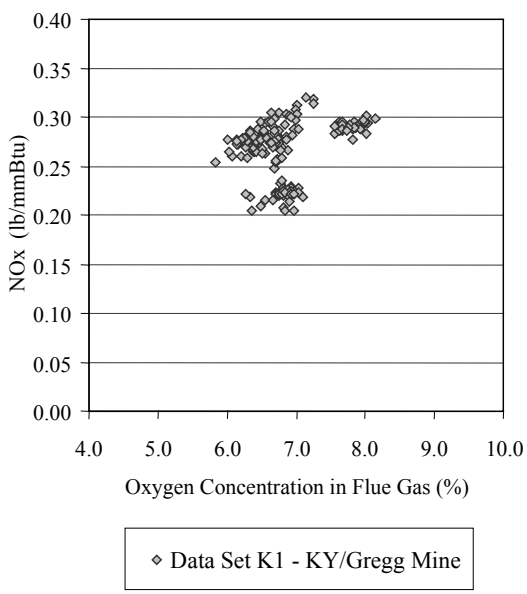

Figure 4.4-8 Effect of Excess Oxygen on NOx Emissions With Kentucky Coal and Gregg Mine Limestone

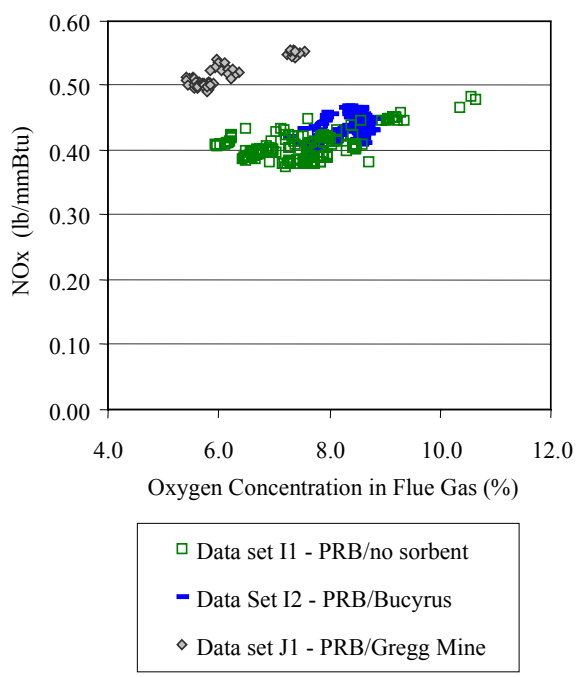

Figure 4.4-9 Effect of Excess Oxygen on NOx Emissions With PRB Coal and Bucyrus and Gregg Mine Limestone

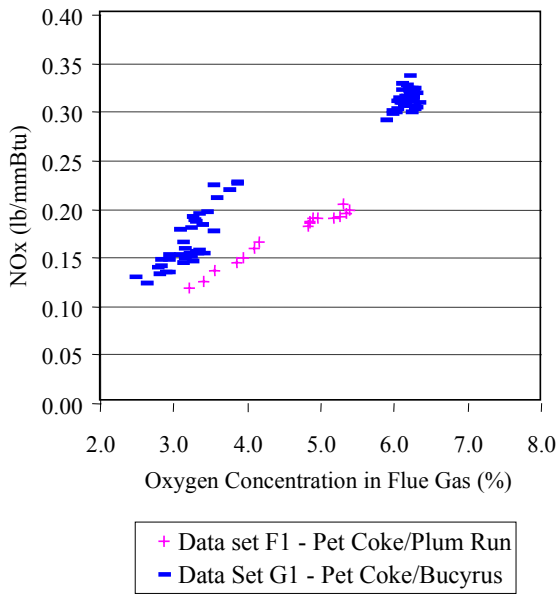

Figure 4.4-10 Effect of Excess Oxygen on NOx Emissions With Pet Coke and Plum Run Dolomite and Bucyrus Limestone

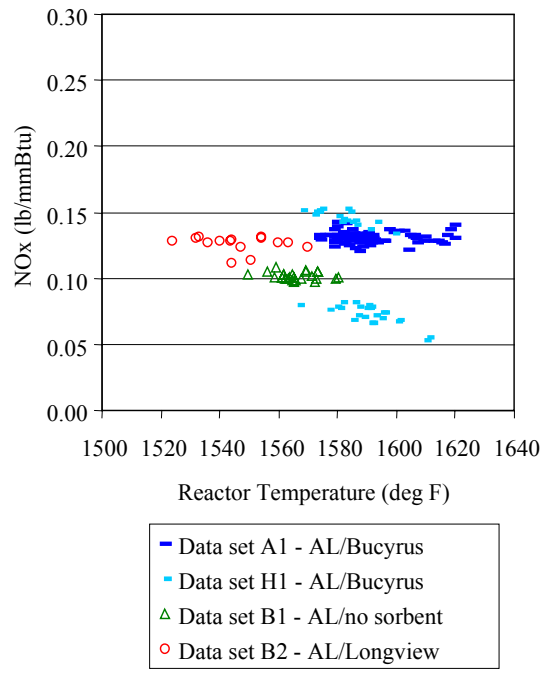

Figure 4.4-11 Effect of Reactor Temperature on NOx Emissions With Alabama Coal and Bucyrus and Longview Limestone

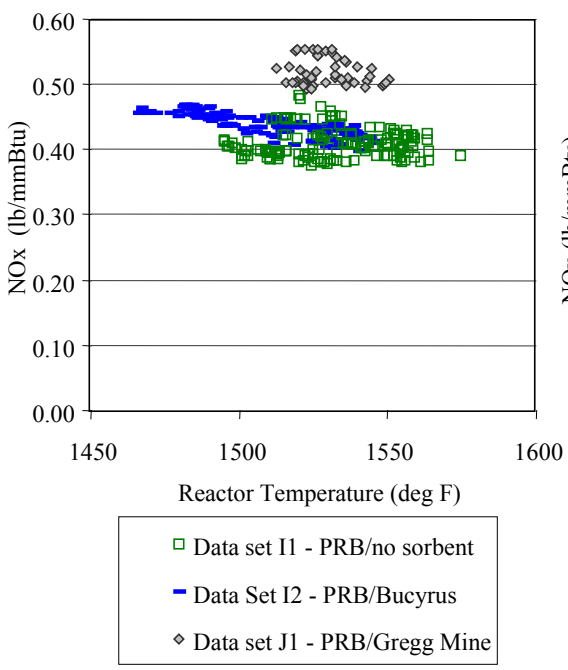

Figure 4.4-12 Effect of Reactor Temperature on NOx Emissions With Illinois Coal and Bucyrus and Longview Limestone and Plum Run Dolomite

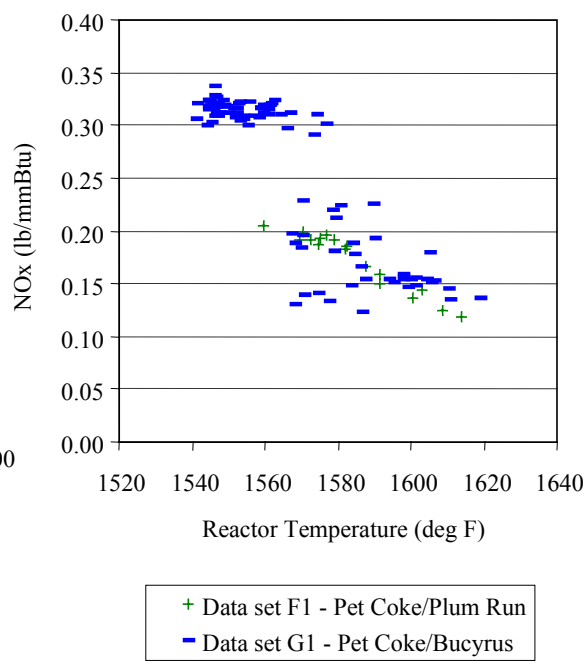

Figure 4.4-13 Effect of Reactor Temperature on NOx Emissions With KY Coal and Gregg Mine Limestone

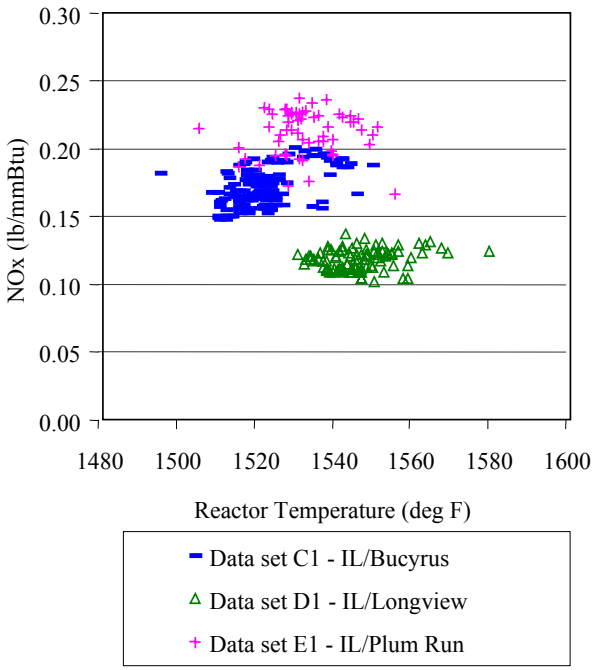

Figure 4.4-14 Effect of Reactor Temperature on NOx Emissions With PRB Coal and Bucyrus and Gregg Mine Limestone

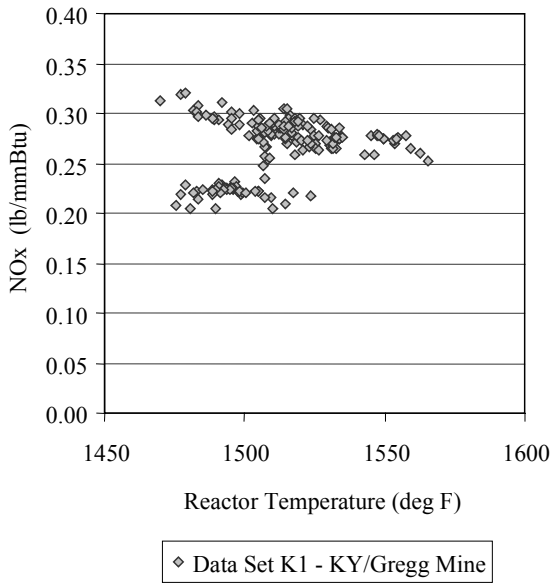

Figure 4.4-15 Effect of Reactor Temperature on NOx Emissions With Pet Coke and Plum Run Dolomite and Bucyrus Limestone

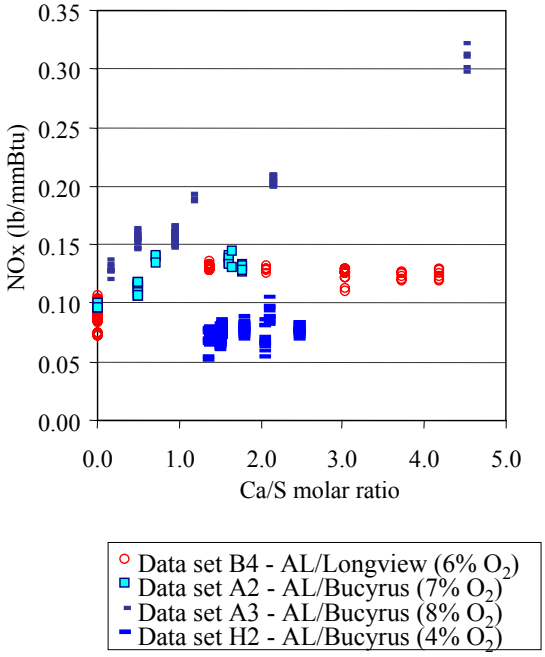

Figure 4.4-16 Effect of Sorbent Feedrate on NOx Emissions With Alabama Coal and Bucyrus and Longview Limestone

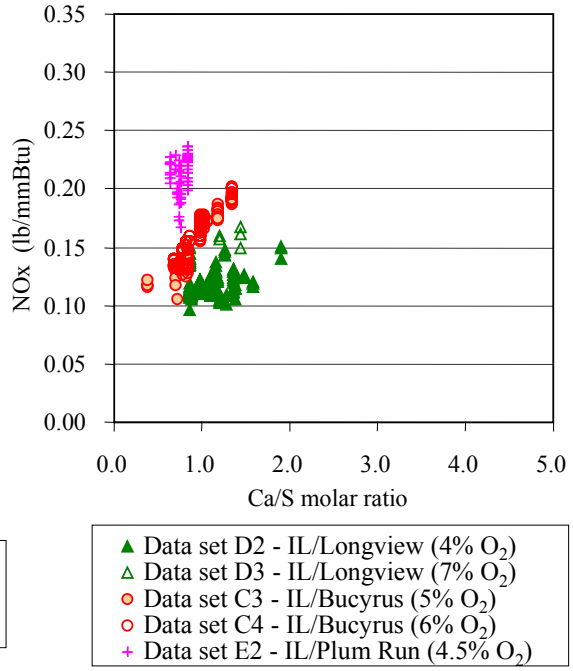

Figure 4.4-17 Effect of Sorbent Feedrate on NOx Emissions With Illinois Coal and Bucyrus and Longview Limestone and Plum Run Dolomite

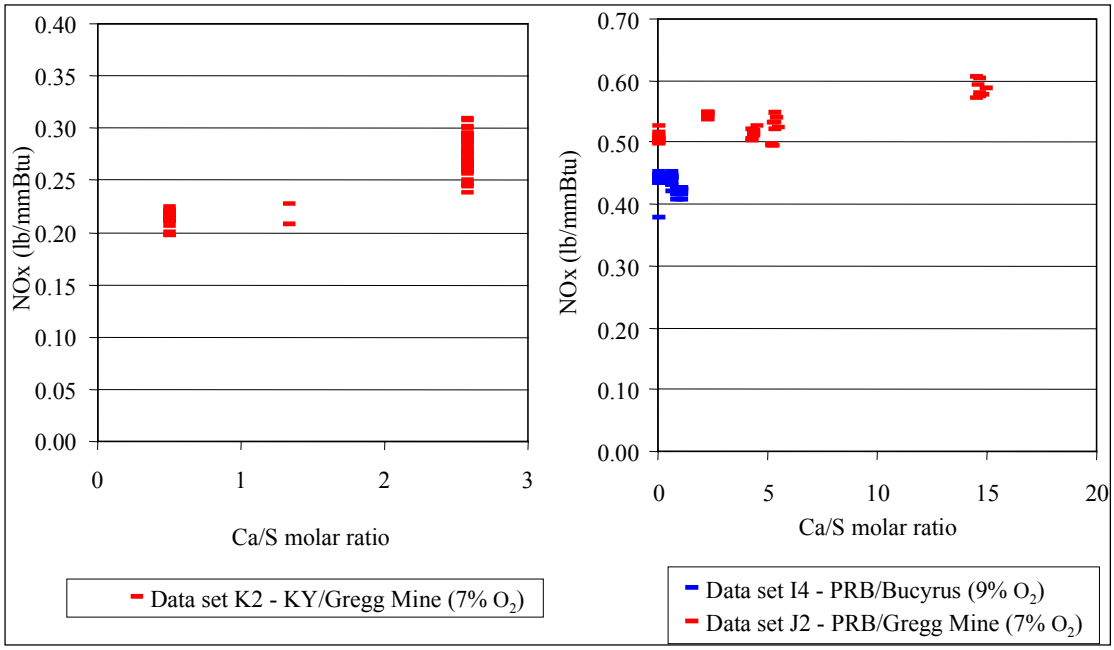

Figure 4.4-18 Effect of Sorbent Feedrate on NOx Emissions With Kentucky Coal and Gregg Mine Limestone

Figure 4.4-19 Effect of Sorbent Feedrate on NOx Emissions With PRB Coal and Bucyrus and Gregg Mine Limestone

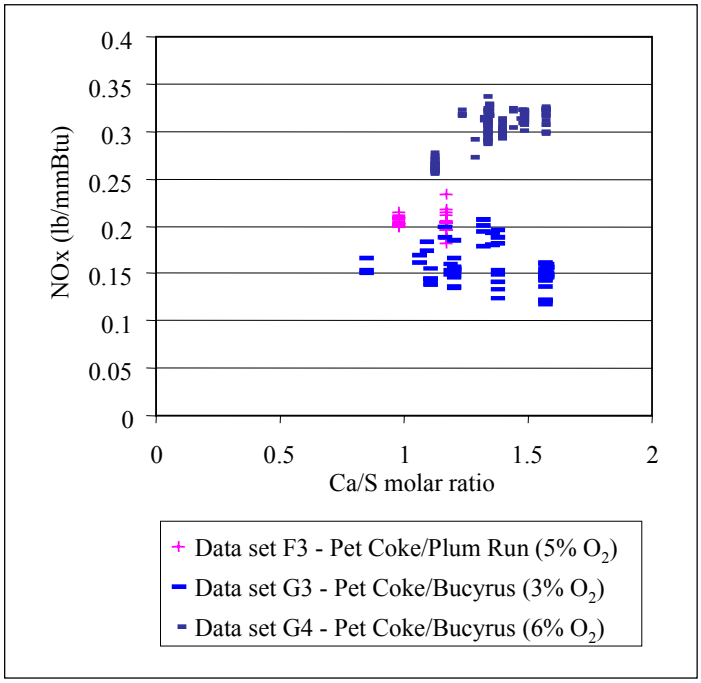

Figure 4.4-20 Effect of Sorbent Feedrate on NOx Emissions With Pet Coke and Plum Run Dolomite and Bucyrus Limestone

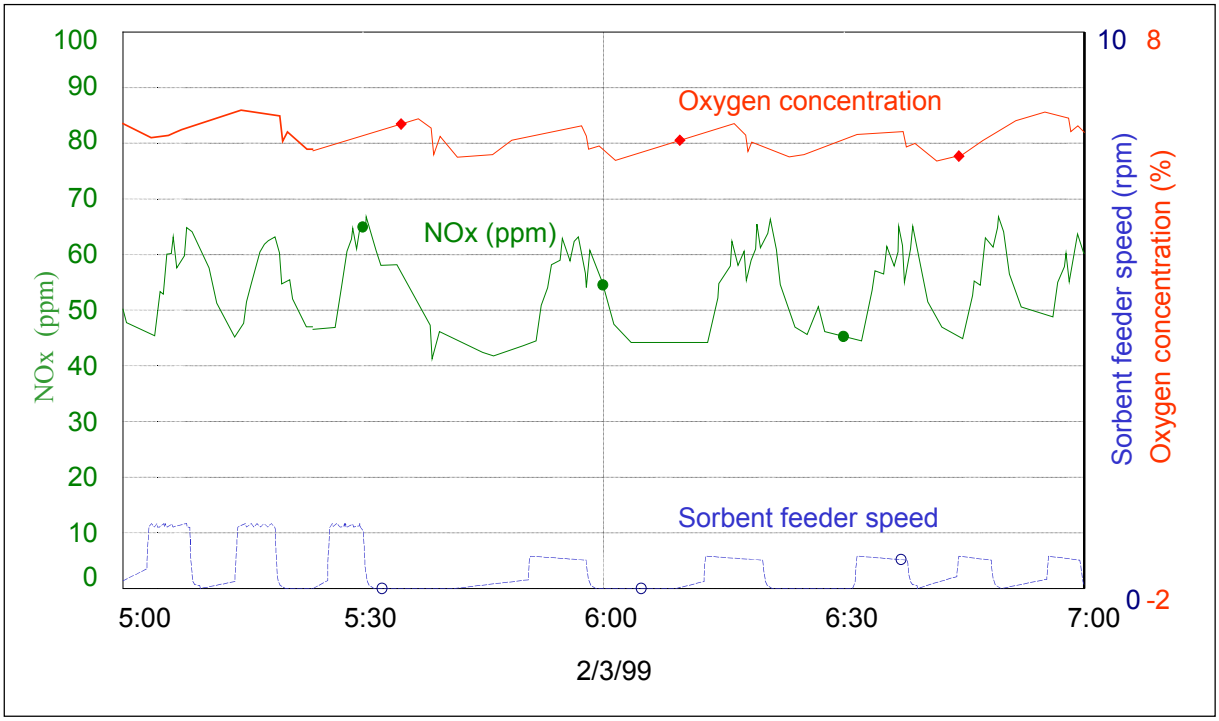

Figure 4.4-21 Effect of Sorbent Feedrate on NOx Emissions With Alabama Coal and Longview Limestone

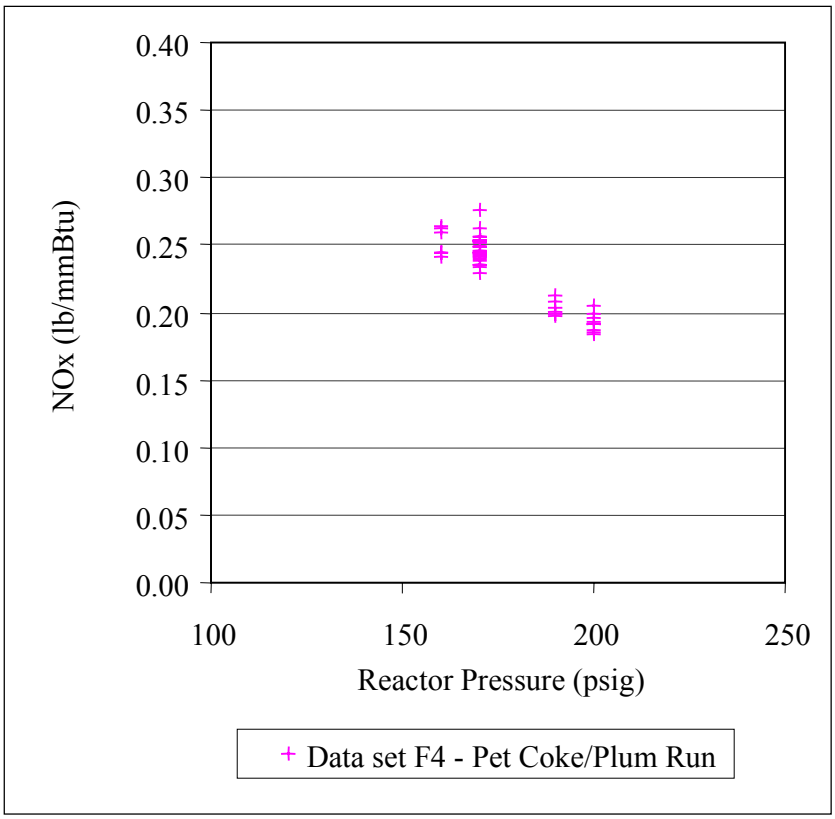

Figure 4.4-22 Effect of Reactor Pressure on NOx Emissions With Pet Coke and Plum Run Dolomite

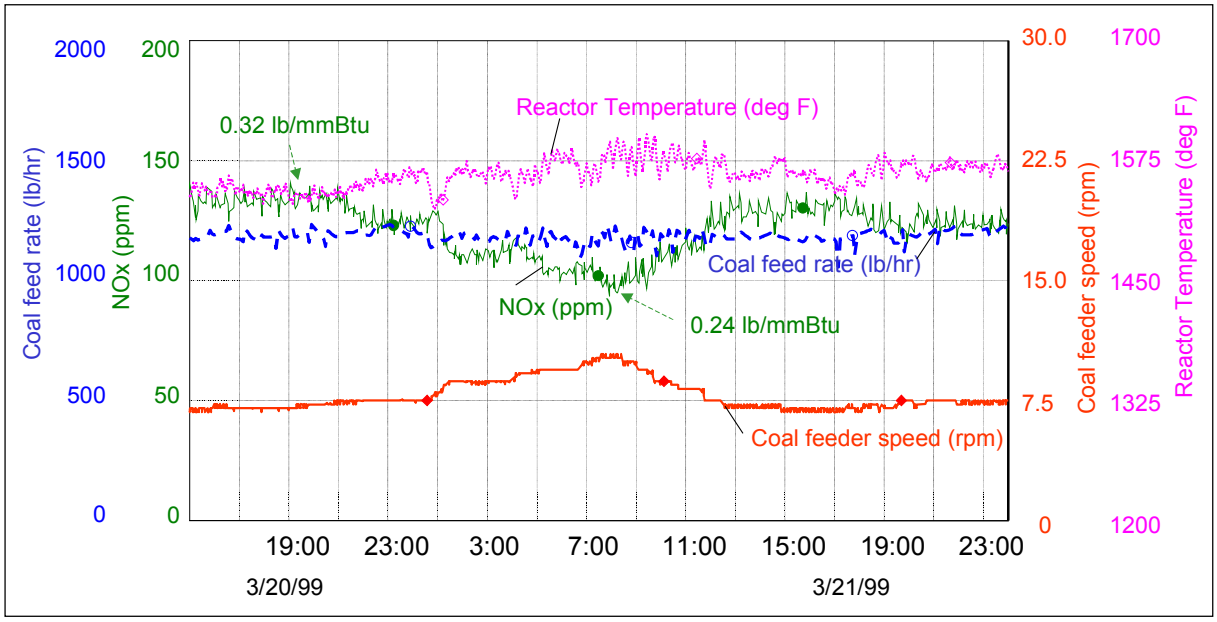

Figure 4.4-23 Effect of Fuel Feed Particle Size on NOx Emissions With Pet Coke and Bucyrus Limestone

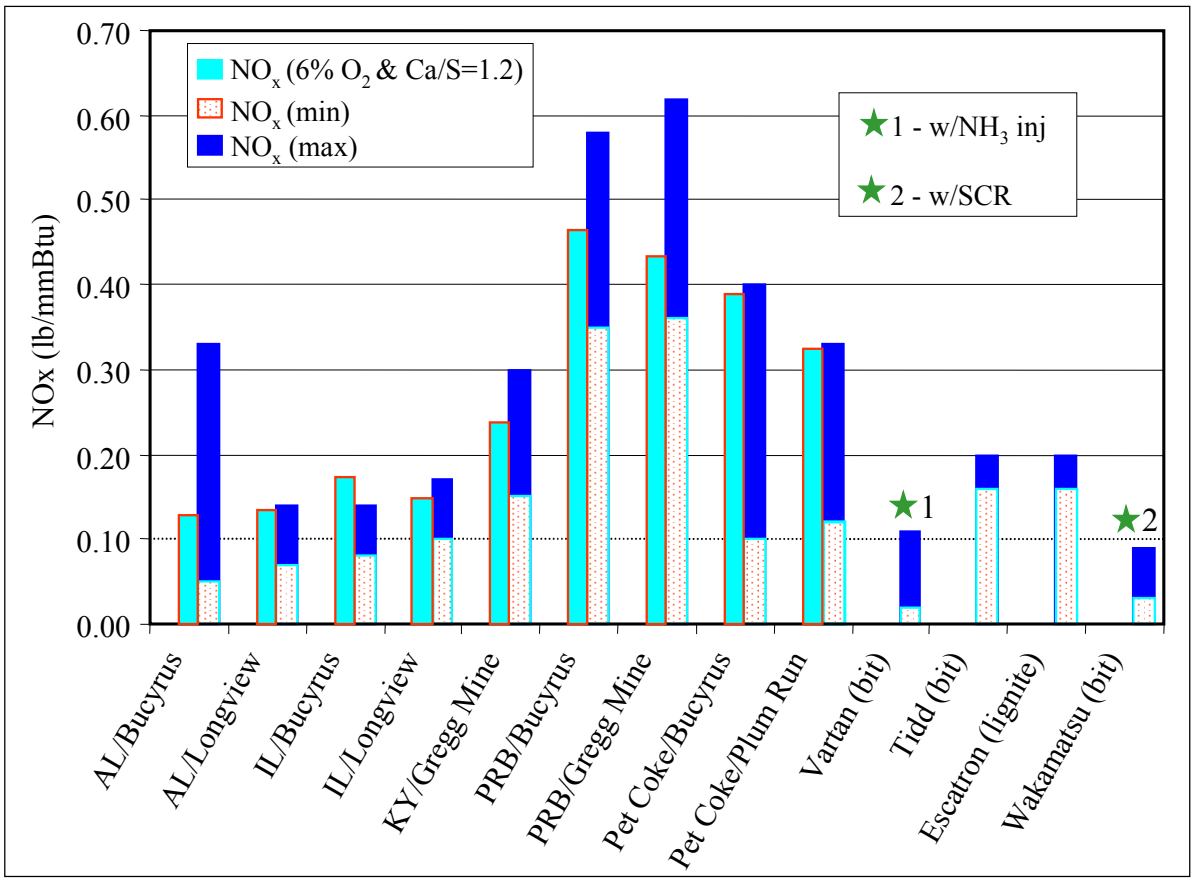

Figure 4.4-24 Range of NOx Emissions With Different Feed Combinations (Data Set L1)

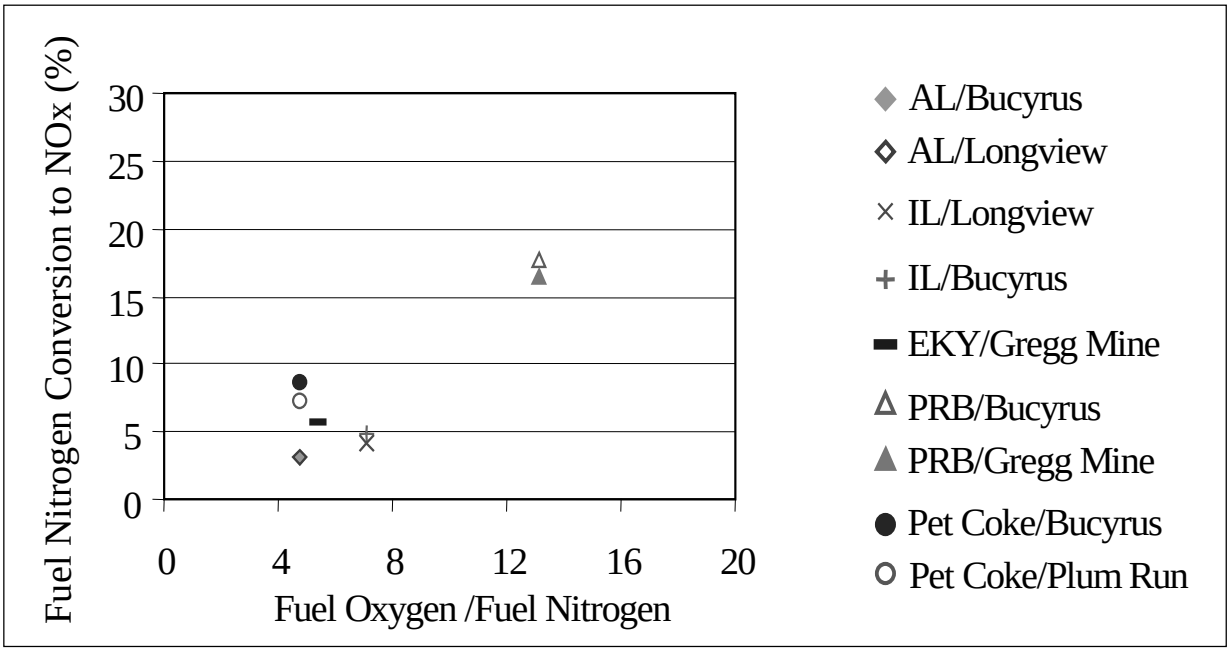

Figure 4.4-25 Relationship Between Fuel Nitrogen Conversion to NOx and Fuel Oxygen and Fuel Nitrogen

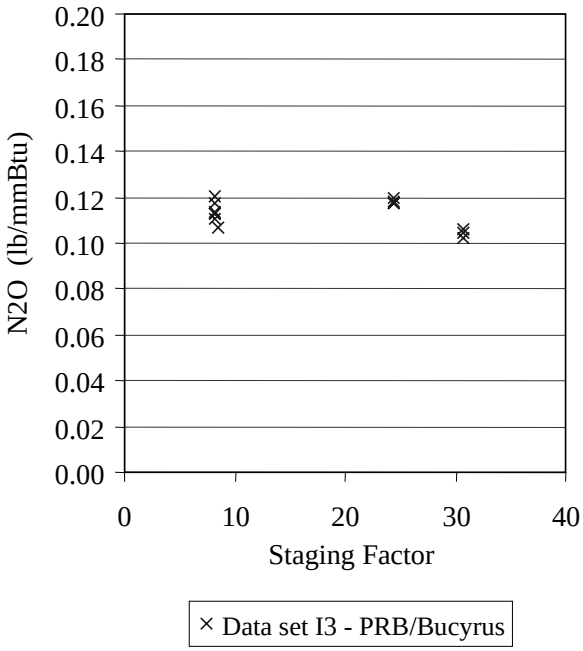

Figure 4.4-26 Effect of Staging Air on N_2O Emissions With PRB Coal and Bucyrus Limestone

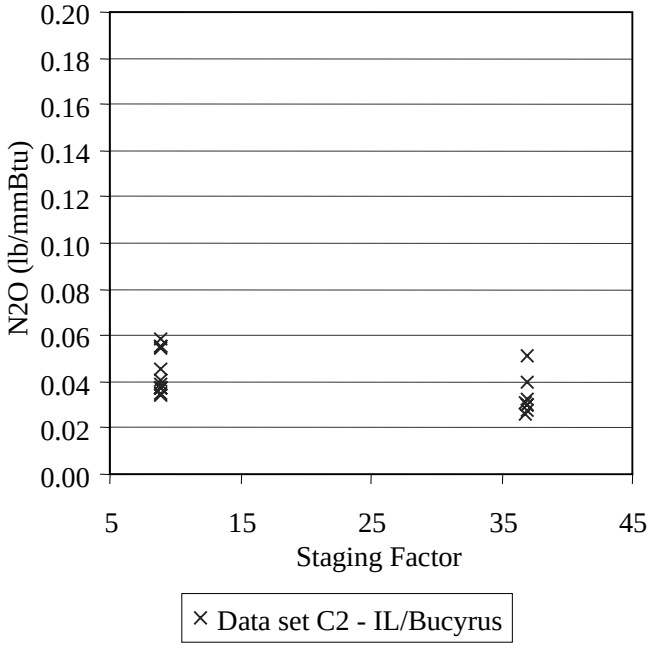

Figure 4.4-27 Effect of Staging Air on N_2O Emissions With Illinois Coal and Bucyrus Limestone

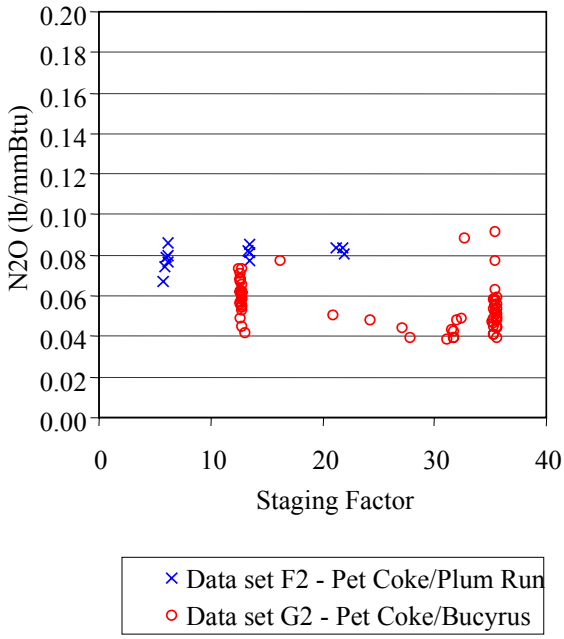

Figure 4.4-28 Effect of Staging Air on N_2O Emissions With Pet Coke and Bucyrus Limestone and Plum Run Dolomite

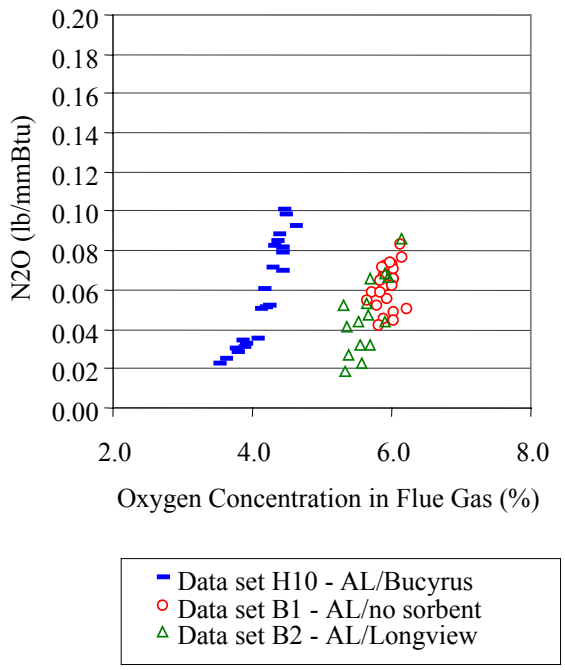

Figure 4.4-29 Effect of Excess Oxygen on N_2O Emissions With Alabama Coal and Bucyrus and Longview Limestone

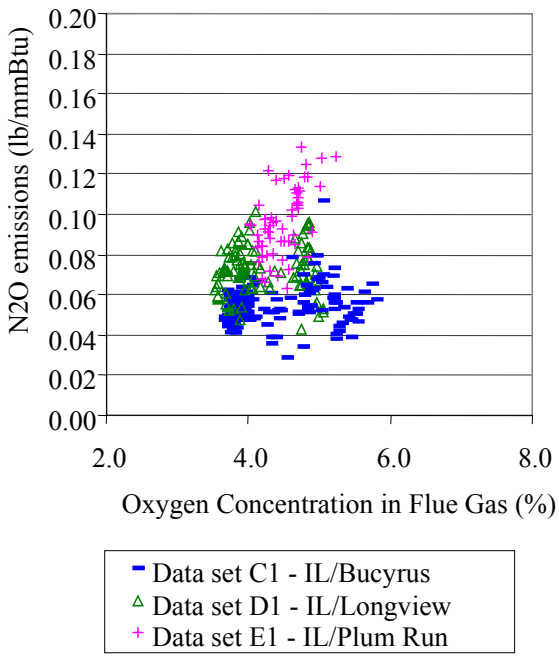

Figure 4.4-30 Effect of Excess Oxygen on N_2O Emissions With Illinois Coal and Bucyrus and Longview Limestone and Plum Run Dolomite

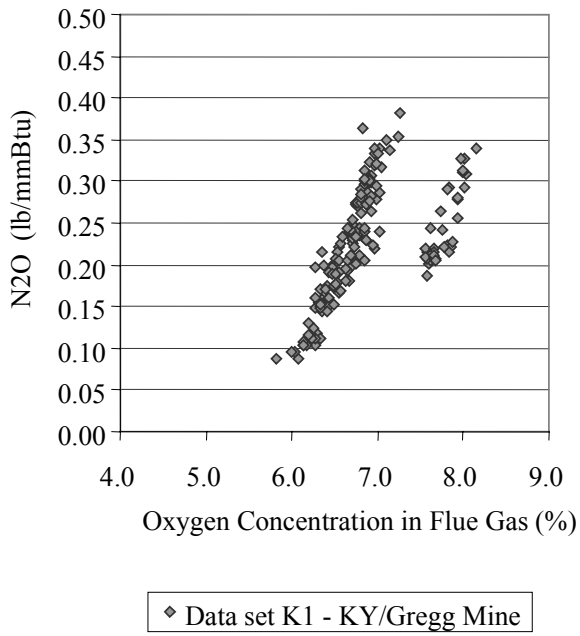

Figure 4.4-31 Effect of Excess Oxygen on N_2O Emissions With Kentucky Coal and Gregg Mine Limestone

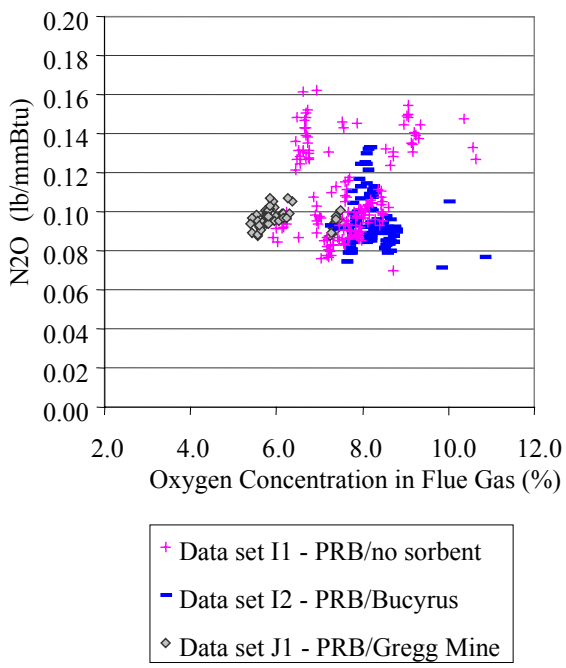

Figure 4.4-32 Effect of Excess Oxygen on N_2O Emissions With PRB Coal and Bucyrus and Gregg Mine Limestone

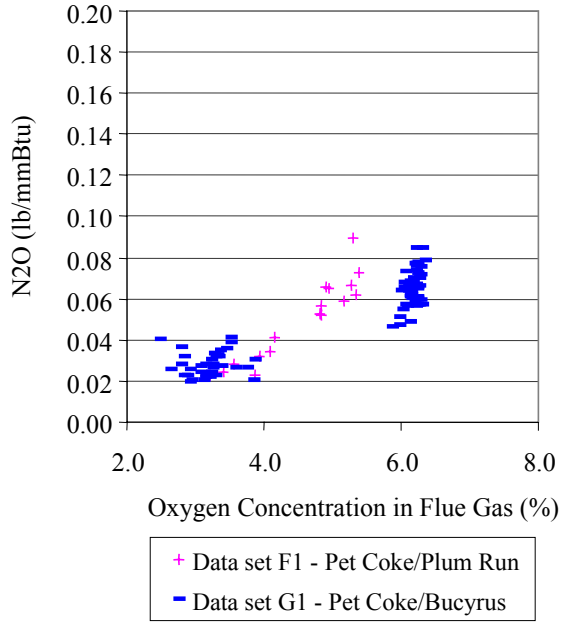

Figure 4.4-33 Effect of Excess Oxygen on N_2O Emissions With Pet Coke and Plum Run Dolomite and Bucyrus Limestone

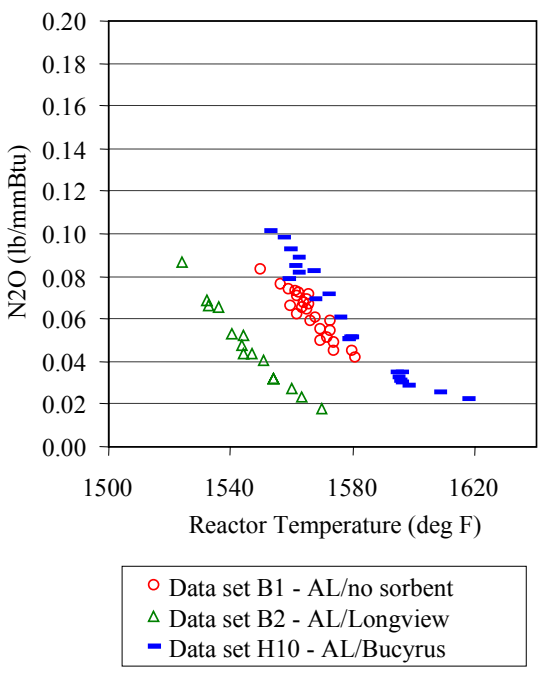

Figure 4.4-34 Effect of Reactor Temperature on N_2O Emissions With Alabama Coal and Bucyrus and Longview Limestone

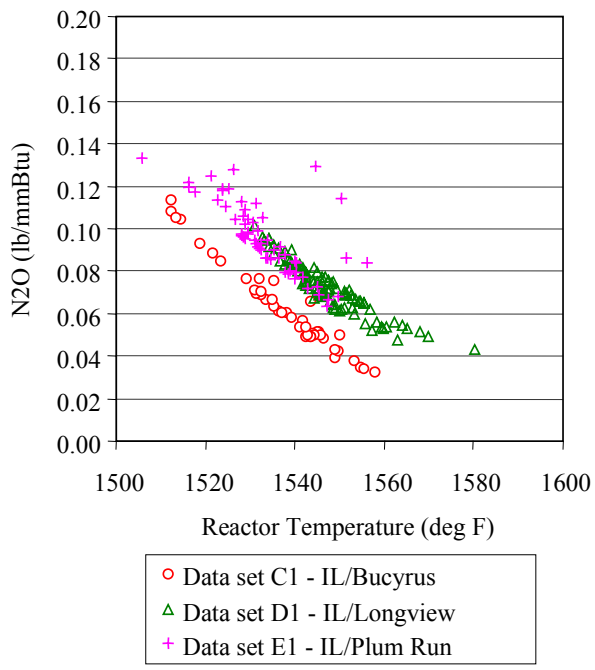

Figure 4.4-35 Effect of Reactor Temperature on N_2O Emissions With Illinois Coal and Bucyrus and Longview Limestone and Plum Run Dolomite

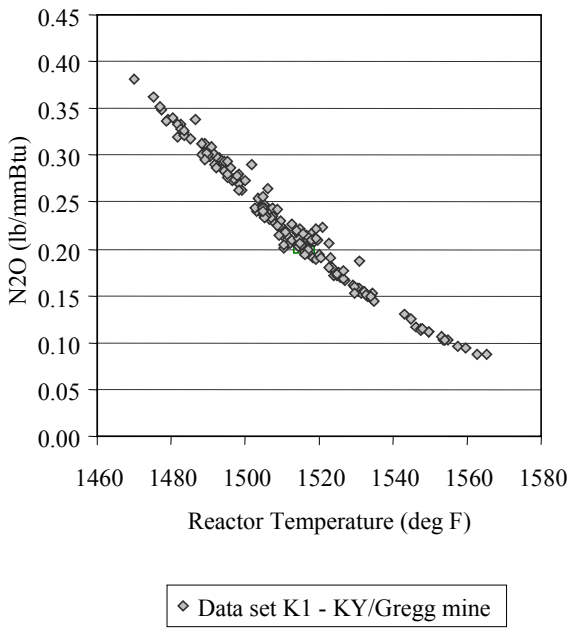

Figure 4.4-36 Effect of Reactor Temperature on N_2O Emissions With Kentucky Coal and Gregg Mine Limestone

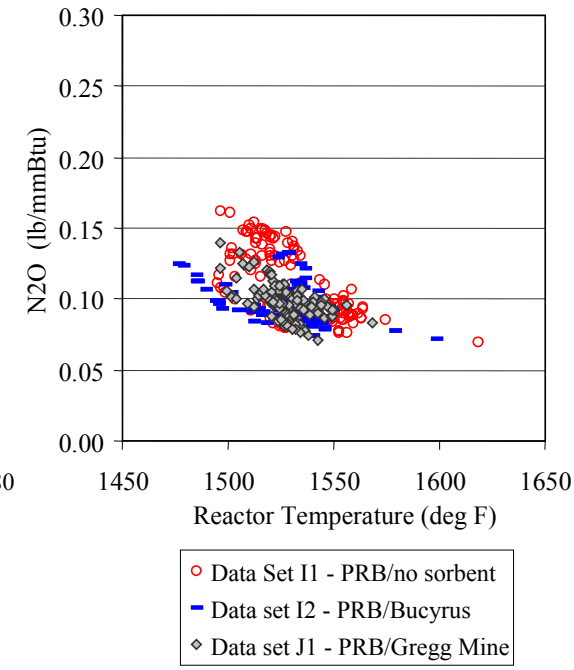

Figure 4.4-37 Effect of Reactor Temperature on N_2O Emissions With PRB Coal and Bucyrus and Gregg Mine Limestone

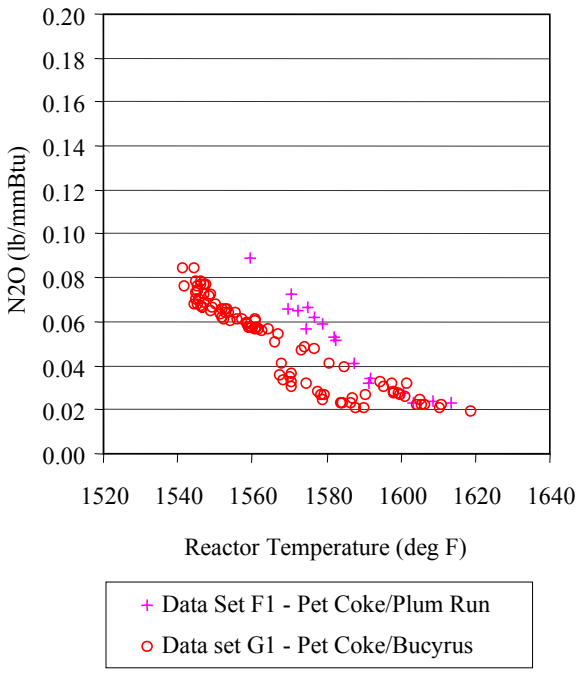

Figure 4.4-38 Effect of Reactor Temperature on N_2O Emissions With PRB Coal and Bucyrus and Gregg Mine Limestone

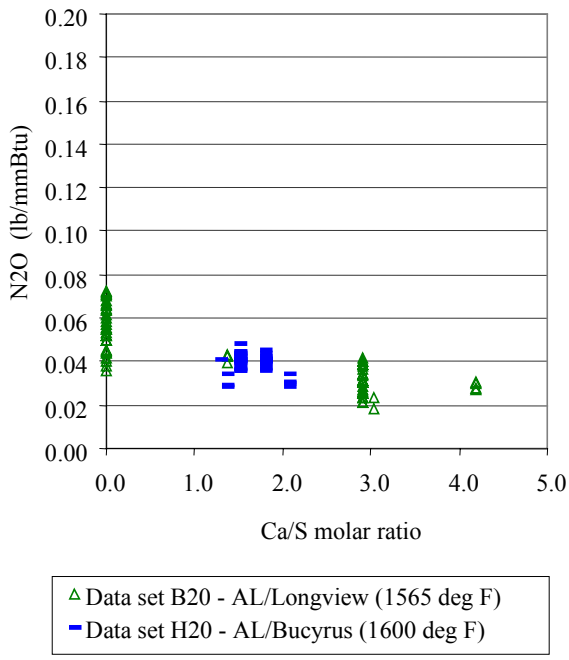

Figure 4.4-39 Effect of Sorbent Feedrate on N_2O Emissions With Alabama Coal and Longview and Bucyrus Limestone

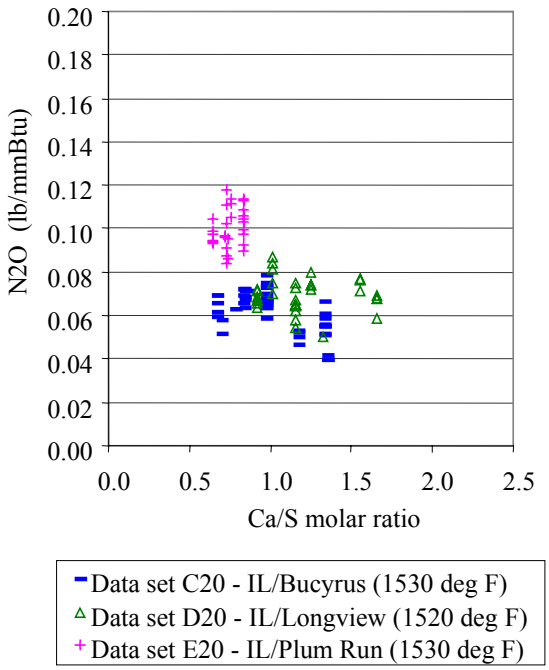

Figure 4.4-40 Effect of Sorbent Feedrate on N_2O Emissions With Illinois Coal and Bucyrus and Longview Limestone and Plum Run Dolomite

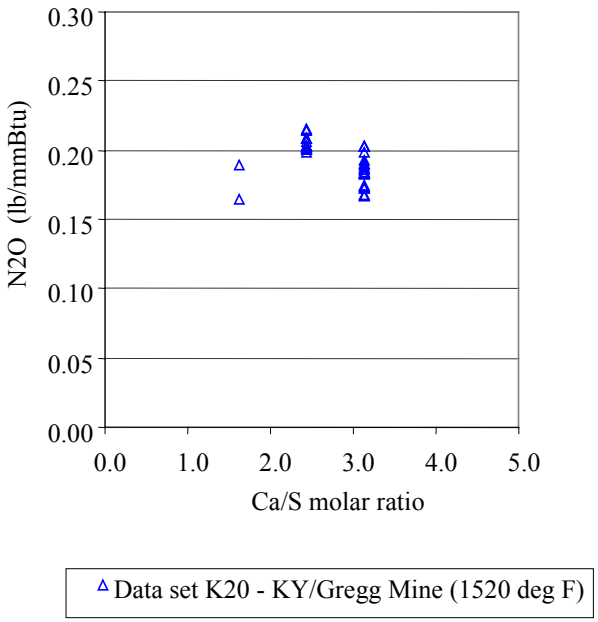

Figure 4.4-41 Effect of Sorbent Feedrate on N_2O Emissions With Kentucky Coal and Gregg Mine Limestone

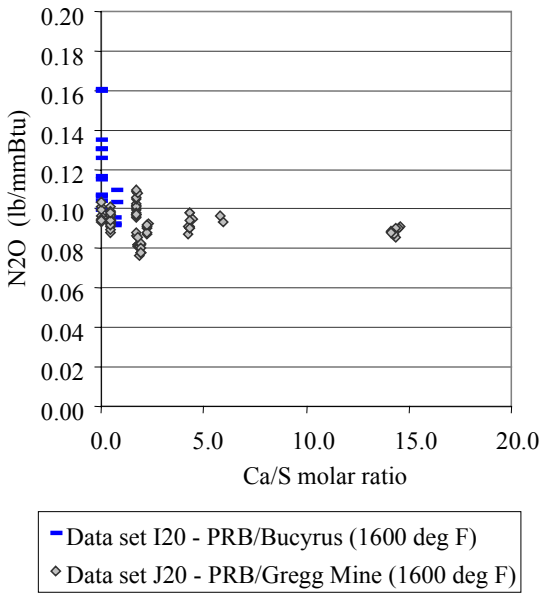

Figure 4.4-42 Effect of Sorbent Feedrate on N_2O Emissions With PRB Coal and Bucyrus and Gregg Mine Limestone

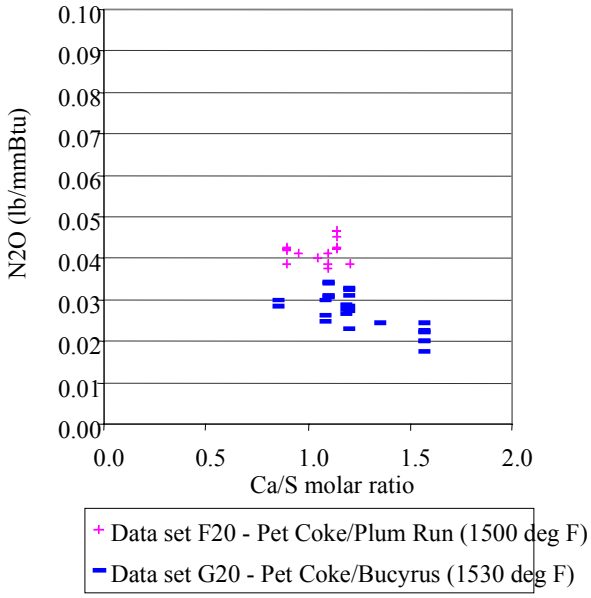

Figure 4.4-43 Effect of Sorbent Feedrate on N_2O Emissions With Pet Coke and Bucyrus Limestone and Plum Run Dolomite

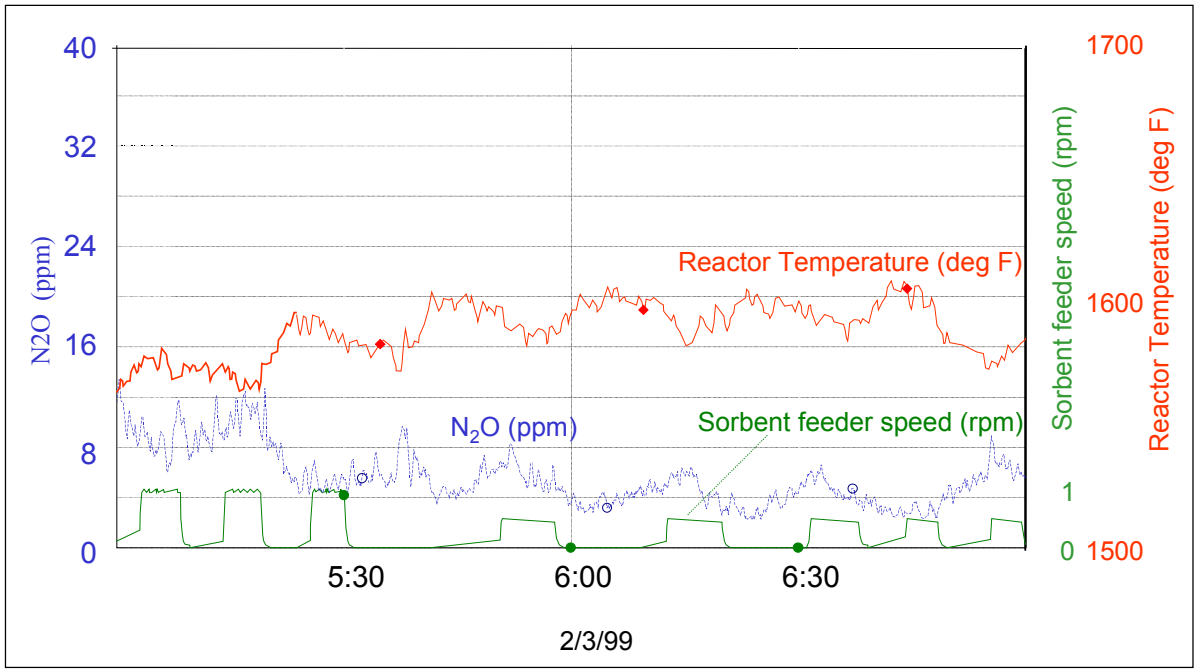

Figure 4.4-44 Effect of Sorbent Feedrate on N_2O Emissions With Alabama Coal and Longview Limestone

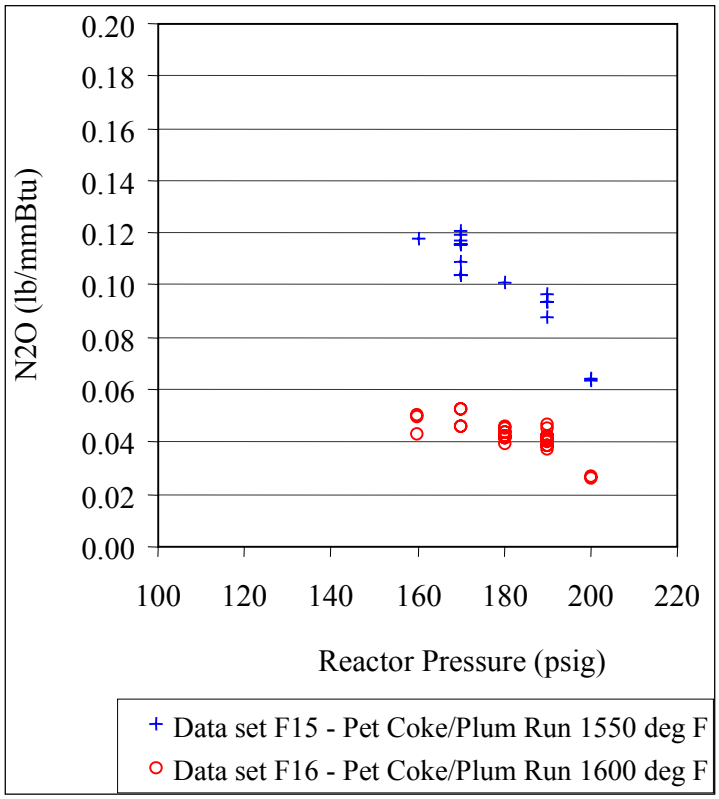

Figure 4.4-45 Effect of Reactor Pressure on N_2O Emissions With Pet Coke and Plum Run Dolomite

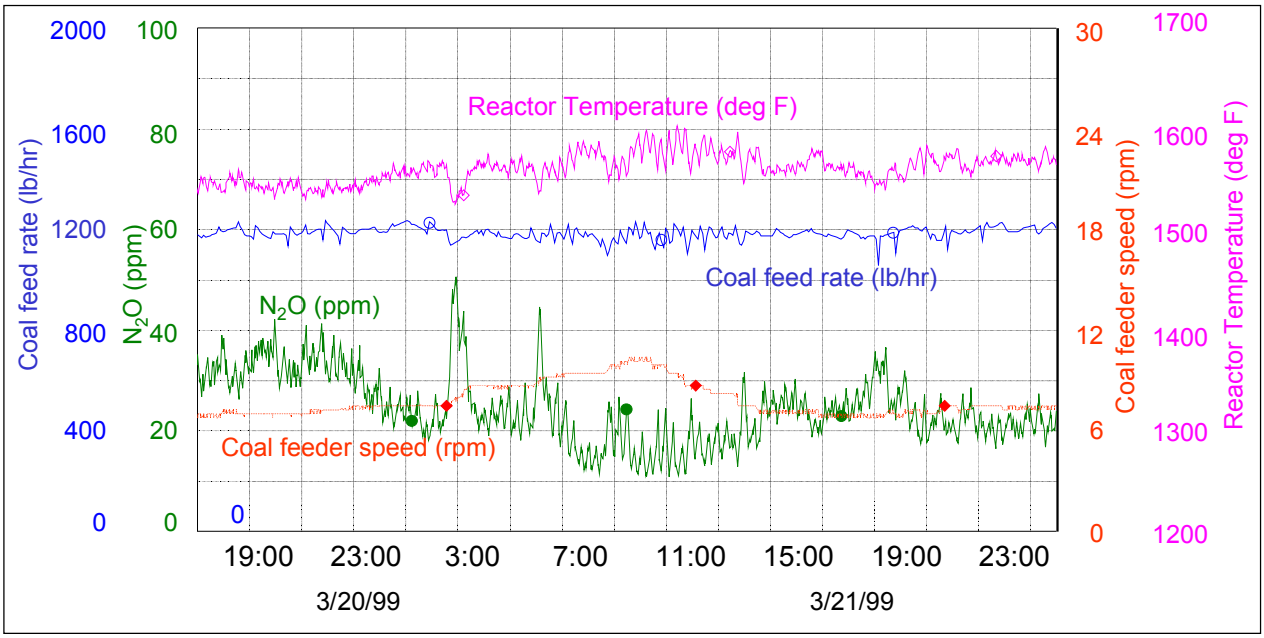

Figure 4.4-46 Effect of Fuel Feed Particle Size on N_2O Emissions Wth Pet Coke and Bucyrus Limestone

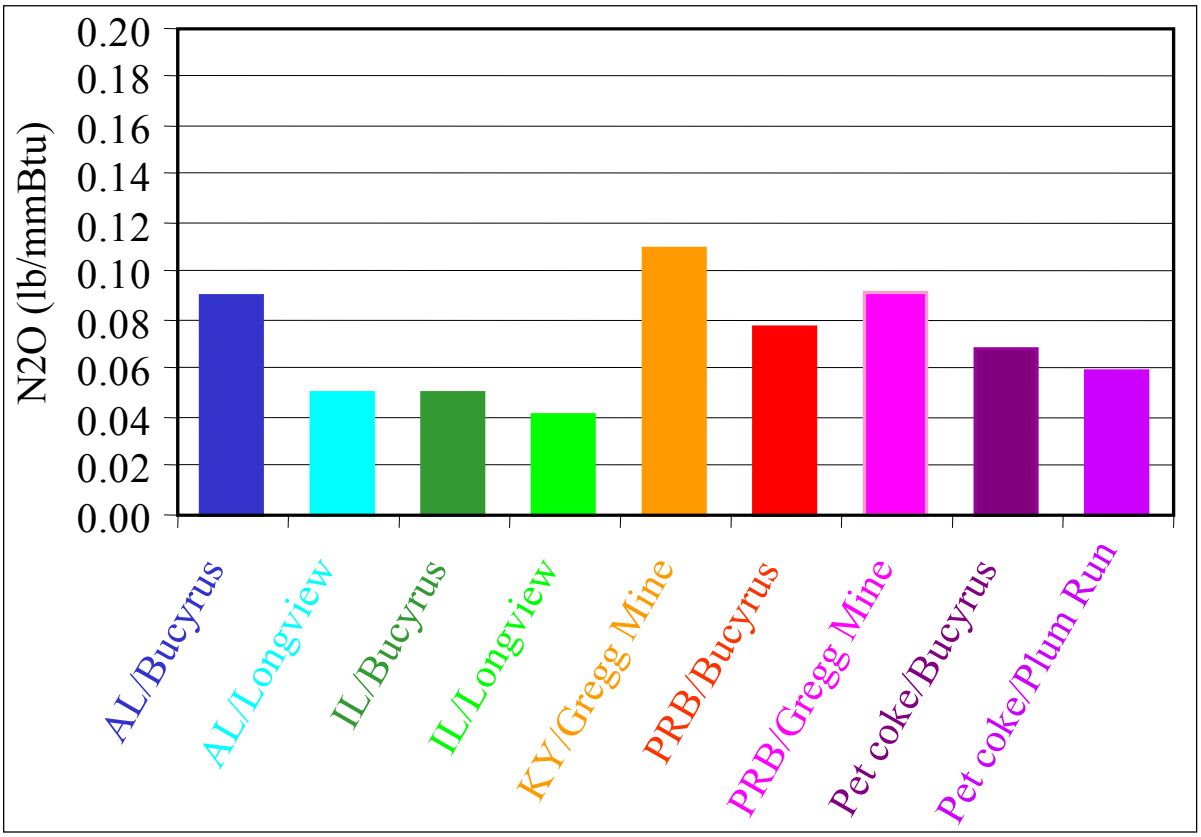

Figure 4.4-47 Range of N_2O Emissions With Different Feed Combinations (Data Set L2)

4.5 TEMPERATURE PROFILE

The transport reactor showed a significant change in temperature profile as different fuels were fired during TC05. Five separate fuels were fired: Alabama Calumet mine bituminous, Illinois #6 bituminous, Eastern Kentucky bituminous, Power River Basin Bell Ayre subbituminous, and petroleum coke. Two of these fuels did not provide suitable data for comparison. The operating temperature for the PRB coal was much lower than the other coals. The mixing zone was partially blocked during the firing of the Eastern Kentucky coal, which led to a distorted temperature profile.

The other three fuels were each burned under similar conditions. The Alabama and Illinois coals are enough alike that they produced comparable temperature profiles as contrast to the petroleum coke temperature profile. Table 4.5-1 gives an analysis at the time of testing of each fuel.

The temperature profile data for the Alabama coal is from February 4, 1999, at 09:00. The Illinois coal data is from February 8, 1999, at 13:00. The petroleum coke data is from March 20, 1999, at 06:00. The circulation rate at each time varied less than ±10 percent from the average circulation rate of the three periods. The average riser temperature for all three cases was around 1,575°F. The reactor pressure in each case was 200 psig.

The mixing zone profiles for all three fuels are very similar. Hot solids from the standpipe mix with cool solids from the combustor heat exchanger are cooled by the addition of the primary combustion air. Above the primary air nozzles and coal feed nozzle the temperature increases steadily to the transition to the riser section. The temperature entering the riser was within a range of 3°F for all three cases.

Figure 4.5-1 shows the riser temperature profile for the Illinois coal and the petroleum coke. The Illinois coal gives a rising temperature until about two-thirds up the riser. After this point the temperature decreases through the remaining riser section and crossover. The solids increase again in temperature as they fall into the upper standpipe from the disengager. The partially cleaned gas exiting the disengager increases in temperature before being cooled at the cyclone entrance by vent gas from the combustor heat exchanger.

The petroleum coke temperature profile shows a decrease in temperature of approximately 100°F in the lower riser, apparently from the addition of secondary air. After the quench effect in the lower riser the temperature increases to the top of the riser before decreasing slightly in the riser crossover. The solids decline in temperature as they move from the crossover through the disengager to the standpipe. The gas shows a large increase in temperature as it leaves the disengager before being cooled by the gas from the heat exchanger.

Figure 4.5-2 gives the standpipe and dipleg temperature profiles for the Alabama coal and the petroleum coke. The Alabama coal gives the normal profile experienced thus far with most fuels and operating conditions. The dipleg temperatures are lower than the standpipe temperatures. The dipleg temperatures decrease as they flow due to heat loss to the surroundings and cooling from aeration. The top two temperatures are from the vertical section

of the dipleg and the second two temperatures are from the slant section. The top temperature of the slant section is generally lower than the bottom temperature due to local aeration effects. The standpipe temperature slowly declines until mixed with the much cooler solids from the dipleg.

With the petroleum coke there is evidently combustion continuing in the standpipe and dipleg. Temperatures in both the dipleg and standpipe increase rather than decrease with the exception of the lowest part of the dipleg. Also unusual is the solids entering the dipleg are hotter than the solids entering the standpipe despite the cool-heat-exchanger vent gas mixed into the cyclone entrance. The petroleum coke profile shows a continued increase in temperature below where the dipleg solids are mixed into the stream.

The differences between the temperature profiles of the bituminous coals and the petroleum coke can best be explained by the lower reactivity of the petroleum coke. The combustion of the bituminous coals was essentially complete by the middle of the riser. The profiles of all of the bituminous and subbituminous coals show another increase in temperature leaving the disengager. This is because of the lower heat transfer away from the burning particles due to loss of most of the solids to the standpipe allows the particles to reach a temperature high enough to complete combustion. With the petroleum coke combustion continued to take place all the way to the top of the riser. There was also 2 to 5 times as much temperature rise from the disengager inlet to outlet with the petroleum coke compared to other fuels. Combustion of the petroleum coke continued into the dipleg and standpipe where other fuels completed combustion before reaching these areas. As a comparison (within the accuracy of sampling and analyses), the petroleum coke ash collected in the PCD for this time had 0.07-percent carbon and the reactor bottom ash had 0.09-percent carbon. For both the Illinois and the Alabama coal these numbers were zero-percent, respectively.

Table 4.5-1

Analysis of Each Fuel

As Received Analysis (%)	Alabama Coal	Illinois Coal	Petroleum Coke
Moisture	3.4	3.3	0.8
Volatiles	36.4	36.8	12.5
Fixed Carbon	45.9	46.0	84.3
Btu/lb	11,900	11,900	14,600
C	67.3	67.2	69.6
H	4.3	4.5	3.5
N	1.4	1.6	1.5
S	2.0	2.0	5.8
O	7.3	7.5	16.4
Ash	14.3	13.9	2.4

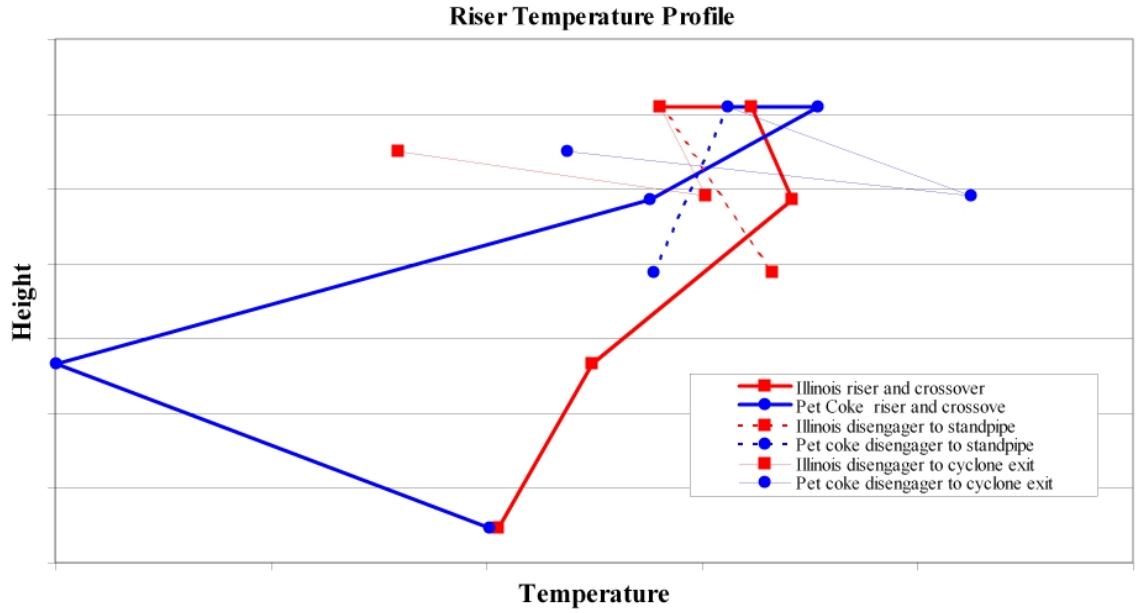

Figure 4.5-1 Riser Temperature Profile for Illinois No. 6 Coal and Petroleum Coke

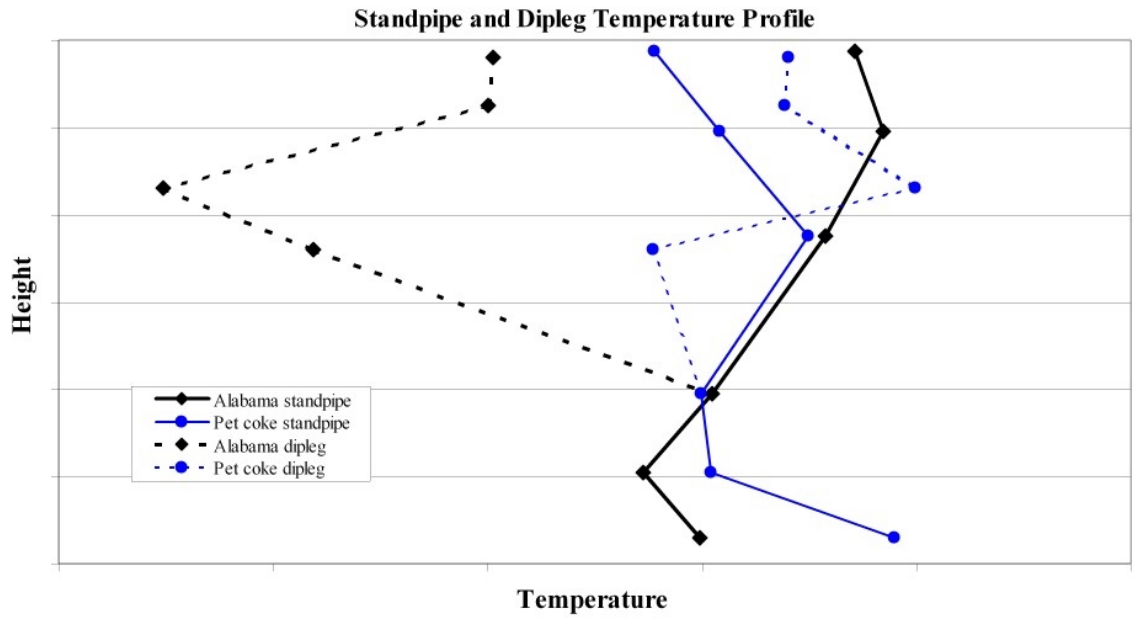

Figure 4.5-2 Standpipe and Dipleg Temperature Profile for Alabama Coal and Petroleum Coke

TERMS

Listing of Abbreviations

AAS	Automated Analytical Solutions
ADEM	Alabama Department of Environmental Management
APC	Alabama Power Company
APFBC	Advance Pressurized Fluidized-Bed Combustion
ASME	American Society of Mechanical Engineers
AW	Application Workstation
BFI	Browning-Ferris Industries
BFW	Boiler Feed Water
BMS	Burner Management System
BOC	BOC Gases
BOP	Balance-of-Plant
BPIR	Ball Pass Inner Race, Frequencies
BPOR	Ball Pass Outer Race, Frequencies
BSF	Ball Spin Frequency
CAD	Computer-Aided Design
CEM	Continuous Emissions Monitor
CFB	Circulating Fluidized Bed
CFR	Code of Federal Regulations
CHE	Combustor Heat Exchanger
COV	Coefficient of Variation (Standard Deviation/Average)
CPC	Combustion Power Compay
CPR	Cardiopulmonary Resuscitation
CTE	Coefficient of Thermal Expansion
DC	Direct Current
DCS	Distributed Control System
DOE	U.S. Department of Energy
E & I	Electrical and Instrumentation
EERC	Energy and Environmental Research Center
EPRI	Electric Power Research Institute
EDX	Energy-Dispersive X-Ray
ESCA	Electron Spectroscopy for Chemical Analysis
FCC	Fluidized Catalytic Cracker
FCP	Flow-Compacted Porosity
FETC	Federal Energy Technology Center
FFG	Flame Front Generator
FI	Flow Indicator
FIC	Flow Indicator Controller
FOAK	First-of-a-Kind
FTF	Fundamental Train Frequency
FW	Foster Wheeler
GBF	Granular Bed Filter
GC	Gas Chromatograph
GEESI	General Electric Environmental Services, Inc.

HP	High Pressure
HRSG	Heat Recovery Steam Generator
HTF	Heat Transfer Fluid
HTHP	High-Temperature, High-Pressure
I/O	Inputs/Outputs
ID	Inside Diameter
IF&P	Industrial Filter & Pump
IGV	Inlet Guide Vanes
IR	Infrared
KBR	Kellogg Brown & Root
LAN	Local Area Network
LIMS	Laboratory Information Management System
LOC	Limiting Oxygen Concentration
LOI	Loss on Ignition
LPG	Liquefied Propane Gas
LSLL	Level Switch, Low Level
MAC	Main Air Compressor
MCC	Motor Control Center
MS	Microsoft Corporation
NDIR	Nondestructive Infrared
NFPA	National Fire Protection Association
NOx	Nitrogen Oxides
NPDES	National Pollutant Discharge Elimination System
NPS	Nominal Pipe Size
OD	Outside Diameter
OSHA	Occupational Safety Health Administration
OSI	OSI Software, Inc.
P&IDs	Piping and Instrumentation Diagrams
PC	Pulverized Coal
PCD	Particulate Control Device
PDI	Pressure Differential Indicator
PDT	Pressure Differential Transmitter
PFBC	Pressurized Fluidized-Bed Combustion
PI	Plant Information
PLC	Programmable Logic Controller
PPE	Personal Protection Equipment
PRB	Powder River Basin
PSD	Particle Size Distribution
PSDF	Power Systems Development Facility
ΔP	Pressure Drop
PT	Pressure Transmitter
RFQ	Request for Quotation
RO	Restriction Orifice
RSSE	Reactor Solid Separation Efficiency
RT	Room Temperature
SCS	Southern Company Services, Inc.
SEM	Scanning Electron Microscopy

SMD	Sauter Mean Diameter
SRI	Southern Research Institute
SUB	Start-up Burner
TCLP	Toxicity Characteristic Leaching Procedure
TR	Transport Reactor
TRDU	Transport Reactor Demonstration Unit
TSS	Total Suspended Solids
UBP	Uncompacted Bulk Porosity
UND	University of North Dakota
UPS	Uninterruptible Power Supply
UV	Ultraviolet
VFD	Variable Frequency Drive
VOCs	Volatile Organic Compounds
WPC	William's Patent Crusher
XRD	X-Ray Diffraction
XXS	Extra, Extra Strong

Listing of Units

acfm	actual cubic feet per minute
Btu	British thermal units
°C	degrees celsius or centigrade
°F	degrees fahrenheit
ft	feet
FPS	feet per second
gpm	gallons per minute
g/cm^3	grams per cubic centimeter
g	grams
GPa	gigapascals
hp	horsepower
hr	hour
in.	inches
inWg	inches, water gauge
°K	degrees kelvin
kg	kilograms
kJ	kilojoules
kPa	kilopascals
ksi	thousand pounds per square inch
m	meters
MB	megabytes
mm	millimeters
MPa	megapascals
msi	million pounds per square inch
MW	megawatts
m/s	meters per second
MBtu	Million British thermal units
m^2/g	square meters per gram
μ or μm	microns or micrometers
dp_{50}	particle size distribution at 50 percentile
ppm	parts per million
ppm (v)	parts per million (volume)
ppm (w)	parts per million (weight)
lb	pounds
pph	pounds per hour
psia	pounds per square inch
psig	pounds per square inch gauge
ΔP	pressure drop
rpm	revolutions per minute
s or sec	seconds
scf	standard cubic feet
scfm	standard cubic feet per minute
V	volts
W	watts

APPENDIX

MECHANICAL AND THERMAL EVALUATION OF SEVERAL CANDLE FILTER MATERIALS

Report to
Southern Company Services, Inc.
Power Systems Development Facility

SRI-ENG-99-019-9386-I-F

MECHANICAL AND THERMAL EVALUATION OF SEVERAL CANDLE FILTER MATERIALS

Report to
Southern Company Services, Inc.
Power Systems Development Facility
P. O. Box 1069
Highway 25 North
Wilsonville, Alabama 35186

Purchase Order Number C-97-001785

May 1999

SRI-ENG-99-019-9386-I-F

Mechanical and Thermal Evaluation of Several Candle Filter Materials

Final Report to

Southern Company Services, Inc.
Power systems Development Facility
P. O. Box 1069
Highway 25 North
Wilsonville, Alabama 35186

Purchase Order Number C-97-001785

Jack D. Spain
Research Engineer

H. Stuart Starrett
Director, Mechanics Research

Date

Date

Southern Research Institute
757 Tom Martin Drive
Birmingham, AL 35211

May 1999

TABLE OF CONTENTS

Page

1.0 BACKGROUND 1

2.0 MATERIAL ISSUES/SYSTEM REQUIREMENTS 2

3.0 MATERIAL DESCRIPTION 4

4.0 TEST MATRICES AND CUTTING PLANS 5

5.0 TEST METHODS 6

6.0 EXPERIMENTAL RESULTS 6

6.1 Coors P-100A-1 6
6.1.1 Hoop Tensile Results 7
6.1.2 Thermal Expansion 7
6.1.3 Thermal Conductivity 8
6.1.4 Thermal and Mechanical Analysis 9
6.1.5 Conclusions 10

6.2 Clay-Bonded SiC Materials – Schumacher TF-20 and T10-20 and Pall 326 and 442T 10
6.2.1 Tensile Results for Schumacher TF20 and T10-20 11
6.2.2 Tensile Results for Pall 442T and 326 12
6.2.3 Thermal and Mechanical Analysis 13
6.2.4 Conclusions 14

6.3 Pall 181 15
6.3.1 Tensile Results 15
6.3.2 Thermal Expansion 15
6.3.3 Thermal Conductivity 16
6.3.4 Conclusions 16

6.4 IF&P (REECER™) Recrystallized SiC 16
6.4.1 Density 17
6.4.2 Tensile Results 17
6.4.3 Thermal Expansion 17
6.4.4 Thermal Conductivity 17
6.4.5 Conclusions 18

6.5 Ensto Aluminum Oxide 18
6.5.1 Density 19
6.5.2 Tensile Results 19

6.5.3 Thermal Expansion 19
6.5.4 Thermal Conductivity 19
6.5.5 Conclusions 19

7.0 MATERIAL COMPARISONS 20

8.0 CONCLUSIONS 22

REFERENCES 22

LIST OF ILLUSTRATIONS

Table **Page**

4.0-1 Cutting Plan for Virgin Coors Filter KC027 24
4.0-2 Cutting Plan for Virgin Coors Filter LC026 25
4.0-3 Cutting Plan for Coors Candle Filter KC005 After 616 Hours at SCS 26
4.0-4 Cutting Plan for Coors Candle Filter KC011 After 616 Hours at SCS 27
4.0-5 Cutting Plan for Coors Candle Filter LC025 After 616 Hours at SCS 28
4.0-6 Cutting Plan for Coors Candle Filter KC007 After 628 Hours at SCS 29
4.0-7 Cutting Plan for Schumacher TF20 Candle Filter 324H12 After 822 Hours at SCS 30
4.0-8 Cutting Plan for Schumacher TF20 Candle Filter 324H13r After 822 Hours at SCS 31
4.0-9 Cutting Plan for Virgin Schumacher T10-20 Candle Filter 360H071 32
4.0-10 Cutting Plan for Schumacher T10-20 Candle Filter 324H016 After 810 Hours at SCS 33
4.0-11 Cutting Plan for Schumacher T10-20 Candle Filter 324H018 After 1239 Hours at SCS 34
4.0-12 Cutting Plan for Pall 326 Candle Filter 3-24A After 429 Hours at SCS 35
4.0-13 Cutting Plan for Pall 326 Candle Filter 1-36A After 429 at SCS 36
4.0-14 Cutting Plan for Pall 326 Candle Filter 4-991 After 1251 Hours at SCS 37
4.0-15 Cutting Plan for Pall 442T Candle Filter 1A-4 After 616 Hours at SCS 38
4.0-16 Cutting Plan for Pall 442T Candle Filter 5-948 After 1438 Hours at SCS 39
4.0-17 Cutting Plan for Pall 442T Candle Filter 2-1018 After 1867 Hours at SCS 40
4.0-18 Cutting Plan for Virgin Pall 181 Candle Filter 7-1405H 41
4.0-19 Cutting Plan for Virgin IF&P REECER Candle Filter FE98073109 42
4.0-20 Cutting Plan for Virgin IF&P REECER Candle Filter FE98073110 43
4.0-21 Cutting Plan for Virgin Ensto Candle Filter 146-97 44

6.1-1 Thermocouple Locations and Configuration 45
6.1-2 Hoop Tensile Strength of Coors P-100A-1 Versus Hours in Operation 46
6.1-3 Failed Specimen Tn-Hoop-7, 8, and 9 47
6.1-4 Axial Thermal Expansion of Coors P-100A-1 48
6.1-5 Probable Axial Tensile Stress-Strain Responses for Coors P-100A-1 49
6.1-6 Radial Thermal Conductivity of Coors P-100A-1 50
6.1-7 I-D, Flat Plate Model for Thermal Transient Analysis 51
6.1-8 Temperature Gradient in Coors P-100A-1 Candle Filter with a Temperature Increase of 320°F in 60 sec On One Surface 52

6.2-1 Hoop Tensile Strength Versus Hours of Operation for Schumacher TF20 and T10-20 53
6.2-2 Room Temperature Axial Tensile Stress-Strain Responses of Schumacher Candle Filter Materials 54
6.2-3 Hoop Tensile Strength Versus Hours of Operation for Pall 326 and 442T 55
6.2-4 Virgin Weight of Pall Candle Filters 56
6.2-5 Hoop Tensile Strength of Pall 326 and 442T Candle Filters 57
6.2-6 Room Temperature Axial Tensile Stress-Strain Responses for Pall 326 58
6.2-7 Room Temperature Axial Tensile Stress-Strain Responses for Pall 442T 59
6.2-8 Unit Thermal Expansion of Schumacher TF20, Pall 326, and Coors P-100A-1 60
6.2-9 Radial Thermal Conductivity of Schumacher TF20 and Pall 326 61
6.2-10 Temperature Gradient in Schumacher TF20 and Pall 326 Candle Filters with a Temperature Increase of 320°F in 60 sec on One Surface 62

6.3-1 Axial Tensile Stress-Strain Responses for Pall 181 63
6.3-2 Axial Tensile Strength Versus Temperature for Pall 181 and 326 64
6.3-3 Young's Modulus Versus Temperature for Pall 181 and 326 65
6.3-4 Strain-to-Failure Versus Temperature for Pall 181 and 326 66
6.3-5 Unit Thermal Expansion of Pall 181 67
6.3-6 Radial Thermal Conductivity of Pall 181 68

6.4-1 Axial Tensile Stress-Strain Responses for IF&P Recrystallized SiC 69
6.4-2 Axial Unit Thermal Expansion of IF&P Recrystallized SiC 70
6.4-3 Radial Thermal Conductivity of IF&P Recrystallized SiC 71

6.5-1 Axial Tensile Stress-Strain Responses for Ensto Candle Filter Material 72
6.5-2 Unit Thermal Expansion of Ensto Candle Filter Material 73
6.5-3 Radial Thermal Conductivity of Ensto Candle Filter Material 74

7.0-1 Room Temperature Tensile Strength of Candidate Candle Filter Materials 75
7.0-2 Maximum Axial Tensile Load Capability of Several Candle Filter Materials 76
7.0-3 Room Tensile Strength of Coors P-100A-1, Schumacher TF20 and T10-20, and Pall 326 and 442T 77
7.0-4 Thermal Expansion of Candle Filter Materials 78
7.0-5 Radial Thermal Conductivity of Candle Filter Materials 79
7.0-6 Temperature Gradient, OD-ID, in Candle Filters During PSDF Thermal Transients 80

LIST OF TABLES

Table **Page**

2.0-1 Material Issues for Candle Filters 81

4.0-1 Test Matrix for Coors P-100A-1 82
4.0-2 Test Matrix for SiC Filter Elements from SCS 83
4.0-3 Test Matrix for Virgin Pall 181 84
4.0-4 Test Matrix for Virgin IF&P Recrystallized SiC 85
4.0-5 Test Matrix for Virgin Ensto 86

6.1-1 Operational History of Coors-100A-1 Candle Filters 87
6.1-2 Room Temperature Hoop Tensile Strength of Coors P-100A-1 Alumina Mullite 88

6.2-1 Operational History of Clay-Bonded Candle Filters 90
6.2-2 Room Temperature Hoop Tensile Strength of Schumacher TF20 T10-20 Candle Filter Material 91
6.2-3 Room Temperature Axial Tensile Properties of Schumacher TF20 and T10-20 93
6.2-4 Room Temperature Hoop Tensile Strength of Pall 326 and 442T Candle Filter Material 94
6.2-5 Room Temperature Axial Tensile Properties of Pall 326 and 442T 96

6.3-1 Room Temperature Hoop Tensile Strength of Pall 181 Candle Filter Material 97
6.3-2 Axial Tensile Properties of Virgin pall 181 Filter Material 98

6.4-1 Room Temperature Hoop Tensile Strength of IF & P Reecer Candle Filter Material 99
6.4-2 Axial Tensile Properties of Virgin IF and P Reecer Filter Material 100

6.5-1 Density of Ensto Candle Filter Material 101
6.5-2 Room Temperature Hoop Tensile Strength of Ensto Candle Filter Material 102
6.5-3 Axial Tensile Properties of Ensto Filter Material 103

1.0 BACKGROUND

This report summarizes test results obtained on several candle filter materials which are candidates for use in the Southern Company Services (SCS) Power Systems Development Facility (PSDF) in Wilsonville, Alabama. The materials evaluated were:
.

Pall 442T, 326, 181
Schumacher TF20, T10-20
Coors P-100A-1
Industrial Filter and Pump (IF&P) Recrystallized SiC (REECER™)
Ensto aluminum oxide

The objectives of this testing were to

- provide material characterization to develop an understanding of the physical, mechanical, and thermal behavior of these materials.
- develop a materials property data base from which the behavior of these materials in the hot gas cleanup environment may be predicted.
- perform testing and analysis of filter materials after operation in the PSDF to determine the effects of the thermal and chemical environments on these materials.
- explain candle filter failures in the PSDF.

SCS has placed instrumentation in the particulate collection device (PCD) to measure many of the operating parameters including temperatures on the inside and outside walls of the candle filters. The measured mechanical and thermal properties are used to explain and predict performance in operation based on the measured operating parameters.

Pall 442T and 326, Schumacher F40 and TF20, and Coors P-100A-1 have been tested in the past and the results presented in several reports to the U.S. Department of Energy (See Ref. 1-8). Experience with Pall 442T and Schumacher F40 in pressurized fluidized bed combustion (PFBC) at the American Electric Power Tidd Demonstration Plant, Brilliant, Ohio and the Foster Wheeler pressurized circulating fluidized bed combustion (PCFBC) facility in Karhula, Finland resulted in failures due to creep and degradation of the clay binder. In an effort to eliminate the creep failures and binder degradation, Pall and Schumacher produced the filter elements designated Pall 326 and Schumacher TF20 with modified binders. Results indicate that these materials do have reduced creep rates; however, the binders still contain glass so creep may still occur above temperatures of ~1300°F to 1,400ºF (700ºC to 760ºC). The reduced creep rates come at the expense of room temperature tensile strength as both Schumacher TF20 and Pall 326 had lower tensile strengths than Schumacher F40 and Pall 442T. The microstructure of Schumacher F40 and Pall 442T were retained in the TF20 and 326 materials. Their microstructures, individual SiC particles or clusters of SiC particles connected by glass bridges, provide an “inherent toughness” which slows propagation of microcracks. Results obtained from these materials indicate they potentially have a long life at temperatures up to 1400ºF(760ºC) in the absence of major process upsets. Testing has been conducted on Schumacher TF20 and Pall 326 and 442T

after operation in the PSDF at temperatures near 1,400ºF (760ºC) to assess lifetime issues and to evaluate their performance during thermal transient events. Two additional clay-bonded SiC materials have been tested in this program, Schumacher T10-20 and Pall 181. Schumacher T10-20 has the same structural support wall as TF20 but with a different surface membrane. The binder in Pall 181 is modified from the 326 binder.

Coors P-100A-1 alumina/mullite has demonstrated operation at 1550°F (840ºC) in the Foster Wheeler PCFBC at Karhula for over 3000 hours without failure. The Coors material eliminates the creep and chemical degradation of the binder observed in the clay-bonded materials and thus allows higher temperature operation. Experience in the SCS-PSDF, however, has resulted in failure of many Coors candles, especially during transition from start-up burner operation to coal. Testing was conducted in the program to explain these failures. Test results showed that Coors P-100A-1 has a much lower thermal conductivity than the clay-bonded SiC materials; therefore under the same thermal transient conditions, more severe temperature gradients develop in the Coors material. Further, the microstructure of the Coors material does not provide the same inherent toughness as the clay-bonded SiC materials so that cracks propagate more readily.

IF&P recrystallized SiC and Ensto alumina oxide are newer candidate materials with little or no prior results available for them. Testing was conducted on these two materials to obtain a quick assessment of whether they can withstand the thermal environment of the PSDF and to develop a database on virgin materials so that degradation during operation may be monitored. Results obtained for IF&P material showed that it has a thermal conductivity of ~130 Btu-in./hr.-ft^2-°F (18.7 W/m-K) at 1,000ºF (540ºC), which is more than twice the conductivity of any other candidate material. Therefore, it may perform better than materials with similar thermal expansion and strain-to-failure during thermal transients because temperature gradients will be less severe than in other materials. Tests are required to address long-term operation issues such as oxidation of the SiC particles. Results obtained for Ensto indicate that it has relatively high coefficient of thermal expansion (CTE) of 4.0 x 10^{-6}/°F (7.2 x 10^{-6}/ºC) from 500°F to 1,500ºF (260ºC to 815ºC) and a low thermal conductivity of ~6 Btu-in./hr.-ft^2-°F (0.86 W/m-K). Therefore, it will be quite susceptible to thermal stress failure during transient events.

2.0 MATERIAL ISSUES/SYSTEM REQUIREMENTS

Based on operating conditions measured in the PSDF, anticipated requirements in future systems, and in-service performance of candle filters tested to date, several critical material issues have been identified and summarized in Table 2.0-1. The material issues are divided in four categories, installation and handling, pulse cleaning, process upsets, and life which place different requirements on the candles.

The candles must have sufficient strength to withstand the mechanical loads and “toughness” to withstand bumps, nicks, scrapes, etc. associated with handling and installation. While the magnitude of the mechanical loads which the candles will experience during installation is not well-defined, an indication of a particular materials ability to handle loads is obtained from the tensile strength. Tensile strain-to-failure provides an indication of

the materials ability to withstand being bumped. There are several additional issues associated with handling and installation which are not addressed effectively through property measurements. For example, the surface of the candles is likely to be scraped or nicked by other candles or by nuts, bolts, wrenches, etc. during installation. A candle with a delicate membrane or other outer surface is unlikely to survive installation intact.

During pulse cleaning, the backpulse imparts a temperature difference on the inside surface of the candle rapidly enough that the temperature distribution through the candle wall is nearly a step function. That is, the surface attains the temperature of the backpulse gas while the rest of the material is still at the nominal operating temperature. Therefore, the thermal stress level during pulse cleaning is determined by candle operating temperature, backpulse gas temperature, and candle filter material properties, including Young's modulus and thermal expansion of the candle. Thermal diffusivity has little influence. In systems operating with the Siemens-Westinghouse failsafe/regenerator, temperature differences between the candle operating temperature and backpulse gas temperature are ~100°F (56ºC) or less. All current candidate materials have survived that temperature difference. Alternate failsafes that do not preheat the backpulse gas may be used in some systems. In this case, the temperature difference between the candle filter and backpulse gas may be enough to cause microcracking in some candle materials. The material properties, tensile strain-to-failure, thermal expansion, and microstructure (do microcracks propagate and lead to failure?) determine which materials are suitable for use in systems where the backpulse gas is not preheated by a failsafe/regenerator. In screening new candidate materials, the initial screening must include testing to determine whether the material can withstand at least the backpulse conditions.

Several different "process upsets" have been observed and others have been theorized. Among those observed and documented so far are coal carryover into and combustion inside of the filter vessel, ash removal system failure, ash bridging, backside blinding, and ash penetration. These events may result in mechanical or thermal stresses or in chemical attack of the candles. The stresses resulting from any of these events are not well understood, at least not quantitatively.

Some qualitative statements can be made as to the types of loads that some of these scenarios will place on the candles so that evaluations may be made, based on material properties, of which materials offer the best chance to survive various upsets. For example, if coal is carried over into and burned inside of the filter vessel, the temperature on the outside surface of the candles will rise rapidly. An increase of ~320°F (160ºC) in ~60 sec was measured at one location in the SCS PSDF during one carryover event. The resulting temperature profile in the candle will depend on the thermal diffusivity of the candle. That is, a material which conducts heating rapidly away from the surface will see a more moderate thermal gradient than a material which stores the heat near the surface. Since the thermal stress level depends on the temperature gradient, the thermal stresses generated will be set by the temperature rise rate, Young's modulus, thermal expansion, and thermal diffusivity of the candle. If ash bridging occurs, mechanical loads in the form of side loads distributed along the candles and axial loads due to the weight of the ash will result. Additionally, strong temperature gradients may result due to ash bridging. Work is ongoing to understand what

demands are placed on candle filters by various process upset events. As these process upsets are understood, dialogue between candle manufacturers and system operators is needed to determine which scenarios the elements must survive and which may be eliminated by the operators.

Candle filters which can operate for up to ~18000 hours will ultimately be required. Clay-bonded SiC particle materials have been subject to creep, chemical attack of the glass binder, and oxidation of the SiC particles in PFBC operation, limiting the life of these materials at temperatures above 1,400ºF (760ºC). Previous experience in PFBC operation and mechanical and thermal property measurements on monolithic oxides have indicated that these materials are subject to more failures during process upsets than clay-bonded materials. In the absence of process upset failures, static fatigue and crack propagation may limit the life of these materials. The all-oxide composite materials have not seen as much exposure in PFBC operation as clay-bonded SiC or monolithic oxide materials; however, based on limited experience and property measurements, creep, degradation, and ash penetration are issues which must be addressed to predict long-term survivability of these materials. All of the lifetime issues are strongly affected by operating temperature. Results at the PSDF have shown that clay-bonded SiC materials may have a long lifetime if the operation temperature is 1,400ºF (760ºC) or less. Some of the candles have been in operation for at least 3000 hours without failure. Continued service along with property testing of these materials is in progress to try to predict their potential service life. If the operating temperature is to be extended up to 1,500ºF (815ºC), 1600ºF(870ºC), or higher, materials other than the clay-bonded SiC will be necessary to obtain the required lifetime. Development and testing of newer materials is in progress to try to achieve an acceptable lifetime at temperatures above 1,400ºF (760ºC).

3.0 MATERIAL DESCRIPTION

All of the Pall and Schumacher filter materials discussed in this report are clay-bonded SiC particle materials manufactured with an I.D. of ~1.575 inch (40 mm) and a wall thickness of ~0.400 inch (10 mm). The filters have a membrane layer of ~100Φm thickness which provides the filtration applied to the outer surface. The microstructure of both Schumacher and Pall materials consists of individual SiC particles connected by clay or glass bridges. The materials differ in SiC particle size, clay binder chemistry, and outer membrane composition. Pall 326 and Schumacher TF20 have higher temperature, creep resistant binders in comparison with Pall 442T and Schumacher F40. Pall 181 is manufactured with a more cyrstalline binder containing more mullite than Pall 326. Schumacher T10-20 is the same as Schumacher TF20 except for the outer surface membrane layer.

Coors P-100A-1 is a monolithic alumina/mullite filter material. The Coors filters have the same nominal dimensions as the Pall and Schumacher clay-bonded SiC particle filters but have no membrane layer applied to the O.D.

IF & P REECER™ consists of SiC grains fused together without the use of a clay binder. Processing consists of heating SiC grains to temperature above 3500°F (1930ºC) in inert environment so that the grains fuse and form a monolithic material.

Ensto candle filters consist of aluminum oxide particles with a mullite binder to form a microstructure similar to the clay-bonded SiC materials.

4.0 TEST MATRICES AND CUTTING PLANS

The testing conducted on Coors P-100A-1 is outlined in Table 4.0-1. The objectives were to: 1.) assess the performance of Coors P-100A-1 at the PSDF and 2.) explain the failures of those filters during operation. This testing provided data on filters from two different batches and three different operation histories. The 616 hour elements included two from the same batch, KC, but one from the top plenum and one from the bottom. Room temperature hoop tensile strength, axial thermal expansion from RT to 1800°F (980ºC), and thermal conductivity from RT to ~1250°F (680ºC) were measured on as-manufactured material. For each filter, as-manufactured or after operation, hoop tensile strength was measured on three specimens from the flanged end, three from the middle, and three from the closed end to evaluate property variations along the length of the element.

The clay-bonded SiC materials, Pall 326 and 442T and Schumacher TF20 and T10-20, were tested according to the test matrix shown in Table 4.0-2. The objective was to assess property degradation during operation at the PSDF. Hoop tensile strength was measured on nine specimens (three from the flanged end, three from the middle, and three from the closed end) from each candle filter. Axial tensile stress-strain responses were measured and light microscopy conducted on selected candles. Properties of as-manufactured Pall 326 and 442T and Schumacher TF20 measured and reported under work performed for DOE/FETC (see Ref. 1 and 2) were used for comparisons to determine the degree of degradation. Schumacher T10-20 is the same as TF20 except for the membrane layer and therefore should have the same as-manufactured properties as TF20; however, one virgin Schumacher T10-20 filter was tested to verify this.

Pall 181, IF&P recrystallized SiC, and Ensto were tested according to the test matrices shown in Tables 4.0-3 through 4.0-5. The objectives of these tests were to 1.) provide an initial look at these materials to determine whether installation in the PSDF was warranted, 2.) provide material properties required to predict performance in the PSDF, and 3.) provide baseline data for comparison with properties measured on these materials after operation. Some of the testing required in these test matrices is still in progress and the results will be reported separately.

Specimens required to conduct the tests outlined were removed from the candle filters as shown in Figures 4.0-1 through 4.0-21. The hoop tensile specimens are taken from the flanged end, the middle, and the closed end of each candle to determine if the strength varies axially along the candles. The hoop tensile strength of each specimen is shown on these cutting plans. The results will be discussed in Section 6. Axial tensile and thermal

expansion specimens, as required, were taken from regions adjacent to the hoop tensile specimens at the closed end.

5.0 TEST METHODS

The tests method used in this program were the same as used in past programs to evaluate these or similar materials. A description of the test methods is given in reports provided to DOE/FETC (Ref. 1 and 2).

6.0 EXPERIMENTAL RESULTS

6.1 Coors P-100A-1

Coors P-100A-1 was tested as-manufactured, after 616 hours of operation in the PSDF, and after 628 hours of operation in the PSDF. The Coors filters tested in this program and their operational history at the PSDF are summarized in Table 6.1-1. The first 19 Coors filter elements were installed in the PSDF in April 1997 and operated with no failures until July 1997. During this period, 616 hours of on-coal operation was accumulated. During the July 1997 shutdown, 11 Coors filter elements were removed from service intact, 8 were left in service, and 10 were installed new. Three of the 11 filters removed were tested at SRI. When operation was restarted in the last week of August 1997, 3 Coors filters broke during transition to coal. After 12 hours on coal, the system was shutdown. During inspection of the system after shutdown, a fourth Coors filter element broke. All four of the failed filters had been in operation from April-July 1997 and were left in service. Two of the remaining four filters which were in operation from April-July were removed (one for material testing at SRI) and two remained in service. The two Coors filters which remained in service subsequently failed September 7 and September 19. The 10 Coors filters installed new during the July shutdown all failed on November 2, 1997. Testing of Coors filters in this program was conducted both to assess performance under PSDF conditions and to explain the failure which occurred.

In order to measure the operating temperatures of the candle filters and to help explain the failures which occurred, one Coors P-100A-1 candle and one Pall 326 candle and two failsafes were instrumented with thermocouples. The configuration and locations of the thermocouples are illustrated in Figure 6.1-1. The instrumented candles and failsafes were installed in March 1998 and operation began in April 1998. When the transport reactor switched from the gas-fired start-up burner to coal feed, pieces of Coors P-100A-1 and Blasch 4-270 (both aluminum oxide materials) were found in the ash removal system. The thermocouple readings on the candle filters showed several sharp spikes, the most severe being a temperature increase of 320°F (180ºC) over a period of 60 sec on the outside surface of the Pall 326 filter. The cause of the temperature spikes is thought to be coal carry-over from the transport reactor to the PCD. If coal carry-over into the PCD was indeed the cause of these spikes, then the severity may have been much worse at other locations than measured by these thermocouples. That is, if the thermocouple that recorded the 320°F

(180ºC)/60 sec temperature increase was several inches from the nearest burning coal particle, then the magnitude of the temperature increase would be greater near the particle. A more detailed summary of the thermocouple installation and recorded temperatures is provided in Reference 11.

6.1.1 Hoop Tensile Results

Room temperature hoop tensile strengths are plotted versus hours in operation in Figure 6.1-2 and summarized in Table 6.1-2. The strengths measured for each individual specimen was also shown in the cutting plans presented in Figures 4.0-1 through 4.0-6. The strength decreased ~12% during 616-628 hours in operation from an average of ~1,800 psi (12.4 MPa) as-manufactured to ~1,600 psi (11.0 MPa) after operation. Some batch-to-batch variability in strengths was also seen as specimens from the LC batch had tensile strengths 10 to 16% greater than specimens from the KC batch. Three specimens from candle KC007, the candle which was installed in April 1997 and remained in operation until September 1, 1997, failed at stress levels of 150 to 450 psi (1.0-3.1 MPa). These three specimens were adjacent to each other near the flanged end of the candle filter as shown in Figure 4.0-6. The failure mode was different for these three specimens than for other specimens. Failure normally occurs along a nearly straight, vertical line. For these specimens, failure was along a wavy line at an angle from vertical. An orientation line drawn on the candle filters before they were cut allowed the failed specimens to be reassembled to their original positions. The reassembled specimens are shown in Figure 6.1-3. A 3/8" (9.5 mm) high ring taken from adjacent to specimen Tn-Hoop-7 for light microscopy failed during bandsawing and this specimen was also reassembled and shown in Figure 6.1-3. These four specimens, Tn-Hoop-7, 8, and 9 and the microscopy sample, failed along a continuous wavy line at an angle from vertical. The failure modes and low tensile strengths of these filters were evidently the results of a pre-existing crack. The crack in candle KC007, the sudden failure of three filters, and the apparent lack of mechanical load suggest a sudden thermal event during the 12 hours of operation between July and September 1, 1997 caused the candle failures and the cracking of candle KC007. The same event which caused the crack in this candle likely caused the failures in four other candles.

6.1.2 Thermal Expansion

Axial unit thermal expansion is plotted in Figure 6.1-4. The coefficient of thermal expansion (CTE) is obtained from the slope of the unit thermal expansion curve. From 500°F (260ºC) to 1,500ºF (815ºC), the average CTE of virgin material was 2.8×10^{-6} in./in./°F (5.0×10^{-6}/ºC). The thermal expansion of Candle KC007, measured after 628 hours in operation, was slightly greater (~3%) than the expansion of virgin Candle KC027. This increase is slight; however, thermal expansion is normally very consistent and a slight change may indicate a difference between candles.

The tensile stress-strain response and unit thermal expansion set thermal stress and strain levels for a given temperature distribution. Thermal expansion and tensile strain-to-failure establish the temperature gradients required to initiate microcracking. If the tensile stress-strain response and thermal expansion are known, then thermal stress and strain levels

for a given temperature distribution may be calculated. The calculated stresses and strains may be compared to the ultimate values measured to determine whether microcracking will occur.

Axial tensile stress-strain responses for Coors P-100A-1 at RT and 1,500ºF (815ºC) were measured and reported under U.S. Dept. of Energy Contract No. DE-AC31-89MC26233 (see Ref. 3) and are shown in Figure 6.1-5. From these properties measured at RT and 1,500ºF (815ºC), the properties at 1,000ºF (540ºC) (the nominal temperature in the PCD when the Coors filters failed) were estimated to be: ultimate tensile strength about 2,400 psi (16.5 MPa) and strain-to-failure about 0.8 mils/inch (0.08%). The relationship between strain-to-failure and thermal expansion is illustrated in Figure 6.1-4. Tensile strain-to-failure at 1,000ºF (540ºC) is shown on the Y-axis and the corresponding temperature gradient (T_{body} - $T_{surface}$) required to cause this tensile strain is shown on the X-axis. This illustration is a reasonable model during the back pulse where the body of the filter is at the operating temperature and the temperature of the back pulse gas is suddenly applied to the surface (see discussion in Section 2.0). Back pulse gas temperature measurements at the PSDF indicated that if the Siemens-Westinghouse failsafe/regenerator is used, back pulse cleaning will not produce large enough temperature gradients to fail the Coors filters. Extended accelerated pulse cycle testing at Siemens-Westinghouse also indicated that Coors elements can survive back pulse cleaning with the use of the failsafe/regenerator (Ref. 8). However, if the system is to be operated with a different failsafe that does not provide preheating of the back pulse gas, then another method of preheating is required or a candle filter which can survive the temperature gradients must be selected.

6.1.3 Thermal Conductivity

Since the measured unit thermal expansion and tensile stress-strain responses, along with measured conditions in the PSDF and extended accelerated pulse cycle testing at Siemens-Westinghouse, indicated that back pulse cleaning was not likely the cause of Coors failures, the effect of thermal transients was considered. As discussed in Section 2.0, the temperature profile in the candle filters during transients depends on the thermal diffusivity, $\alpha = k/\Delta Cp$

where α = thermal diffusivity
k = thermal conductivity
Δ = density
Cp = specific heat

Thermal conductivity of Coors P-100A-1 in the radial direction was measured and is plotted versus temperature in Figure 6.1-6. Thermal conductivity decreased slightly with temperature from 12.5 Btu-in./hr-ft^2-°F (1.8 W/m-K)at RT to 10.9 Btu-in./hr-ft^2-°F (1.6 W,-K) at 1220°F (660ºC). At 1,000ºF (540ºC), the nominal temperature in the PSDF when the Coors filters failed, the thermal conductivity was 11 Btu-in./hr-ft^2-°F (1.6 W/m-K). Thermal diffusivity at 1,000ºF (540ºC) is therefore 0.031 ft^2/hr (8.0 x 10^{-7} m^2/sec based on the measured thermal conductivity and density (101 lb/ft^3, 1.62 gr/cm^3) and a literature value of specific heat (0.29 Btu/lb.-°F, 1.21 KJ/Kg-°K).

6.1.4 Thermal and Mechanical Analysis

As a first approximation of the temperature gradients in a Coors P-100A-1 candle filter with the properties as measured at 1,000ºF (540ºC), a simple, 1-D flat plate model with appropriate boundary conditions was assumed. The model, with boundary and initial conditions, is shown in Figure 6.1-7. As shown, the model was a flat plate, 0.40 in. (10 mm) thick, initially at a uniform temperature. A temperature ramp rate of 320°F(180ºC)/60 sec was applied to one surface while the other surface was insulated. Results from these calculations are shown in Figure 6.1-8 which is a plot of the temperature difference between the surfaces versus time. For a candle filter, this represents T_{OD}-T_{ID} versus time. The maximum temperature gradient was calculated to be ~210°F (99ºC).

The temperature difference between the O.D. and I.D. does not tell the whole story of whether microcracking or candle failure will occur. The temperature distribution will have some effect. The case discussed in Section 6.1.2 for back pulse cleaning, that is, the candle wall at a uniform temperature and then one surface suddenly brought to a different temperature, results in the most severe thermal stresses for a given $T_{OD} – T_{ID}$. The least severe thermal stresses for a given $T_{OD} – T_{ID}$ occurs in the case of the steady-state temperature profile where the temperature changes gradually across the wall thickness. For this case, Coors could withstand nearly a 500°F (260ºC) ID to OD gradient before microcracking would occur. For the thermal transients seen in the PSDF, the gradients were in between these two extreme cases.

While the calculated gradient of 210°F (99ºC) was not severe enough to cause cracking for either case, back pulsing or steady-state, it was close. If the surface heating rate of 320°F (180ºC)/60 sec was some distance from the location of the most severe heating rates, then gradients sufficient to cause failure of Coors filters were likely. Another important consideration is that the gradients required to cause cracking were calculated based on average properties of virgin material. Property degradation after operation could lead to greater susceptibility for cracking. More importantly, cracking will initiate selectively at the weakest locations, or at least the locations where strain-to-failure is lowest. At these selected locations, cracking will occur at gradients less severe than those calculated based on average properties.

If the data and analysis presented above indicate that microcracking of Coors P-100A-1 candles will occur under the thermal transient conditions at the PSDF, the question of whether these microcracks lead to failure remains. The Coors candles tested in this program were in the PCD during several startups and transitions to cool during the 616 hours of operation from April to July. Also, several new Coors filters were in operation in September when failure of the filters which remained in operation from April occurred. These new filters subsequently failed in November after 822 hours of operation. Mr. C. D. Pears investigated the fracture patterns of Coors P-100A-1 from the PSDF and his results are presented in Ref. 10. These results indicate fracture of these filters results from numerous microcracks which form and progress to the point that the cracks “link” and become severe enough to cause fracture. The cracks could be initiated by several chemical or thermal events

including pulsing, asymmetric thermal and mechanical load, or multiple startups with coal carry-over. Given the mechanical and thermal properties of Coors filters and the temperatures measured on the surface of candles in the PCD, coal carry-over into the PCD is certainly the likely cause.

6.1.5 Conclusions

Coors P-100A-1 eliminates several problems which face clay-bonded SiC materials in hot gas cleanup applications. Because there is no clay or glass binder, creep and chemical degradation of the binder are reduced. Oxidation is also avoided. The Coors filters have operated successfully at Karhula for over 3000 hours. However, during operation of the SCS-PSDF, several candles have failed during transition from startup burner to coal. Test results and observation of failed Coors filters from the PSDF indicated that failure was likely due to accumulated microcracking caused by coal burn in the PCD during several transitions to coal.

The average tensile properties and thermal expansion indicate that Coors P-100A-1 can withstand I.D. to O.D. temperature gradients of ~280°F (160ºC) to 500°F (280ºC), depending on the temperature distribution, without microcracking. However, microcracking will initiate selectively at locations where the strain-to-failure is a minimum. Therefore, the temperature gradient required to initiate microcracks is somewhat less than the values shown above. While these properties show that the Coors material can withstand the temperature gradients of normal operation, even during back pulsing, the low thermal diffusivity will lead to severe temperature gradients during the thermal transients observed at the PSDF. Calculations have indicated that the temperature gradients encountered during transients at the PSDF were severe enough to cause microcracking. The microstructure is also an important factor in determining whether microcracks will propagate and damage accumulation during several transients will lead to failure of the candle filters. Coors P-100A-1 has a relatively homogeneous microstructure which will propagate cracks, once they develop, much more readily than the clay-bonded SiC materials.

6.2 Clay-Bonded SiC Materials – Schumacher TF-20 and T10-20 and Pall 326 and 442T

Hoop and axial tensile testing was conducted on Schumacher TF20 and T10-20 and Pall 326 and 442T candle filters after operation at the PSDF. Individual candles tested and their hours in operation and maximum operating temperature are summarized in Table 6.2-1. Properties of virgin Schumacher TF20 and Pall 326 and 442T have been measured and reported under DOE contract (see Ref. 1 and 4). Properties measured after operation are compared to those virgin properties to determine whether degradation is occurring during operation at the PSDF. Virgin properties have not been measured on Schumacher T10-20 in any previous efforts. Since this material is the same as Schumacher TF20 except for the membrane layer, the properties of the structural wall should be the same; however, testing was conducted on one virgin T10-20 candle filter in this effort.

In operation at the PSDF, these clay-bonded SiC materials have proven better able to withstand thermal transients than monolithic aluminum oxides. However, on two occasions, one in April 1997 and one in October 1998, clay-bonded SiC materials have failed due to coal burning in the PCD. Material properties measured under DOE contract, and operating conditions measured at the PSDF have been used to perform the same type of analysis on Schumacher and Pall materials that was presented for Coors in the previous section. The objective of this analysis was to explain why the clay-bonded SiC materials have withstood thermal transients, including coal carry-over into the PCD, better than aluminum oxides and to look at what level of thermal transient will cause failure of clay-bonded SiC.

6.2.1 Tensile Results for Schumacher TF20 and T10-20

Room temperature hoop tensile strengths are plotted versus hours in operation in Figure 6.2.1 and summarized in Table 6.2-2. Individual specimen strengths are also shown on the cutting plans in Figure 4.0-7 through 4.0-11. Strength was measured under DOE/FETC contract on TF20 in virgin condition and after operation at Karhula for 540 hours at 1550°F (840ºC). These results are included for comparison in Figure 6.2-1. Results for virgin material show a higher strength for T10-20 than for TF20. While the overall coefficient of variation (COV) (i.e., standard deviation/average) of tensile strengths of virgin material was low, some indication of variability was seen. The measured strengths of three specimens from TF20 Candle 344E-309 were ~9% greater than the strengths of three specimens from Candle 344E-295. Only one virgin T10-20 filter was tested but the strength of three specimens nearest the flange was ~23% lower than the strength of the specimens from the middle or near the closed end of the filter. Given the data scatter seen (see especially axial tensile results in the next section) and that TF20 and T10-20 should be the same material except for the membrane, the apparent strength difference is most likely due to variability. This should be confirmed by additional testing of virgin T10-20. These results indicate a decrease in strength during operation at the PSDF. While the strength was lower after operation than in virgin condition, it appeared to level off and was the same after 810, 822, or 1239 hours of operation. Strength values obtained on one TF20 candle filter from operation at a nominal temperature of 1550°F (840ºC) at Karhula are also shown in Figure 6.2-1. These results were obtained and reported under contract with DOE/FETC, see Ref. 4.

Room temperature axial tensile stress-strain responses are shown in Figure 6.2-2 and the results are summarized in Table 6.2-3. Stress-strain responses measured under DOE/FETC contract on virgin TF20 material are included for comparison. These results show the strength in the axial direction is about half the strength in the hoop direction. This strength difference has not yet been explained. The measured axial tensile strengths and Young's modulus values are nearly the same after operation at the PSDF or at Karhula as for virgin materials. However, the stress-strain curves after operation show a slight "roll over" not seen for virgin material. This slight change in stress-strain response after operation was likely due to degradation of the binder. Evidence of binder degradation was seen during microscopic examination of the material from Karhula, see Ref. 4.

6.2.2 Tensile Results for Pall 442T and 326

Room temperature hoop tensile strengths are plotted versus hours in operation in Figure 6.2-3 and summarized in Table 6.2-4. Individual specimen strengths are also shown on the cutting plans presented in Figures 4.0-12 and 4.0-17. Strength was measured under DOE/FETC contract on virgin 326 and 442T filters and on one filter operated at Karhula for 540 hours at 1550°F (840ºC). These results are included for comparison in Figure 6.2-3. The individual specimen strengths from any one particular candle filter were very consistent; however, considerable candle-to-candle variability was seen. These results do not show any change in strength during operation at the PSDF although the candle-to-candle variability could obscure any change that may have occurred.

Weights of all Pall elements were measured before shipment to SCS. The virgin weight of each element is plotted in Figure 6.2-4. The X-axis on this plot represents a candle number assigned at the PSDF when the candles were received. The weight of each filter tested at SRI is also shown on the tensile strength plot of Figure 6.2-3. Again, note that all of these weights were obtained on the filters in virgin condition before installation in the PCD. The COV in weights was 2.8% for 326 candles and 2.2% for 442T candles. Hoop tensile strengths are plotted versus virgin candle weight in Figure 6.2-5. Hours of operation are also shown in this figure. Results for 442T filters show that the effect of weight overpowers any effect which operation at the PSDF may have had. These results also show that the strength of the 326 candle filters increased with weight. However, the 326 results do indicate a possible strength change during operation. Based on the strength-weight correlation seen in the other filters, the strength of Candle 4-991 might have been greater if it had not been in operation longer than any other 326 filter tested. Three virgin 326 filters of different weights will be tested to try to determine whether the weight difference could be due to dimensional differences in the candles. Three virgin 326 filters of different weights will be tested to try to separate the effect of operation from the effect of weight.

Room temperature axial tensile stress-strain responses are shown in Figure 6.2-6 for 326 and Figure 6.2-7 for 442T and the results are summarized in Table 6.2-5. Stress-strain responses were measured on virgin material under DOE/FETC contract and are included for comparison. As with the hoop tensile results, candle-to-candle variability was the most obvious observation in the axial strength measurements. A quick look at the stress-strain curves would indicate that both ultimate strength and strain-to-failure of Pall 326 increased during operation at the PSDF while the properties of 442T did not change. However, the hoop tensile strength results showed that candle weight may drive the tensile strength and weights were not available for the virgin candles. In fact, the highest strength Pall 326 candle, Candle 4-991 with 1251 hours of operation, was also the 326 candle with the highest weight (Figure 6.2-5). If indications of property degradation are to be obtained from the tensile stress-strain responses, the effect of candle weight and any other sources of large variability must be understood so that these effects may be sorted from material degradation.

The tensile properties measured were inconclusive in determining whether degradation of Pall 326 and 442T occurred during operation at the PSDF. A decrease in tensile strength coupled with greater nonlinearity in the axial stress-strain curves was

measured after operation at 1550°F (840ºC) at Karhula. These property changes were supported by evidence of binder degradation observed in low powered photomicrographs. The higher operating temperatures at Karhula may result in greater property degradation for the Pall material than the PSDF operating temperatures. However, this apparent effect could be due to candle-to-candle variability. Light microscopy is part of this program but has not been completed due to equipment problems. These problems have now been eliminated and microscopy is in progress. These results may provide an indication of whether binder degradation is occurring during operation at the PSDF.

6.2.3 Thermal and Mechanical Analysis

Elevated temperature axial tensile properties, thermal expansion, and thermal conductivity of Schumacher TF20 and Pall 326 have been measured under DOE/FETC contract. These properties will be used with the temperature measurements on Coors P-100A-1 and Pall 326 in the PSDF to understand why the clay-bonded SiC materials have withstood these thermal transients better than monolithic aluminum oxides and to assess what severity of thermal transients these materials can withstand.

Unit thermal expansions of Schumacher TF20 and Pall 326 are shown in Figure 6.2-8. Coors P-100A-1 is included in this figure for comparison. The strain-to-failure at 1,000ºF (540ºC) was estimated for each material based on measured values at RT, 1,400ºF(760ºC), 1,500ºF (815ºC), and 1,600ºF (870ºC) and these values are shown on Figure 6.2-8. From the thermal expansion and strain-to-failure, the back pulse ΔT (difference between candle operating and back pulse gas temperature) which will initiate microcracking was calculated to be ~170°F (95ºC) for TF20 and ~210°F (115ºC) for 326. As shown in Section 6.1.2, the value for Coors was ~280°F (160ºC). These results indicate that the clay-bonded SiC materials are more susceptible to microcracking due to back pulsing than Coors. However, during thermal transients such as coal burn in the PCD, thermal conductivity plays a role in the materials ability to dissipate heat throughout the filter wall.

Thermal conductivity of Schumacher TF20 and Pall 326 are plotted in Figure 6.2-9. At 1,000ºF (540ºC), the thermal conductivity of TF20 was 51 Btu-in./hr-ft^2-°F (7.3 W/m-K) and the thermal conductivity of 326 was 38 Btu-in./hr-ft^2-°F (5.5 W/m-K). Using measured density values of 119 lb/ft^3 (1.91 gr/cm^3) for TF20 and 115 lb/ft^3 (1.84 gr/cm^3) for 326 and literature values of specific heat of 0.29 Btu/lb.-°F (1.2 KJ/Kg-K) for both materials, thermal diffusivity at 1,000ºF (540ºC) was 0.126 ft^2/hr (3.3 x 10^{-6} m^2/sec) for TF20 and 0.095 ft^2/hr (2.5 x 10^{-6} m^2/sec) for 326. These thermal diffusivity values are 3-4 times greater than the thermal diffusivity of Coors P-100A-1.

The same 1-D, flat plate model with the same boundary conditions used to estimate the O.D. to I.D. temperature gradient in Coors filters was used to estimate the gradients in Schumacher and Pall filters. Results are shown in Figure 6.2-10. For a surface heating rate of 320°F(180ºC)/60 sec, the maximum gradient, T_{OD} - T_{ID}, was calculated to be ~75°F (42ºC) for Schumacher TF20 and ~95°F (53ºC) for Pall 326. These calculations show the role of thermal conductivity in establishing the temperature gradients which a candle

filters will see during a thermal transient event. The tensile strain-to-failure and thermal expansion of Schumacher and Pall filters indicate that a slightly less severe thermal gradient will cause microcracking in these materials than in Coors. However, the thermal diffusivity of 3-4 times greater in TF20 and 326 will lead to much less severe gradients than in Coors during transient events. Therefore, more severe thermal transients are required to cause microcracking in TF20 and 326. As the events in the PSDF during April 1997 and October 1998 showed, thermal transients severe enough to fail the clay-bonded SiC materials are possible in the PSDF.

Another important difference between the Schumacher and Pall materials and the Coors material is the microstructure. The clay-bonded SiC materials consist of SiC particles connected by clay binder material. The binder material does not typically cover the entire particle but forms bridges between adjacent particles. When microcracking occurs it is in the binder bridges. A large amount of energy is required to propagate a crack from one binder bridge to an adjacent bridge. Coors filters have a much different microstructure. Although the material is quite porous, it is much closer to a homogeneous, monolithic ceramic. If microcracks start in this material, they propagate much more readily than in the clay-bonded SiC, making failure more likely.

6.2.4 Conclusions

Schumacher TF20 and T10-20

The tensile strength of Schumacher TF20 and T10-20 decreased during the first 800 hours of operation of the PSDF and remained the same through 1200 hours of operation. These observations are based on testing of a limited number of elements and may be altered or confirmed with additional testing. Microscopic examination of these materials is in progress in hopes of determining the cause of the strength loss measured (binder degradation, damage during thermal transients, etc.) and whether greater degradation is evident after 1200 hours of operation than after 800 hours of operation.

Pall 326 and 442T

Candle-to-candle variability was the most obvious feature of the strength measurements on Pall 326 and 442T. There was a strong correlation between measured strength and candle weight. If any strength change occurred during operation, it was obscured by the effect of weight.

Thermal expansion and strain-to-failure measurements show that, given the same temperature gradient the Pall and Schumacher clay-bonded materials are just as susceptible or maybe even more susceptible to thermal stress induced microcracks than Coors P-100A-1. However, the microstructure of the clay-bonded materials provides an “inherent toughness” which makes propagation of microcracks, leading to candle failure, less likely than in the more homogeneous Coors material.

Thermal conductivity plays a big role in setting the severity of temperature gradients in the candle filters during thermal transients. The Schumacher and Pall clay-bonded SiC materials have a greater thermal conductivity than the aluminum oxide materials; therefore, the temperature gradients are less severe during thermal transients.

Overall, the results indicate that in the absence of major thermal transients and temperature excursions, Schumacher and Pall clay-bonded materials have a long life (thousands of hours) at operating temperatures up to 1,400ºF (760ºC). Lifetime predictions for 9000 hours, 18000 hours, etc. will require more experience in PFBC service. Above 1,400ºF (760ºC), creep, static fatigue, and degradation will limit the use of these materials.

6.3 Pall 181

A new clay-bonded SiC particle material from Pall, denoted Pall 181, has been tested and the results are given in this section. The clay binder of Pall 326 was modified to form Pall 181. Properties of virgin 181 were measured to 1.) provide screening before this material is installed for operation at the PSDF, 2.) begin development of a material property database to conduct mechanical and thermal analysis, and 3.) obtain baseline data for comparisons with properties measured after operation.

6.3.1 Tensile Results

Hoop tensile results are summarized in Table 6.3-1. Individual values are shown on the cutting plans of Figure 4.0-18. The average hoop tensile strength of Pall 181 was 2,800 psi (19.3 MPa), ~30% greater than the average value for Pall 326 and ~15% greater than Pall 442T. Since only one Pall 181 candle has been tested, candle-to-candle variability has not been assessed.

Axial tensile stress-strain responses at RT, 1,400ºF (760ºC) F, 1,500ºF (815ºC), and 1,600ºF (870ºC) are shown in Figure 6.3-1. Results are summarized in Table 6.3-2. Properties are plotted versus temperature in Figures 6.3-2, 3, and 4. Properties of Pall 326 are included in these figures for comparison. The average ultimate tensile strength was ~2,570 psi (17.7 MPa) at RT and 1,400ºF (760ºC) and then decreased to ~2,130 (14.7 MPa) psi at 1,600ºF (870ºC). The average strain-to-failure was ~0.45 mils/inch (0.045%) from RT to 1,500ºF (815ºC), then increased to ~0.83 (0.083%) mils/inch at 1,600ºF (870ºC). The ultimate strength of Pall 181 was greater than the strength of Pall 326 except at 1,500ºF (815ºC) where 326 reached a peak value in strength. Strain-to-failure of 181 was greater than 326 at RT but less from 1,400ºF (760ºC) to 1,600ºF (870ºC).

6.3.2 Thermal Expansion

Unit thermal expansion of Pall 181 is shown in Figure 6.3-5. Except for the "bump" in the 326 curve at ~300°F (150ºC) to 500°F (260ºC), probably due to phase change in the binder, the thermal expansion of Pall 181 and 326 are nearly identical. The average CTE from 500°F (260ºC) to 1,500ºF (815ºC) was 2.8 x 10^{-6} in./in./°F

(5.0×10^{-6}/ºC). Taken together, the thermal expansion and strain-to-failure results suggest that at temperatures of 1,500ºF (815ºC) to 1,600ºF (870ºC) Pall 181 may be more sensitive to thermal stresses than Pall 326 but in the range of 1,000ºF (540ºC) the materials are similar. Material variability will also play a role.

6.3.3 Thermal Conductivity

Thermal conductivity of Pall 181 is plotted versus temperature in Figure 6.3-6. Conductivity decreased with temperature from 38 Btu-in./hr-ft^2-°F (5.5 W/m-K) at RT to 30 Btu-in./hr-ft^2-°F (4.3 W/m-K) at 1240°F (670ºC). At 1,000ºF (540ºC)°F, the thermal conductivity was ~31 Btu-in./hr-ft^2-°F (4.5 W/m-K). Thermal conductivity of Pall 181 was slightly lower than for Pall 326, 31 Btu-in./hr-ft^2-ºF (4.5 W/m-K) compared to 38 Btu-in./hr-ft^2-ºF (5.5 W/m-K)at 1,000ºF (540ºC). This will lead to a slightly more severe temperature gradient for Pall 181. By the same thermal model used in the previous sections, the maximum gradient, $T_{OD} - T_{ID}$, for a Pall 181 candle with a 320°F(180ºC)/60 sec temperature increase on one surface would be 110°F (60ºC) compared to 95°F (53ºC) for Pall 326. Again, this calculation is based on the measured thermal conductivity and density values and the literature value of specific heat, 0.29 Btu/lb.-°F (1.2 KJ/Kg-K).

6.3.4 Conclusions

Tensile results show that Pall 181 has a higher strength than Pall 326 in both the axial and hoop directions. At RT, the strain-to-failure was also greater for Pall 181; however, at 1,400°F (760°C) the strain-to-failure was greater for Pall 326. Properties were not measured at any temperatures between RT and 1,400°F (760°C). Pall 181 also has a slightly lower thermal conductivity than Pall 326. The lower strain-to-failure, at least at 1,400°F (760°C) and above, and thermal conductivity make Pall 181 more susceptible to cracking due to thermal stress; however, the property differences are small so the increased susceptibility to thermal stress cracking will also be small. The microstructure of Pall 181 is similar to the other clay-bonded SiC materials (that is, individual SiC particles connected by bridges of binder material). This microstructure makes crack propagation, leading to failure of the candle filter, less likely than in materials with a more homogenous microstructure.

6.4 IF&P (REECER™) Recrystallized SiC

Particular interest in IF & P recrystallized SiC has developed since two of the candle filters survived the October 1998 thermal transient which failed the clay-bonded SiC and monolithic oxide Ensto filters. The IF & P filters were in the bottom plenum where all the failures occurred. Properties were measured to 1.) begin development of a material property database to conduct mechanical and thermal analysis, 2.) obtain baseline data for comparisons with properties measured after operation, and 3.) explain why this material withstood the same thermal transient which caused failure of the clay-bonded SiC filters. The filters tested had several process related “bubbles” in the wall up to ~1/8 inch (3 mm)

diameter. Some of these bubbles were internal and others extended to the inside surface. None extended to the outside surface.

6.4.1 Density

Bulk density was measured on one specimen, Tn-Hoop-127, (which was used to measure axial thermal expansion, not hoop tension) and a bulk density of 144 lb./ft^3 (2.30 gr/cm^3) was obtained. Bulk density was also measured on four individual specimens, two axial thermal expansion and two thermal conductivity, and the density values ranged from 134 lb./ft^3 (2.15 gr/cm^3) to 137 lb./ft^3 (2.20 gr/cm^3).

6.4.2 Tensile Results

Hoop tensile results are summarized in Table 6.4-1. Individual values are shown on the cutting plans of Figures 4.0-19 and 20. The average hoop tensile strength was 2,030 psi (14 MPa). Specimen dimensions, shown in Table 6.4-1, indicate that the inside diameter varied from 1.72 in. (43.7 mm) to 1.83 in. (46.5 mm) in Candle FE98073109 and from 1.60 in. (40.6 mm) to 1.78 in. (45.2 mm) in Candle FE 98073110. In each case the largest I.D., thinnest wall, was nearest the flanged end. Because of the dimensional variation, some specimens had a higher hydrostatic pressure but lower strength than other specimens. Several specimens, including the weakest three, failed at a hole. However, the effect of the holes on strength was unclear as the strongest and third strongest specimens also failed at a hole. One specimen, Tn-Hoop-132, had a hole visible on the I.D. but did not fail there and other specimens had holes visible on the top or bottom surfaces but did not fail at them. Factors other than simply the presence of a hole, including the size and location of the hole, would likely play a role in determining the effect, if any, on strength.

Axial tensile stress-strain responses at RT and 1,500ºF (815ºC) F are shown in Figure 6.4-1 and the results are summarized in Table 6.4-2. The average tensile strength was 2,120 psi (14.6 MPa) at RT and changed little to 1,980 psi (13.6 MPa) at 1,500ºF (815ºC). However, Young's modulus increased from an average of 13.7 Msi (94.4 MPa) at RT to 18.8 Msi (129.5 GPa) at 1,500ºF (815ºC) F and strain-to-failure decreased from an average of 0.16 mils/inch (0.016%) at RT to 0.10 mils/inch (0.010%) at 1,500ºF (815ºC). One specimen, Tn-Ax-75, tested at 1,500ºF (815ºC) failed at an ultimate strength of 950 psi (6.6 MPa) and strain-to-failure of 0.06 mils/inch (0.006%). These two values were not included in calculations of average properties at 1,500ºF (815ºC).

6.4.3 Thermal Expansion

Unit thermal expansion is shown in Figure 6.4-2. The average CTE from 500°F (260ºC) to 1,500ºF (815ºC) was 2.4 x 10^{-6} in./in./°F (4.3 x 10^{-6}/ºC). The strain-to-failure and thermal expansion together indicate a temperature difference of between 42°F (25ºC) (based on the 1,500ºF (815ºC) strain-to-failure) and 67°F (35ºC) (based on the RT strain-to-failure) required to cause microcracking under the back pulse cleansing model discussed previously.

6.4.4 Thermal Conductivity

Thermal expansion and strain-to-failure measurements indicate that smaller temperature gradients are required to cause cracking in the IF&P recrystallized SiC than in the clay-bonded SiC materials, yet the IF&P material survived the same thermal transient which failed the other materials. An explanation may be found in the thermal conductivity. Thermal conductivity of the IF&P materials is plotted in Figure 6.4-3. The conductivity decreased with temperature from 245 Btu-in./hr-ft^2-°F (35.3 W/m-K) at RT to 100 Btu-in./hr-ft^2-°F (14.4 W/m-K) at 1,500ºF (815ºC). At 1,000ºF (540ºC), the conductivity of IF&P was 125 Btu-in./hr-ft^2-°F (18.0 W/m-K), compared to 51 Btu-in./hr-ft^2-ºF (7.3 W/m-K) for Schumacher TF20 and 38 Btu-in./hr-ft^2-°F (5.5 W/m-K) for Pall 326. The maximum temperature gradient, T_{OD}-T_{ID}, calculated for IF&P recrystallized SiC with a 320°F (180ºC)/60 sec heating rate on one surface would be 40°F (20ºC).

6.4.5 Conclusions

Tensile results indicate that as-manufactured IF&P recrystallized SiC has sufficient strength—2,030 psi (14.0 MPa) in the hoop direction and 2,120 psi (14.6 MPa) in the axial direction —for operation in the hot gas filtration environment. Because the IF&P material has no clay or glass binder, strain-to-failure does not increase with temperature to 1,500ºF (815ºC) as for Schumacher and Pall materials. Therefore, less severe temperature gradients under back pulse cleansing conditions are required to cause cracks in the IF&P material based on 1,500ºF (815ºC) properties. Properties of all materials are needed to evaluate thermal stress sensitivity in the range of 1,000ºF (540ºC) to 1,400ºF (760ºC). The lack of clay binder which leads to lower strain-to-failure at 1,500ºF (815ºC) also leads to much higher thermal conductivity of IF&P, 125 Btu-in./hr ft^2-°F (18.0 W/m-K) at 1,000ºF (540ºC) compared to 38 Btu-in./hr-ft^2-°F (5.5 W/m-K) for Pall 326 and 51 Btu-in./hr-ft^2-°F (7.3 W/m-K) for Schumacher TF20. The greater thermal conductivity means that under thermal transient conditions, the temperature gradients will be less severe in IF&P than in the clay-bonded SiC materials. The higher conductivity was sufficient during the October 1998 thermal transient at the PSDF to prevent failure of the IF&P filters when the clay-bonded SiC filters failed.

The relatively higher thermal conductivity and the recent success during the thermal transient at the PSDF indicate that additional materials characterization as well as operational experience are warranted for IF&P recrystallized SiC. Several issues remain which affect long-term performance. These issues include 1.) the low strain-to-failure at elevated temperature, 2.) “inherent toughness” or resistance to microcrack propagation, and 3.) chemical compatibility, including SiC oxidation in PFBC operation, in the hot gas cleanup environment.

6.5 Ensto Aluminum Oxide

Ensto has manufactured aluminum oxide candle filters with a microstructure similar to the clay-bonded SiC materials. That is, individual particles connected by bridges.

The hope is for this material to provide the same chemical advantages as Coors P-100A-1, no oxidation of SiC particles and no degradation of clay binder, with the "inherent toughness" provided by Schumacher and Pall materials. Properties of the Ensto material were measured to 1.) provide screening before this material is installed for operation at the PSDF, 2.) begin development of a material property database to conduct mechanical and thermal analysis, and 3.) obtain baseline data for comparisons with properties measured after operation.

6.5.1 Density

Bulk density was measured on nine hoop tensile specimens and the results are summarized in Table 6.5-1. The average density was 117.6 lb./ft^3 (1.885 gr/cm^3). Three adjacent specimens removed from near the flanged end and all had densities ~1.0% greater than any of the other six specimens.

6.5.2 Tensile Results

Hoop tensile results are summarized in Table 6.5-2. Individual values are shown on the cutting plans of Figure 4.0-21. The average hoop tensile strength was 940 psi (6.5 MPa). The three specimens from near the flanged end which had the highest density also had the highest tensile strength, ~15% greater than the average of the other six. Strain gages were mounted on two specimens and Young's modulus values of 2.2 Msi (15.2 GPa) and 2.8 Msi (19.3 GPa) and strain-to-failure values of 0.41 mils/inch (0.041%) and 0.40 mils/inch (0.040%) were obtained.

Axial tensile stress-strain responses at RT and 1,500ºF (815ºC) are shown in Figure 6.5-1. Results are summarized in Table 6.5-3. The tensile properties were near the same at RT and 1,500ºF (815ºC) with the tensile strength ranging from 740 psi (5.1 MPa) to 980 psi (6.8 MPa) and strain-to-failure ranging from 0.35 mils/inch (0.035%) to 0.55 mils/inch (0.055%).

6.5.3 Thermal Expansion

Unit thermal expansion is shown in Figure 6.5-2. The average CTE from 500°F (260ºC) to 1,500ºF (815ºC) was 4.0 x 10^{-6} in./in./°F (7.2 x 10^{-6}/ºC). The strain-to-failure and thermal expansion together indicate a temperature gradient (T_{body} - $T_{surface}$) of ~110°F (60ºC) required to cause microcracking under back pulse conditions discussed previously.

6.5.4 Thermal Conductivity

Thermal conductivity is plotted in Figure 6.5-3. The measured conductivity was 6.8 Btu-in.-hr-ft^2-°F (1.0 W/m-K) at RT and 6.0 Btu-in.-hr-ft^2-°F (0.9 W/m-K) at 1280°F (690ºC). The maximum temperature gradient, T_{OD}-T_{ID}, calculated for Ensto with a 320°F(180ºC)/60 sec heating rate on one surface would be ~290°F (160ºC).

6.5.5 Conclusions

Ensto has higher thermal expansion than Coors, CTE of ~4.0 x 10^{-6}/°F (7.2 x 10^{-6}/ºC) from 500°F (260ºC) to 1,500ºF (815ºC) compared to ~2.8 x 10^{-6}/°F (5.0 x 10^{-6}/ºC), and lower strain-to-failure than Coors, ~0.45 mils/inch (0.045%) at 1,000ºF (540ºC) compared to ~0.80 mils/inch (0.080%). This combination will lead to microcracking of Ensto at less severe temperature gradients than Coors. Thermal conductivity of Ensto is also lower than Coors, ~6 Btu-in./hr-ft^2-°F (0.9 W/m-K) at compared to ~10 Btu-in./hr-ft^2-°F (1.4 W/m-K)at 1,000ºF (540ºC)°F, which leads to more severe temperature gradients during thermal transients. The properties obtained indicate that microcracking due to thermal stress is likely to occur during the thermal transients encountered at the PSDF.

7.0 Material Comparisons

As-manufactured room temperature tensile strengths of eleven candidate candle filter materials are compared in Figure 7.0-1. Test results obtained under this contract and under contract to DOE/FETC are included for comparison. This figure shows a wide range of tensile strengths of the various materials. Because the mechanical loads encountered during operation have not been quantified, the maximum strength requirements have not been determined. When mechanical loads on the candle filters are identified and quantitized, it is the ability to carry these loads, not the value of tensile strengths which will be critical. From the average axial tensile strengths, the maximum load each candle filter can withstand has been calculated and the results are plotted in Figure 7.0-2. These maximum load capability values could allow some manufacturers options for improving the performance of their elements. If a particular element can withstand a specified load easily, then the manufacturer would have options such as decreasing the wall thickness or varying density and porosity while maintaining acceptable permeability if these changes would improve the thermal performance.

Tensile strength has been used to monitor candle filter degradation during operation. The tensile strengths of Coors, Schumacher, and Pall elements are plotted versus hours of operation in the PSDF in Figure 7.0-3. The strength of Coors elements decreased ~10-15% during ~615 hours of operation. Longer term operation of Coors elements was not obtained because of the failures. The hoop tensile strength of Schumacher TF20 and T10-20 decreased during the first 800 hours but results from one T10-20 element tested after 1239 hours of operation indicate that the strength may level off after this initial decrease. Testing of elements with more hours of operation will confirm this. Little change was seen in the axial tensile strength of Schumacher materials for up to 1250 hours of operation in the PSDF. Candle-to-candle variability in Pall 326 and 442T make conclusions about strength degradation of these materials during operation impossible.

Failures in the PSDF to date have resulted from thermal stresses during transient events, primarily coal combustion inside the PCD. Susceptibility of an element to failure during these events depends on

1. thermal expansion and tensile strain-to-failure which determine the temperature gradient required to initiate microcracking,
2. thermal conductivity (diffusivity) which determines the magnitude of the temperature gradients during a thermal transient, and
3. the microstructure which determines whether microcracks are likely to propagate and result in candle failure.

Thermal expansions of candle filter materials, some measured under this contract and some under DOE/FETC contract, are shown in Figure 7.0-4. From the thermal expansions and strain-to-failure, the gradients (T_{body}-$T_{surface}$) required to initiate microcracking were estimated and are tabulated below. These temperature gradients were calculated assuming a flat plate initially at a uniform temperature and the temperature of one surface suddenly decreased by the amount shown. As discussed earlier, the calculation is a good approximation of pulse cleaning but not good during thermal transients. Also, the strain-to-failure values used in the calculation were based on elevated temperature measurements for some materials and room temperature values for others. Because of the assumptions in making the calculations the gradients shown represent only a relative comparison of different candle filters. Even with the shortcomings discussed, this table illustrates that a large strain capability and low thermal expansion help decrease the likelihood of microcracking for a given temperature gradient.

Material	Average CTE 500°F (260ºC) - 1,500ºF (815ºC)		Strain-to-Failure		Temperature Gradient	
	(10^{-6}/°F)	(10^{-6}/°C)	mils/inch	(%)	°F	(ºC)
Pall 326	2.8	(5.0)	0.60[1]	(0.060)	210	(120)
Pall 181	2.8	(5.0)	0.46[1]	(0.046)	160	(90)
Schumacher TF20	2.5	(4.5)	0.40[1]	(0.040)	170	(95)
IF&P REECER™	2.7	(4.9)	0.13[1]	(0.013)	50	(30)
Coors P-100A-1	2.8	(5.0)	0.80[1]	(0.080)	280	(160)
Ensto	4.0	(7.2)	0.46[1]	(0.046)	120	(70)
Blasch 4-270	4.1	(7.4)	0.30[2]	(0.030)	70	(40)
Dupont PRD-66C	2.2	(4.0)	1.65[2]	(0.165)	750	(420)
McDermott	4.6	(8.3)	2.10[2]	(0.210)	460	(260)

Notes: 1. Probable value at 1,000ºF (540ºC).
2. Probable value at RT.

During the thermal transients encountered at the PSDF, Coors P-100A-1 failed despite a relatively large temperature gradient required to initiate microcracking where IF&P survived despite relatively small temperature gradient required to initiate microcracking. This is due, at least in part, to thermal conductivity differences. The thermal conductivity of several candle filter materials is shown in Figure 7.0-5. Based on the thermal conductivity shown and the wall thickness of each candle, the temperature gradient generated during a 320°F (180ºC) increase in surface temperature over a one minute period was estimated. The results are plotted in Figure 7.0-6. The temperature gradients generated in low conductivity materials is much more severe than in high conductivity materials. For example, the temperature gradient in a Coors element is ~225°F (125ºC) while the gradient in an IF&P

REECER element is ~40°F (20ºC). Therefore, while the Coors material can accommodate more thermally induced strain than IF&P, the more severe temperature gradients encountered during the thermal transients lead to failure of Coors elements where IF&P REECER elements survived. Relatively large temperature gradients are generated in the McDermott and PRD-66 composite material also. However, these materials have ~3 to 4 times the strain capability (based on RT values) of Coors P-100A-1 and therefore have survived the thermal transients at the PSDF so far. Materials with a relatively low thermal conductivity, low strain-to-failure, and high thermal expansion, such as Blasch 4-270 and Ensto, will fail if the transient events which lead to large temperature gradients occur.

The microstructure of the materials also plays a role in determining whether microcracks which develop due to either thermal or mechanical stresses propagate and lead to failure of the candle. The clay-bonded SiC particle structure of Schumacher and Pall candles provides an inherent toughness in comparison with more homogeneous materials such as Coors P-100A-1 and Blasch 4-270. That is, more energy is required to drive a microcrack in the clay-bonded materials. The as-manufactured ceramic composite materials also have the toughness to resist microcrack propagation. Testing of these materials after operation will indicate whether that toughness is retained.

8.0 Conclusions

Based on the test results obtained in this program the following conclusions were obtained:

- Coors P-100A-1 elements failed during operation at the PSDF due to accumulated microcracking most likely caused by coal burning in the PCD during several transitions to coal.
- Thermal transients are likely to cause microcracking in Coors P-100A-1, Blasch 4-270, and Ensto candles because of their low-thermal conductivities.
- For operation at up to 1,400ºF (760ºC), the clay-bonded SiC particle materials from Schumacher and Pall potentially have a long life (thousands of hours) in the absence of major process upsets and temperature excursions.

References

1. Spain, J. D. and Starrett, H. S., “Physical, Mechanical and Thermal Properties of Refractron SiC Filter Material,” Report No. SRI-MME-94-253-6938.20.1-I-F, prepared for DOE/METC under Contract No. DE-AC21-89MC26233.

2. Spain, J. D. and Starrett, H. S., “Physical, Mechanical and Thermal Properties of Schumacher SiC Filter Material,” Report No. SRI-MME-94-253-6938.20.1-I-F, prepared for DOE/METC under Contract No. DE-AC21-89-MC26233.

3. Spain, J. D. and Starrett, H. S., "Physical, Mechanical and Thermal Properties of Coors Alumina Mullite Filter Material," Report No. SRI-MME-94-480-6938.20.1-I-F, prepared for DOE/METC under Contract No. DE-AC21-89-MC26233.

4. Spain, J. D. and Starrett, H. S., "Properties of Ceramic Candle Filters." Advanced Coal-Based Power and environmental Systems '97 Conference, Pittsburgh, Pennsylvania, July 22-24, 1997.

5. Spain, J. D. and Starrett, H. S., "Creep of Schumacher, Refractron, and Coors Ceramic Filter Materials," Report No. SRI-ENG-94-904-6938.20.1-IV-F, prepared for DOE/METC under Contract No. DE-AC21-89MC26239.

6. Pears, C. D. "A Model for the Response of Schumacher Glass Bonded-Silicon Carbide." Technical Note prepared for DOE/METC under Contract No. DE-AC21-89MC26239.

7. Pears, C. D., "A Model for the Response of Refractron Glass Bonded-Silicon Carbide," Technical Note prepared for DOE/METC under Contract No. DE-AC21-89MC26239.

8. Alvin, M. A., "Thermal/Chemical Degradation of Ceramic Cross-Flow Filter Materials – Final Report," DOE/METC Contract No. DE-AC21-88MC25034.

9. Alvin, M. A., "Filter Component Assessment," Advanced Coal-Based Power and Environmental Systems '97 Conference, Pittsburgh, Pennsylvania, July 22-24, 1997.

10. Pears, C. D., "Technical Note on Fracture Patterns in Coors P-100A-1 Alumina/Mullite Filter," Technical Note prepared for Southern Company Services under P. O. C-97-001785.

11. Technical Progress Report for M. W. Kellogg Transport Reactor Train With Westinghouse Particulate Control Device. TC02 Run Report, Section 3.8, prepared by Southern Company Services, DOE Cooperative Agreement Number DE-FC21-90MC25140, Final Report To Be Released in February 1999.

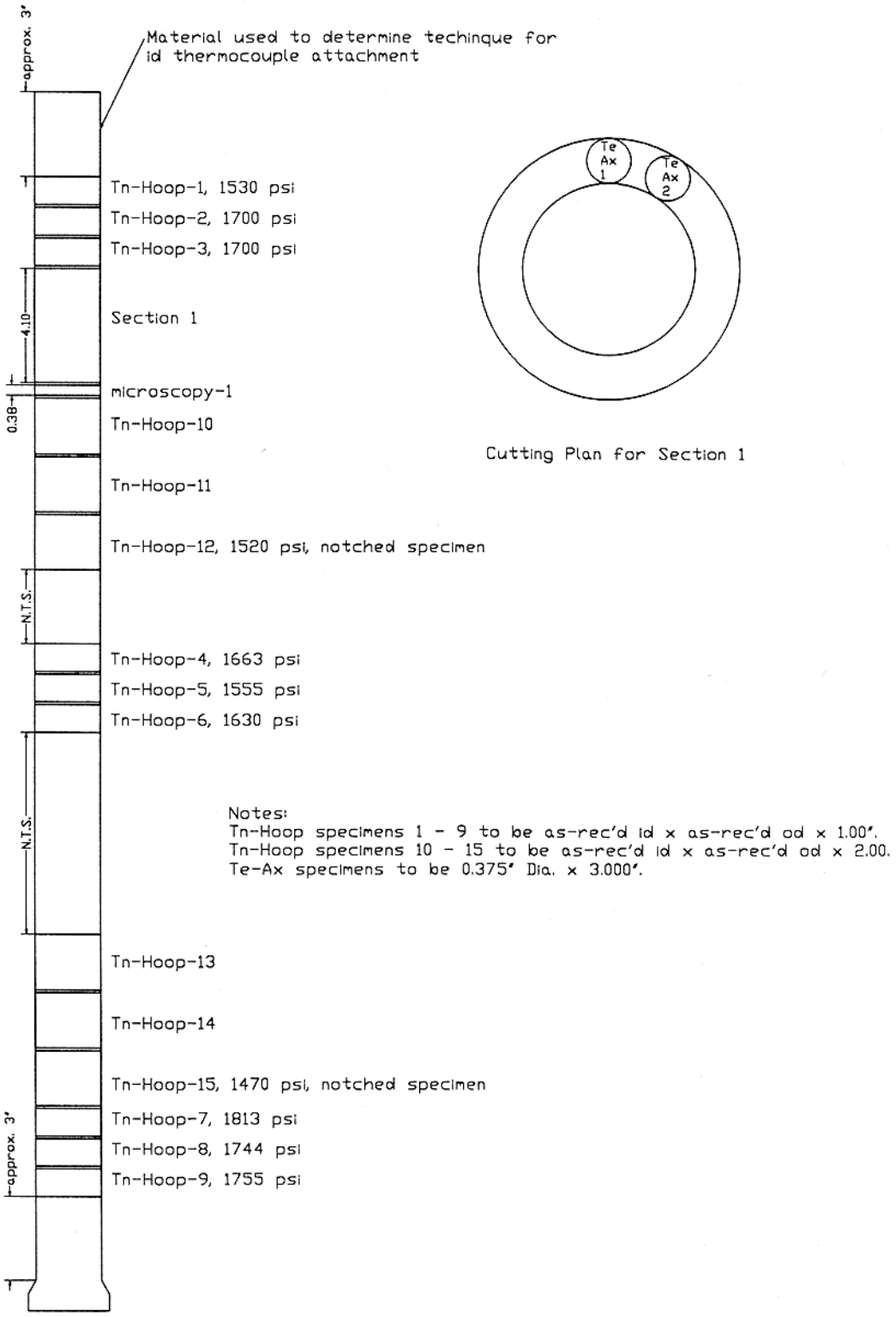

Figure 4.0-1. Cutting Plan for Virgin Coors Filter KC027

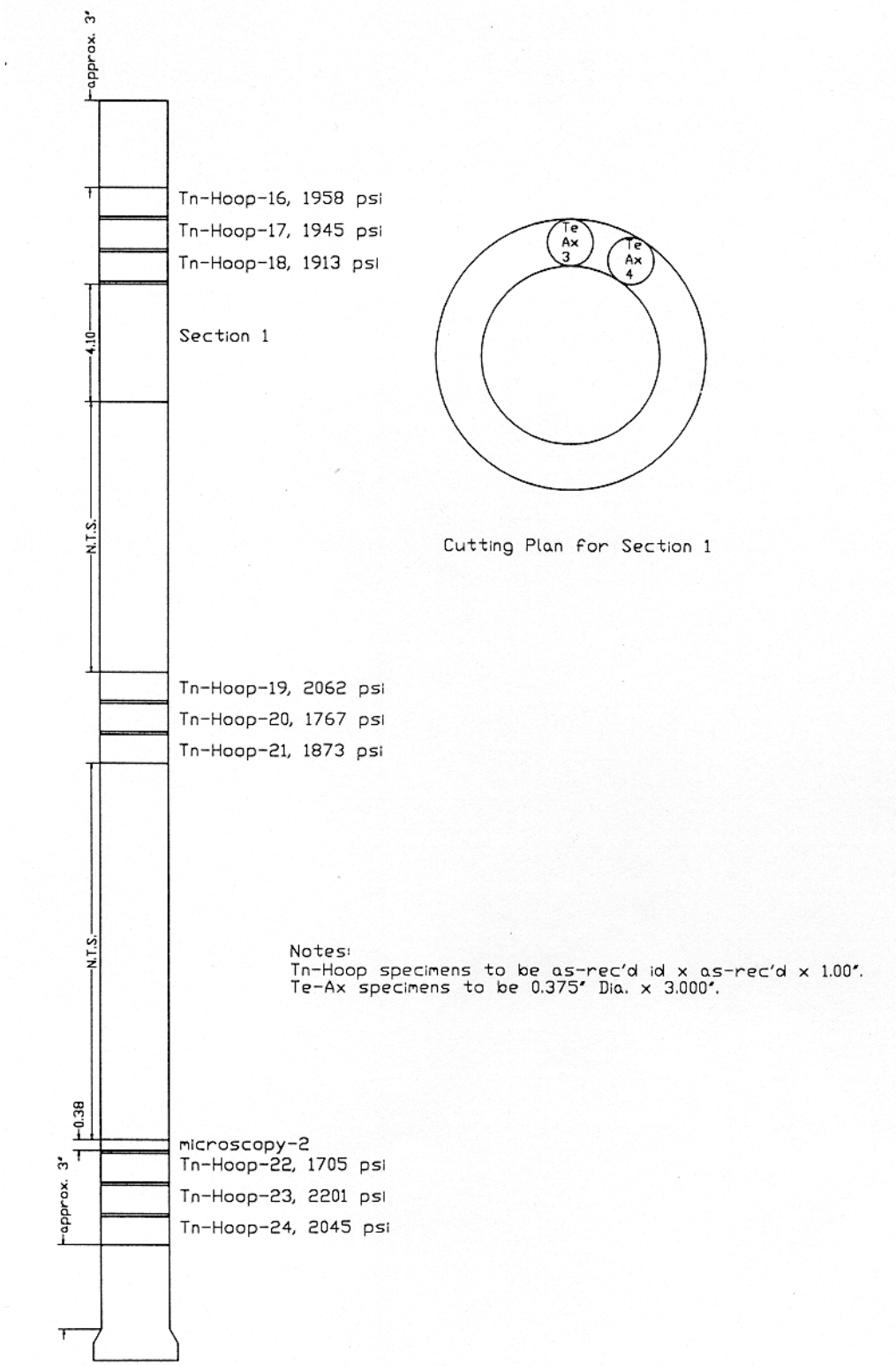

Figure 4.0-2. Cutting Plan for Virgin Coors Filter LC026

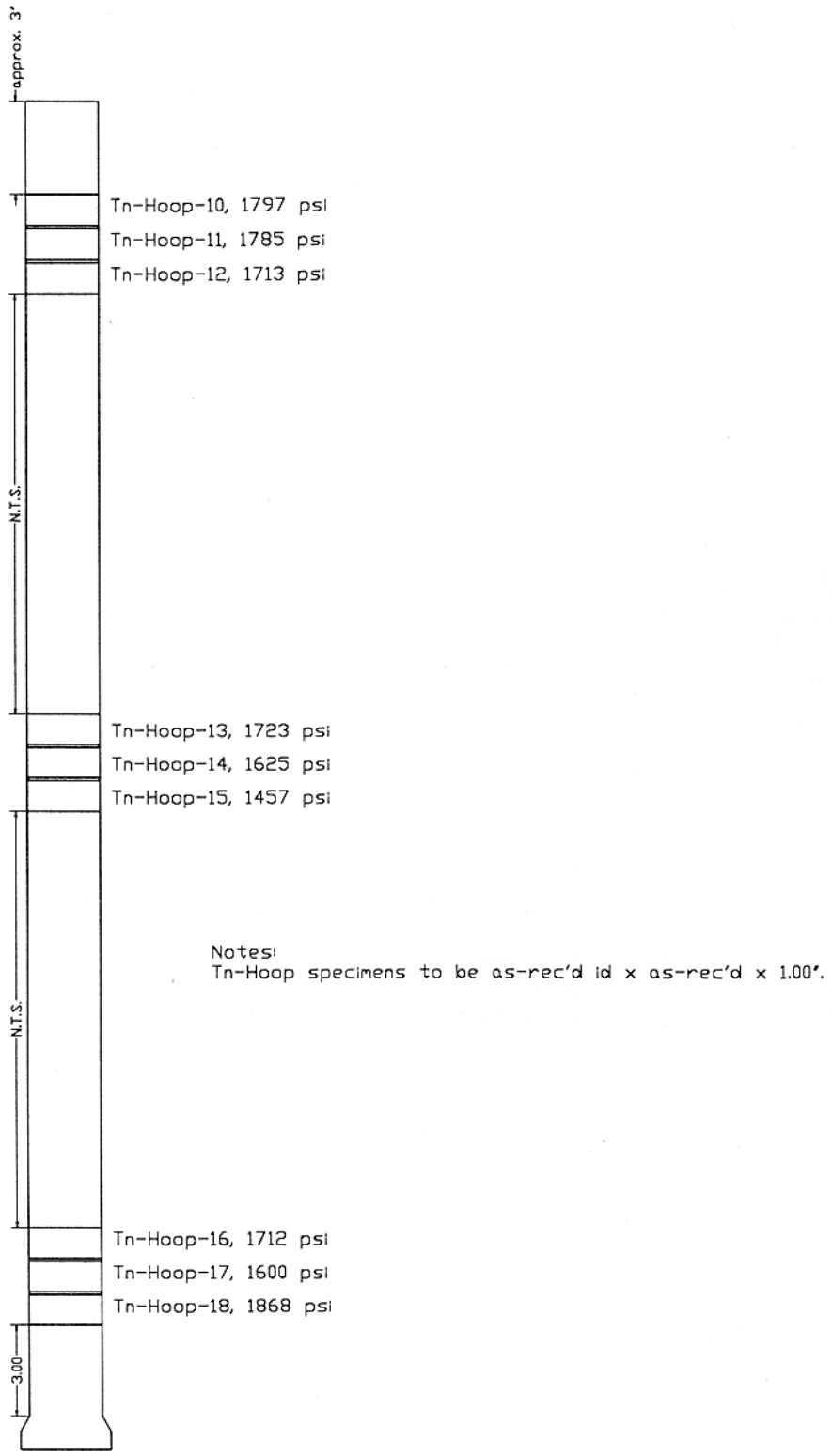

Figure 4.0-3. Cutting Plan for Coors Candle Filter KC005 after 616 Hrs at SCS

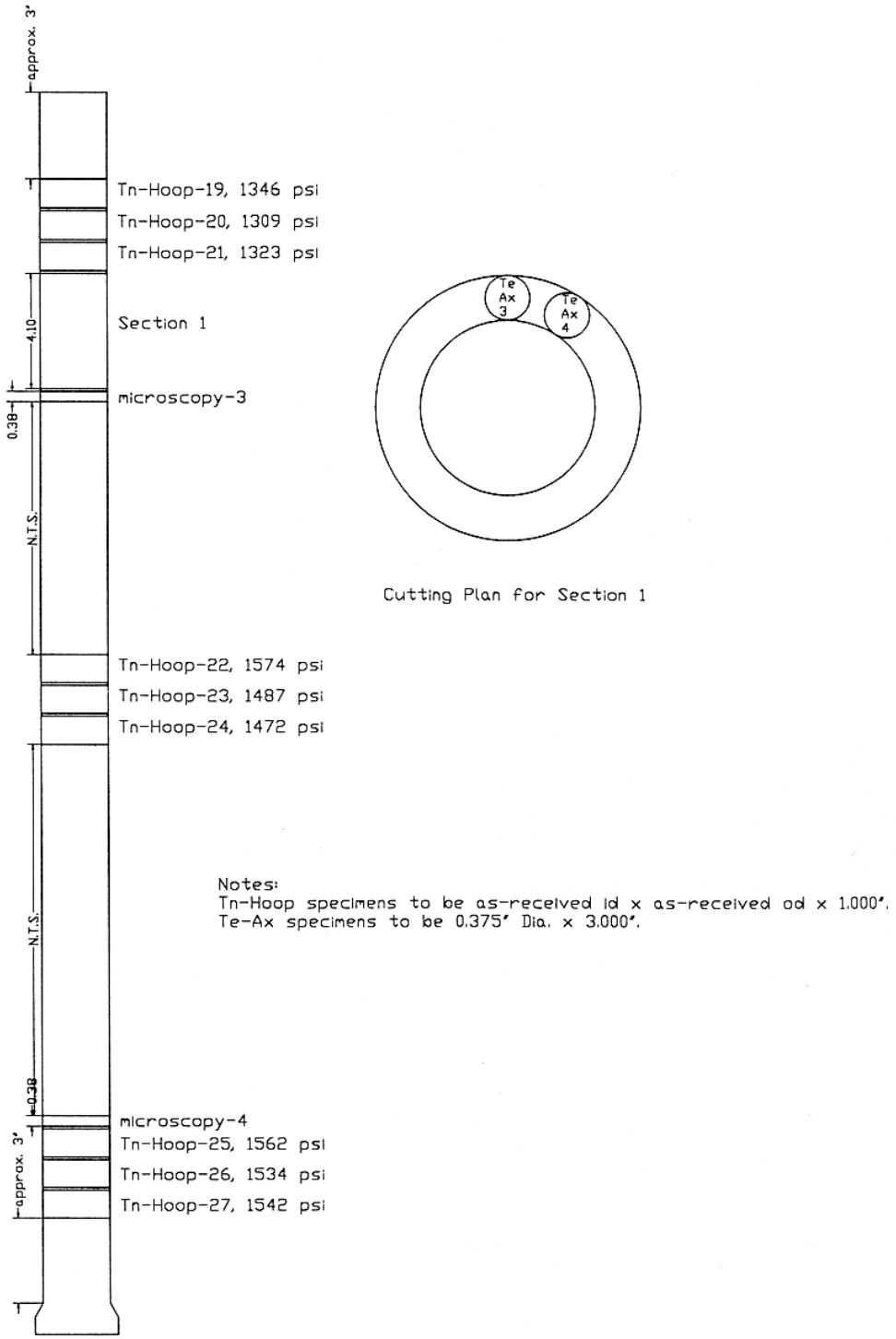

Figure 4.0-4. Cutting Plan for Coors Candle Filter KC011 after 616 Hrs at SCS

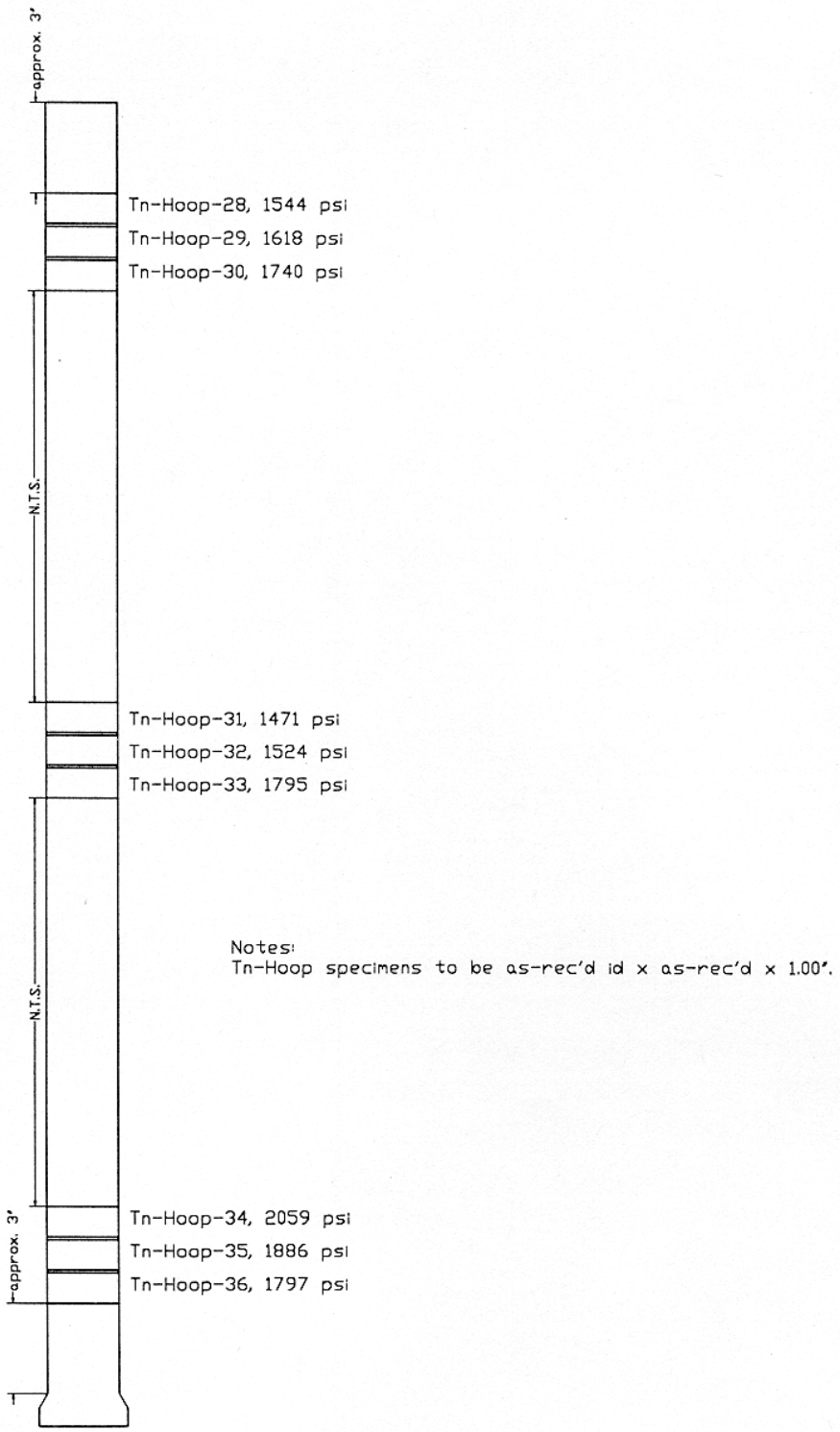

Figure 4.0-5. Cutting Plan for Coors Candle Filter LC025 after 616 Hrs at SCS

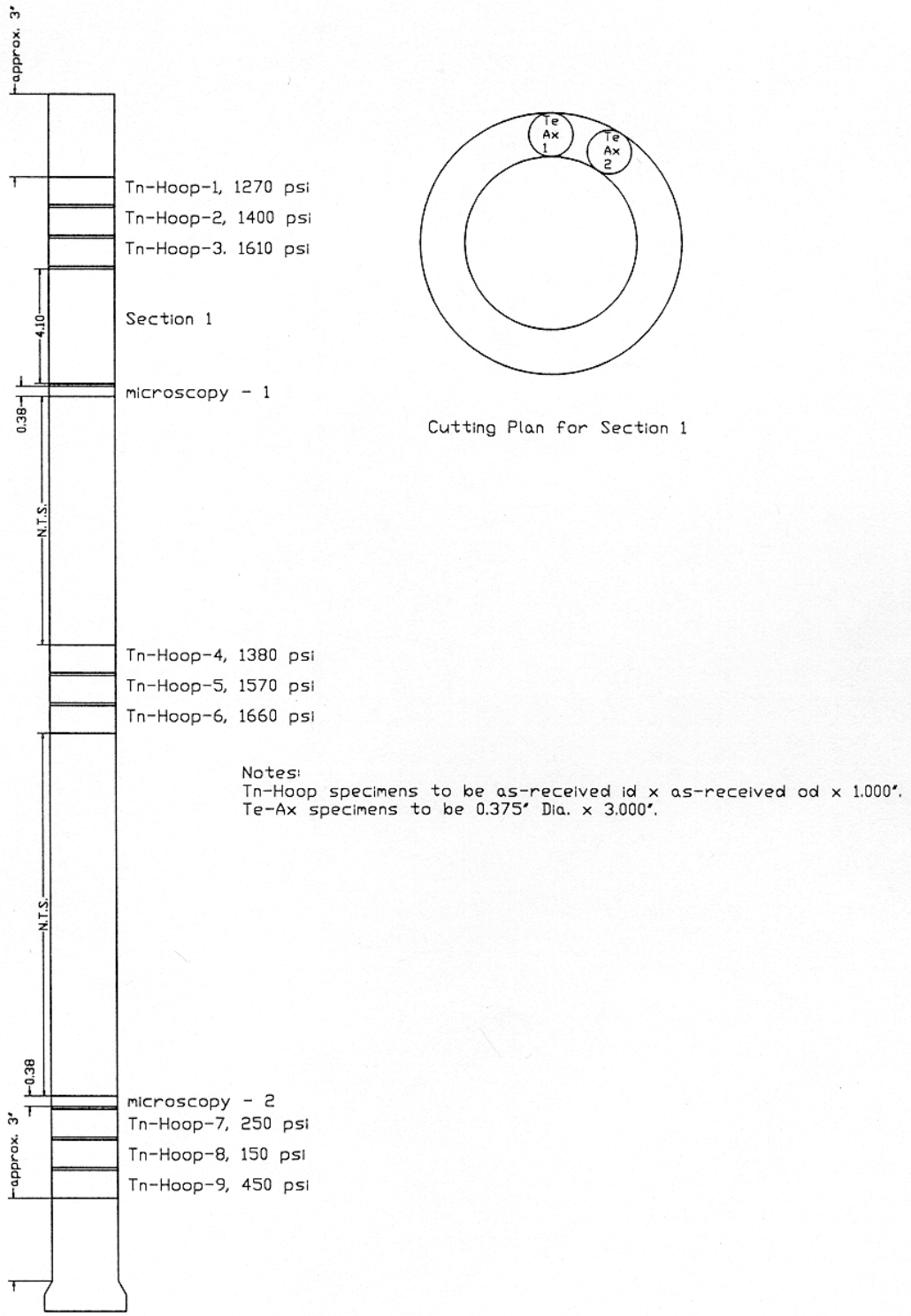

Figure 4.0-6. Cutting Plan for Coors Candle Filter Candle KC007 after 628 Hrs at SCS

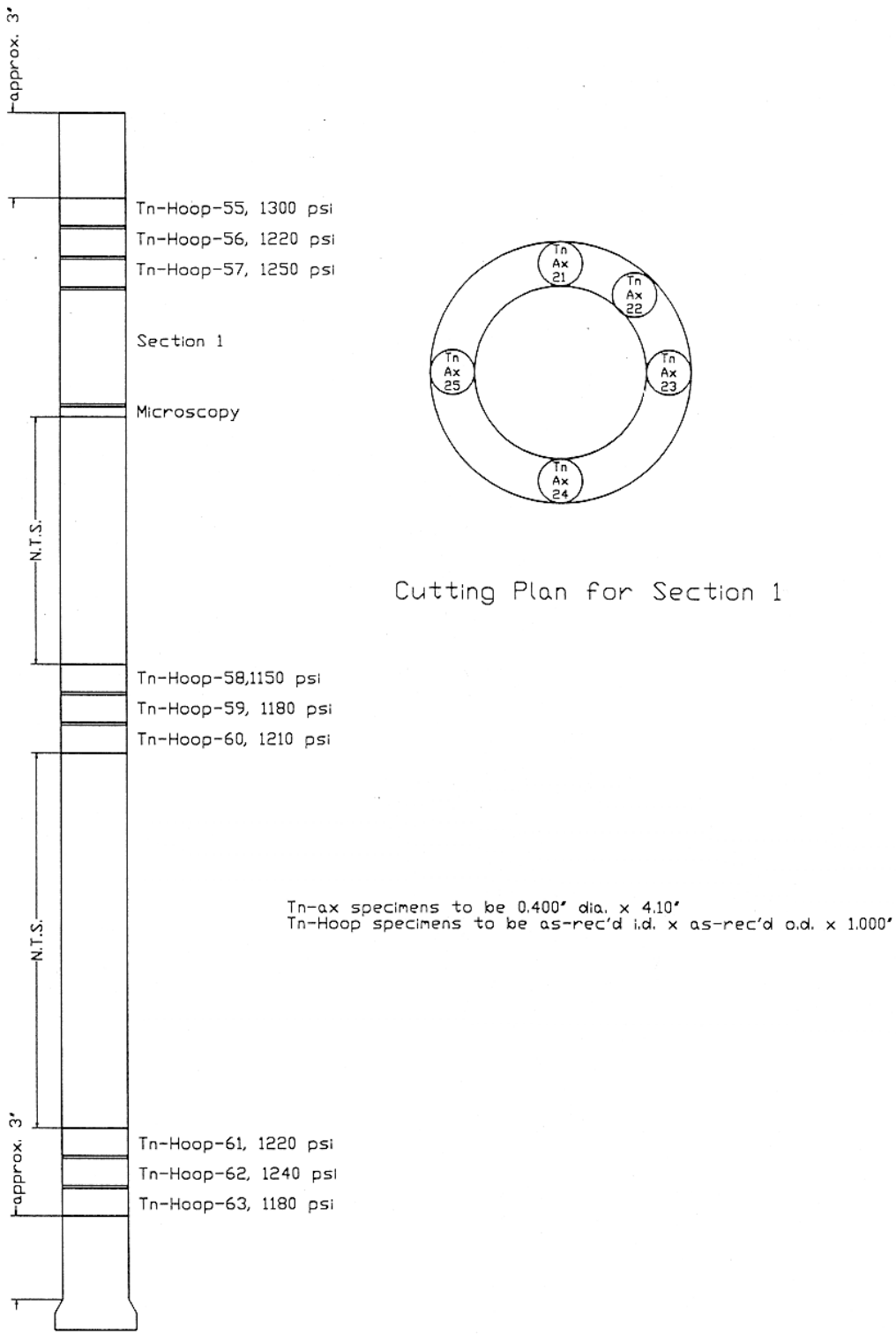

Figure 4.0-7. Cutting Plan for Schumacher TF20 Candle Filter 324H12 after 822 Hrs at SCS

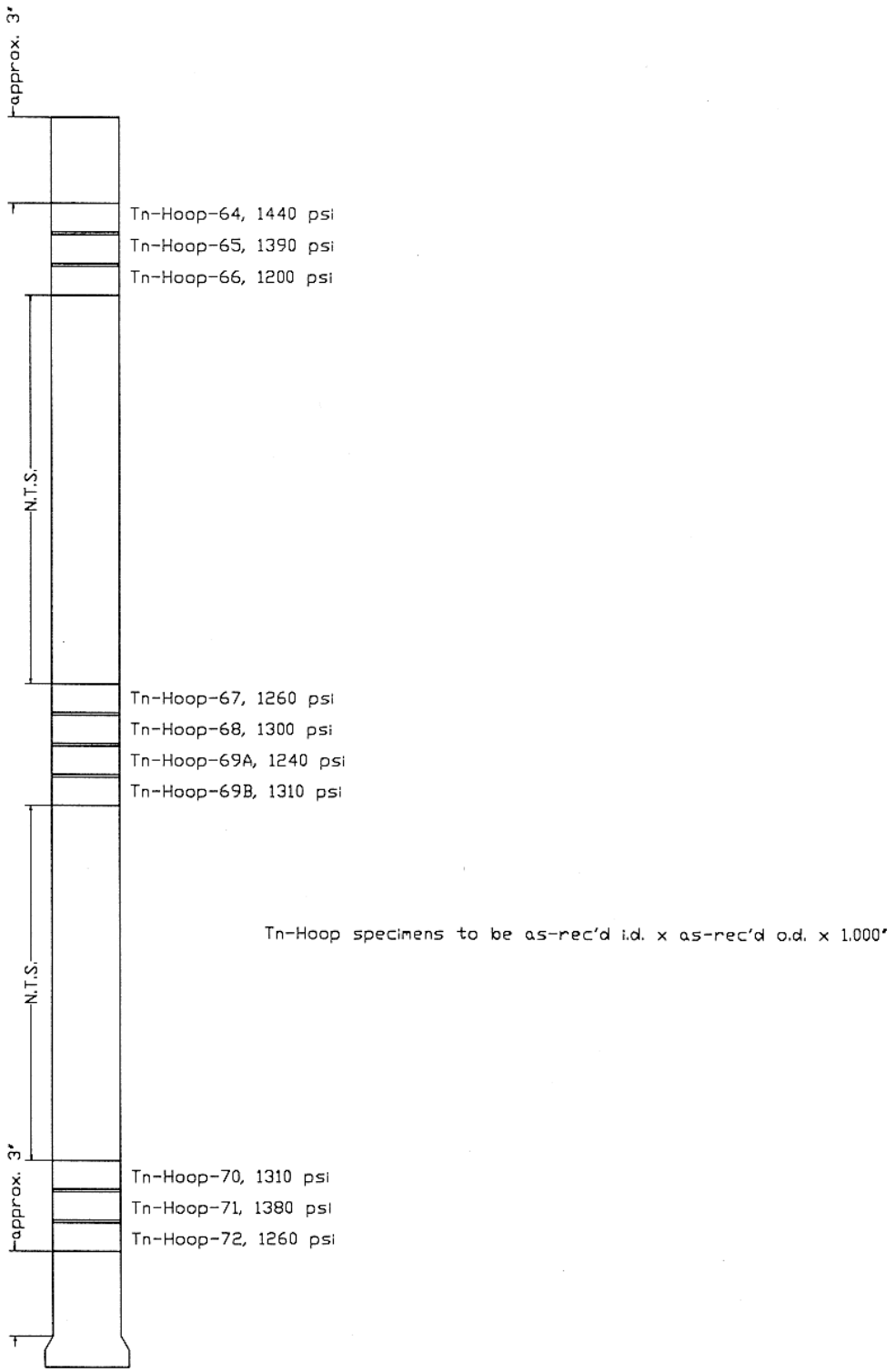

Figure 4.0-8. Cutting Plan for Schumacher TF20 Candle Filter 324H13r after 822 Hrs at SCS

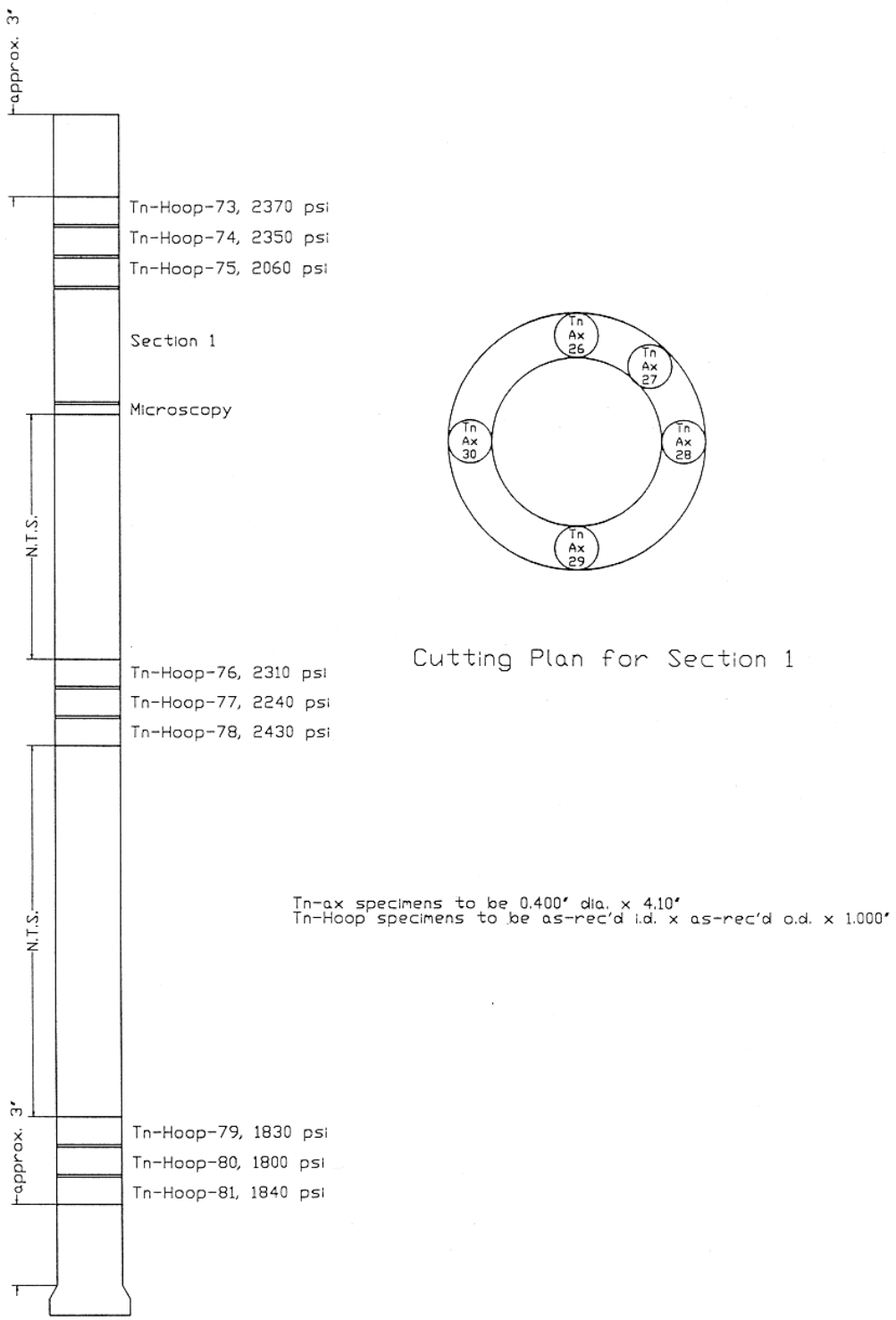

Figure 4.0-9. Cutting Plan for Virgin Schumacher T10-20 Candle Filter 360H071

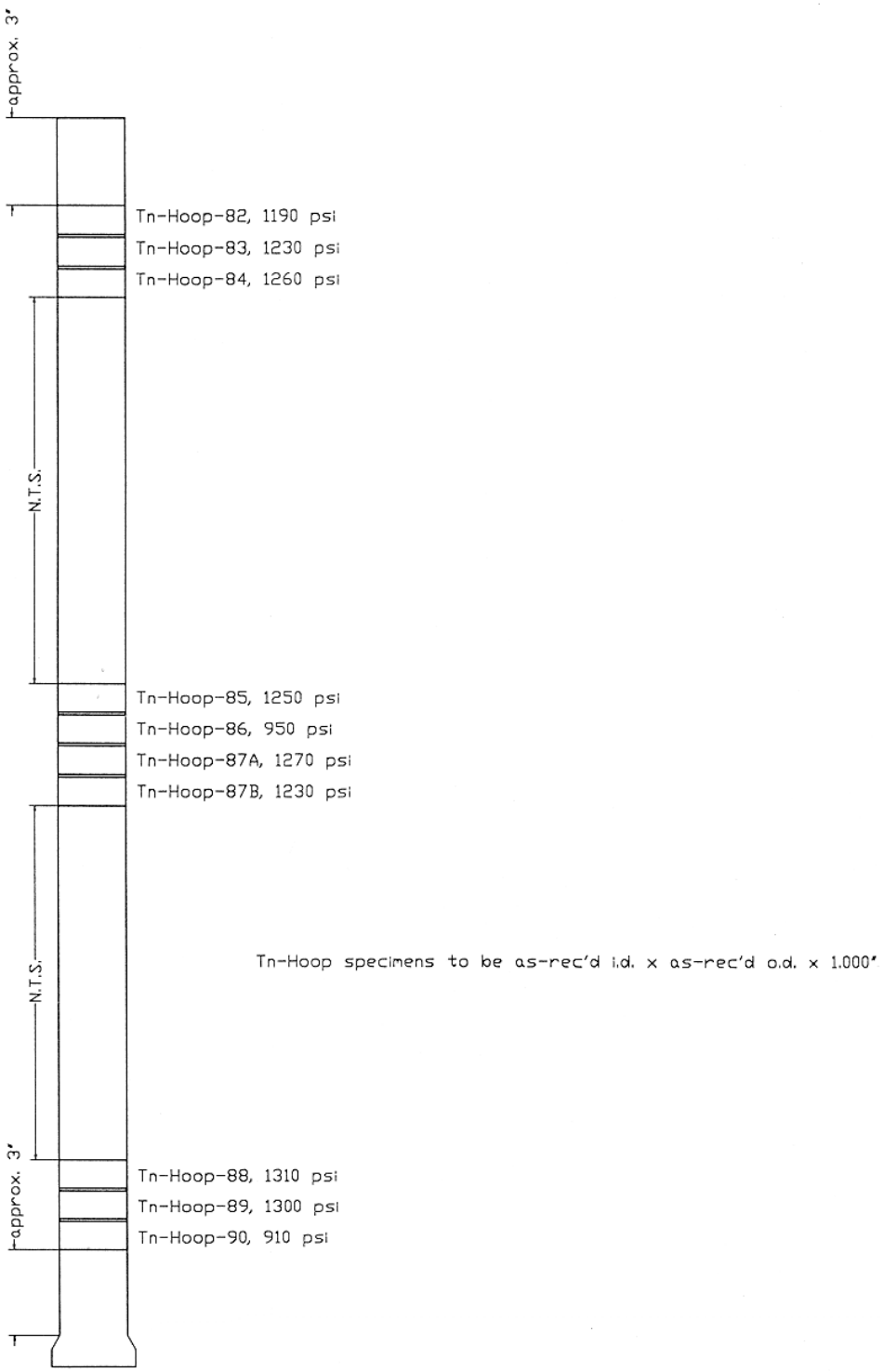

Figure 4.0-10. Cutting Plan for Schumacher T10-20 Candle Filter 324H016 after 810 Hrs at SCS

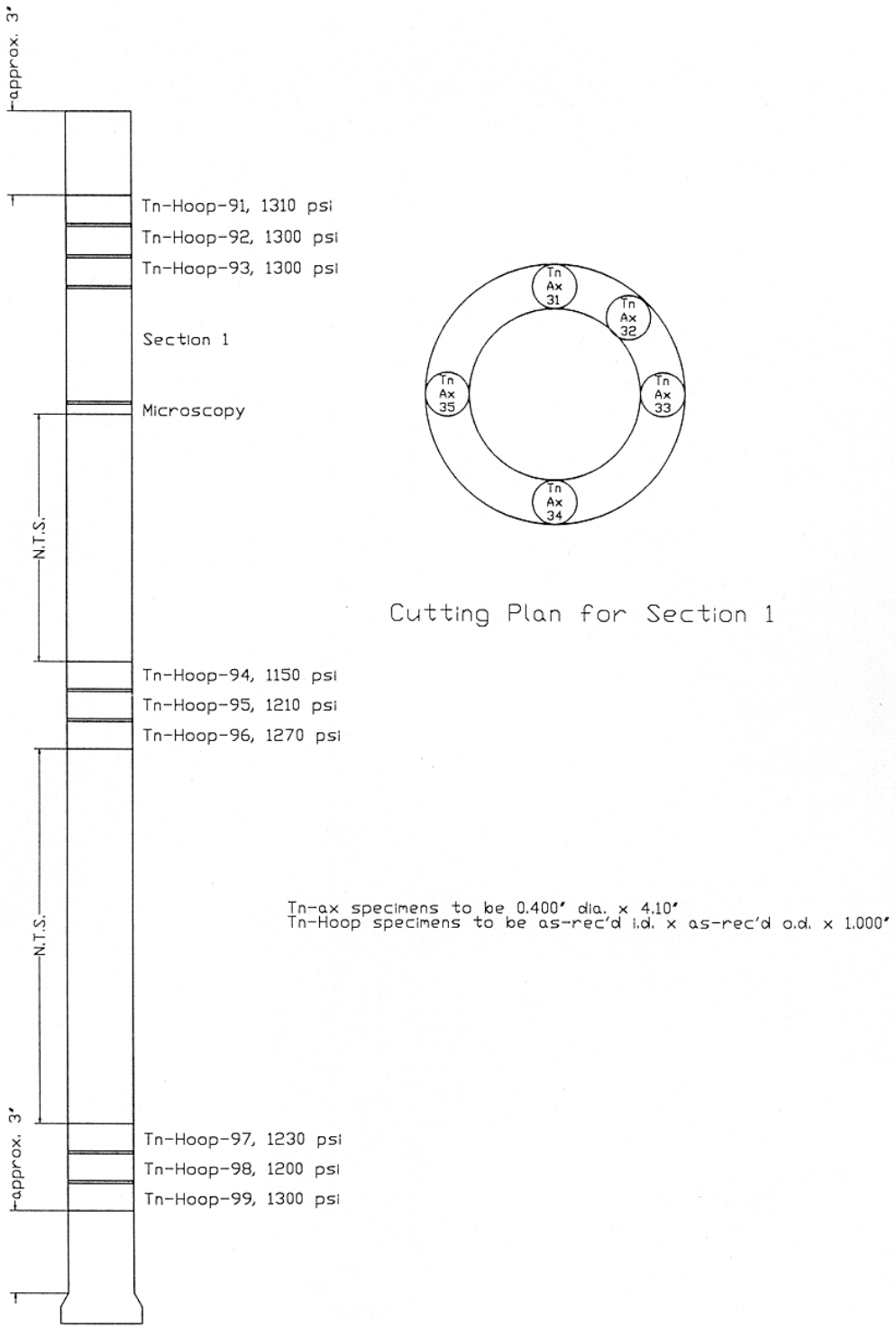

Figure 4.0-11. Cutting Plan for Schumacher T10-20 Candle Filter 324H018 after 1239 Hrs at SCS

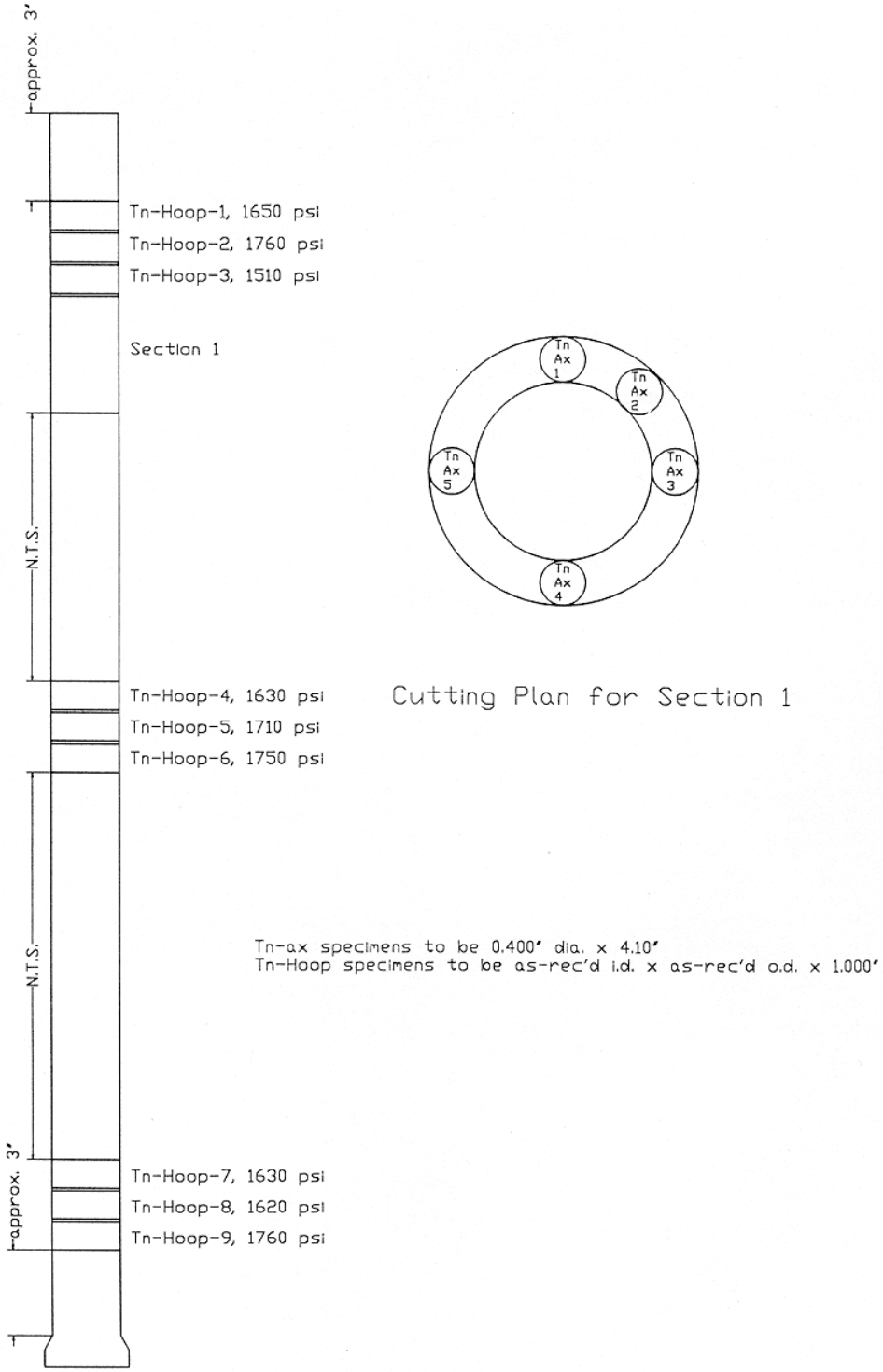

Figure 4.0-12. Cutting Plan for Pall 326 Candle Filter 3-24A after 429 Hrs at SCS

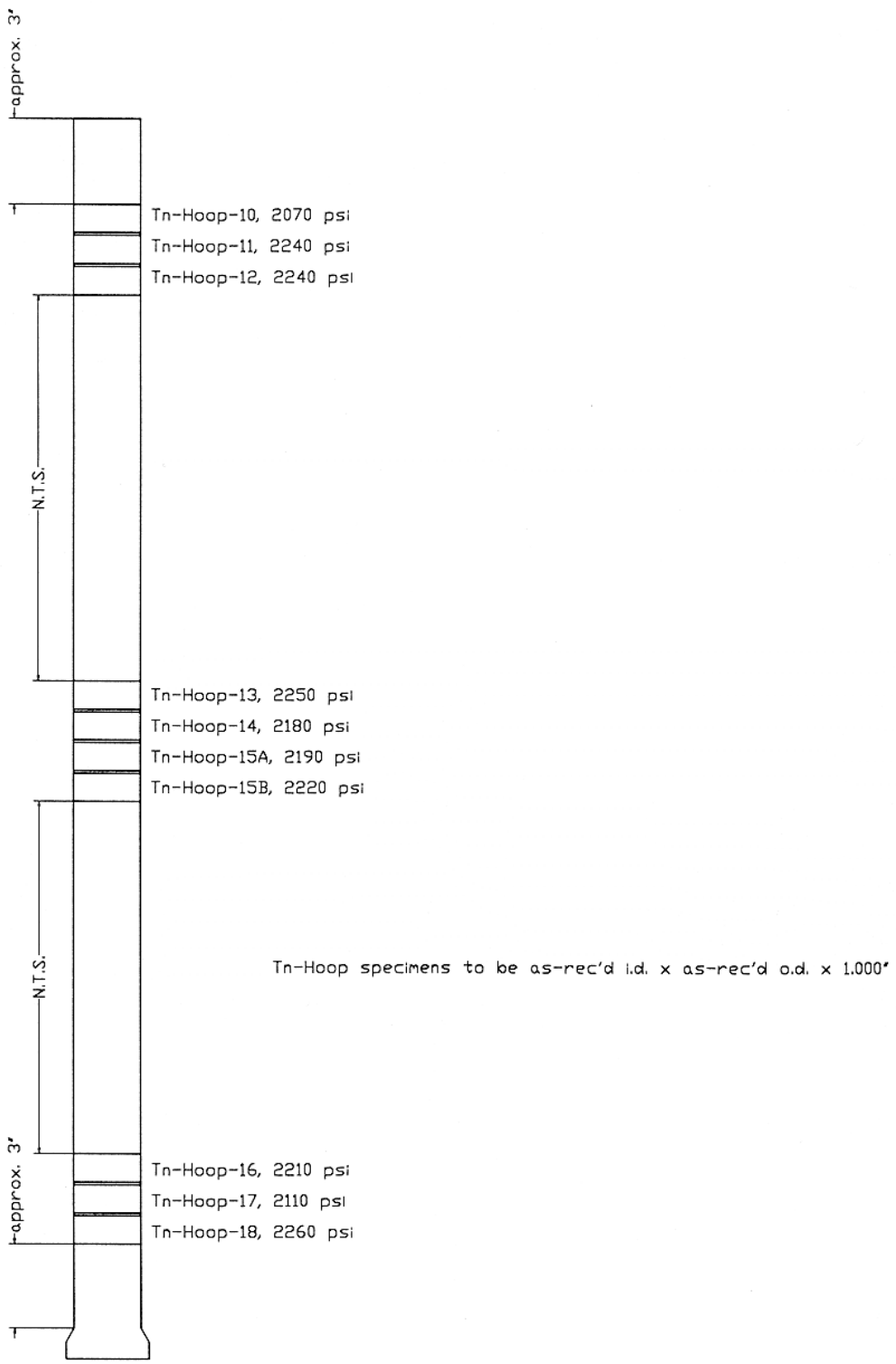

Figure 4.0-13. Cutting Plan for Pall 326 Candle Filter 1-36A after 429 Hrs at SCS

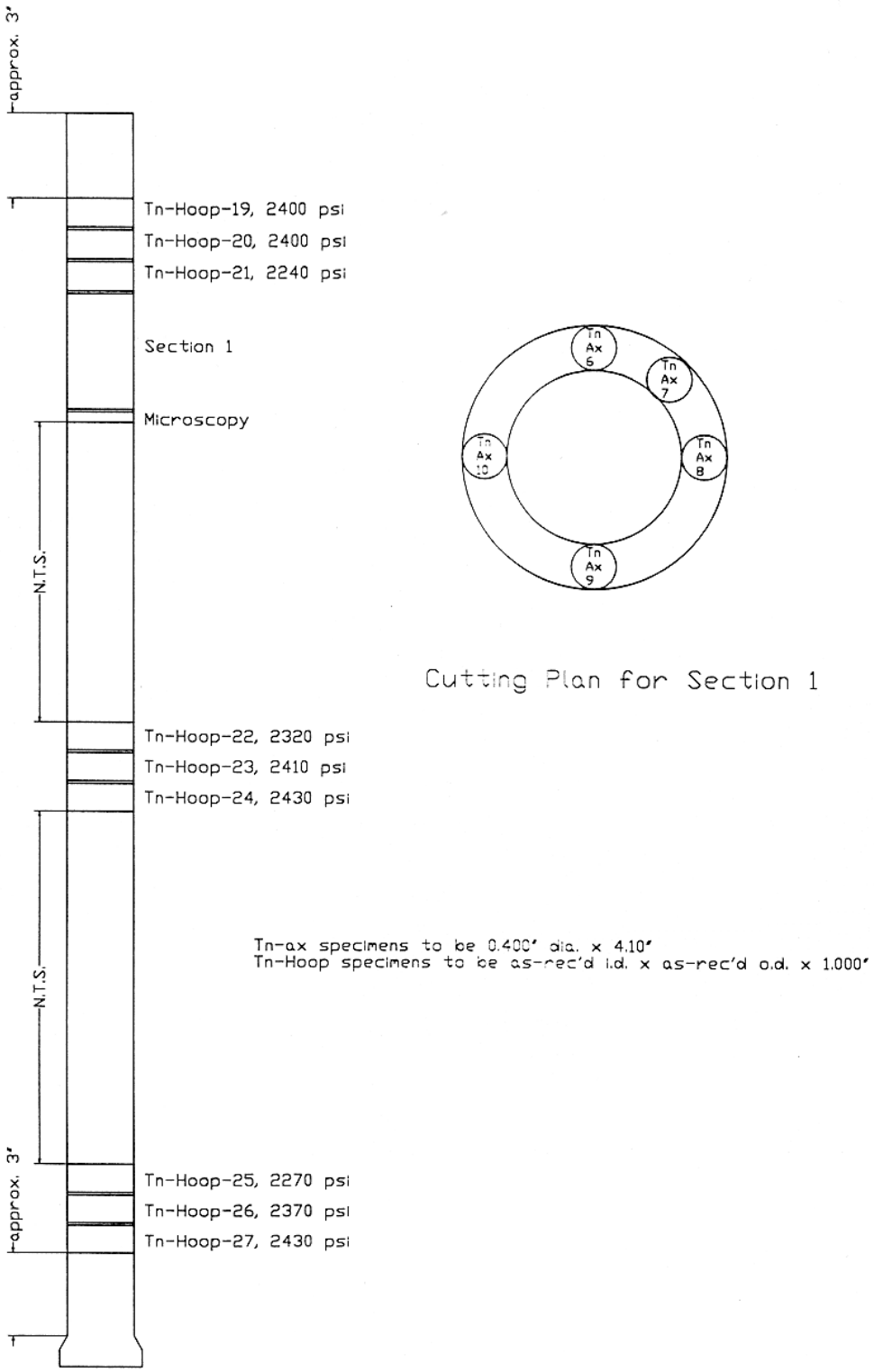

Figure 4.0-14. Cutting Plan for Pall 326 Candle Filter 4-991 after 1251 Hrs at SCS

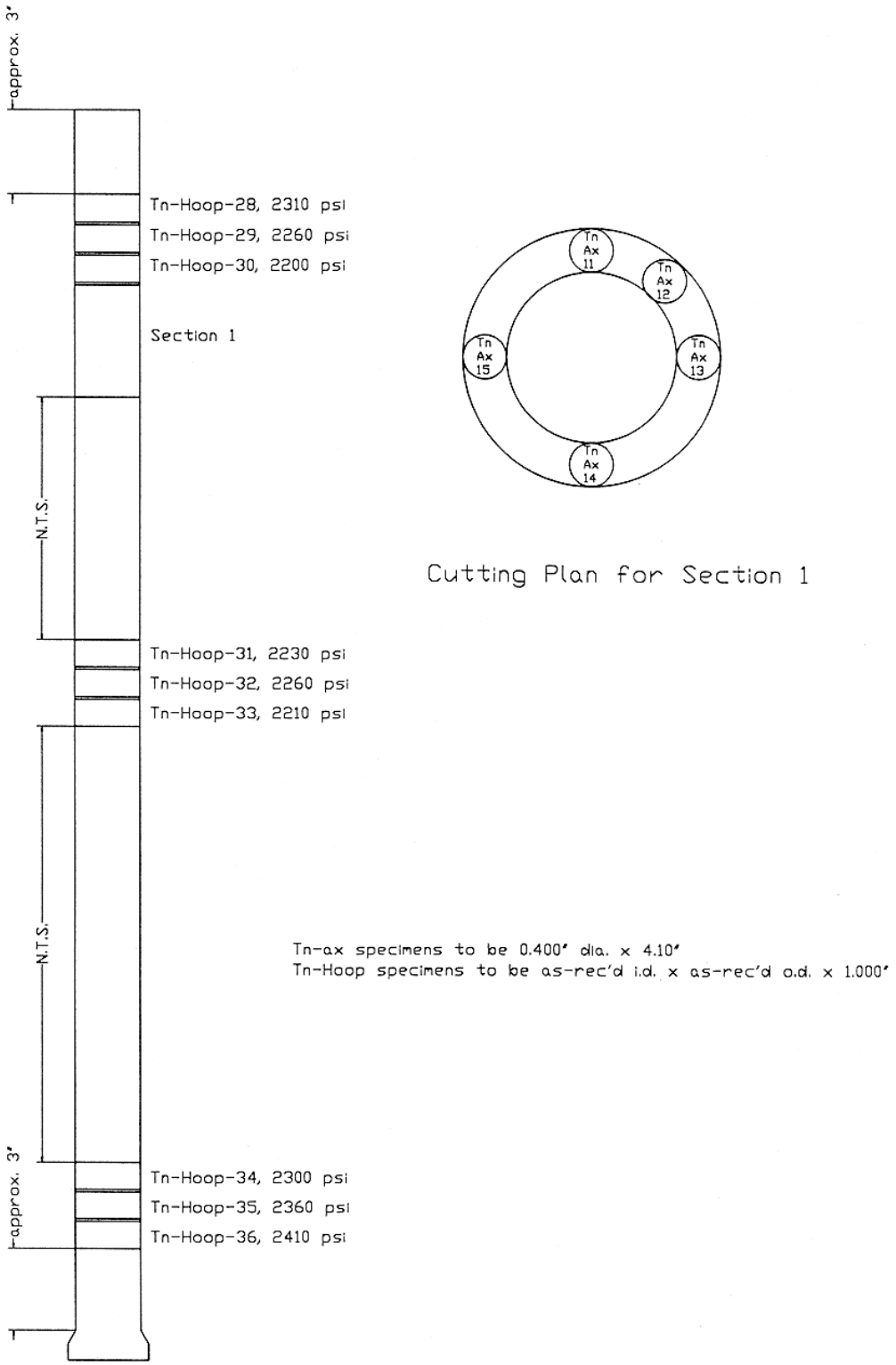

Figure 4.0-15. Cutting Plan for Pall 442T Candle Filter 1A-4 after 616 Hrs at SCS

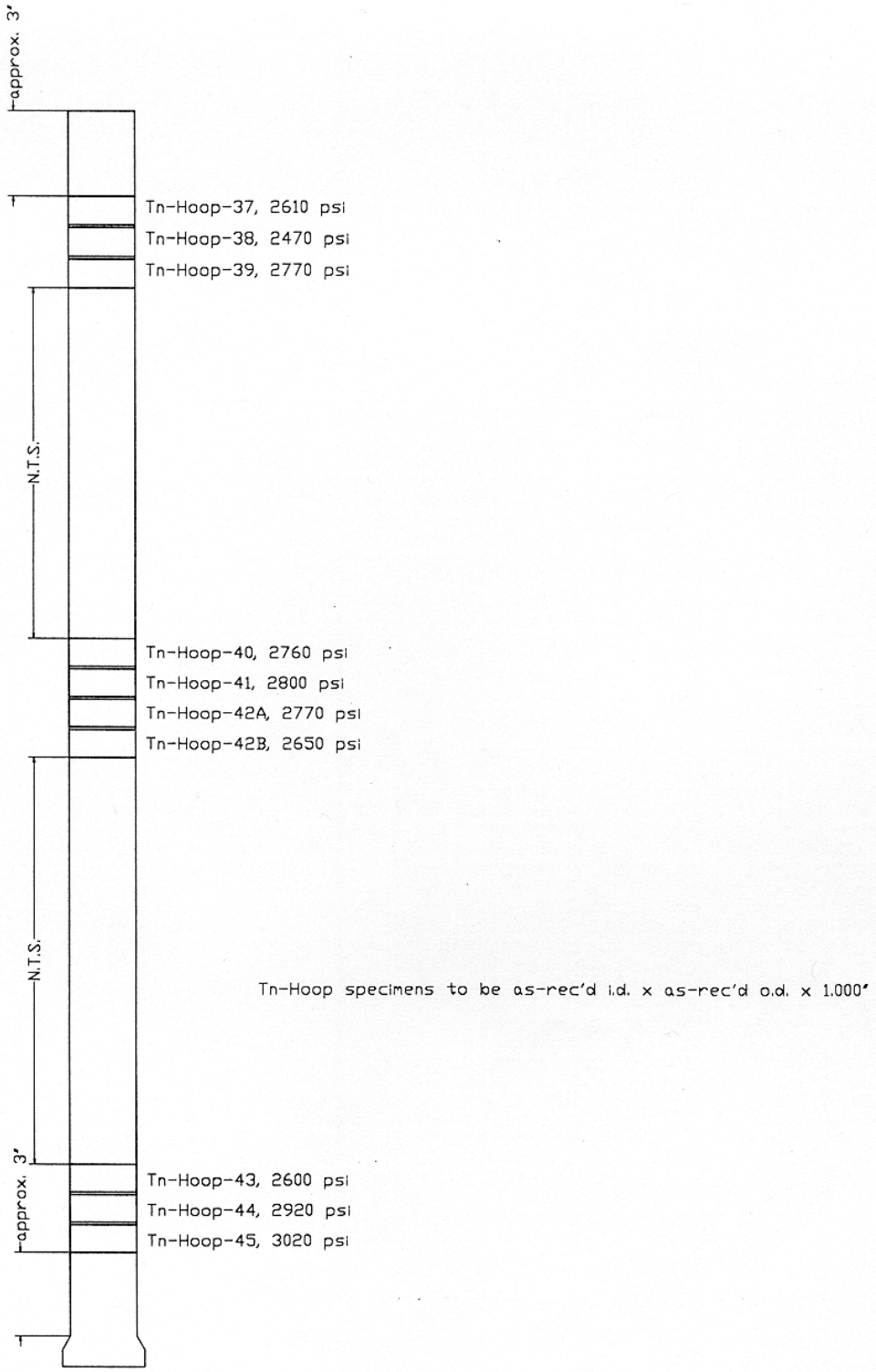

Figure 4.0-16. Cutting Plan for Pall 442T Candle Filter 5-948 after 1438 Hrs at SCS

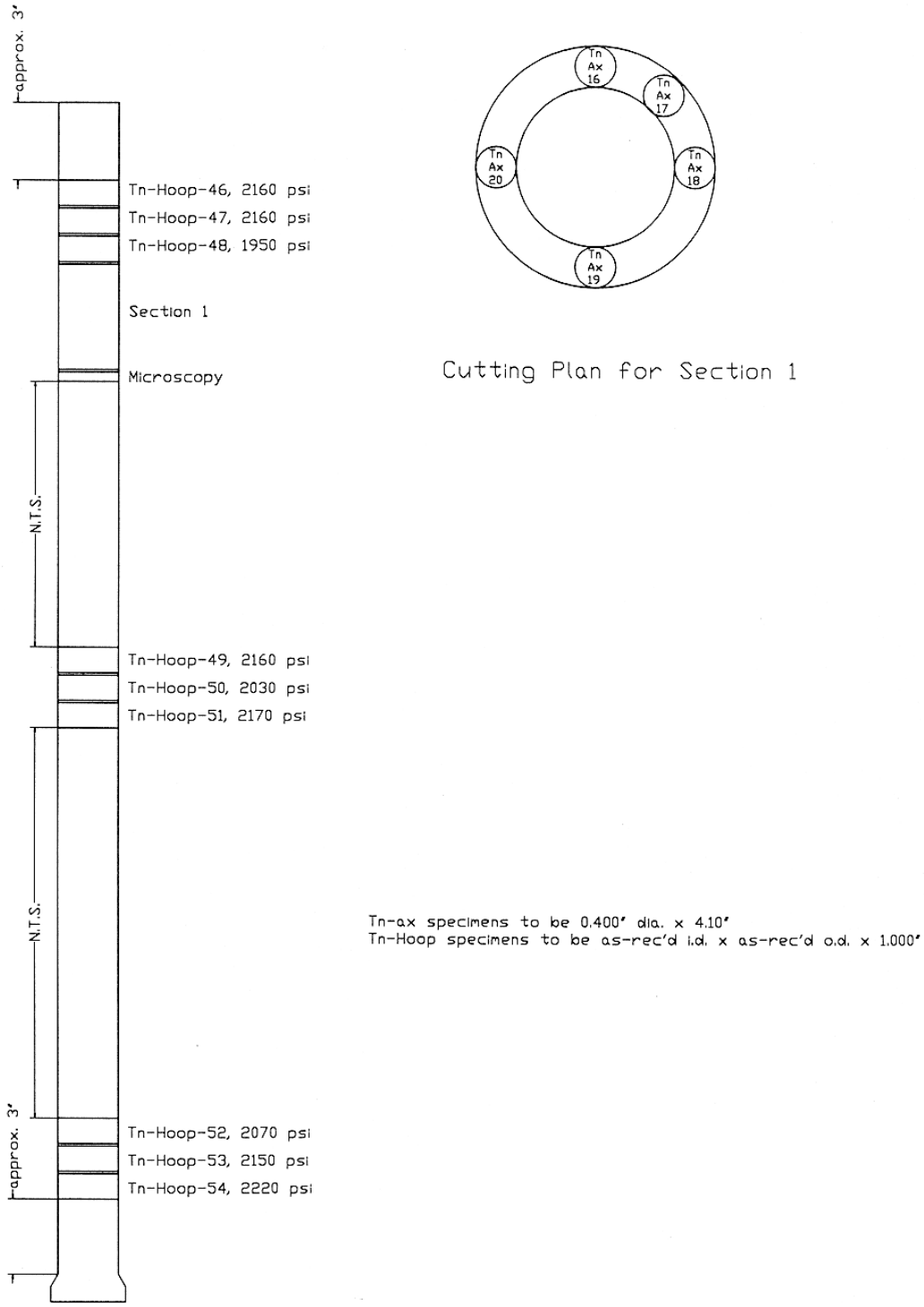

Figure 4.0-17. Cutting Plan for Pall 442T Candle Filter 2-1018 after 1867 Hrs at SCS

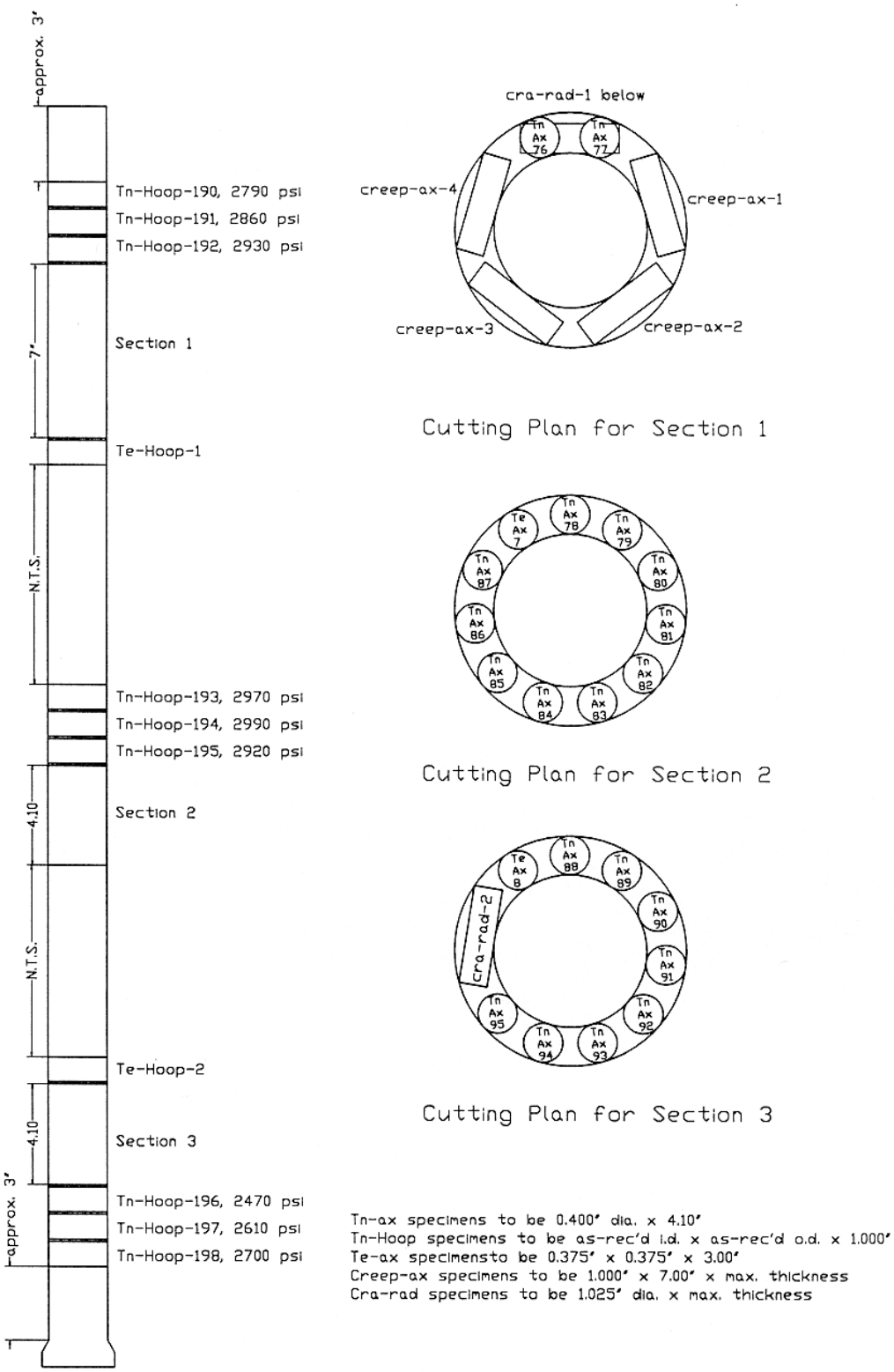

Figure 4.0-18. Cutting Plan for Virgin Pall 181 Candle Filter 7-1405H

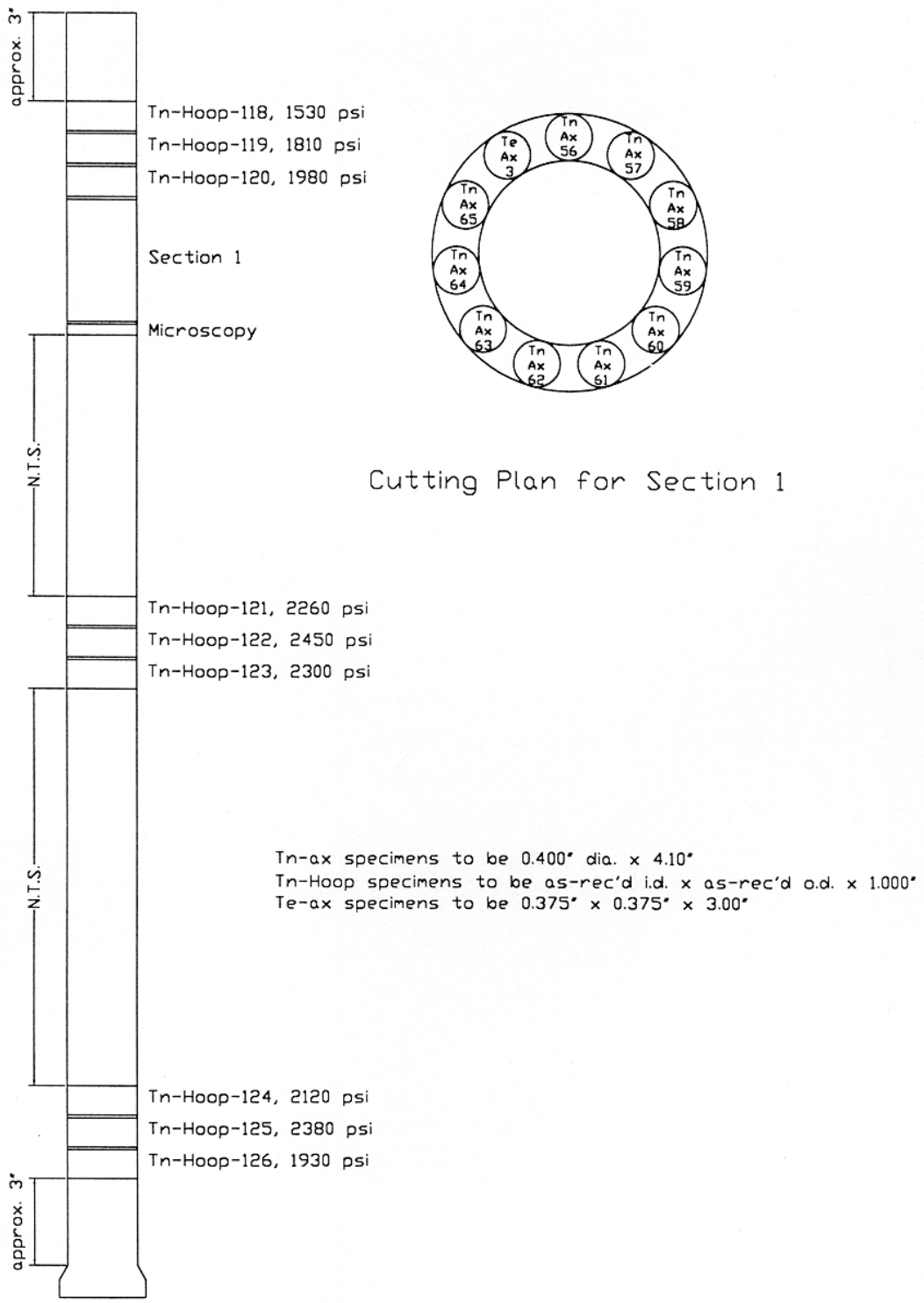

Figure 4.0-19. Cutting Plan for Virgin IF&P REECER Candle Filter FE98073109

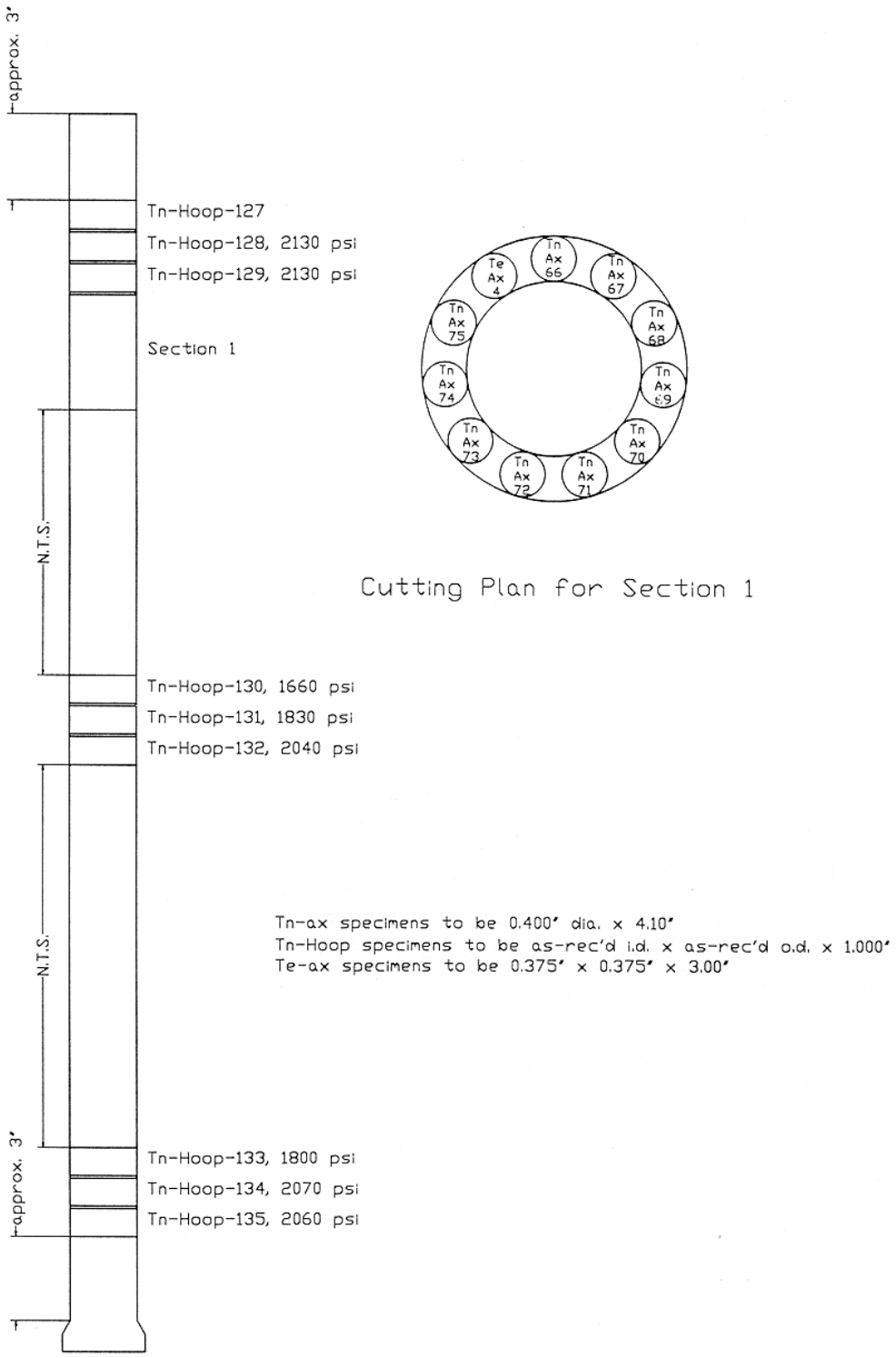

Figure 4.0-20. Cutting Plan for Virgin IF&P REECER Candle Filter FE98073110

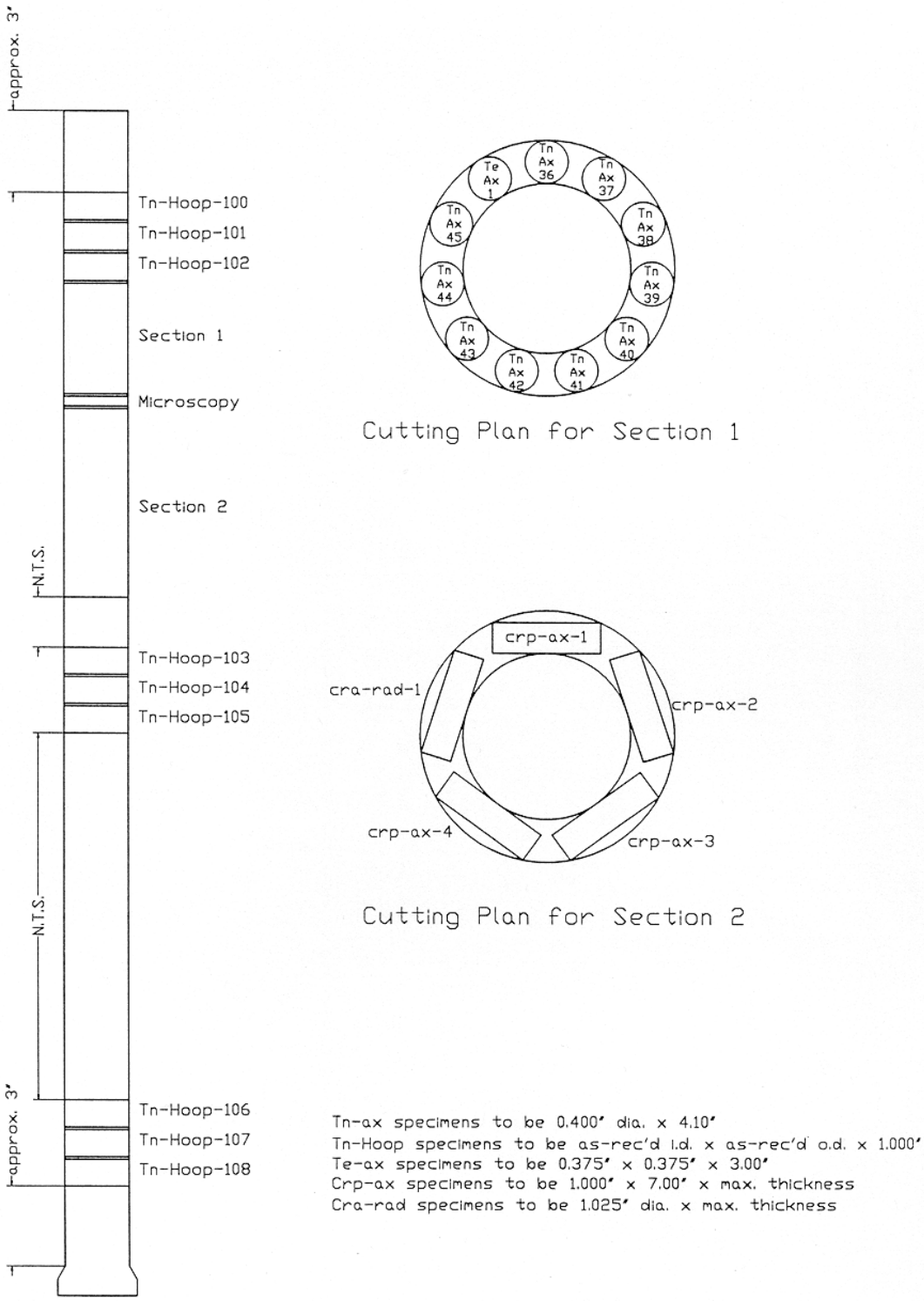

Figure 4.0-21. Cutting Plan for Virgin Ensto Candle Filter 146-97

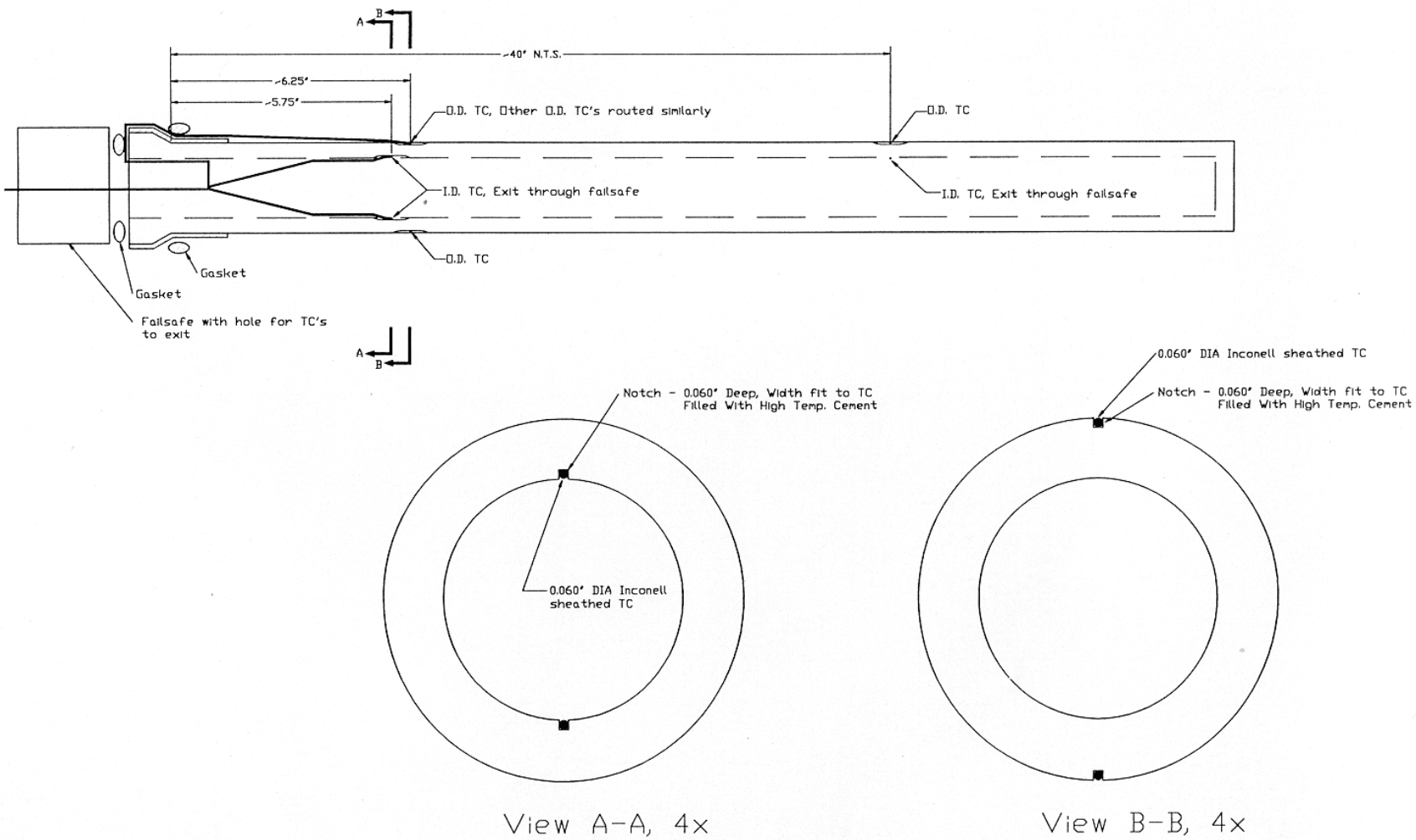

Figure 6.1-1. Thermocouple Locations and Configuration

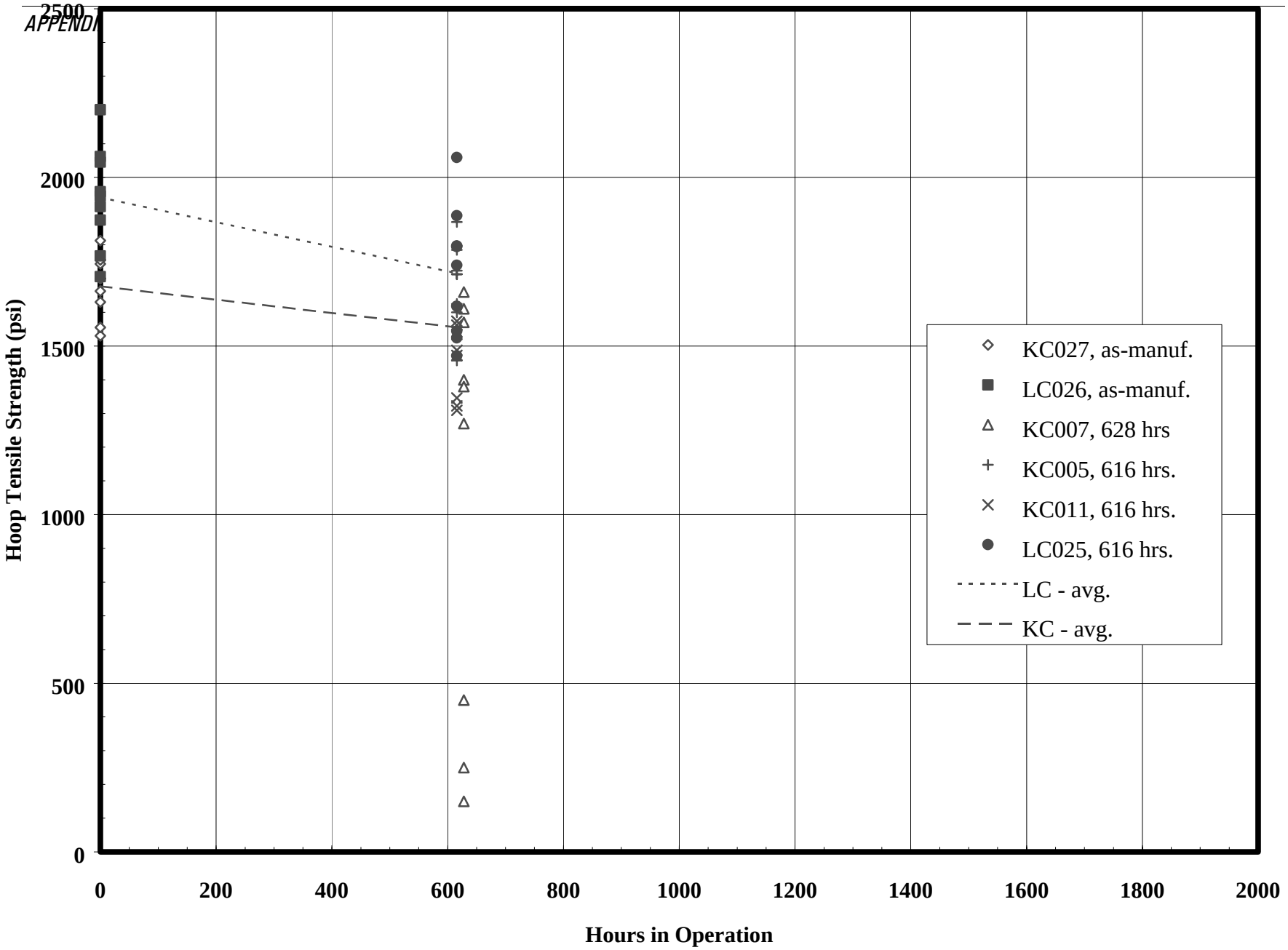

Figure 6.1-2 Hoop Tensile Strength of Coors P-100A-1 Versus Hours in Operation

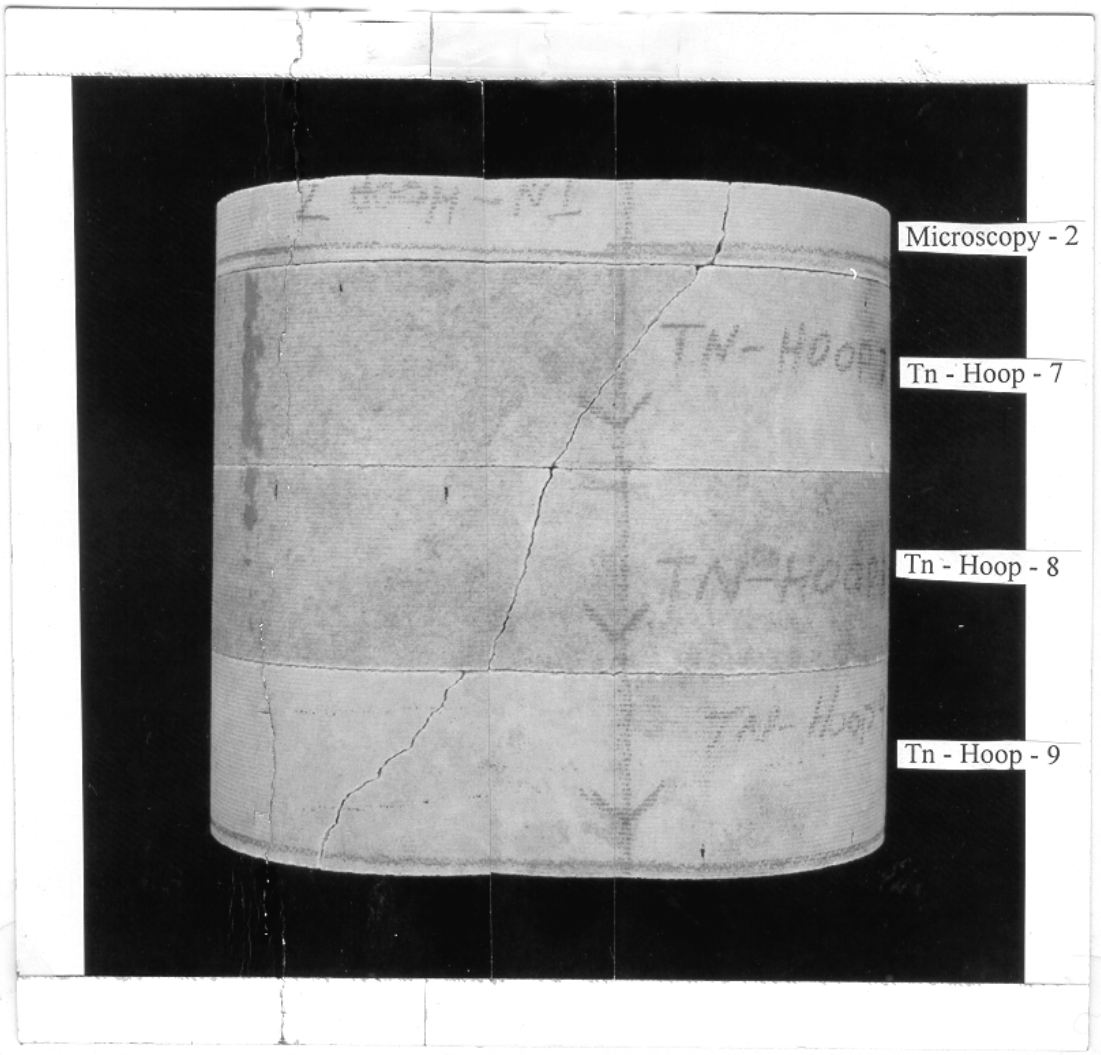

Figure 6.1-3. Failed Specimen Tn-Hoop-7, 8, and 9

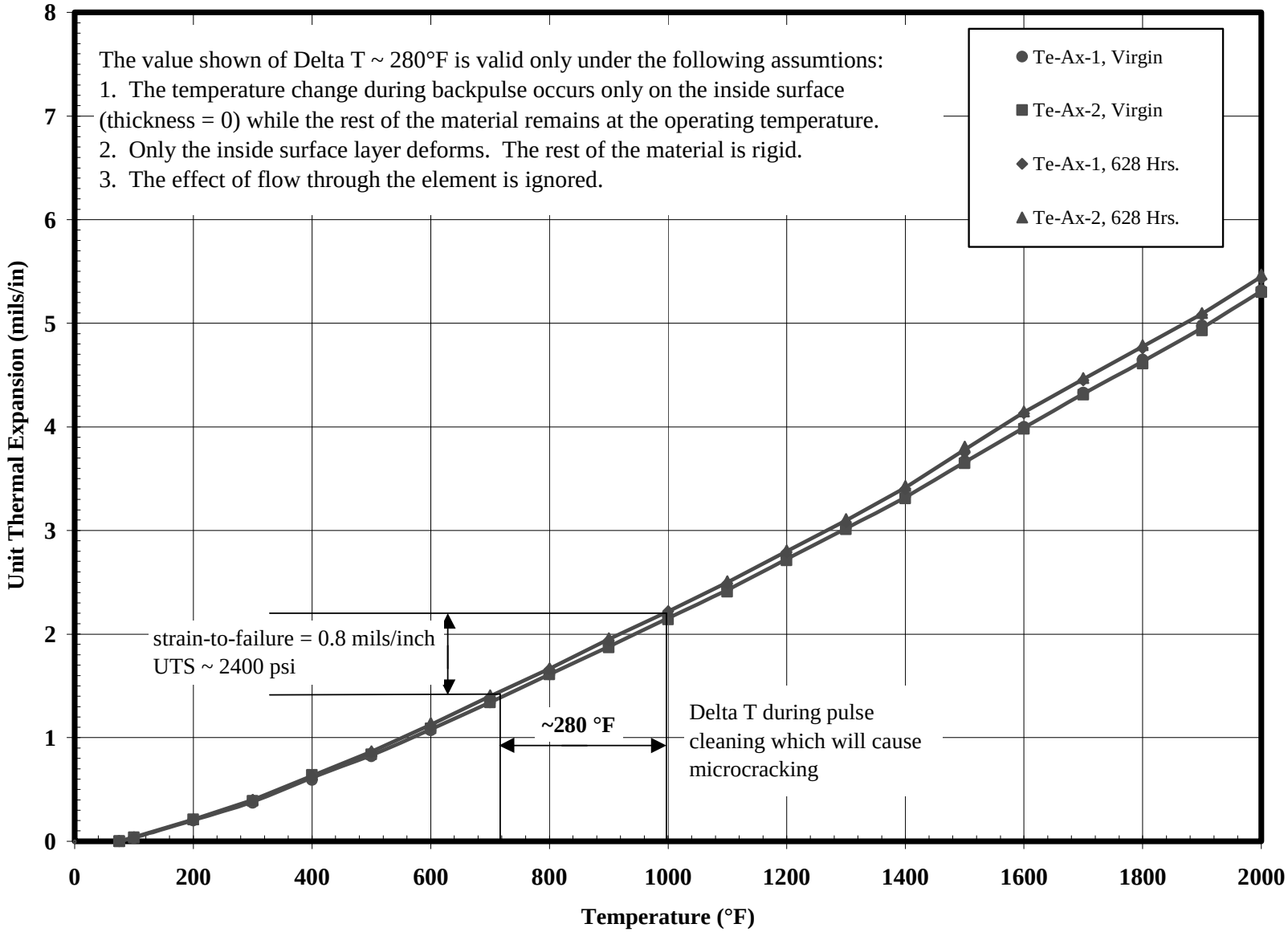

Figure 6.1-4 Axial Thermal Expansion of Coors P-100A-1

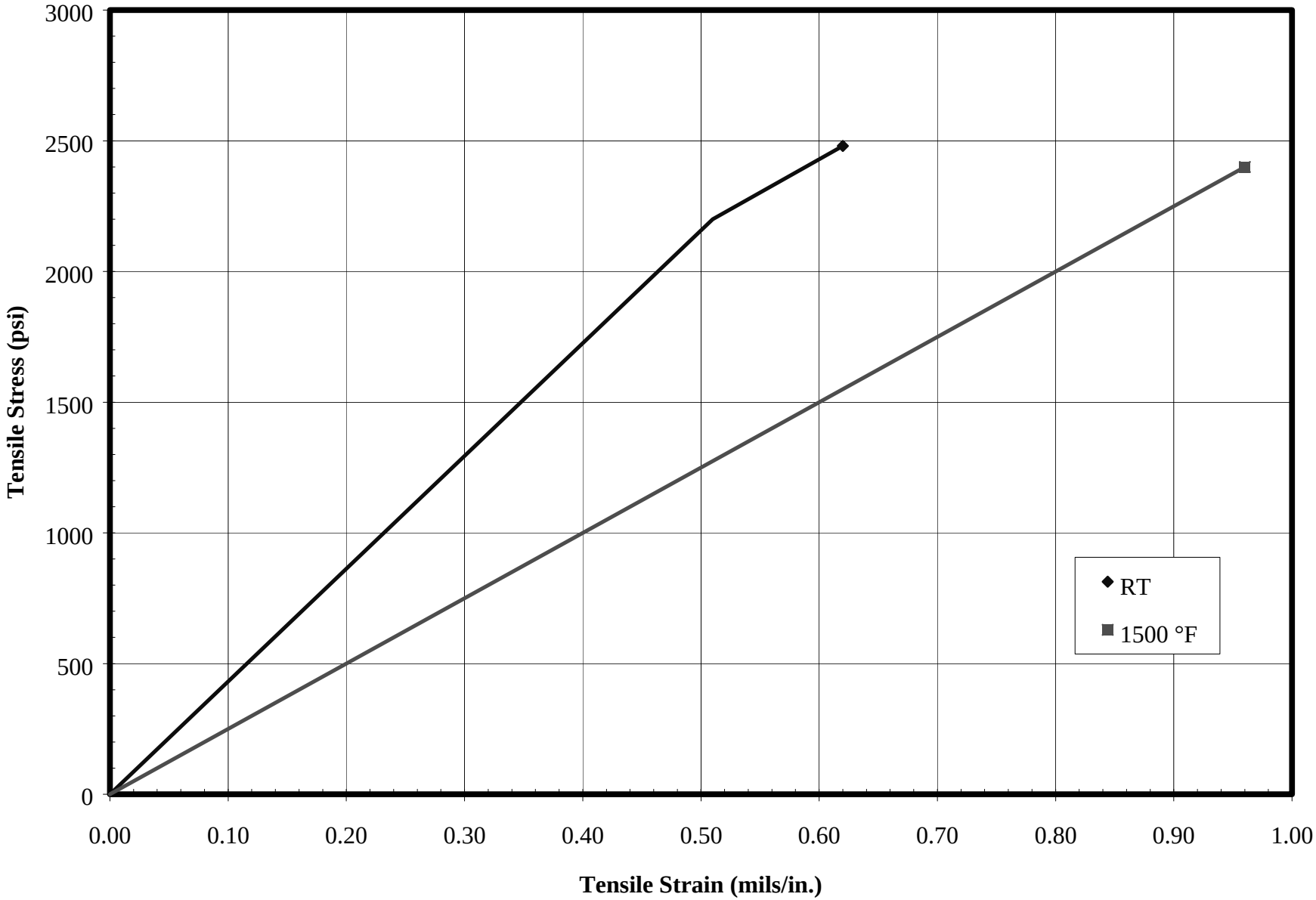

Figure 6.1-5 Probable Axial Tensile Stress-Strain Responses for Coors P-100A-1

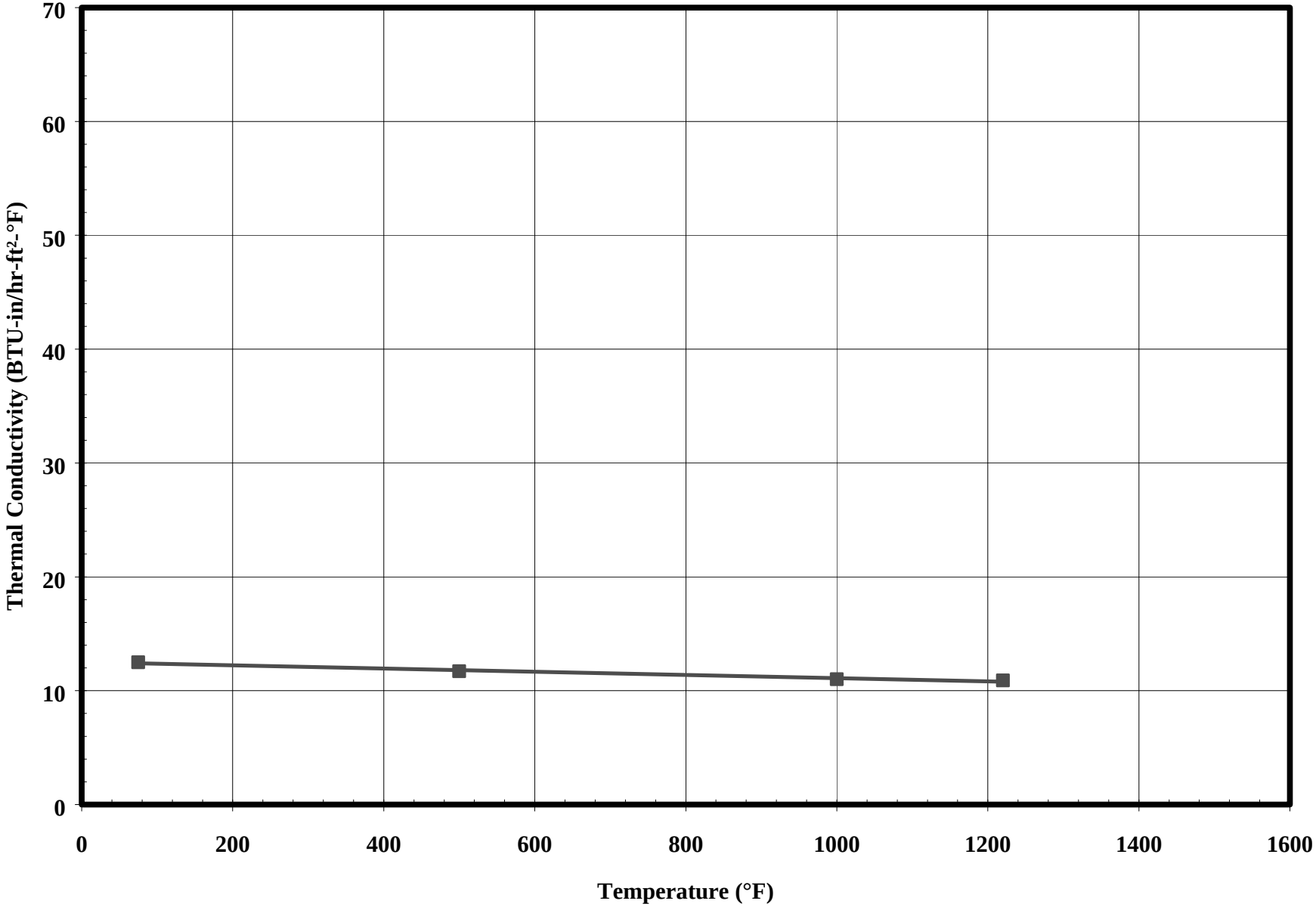

Figure 6.1-6 Radial Thermal Conductivity of Coors P-100A-1

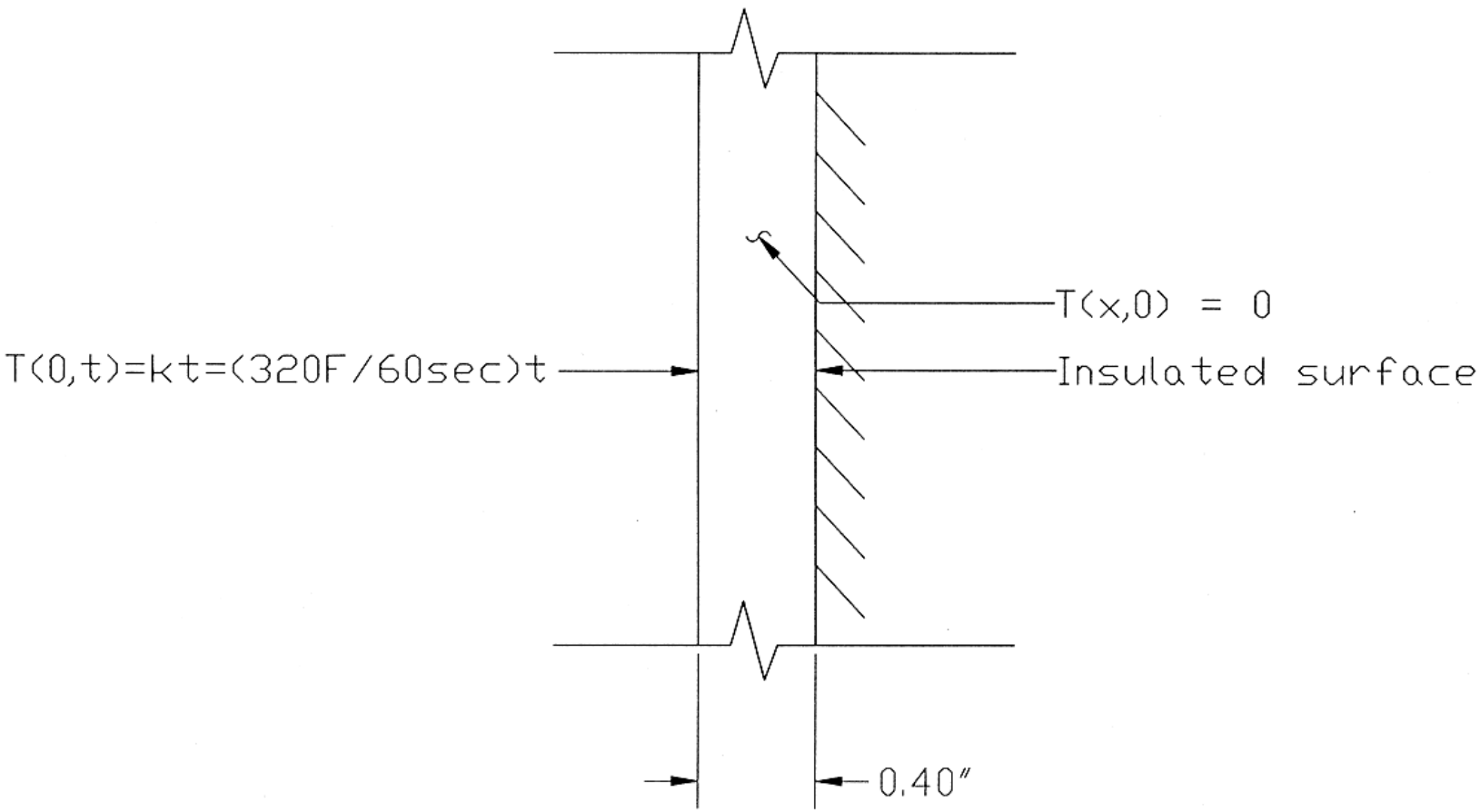

Figure 6.1-7. 1-D, Flat Plate Model for Thermal Transient Analysis

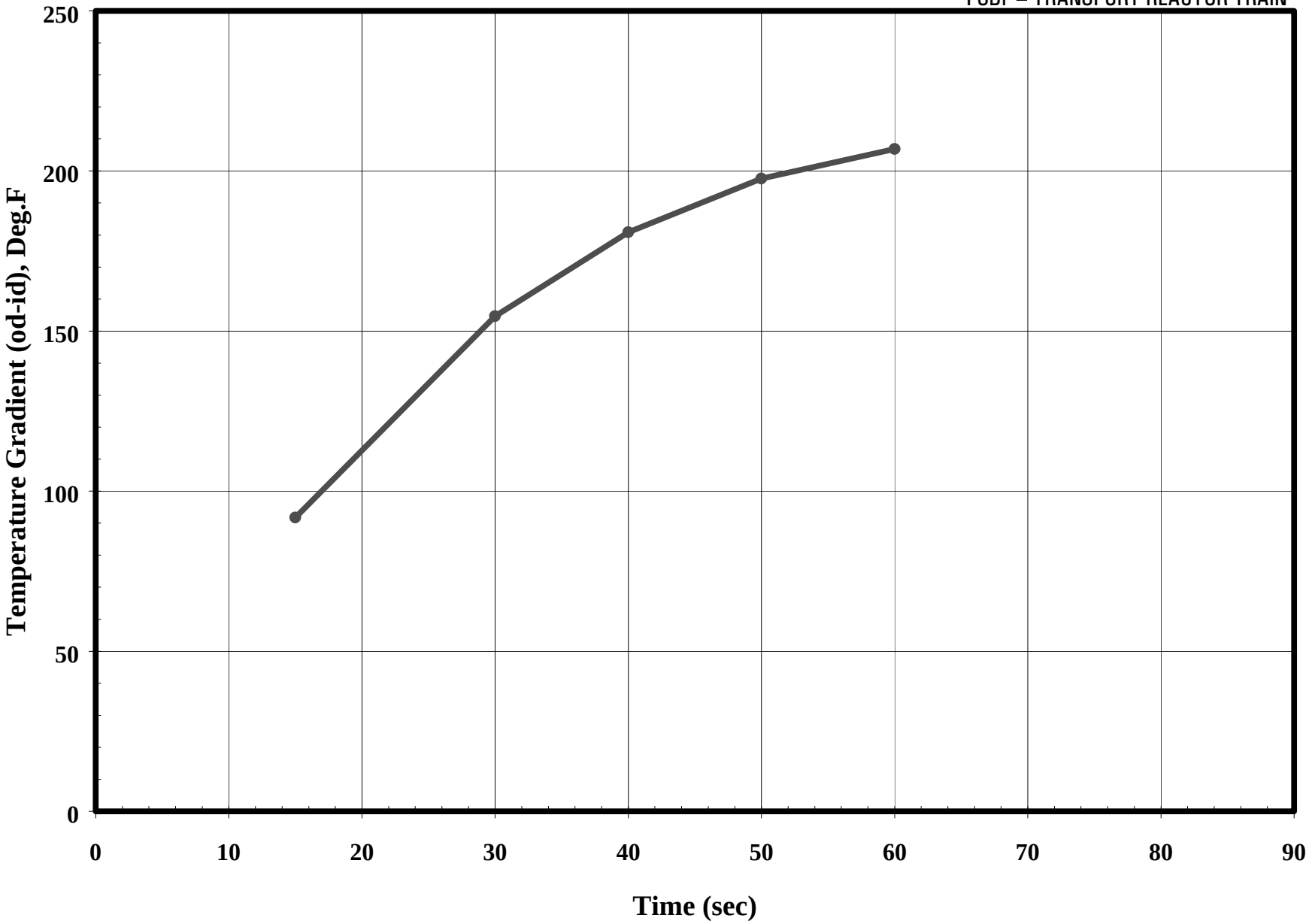

Figure 6.1-8 Temperature Gradient in Coors P-100A-1 Candle Filter
With a Temperature Increase of 320 °F in 60 sec. on One Surface

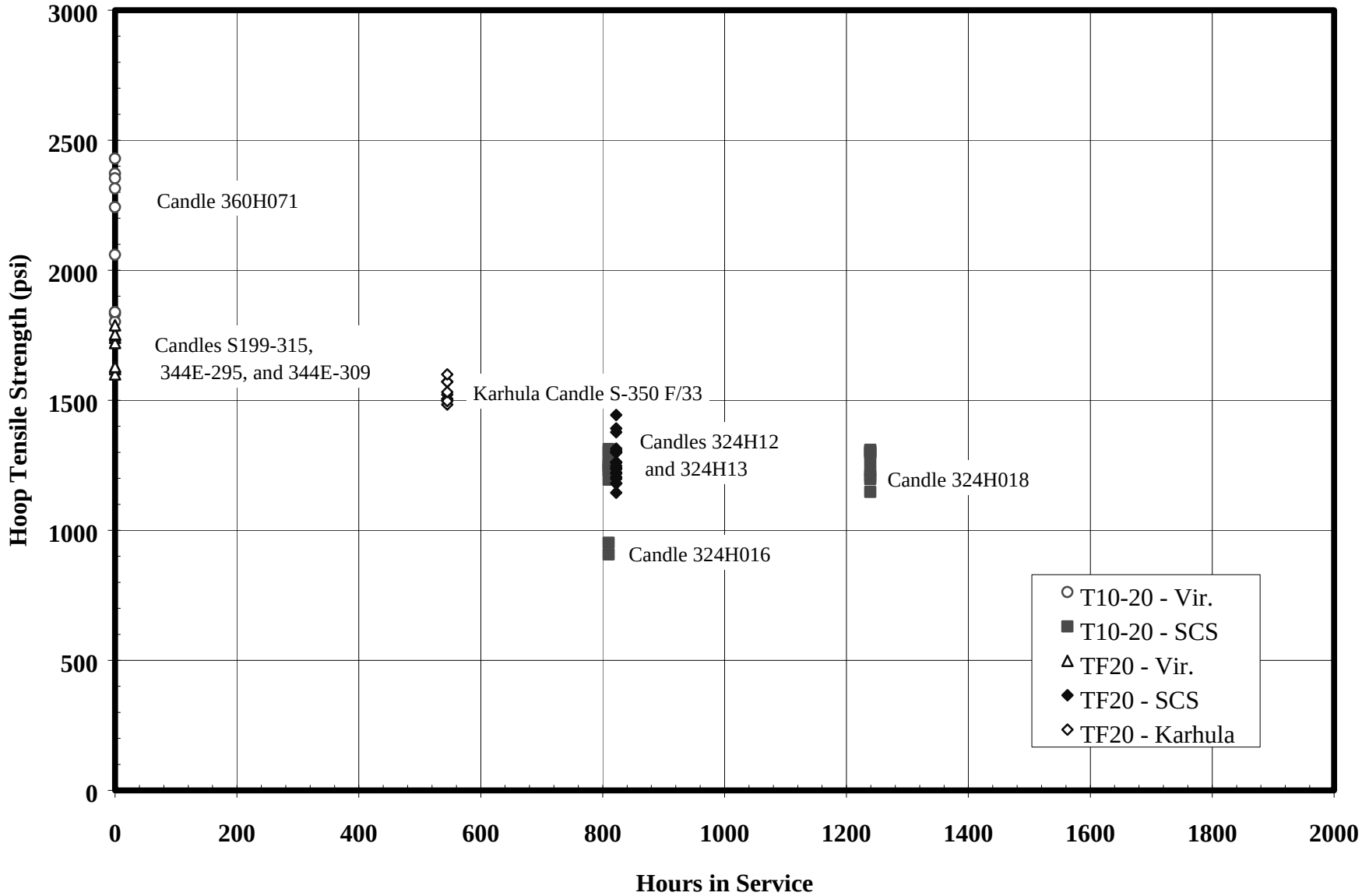

Figure 6.2-1 Hoop Tensile Strength Versus Hours of Operation for Schumacher TF20 and T10-20

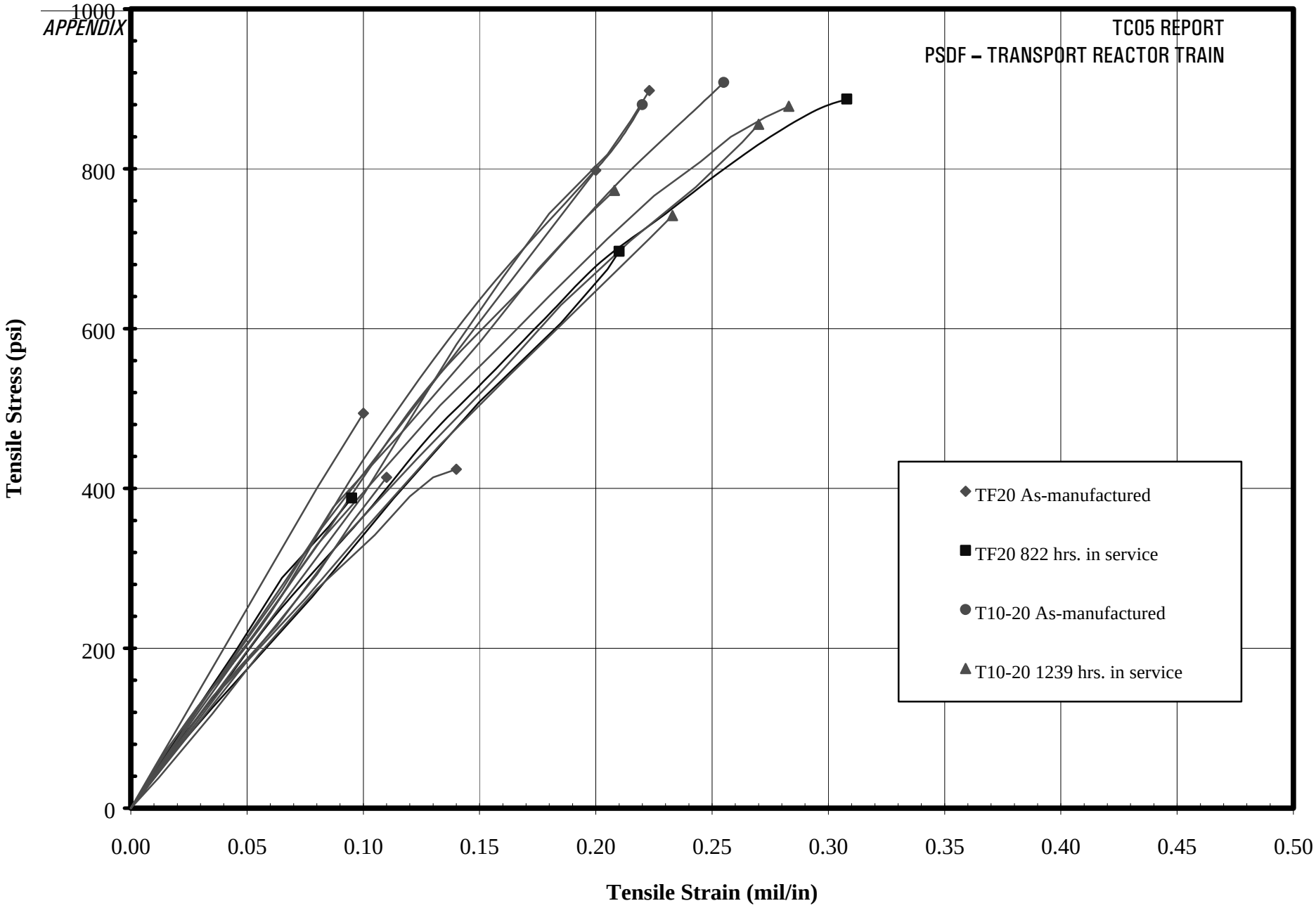

Figure 6.2-2 Room Temperature Axial Tensile Stress-Strain Responses of Schumacher Candle Filter Materials

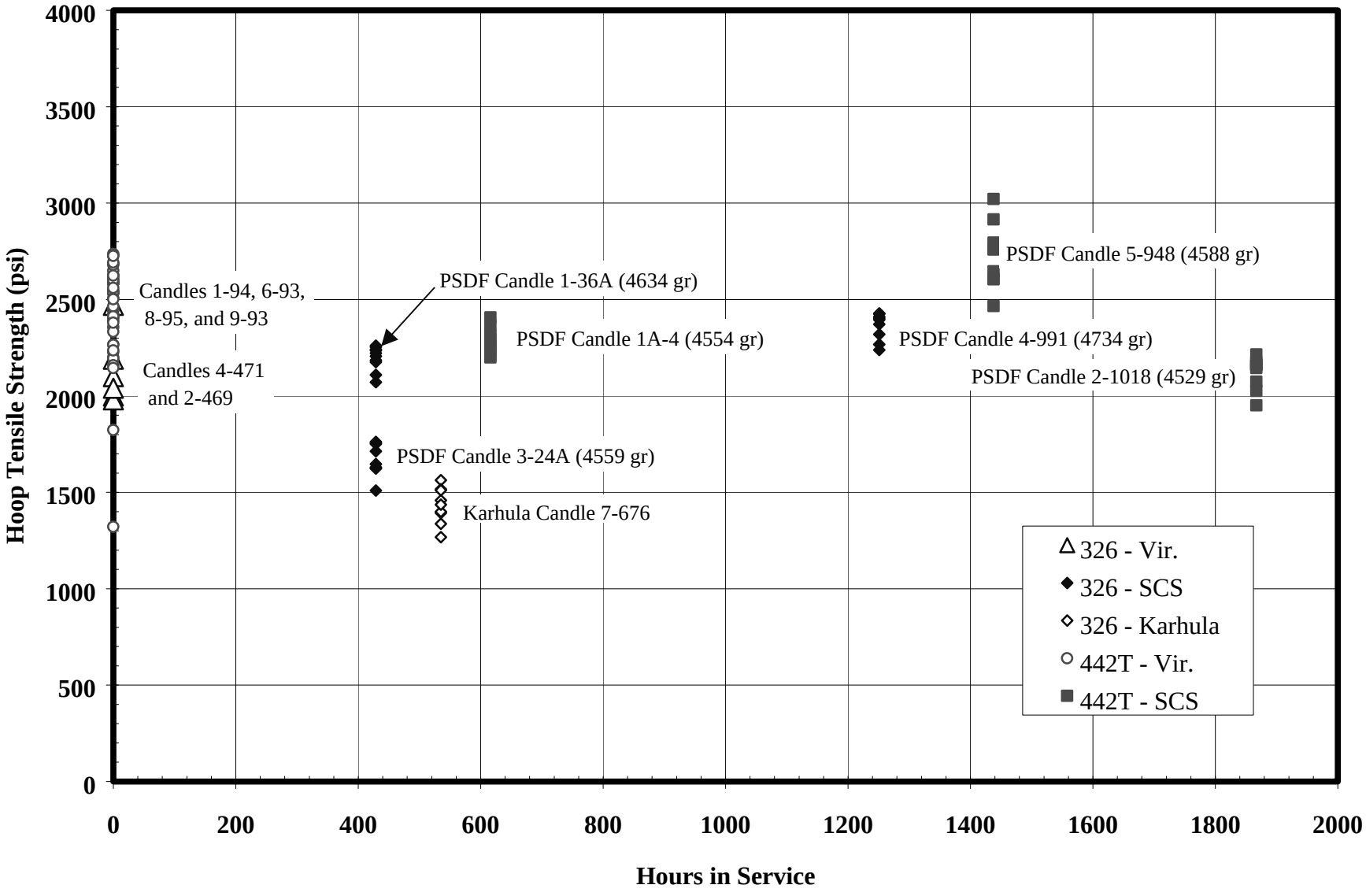

Figure 6.2-3 Hoop Tensile Strength Versus Hours of Operation for Pall 326 and 442T

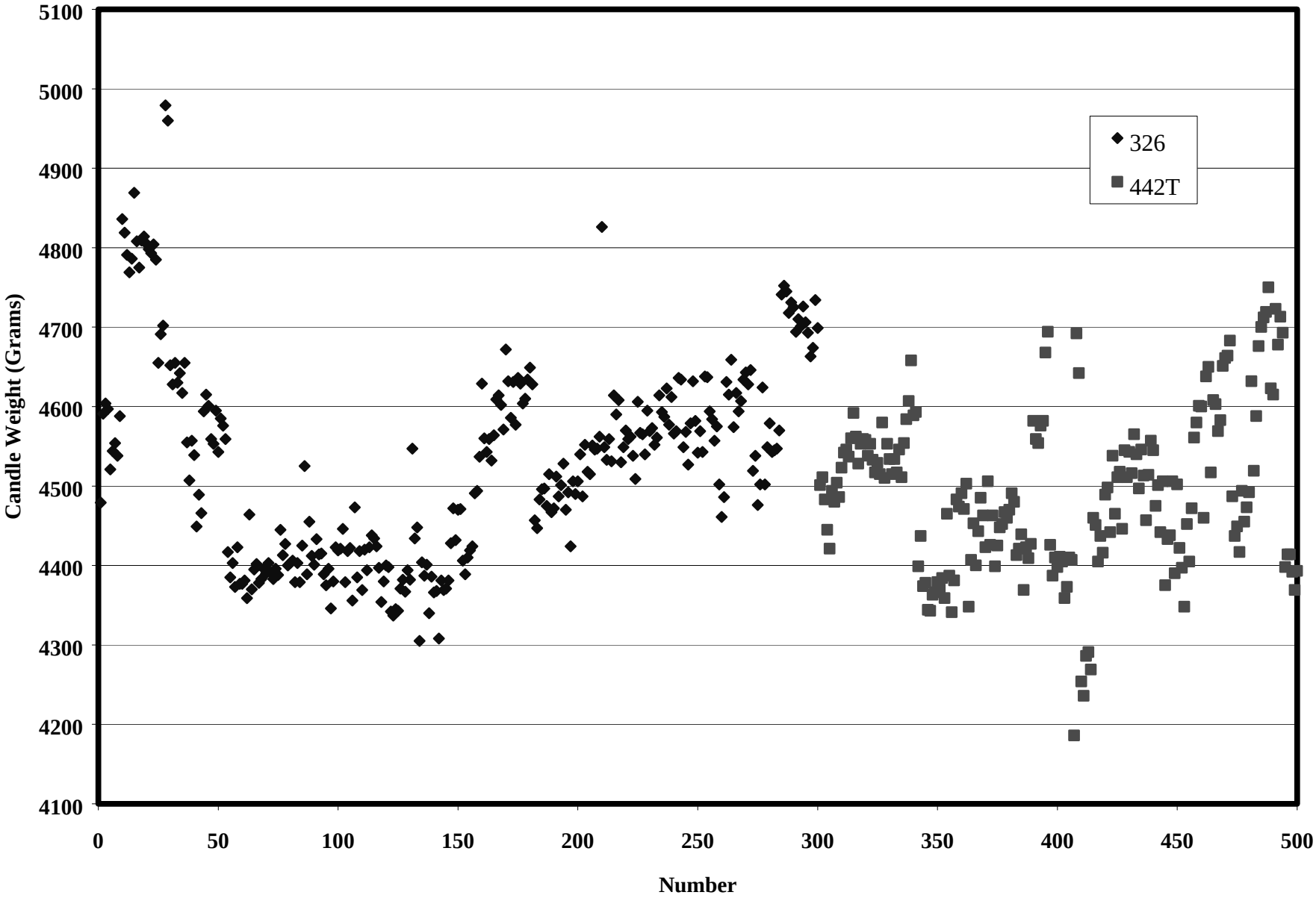

Figure 6.2-4 Virgin Weight of Pall Candle Filters

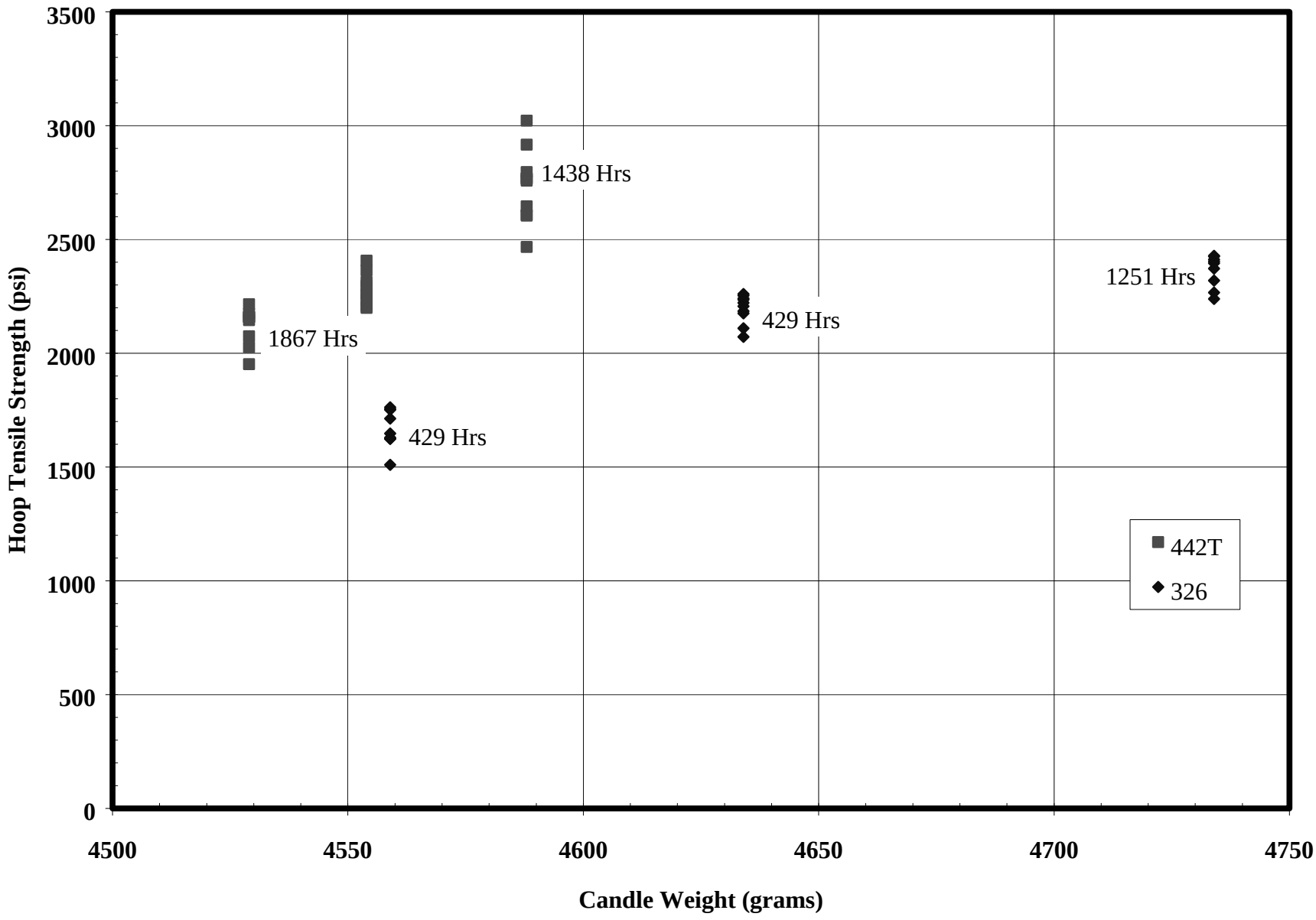

Figure 6.2-5 Hoop Tensile Strength of Pall 326 and 442T Candle Filters

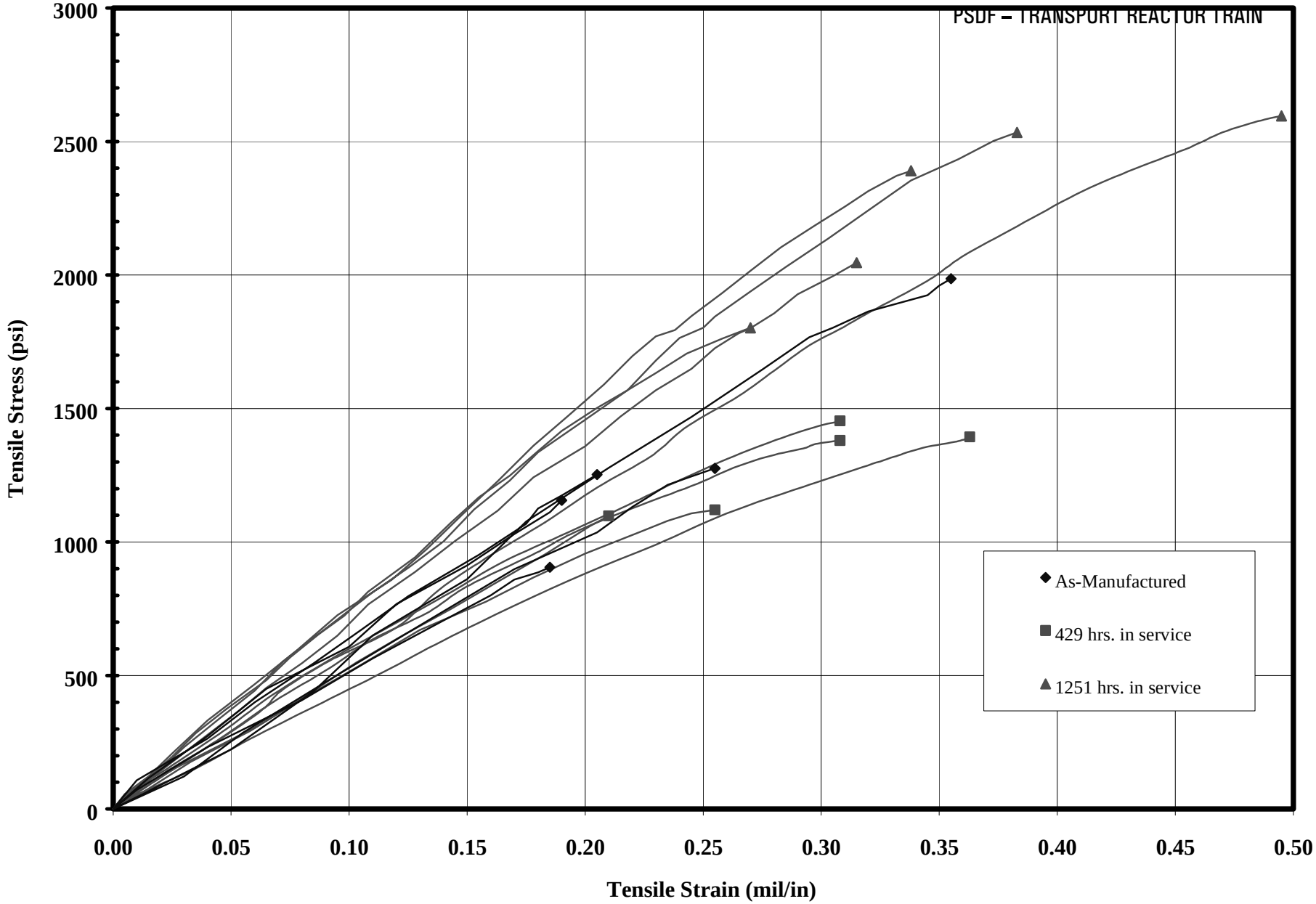

Figure 6.2-6 Room Temperature Axial Tensile Stress-Strain Responses for Pall 326

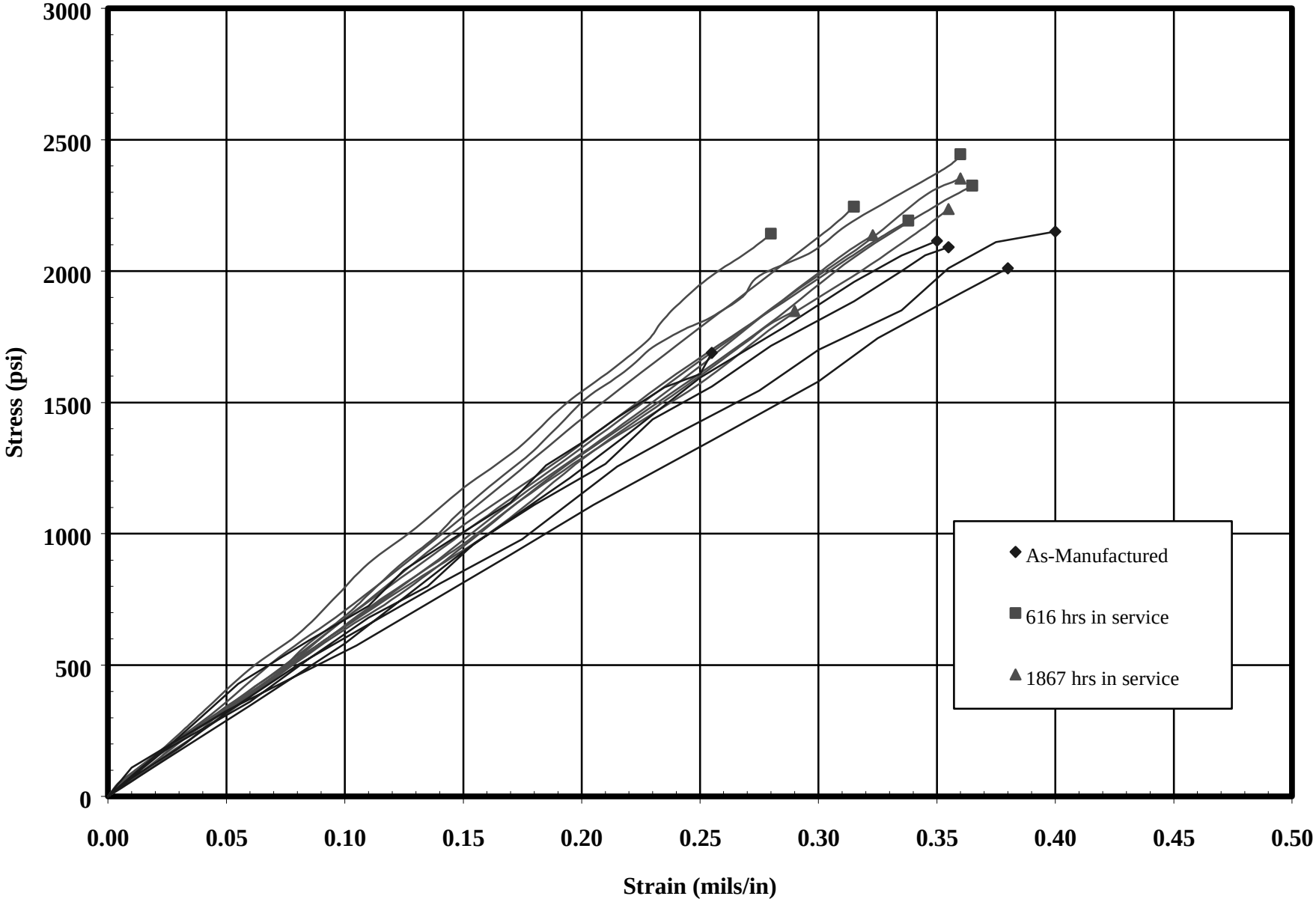

Figure 6.2-7 Room Temperature Axial Tensile Stress-Strain Responses for Pall 442T

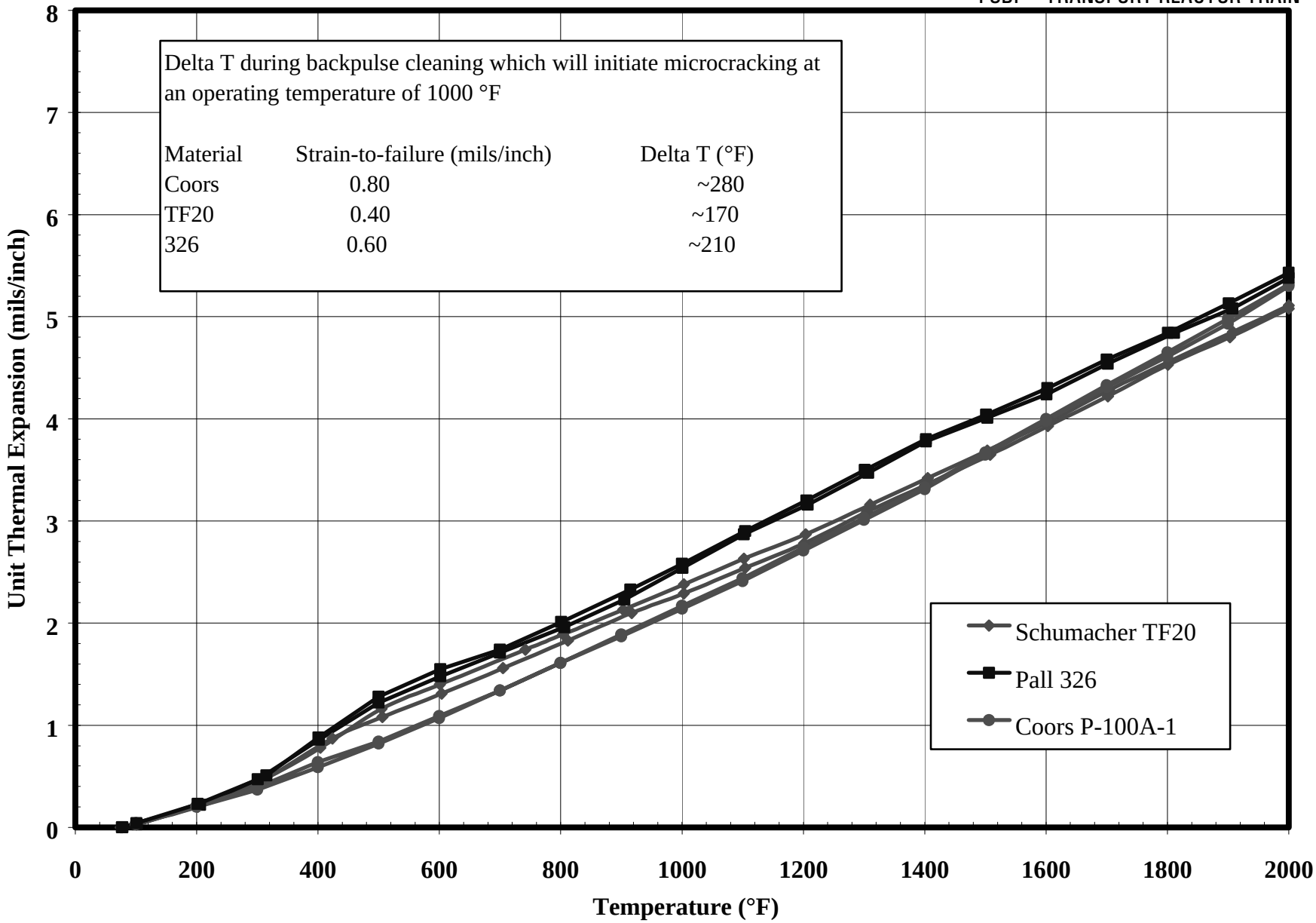

Figure 6.2-8 Unit Thermal Expansion of Schumacher TF20, Pall 326, and Coors P-100A-1

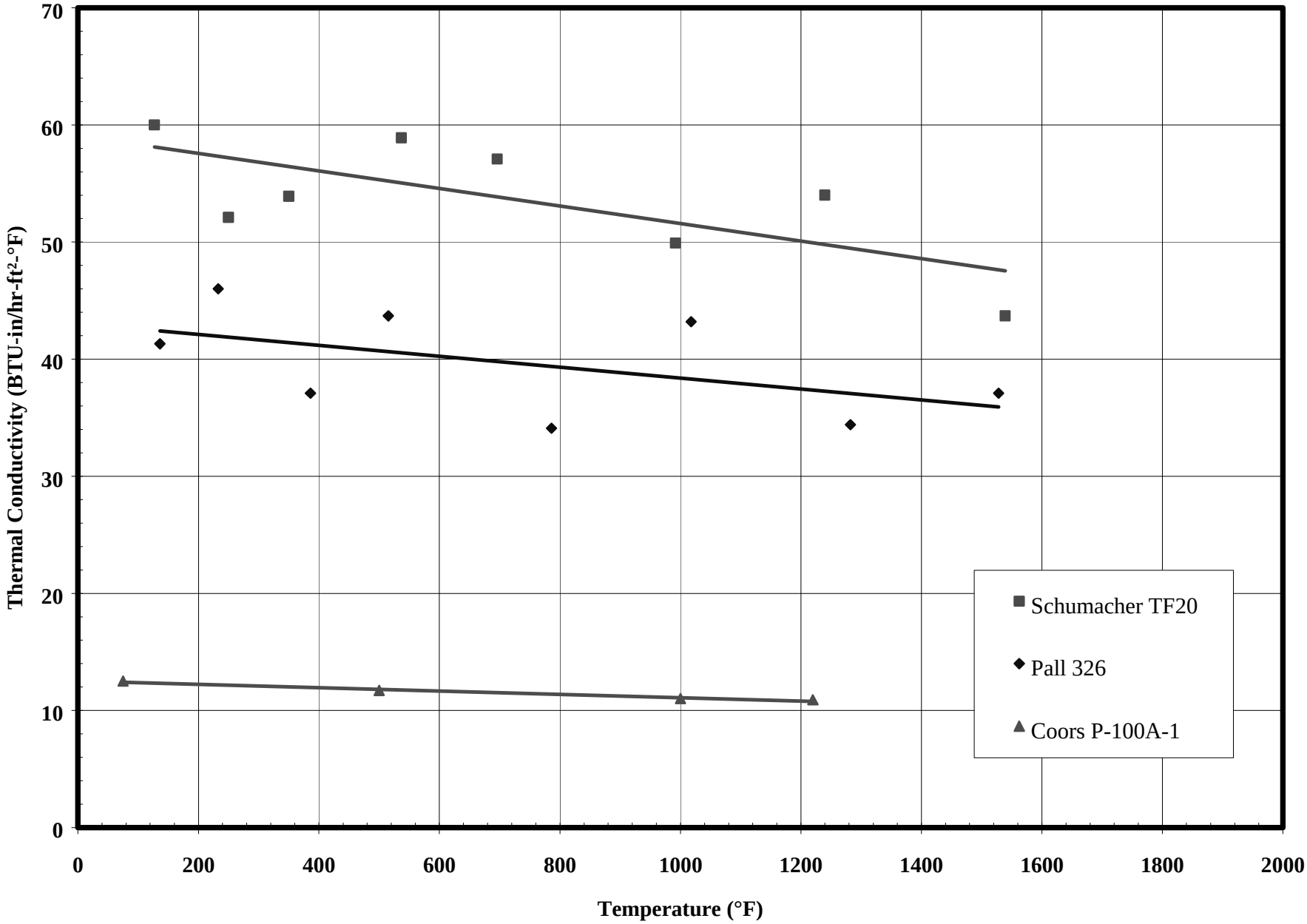

Figure 6.2-9 Radial Thermal Conductivity of Schumacher TF20 and Pall 326

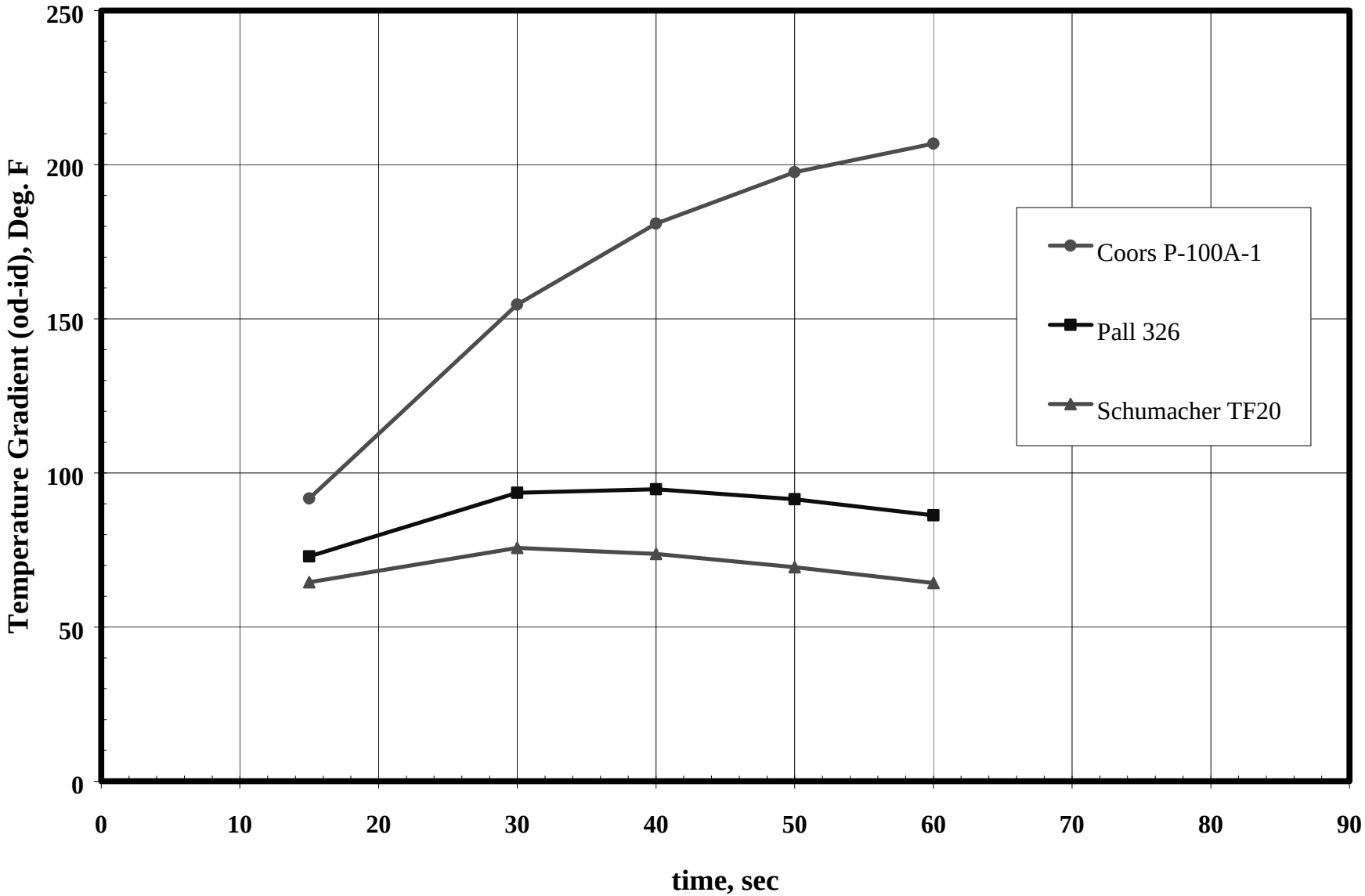

Figure 6.2-10 Temperature Gradient in Schumacher TF20 and Pall 326 Candle Filters With a Temperature Increase of 320 °F in 60 sec. on One Surface

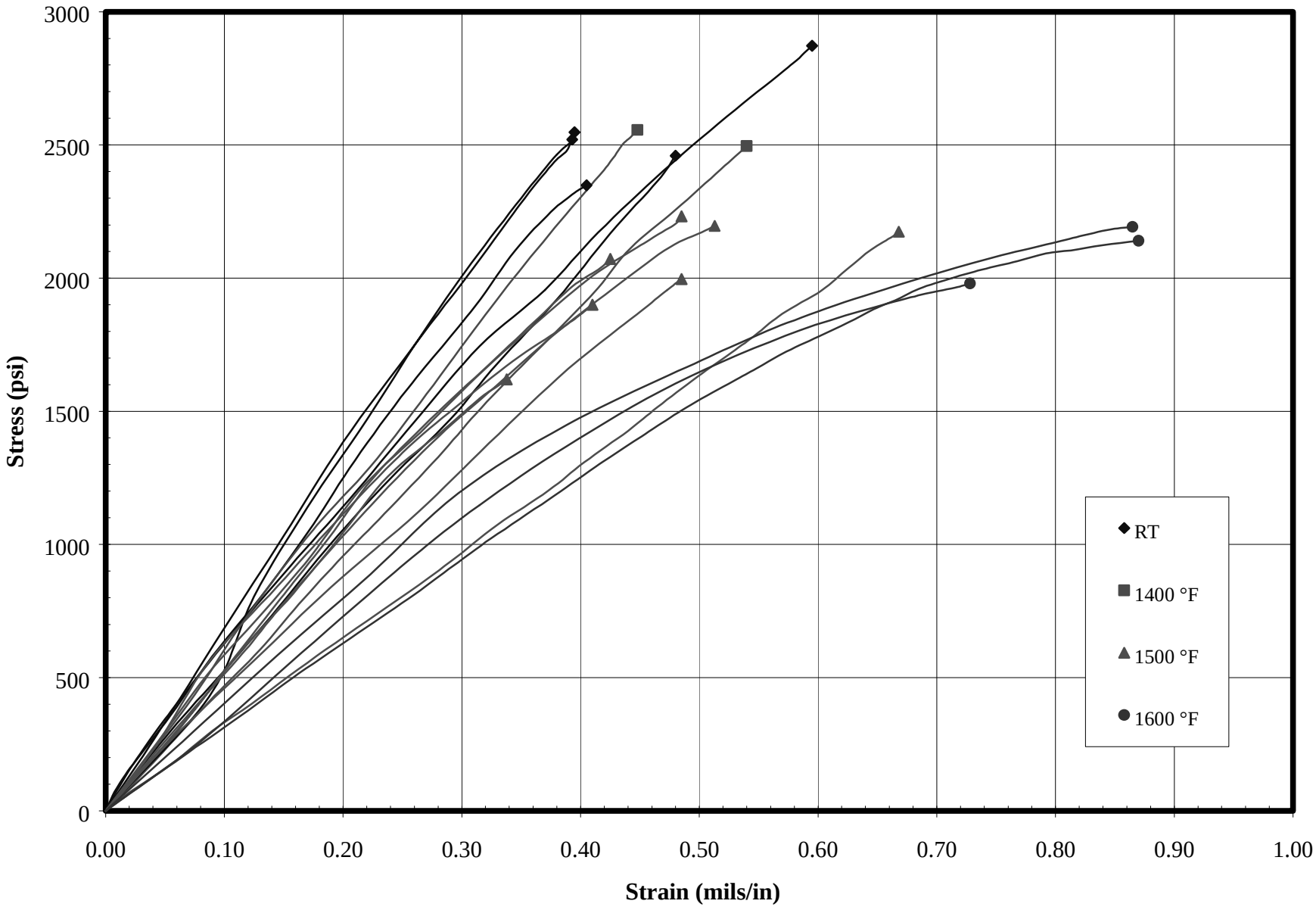

Figure 6.3-1 Axial Tensile Stress-Strain Responses for Pall 181

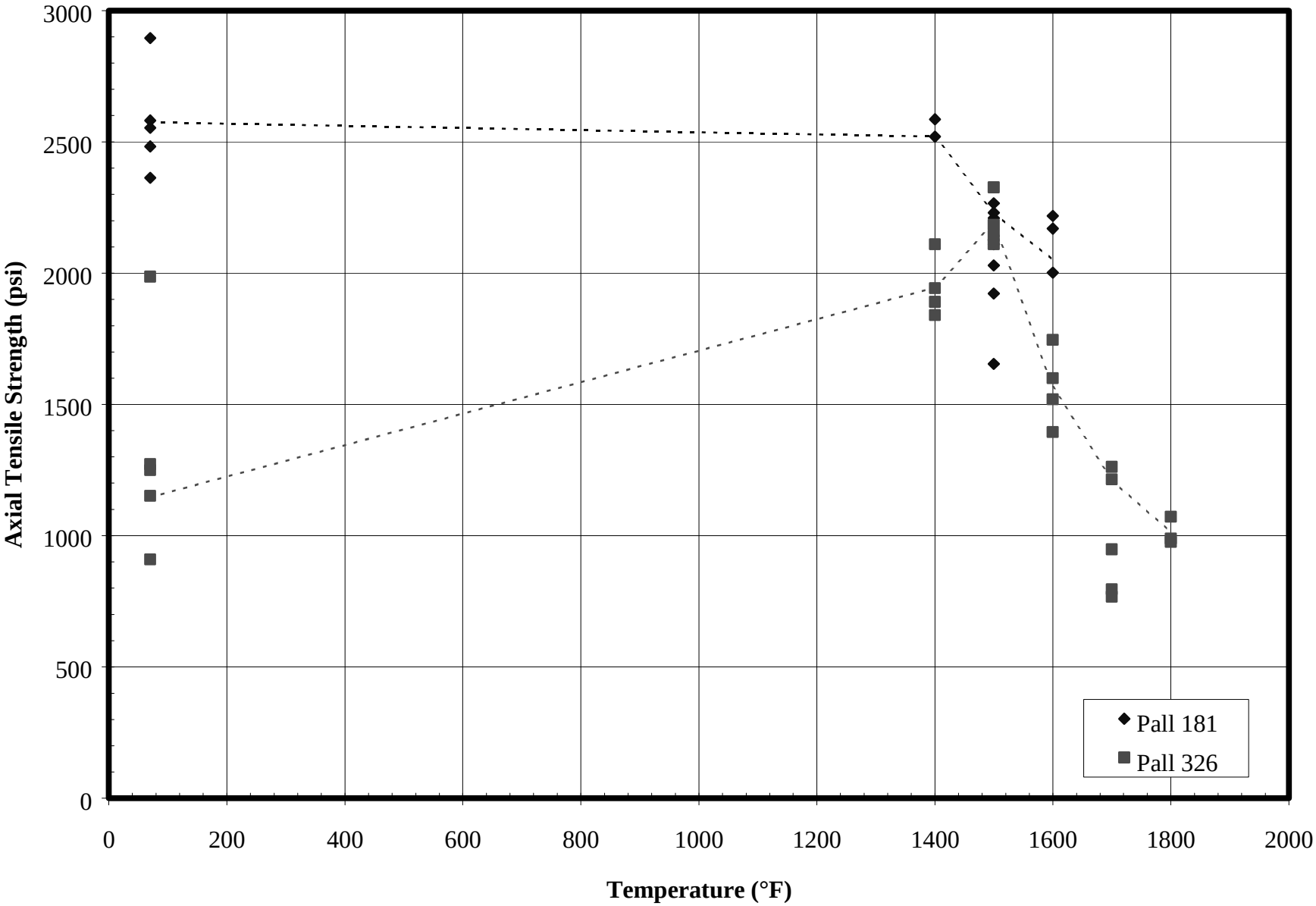

Figure 6.3-2 Axial Tensile Strength Versus Temperature for Pall 181 and 326

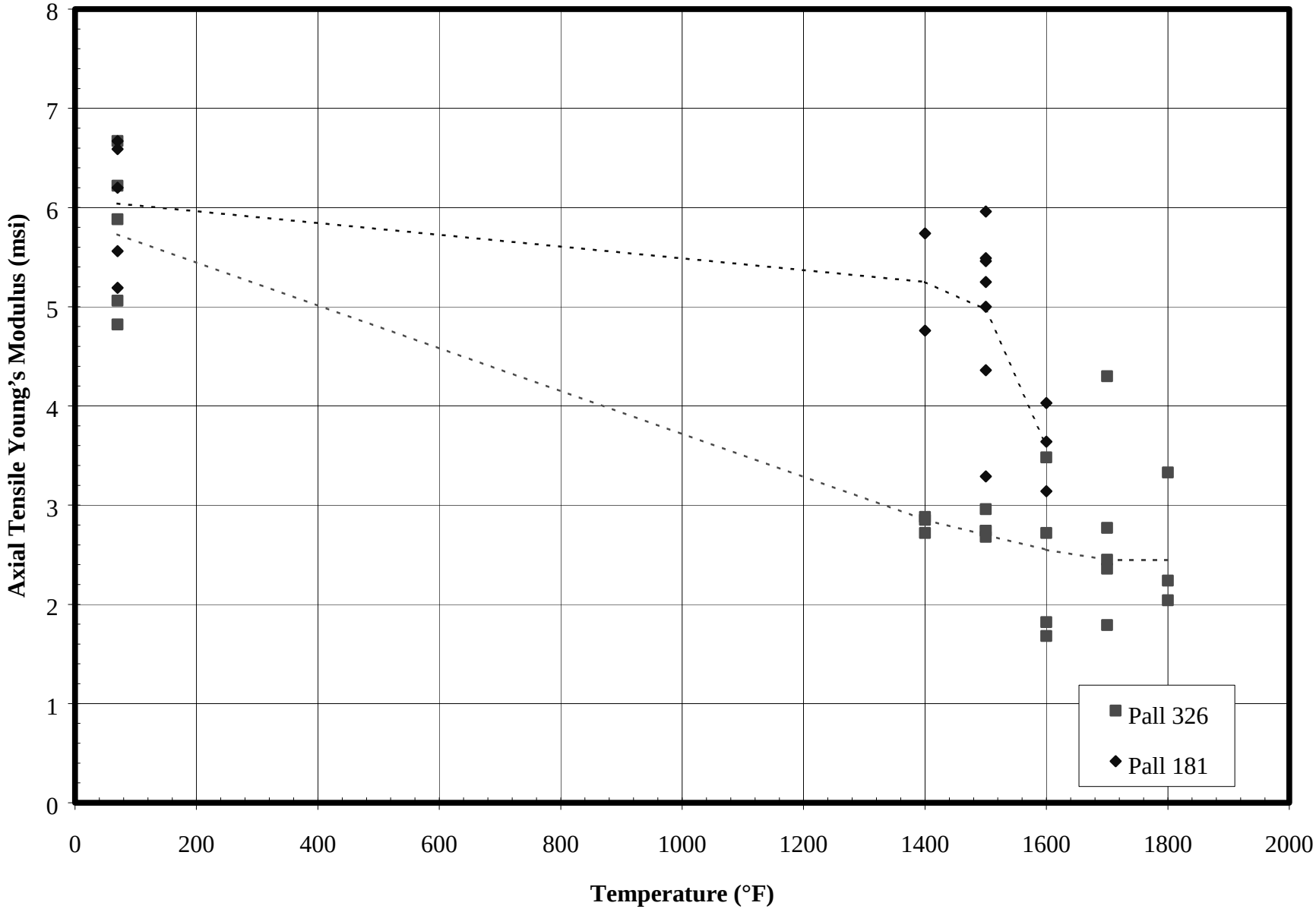

Figure 6.3-3 Young's Modulus Versus Temperature for Pall 181 and 326

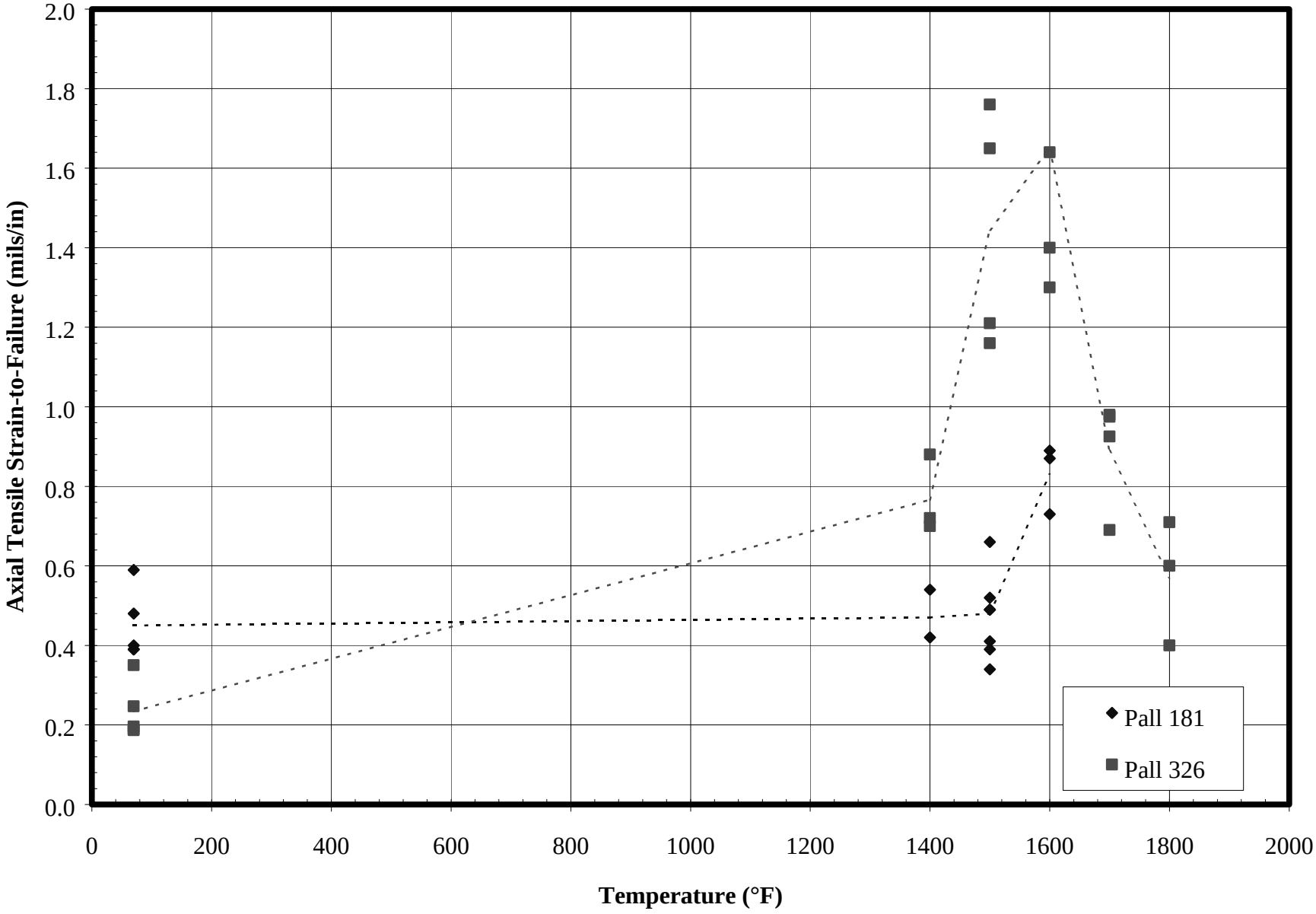

Figure 6.3-4 Strain-to-Failure Versus Temperature for Pall 181 and 326

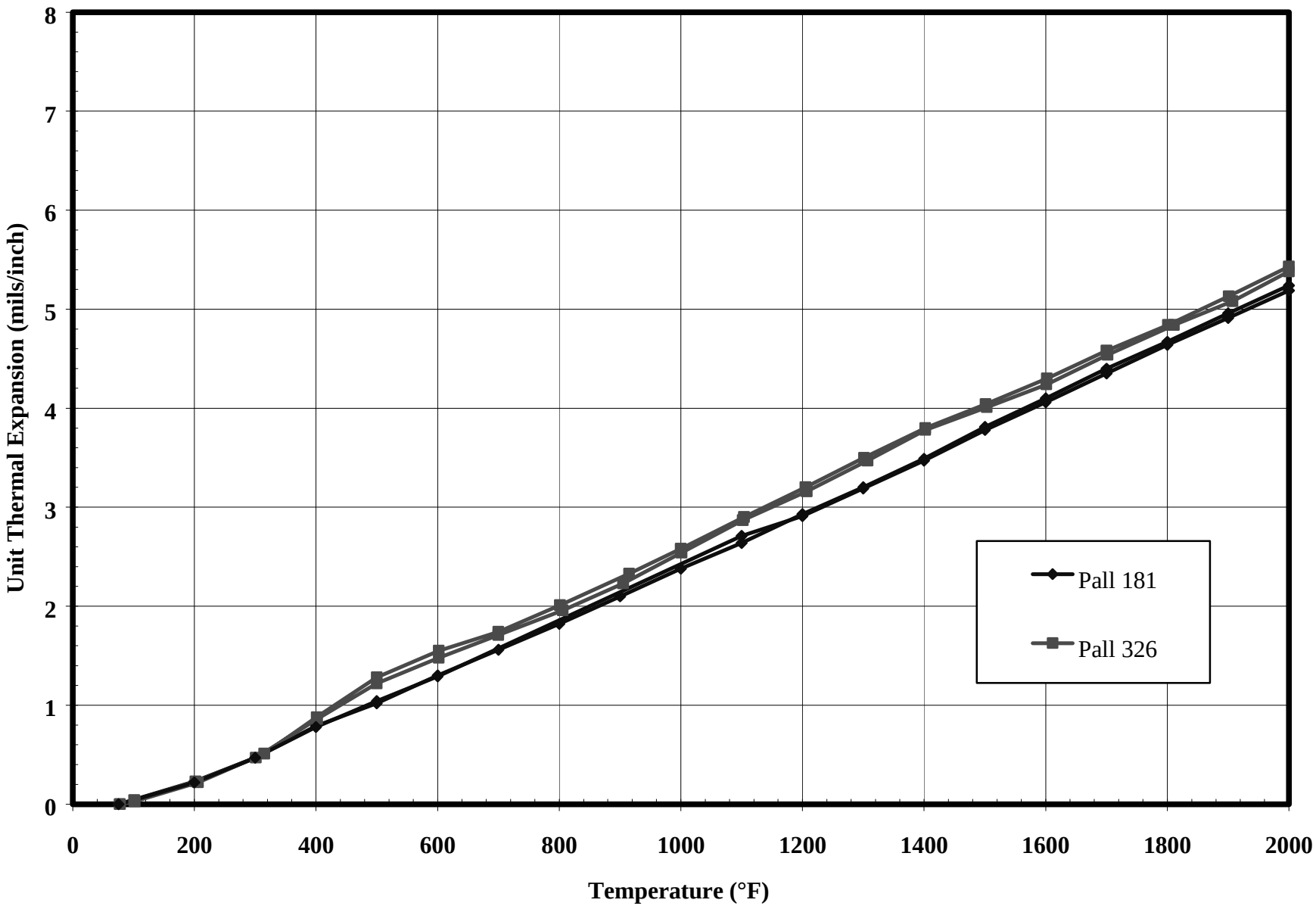

Figure 6.3-5 Unit Thermal Expansion of Pall 181

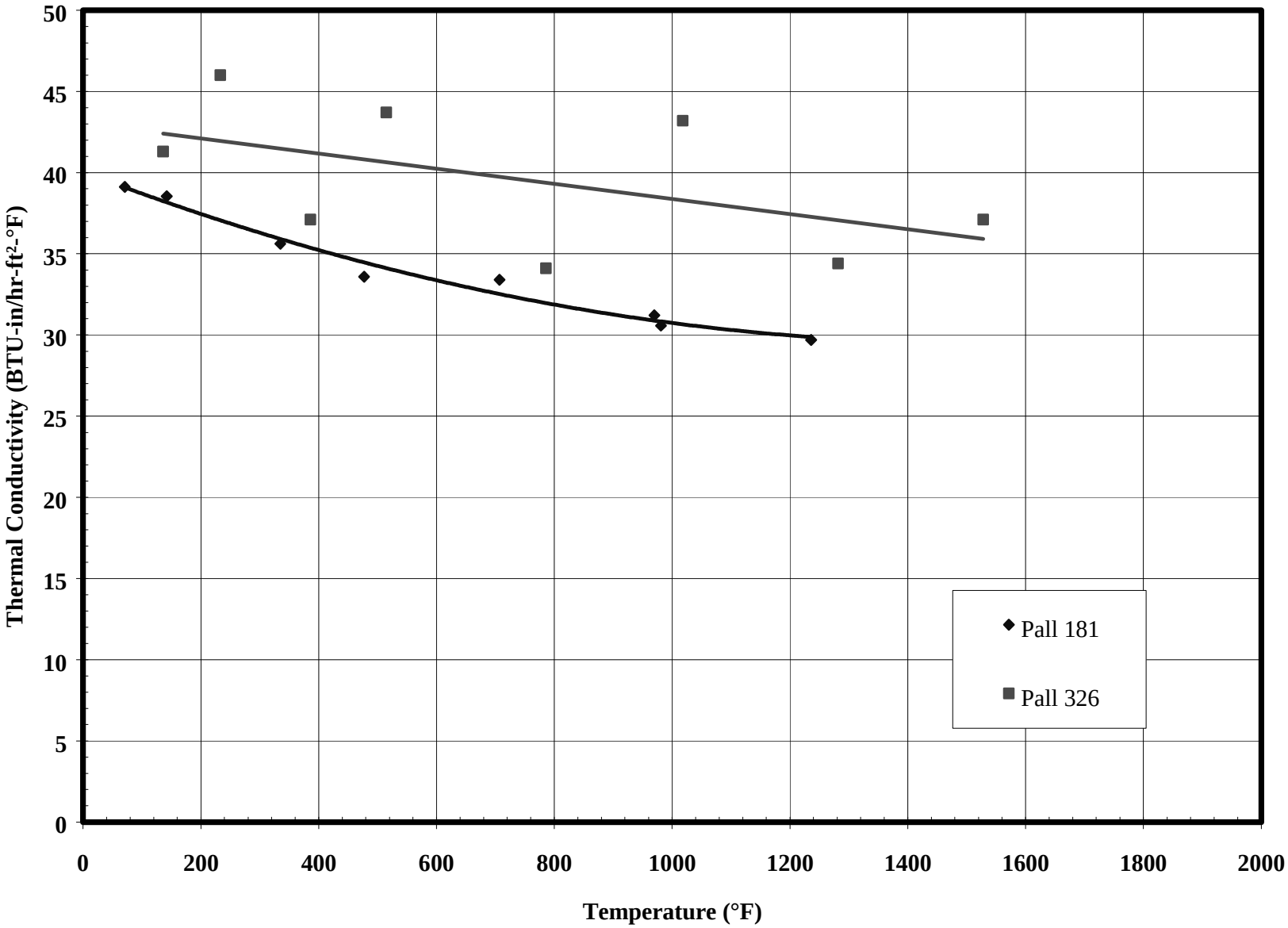

Figure 6.3-6 Radial Thermal Conductivity of Pall 181

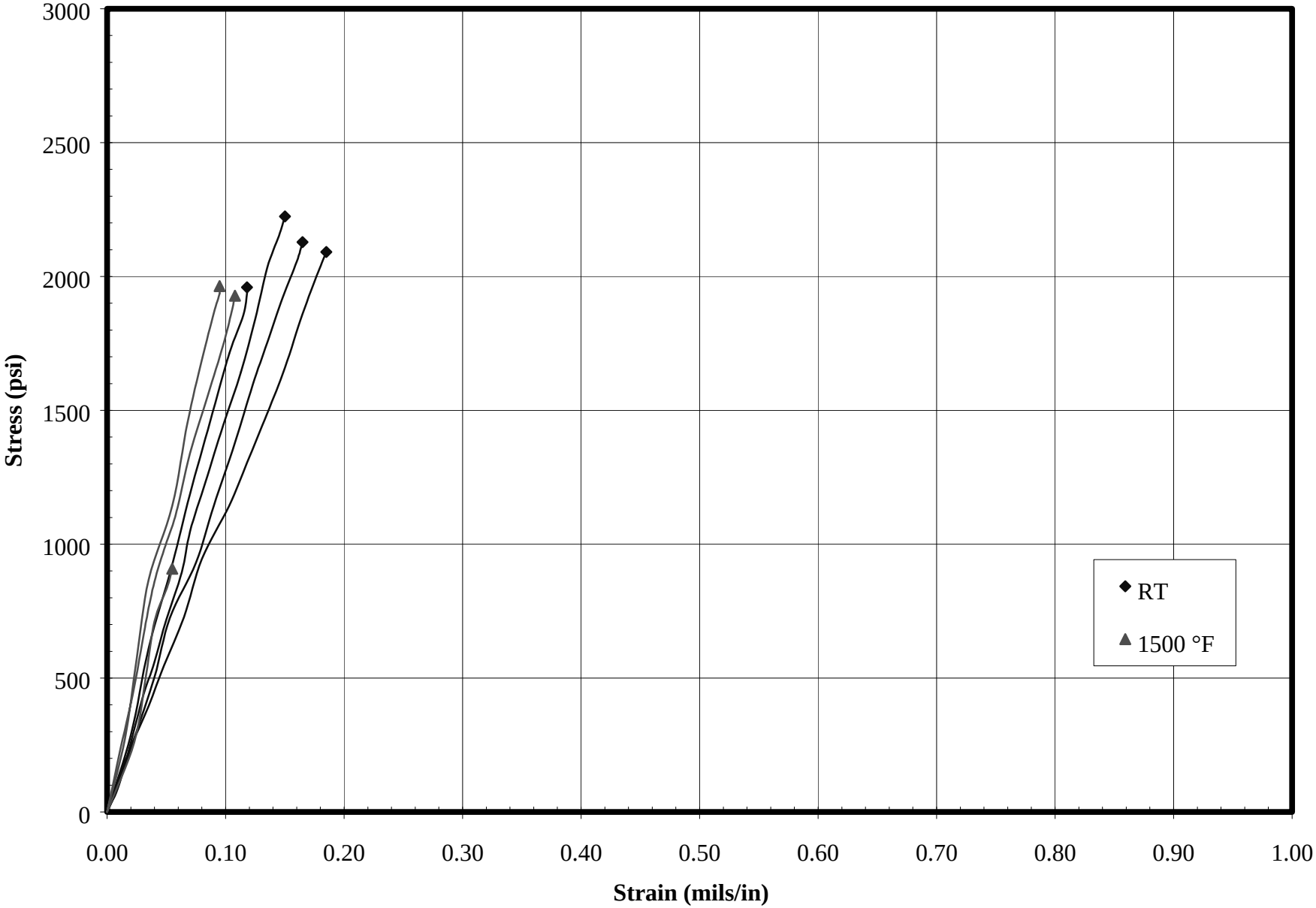

Figure 6.4-1. Axial Tensile Stress-Strain Responses for IF&P Recrystallized SiC

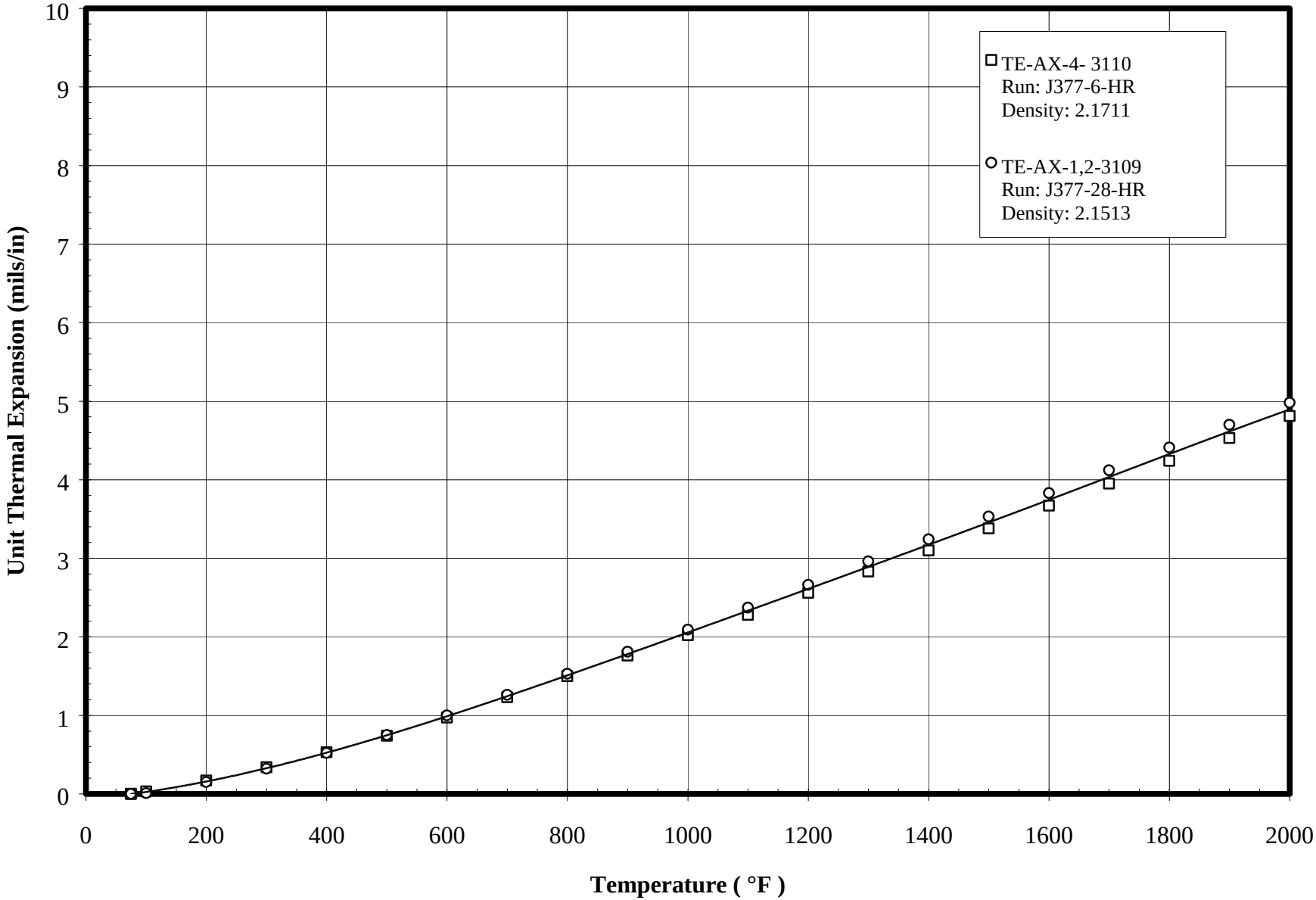

Figure 6.4-2 Axial Unit Thermal Expansion of IF&P Recrystallized SiC

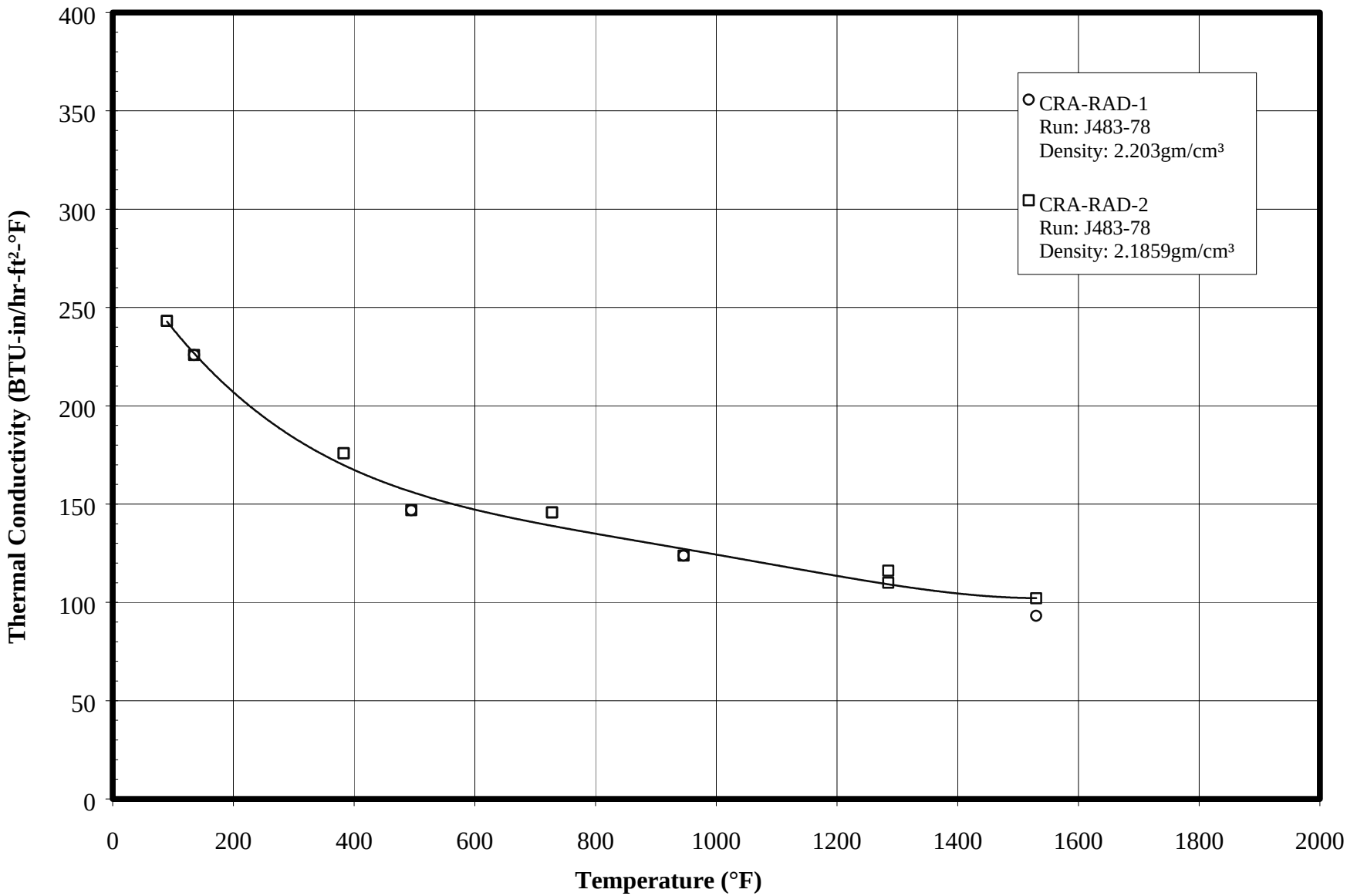

Figure 6.4-3 Radial Thermal Conductivity of IF&P Recrystallized SiC

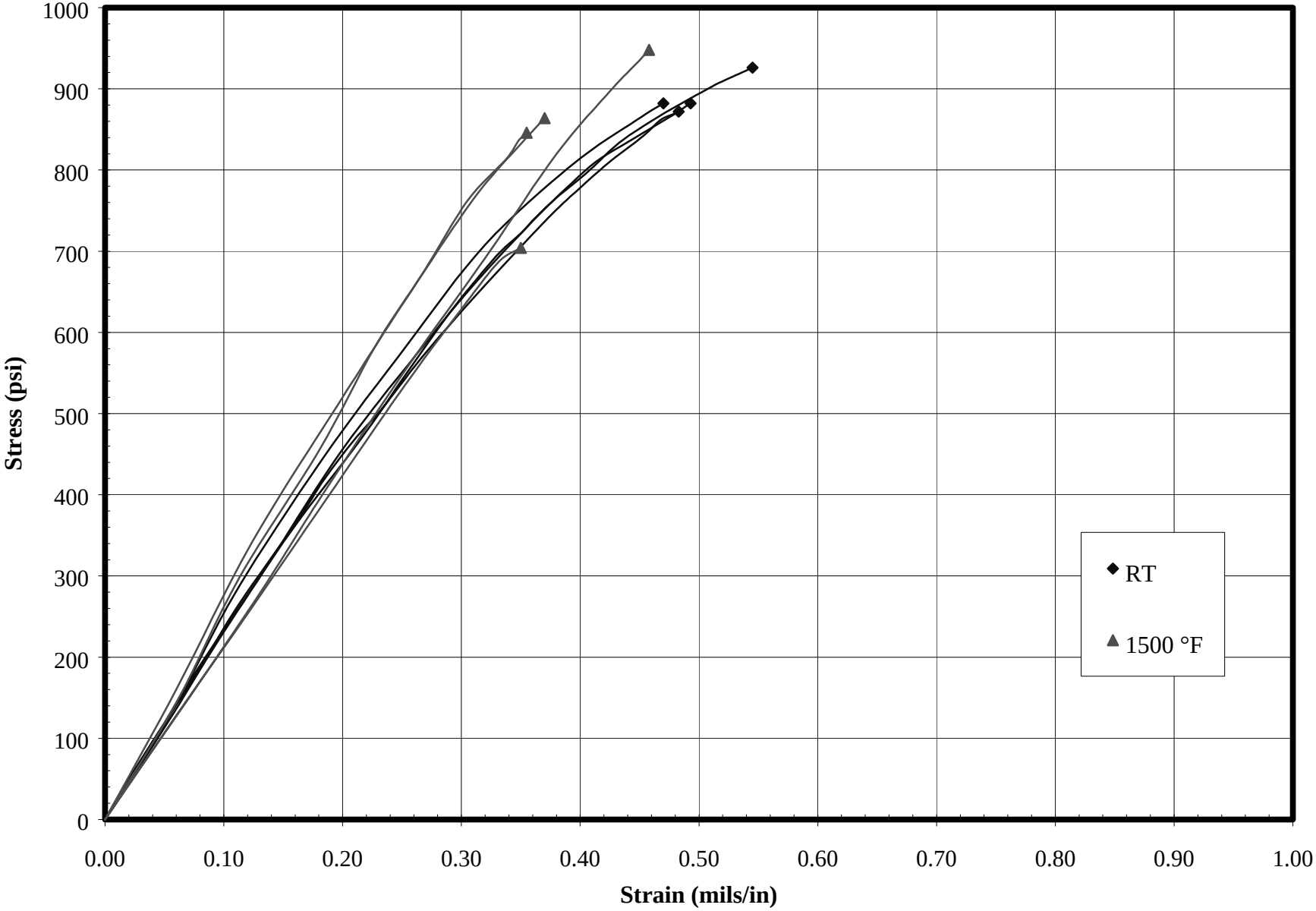

Figure 6.5-1 Axial Tensile Stress-Strain Responses for Ensto Candle Filter Material

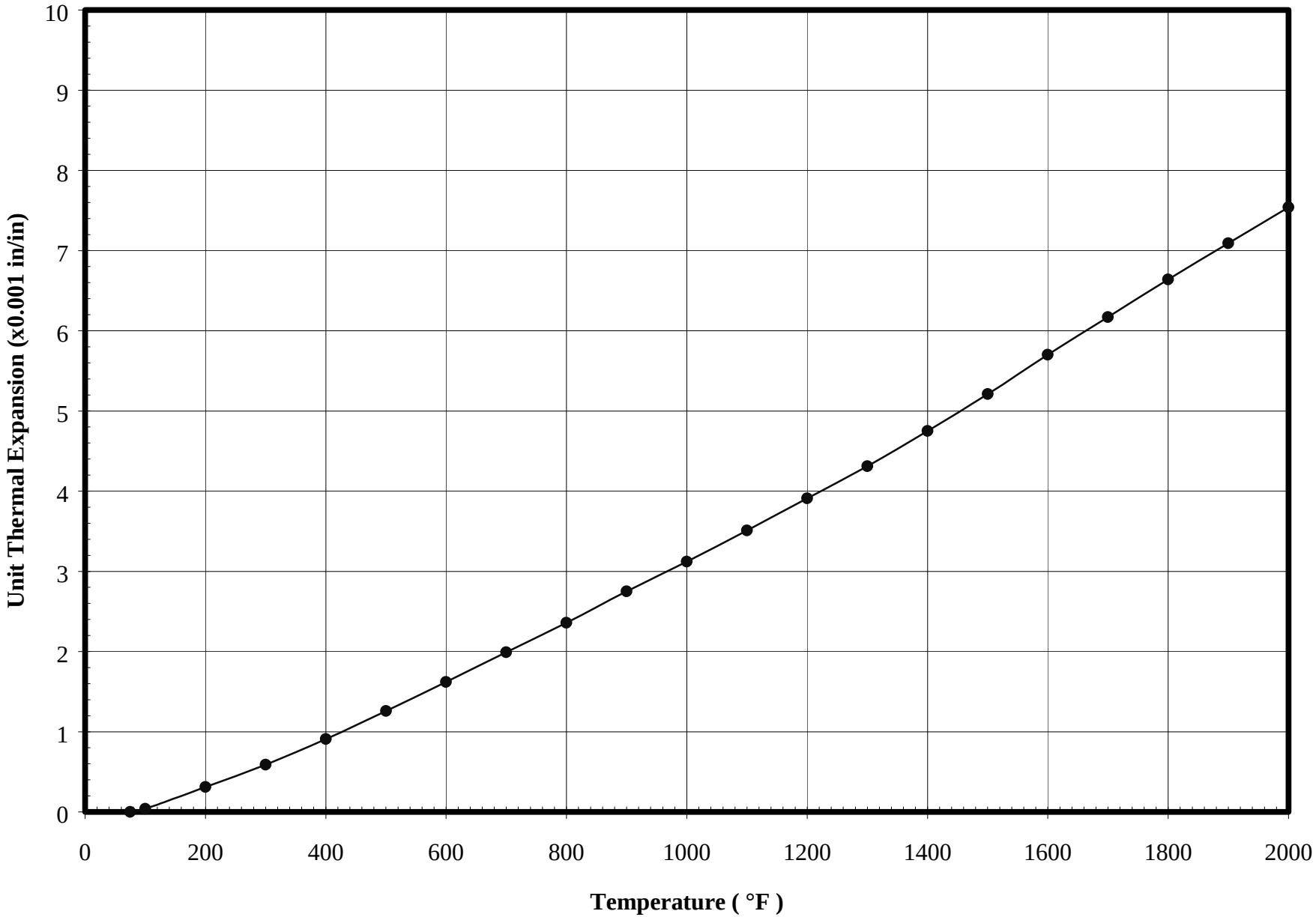

Figure 6.5-2 Unit Thermal Expansion of Ensto Candle Filter Material

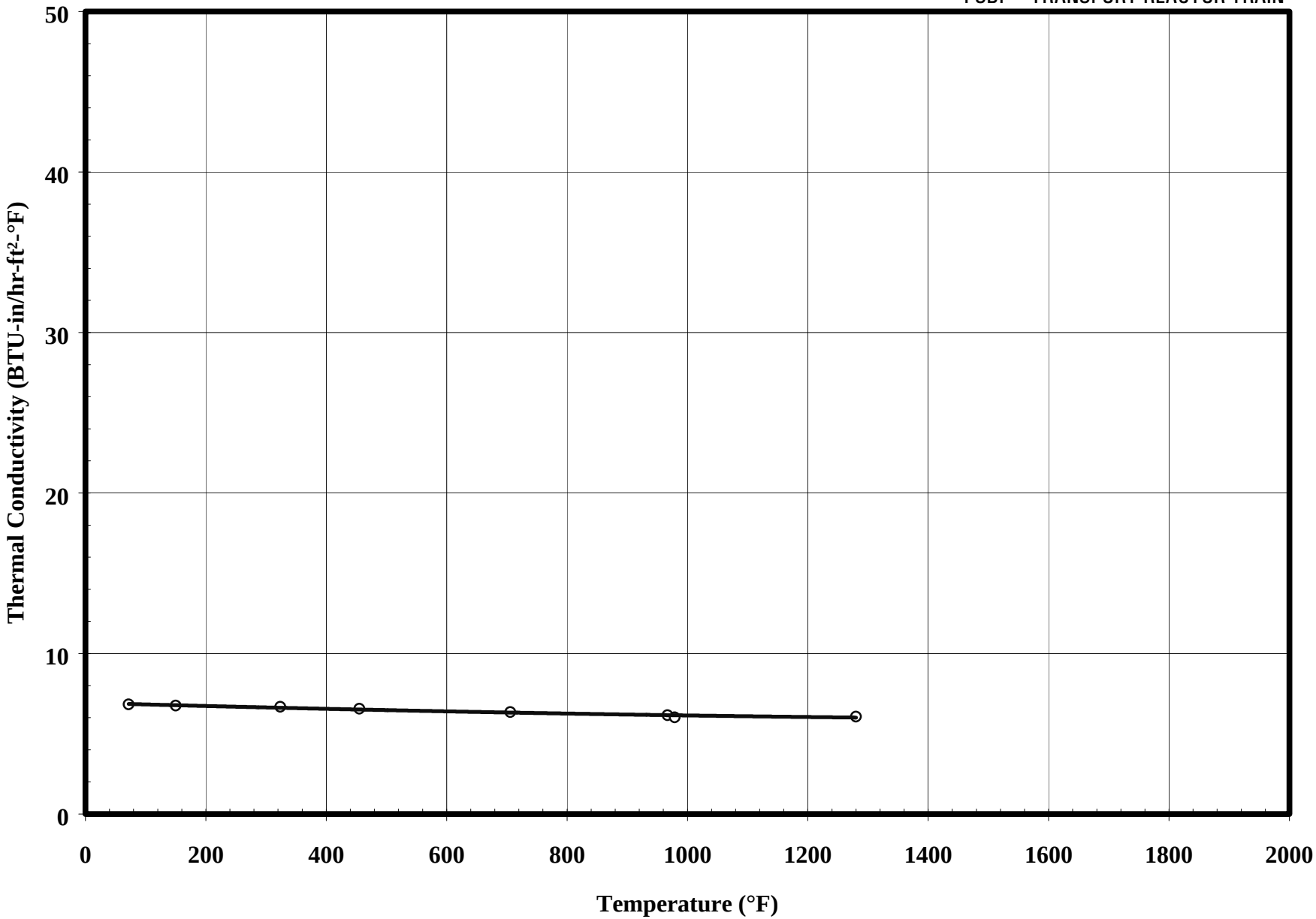

Figure 6.5-3 Radial Thermal Conductivity of Ensto Candle Filter Material

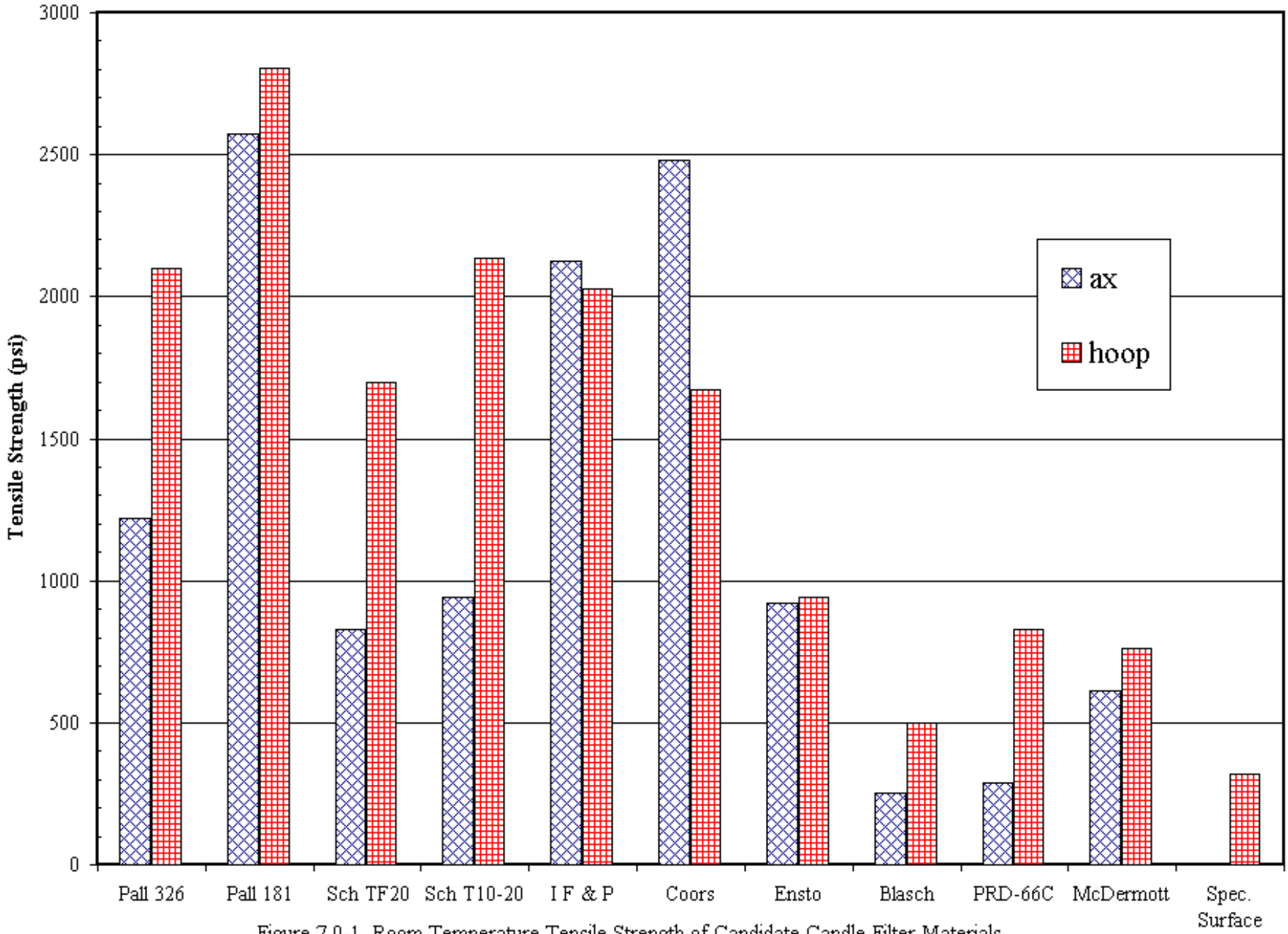

Figure 7.0-1 Room Temperature Tensile Strength of Candidate Candle Filter Materials

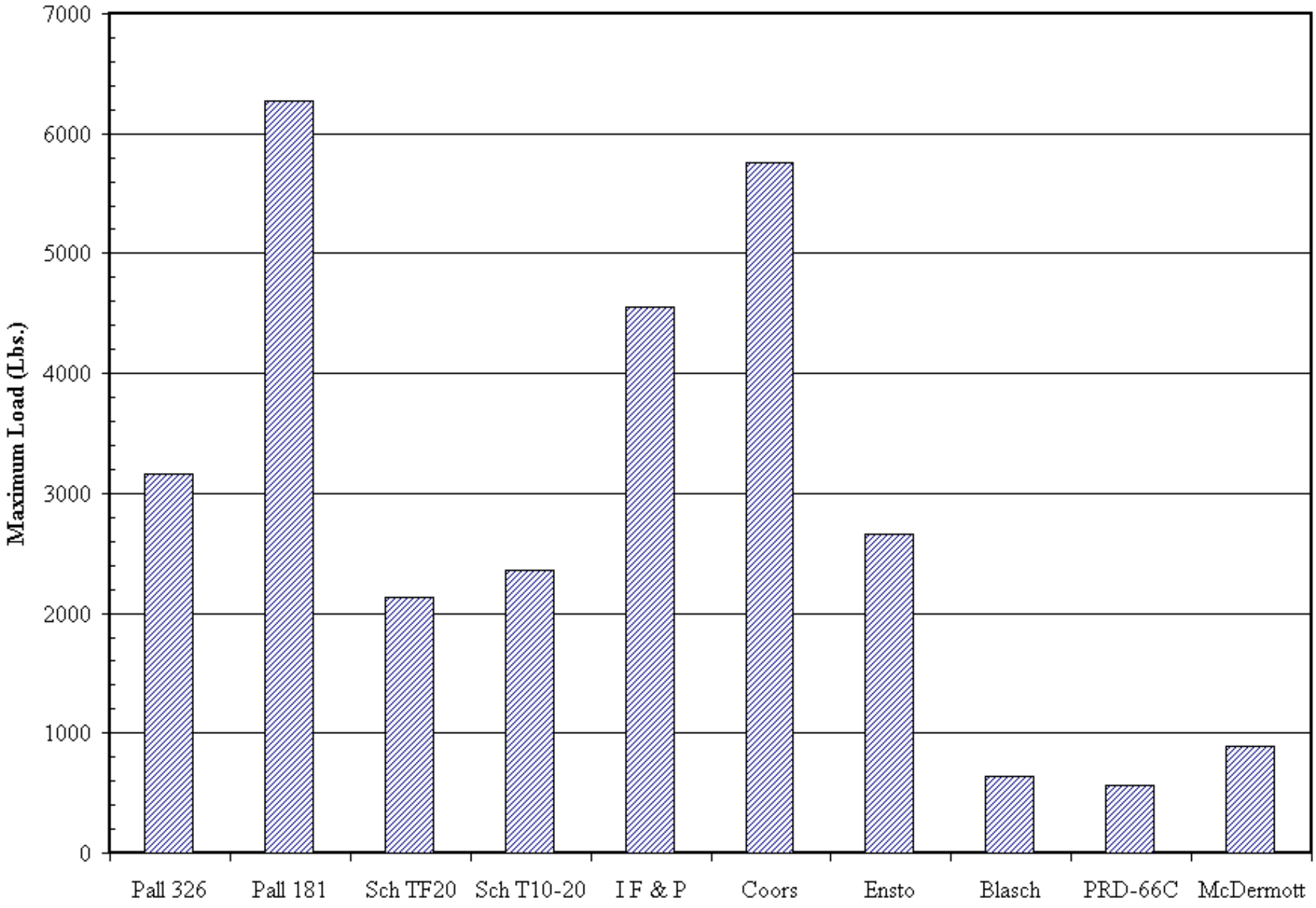

Figure 7.0-2. Maximum Axial Tensile Load Capability of Several Candle Filter Materials

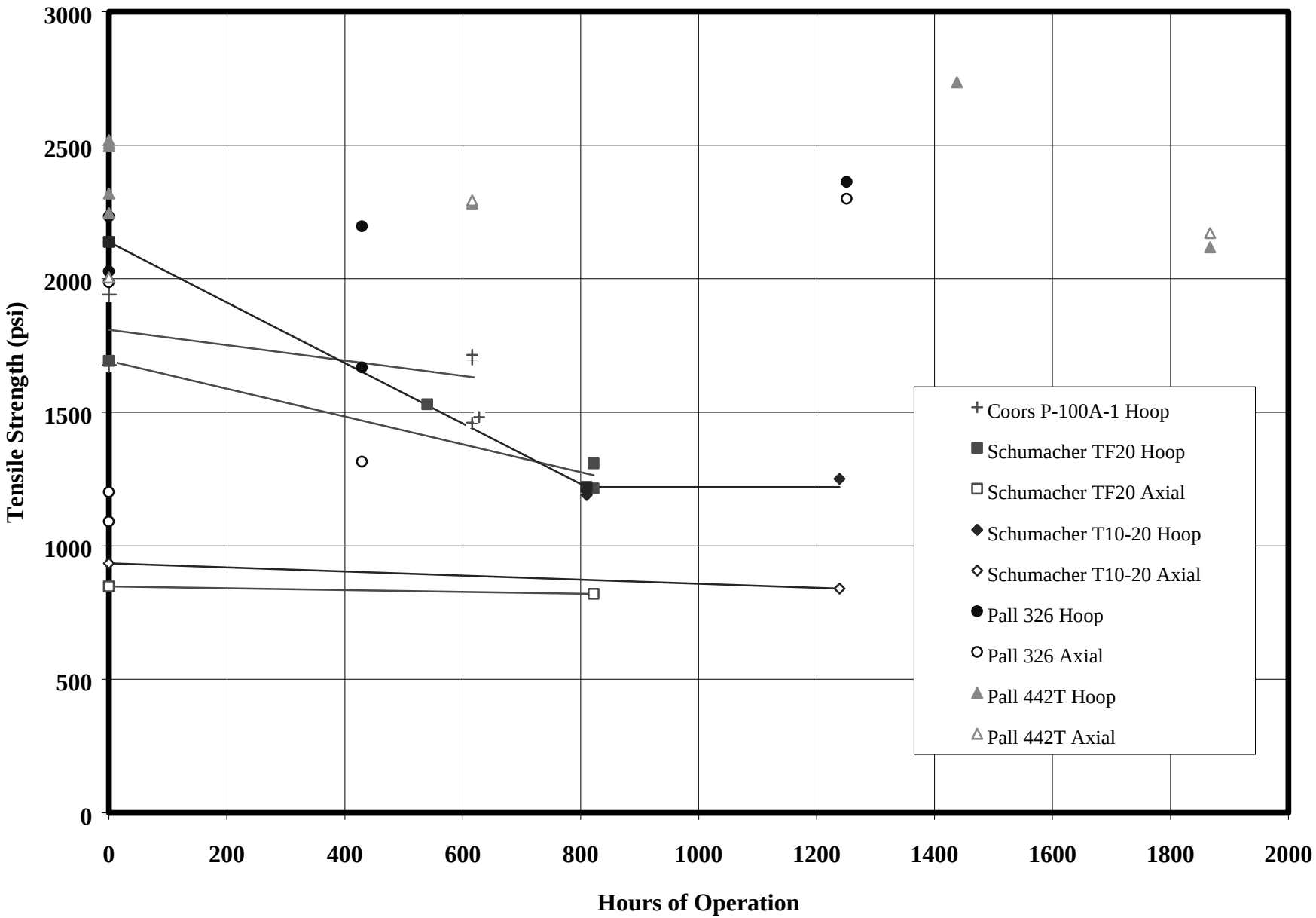

Figure 7.0-3 Room Tensile Strength of Coors P-100A-1, Schumacher TF20 and T10-20, and Pall 326 and 442T

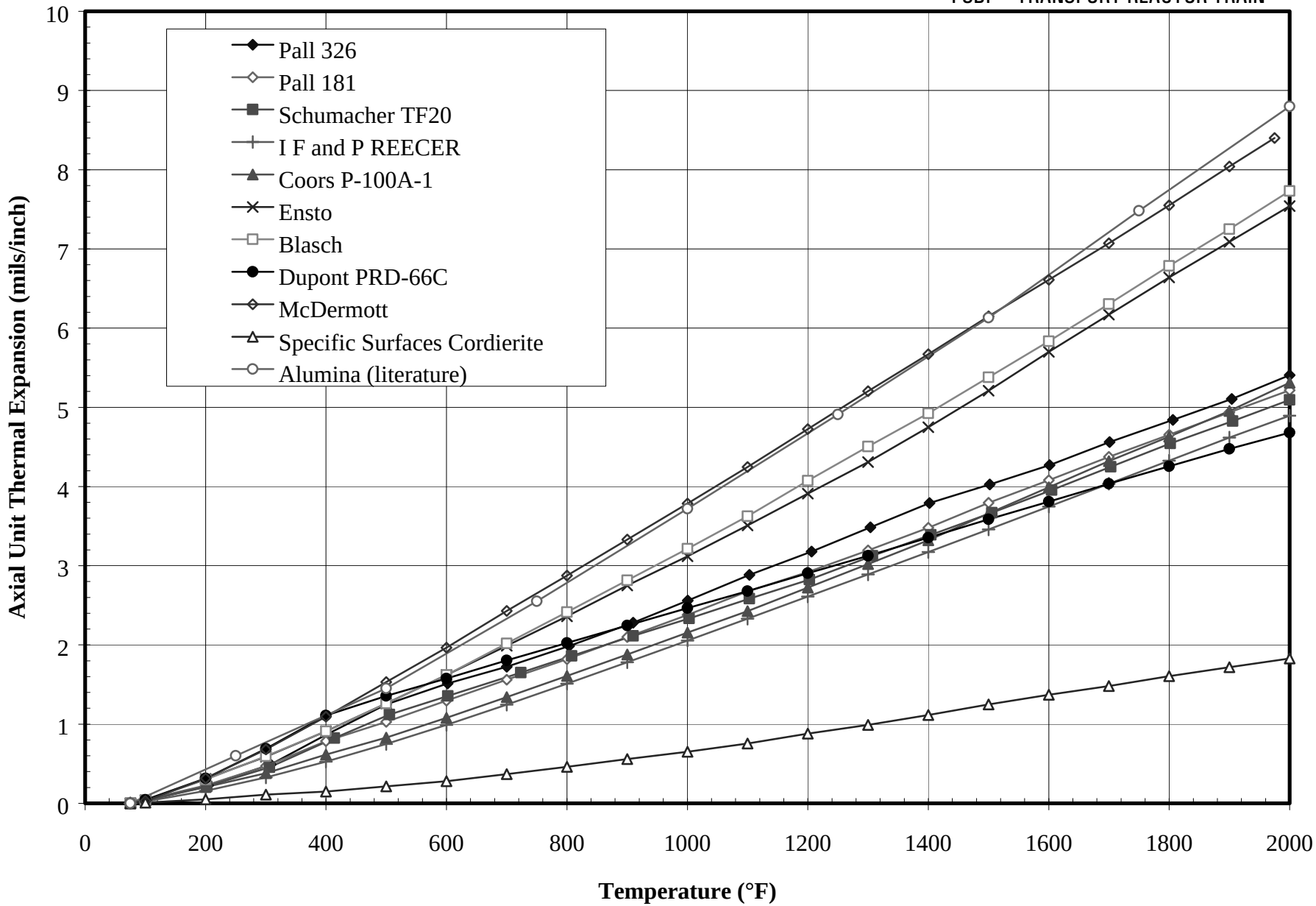

Figure 7.0-4. Thermal Expansion of Candle Filter Materials

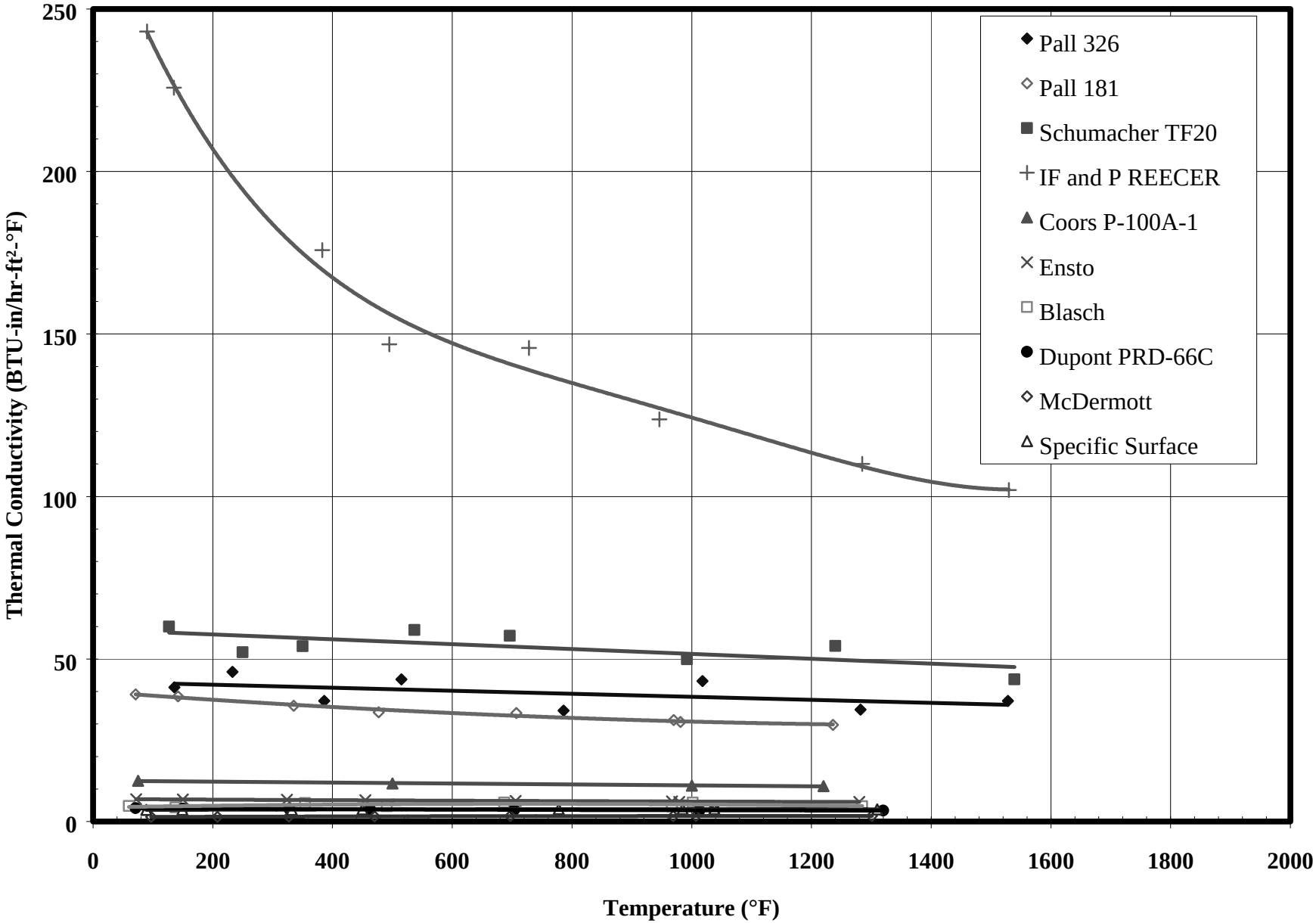

Figure 7.0-5 Radial Thermal Conductivity of Candle Filter Materials

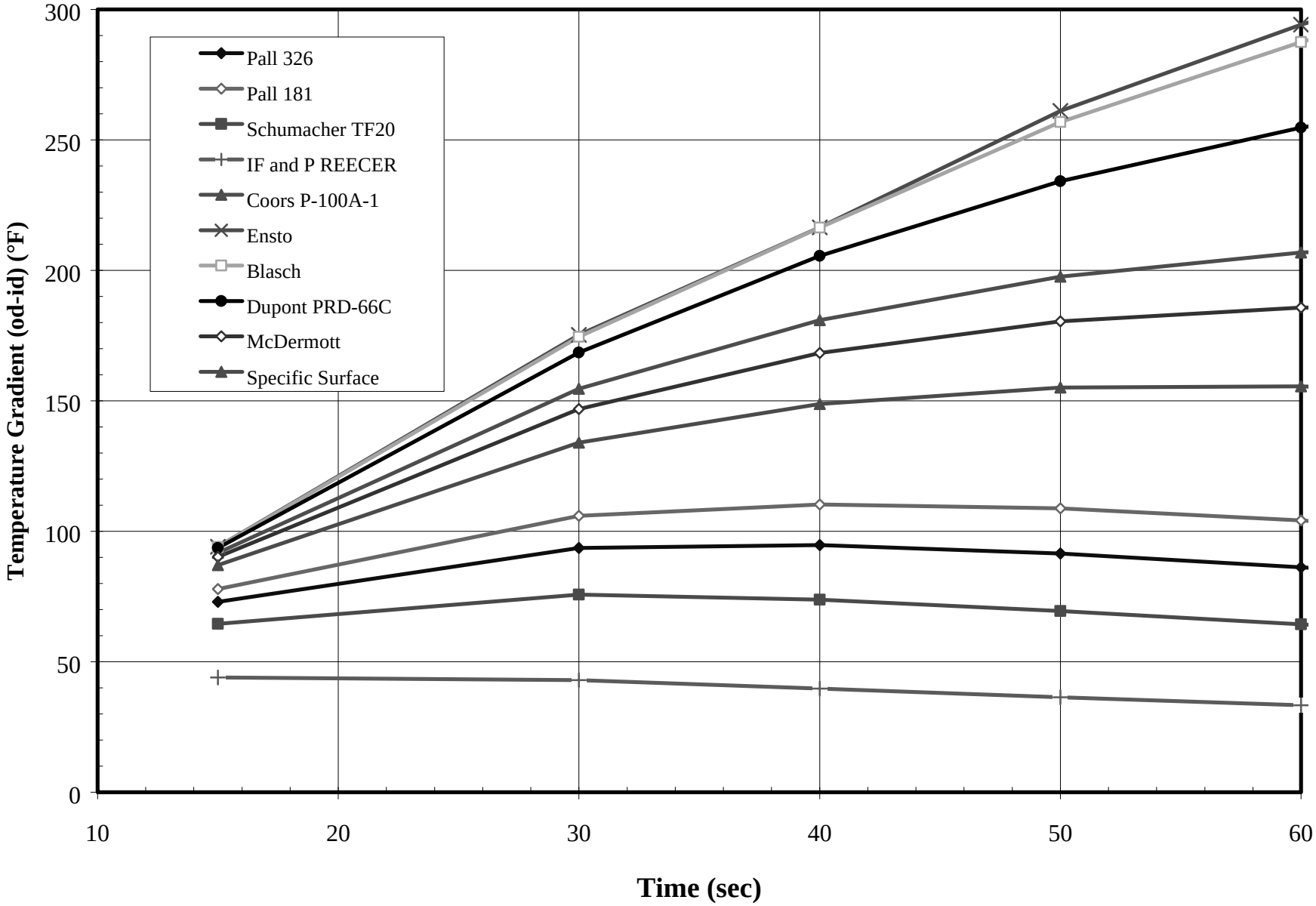

Figure 7.0-6. Temperature Gradient, OD-ID, in Candle Filters During PSDF Thermal Transients

Table 2.0-1
Material Issues for Candle Filters

Pulse Cleaning (thermal stress)	**Process Upsets** (thermal stress and other loads)	**Life** (creep, static fatigue, degradation)	**Installation and Handling**
Thermal expansion	Thermal expansion	Creep	Tensile Strength
Tensile strain-to-failure	Tensile strain-to-failure	Static Fatigue / crack propagation	"Toughness"
"Toughness"	Thermal conductivity	Degradation	
	Tensile Strength	Natural frequency	
	"Toughness"		

Table 4.0-1

Test Matrix for Coors P-100A-1

				Replications at Temp. (°F)	
Element	**Service**	**Test**	**Orientation**	**RT**	**1800**
KC027	as-manuf.	Tn	Hoop	3/3/3	
		TE	Axial	2---------->	
		Light Mic.		Yes	
LC026	as-manuf.	Tn	Hoop	3/3/3	
		TE	Axial	2---------->	
		K	Radial	2---------->	(to ~1250 °F)
		Light Mic.		Yes	
KC005	616 hrs.	Tn	Hoop	3/3/3	
KC011	616 hrs.	Tn	Hoop	3/3/3	
		TE	Axial	2---------->	
		Light Mic.		Yes	
LC025	616 hrs.	Tn	Hoop	3/3/3	
KC007	628 hrs.	Tn	Hoop	3/3/3	
		Light Mic.		Yes	

Legend: Tn - Tensile
TE - Thermal Expansion
K - Thermal Conductivity
Light Mic. - Light Microscopy
3/3/3 - 3 specimens from the bottom section, 3 from the middle and 3 from the top.

Table 4.0-2

Test Matrix for SiC Filter Elements from SCS

		Number of Tests After Exposure at PSDF								
Material	**Test**	**As-Manuf**	**429 Hrs**	**616 Hrs**	**810 Hrs**	**822 Hrs**	**1239 Hrs**	**1251 Hrs**	**1438 Hrs**	**1867 Hrs**
Pall 326	Tn-hoop		18 tests					9 tests		
	Tn-axial		5 tests					5 tests		
	Thermal expansion RT-1800F									
	Microscopy							Yes		
Pall 442T	Tn-hoop			9 tests					9	9
	Tn-axial			5 tests						5
	Thermal expansion RT-1800F									
	Microscopy									Yes
Sch TF20	Tn-hoop					18 tests				
	Tn-axial					5 tests				
	Thermal expansion RT-1800F									
	Microscopy					Yes				
Sch T10-20	Tn-hoop	9 tests			9 test		9 test			
	Tn-axial	5 tests					5 test			
	Thermal expansion RT-1800F	2 tests								
	Microscopy	Yes					Yes			

Table 4.0-3

Test Matrix for Virgin Pall 181

		Replications at			
Test	**Orientation**	**RT**	**1400F**	**1500F**	**1600F**
Tn	Hoop	3/3/3			
	Ax	5	5	5	5
TE	Ax	2----------->(to 2000 °F)			
K	Rad	2----------->(to ~1250 °F)			
Cp		Yes----------->(to ~1500 °F)			
Light Mic.		Yes			

Legend:
Tn - Tensile
TE - Thermal Expansion
K - Thermal Conductivity
Light Mic. - Light Microscopy
3/3/3 - 3 specimens from bottom section, 3 from middle, and 3 from top

Table 4.0-4

Test Matrix for Virgin IF & P Recrystallized SiC

		Replications at			
Test	**Orientation**	**RT**	**1400F**	**1500F**	**1600F**
Tn	Hoop	3/3/3, 2 candles (18 total tests)			
	Ax	5		5	
TE	Ax	2----------->(to 2000 °F)			
K	Rad	2----------->(to ~1500 °F)			
Cp		Yes----------->(to ~1500 °F)			
Light Mic.		Yes			

Legend:
Tn - Tensile
TE - Thermal Expansion
K - Thermal Conductivity
Light Mic. - Light Microscopy
3/3/3 - 3 specimens from bottom section, 3 from middle, and 3 from top

Table 4.0-5

Test Matrix for Virgin Ensto

		Replications at			
Test	**Orientation**	**RT**	**1400F**	**1500F**	**1600F**
Tn	Hoop	3/3/3			
	Ax	5		5	
TE	Ax	2---------->		(to 2000 °F)	
K	Rad	2---------->		(to ~1280 °F)	
Cp		Yes---------->		(to ~1500 °F)	
Light Mic.		Yes			

Legend:
Tn - Tensile
TE - Thermal Expansion
K - Thermal Conductivity
Light Mic. - Light Microscopy
3/3/3 - 3 specimens from bottom section, 3 from middle, and 3 from top

Table 6.1-1

Operational History of Coors P-100A-1 Candle Filters

Candle	Plenum Location	Maximum Temp. (°F)	Hours in Operation
KC027			as-manufactured
LC026			as-manufactured
KC005	B12	1506	616
KC011	T05	1506	616
LC025	T03	1506	616
KC007	B10	1506	628

Table 6.1-2

Room Temperature Hoop Tensile Strength of Coors P-100A-1 Alumina Mullite

Candle	Specimen No.	Hours in Operation	ID, inches	OD, inches	Ultimate Strength, psi	Remarks
KC027	TN-Hoop-1	As-Manuf.	1.63	2.35	1530	
KC027	TN-Hoop-2	As-Manuf.	1.63	2.36	1700	
KC027	TN-Hoop-3	As-Manuf.	1.62	2.36	1700	
KC027	Tn-Hoop-4	As-Manuf.	1.61	2.35	1663	
KC027	Tn-Hoop-5	As-Manuf.	1.60	2.35	1555	
KC027	Tn-Hoop-6	As-Manuf.	1.64	2.36	1630	
KC027	Tn-Hoop-7	As-Manuf.	1.63	2.36	1813	
KC027	Tn-Hoop-8	As-Manuf.	1.64	2.38	1744	
~~KC027~~	~~Tn-Hoop-9~~	~~As-Manuf.~~	~~1.64~~	~~2.38~~	~~1755~~	
			Average		1677	
			Standard Deviation		88	
			COV		5%	
LC026	Tn-Hoop-16	As-Manuf.	1.61	2.37	1958	
LC026	Tn-Hoop-17	As-Manuf.	1.60	2.37	1945	
LC026	Tn-Hoop-18	As-Manuf.	1.62	2.38	1913	
LC026	Tn-Hoop-19	As-Manuf.	1.63	2.35	2062	
LC026	Tn-Hoop-20	As-Manuf.	1.63	2.36	1767	
LC026	Tn-Hoop-21	As-Manuf.	1.60	2.37	1873	
LC026	Tn-Hoop-22	As-Manuf.	1.59	2.39	1705	
LC026	Tn-Hoop-23	As-Manuf.	1.63	2.35	2201	
~~LC026~~	~~Tn-Hoop-24~~	~~As-Manuf.~~	~~1.63~~	~~2.37~~	~~2045~~	
			Average		1941	
			Standard Deviation		143	
			COV		7%	
KC005	Tn-Hoop-10	616	1.60	2.33	1797	
KC005	Tn-Hoop-11	616	1.60	2.34	1785	
KC005	Tn-Hoop-12	616	1.62	2.36	1713	
KC005	Tn-Hoop-13	616	1.64	2.35	1723	
KC005	Tn-Hoop-14	616	1.65	2.39	1625	
KC005	Tn-Hoop-15	616	1.62	2.35	1457	
KC005	Tn-Hoop-16	616	1.64	2.37	1712	
KC005	Tn-Hoop-17	616	1.62	2.37	1600	
~~KC005~~	~~Tn-Hoop-18~~	~~616~~	~~1.63~~	~~2.35~~	~~1868~~	
			Average		1698	
			Standard Deviation		116	
			COV		7%	

Table 6.1-2 (Cont'd)

Room Temperature Hoop Tensile Strength of Coors P-100A-1 Alumina Mullite

Candle	Specimen No.	Hours in Operation	ID, inches	OD, inches	Ultimate Strength, psi	Remarks
KC011	Tn-Hoop-19	616	1.60	2.39	1346	
KC011	Tn-Hoop-20	616	1.60	2.39	1309	
KC011	Tn-Hoop-21	616	1.61	2.36	1323	
KC011	Tn-Hoop-22	616	1.61	2.36	1574	
KC011	Tn-Hoop-23	616	1.64	2.39	1487	
KC011	Tn-Hoop-24	616	1.61	2.36	1472	
KC011	Tn-Hoop-25	616	1.63	2.36	1562	
KC011	Tn-Hoop-26	616	1.64	2.39	1534	
~~KC011~~	~~Tn-Hoop-27~~	~~616~~	~~1.61~~	~~2.37~~	~~1542~~	
			Average		1461	
			Standard Deviation		101	
			COV		7%	
LC025	Tn-Hoop-28	616	1.63	2.36	1544	
LC025	Tn-Hoop-29	616	1.59	2.35	1618	
LC025	Tn-Hoop-30	616	1.60	2.33	1740	
LC025	Tn-Hoop-31	616	1.59	2.36	1471	
LC025	Tn-Hoop-32	616	1.60	2.33	1524	
LC025	Tn-Hoop-33	616	1.64	2.35	1795	
LC025	Tn-Hoop-34	616	1.61	2.33	2059	
LC025	Tn-Hoop-35	616	1.63	2.34	1886	
~~LC025~~	~~Tn-Hoop-36~~	~~616~~	~~1.60~~	~~2.37~~	~~1797~~	
			Average		1715	
			Standard Deviation		181	
			COV		11%	
KC007	TN-Hoop-1	628	1.63	2.40	1270	
KC007	TN-Hoop-2	628	1.63	2.40	1400	
KC007	TN-Hoop-3	628	1.63	2.40	1610	
KC007	TN-Hoop-4	628	1.57	2.37	1380	
KC007	TN-Hoop-5	628	1.63	2.40	1570	
KC007	TN-Hoop-6	628	1.63	2.35	1660	
KC007	TN-Hoop-7	628	1.61	2.38	250	not included in statistics
KC007	TN-Hoop-8	628	1.63	2.35	150	not included in statistics
~~KC007~~	~~TN-Hoop-9~~	~~628~~	~~1.65~~	~~2.38~~	~~450~~	not included in statistics
			Average		1482	
			Standard Deviation		140	
			COV		9%	

Table 6.2-1

Operational History of Clay-Bonded Candle Filters

Material	Candle	Plenum Location	Maximum Temp. (F°)	Hours in Operation
Schumacher TF20	324H12	B47	1463	P22
Schumacher TF20	324H13	B19	1463	P22
Schumacher T10-20	360H071			As-manufactured
Schumacher T10-20	324H016	B27	1463	810
Schumacher T10-20	324H018	T24	1477	1239
Pall 326	1-36A	T2	1477	429
Pall 326	3-24A	B48	1477	429
Pall 326	4-991	T28	1477	1251
Pall 442T	1A-4	B36	1506	616
Pall 442T	5-948	B13	1506	1438
Pall 442T	2-1018	B14	1506	1867

Table 6.2-2

Room Temperature Hoop Tensile Strength of Schumacher TF20 T10-20 Candle Filter Material

Material	Candle	Specimen Number	Hours in Operation	I.D. (in.)	O.D. (in.)	Ultimate Strength (psi)	Remarks
TF20	S199/315E PT-20	TN-Hoop-1	As-Manuf.	1.54	2.37	1740	See Note 1
TF20	S199/315E PT-20	TN-Hoop-2	As-Manuf.	1.54	2.37	1720	See Note 1
TF20	S199/315E PT-20	TN-Hoop-3	As-Manuf.	1.53	2.37	1620	See Note 1
TF20	344E-295	TN-Hoop-1	As-Manuf.	1.54	2.38	1600	See Note 1
TF20	344E-295	TN-Hoop-2	As-Manuf.	1.54	2.38	1628	See Note 1
TF20	344E-295	TN-Hoop-3	As-Manuf.	1.54	2.38	1628	See Note 1
TF20	344E-309	TN-Hoop-4	As-Manuf.	1.53	2.38	1750	See Note 1
TF20	344E-309	TN-Hoop-5	As-Manuf.	1.53	2.38	1754	See Note 1
~~TF20~~	~~344E-309~~	~~TN-Hoop-6~~	~~As-Manuf.~~	~~1.53~~	~~2.38~~	~~1788~~	~~See Note 1~~
				Average		1692	
				Standard Deviation		68	
				COV		4%	
TF20	324H12	TN-Hoop-55	822	1.552	2.371	1299	
TF20	324H12	TN-Hoop-56	822	1.543	2.370	1222	
TF20	324H12	TN-Hoop-57	822	1.564	2.368	1248	
TF20	324H12	TN-Hoop-58	822	1.584	2.374	1145	
TF20	324H12	TN-Hoop-59	822	1.583	2.373	1181	
TF20	324H12	TN-Hoop-60	822	1.586	2.378	1205	
TF20	324H12	TN-Hoop-61	822	1.605	2.374	1218	
TF20	324H12	TN-Hoop-62	822	1.600	2.368	1240	
~~TF20~~	~~324H12~~	~~TN-Hoop-63~~	~~822~~	~~1.602~~	~~2.368~~	~~1180~~	
				Average		1215	
				Standard Deviation		42	
				COV		3%	
TF20	324H13	TN-Hoop-64	822	1.551	2.376	1444	
TF20	324H13	TN-Hoop-65	822	1.552	2.372	1392	
TF20	324H13	TN-Hoop-66	822	1.560	2.374	1199	
TF20	324H13	TN-Hoop-67	822	1.585	2.375	1260	
TF20	324H13	TN-Hoop-68	822	1.586	2.377	1300	
TF20	324H13	TN-Hoop-69a	822	1.583	2.379	1236	
TF20	324H13	TN-Hoop-69b	822	1.590	2.385	1306	
TF20	324H13	TN-Hoop-70	822	1.604	2.376	1314	
TF20	324H13	TN-Hoop-71	822	1.602	2.376	1378	
~~TF20~~	~~324H13~~	~~TN-Hoop-72~~	~~822~~	~~1.604~~	~~2.374~~	~~1262~~	
				Average		1309	
				Standard Deviation		72	
				COV		6%	

Table 6.2-2 (continued)

Room Temperature Hoop Tensile Strength of Schumacher TF20 T10-20 Candle Filter Material

Material	Candle	Specimen Number	Hours in Operation	I.D. (in.)	O.D. (in.)	Ultimate Strength (psi)	Remarks
T10-20	360H071	TN-Hoop-73	As-manuf.	1.54	2.38	2372	
T10-20	360H071	TN-Hoop-74	As-manuf.	1.55	2.37	2354	
T10-20	360H071	TN-Hoop-75	As-manuf.	1.56	2.38	2059	
T10-20	360H071	TN-Hoop-76	As-manuf.	1.58	2.38	2314	
T10-20	360H071	TN-Hoop-77	As-manuf.	1.59	2.38	2242	
T10-20	360H071	TN-Hoop-78	As-manuf.	1.59	2.39	2429	
T10-20	360H071	TN-Hoop-79	As-manuf.	1.56	2.39	1832	
T10-20	360H071	TN-Hoop-80	As-manuf.	1.60	2.39	1801	
~~T10-20~~	~~360H071~~	~~TN-Hoop-81~~	~~As-manuf.~~	~~1.59~~	~~2.37~~	~~1839~~	
				Average		2138	
				Standard Deviation		243	
				COV		11%	
T10-20	324H016	TN-Hoop-82	810	1.55	2.37	1194	
T10-20	324H016	TN-Hoop-83	810	1.56	2.37	1229	
T10-20	324H016	TN-Hoop-84	810	1.56	2.37	1257	
T10-20	324H016	TN-Hoop-85	810	1.58	2.37	1246	
T10-20	324H016	TN-Hoop-86	810	1.59	2.38	952	
T10-20	324H016	TN-Hoop-87A	810	1.59	2.38	1270	
T10-20	324H016	TN-Hoop-87B	810	1.59	2.38	1233	
T10-20	324H016	TN-Hoop-88	810	1.60	2.37	1313	
T10-20	324H016	TN-Hoop-89	810	1.60	2.37	1301	
~~T10-20~~	~~324H016~~	~~TN-Hoop-90~~	~~810~~	~~1.60~~	~~2.38~~	~~907~~	
				Average		1190	
				Standard Deviation		135	
				COV		11%	
T10-20	324H018	TN-Hoop-91	1239	1.56	2.37	1309	
T10-20	324H018	TN-Hoop-92	1239	1.56	2.37	1296	
T10-20	324H018	TN-Hoop-93	1239	1.57	2.37	1303	
T10-20	324H018	TN-Hoop-94	1239	1.58	2.37	1147	
T10-20	324H018	TN-Hoop-95	1239	1.59	2.37	1208	
T10-20	324H018	TN-Hoop-96	1239	1.59	2.37	1271	
T10-20	324H018	TN-Hoop-97	1239	1.61	2.39	1230	
T10-20	324H018	TN-Hoop-98	1239	1.60	2.37	1196	
~~T10-20~~	~~324H018~~	~~TN-Hoop-99~~	~~1239~~	~~1.61~~	~~2.38~~	~~1303~~	
				Average		1251	
				Standard Deviation		55	
				COV		4%	

Table 6.2-3

Room Temperature Axial Tensile Properties of Schumacher TF20 and T10-20

Material	Candle	Specimen Number	Hours in Operation	Ultimate Strength (psi)	Young's Modulus (Msi)	Strain-to-Failure mils./in.	Remarks
TF20	344E-295	TN-AX-3	As-Manuf.	426	3.22	0.15	
TF20	344E-295	TN-AX-7	As-Manuf.	414	3.70	0.11	
TF20	344E-309	TN-AX-12	As-Manuf.	798	4.28	0.20	
TF20	344E-309	TN-AX-17	As-Manuf.	496	5.00	0.10	
~~TF20~~	~~344E-309~~	~~TN-AX-21~~	~~As-Manuf.~~	~~898~~	~~3.92~~	~~0.23~~	
		Average		606	4.02	0.16	
		Standard Deviation		202	0.6	0.05	
		COV		33%	15%	32%	
TF20	S-350 F/33	TN-AX-1	540				Broke during assembly
TF20	S-350 F/33	TN-AX-2	540	796	3.22	0.32	Karhula
~~TF20~~	~~S-350 F/33~~	~~TN-AX-3~~	~~540~~	~~825~~	~~3.83~~	~~0.31~~	~~Karhula~~
		Average		811	3.53	0.32	
TF20	324H12	TN-AX-21	822				Broke in handling
TF20	324H12	TN-AX-22	822				Broke in handling
TF20	324H12	TN-AX-23	822	415	4.12	0.09	SCS
TF20	324H12	TN-AX-24	822	725	3.39	0.22	SCS
~~TF20~~	~~324H12~~	~~TN-AX-25~~	~~822~~	~~916~~	~~3.72~~	~~0.30~~	~~SCS~~
		Average		685	3.74	0.20	
		Standard Deviation		206	0.3	0.09	
		COV		30%	8%	43%	
TF20	S-350 F/30	TN-AX-1	1166				Specimen was cracked; broke during assembly
TF20	S-350 F/30	TN-AX-2	1166	834	3.52	0.26	Karhula
~~TF20~~	~~S-350 F/30~~	~~TN-AX-3~~	~~1166~~	~~827~~	~~4.09~~	~~0.28~~	~~Karhula~~
		Average		831	3.81	0.27	
T10-20	360H071	TN-AX-26	0				Broke in handling
T10-20	360H071	TN-AX-27	0				Broke in handling
T10-20	360H071	TN-AX-28	0	967	3.85	0.26	SCS
T10-20	360H071	TN-AX-29	0	903	4.10	0.22	SCS
~~T10-20~~	~~360H071~~	~~TN-AX-30~~	~~0~~	—	—	—	Broke in handling
		Average		935	3.98	0.24	
T10-20	324H018	TN-AX-31	1239	801	4.19	0.21	SCS
T10-20	324H018	TN-AX-32	1239	905	4.04	0.28	SCS
T10-20	324H018	TN-AX-33	1239	884	3.60	0.27	SCS
T10-20	324H018	TN-AX-34	1239				Broke in handling
~~T10-20~~	~~324H018~~	~~TN-AX-35~~	~~1239~~	~~768~~	~~3.53~~	~~0.24~~	~~SCS~~
		Average		840	3.84	0.25	
		Standard Deviation		57	0.3	0.03	
		COV		7%	7%	11%	

Table 6.2-4

Room Temperature Hoop Tensile Strength of Pall 326 and 442T Candle Filter Material

Material	Candle	Specimen Number	Hours in Operation	ID (in.)	OD (in.)	Ultimate Strength (psi)	Remarks
326	3-24A	TN-Hoop-1	429	1.55	2.37	1647	
326	3-24A	TN-Hoop-2	429	1.55	2.38	1762	
326	3-24A	TN-Hoop-3	429	1.56	2.38	1510	
326	3-24A	TN-Hoop-4	429	1.58	2.38	1629	
326	3-24A	TN-Hoop-5	429	1.58	2.38	1713	
326	3-24A	TN-Hoop-6	429	1.58	2.38	1751	
326	3-24A	TN-Hoop-7	429	1.60	2.38	1625	
326	3-24A	TN-Hoop-8	429	1.60	2.38	1624	
326	3-24A	TN-Hoop-9	429	1.60	2.38	1755	
326	1-36A	TN-Hoop-10	429	1.55	2.37	2072	
326	1-36A	TN-Hoop-11	429	1.55	2.37	2236	
326	1-36A	TN-Hoop-12	429	1.55	2.38	2241	
326	1-36A	TN-Hoop-13	429	1.57	2.38	2254	
326	1-36A	TN-Hoop-14	429	1.57	2.39	2175	
326	1-36A	TN-Hoop-15a	429	1.58	2.39	2185	
326	1-36A	TN-Hoop-15b	429	1.58	2.39	2221	
326	1-36A	TN-Hoop-16	429	1.60	2.37	2206	
326	1-36A	TN-Hoop-17	429	1.60	2.37	2109	
~~326~~	~~1-36A~~	~~TN-Hoop-18~~	~~429~~	~~1.60~~	~~2.36~~	~~2260~~	
				Average		1946	
				Standard Deviation		272	
				COV		14%	
326	4-991	Tn-Hoop-19	1251	1.55	2.36	2396	
326	4-991	Tn-Hoop-20	1251	1.55	2.36	2404	
326	4-991	Tn-Hoop-21	1251	1.55	2.37	2239	
326	4-991	Tn-Hoop-22	1251	1.58	2.37	2319	
326	4-991	Tn-Hoop-23	1251	1.57	2.37	2411	
326	4-991	Tn-Hoop-24	1251	1.57	2.37	2425	
326	4-991	Tn-Hoop-25	1251	1.60	2.37	2267	
326	4-991	Tn-Hoop-26	1251	1.59	2.37	2372	
~~326~~	~~4-991~~	~~Tn-Hoop-27~~	~~1251~~	~~1.60~~	~~2.36~~	~~2428~~	
				Average		2362	
				Standard Deviation		66	
				COV		3%	

Table 6.2-4 (continued)

Room Temperature Hoop Tensile Strength of Pall 326 and 442T Candle Filter Material

Material	Candle	Specimen Number	Hours in Operation	ID (in.)	OD (in.)	Ultimate Strength (psi)	Remarks
442T	1A-4	TN-Hoop-28	616	1.54	2.36	2313	
442T	1A-4	TN-Hoop-29	616	1.53	2.35	2257	
442T	1A-4	TN-Hoop-30	616	1.53	2.36	2199	
442T	1A-4	TN-Hoop-31	616	1.55	2.37	2233	
442T	1A-4	TN-Hoop-32	616	1.56	2.37	2262	
442T	1A-4	TN-Hoop-33	616	1.56	2.37	2206	
442T	1A-4	TN-Hoop-34	616	1.58	2.37	2296	
442T	1A-4	TN-Hoop-35	616	1.58	2.36	2363	
~~442T~~	~~1A-4~~	~~TN-Hoop-36~~	~~616~~	~~1.58~~	~~2.36~~	~~2406~~	
				Average		2282	
				Standard Deviation		66	
				COV		3%	
442T	5-948	TN-Hoop-37	1438	1.52	2.35	2607	
442T	5-948	TN-Hoop-38	1438	1.53	2.35	2466	
442T	5-948	TN-Hoop-39	1438	1.55	2.36	2766	
442T	5-948	TN-Hoop-40	1438	1.55	2.36	2759	
442T	5-948	TN-Hoop-41	1438	1.55	2.36	2795	
442T	5-948	TN-Hoop-42a	1438	1.55	2.36	2769	
442T	5-948	TN-Hoop-42b	1438	1.55	2.36	2646	
442T	5-948	TN-Hoop-43	1438	1.57	2.36	2604	
442T	5-948	TN-Hoop-44	1438	1.57	2.35	2916	
~~442T~~	~~5-948~~	~~TN-Hoop-45~~	~~1438~~	~~1.59~~	~~2.35~~	~~3021~~	
				Average		2735	
				Standard Deviation		153	
				COV		6%	
442T	2-1018	TN-Hoop-46	1867	1.52	2.36	2159	
442T	2-1018	TN-Hoop-47	1867	1.53	2.36	2157	
442T	2-1018	TN-Hoop-48	1867	1.53	2.36	1951	
442T	2-1018	TN-Hoop-49	1867	1.55	2.37	2160	
442T	2-1018	TN-Hoop-50	1867	1.55	2.37	2026	
442T	2-1018	TN-Hoop-51	1867	1.55	2.37	2174	
442T	2-1018	TN-Hoop-52	1867	1.57	2.36	2074	
442T	2-1018	TN-Hoop-53	1867	1.59	2.37	2145	
~~442T~~	~~2-1018~~	~~TN-Hoop-54~~	~~1867~~	~~1.56~~	~~2.34~~	~~2215~~	
				Average		2118	
				Standard Deviation		79	
				COV		4%	

Table 6.2-5

Room Temperature Axial Tensile Properties of Pall 326 and 442T

Material	Candle	Specimen Number	Hours in Operation	Ultimate Strength (psi)	Modulus (Msi)	Strain-to-Failure (in./in.)	Remarks
326	4-471	TN-AX-12	As-Manuf.	1152	5.88	0.20	See Note 1
326	4-471	TN-AX-17	As-Manuf.	1250	6.67	0.19	See Note 1
326	2-469	TN-AX-5	As-Manuf.	910	4.82	0.19	See Note 1
326	2-469	TN-AX-11	As-Manuf.	1272	5.06	0.25	See Note 1
~~326~~	~~2-470~~	~~TN-AX-22~~	~~As-Manuf.~~	~~1987~~	~~6.22~~	~~0.35~~	~~See Note 1~~
		Average		1314	5.73	0.24	
		Standard Deviation		360	0.7	0.06	
		COV		27%	12%	26%	
326	3-24A	TN-AX-1	429	1151	5.12	0.26	
326	3-24A	TN-AX-2	429	1120	5.30	0.21	
326	3-24A	TN-AX-3	429	1476	5.86	0.31	
326	3-24A	TN-AX-4	429	1422	4.55	0.36	
~~326~~	~~3-24A~~	~~TN-AX-5~~	~~429~~	~~1405~~	~~5.37~~	~~0.31~~	
		Average		1315	5.24	0.29	
		Standard Deviation		149	0.4	0.05	
		COV		11%	8%	18%	
326	4-991	TN-AX-6	1251	2560	7.27	0.38	
326	4-991	TN-AX-7	1251	2417	7.55	0.33	
326	4-991	TN-AX-8	1251	2621	5.84	0.50	
326	4-991	TN-AX-9	1251	1825	7.34	0.27	
~~326~~	~~4-991~~	~~TN-AX-10~~	~~1251~~	~~2071~~	~~7.21~~	~~0.32~~	
		Average		2299	7.04	0.36	
		Standard Deviation		304	0.6	0.08	
		COV		13%	9%	22%	
442T	1-94	TN-AX-1	As-Manuf.	1678	6.63	0.26	See Note 1
442T	1-94	TN-AX-6	As-Manuf.	2001	5.38	0.38	See Note 1
442T	1-94	TN-AX-8	As-Manuf.	2118	6.22	0.35	See Note 1
442T	1-94	TN-AX-15	As-Manuf.	2145	5.68	0.40	See Note 1
~~442T~~	~~1-94~~	~~TN-AX-21~~	~~As-Manuf.~~	~~2081~~	~~6.10~~	~~0.35~~	~~See Note 1~~
		Average		2005	6.00	0.35	
		Standard Deviation		170	0.43	0.05	
		COV		8%	7%	14%	
442T	1A-4	TN-AX-11	616	2471	7.34	0.36	
442T	1A-4	TN-AX-12	616	2169	7.84	0.27	
442T	1A-4	TN-AX-13	616	2270	7.17	0.32	
442T	1A-4	TN-AX-14	616	2340	6.45	0.36	
~~442T~~	~~1A-4~~	~~TN-AX-15~~	~~616~~	~~2215~~	~~6.81~~	~~0.34~~	
		Average		2293	7.12	0.33	
		Standard Deviation		106	0.5	0.03	
		COV		5%	7%	10%	
442T	2-1018	TN-AX-16	1867	1880	6.35	0.29	
442T	2-1018	TN-AX-17	1867	2390	6.64	0.36	
442T	2-1018	TN-AX-18	1867	2255	6.25	0.36	
442T	2-1018	TN-AX-19	1867	2160	6.61	0.32	
~~442T~~	~~2-1018~~	~~TN-AX-20~~	~~1867~~	~~—~~	~~—~~	~~—~~	~~Broke in handling~~
		Average		2171	6.46	0.33	
		Standard Deviation		187	0.2	0.03	
		COV		9%	3%	9%	

Note 1: Measured under DOE/FETC contract.

Table 6.3-1

Room Temperature Hoop Tensile Strength of Pall 181 Candle Filter Material

Candle	Specimen Number	Hours in Operation	I.D. (in.)	O.D. (in.)	Ultimate Strength (psi)	Remarks
7-1405H	Tn-Hoop-190	As-Manuf.	1.55	2.36	2790	
7-1405H	Tn-Hoop-191	As-Manuf.	1.55	2.37	2860	
7-1405H	Tn-Hoop-192	As-Manuf.	1.55	2.37	2930	
7-1405H	Tn-Hoop-193	As-Manuf.	1.57	2.36	2970	
7-1405H	Tn-Hoop-194	As-Manuf.	1.57	2.37	2990	
7-1405H	Tn-Hoop-195	As-Manuf.	1.57	2.36	2920	
7-1405H	Tn-Hoop-196	As-Manuf.	1.57	2.36	2470	
7-1405H	Tn-Hoop-197	As-Manuf.	1.60	2.33	2610	
~~7-1405H~~	~~Tn-Hoop-198~~	~~As-Manuf.~~	~~1.60~~	~~2.35~~	~~2700~~	
			Average		2804	
			Standard Deviation		168	
			COV		6%	

Table 6.3-2

Axial Tensile Properties of Virgin Pall 181 Filter Material

Candle	Specimen Number	Test Temperature (°F)	Ultimate Strength (psi)	Young's Modulus (Msi)	Strain-to-Failure (mils/in.)	Remarks
7-1405H	TN-AX-76	RT				Broke in handling
7-1405H	TN-AX-80	RT	2483	5.19	0.48	
7-1405H	TN-AX-84	RT	2895	5.56	0.59	
7-1405H	TN-AX-87	RT				Broke in handling
7-1405H	TN-AX-90	RT	2363	6.20	0.40	
7-1405H	TN-AX-92	RT	2554	6.59	0.39	
7-1405H	TN-AX-93	RT				Broke in handling
~~7-1405H~~	~~TN-AX-94~~	~~RT~~	~~2582~~	~~6.67~~	~~0.39~~	
	Average		2575	6.04	0.45	
	Standard Deviation		177	0.6	0.08	
	COV		7%	10%	17%	
7-1405H	TN-AX-77	1400	2520	4.76	0.54	
~~7-1405H~~	~~TN-AX-85~~	~~1400~~	~~2586~~	~~5.74~~	~~0.42~~	
	Average		2553	5.25	0.48	
7-1405H	TN-AX-78	1500	2210	3.29	0.66	
7-1405H	TN-AX-81	1500	2110	5.46	0.39	
7-1405H	TN-AX-82	1500	1654	5.25	0.34	
7-1405H	TN-AX-83	1500	2266	5.49	0.49	
7-1405H	TN-AX-86	1500	2030	4.36	0.49	
7-1405H	TN-AX-89	1500	1922	5.96	0.41	
~~7-1405H~~	~~TN-AX-91~~	~~1500~~	~~2230~~	~~5.00~~	~~0.52~~	
	Average		2060	4.97	0.47	
	Standard Deviation		200	0.8	0.10	
	COV		10%	17%	21%	
7-1405H	TN-AX-79	1600	2170	3.14	0.87	
7-1405H	TN-AX-88	1600	2218	4.03	0.89	
~~7-1405H~~	~~TN-AX-95~~	~~1600~~	~~2002~~	~~3.64~~	~~0.73~~	
	Average		2130	3.60	0.83	
	Standard Deviation		93	0.4	0.07	
	COV		4%	10%	9%	

Table 6.4-1

Room Temperature Hoop Tensile Strength of I F & P Reecer Candle Filter Material

Candle	Specimen Number	Hours in Operation	I.D. (in.)	O.D. (in.)	Max. Hydrostatic Pressure (psig)	Ultimate Strength (psi)	Remarks
FE98073109	TN-Hoop-118	As-Manuf.	1.72	2.41	493	1530	Failed at hole
FE98073109	TN-Hoop-119	As-Manuf.	1.72	2.40	587	1810	Failed at hole
FE98073109	TN-Hoop-120	As-Manuf.	1.73	2.40	628	1980	Failed at hole
FE98073109	TN-Hoop-121	As-Manuf.	1.78	2.40	657	2260	
FE98073109	TN-Hoop-122	As-Manuf.	1.78	2.41	711	2450	Failed at hole
FE98073109	TN-Hoop-123	As-Manuf.	1.80	2.40	645	2300	Failed at hole
FE98073109	TN-Hoop-124	As-Manuf.	1.82	2.39	564	2120	
FE98073109	TN-Hoop-125	As-Manuf.	1.83	2.40	626	2380	
~~FE98073109~~	~~TN-Hoop-126~~	~~As-Manuf.~~	~~1.82~~	~~2.39~~	~~519~~	~~1930~~	Failed at hole
			Average			2084	
			Standard Deviation			282	
			COV			14%	
FE98073110	TN-Hoop-127	As-Manuf.	1.59	2.40	882	2260	
FE98073110	TN-Hoop-128	As-Manuf.	1.60	2.41	819	2130	
FE98073110	TN-Hoop-129	As-Manuf.	1.62	2.43	824	2130	
FE98073110	TN-Hoop-130	As-Manuf.	1.68	2.40	570	1660	Failed at hole
FE98073110	TN-Hoop-131	As-Manuf.	1.70	2.40	605	1830	
FE98073110	TN-Hoop-132	As-Manuf.	1.71	2.41	671	2040	Failed away from hole
FE98073110	TN-Hoop-133	As-Manuf.	1.76	2.40	548	1800	
FE98073110	TN-Hoop-134	As-Manuf.	1.75	2.39	626	2070	
~~FE98073110~~	~~TN-Hoop-135~~	~~As-Manuf.~~	~~1.78~~	~~2.39~~	~~595~~	~~2060~~	
			Average			1998	
			Standard Deviation			181	
			COV			9%	

Table 6.4-2

Axial Tensile Properties of Virgin I F and P Reecer Filter Material

Candle	Specimen Number	Test Temperature (°F)	Ultimate Strength (psi)	Young's Modulus (Msi)	Strain-to-Failure (mils/in.)	Remarks
FE98073110	TN-AX-66	RT	2150	12.8	0.17	
FE98073110	TN-AX-68	RT	1990	16.3	0.12	
FE98073110	TN-AX-69	RT	2240	14.5	0.16	
FE98073110	TN-AX-70	RT				Broke in handling
FE98073110	TN-AX-72	RT				Broke in handling
FE98073110	TN-AX-73	RT				Broke in handling
~~FE98073110~~	~~TN-AX-74~~	~~RT~~	~~2110~~	~~11.1~~	~~0.19~~	
	Average		2123	13.7	0.16	
	Standard Deviation		90	1.9	0.03	
	COV		4%	14%	16%	
FE98073110	TN-AX-67	1500	1960	20.0	0.11	
FE98073110	TN-AX-71	1500	1990	20.0	0.09	
~~FE98073110~~	~~TN-AX-75~~	~~1500~~	~~950[1]~~	~~16.3~~	~~0.06[1]~~	
	Average		1975	18.8	0.10	

Note 1: Data not included in statistics

Table 6.5-1

Density of Ensto Candle Filter Material

Candle	Specimen Number	I.D. (in.)	O.D. (in.)	Height (in.)	Weight (gr)	Density (gr/cm³)	Density (lb/ft³)
146-97	TN-Hoop-100	1.45	2.40	0.999	89.12	1.885	117.6
146-97	TN-Hoop-101	1.45	2.40	0.999	89.16	1.888	117.8
146-97	TN-Hoop-102	1.45	2.40	0.999	88.92	1.886	117.7
146-97	TN-Hoop-103	1.45	2.39	0.999	88.04	1.884	117.6
146-97	TN-Hoop-104	1.45	2.40	0.999	88.13	1.880	117.3
146-97	TN-Hoop-105	1.45	2.39	0.999	88.17	1.886	117.7
146-97	TN-Hoop-106	1.46	2.42	0.999	91.14	1.903	118.8
146-97	TN-Hoop-107	1.46	2.42	0.999	91.05	1.904	118.8
~~146-97~~	~~TN-Hoop-108~~	~~1.46~~	~~2.42~~	~~0.999~~	~~91.08~~	~~1.905~~	~~118.9~~
			Average			1.885	117.6
			Standard Deviation			0.002	0.150
			COV			0.13%	0.13%

Table 6.5-2

Room Temperature Hoop Tensile Strength of Ensto Candle Filter Material

Candle	Specimen Number	Hours in Operation	I.D. (in.)	O.D. (in.)	Max. Hydrostatic Pressure (psig)	Ultimate Strength (psi)	Remarks
146-97	TN-Hoop-100	As-Manuf.	1.45	2.40	421	895	E=2.2 msi, stf=0.41 mils/in.
146-97	TN-Hoop-101	As-Manuf.	1.45	2.40	423	910	
146-97	TN-Hoop-102	As-Manuf.	1.45	2.40	441	950	
146-97	TN-Hoop-103	As-Manuf.	1.45	2.39	467	1005	
146-97	TN-Hoop-104	As-Manuf.	1.45	2.40	456	990	E=2.8 msi, stf=0.40 mils/in.
146-97	TN-Hoop-105	As-Manuf.	1.45	2.39	412	890	
146-97	TN-Hoop-106	As-Manuf.	1.46	2.42	510	1090	
146-97	TN-Hoop-107	As-Manuf.	1.46	2.42	514	1100	
~~146-97~~	~~TN-Hoop-108~~	~~As-Manuf.~~	~~1.46~~	~~2.42~~	~~500~~	~~1070~~	
			Average			940	
			Standard Deviation			45	
			COV			5%	

Table 6.5-3

Axial Tensile Properties of Ensto Filter Material

Candle	Specimen Number	Test Temperature (°F)	Ultimate Strength (psi)	Young's Modulus (Msi)	Strain-to-Failure (mils/in.)	Remarks
46-97	TN-AX-36	RT	900	2.25	0.49	
46-97	TN-AX-39	RT	960	2.18	0.55	
46-97	TN-AX-42	RT				Broke in handling
46-97	TN-AX-43	RT	900	2.26	0.50	
~~46-97~~	~~TN-AX-45~~	~~RT~~	~~919~~	~~2.44~~	~~0.47~~	
	Average		920	2.28	0.50	
	Standard Deviation		24	0.10	0.03	
	COV		3%	4%	6%	
46-97	TN-AX-37	1500	740	2.11	0.35	
46-97	TN-AX-38	1500	880	2.53	0.36	
46-97	TN-AX-40	1500	980	2.14	0.46	
~~46-97~~	~~TN-AX-44~~	~~1500~~	~~900~~	~~2.64~~	~~0.37~~	
	Average		875	2.36	0.39	
	Standard Deviation		86	0.23	0.04	
	COV		10%	10%	11%	